#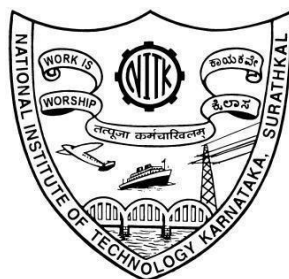 DESIGN, SYNTHESIS AND CHARACTERIZATION OF COLORIMETRIC RECEPTORS FOR THE DETECTION OF BIOLOGICALLY AND ENVIRONMENTALLY IMPORTANT ANIONS AND ITS APPLICATIONS

Thesis

Submitted in partial fulfilment of the requirements for the degree of
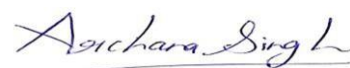
DOCTOR OF PHILOSOPHY

by

ARCHANA SINGH

DEPARTMENT OF CHEMISTRY

NATIONAL INSTITUTE OF TECHNOLOGY KARNATAKA,

SURATHKAL, MANGALORE-575025

May, 2020

DECLARATION

by the Ph.D. Research Scholar

I hereby *declare* that the Research Thesis entitled **"Design, Synthesis and Characterization of Colorimetric Receptors for the Detection of Biologically and Environmentally Important Anions and its Applications"** Which is being submitted to the National Institute of Technology Karnataka, Surathkal in partial fulfilment of the requirements for the award of the Degree of Doctor of Philosophy in **Chemistry** is a *bonafide report of the research work carried out by me*. The material contained in this Research Thesis has not been submitted to any University or Institution for the award of any degree.

Archana Singh

Archana Singh

Reg. No.: 155069CY15F02

Department of Chemistry

Place: Surat, Gujarat

Date:06/09/2020

CERTIFICATE

This is to certify that the Research Thesis entitled "**Design, Synthesis and Characterization of Colorimetric Receptors for the Detection of Biologically and Environmentally Important Anions and its Applications**" submitted by **Ms. Archana Singh** (Register Number: **155069CY15F02**) as the record of the research work carried out by her, is *accepted as the Research Thesis submission* in partial fulfilment of the requirements for the award of degree of Doctor of Philosophy.

Dr. Darshak R. Trivedi

Research Guide(s)

Date:

Chairman - DRPC

Date:

DEDICATED TO MY

MOTHER

FATHER

BROTHERS

SISTER

FRIENDS

&

NANI

One book,
One pencil,
One Pen, and
One teacher
can change the life………

Dr. Darshak R. Trivedi

Associate Professor

Research Guide

N.I.T.K

ACKNOWLEDGEMENT

"Experience is the best teacher"

It has been a great experience pursuing research career at National Institute of Technology Karnataka (NITK) Surathkal with proficient and unique individuals who have helped me to achieve what I have up to this point. I would like to express my deepest appreciation for the help and support of the kind people around me, to only some of whom it is possible to give a particular mention here.

My first gratitude must go to my advisor, **Dr. Darshak R. Trivedi** who patiently provided me the vision and necessary guidance as well as support to reach the vision. This work would not have been possible without his supervision and encouragement throughout the research program. Along with the subject he taught me how to tackle the difficulties of life and ultimately to reach the goals successfully. I am sure it will support me to move forward in my career and life as well.

I am grateful to NITK for the research infrastructure and fellowship that allowed me to work at a smoother pace. I am grateful to Prof. Arun M. Isloor, Head, Department of Chemistry and Chairman-DRPC, prof. D. Krishna Bhatt, and Prof. B. Ramachandra Bhat, Former Head, Department of Chemistry for their kind support. I am thankful to the RPAC members, Prof. Vidya Shetty K, Department of Chemical Engineering for the continuous guidance during my seminars that helped me shape my research work. I am also thankful to Dr. Debashree Chakraborty, Department of Chemistry for his encouragement and inspiration all throughout my work.

I thank Prof. A. Vasudeva Adhikari, Prof. A. Nityananda Shetty, Prof. A. Chitharanjan Hegde, Dr. Udaya Kumar D., Dr. Sib Sankar Mal, Dr. Beneesh P.B., Dr. Saikat Datta, Dr. Lakshmi Vellanki and Dr. Vijayendra S. Shetti for their support during the research work. I wish to convey my sincere thanks to Dr. Ajith K. M., Assistant Professor, Department of Physics, NITK Surathkal for his support in providing access to Gaussian 09 package.

I am thankful to Dr. Suban K. Sahoo, Department of Applied Chemistry, S.V. National Institute Technology Surat, Gujarat for the kind help and productive discussions on

<div align="right">**ARCHANA SINGH**</div>

ABSTRACT

Nature in its fullest form is a reservoir of biochemical processes regulated by various ionic species, which are primarily known to sustain ecological balance in the living system. Among them, anions such as fluoride (F^-), acetate (AcO^-), dihydrogen phosphate ($H_2PO_4^-$), carbonate (CO_3^{2-}), arsenite (AsO_2^-), arsenate (AsO_4^{2-}), and dicarboxylates have a profound impact on human health, which are both beneficial and detrimental, depending on the amount present in the living system. Apart from the above anions detection, the detection of sodium fluoride and acetate ions in aqueous medium is important due its importance in household usage in the form of food, medicine, and cosmetics. Beyond an optimum amount, anions can lead to health issues. In this direction, the design and synthesis of artificial organic receptors has garnered great attention due to its ability to mimic molecular recognition at the physiological level. Owing to the profound utility of artificial receptors, this work–focuses on the rational design of organic receptors, which can aid the colorimetric detection of anions. Seven different series of receptors based on various backbones, following binding site-signalling unit approach, has been designed, synthesized, and characterized by standard spectroscopic techniques. The anion binding ability of the receptors is evaluated in appropriate solvent systems and confirmed by UV-Vis titration, ^{1}H-NMR titration, Cyclic voltammetric, and DFT studies. The binding constant for the receptor-anion complex is calculated using the Benesi–Hildebrand equation. The binding mechanism is proposed based on UV-Vis titration and the same is confirmed by ^{1}H NMR titration. The lower detection limit valves of the receptors achieved towards active anions signifies their efficacy in real- life application. Based on the experimental results, it is concluded that simple organic molecules can act as very good colorimetric receptors for biologically important anions such as F^-, AcO^-, $H_2PO_4^-$, dicarboxylate, and CO_3^{2-}. Along with colorimetric detection, these receptors exhibited practical application such as detection of F^- ion in sea water, commercially available mouthwash and toothpaste, detection of AcO^- ion in vinegar solution and test strip application.

Keywords: Anion Receptors, Colorimetric detection, Solvatochromism, Aqueous media, Deprotonation, Intramolecular charge transfer

CONTENTS

CHAPTER 1: INTRODUCTION AND LITERATURE REVIEW

CHAPTER 2: COLORIMETRIC ANION SENSORS BASED ON POSITIONAL EFFECT OF NITRO GROUP FOR RECOGNITION OF BIOLOGICALLY RELEVANT ANIONS IN ORGANIC AND AQUEOUS MEDIUM, INSIGHT REAL - LIFE APPLICATION AND DFT STUDIES

CHAPTER 3: SUBSTITUENT EFFECT FOR COLORIMETRIC DETECTION OF BIOLOGICALLY AND ENVIRONMENTALLY RELEVANT ANIONS: INSIGHT IN REAL LIFE APPLICATION

CHAPTER 4: DESIGN AND SYNTHESIS NEW COLORIMETRIC RECEPTORS FOR NAKED-EYE DETECTION OF BIOLOGICALLY IMPORTANT FLUORIDE AND ACETATE ANIONS IN ORGANIC AND ARSENITE IN AQUEOUS MEDIUM BASED ON ICT MECHANISM: DFT STUDY AND TEST STRIP APPLICATION

CHAPTER 5: CHEMOSENSOR BASED ON HYDRAZINYL PYRIDINE FOR SELECTIVE DETECTION OF F ⁻ ION IN ORGANIC MEDIA AND CO₃²⁻ IONS IN AQUEOUS MEDIA: DESIGN, SYNTHESIS, CHARACTERIZATION AND PRACTICAL APPLICATION

CHAPTER 6: DESIGN AND SYNTHESIS OF MALONOHYDRAZIDE BASED COLORIMETRIC RECEPTORS FOR DISCRIMINATION OF MALEATE OVER FUMARATE AND DETECTION OF F⁻, ACO⁻ AND ASO₂⁻ IONS

CHAPTER 7: SPECTROSCOPIC STUDIES OF COLORIMETRIC RECEPTORS FOR RECOGNITION OF BIOLOGICALLY IMPORTANT F⁻, ACO⁻ AND $H_2PO_4^-$ ANIONS IN ORGANO-AQUEOUS MEDIUM: REAL-LIFE APPLICATION

CHAPTER 8 : SUMMARY AND CONCLUSIONS

NOMENCLATURE

ABBREVIATION

ACN	Acetonitrile
AcOH	Acetic acid
AcO^-	Acetate ion
AsO_2^-	Arsenite
AsO_4^{2-}	Arsenate
B-H	Benesi-Hildebrand
Br^-	Bromide
^{13}C-NMR	Carbon-13 nuclear magnetic resonance
Cl^-	Chloride
DCM	Dichloromethane
DFT	Density Functional Theory
DMF	Dimethylsulfoxide
DMSO-d_6	Dimethylsulfoxide-deuterated
ESI	Electron Spray Ionized
EtOH	Ethyl alcohol
Equiv.	Equivalence
Fig	Figure
F^-	Fluoride
FT-IR	Fourier Transform Infra-Red
HOMO	Highest Occupied Molecular Orbital
^1H-NMR	Proton Nuclear Magnetic Resonance
$H_2PO_4^-$	Dihydrogen phosphate
HSO_4^-	Hydrogen sulfate
I^-	Iodide
ICT	Intramolecular Charge Transfer
LUMO	Lowest Unoccupied Molecular Orbital
MeOH	Methanol
mp	Melting point

MS	Mass Spectra
NO_3^-	Nitrate
$NaCO_3^{2-}$	Sodium bicarbonate
NaF	Sodium Fluoride
NaAcO	Sodium Acetate
RT	Room temperature
TBA	Tetra Butyl Ammonium
THF	Tetramethylsilane
TMS	Tetramethylsilane
TLC	Thin Layer Chromatography
UV-Vis	Ultraviolet-Visible
WHO	World Health Organization

SYMBOLS AND UNITS

α	Alpha
β	Beta
cm	Centimetre
°	Degree
°C	Degree Celsius
δ	Delta
γ	Gamma
g	Gram
>	Greater than
h	Hour
Hz	Hertz
-1	Inverse
λ	Lamda
<	Less than
L	Litre
MHz	Mega hertz
mL	millilitre
mmol	millimole
min	Minute
M	Molar
μ	Mu
nm	Nanometre
ppm	Parts per million
θ	Theta

CHAPTER 1

INTRODUCTION AND LITERATURE REVIEW
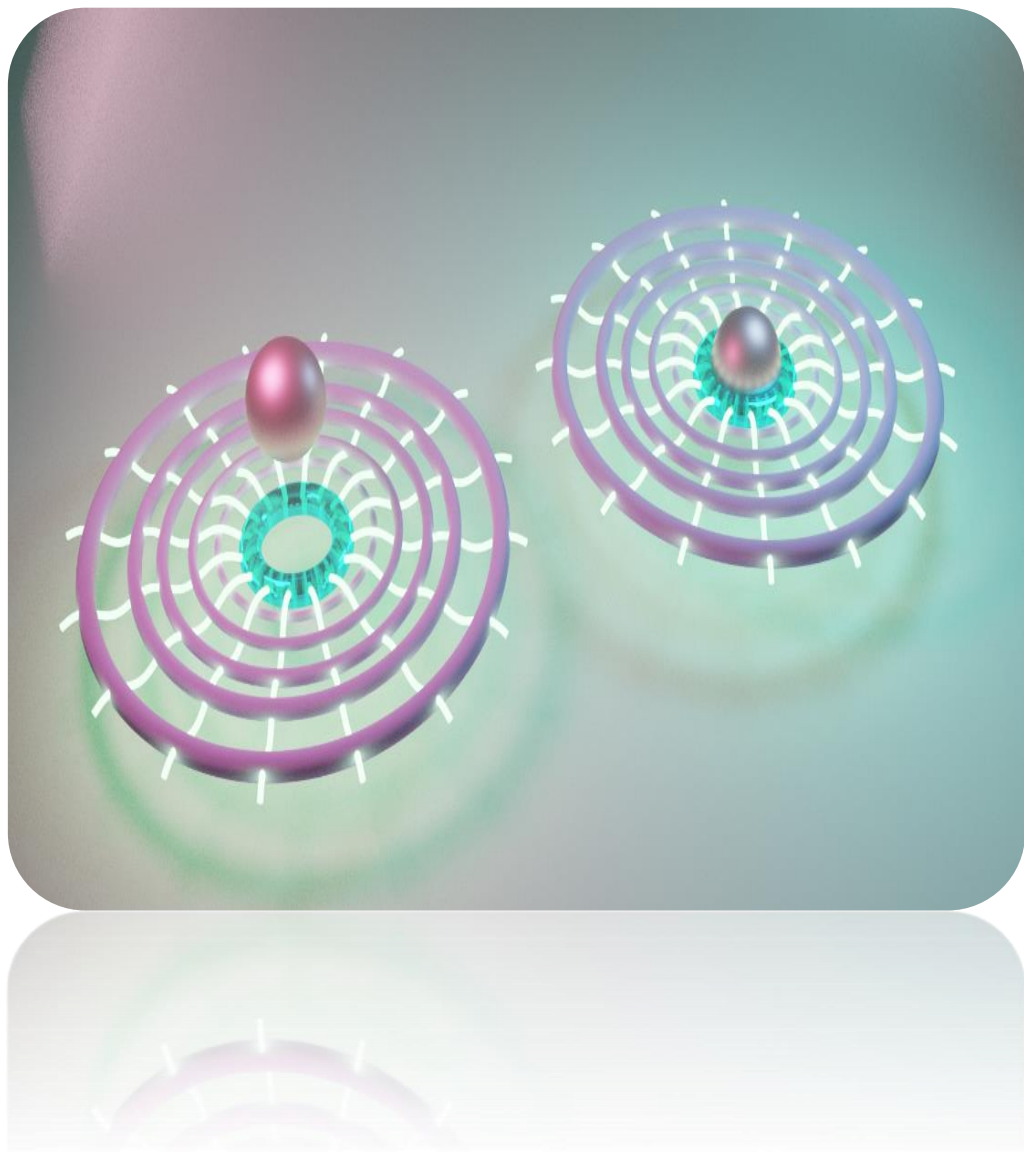
Abstract: In this chapter, a brief introduction about supramolecular chemistry and anion is given. In addition, challenges in anion detection, colorimetric chemosensor, a brief review of literature, and scope and objectives of the current work have been presented.

1.1   SUPRAMOLECULAR CHEMISTRY

Supramolecular chemistry as defined by Jean-Marie Lehn, who shared the Nobel Prize for this work in the year 1987, is the chemistry of the intermolecular bond covering the structure and functions of the association of two or more chemical species. It can also be defined as 'the chemistry of the non-covalent bond' and 'non-molecular chemistry'. Supramolecular chemistry is defined in terms of the non-covalent interaction between a 'host' and a 'guest' molecule where the large host molecule is capable of enclosing the smaller guest molecular via non-covalent interaction. Thus, supramolecular chemistry is spontaneous, self-assembly, and reversible association of two or more components to form large non-covalent bound aggregates. The general structure aspects of supramolecular chemistry are shown in Fig. 1.1.
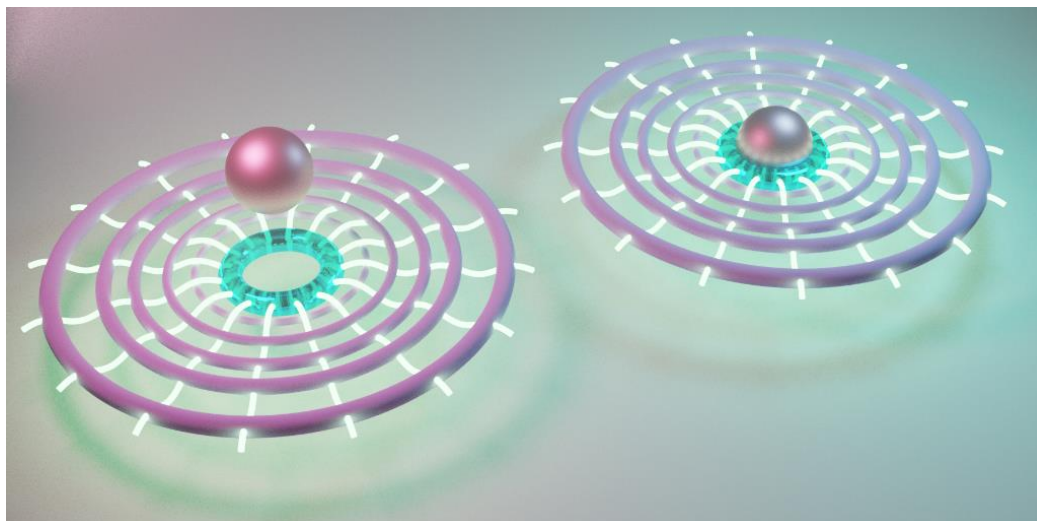
Fig. 1.1 Representation of the structural aspects of supramolecular chemistry

1.2   HOST-GUEST CHEMISTRY

Supramolecular chemistry involves the interaction of two or more components. The term 'Host-Guest chemistry' can be correlated to the complexation phenomenon. It involves the binding of the host molecule with the guest molecule forming a host-guest complex. An ion or an organic molecule whose binding sites converge in the complex is called as the host component. An ion or molecule whose binding site diverges in a complex is called as the guest component. A region of the host or guest that is of the correct size, geometry, and chemical nature and can interact through non-covalent interactions is referred to as the binding site. In supramolecular chemistry, a molecular complex is said to be highly structured if it is composed of at least one host and one guest component. For an efficient host-guest relationship, there should be complementary stereo-electronic arrangement of the binding sites for the host and the guest. Simple guests are quite abundant because the location of divergent binding sites does not involve complex organization. Hosts with appropriate binding sites are rare to find, which necessitates them to be designed and synthesized. In other words, the binding and supporting parts of the hosts when compared with the guests have to be quite large.

1.3   ANIONS

By definition, anions are species that have gained an electron and are negatively charged. They possess more number of electrons than protons. Though there are many elements from stable atomic cations or positively charged ions, only a handful form stable atomic anions. Elements belonging to Group 17 or the halides F, Cl, Br, and I readily form anions bearing -1 charge (F^-, Cl^-, Br^-, and I^-), while Group 16 elements O and S form atomic anions with -2 charge (O^{2-} and S^{2-}). Molecular ions or polyatomic ions are abundant in nature. They are stable chemical species, which retain their structure in crystals as well as in solution. Mostly, polyatomic ions are classified into three categories: (i) Diatomic anions, e.g., OH^- and CN^-, (ii) Anions with carbon, e.g., CO_3^-, CH_3COO^-, and $C_2O_4^{2-}$, and (iii) Oxoanions which possess a central atom surrounded by one to four oxygen atoms, e.g., SO_4^{2-}, SO_3^{2-}, NO_3^-, NO_2^-, ClO_4^- , etc.

1.3.1 Environmentally and biologically important anions

Anions are responsible for many biological processes as well as in regulating several environmental processes. Generally, an anion is directly involved in various biological parameters such as retaining cell volume, osmotic pressure, production of electrical signals, activation of pathways to transfer genetic information, etc. (Alberts et al.1994). Thus, anions directly influence many genetic disorders such as Pendred's syndrome (Scott et al. 1999; Yoshida et al. 2002), Bartter's syndrome (Simon et al.,1997) Dent's disease (Devuyst et al. 1999), cystic fibrosis (Anderson et al.1991), and osteoporosis (Kornak et al. 2001). Anions are an indispensable component in the interaction between RNA/DNA and proteins as well as in many enzymatic complexes and are the energy source for enzymatic transformation. Further, anions act as environmental pollutants, which includes contamination of drinking water with fluoride, carcinogenesis (the process by which normal cells are transformed in to cancer cells) by metabolites of acetate, and eutrophication (uncontrolled growth of algae due to excess of nutrients in water bodies) caused by phosphate/nitrates containing fertilizers (Moss 1996). Though there are many disadvantages associated with anions, some of them are still essential for normal health.

1.3.1.1 Fluoride (F^-)

Fluoride is known to have multiple implications on human health. It gains entry into the human body through the gastrointestinal tract and is readily absorbed in the stomach (Whitford 1996). Fluoride is known to decrease the incidence of dental carries and enhance the rate of enamel remineralization (Bratthall et al. 1996; Margolis and Moreno 1990; Murray 1993). However, excessive fluoride ingestion during tooth formation can lead to hypominerlization of dental enamel leading to dental fluorosis (Fejerskov et al. 1987; Richards et al. 1986). Long- term exposure to small amounts of fluoride in drinking water can lead to skeletal fluorosis (Evans and Darvell 1995)

1.3.1.2 Acetate (AcO^-)

Acetate, being a planar oxy-anion, plays an important role in the chemical, environmental, and biochemical metabolic processes. Acetates are a common building

block for biosynthesis. The fatty acids are produced by connecting C2 units derived from acetate (March 1992). It is mainly used by organisms in the form of acetyl coenzyme A. They play an important role in the nylon industry and also in the manufacture of paper, paints, dyes, and plastics. They exhibit special biochemical behaviour in enzymes and antibodies. The LD50-value of acetate is found to be 3530 mg/kg. Acetate is used as an indicator of organic decomposition in marine sediments based on the rate of acetate production and oxidation (Christensen 1984; Sørensen et al. 1981). Also, it exhibits specific biochemical behaviour in enzymes and antibodies (Vella 1990). In addition, sodium salts of acetate are used in foodstuffs including meat, poultry, and fish (Suganya et al. 2014).

1.3.1.3 Dihydrogen Phosphate ($H_2PO_4^-$)

Dihydrogen phosphate is ubiquitous in biochemical. It is usually the leaving group in metabolic reactions (Preiss and Handler 1958). Inorganic phosphates, commonly used as fertilizer in agriculture, are a potent cause for the eutrophication of the aquatic system when they runoff into the river (Greenhalgh and Selman 2012). Dihydrogen phosphate plays key roles in signal transduction, energy storage of the biological system, and gene construction. The maintenance of the phosphate level at physiological condition is crucial as it is one of the prime factors influencing bone health (Marks et al. 2010).

1.3.1.4 Arsenic (As)

Arsenic is a potent source of toxicity to the living system as it presents severe health issues such as skin cancer, skin lesions, neurotoxicity, cardiovascular diseases, and diabetes. Researches have extensively studied the biogeochemistry of arsenic (Ferguson and Gavis 1972) and found that arsenate is predominant in well-oxidized water and arsenite is predominant in reduced environments. Research indicates arsenite to be almost 25-60 times more toxic than arsenate and more mobile in the environment (Asadollahzadeh et al. 2014; Korte and Fernando 1991).

1.3.1.5   Carbonate ion (CO_3^{2-})

The detection and quantification of carbonate is of great importance due to its abundance and ubiquity in natural water and soil environments, mainly as metal carbonates (Chen et al. 2011). Carbonate compounds are extensively used in the manufacture of glass, rayon, rubber, plastic, paper, printing, ink, and food industries (Ghorai et al. 2016; Tas 2009). In spite of these wide applications in various processes, the carbonate ion is toxic in large doses. The strong caustic effect of carbonate to the gastrointestinal tract can cause severe abdominal pain, vomiting, diarrhoea, collapse, and even death (Jain et al. 2006).

1.3.1.6   Dicarboxylate ions

Generally, dicarboxylates are anions which contain two carboxylic acid functional groups in a molecule. Dicarboxylic acids have gained significance due to their widespread application in pharmaceutical and food industries. Apart from these, dicarboxylates are used in fragrances, polyamides/nylons, adhesive, lubricants, polyurethane foams, leather tanning, and polyesters. Furthermore, they are biologically very important as they play a crucial role in numerous metabolic processes such as glyoxalate cycle, generation of high energy phosphate bonds, and in dicarboxylate cycle for autotrophic carbon dioxide (CO_2) fixation (Berg et al. 2012). Dicarboxylate isomers such as maleate and fumarate play a significant role in many biological processes. For example, fumarate is generated in the krebs cycle and maleate is used to inhibit the krebs cycle (Gougoux at al.1976; EiamOng et al. 1995). The cis-aconitate is produced during the citric acid cycle, whereas trans-aconitate is a good inhibitor of both aconitase and fumarase (Katz et al. 2004).

1.4   ANION RECEPTOR CHEMISTRY

The prominent feature of anions is their negative electrostatic changes which distinguished themselves from other guest species. Also, the pre-organized placement of complementary binding sites on the receptors constitutes the basic design criteria. Combining above two features, it could be said that anion receptors chemistry involves

in designing new synthetic receptors for quantifying and sensing anions (Sessler et al. 2006)

1.4.1   Challenges of anion receptor chemistry

The design of anion receptors involves the criteria of specificity arising from the preorganized placement of complementary binding sites. Even if the above necessity is fulfilled, certain properties of anions make the task slightly more challenging. These could be summarized as follows:

❖   Anions being larger than cations require larger receptors, which can accommodate them. F^- (1.33A^0), being the smallest anion, has a radius comparable to that of K^+ (1.388A^0) (Shannon 1976). Cations are generally spherical in shape, with the exception of organic cations, while anions exist in many shapes and sizes. For example, halides (F^-, Cl^-, Br^-, I^-) are spherical, SCN^- are linear, NO_3^- are planar, HPO_4^- are tetrahedral, and PF_6 are octahedral. On the other hand, biologically important anions like nucleotides and proteins have complex shapes. The different shapes of anions are shown in Fig. 1.2.

F^-, Cl^-, Br^-, I^- CN^-, SCN^-, OH^- CN^-, SCN^-, OH^-

Spherical   *Linear*   *Trigonal planar*

$PO_4{}^{3-}$, $VO_4{}^{3-}$, $MnO_4{}^{3-}$, $ClO_4{}^{3-}$

Tetrahedral

$[Fe(CN)6]^{4-}$, $[Co(CN)_6]^{3-}$

Octahedral
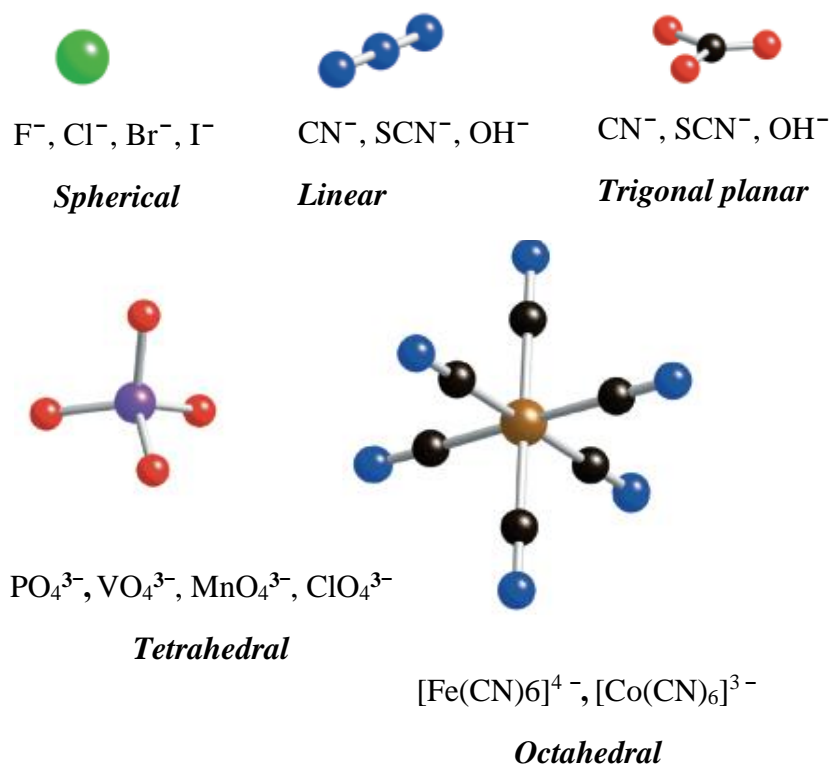
Fig. 1.2 Different shapes and sizes of anions

❖ Anions have high free energy of solvation and thus, the nature of the solvent interferes in the anions binding event through factors such as binding strength and selectivity. Electrostatic interaction stabilizes the anions in solution dwarfing other recognition forces. Hydroxylic solvents are potent enough to form a strong hydrogen bond with anions. Therefore, a potential anion receptor has to face tough competition with the solvent environment in an aqueous recognition event. Considering the example of a neutral receptor where the interaction with the anion is primarily hydrogen bonding, it is less likely to compete with the polar protic solvation shell present around the target anion in a hydroxylic solvent. Thus, it only functions as an anion receptor in aprotic organic solvents. On the other hand, a charged receptor incurs benefit from electrostatic effects and as a result, competes more effectively with polar protic solvents. Lastly, it is the anion receptor that not only competes with the solvent, but also with the counter anions paired with the target anion.

❖ Anions are pH sensitive and easily get protonated at low pH to lose their negative charge. Thus, receptors must function within the pH range of the target anions.

❖ Anions are usually co-ordinatively saturated. Therefore, the binding of anions should take place only through weak forces such as hydrogen bonding or van der Waals interactions.

❖ Hydrophobicity is one of the factors influencing the selectivity of the receptor. It could be well -explained with the Hofmeister series (Hofmeister 1888), which is the result of studies on the effects of salts on the solubility of the proteins. This series orders anions by their decreasing hydrophobicity and consequently increases in the degree of aqueous solvation. Hydrophobicity can be used in the design of anion receptors to bias selectivity towards large anions with low charge. Both hydrophobicity and the Hofmeister series can be used in solvent extraction of anions from an aqueous solution. The anion receptors, which perturb (or bias) the Hofmeister series from its normal order, help in the selective extraction of a particular anion as shown in (Scheme 1.1).

Organic anions $> ClO_4^- > SCN^- > I^- >$ Salicylate $> NO_3^- > Br^- > Cl^- > HCO_3^- > H_2PO_4^- > F^- > SO_4^{2-} > H_2PO_4^-$

Scheme 1.1 Representation of the Hofmeister series

1.4.2 History of anion receptor chemistry

The first synthetic anion receptor was reported by Park and Simmons in the later '60s (park and simmons 1968). Their work highlighted the halide binding properties of a macrobicyclic receptor containing two ammonium centres bridged by three alkyl linkers. (Scheme 1.2)

Following this, Lehn and co-worker (Graf and Lehn 1976) designed a variety of macrobicyclic and macrotricyclic ammonium- based receptors (cryptands), which demonstrated the optimization of an anion fit for a given charged cavity for stronger binding (Scheme 1.3). Further, they extended their work to the synthesis of protonated cryptands to bind linear species like azide (Scheme 1.4). The crystal structure of the azide bound receptor showed the presence of hydrogen-bonding interaction.

Later in early '80s, Schimidtchen designed and synthesized a series of receptors having quaternary ammonium groups arranged in a tetrahedral fashion that bind anions in their cage- like structure through electrostatic interactions. The selectivity towards anions was increased by altering the alkyl chain length between the ammonium centres (Scheme 1.5). Positively charged ammonium- based receptors with appropriate counter anions resulted in a competitive effect with the anions in the binding process (Scheme 1.6).

In 1980s, Sesslers reported the role of porphyrin- based receptors like sapphyrin, a pentapyrrolic macrocycle (Scheme 1.7). As it was readily susceptible to protonation the generation of monopositive and dipositive macrocycles was much easier. Macrocyclic core based doubly protonated sapphyrin proved to be the binding of the fluoride ion. Pyrroles- based cyclic and acyclic receptors, having relatively good anion binding properties, have been extensively studied. With this rich anion complexation chemistry, pyrroles- based receptors have been extensively worked upon by Gale, Sessler, and others.

Pascal and co-worker in 1986 reported hydrogen bonding between neutral receptors and anions, wherein the receptors included groups like amide, urea, and pyrroles within the cyclophane host (Scheme 1.8).

In 1993, a series of acyclic tripodal receptors containing amide groups were synthesized by Reinhoudt and co-worker for anions such as HSO_4^-, $H_2PO_4^-$, and Cl^- (Scheme 1.9). The binding constant was measured by conductivity measurement in acetonitrile. Prior to this work, Wilcox and co-workers designed and synthesized receptors with built- in urea subunits for detection of oxoanions (Scheme 1.10). According to them, the presence of hydrogen bonding between urea and oxoanions assisted the binding process, and UV-Vis titration was performed in chloroform solution using the receptors and a variety of oxoanions.
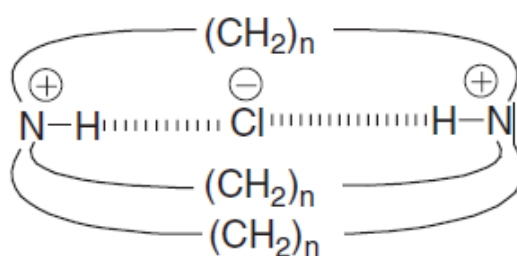
Scheme 1.2 Macrobicyclic receptors with ammonium bridgehead centres and alkyl linkers
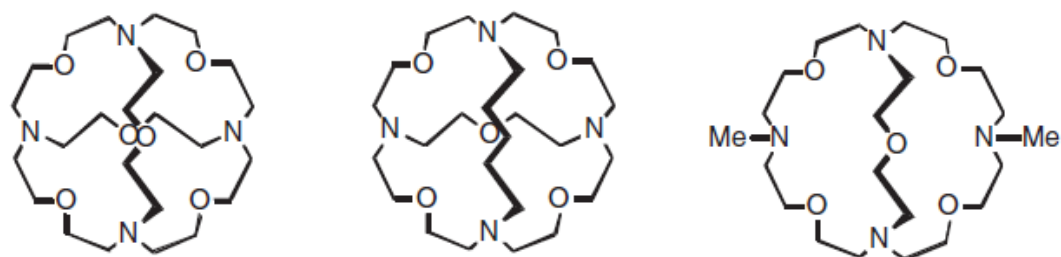
Scheme 1.3 Macrobicyclic and macrotricyclic ammonium based receptors (cryptands)
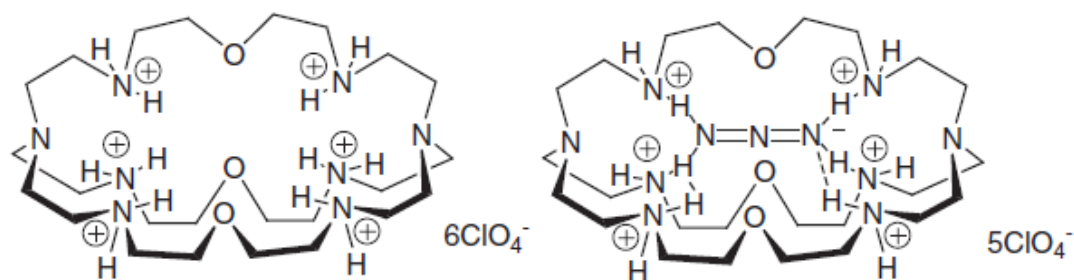
Scheme 1.4 Protonated cryptands

Me
N⊕

X   X
X
Me~N
-X-
N·Me
X   X
N⊕
Me

X = –(CH₂)₆–
X = –(CH₂)₈–

$$X = -(CH_2)_6-$$
$$X = -(CH_2)_8-$$
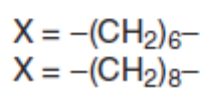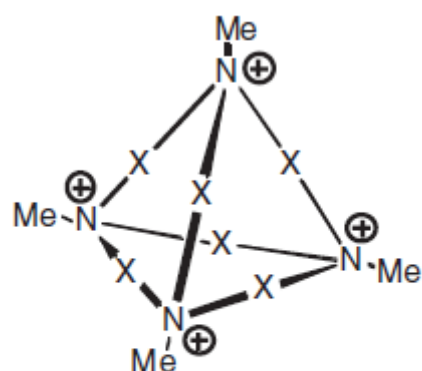
Scheme 1.5 Receptors bearing quaternary ammonium groups and alkyl linkers

⊖BH₃
N⊕

X   X
X
H₃B—N
-X-
N—BH₃
X   X
N⊕
H₃B⊖

$$X = -(CH_2)_6-$$
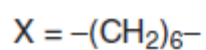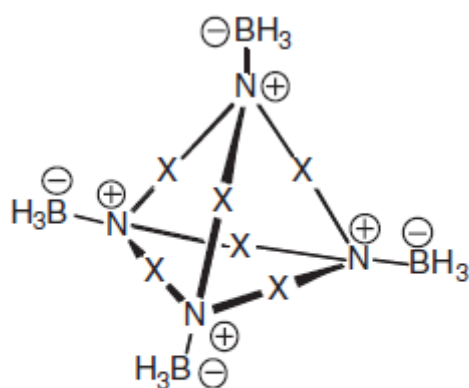
Scheme 1.6 Neutral zwitterionic receptors

S
S
S
N
H
N—H   H—N
O
O=
O
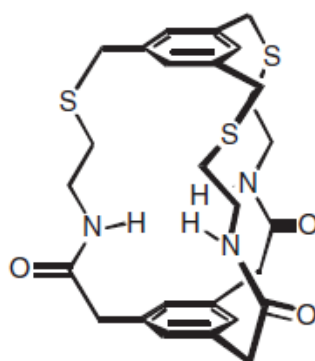
Scheme 1.7 Neutral cyclophane- based receptors

R = CH₂Cl
R = (CH₂)₄CH₃
R = C₆H₅
R = 4-MeOC₆H₄

R = 4-MeC₆H₅
R = 2-naphthyl
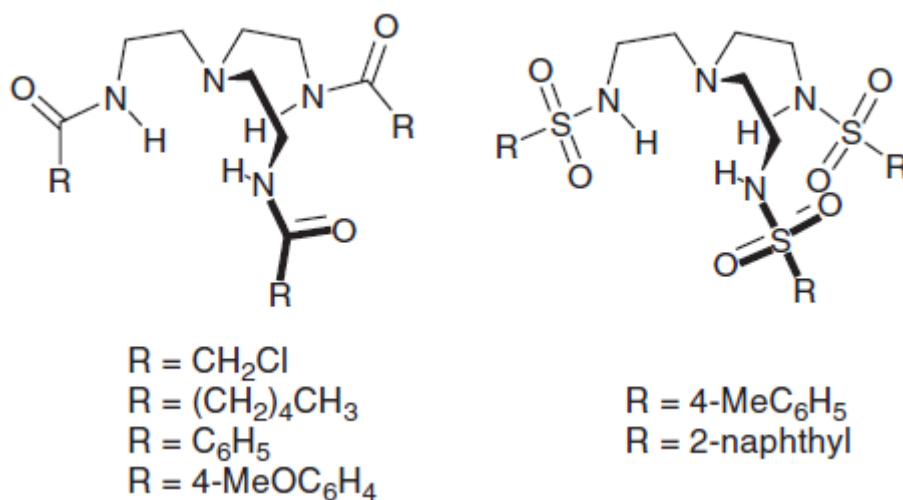
Scheme 1.8 A series of acyclic tripodal receptors bearing amide groups

X = O
X = S
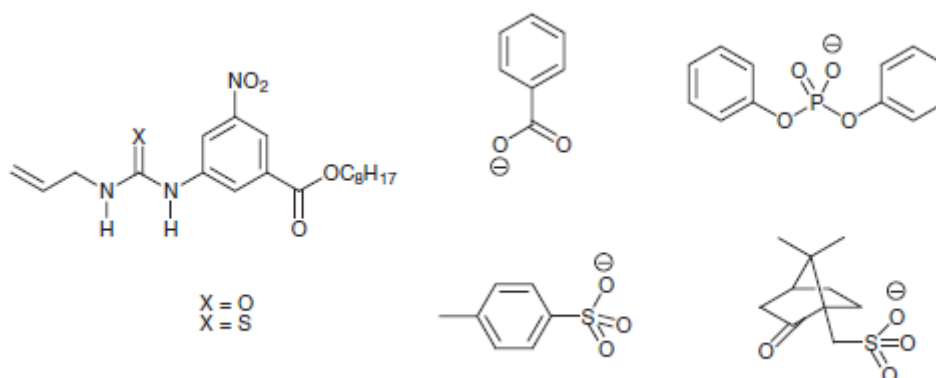
Scheme 1.9 A series of synthetic receptor containing a built in urea subunit and oxo-anionic guests
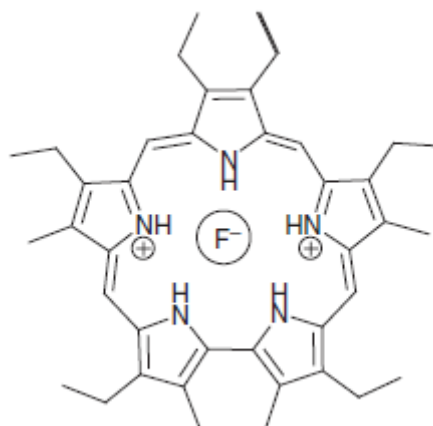
Scheme 1.10 Porphyrin- based receptor

1.5 COLORIMETRIC CHEMOSENSOR

Since its inception, the design and synthesis of new receptors has been focused on practical applications. Molecular sensing is one such field, which has received more attention in the last decade. According to analytical chemistry, sensor is a device that can detect and quantify the concentration of the analyte. In the field of supramolecular chemistry, molecular biology, and biochemistry, the term 'sensor' is closely associated with a molecular event. A receptor can be called a sensor when the chemical receptor gives a measurable signal in response to the binding of an analyte. It was Antony Czarnick, who coined the term 'chemosensor' to differentiate between a designed chemical receptor and biosensors (Czarnik 1994).

The design of new synthetic receptors for sensing applications can be a fertile ground for the creativity of supramolecular chemists. A receptor design is vital for the sensing process, but its binding strategy is more important. Depending on the type of signal produced on the binding event, chemosensors can be classified into two categories as electronic sensors and optical sensors. Electronic sensors exhibit changes in its electrochemical properties, while optical sensors exhibit change in the optical signals on binding events. In general, three components get together in the construction of an optical anion sensor, namely, the anion binding site, the chromophore or signalling unit, and the method of measuring the change and converting it into useful information (Suksai and Tuntulani 2003).

Optical sensors can be further classified as

i) **Chromogenic / Colorimetric chemosensor**: Here, the signalling unit results in colour change on the binding of the guest moiety by the receptor as depicted in Fig. 1.3.
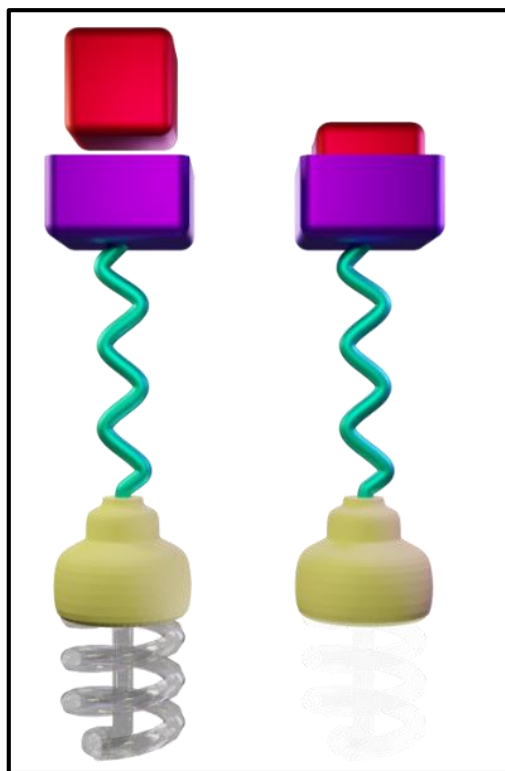
Fig. 1.3 Principle of chromogenic anion sensors

ii) **Fluorogenic / Fluorometric chemosensor**: In this type, the interaction between the guest moiety and the receptor results in changes in the fluorescence behaviour of the signalling unit as given in Fig. 1.4.

Optical approaches like colorimetric and fluorometric are commonly used techniques to quantify and sense anions. The simple instrumentation involved with the colorimetric techniques and the possibility of achieving lower detection limits through fluorimetry have made them much more appealing.
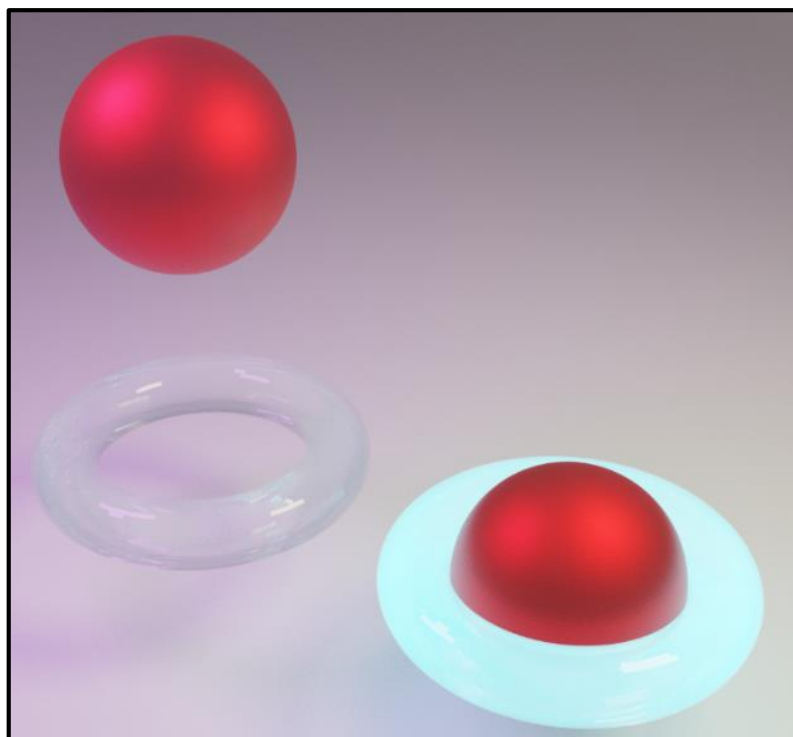
Fig. 1.4 Fluorometric chemosensor

1.5.1 Types of colorimetric chemosensors

Depending on the nature of interaction of the binding site with the signalling unit, three different approaches have been used by various groups in pursing synthetic receptors.

i)   Binding site- signalling unit approach

This involves the attachment of binding sites to the signalling unit through covalent bonds. The interaction of the anion with the binding site changes the electronic property of the signalling unit. This leads to the sensing of the target anion through colour or emission modulation. And, in this approach, the sensing feature could be observation, but only in organic solvents. The colour change could be related to the basicity of the anions that either form hydrogen bond interaction or/ and induced deprotonation of the receptor (Amendola et al. 2006). A schematic representation of the binding site- signalling unit approach is shown in Fig. 1.5.
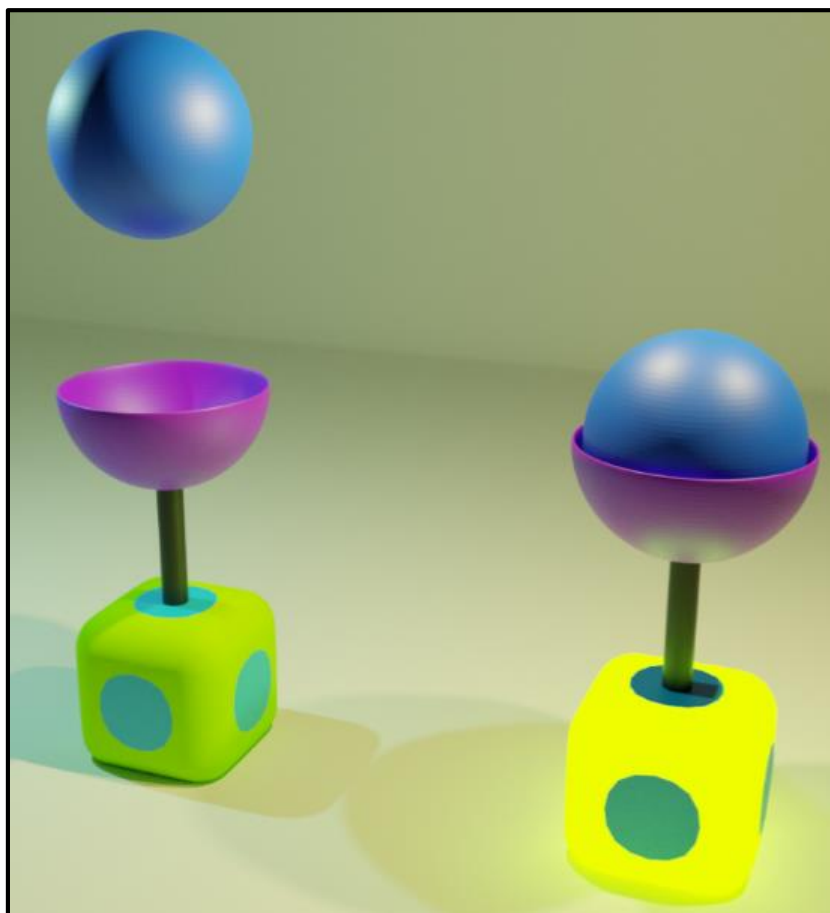
Fig. 1.5 Schematic representation of anion recognition through subunit approach

ii)   The Displacement assay approach

The displacement assay approach consists of a receptor, which contains a binding site and a signalling unit non-covalently bound together to form complex molecules. When an anion is introduced to the solution of this complex molecule, it substitutes the signalling unit and a free signalling unit in the solution incorporates the colour change in the system. The general representation of the diaplacement assay approach is depicted in Fig. 1.6.
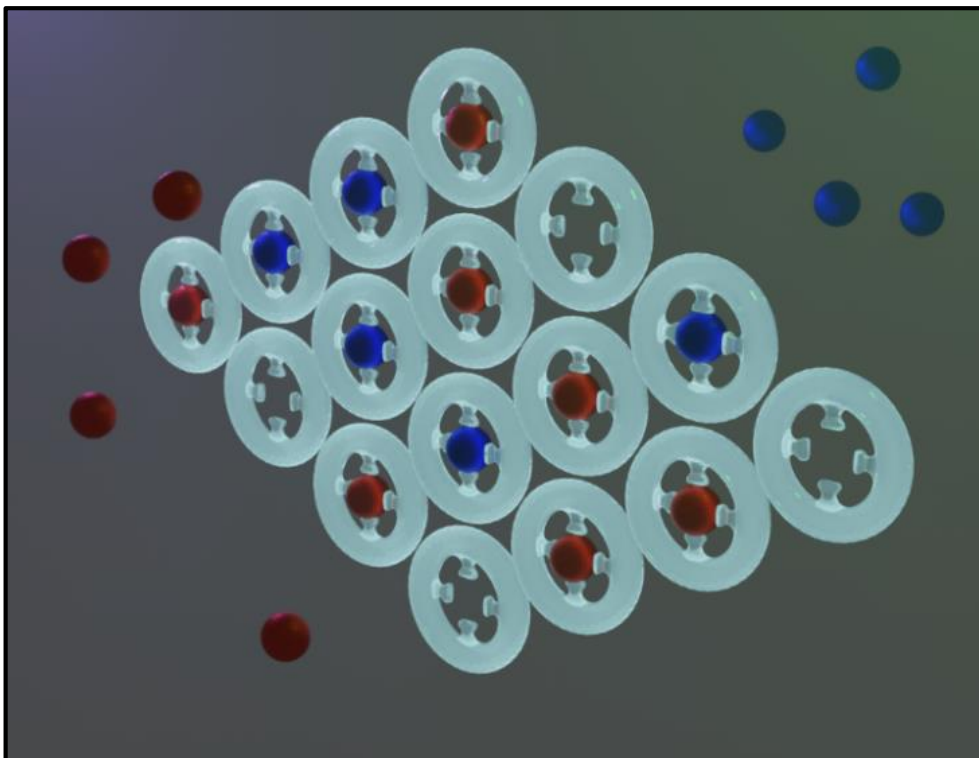
Fig. 1.6 Schematic representation of anion recognition through displacement assay approach

iii) Chemodosimeter approach

This represents a well-established procedure for the design of an anion receptor. It involves specific anion-induced reactions involving the rupture and formation of covalent bonds. It results in major chemical changes in the receptor along with remarkable spectroscopic changes. This approach involves the nucleophilic attack of the target species to electron density in the entire molecule and results in colour change (Xu et al. 2010). A general representation of the chemodosimeter approach is shown in Fig. 1.7.
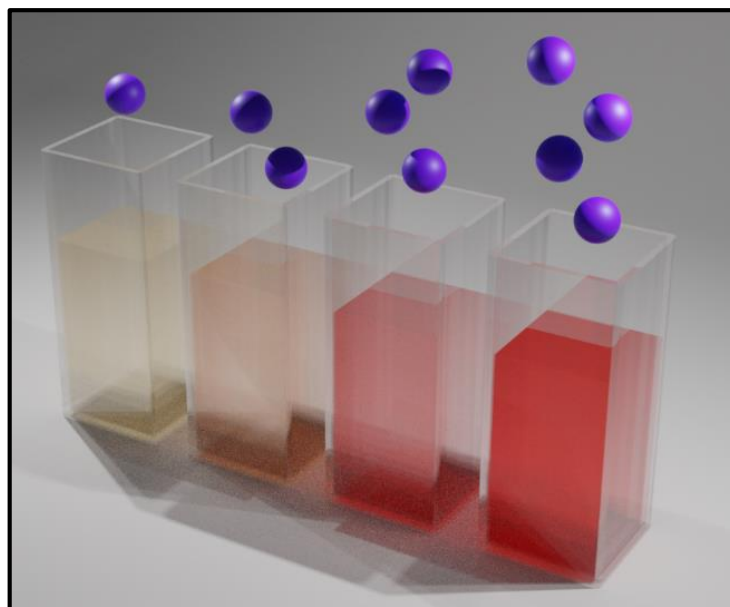
Fig. 1.7 Schematic representation of anion recognition through chemodosimeter approach

1.6   LITERATURE REVIEW

Anions receptors with numerous binding sites based on amide, thioamide, sulfonamide, urea, thiourea, indole, and pyrrole subunits have been reported in literature from several years. However, the selectivity binding of biologically important anions is still a challenging task and needs to be explored further. Despite there being challenges towards the anion detection process, researchers have extensively worked upon designing artificial receptors, which can bind anions through various non-covalent interaction such as hydrogen bonding and anion-π and through reactions like hydrogen abstraction and electron transfer (Beer et al. 2003). Since the current research is focused on colorimetric and detection of biologically important anions such as F^-, AcO^- and $H_2PO_4^-$ ions a brief literature survey relevant to the present study has been conducted.

1.6.1   Literature on F^-, AcO^- and $H_2PO_4^-$ ions detection

Mahapatra et al. 2011 developed a series of colorimetric receptors (**L 1.1-L 1.5**) with different substituted groups containing electron withdrawing and donating group. Among them, receptor **L 1.2** displayed high selectivity for F^- ion with intense colour change from pale yellow to purple due to the presence of electron withdrawing

nitro group which enhance acidity of azophenol moiety and displayed higher bathochromic shift ($\Delta\lambda_{max}$) of 122 nm with detection limit of 1.00×10^{-5} M. When the F^- ion binds to azophenol form hydrogen bonds which affect the electronic properties of chromophores, the result is a change of colour with a subsequent new internal charge transfer (ICT) between the F^- bound hydroxyl group and the electron deficient azo moiety which is confirmed by the ^{1}H-NMR titration. For analytical application, a test strip of the receptor **L 1.2** was used to detect the F^- ion.
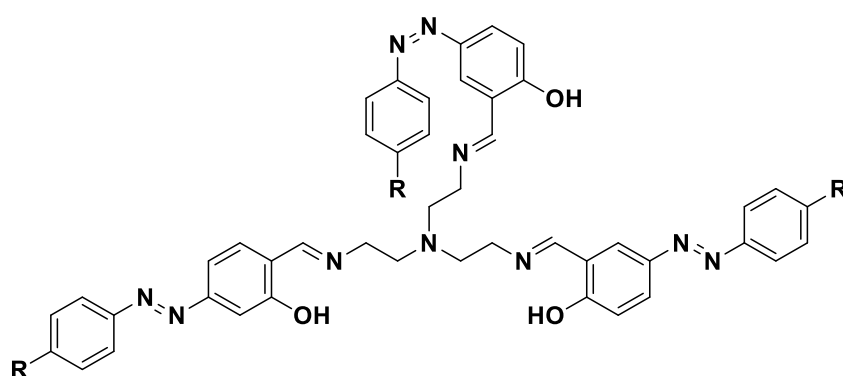
R= H   L 1.1
R=NO$_2$ L 1.2
R=COOEt   L 1.3
R=OMe   L 1.4
R=Me   L 1.5

L 1.1-L 1.5

Park et al. 2011 designed and synthesized a novel colorimetric receptor **L 1.6** based on the anthracene and nitrophenyl group as the signalling unit. The receptor **L1.6** utilized amide NH, amine NH, and 9-anthracenyl hydrogen to bind F^- and the $H_2PO_4^-$ ions. The Job's plot showed 1:1 stoichiometry between the receptor and F^- and the $H_2PO_4^-$ ions. The receptor **L1.6** selectively binds with F^- and $H_2PO_4^-$ ions with naked eye change from colourless to yellow in the DMSO, while the other anions did not show obvious colour change. The binding constants were found to be 7.0×10^2 M^{-1} and 5.0×10^2 M^{-1} in the DMSO.
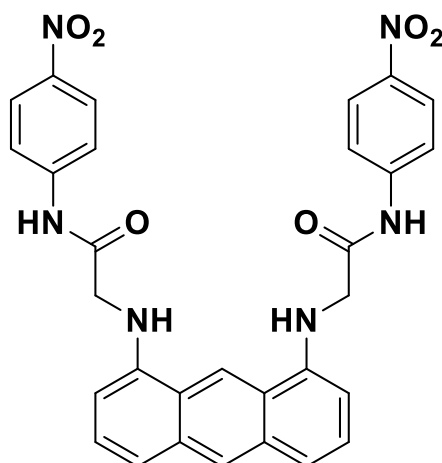
L 1.6

Bose et al. 2011 designed and synthesized a series of new symmetrically functionalized guanidinium chloride (**L 1.7, L 1.8, L 1.9, L 1.10, L 1.11, L 1.12, L 1.13, L 1.14, L 1.15,** and **L 1.16),** wherein the reactivity towards anions was tuned by varying the functional groups attached to the guanidium moiety with respect to (i) aromaticity (**L 1.7-L 1.10**) (ii) induction effect (**L 1.11- L. 1.15**) (iii) Positional isomeric effect (**L 1.13- L 1.15**) and (iv) Indole functionality (**L 1.16**) of the conjugated aryl unit. Receptor (**L 1.7-L 1.10**), fluoride induced vivid colour change from pale yellow to red to reddish orange and finally to blue irrespective of the increasing aromaticity and positional isomeric effect of the substituent that is attached to the guanidium moiety. Interestingly, **L 1.15** has shown the ability to sense distinctly both F and AcO ion colourimetrically. Further, **L 1.16** a sensor attached with indole functionality shows selectivity sensing of F ion colourimetrically. UV-Vis experiment performed to support the binding mechanism between the receptors and F⁻ ion. Single crystal X-ray analyses supported -NH deprotonation in the presence of the highly basic F⁻ and 1:1 binding in the presence of the less basic anion benzoate.

R = (phenyl) **L 1.7**

R= (naphthyl) **L 1.8**

R= (anthracenyl) **L 1.9**

R= (pyrenyl) **L 1.10**

R= (4-methoxyphenyl) —OMe **L 1.11**

R = (pentafluorophenyl) **L 1.12**

R= (2-nitrophenyl, O_2N) **L 1.13**

R= (3-nitrophenyl, NO_2) **L 1.14**

R= (4-nitrophenyl, NO_2) **L 1.15**

R= (3-methylindolyl) **L 1.16**
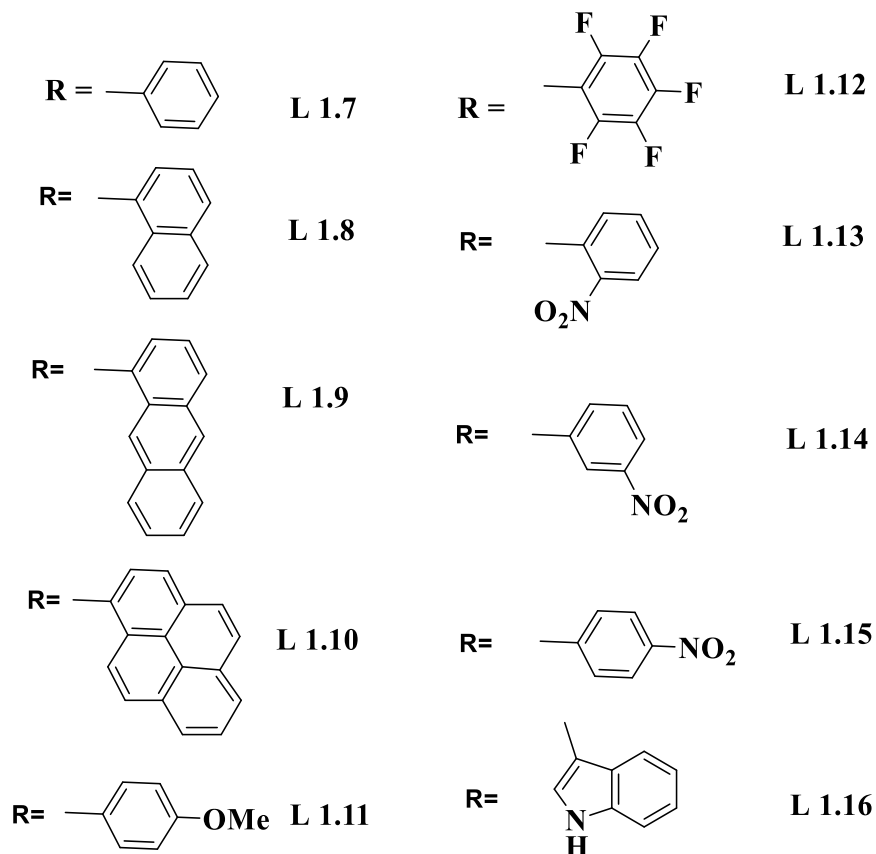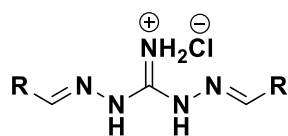
L 1.7- L 1.16

Santos-Figueroa et al. 2012 synthesized a family of heterocyclic thiosemicarbazone dyes (**L 1.17- L 1.23** and **L 1.24**) containing furyl groups, and their response in acetonitrile in the presence of selected anions was studied. The acetonitrile solution of the receptors showed absorption band in the 335-396 nm range, which was modulated by the electron donor or acceptor strength of the heterocyclic system appended to the thiosemicarbazone moiety. F^-, Cl^-, Br^-, I^-, $H_2PO_4^-$, HSO_4^-, NO_3^-, AcO^-, and CN^- anions were used in the recognition studies. From these anions, only the sensing feature was observed for F^-, CN^-, AcO^-, and $H_2PO_4^-$ ions.

L 1.17- L 1.23

L 1.24

R=Br   **L 1.17**   R= ⬡—Br   **L 1.21**

R=NO$_2$ **L 1.18**   R= ⬡—NO$_2$ **L 1.22**

R= ⬡   **L 1.19**   R= ⬡—CHO   **L 1.23**

R= ⬡—O⌒   **L 1.20**
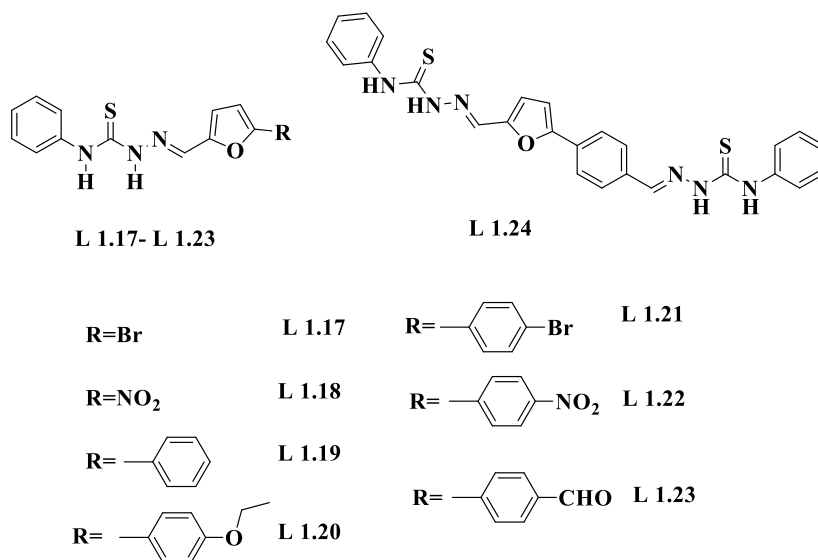
Suganya et al. 2013 synthesized azo- based anion sensors (**L 1.25- L 1.27**) based on the 4-amino azo benzene and three different aldehydes. The receptors (**L 1.25- L 1.27**) displayed high selectivity towards the F⁻ and AcO⁻ ions in 9:1 (DMSO-H$_2$O) (v/v). The binding constant and detection limit results showed that among all the synthesized receptors, **L 1.27** presented strong affinity towards the F⁻ and AcO⁻ ions in the semi-aqueous medium due to the presence of the chromogenic signalling unit in it. Receptor **L 1.26** and **L 1.27** displayed colour change from yellow to pink and yellow to orange, respectively. Anion sensing ability of all receptors was further investigated by 1H-NMR titration, UV-Vis experiment and fluorescence titration. Finally, the receptor **L1.27** was applied for practical application for quantitative detection of F⁻ in the toothpaste sample.

L 1.25   **L 1.26**

L 1.27
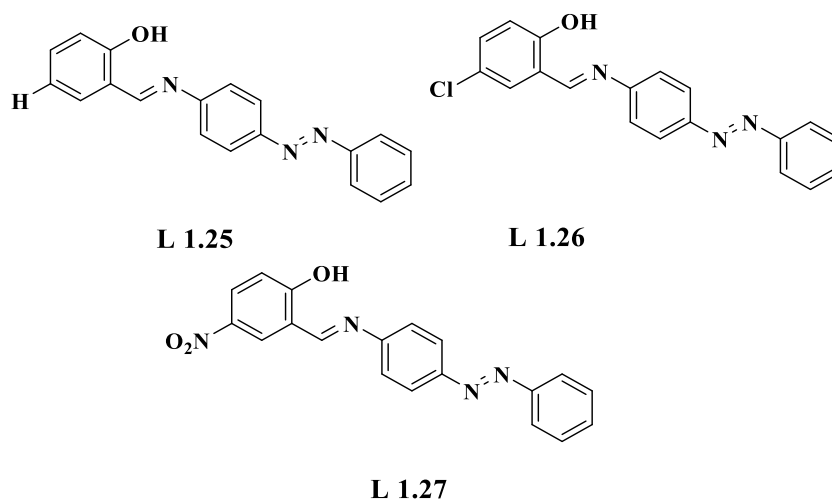
Sharma et al. 2013 synthesized a receptor **L 1.28** by combining vitamin B_6 cofactor pyridoxal with 2-aminophenol. The receptor displayed colour change from yellow to red in the presence of F^- and AcO^- owing to the formation of the polymeric complex 1:1 stoichiometry through multiple hydrogen bonding. This polymeric complex formation locked the C=N bond of the receptor to prevent its rapid isomerization resulting in 'turn-on' of fluorescence only in the presence of F^- ions. The detection limit of this receptor was found to be 7.39×10^{-8} M.
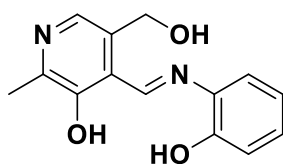
L 1.28

Dalapati et al. 2013 synthesized receptor **L 1.29** for selective detection of F^- and AcO^- ions over other interference anions in aqueous-acetonitrile. The UV-Vis absorption spectra exhibited strong absorption bands at 288 nm and 345 nm for free receptor, and the absorption red bands shifted to 397 nm and 455 nm upon incremental addition of the anions. The B-H plot indicated 1:2 binding stoichiometry between the receptor and the F^- and AcO^- ions. A test-paper coated with receptor **L 1.29** could selectively detect F^- and AcO^- ions by developing yellow colour in aqueous-acetonitrile. The colorimetric and UV-Vis spectral analysis were in well- agreement with the ^{1}H-NMR titration.
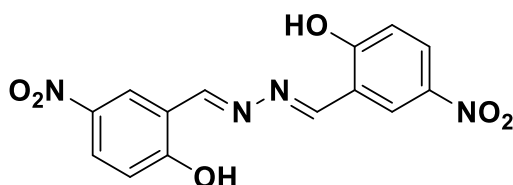
L 1.29

Yong et al. 2013 synthesized a chemosensor **L 1.30** based on 2-thiohydantoin, which showed high selectivity for F^- ion over other anions. The receptor followed the two- step binding process, initially with the hydroxyl functionality of the receptor,

followed by the involvement of the NH unit at higher concentration. This resulted in two- step colour change, initially from colourless to yellow upon addition of F⁻ ions (0-3 equiv.), and secondly from yellow to purple (3 to 6 equiv.). The receptor was further used to develop a test paper to detect F⁻ ions in solid state, wherein it showed detection limit as low as 1.9 ppm.
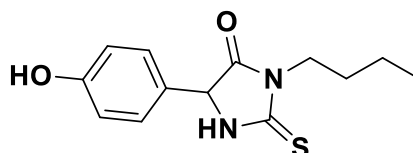
L 1.30

Basu et al. 2013 developed two amidothiourea- based receptors, **L 1.31** and **L 1.32** containing π-acidic 3,5-dibitrophenyl chromophore in good yield, and their anion recognition properties were evaluated both in organic and aqueous organic environment by spectroscopic techniques. Anions such as F⁻, AcO⁻, and $H_2PO_4^-$ were examined as suitable analytes for the receptor molecules, displaying optical signalling from colourless to orange/red, whereas the anions of lesser basicity such as Cl⁻, Br⁻, I⁻, NO_3^-, and HSO_4^- did not show any discernible spectral changes. Highly basic OH⁻ ions induced stepwise change with increasing equivalence from red to green, and anion-π interaction was confirmed.
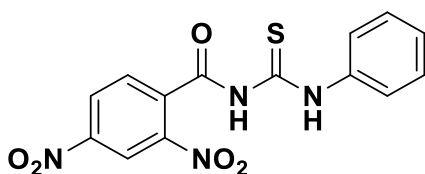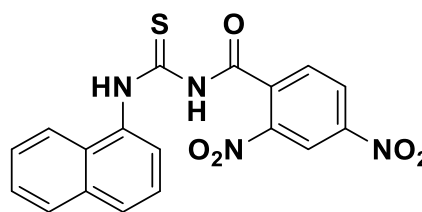
L 1. 31   **L 1.32**

Agarwalla et al. 2014 reported the synthesis of two new receptors, **L 1.33** and **L 1.34** bearing positively charged phosphonium ions aiding the binding of F⁻ and AcO⁻ to the methylene functionality. The role of hydrogen bonding interaction between the

hydrogen atoms of the active methylene group and anionic analyte were explored, and the experiment results were rationalized with detailed computational studies.

L 1.33   **L 1.34**
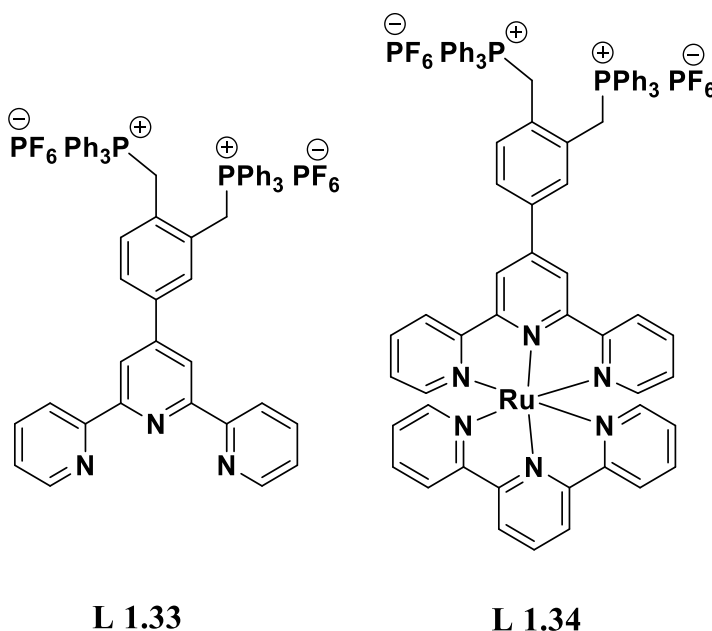
Gunupuru et al. 2014 studied the anion binding properties of dipicrylamine (DPA), **L 1.35**, wherein the –NH group solely acted as binding site and the NO_2 functionality acted as the signalling unit. This suggested that the acidic nature of the NH group was sufficient to bind the anion through single hydrogen bond interaction. The interaction of DPA in acetonitrile with a wide range of anions revealed strong interaction with F^-, AcO^-, and $H_2PO_4^-$ ions with sharp colour change from yellow to red. The UV-Vis titration studies performed with the additions revealed significant red shift of the original absorption band of the receptor with clear isosbestic point. The ^{1}H-NMR titration and computational studies of DPA in the presence of anions revealed the binding of anions by the NH functionality, followed by the deprotonation process.
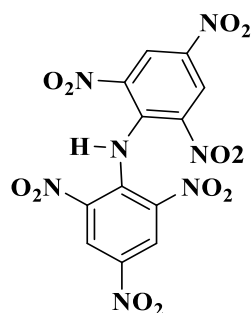
L 1.35

Zang and Jiang 2015 designed and synthesized a series of colorimetric anions **L 1.36**, **L 1.37**, **L 1.38**, and **L 1.39** with different substituent groups including electron donating group (tert-butyl), conjugated group (naphthyl), and electron withdrawing group (chlorine). The substituent effect had great impact on the chromogenic signal output, and also tuned the selectivity and sensitivity of the anion binding through the push-pull mechanism. Real-life analysis of the receptor successfully achieved qualitative estimation of the fluoride in commercially available toothpaste in aqueous media by a simple and easy colorimetric method.
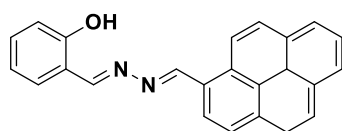
L 1.36
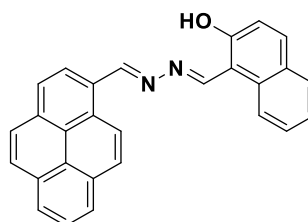
L 1.37
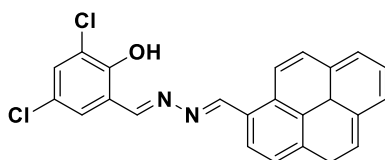
L 1.38
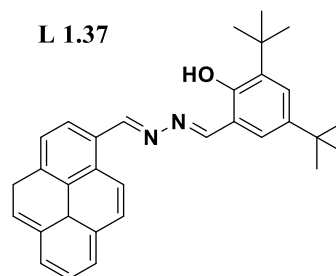
L 1.39

Zou et al. 2015 designed and synthesized anion sensor **L 1.40** based on indole and hydrazide which exhibited colorimetric response towards F^-, AcO^- and $H_2PO_4^-$ ions in DMSO with a significant colour change from colourless to yellow.^{1}H-NMR titration confirmed deprotonation of NH proton on excess addition of F^- ion, whereas

a hydrogen bonding complex in the presence of AcO⁻ and H₂PO₄⁻ ions. Binding constant was found to be $(1.15\pm0.15) \times 10^9\,M^{-2}$ with F⁻ ion, $(3.44\pm0.40) \times 10^4\,M^{-1}$ and $(7.38\pm0.38) \times 10^4\,M^{-1}$ with AcO⁻ and H₂PO₄⁻ ion.
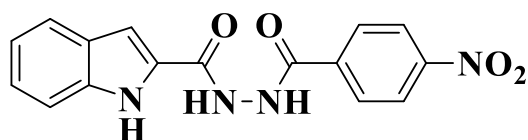
L 1.40

Zhao et al. 2016 designed and synthesized anion receptor **L 1.41** having nitro moiety as a signalling unit and phenolic hydroxyl as an anion-binding site. The synthesized product was characterized by mass spectra and FT-IR. The receptor induced colour change upon addition of F⁻, AcO⁻, and H₂PO₄⁻ from pale yellow to blue, while no obvious colour change was observed upon addition of other tested anions such as Cl⁻, Br⁻, and I⁻ in the DMSO.
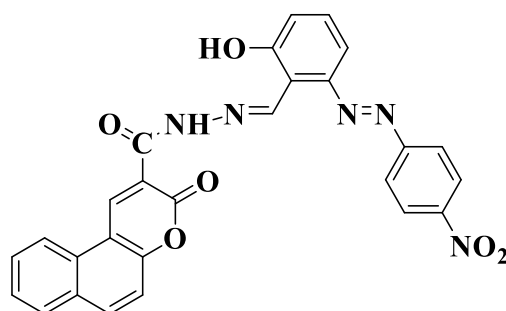
L 1.41

Nie et al. 2017 reported three hydrazine derivatives **L 1.42, L 1.43**, and **L 1.44** possessing electron withdrawing groups, which could selectively detect F⁻ ion. In particular, receptor **L 1.43** exhibited high colorimetric selectivity towards F⁻ ion with colour change from yellow to blue due to the presence of two electron withdrawing nitro groups. The binding mechanism was studied in detailed by UV-Vis studies, ¹H-NMR titration, and Job's plot.
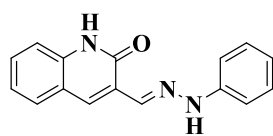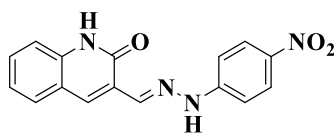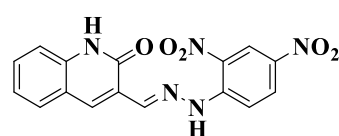
L 1.42   **L 1.43**   **L 1.44**

Arslan et al. 2017 designed and synthesized a novel colorimetric chemosensor based on push-pull for recognition of anions in DMSO. The optical response of the receptor **L 1.45** was studied using colorimetric, UV-Vis, and ^{1}H-NMR titration. It showed high selectivity for F^-, AcO^-, $H_2PO_4^-$, and CN^- over other competing anions such as Cl^-, and HSO_4^- in the DMSO. Upon addition of F^- and AcO^-, it resulted in colour change from yellow to purple, whereas a yellow to pink and yellow to green colour were observed in the case of CN^- and $H_2PO_4^-$, respectively. DFT and TD-DFT calculations were carried out to understand the molecular and electronic structure of **L1.45** as well as the molecular complex of **L 1.45** formed with the anions.
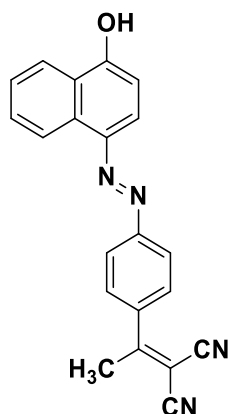
L 1.45

Patil et al 2018 developed rhodamine 6G based colorimetric receptor **L 1.46** for real-time sensing of the F^- ion. The receptor **L 1.46** exhibited significant colour change from pale yellow to pink over other interference anions such as Cl^-, Br^-, I^-, HSO_4^-, $H_2PO_4^-$, and AcO^- in the form of TBA salts in the DMSO. Receptor **L 1.46** was used to detect and quantify the F^- ion present in commercially available mouthwash and the detection limit was estimated to be 4.02 μM. The ^{1}H-NMR titration confirmed the deprotonation of the hydrazone proton (-C=N-NH) upon interaction with the F^- ion in the DMSO-d$_6$ solvent.

L 1.46
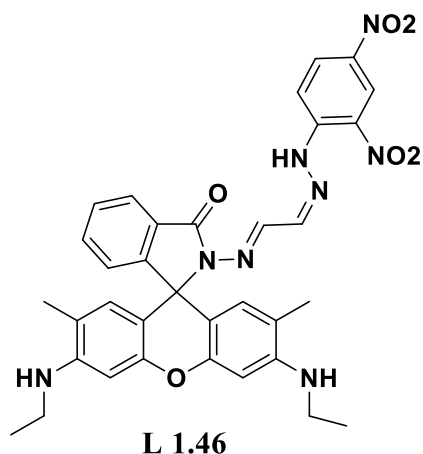
Li et al. 2018 designed and synthesized a new colorimetric chemosensor based on phenolic and acylhydrazine binding units characterized by FT-IR, ^{1}H-NMR, ^{13}C-NMR, and HRMS method. The anion binding properties of **L 1.47** towards different anions was studied using colorimetric, UV-Vis, and ^{1}H-NMR titration methods. The receptor **L 1.47** showed selective colorimetric sensing ability for biologically important F^-, AcO^-, and $H_2PO_4^-$ ions by changing colour from pale yellow to blue in the CH_3CN solution. The detection limit of the receptor **L 1.47** towards F^-, AcO^-, and $H_2PO_4^-$ ions was determined to be 2.94 μM, 4.12 μM, and 12 μM respectively. The binding constant was calculated using the Benesi-Hildebrand equation and was estimated to be 6.85×10^8 M^{-2}, 1.54×10^9 M^{-2}, and 2.37×10^9 M^{-1} (for F^-, AcO^-, $H_2PO_4^-$) in the CH_3CN solution.

L 1.47
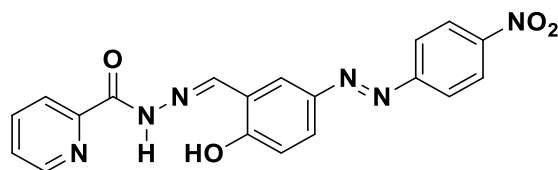
Kodlady et al. 2019 designed and synthesized a series of new aromatic aldehyde with –NH as a hydrogen donor (**L 1.48, L 1.49, L 1.50, L 1.51**) by the simple condensation reaction and their anion sensing properties were investigated by UV-Vis titration. The receptor **L 1.48** showed a dramatic colour change from pale yellow to purple and (**L 1.49, L 1.50 and L 1.51**) pink upon addition of fluoride and cyanide in DMSO medium and (**L 1.48**) showed drastic colour change from yellow to pink in organo-aqueous (DMSO: H_2O, 9:1) medium. ^{1}H-NMR titration performed between the receptors (**L 1.48, L 1.49, L 1.50, L 1.51**) and F^-/CN^- ions, which indicated the

deprotonation of electron in the system through intermolecular charge transfer. Finally, economically visible paper based colorimetric test strip of receptors (**L 1.48, L 1.49, L 1.50, L 1.51**) were fabricated to the detection of F$^-$ and CN$^-$ ions in 100% aqueous solution.

L 1.48

R=

L 1.49

R=

L 1.50

R=

L 1.51

R=
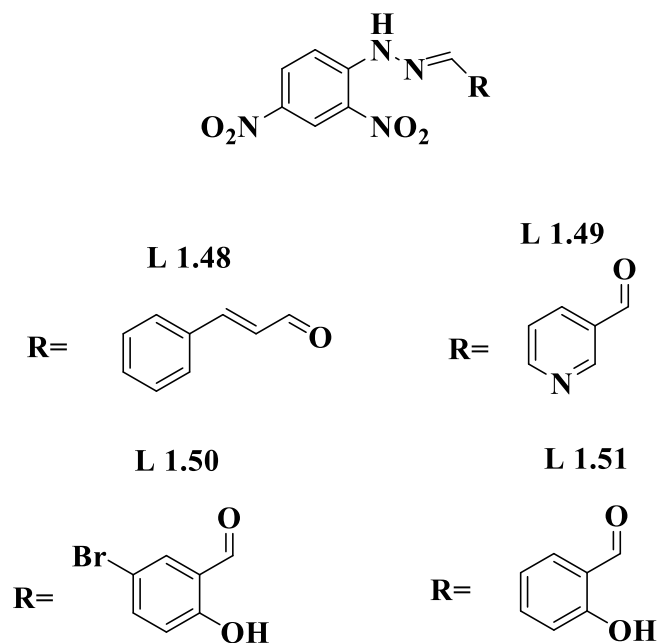
Xiao et al. 2019, developed colorimetric/fluorometric receptor (**L 1.52**) for detection of F$^-$ ion by introducing naphthaldehyde to 1,8-naphthalimide framework. The colorimetric colour change from pale yellow to blue and fluorescent quenching of receptor (**L 1.52**) observed in presence of the F$^-$ ion in DMSO-water (volume ratio 7:1) solution. Receptor (**L 1.52**) bound to F$^-$ ion in 1:1 stoichiometric ratio. The detection limit of receptor (**L 1.52**) towards F$^-$ ion was found to be $8.09 \times 10\text{-}7$ mol L^{-1}.

L 1.52
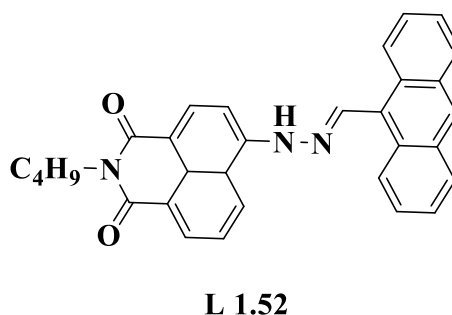
Alreja et al 2019, synthesized and demonstrated novel colorimetric chemosensor (**L 1.53**) based on 1,10-phenanthroline and naphthalene. The anion binding properties was investigated by colorimetric, UV-Visible and ^{1}H-NMR titration

method. Receptor (**L 1.53**) behaved as colorimetric sensor for F⁻ and CN⁻ ion over the other interference anions, and showed naked-eye detectable colour change based on hydrogen bonding interaction followed by the deprotonation. The detection limit of receptor (**L 1.53**) towards F⁻ ion was turned out to be 2.8×10^{-7} M. The receptor (**L 1.53**) conveniently and effectively used as test kit for sensing F⁻ ion in the solid state.
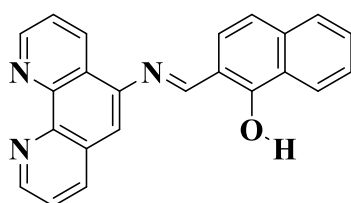
L 1.53

Dwivedi et al 2019, developed a colorimetric receptor (**L 1.54**) based on 2-aminothiazolyl coumarin and naphthalene conjugated as a molecular proble. The receptor (**L 1.54**) upon interaction with the anion exhibited naked eye sensitive colorimetric response to detect AcO⁻ ion in 50% aqueous-ethanol (EtOH: H_2O, v/v, 1:1) solution. The limit of detection for acetate ion was found to be 0.916 μM.
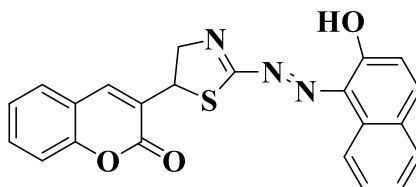
L 1.54

1.6.2 Literature on carboxylate ion detection

Tseng et al. in 2007 designed an organic receptor **L 1.54** for the discriminative detection of isomeric dicarboxylates such as maleate ion over fumarate ion. Upon the addition of maleate ion to the receptor in the DMSO, the receptor showed significant colour change from dark-blue to dark-red distinguishable by the naked eye. This prominent colour change was perhaps due to the deprotonation of the thiourea moiety of the 4-nitronapthyl chromophore. However, upon addition of fumarate ion to the same receptor, the colour of the receptor solution changed from dark-blue to bright yellow.

Thus, these receptors proved to be very good optical chemosensor for selective recognition of maleate ion over fumarate ion.
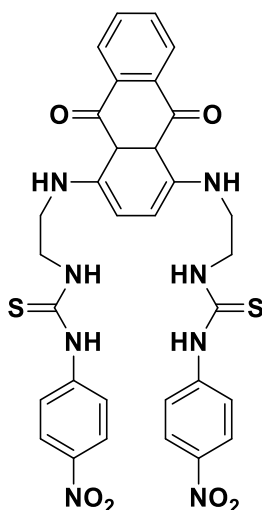
L 1.54

The colour change observed was owing to the formation of a stable complex between the maleate ion and the receptor. The receptor was designed in such a way that during complexation the maleate ion with its cis- conformation exactly fit in the Fig 1.8. On the other hand, fumarate ion has trans- conformation and hence, it weakly bonded with the receptor resulting in weak colour change.
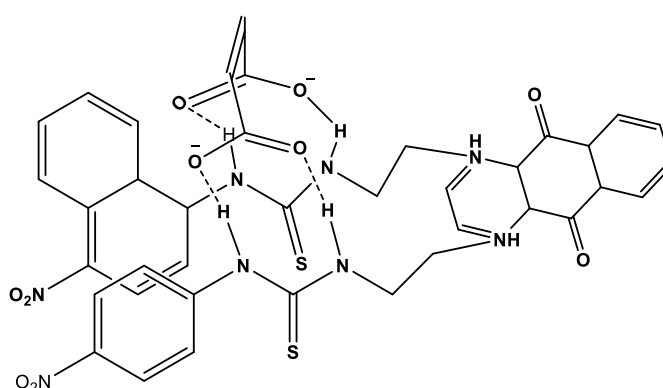
Fig. 1.8 Possible binding model of receptor with maleate ion

A thiourea- based molecular clip was synthesized by Lin et al. (2007), which could fluorometrically discriminate isomeric dicarboxylates. The receptor **L 1.55** comprised of two thiourea-based binding groups and two naphthalene fluorophores units, which

acted as fluorescent chemosensor to distinguish *o*-phthalate from its two other isomers. Upon the addition of *o*-phthalate, the emission intensity at 420 nm decreased drastically through Photoinduced electron transfer (PET) and when the system excited at 380 nm, a new emission band at 480 nm gradually developed upon the addition of the *o*-phthalate ion. However, no such observation was observed with the addition of two isomers.
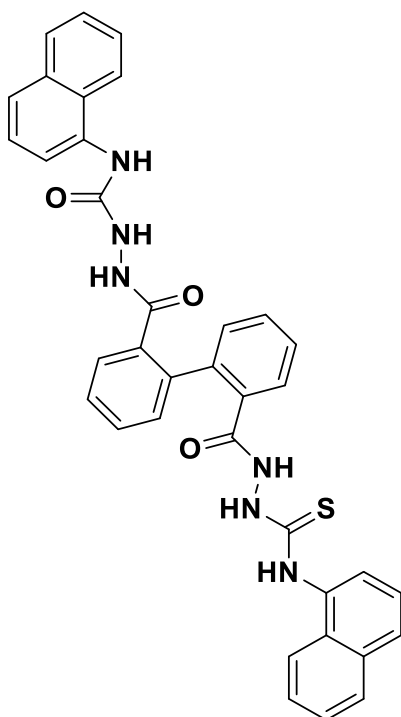
L 1.55

A new triphenylamine-based receptor **L 1.56** for the recognition of aliphatic dicarboxylates with varying chain lengths was synthesized by Ghosh et al. (2010). The receptor was designed in such a way that it could utilize the amide-urea conjugate system. The receptor was found to bond with the dicarboxylates under a semi- rigid, propeller shaped, fluorescent triphenylamine spacer.

L 1.56
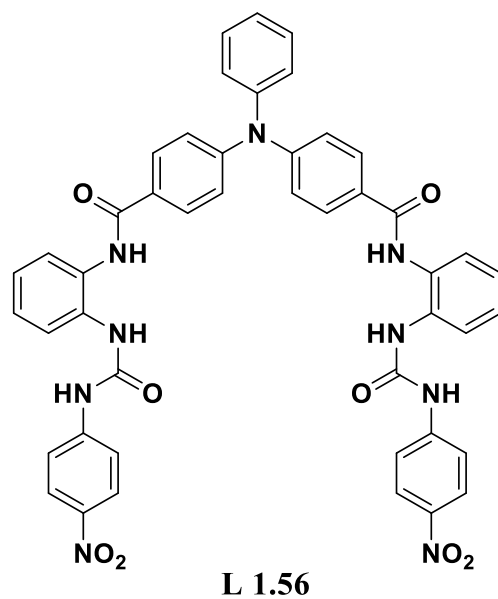
The binding strength of the receptor increased along with the chain length of the dicarboxylates. The binding of these dicarboxylates was achieved via hydrogen bonding and is shown in Fig.1.9.

n=1,2,3,4,5,6
R=p-nitrophenyl
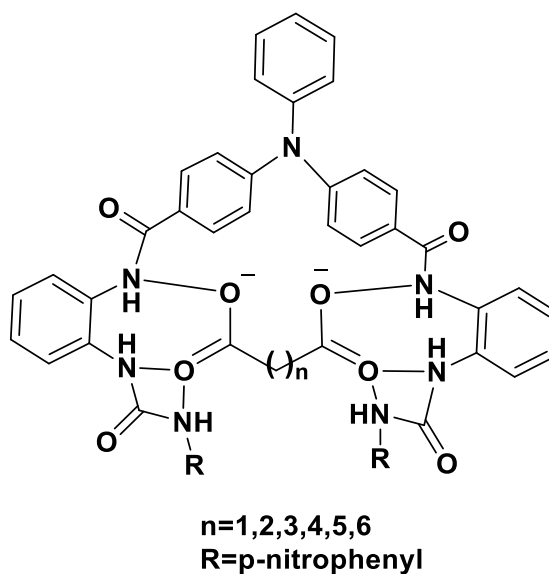
Fig. 1.9 Proposed hydrogen bonding structure of receptor with dicarboxylates

1.7   SCOPE OF THE PRESENT WORK

Anions, though ubiquitous in the biological system, have to be present in optimum amount because too much or too less impact equally on human health. Right from its pioneering work, researches have employed fluorometric and colorimetric methods in the detection of anions. Though being a reliable area of research, fluorometric is accompanied with complications in the detection process owing to its sensitivity towards environmental changes. The light used for excitation can even lead to photochemical changes. In this scenario, there is a lot of opportunity to look into the colorimetric sensing method, where quantitative detection of anions is relatively easier by virtue of the simple instrumentation used. Water is unique with its property to form a highly structured infinite dynamic network of hydrogen bonds. In general, the formation of a hydrogen bond between the anions and the water molecules is possible due to the hydrogen bond donor or the acceptor nature of water. In a biological system, natural receptors such as enzymes and antibodies interact with guest molecules through non-covalent interactions, which are specific and mediated through the functional groups present on them. Mimicking this naturally occurring system, model compounds have been designed by researchers, which can recognize the host-guest complexation event in an organic, non-polar solvent.

For practical application like the detection of anions in seawater or commercial available mouthwash, there is need for organic receptors that are active in an aqueous medium. Water being a competitive solvent, it mediates an interaction between the receptor and the anions. The detection of anions in water is highly challenging in the field of research by virtue of the high solvation energy, large size of anions, and its tendency to be involved in protonation equilibrium in the aqueous solution. Researchers have reported of a positively charged receptor and a neutral anion receptor as being capable of detecting anions, mostly in non-competitive organic solvents such as DMSO, CH_3CN, etc., and in solvent mixtures such as $DMSO-H_2O$, but very few reports on anion recognition are available in purely aqueous media. This drives the need to develop new receptors, which can detect anions in aqueous media.

1.8   OBJECTIVES

❖   To design and synthesize organic receptors with suitable binding sites;

❖   To synthesize simple organic receptors for colorimetric detection of fluoride and acetate ions and for discriminative detection of dicarboxylate isomers, namely, maleate and fumarate ion;

❖   To synthesize simple organic receptors for the detection of biologically important anions like fluoride, acetate and phosphate in aqueous media;

❖   To characterize the synthesized receptors by various spectroscopic techniques like ^{1}H-NMR, ^{13}C-NMR, FT-IR, and Mass analysis;

❖   To monitor colour change through naked eye on addition of appropriate equivalent of anions to the receptor and quantify the colour change by UV-Vis spectrophotometric titration by monitoring the shift in the λ_{max};

❖   To analyze the binding event through ^{1}H-NMR titration experiments and DFT calculation;

❖   To determine the binding constant through the Benesi-Hildebrand (B-H) method, and the binding ratio either by method of continuous variation (Job's plot) or the B-H plot;

❖   To apply the designed receptors to realized real- life applications like detection of fluoride and acetate in seawater, commercially available mouthwash, toothpaste and vinegar;

❖   To arrive at the binding mechanism for selective receptors;

❖   To calculate the detection limit of the receptors towards particular anions; and

❖   To study the quantitative analysis of anion complexation with the receptor molecular using UV-Vis titration.

Overall, the current research work on the synthesis of new and simple organic receptors is aimed towards biological and environmental applications. Further, the practical applications of these receptors involve studies in organic and aqueous medium. In this regard, six different series of receptors have been synthesized and analyzed for the detection of anions. *Chapter 2* describes the synthesis and characterization of five organic receptors with varied positional substitution of the nitro group having hydroxyl functionality as the hydrogen bond donor site. Solvatochromism

properties of one of the receptor was studied in the presence of the acetate ion. The UV-Vis titration, fluorescence, ^{1}H-NMR titration, and DFT studies are discussed in detail. *Chapter* **3** deals with the synthesis of four novel colorimetric anion receptors based on hydrazide derivatives having -NH binding site with different substituents for the colorimetric detection of fluoride and acetate ions in an organic medium. The colorimetric anion sensing properties and the detection mechanism were explored and the real-life application of these receptors was demonstrated by detecting fluoride ions in commercial mouthwash as well as in seawater. In *Chapter 4*, a synthesis of three hydrazine-based colorimetric anion receptors with a NO_2 group and extended π-conjugation (as signaling units) and a naphthy moiety carrying a hydroxyl functionality (as anion binding site) at ortho and para-position for fluoride and acetate ion detection was discussed. The colorimetric anion sensing properties, electrochemical studies, detection mechanism, solvatochromic effect, and DFT calculation have been discussed in detail. In addition, the receptors were successfully demonstrated for the detection of fluoride and arsenite ions using a test strip. In *Chapter 5* the synthesis of hydrazinyl pyridine-based colorimetric receptors owning the NH group as a binding site and the NO_2 group as a signalling unit for the detection of fluoride ion in DMSO and carbonate ion in the aqueous medium is shown. The electrochemical, ^{1}H-NMR titration, and DFT studies have been performed to confirm the anion binding process. Furthermore, the real-life applicability of these receptors has been studied using test strips to detect fluoride and carbonate ions. The receptor in this *Chapter 6* encompasses malonohydrazide functionality with two NH groups as binding sites for colorimetric differentiation of maleate ion over fumarate ion. In addition, the receptors were studied for colorimetric detection of other biologically important anions such as fluoride and acetate ions in DMSO and sodium fluoride, sodium acetate, and arsenite in an organo-aqueous medium. *Chapter 7* deals with the syntheses of new colorimetric receptors for the detection of fluoride, acetate, and phosphate in the form of TBA salts in organic media. Buffer studies were performed for one of the receptors in the presence of acetate ion. Further, the real–life applicability of these receptors was been examined by the detection of fluoride and acetate ions in a toothpaste and vinegar solution. Towards the ends, *Chapter 8* presents the conclusion and outcome of the present research work along with scope for future studies.

CHAPTER 2

COLORIMETRIC ANION SENSORS BASED ON POSITIONAL EFFECT OF NITRO GROUP FOR RECOGNITION OF BIOLOGICALLY RELEVANT ANIONS IN ORGANIC AND AQUEOUS MEDIUM, INSIGHT REAL - LIFE APPLICATION AND DFT STUDIES
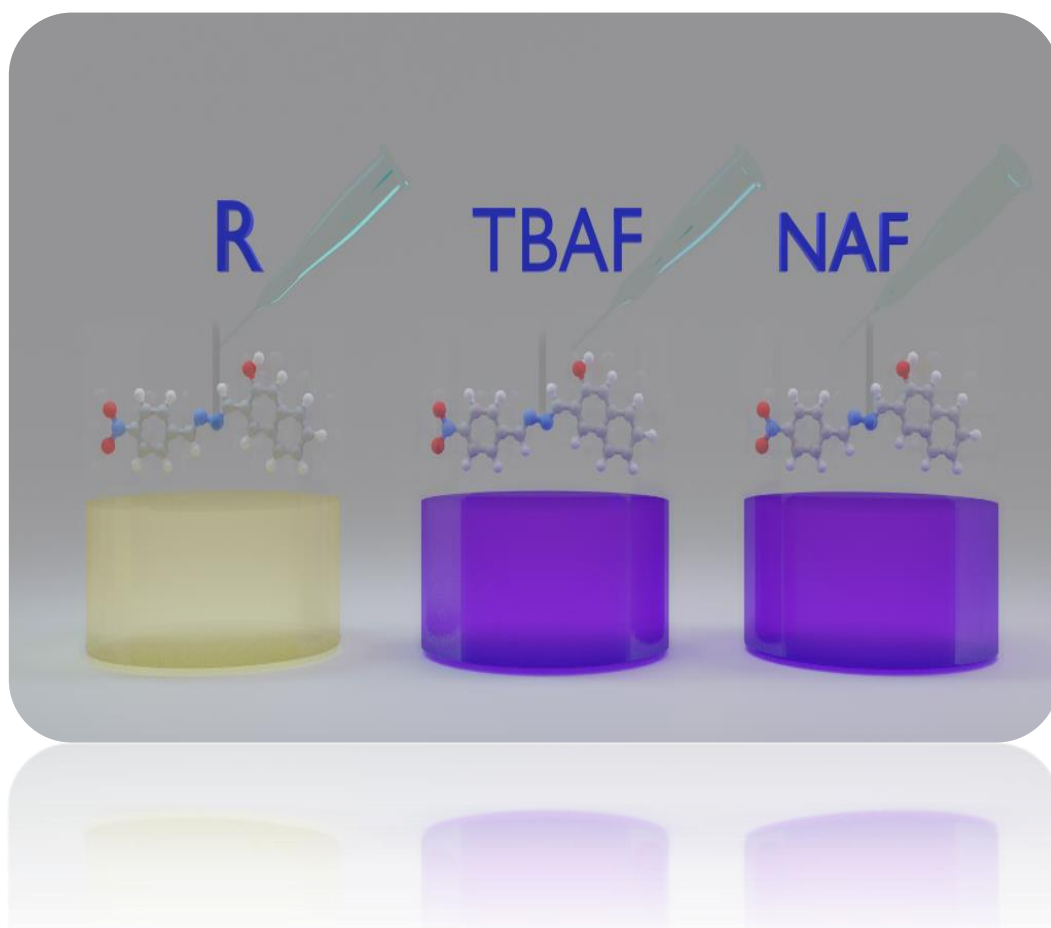
*Abstract: Design, syntheses, and characterization of six new receptors **L1R1-L1R6** is described in this chapter. Anion induced* colour *change of the receptors is monitored via UV-Vis titration and fluorescence titration. The plausible binding mechanism of the receptors towards anion is proposed by ^{1}H-NMR titration and DFT studies.*

2.1 INTRODUCTION

The detection and sensing of anions via organic receptors are of key interest in analytical and environmental chemistry because of their importance in chemical, agricultural, industrial, and biological processes [Gale et al. 2010; Wang et al. 2010; Gunnlaugsson et al. 2006]. Among the anions in particular, fluoride and acetate ions play an important role in dental care, treatment of osteoporosis, and are critical components of numerous metabolic processes in a wide range of industrial and pharmaceutical products [Huang et al. 2011; Jung et al. 2009; Park et al. 2014]. However, excessive intake of ions can cause series damage to humans, especially fluoride ion as it can often lead to fluorosis [Yu et al. 2008; Simon et al. 2016], urolithiasis [Ozsvath et al. 2009; Singh et al. 2001], and even cancer [Grice et al. 2007]. According to the World Health Organization (WHO) and the Environmental Protection Agency, the permissible level of fluoride in drinking water should be 1.5 ppm [Saha and Ghosh et al. 2010]. Although many approaches have been developed for the detection of fluoride and acetate ions including atomic-fluorescence spectrometry (AFS) [Miao et al. 2014; Chen et al. 2013], inductively coupled plasma mass spectrometry (ICP-MS) [Li et al. 2014], electro thermal atomic absorption spectrometry (ETAAS) [Pasias et al. 2013], etc., these methods have their own limitations like low selectivity, difficulty in sample preparation, complicated handling, longer time, and expensive instrumentation [Kumar et al. 2018]. However, colorimetric chemosensor is considered to be the most attractive and interesting to researchers due to its low cost, rapid response rate, easy method, high selectivity, and naked-eye detection of colour change without use of any expensive instruments [Yoshino et al. 2009; Divya et al. 2010; Yu et al. 2010; Lv et al. 2011; Ding et al. 2012; Kim et al. 2013; Anzenbacher et al. 2000]. In recent years, various colorimetric chemosensors have been reported in literature with different functional groups such as urea [Amendola et al. 2006], thiourea

[Liu et al. 2007], amides, benzimidazoles [Cui et al. 2007], etc. to detect biologically important anions via hydrogen bonding interaction or deprotonation. However, most of these receptors have proven to detect anions in a less polar solvent such as (CH_2Cl_2, DMSO, CH_3CN, etc.) [Yu et al. 2007]. Until now, few reports on detection of anions in an aqueous medium are available because anions can strongly solvate in aqueous media because of their highly hydration-free energy, making it difficult to detect anions in aqueous media [Sharma et al. 2014]. Additionally, the selectivity and sensitivity of a receptor depends on the acidity of the proton where the anion binds. In case the acidity of these protons is less than that of water, then the anion gets solvated. However, this shortcoming can be solved to some extent by designing a receptor whose anion binding proton is more acidic than water or by introducing a base-labile group such as hydroxyl (OH) functionality with electron withdrawing –NO_2 group to increase the acidity of the OH proton, which can easily deprotonate with relative basic ions such as F^- and AcO^- [Kigga et al. 2014; Reena et al. 2013].

In the present research paper, six colorimetric receptors **L1R1-L1R6** have been designed and synthesized as shown in Scheme 2.1. Among all synthesized receptors (**L1R1-L1R6**), **L1R1** exhibited high selectivity towards the TBA salts of F^- and AcO^- ions in the DMSO, along with the sodium salts of F^- and AcO^- ions in the organo-aqueous mixture DMSO: H_2O (9:1 v/v) due to the presence of the NO_2 group at the para position and the extended π-conjugation (naphthyl group), which increases the acidity of the -OH proton.
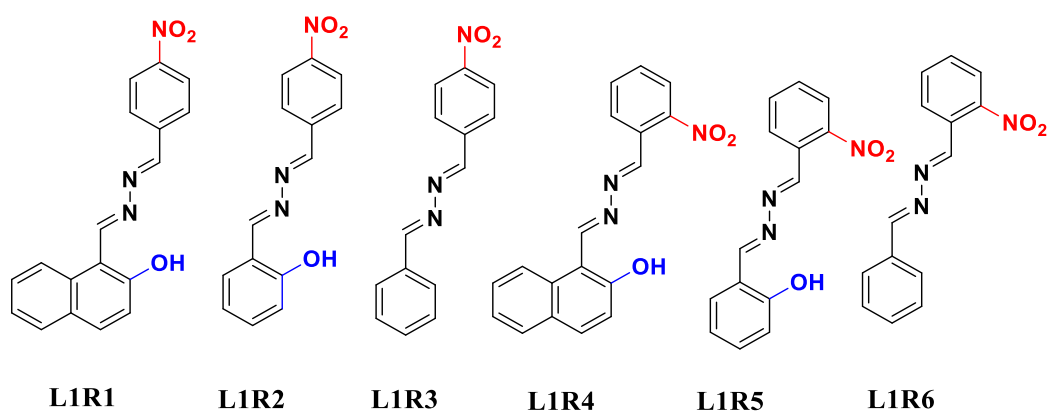
Scheme 2.1 Designed colorimetric receptors **L1R1-L1R6**

2.2 EXPERIMENTAL SECTION

2.2.1 Material and methods

All the chemicals and solvent were purchased from Sigma-Aldrich, Alfa Aesar or from Spectrochemical and used without further purification. The ^{1}H-NMR spectra of the pure samples were recorded using a Bruker Avance (500 MHz) spectrophotometer where tetramethylsilane (TMS) was used as the internal standard and the DMSO-d_6 as the solvent. ^{13}C-NMR spectra were recorded on Bruker Ascend (125 MHz) instrument using TMS as internal references DMSO-d_6 as solvent. The resonance multiplicities were explained as s (singlet), d (doublet), t (triplet), and m (multiplet). The IR spectra were recorded on the Jasco FT-IR spectrometer. The ESI-MS spectra were analysed on a Waters Micromass Q-Tofmicro spectrometer with ESI source. The UV-Vis spectra were recorded with the AnalytikjenaSpecsord S600 Spectrometer in standard 3.5 ml quartz cells with 1 cm path length, and the fluorescence study was monitored using the JASCO-FP-6200 spectrometer. All the reactions were studied by TLC on pre-coated silica gel 60 F254 plates. The melting point was recorded on a struart-SMPS melting-point apparatus in open capillaries.

2.2.2 Synthesis of intermediates S 2.1 and S 2.2

A solution of 4-Nitro-benzaldehyde (0.344 g, 2 mmol) in 5 ml ethanol taken in round bottom (RB) flask and hydrazine hydrate (3 mL, 3 mmol) was added **(S 2.1).** Likewise, in 5mL ethanol, 2-nitrobenzaldehyde (0.344 g, 2 mmol) and hydrazine hydrate (3 mL, 3 mmol) was taken and dissolved **(S 2.2).** The mixture was kept for stirring over night at room temperature. The yellow colour solid product was collected by filtration and washed with cold ethanol to obtain the target intermediate **S 2.1** and **S 2.2** as shown in Scheme 2.2.
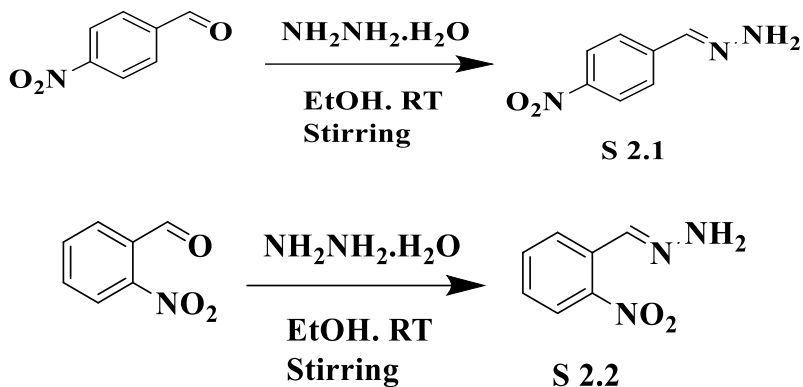
Scheme 2.2 Synthesis of intermediates **S 2.1** and **S 2.2**

2.2.3 Synthesis of receptors L1R1-L1R6

A mixture of different aldehyde (0.346 g, 2 mmol) and intermediate (4-nitro-benzylidene)-hydrazine (**S 2.1**) (0.374 g, 2 mmol) was kept for reaction in an RB flask using 5 ml ethanol under reflux at 60°C for 5h. A mixture of (2-nitro-benzylidene)-hydrazine (**S 2.2**) (0.374 g, 2 mmol) and different aldehyde (0.346 g, 2 mmol) reacted in ethanol under reflux at 60°C for 5h. The reaction mixture was catalysed by a (2-3) drop of acetic acid (CH₃CO₂H). The reaction mixture was cooled to room temperature. The solid formed was filtered and washed with ethanol to obtain the pure target compounds **L1R1, L1R2, L1R3, L1R4, L1R5,** and **L1R6** as shown in Scheme 2.3.
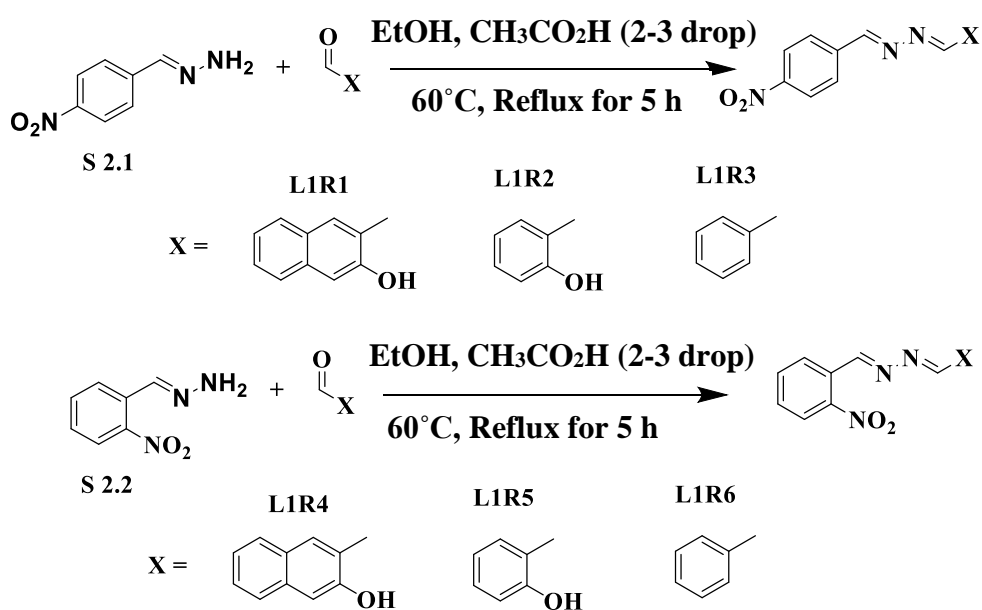
Scheme 2.3 Synthesis of receptors **L1R1-L1R6**

2.2.4 Characterization data

The purity and structure of the intermediate **S 2.1** and **S 2.2** and receptors **L1R1, L1R2, L1R3, L1R4, L1R5,** and **L1R6** were confirmed by FT-IR, ^{1}H-NMR, ^{13}C-NMR, and mass spectroscopic methods. The characterization data has been compiled and given below.

(E)-(4-nitrobenzylidene) hydrazine (S 2.1)
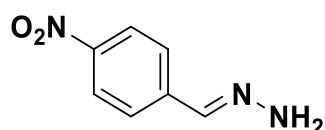
Data obtained for intermediate (S 2.1): Yield 90%., m.p. 130°C. ^{1}H NMR (DMSO-d_6, 500 MHz, Me$_4$Si): δ_{ppm} 7.544 (s,2H), 7.691 (d, J=8Hz, 2H), 7.750 (s, 1H), 8.177 (d, J=8Hz, 2H). ^{13}C NMR (DMSO-d_6, 125 MHz, Me$_4$Si): δ_{ppm} 146.20, 143.83, 135. 03, 125.85, 124.44. Mass (ESI): m/z calculated for $C_7H_7N_3O_2$:165.15 Obtained: 166.0602 [M+H]$^+$.

(E)-(2-nitrobenzylidene) hydrazine (S 2.2)
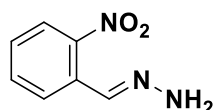
Data obtained for intermediate (S 2.2): Yield 89%., m.p. 125°C. ^{1}H NMR (DMSO-d_6, 500 MHz, Me$_4$Si): δ_{ppm} 7.419- 7.447 (m, 1H), 7.524 (s, 2H), 7.623-7.654 (m, 1H), 7.961 (d, J= 8H, 1H), 8.006 (s, 1H). ^{13}C NMR (DMSO-d_6, 125 MHz, Me$_4$Si): δ_{ppm} 159.01,149.37, 147.04, 134.38, 133.34, 133.34, 132.62, 131.26, 131.02, 129.91, 128.29, 127.95, 126.82, 125.24, 124.69. Mass (ESI): m/z calculated for $C_7H_7N_3O_2$:165.15 Obtained: 166.0602 [M+H]$^+$.

1-((E)-(((E)-4-nitrobenzylidene) hydrazono) methyl) naphthalene-2-ol (L1R1)
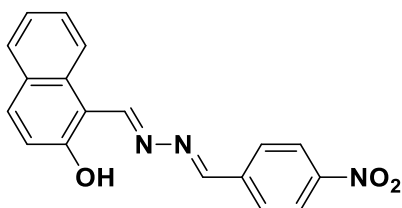
Data obtained for receptor L1R1: Yield 80%, m.p. 330 °C. ^{1}H NMR (DMSO-d$_6$, 500 MHz, Me$_4$Si): δ_{ppm} 7.2495 (d, J= 8.5 Hz, 1H), 7.387-7.417 (m, 1H), 7.556-7.589 (m, 1H), 7.627-7.661 (m,1H), 7.734-7.764 (m,1H), 7.805 (d, J= 8.5 Hz, 1H), 7.8905 (d, J= 8.5 Hz, 1H), 8.094-8.113 (m,1H), 8.1545 (d, J= 9 Hz, 1H) 8.301-8.319 (m, 1H),9.165 (s, 1H), 9.752 (s, 1H), 13.106 (s, 1H). ^{13}C NMR (DMSO-d$_6$, 125 MHz, Me$_4$Si): δ_{ppm} 107.99, 119.32, 119.96, 123.81, 124.84, 123.04, 128.23, 128.79, 129.26, 129.41, 129.59, 131.34, 132.90, 133.37, 135.30, 156.90, 161.81, 163.28. Mass (ESI): m/z calculated for C$_{18}$H$_{13}$N$_3$O$_3$: 319.31 Obtained: 320.1073 [M+H]$^+$.

1-((E)-((E)-4-nitrobenzylidene) hydrazono) methyl) phenol (L1R2)
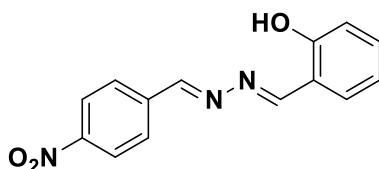
Data obtained for receptor L1R2: Yield 80%, m.p. 230 °C. ^{1}H NMR (DMSO-d$_6$, 500 MHz, Me$_4$Si): δ_{ppm} 6.958-6.988 (m, 1H), 7.029-7.056 (m, 1H), 7.354-7.413 (m, 2H), 7.627-7.660 (m, 1H), 8.0975 (d, J= 8Hz, 1H), 8.298 (d, J=8Hz, 1H), 8.719 (s, 1H), 9.114 (s, 1H), 11.373 (s,1H). ^{13}C NMR (DMSO-d$_6$, 125 MHz, Me$_4$Si): δ_{ppm} 117.22, 117.36, 119.71, 124.06, 129.24, 132.17, 133.43, 139.43, 149.46, 156.90, 159.47, 160.19, 164.67, 166.97. Mass (ESI): m/z calculated for C$_{14}$H$_{11}$N$_3$O$_3$: 269.08 Obtained: 270.092 [M+H]$^+$.

1-(((E)-benzylidene-2-((E)-4-nitrobenzylidene) hydrazine (L1R3)
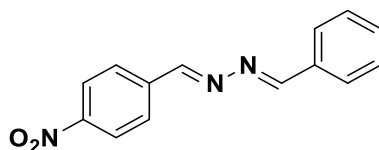
Data obtained for receptor L1R3: Yield 80%, m.p. 180 $^{\circ}$C. ^{1}H NMR (DMSO-d_6, 500 MHz, Me$_4$Si): δ_{ppm} 7.455-7.497 (m, 1H), 7.594-7.630 (m, 2H), 7.594-7.757 (m, 2H), 8.088-8.106 (m, 2H), 8.289-8.306 (m, 2H), 9.114 (s, 1H). ^{13}C NMR (DMSO-d_6, 125 MHz, Me$_4$Si): δ_{ppm} 118.30, 119.00, 124.55, 129.75, 129.82, 130.04, 1313, 137.42, 138.89, 139.92, 149.49, 150.89, 160.30, 161.91. Mass (ESI): m/z calculated for C$_{14}$H$_{11}$N$_3$O$_3$: 253.09 Obtained: 254. 0993 [M+H]$^+$.

1-((E)-(((E)-2-nitrobenzylidene) hydrazono) methyl) naphthalene-2-ol (L1R4)
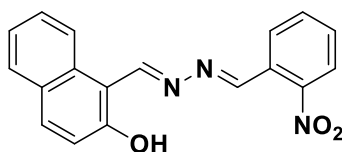
Data obtained for receptor L1R4: Yield 80%, m.p. 300 $^{\circ}$C. ^{1}H NMR (DMSO-d_6, 500 MHz, Me$_4$Si): δ_{ppm} 7.246 (d, J=12Hz, 1H), 7.4225 (d, J= 7.5Hz, 1H), 7.574-7.607 (m,1H), 7.811 (d, J= 8Hz, 1H), 7.9 (d, J= 9Hz, 1H), 8.052 (d, 9Hz, 2H), 8.1725 (d, J= 8.5Hz, 1H), 8.337 (d, J= 9Hz, 2H), 8.732 (s, 1H), 9.774 (s, 1H), 13.148 (s,1H).^{13}C NMR (DMSO-d_6, 125 MHz, Me$_4$Si): δ_{ppm} 117.18, 117.26, 117.32, 119.71, 124.73, 124.79, 128.71, 129.46, 129.59,131.48, 132.53, 133.42, 133.45, 157.78, 158.16, 159.87, 164.68, 166.72. Mass (ESI): m/z calculated for C$_{18}$H$_{13}$N$_3$O$_3$: 319.31 Obtained: 320.1073 [M+H]$^+$.

2-((E)-((E)-2-nitrobenzylidene) hydrazono) methyl) phenol (L1R5)
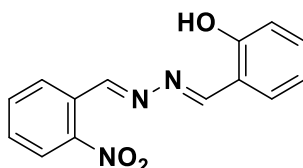
Data obtained for receptor L1R5: Yield 80%, m.p. 205 $^\circ$C. ^{1}H NMR (DMSO-d$_6$, 500 MHz, Me$_4$Si): δ_{ppm} 7.457-7.491 (m, 4H), 7.840-7.875 (m, 2H), 8.0155 (d, J= 8.5Hz, 2H), 8.309 (d, J=9Hz, 1H), 8.669-8.700 (m, 2H). ^{13}C NMR (DMSO-d$_6$, 125 MHz, Me$_4$Si): δppm 108.09, 119.22, 119.98, 123.92, 124.08, 128.15, 128.25, 129.14, 129.28, 132.87, 135.46, 158.52, 161.84, 163.46. Mass (ESI): m/z calculated for C$_{14}$H$_{11}$N$_3$O$_3$: 269.08 Obtained: 270.095 [M+H]$^+$.

1-(((E)-benzylidene-2-((E)-2-nitrobenzylidene) hydrazine (L1R6)
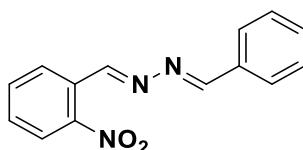
Data obtained for receptor L1R6: Yield 80%, m.p. 160 $^\circ$C. ^{1}H NMR (DMSO-d$_6$, 500 MHz, Me$_4$Si): δ_{ppm} 7.489 (d, J=8Hz, 1H), 7.539-7.570 (m, 1H), 8.2125 (d, J=8.5Hz, 3H), 8.389 (d, J=9Hz, 2H), 8.4495 (d, J=8.5Hz, 1H), 8.751 (s, 1H), 8.908 (s, 1H). ^{13}C NMR (DMSO-d$_6$, 125 MHz, Me$_4$Si): δ_{ppm} 124.09, 125.24, 126.82, 127.95, 128.29, 129.91, 131.02, 131.26,133.34, 134.38, 147.04, 149.37, 149.37, 159.01. Mass (ESI): m/z calculated for C$_{14}$H$_{11}$N$_3$O$_3$: 253.09 Obtained: 254. 0993 [M+H]$^+$.

The representative spectrum of synthesized intermediate **(S 2.1-S 2.2)** and receptors **L1R1-L1R6** is shown below.
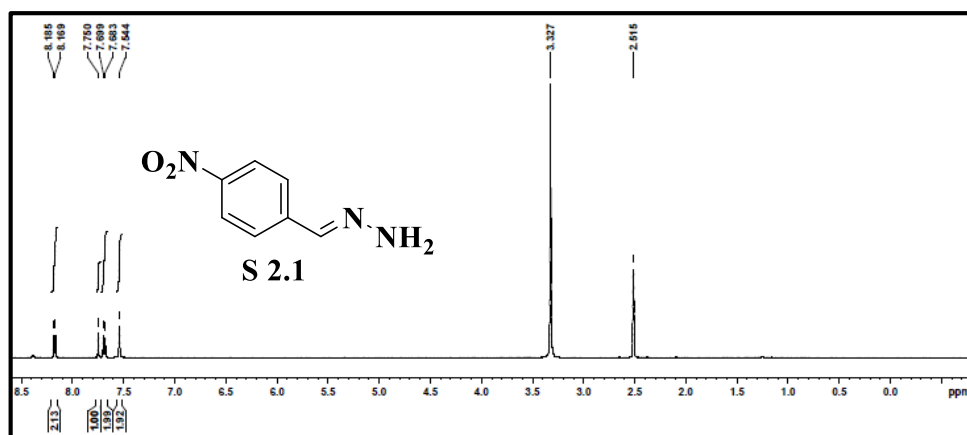
Fig. 2.1 ^{1}H-NMR spectrum of **S 2.1**
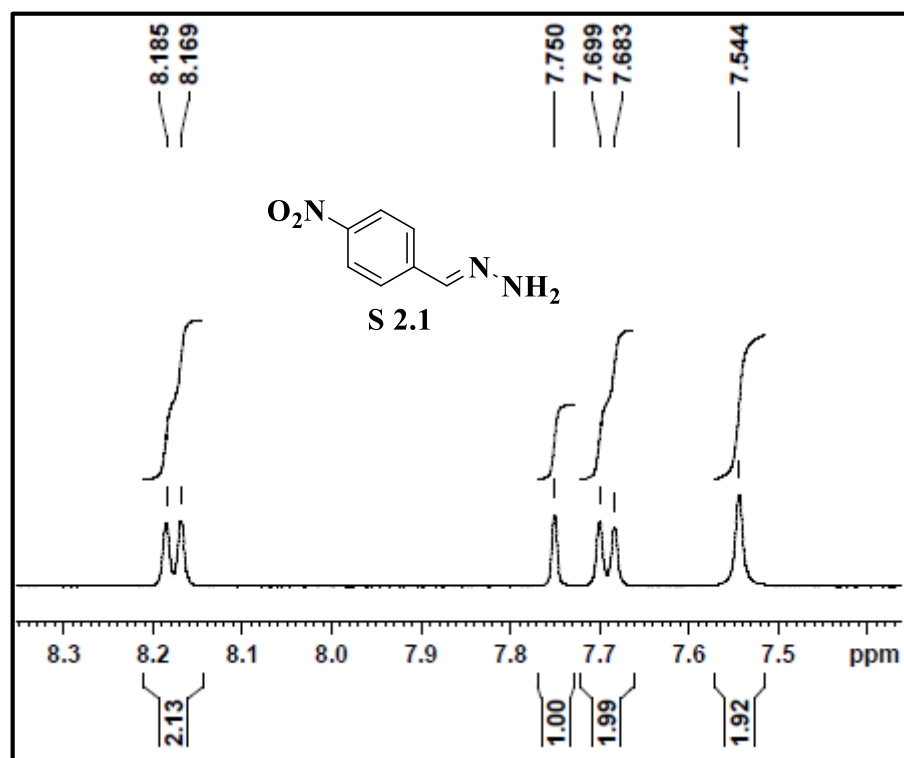
Fig. 2.2 ^{1}H-NMR spectrum of aromatic region of **S 2.1**
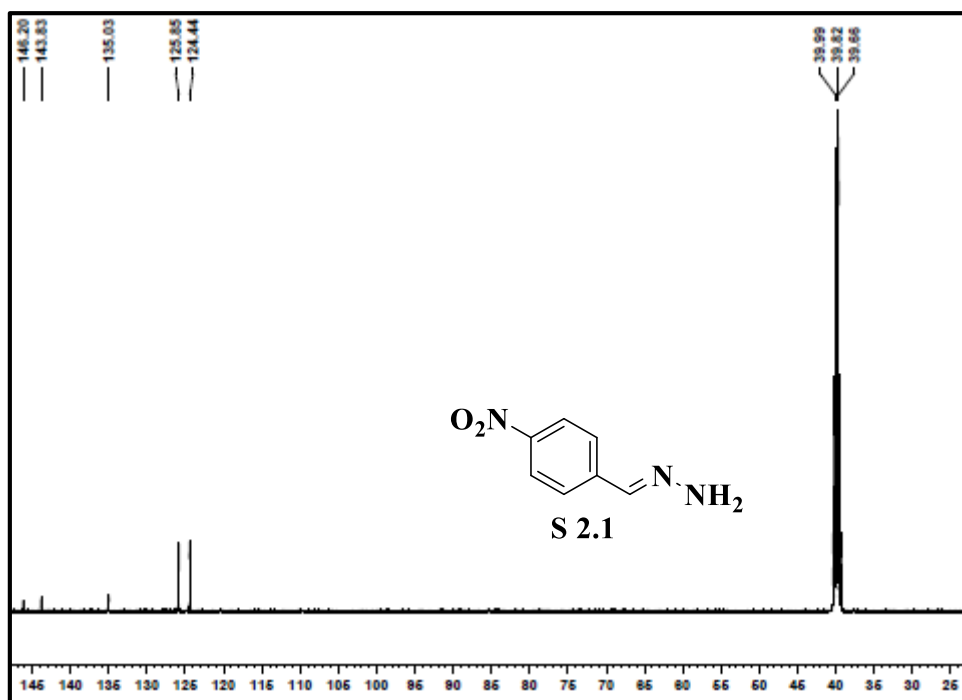
Fig. 2.3 ^{13}C-NMR spectrum of **S 2.1**
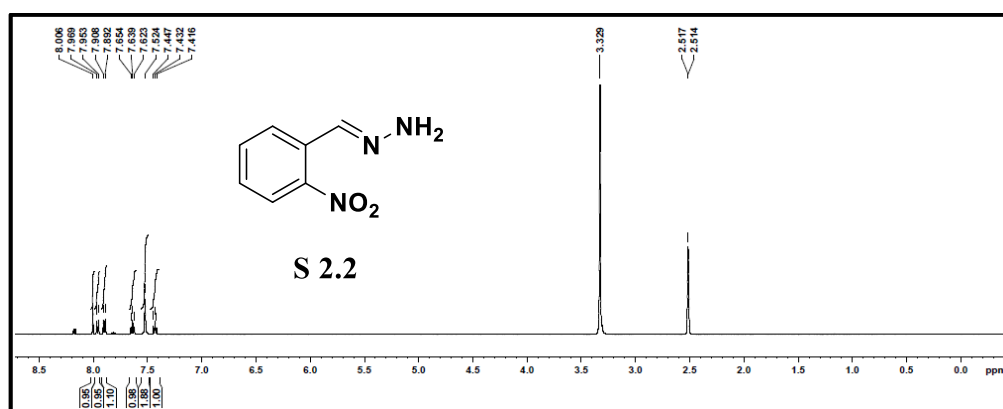
Fig. 2.4 ^{1}H-NMR spectrum of **S 2.2**
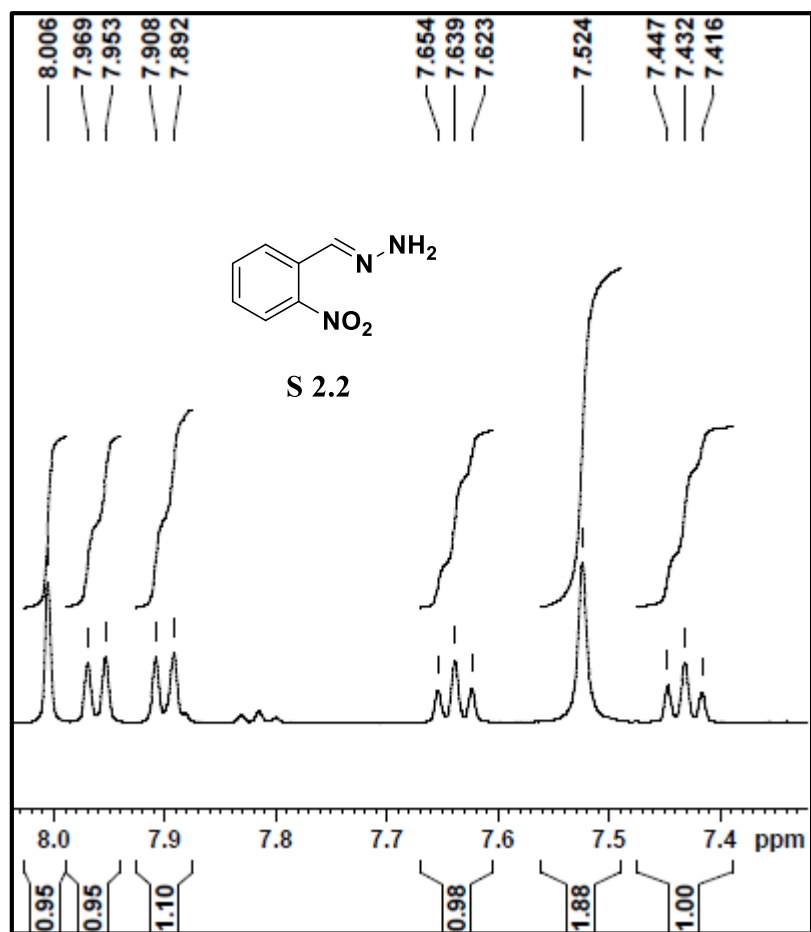
Fig. 2.5 Expanded ^{1}H-NMR spectrum of aromatic region of **S 2.2**
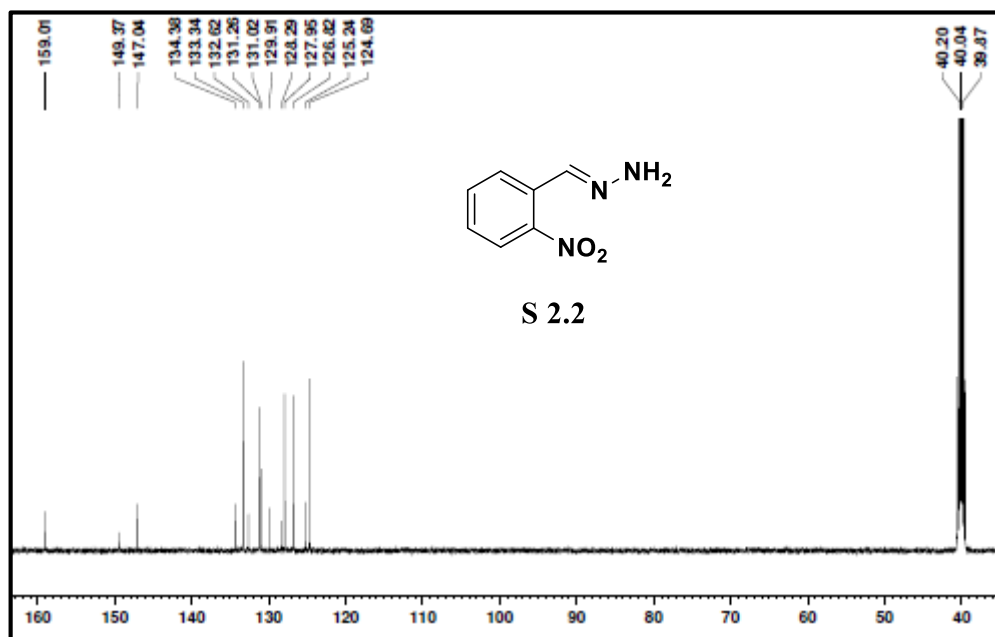
Fig. 2.6 ^{13}C-NMR spectrum of **S 2.2**
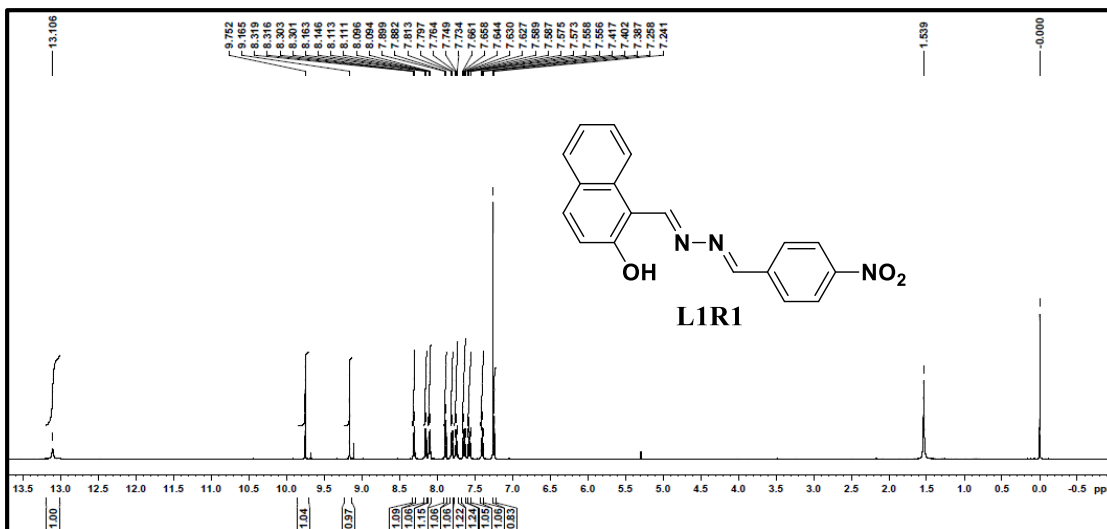
Fig. 2.7 ^{1}H-NMR spectrum of **L1R1**
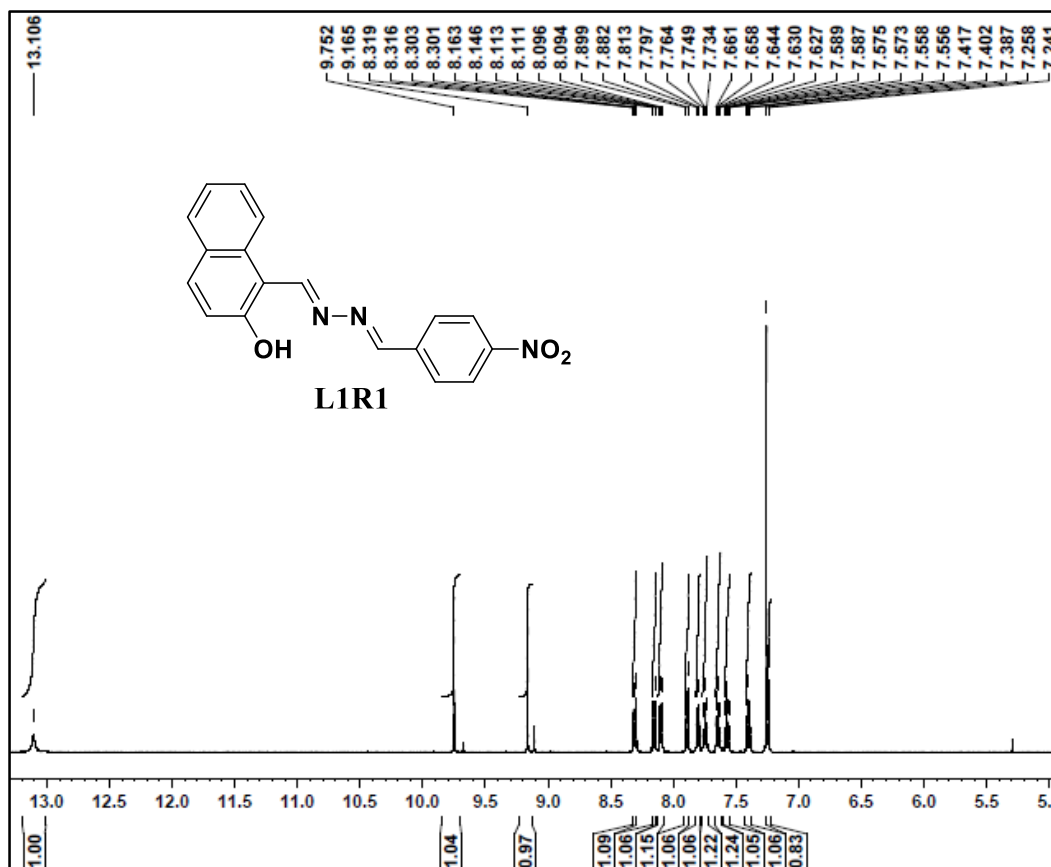
Fig. 2.8 ^{1}H-NMR spectrum of aromatic region of **L1R1**
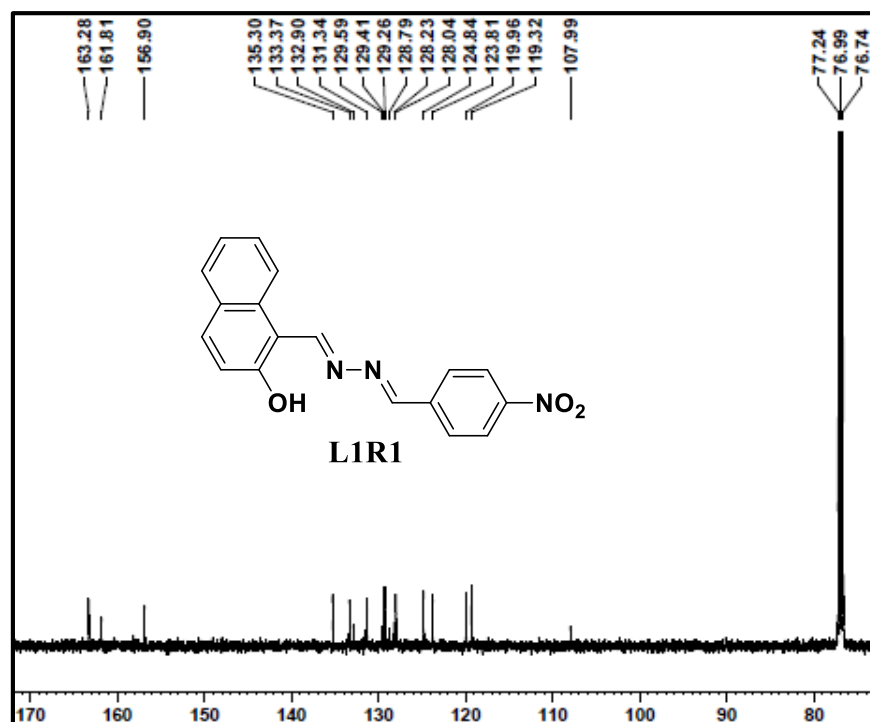
Fig. 2.9 ^{13}C-NMR spectrum of **L1R1**
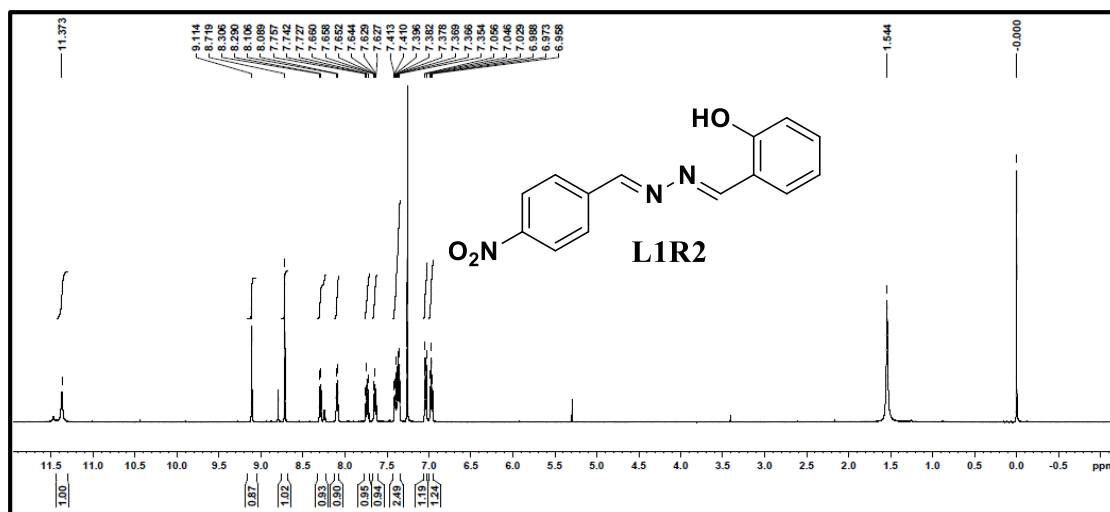
Fig. 2.10 ^{1}H-NMR spectrum of **L1R2**
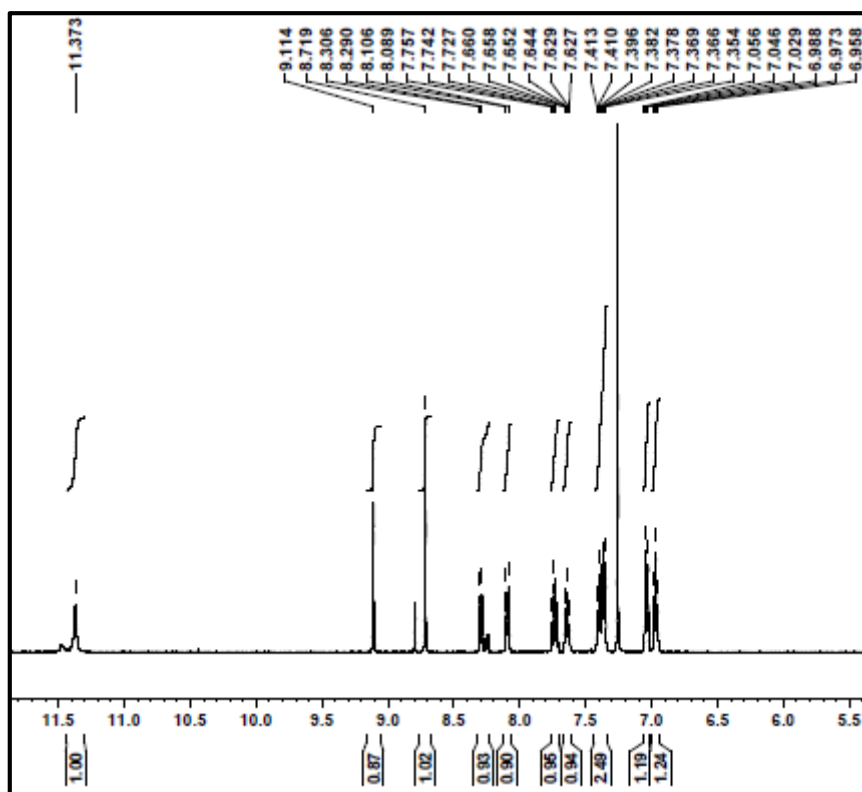
Fig. 2.11 ^{1}H-NMR spectrum of aromatic region of **L1R2**
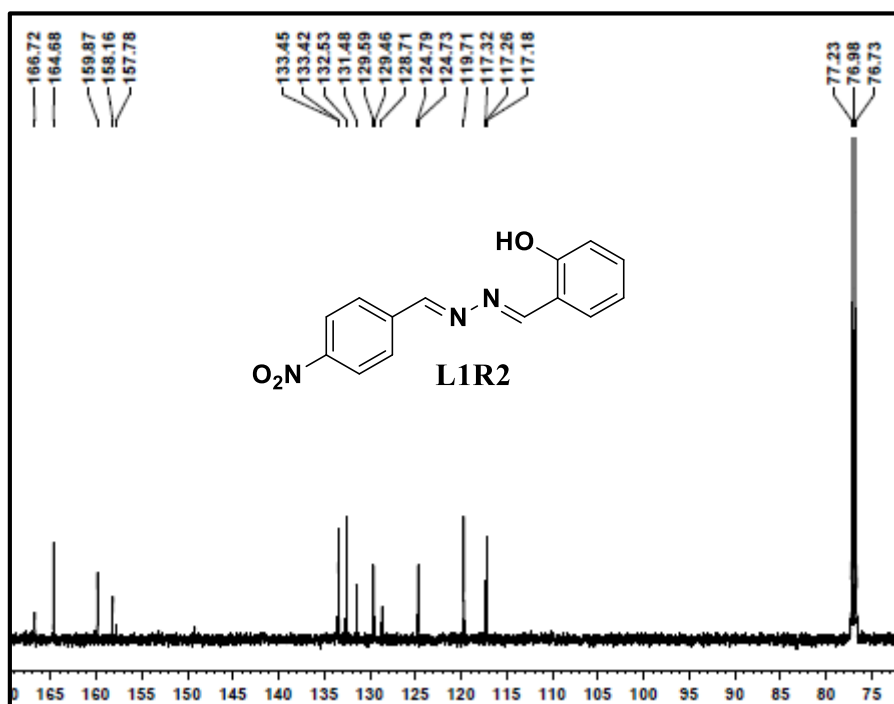
Fig. 2.12 ^{13}C-NMR spectrum of **L1R2**
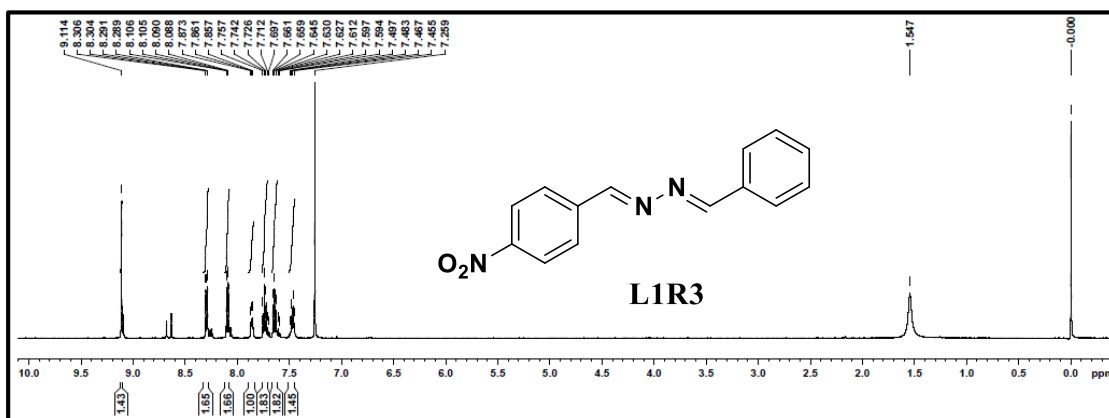
Fig. 2.13 ^{1}H-NMR spectrum of **L1R3**
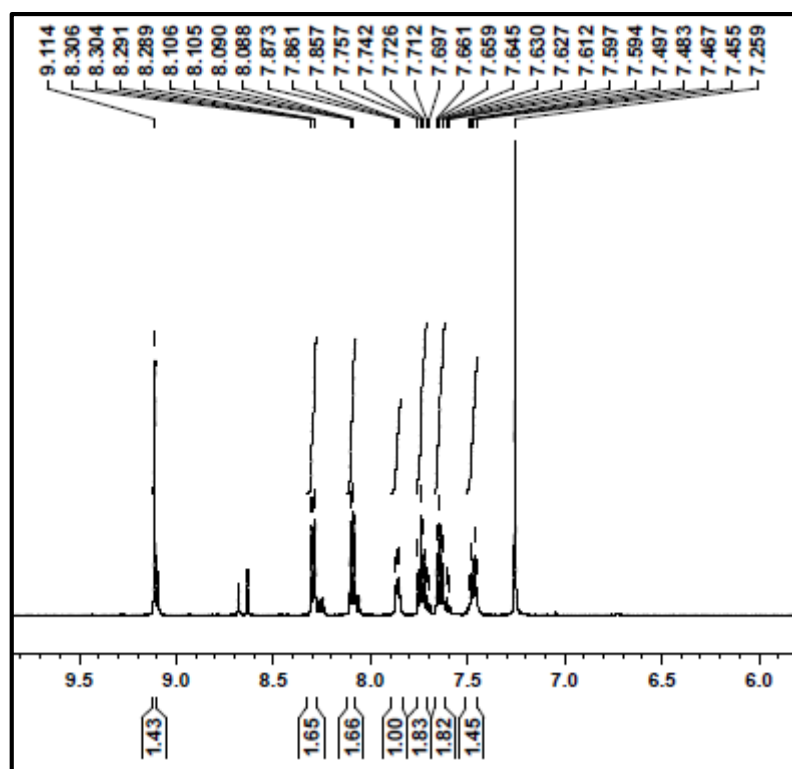
Fig. 2.14 ^{1}H-NMR spectrum of aromatic region of **L1R3**
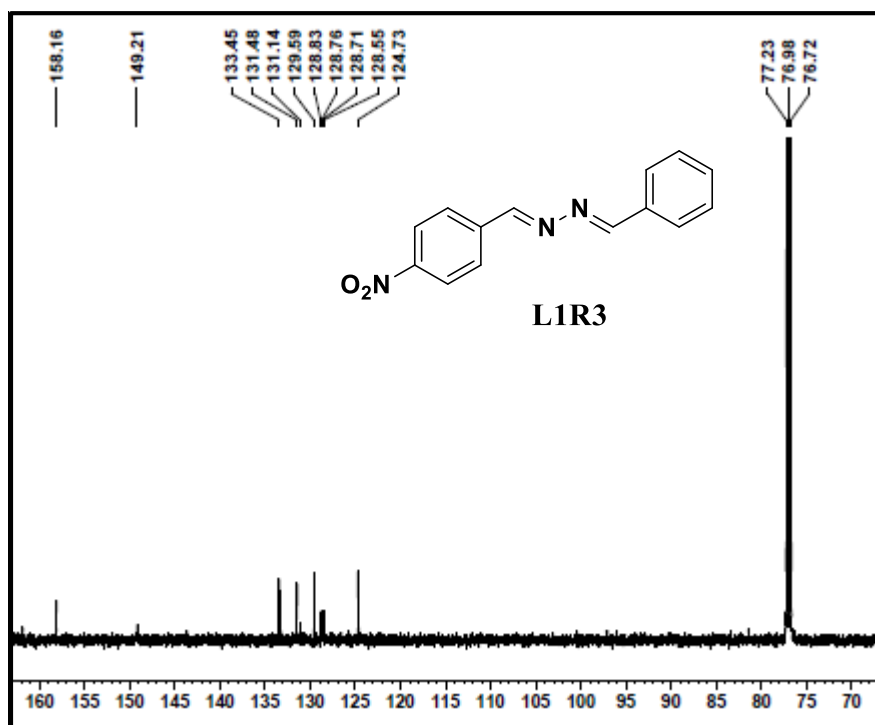
Fig. 2.15 ^{13}C-NMR spectrum of **L1R3**
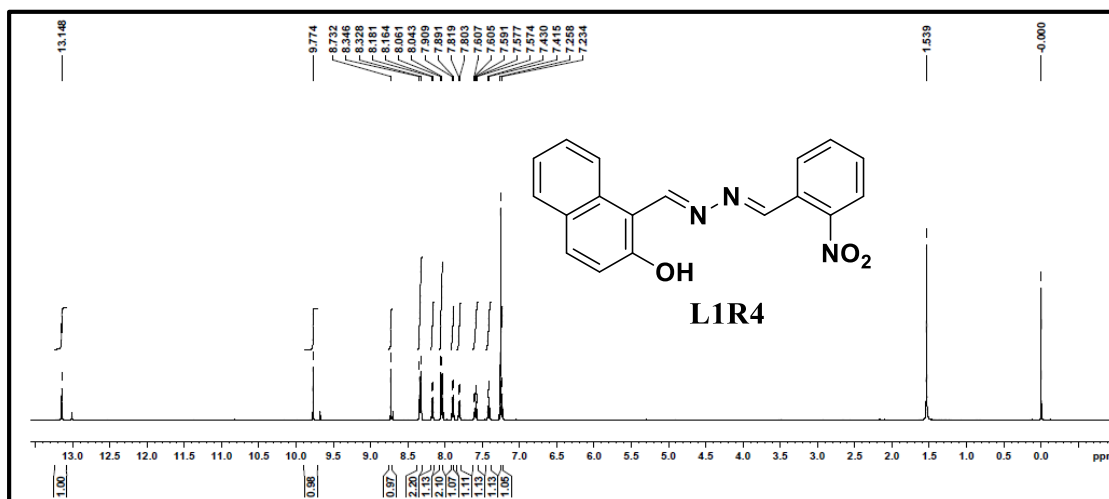
Fig. 2.16 ^{1}H-NMR spectrum of **L1R4**
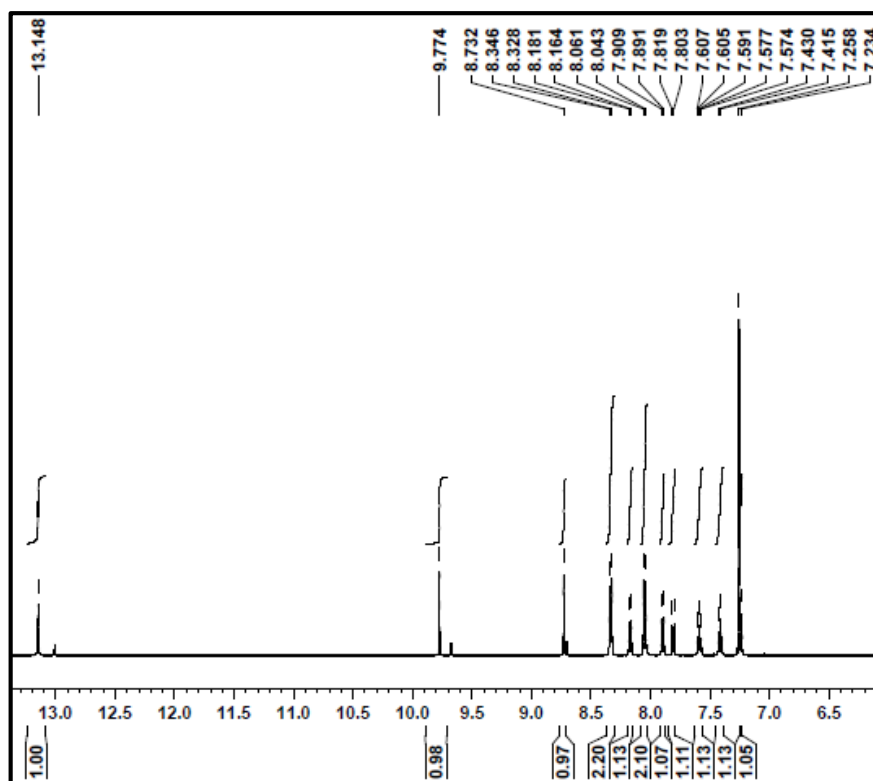
Fig. 2.17 ¹H-NMR spectrum aromatic region of **L1R4**
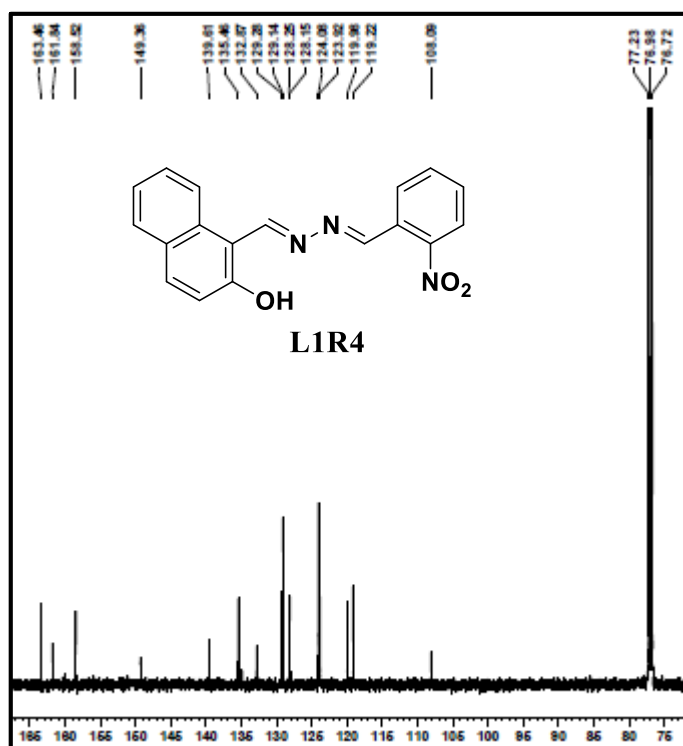
Fig. 2.18 ¹³C-NMR spectrum of **L1R4**
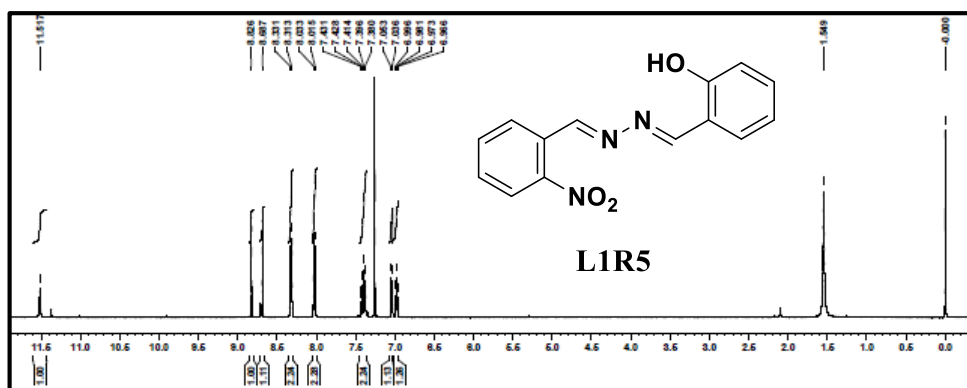
Fig. 2.19 ^{1}H-NMR spectrum of **L1R5**
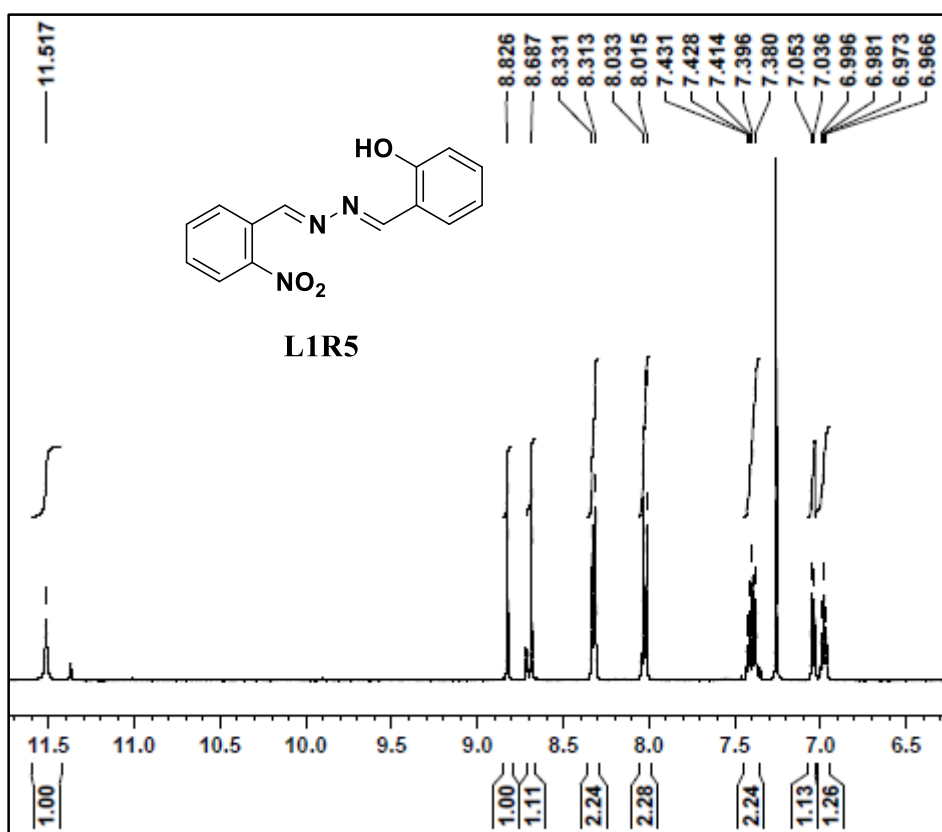
Fig. 2.20 Expanded ^{1}H-NMR spectrum of aromatic region of **L1R5**
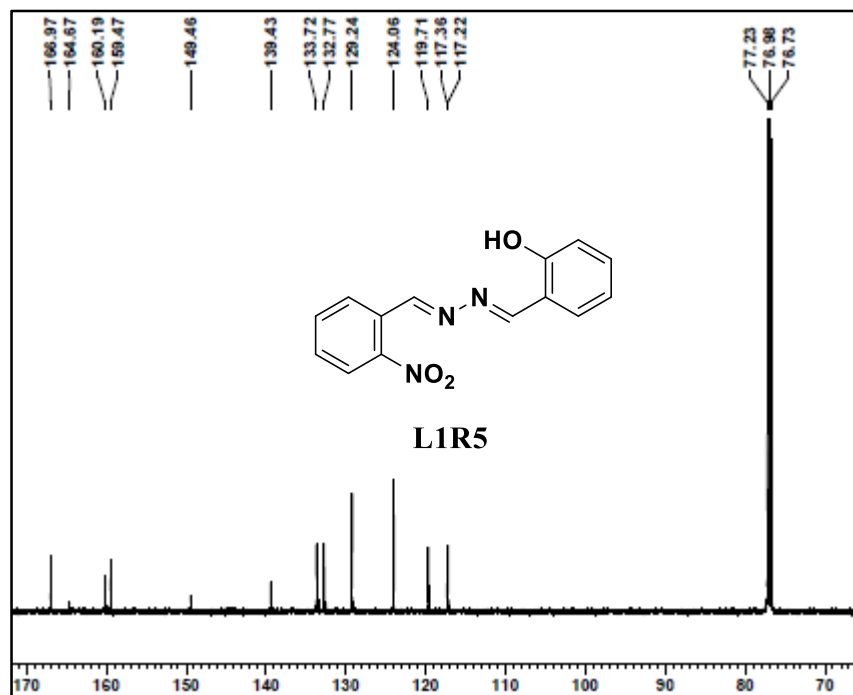
Fig. 2.21 ^{13}C-NMR spectrum of **L1R5**
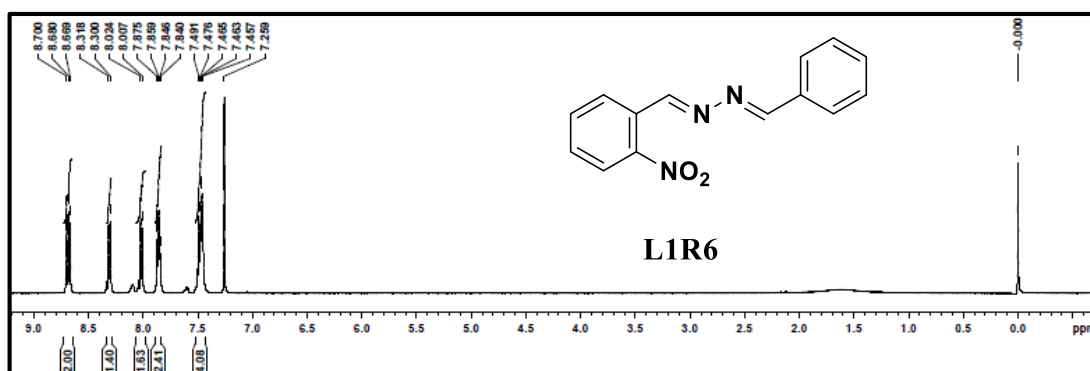
Fig. 2.22 ^{1}H-NMR spectrum of **L1R6**
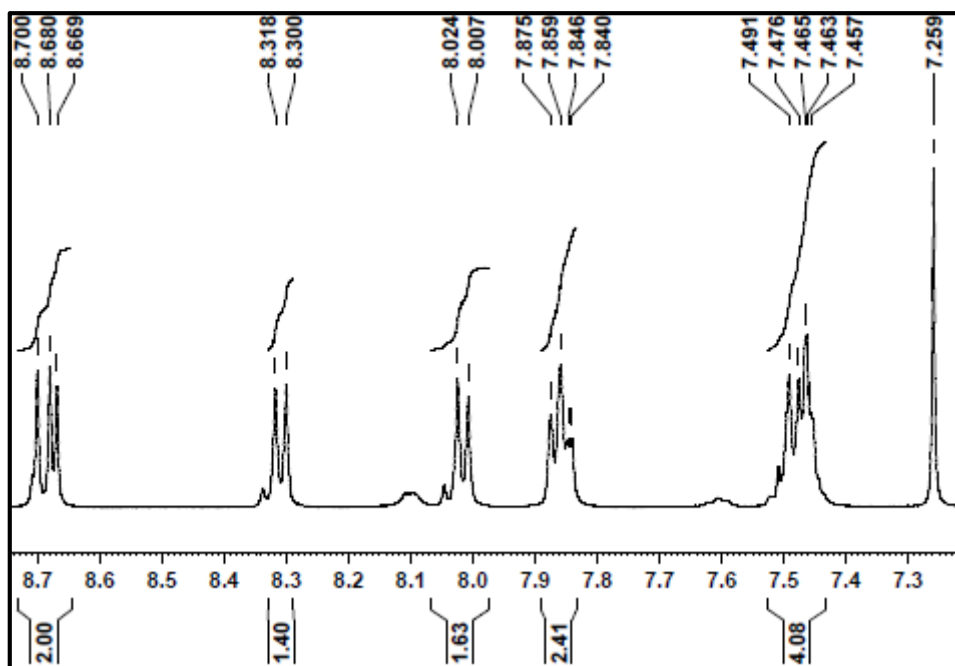
Fig. 2.23 ^{1}H-NMR spectrum of aromatic region of **L1R6**
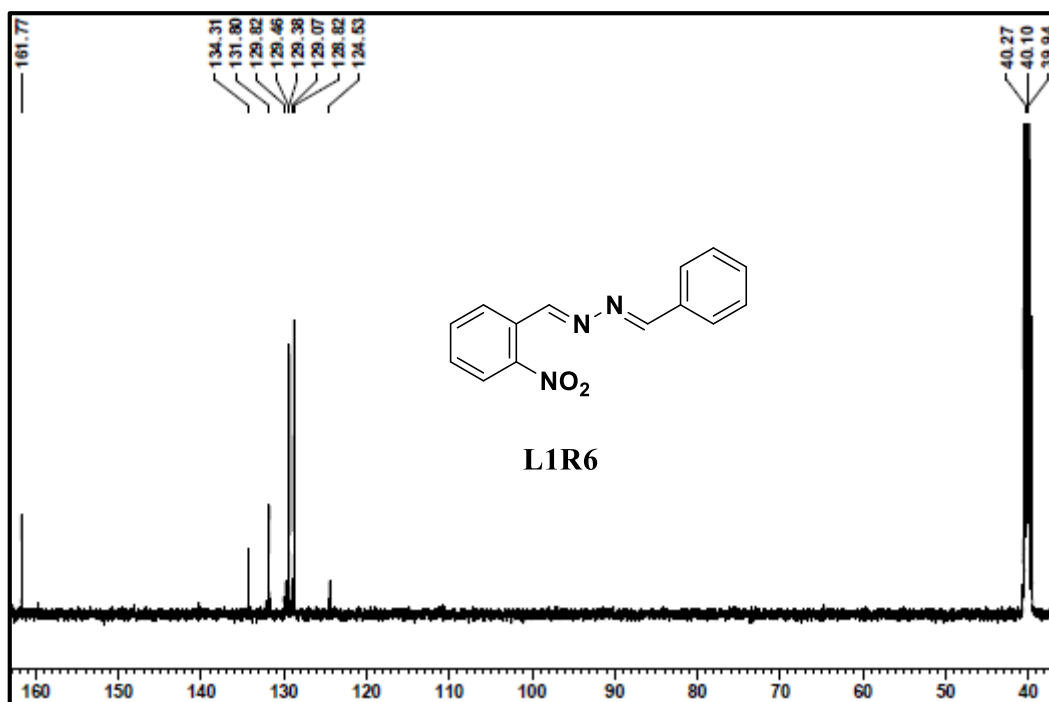
Fig. 2.24 ^{13}C-NMR spectrum of **L1R6**

2.3 RESULTS AND DISCUSSION

2.3.1 Colorimetric responses and comparative study of the receptors L1R1-L1R6 in DMSO

Initially investigated for qualitative analysis to figure out the interaction of various anions with the receptors, the receptors **L1R1- L1R6** solutions were prepared in DMSO of (4.5×10^{-5}M in DMSO). The standard solution of anions in the form of (Tetrabutylammonium salts of F^-, Cl^-, Br^-, I^-, NO_3^-, HSO_4^-, $H_2PO_4^-$, and AcO^-) as (1×10^{-2} M) was prepared in DMSO. With the addition of 2 equiv. of the test anions to the receptors **L1R1-L1R6** solutions, visible colour change was observed only for F^- and AcO^- ions, from pale yellow to purple, light pink, orange, and light yellow as shown in Fig. 2.25 (a, b, d, and e). There was no appreciable colour response upon the addition of the other anions. In this regard, the receptors could serve the purpose of detecting F^- and AcO^- ions among all the tested anions.
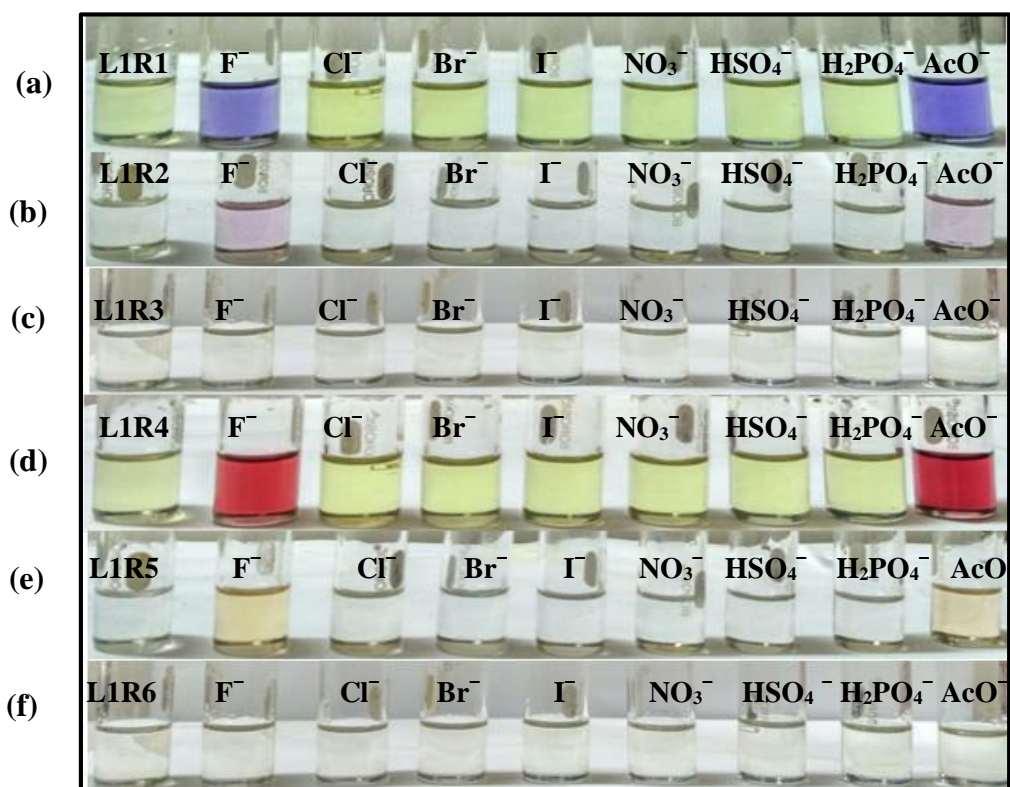
Fig. 2.25 Colour of the receptors (a) **L1R1**(b) **L1R2** (c) **L1R3** (d) **L1R4** (e) **L1R5** (f) **L1R6** (4.5×10^{-5} M in DMSO) after addition of 2 equiv. of various anions (1×10^{-2} M in DMSO)

The UV-Vis absorption spectra were recorded to confirm the colour change, with the addition of test anions to the receptors' solutions. As shown in Fig. 2.26 (a and b), Fig. 2.27 (d), and 2.28 (e), **L1R1, L1R2, L1R4,** and **L1R5** exhibited high selectivity towards F^- and AcO^- ions over the other interference anions. In contrast, **L1R3** and **L1R6,** which lacked the OH group, showed neither colour change nor shift in the absorption band even on addition of excess amounts of F^- and AcO^- ions confirming the role of the -OH group in the binding process with anions as shown in Fig. 2.43(c) and Fig. 2.44 (f). In contrast, no shift in the UV-Vis spectra were recorded for the other anions due to their weak basicity or weak interaction with the receptors (Dini and Khanmohammadi 2019).
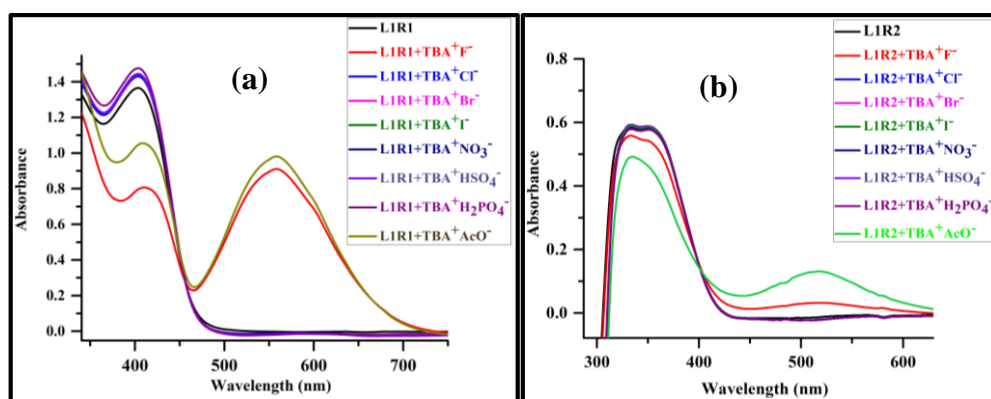
Fig. 2.26 UV-Vis spectral change of the receptors (4.5 ×10^{-5} M in DMSO) in the presence of 2 equiv. of various anions (1 ×10^{-2} M in DMSO) (a) **L1R1** (b) **L1R2**
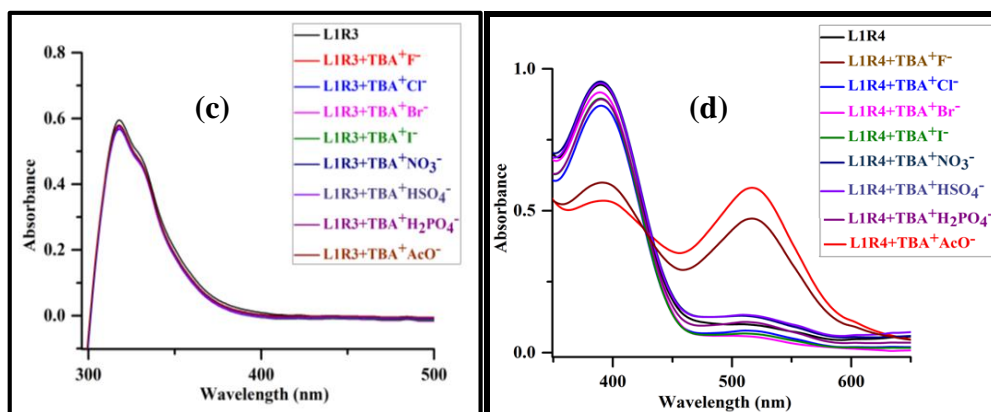
Fig. 2.27 UV-Vis spectral change of the receptors (4.5 ×10^{-5} M in DMSO) in the presence of 2 equiv. of various anions (1 ×10^{-2} M in DMSO) (c) **L1R3** (d) **L1R4**
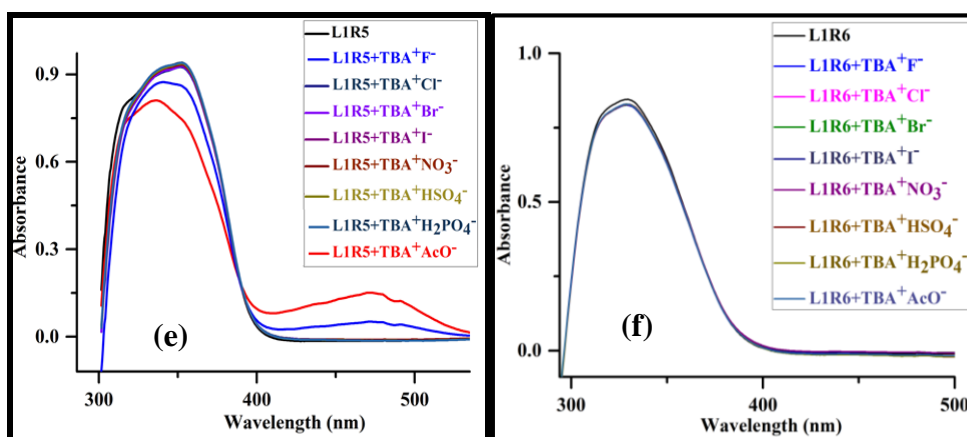
Fig. 2.28 UV-Vis spectral change of the receptors (4.5 ×10⁻⁵ M in DMSO) in the presence of 2 equiv. of various anions (1 ×10⁻² M in DMSO) (e) **L1R5** (f) **L1R6**

2.3.2   UV-Vis titration studies

The UV-Vis absorption spectra were recorded to investigate the qualitative anion binding ability of the receptor **L1R1** (4.5 ×10⁻⁵ M) with the F⁻ and AcO⁻ ions in the DMSO. As depicted in Fig. 2.29 and Fig. 2.30, the receptor **L1R1** showed a strong characteristic band at 404 nm in the DMSO, assigned to the π-π* transition of the p-nitro phenyl chromophore (Rezaeian and Khanmohammadi 2014). With the incremental addition of 0.1 equiv. of F⁻ and AcO⁻ ions to the receptor **L1R1** solution, the intensity of the absorption band at 404 nm decreased with the simultaneous appearance of new bands at 545 nm and 547 nm, which gradually increased. This spectrum shift clearly supports the fact that the receptor **L1R1** bonded strongly with the F⁻ and AcO⁻ ions. Well-defined isosbestic points at 454 nm and 456 nm was observed indicating the formation of a new species in the medium. This bathochromic shift of 141 nm and 143 nm was recorded and attributed to the intramolecular charge transfer (ICT) between the electron deficient NO_2 group at the p-position and the electron rich naphthyl -OH moiety (Bhardwaj et al. 2009).
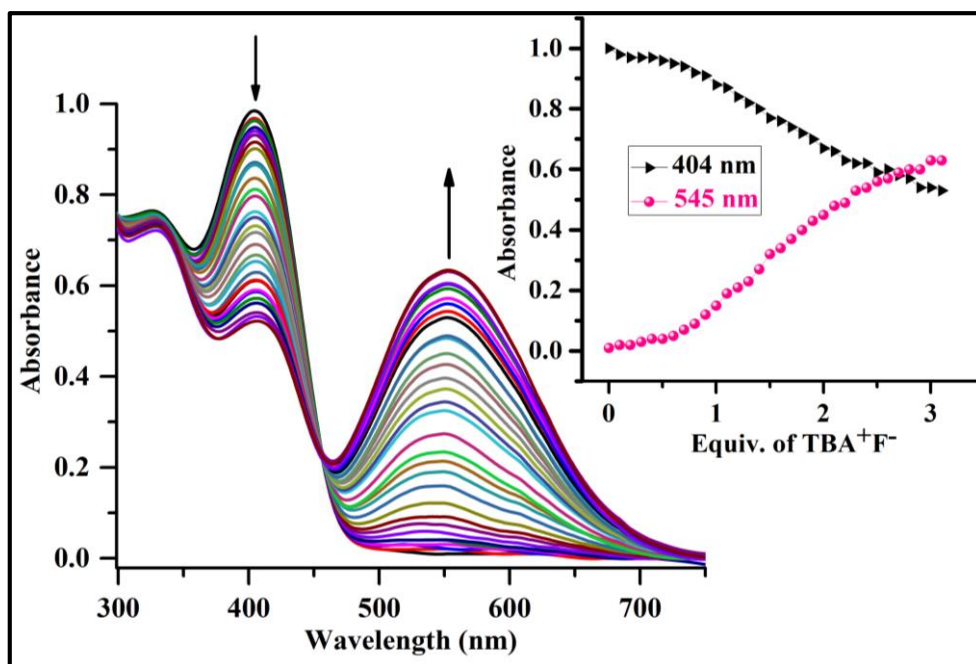
Fig. 2.29 UV-Vis titration spectra of receptor **L1R1** (4.5 ×10^{-5} M in DMSO) with incremental addition of TBA$^+$F$^-$ (10^{-2} M in DMSO); Inset plot representing the variation of absorbance with increasing concentration of TBA$^+$F$^-$
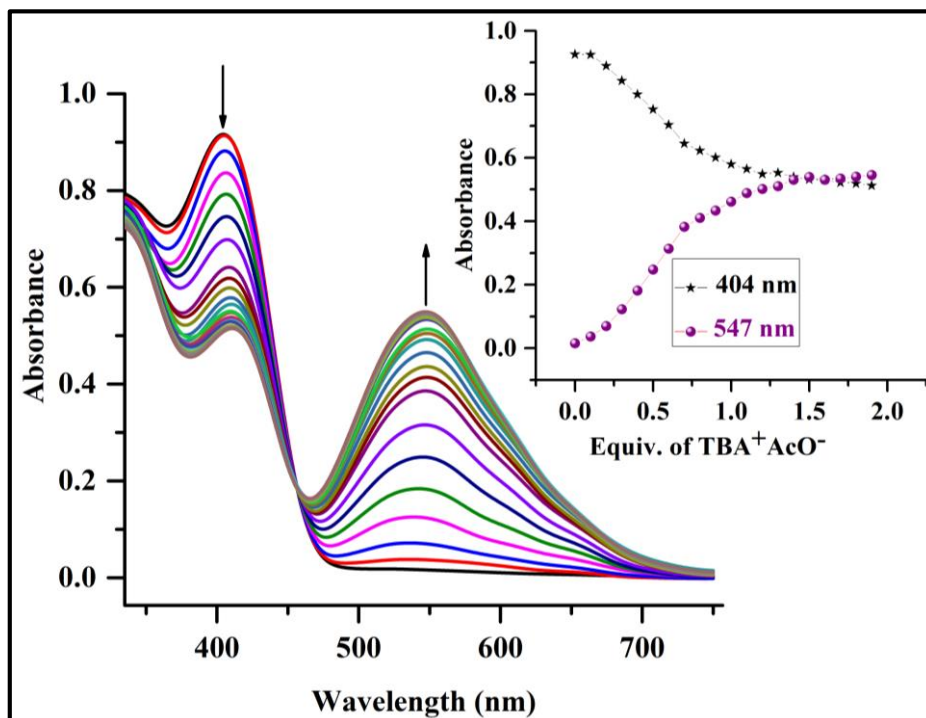
Fig. 2.30 UV-Vis titration spectra of receptor **L1R1** (4.5 ×10^{-5} M in DMSO) with incremental addition of TBA$^+$AcO$^-$ (10^{-2} M in DMSO); Inset plot representing the variation of absorbance with increasing concentration of TBA$^+$AcO$^-$

To understand the positional effect of the nitro group on the anion binding phenomena, receptor **L1R4** was synthesized with a nitro substituent at the ortho position of the phenyl ring. The UV-Vis titration experiment was performed for the receptor **L1R4** in the presence of F^- and AcO^- ions. As illustrated in Fig. 2.31 and Fig. 2.32, the receptor exhibited strong absorption band at 388 nm. Upon incremental addition of F^- and AcO^- ions, the absorption band centred at 388 nm red shifted to 508 nm and 510 nm, which well supported the colour change observed in the naked-eye experiment. This change was associated with the appearance of one isosbestic point at 424 nm and 426 nm, indicating complex formation between the receptor and the added anions F^- and AcO^-. For receptors **L1R2** and **L1R5** with the phenolic -OH groups as the binding sites, the UV-Vis titration experiment was conducted with F^- and AcO^- ions. As shown in Fig. 2.33 (a and b) and Fig. 2.34 (c and d), the receptors, in the absence of anions, exhibited strong absorption bands at 370 nm and 360 nm. A bathochromic shift was observed with the rise of new bands at 465 nm and 470 nm (for the **L1R2** receptor) and 455 nm and 457 nm for the receptor **L1R5** with the addition of F^- and AcO^- ions.
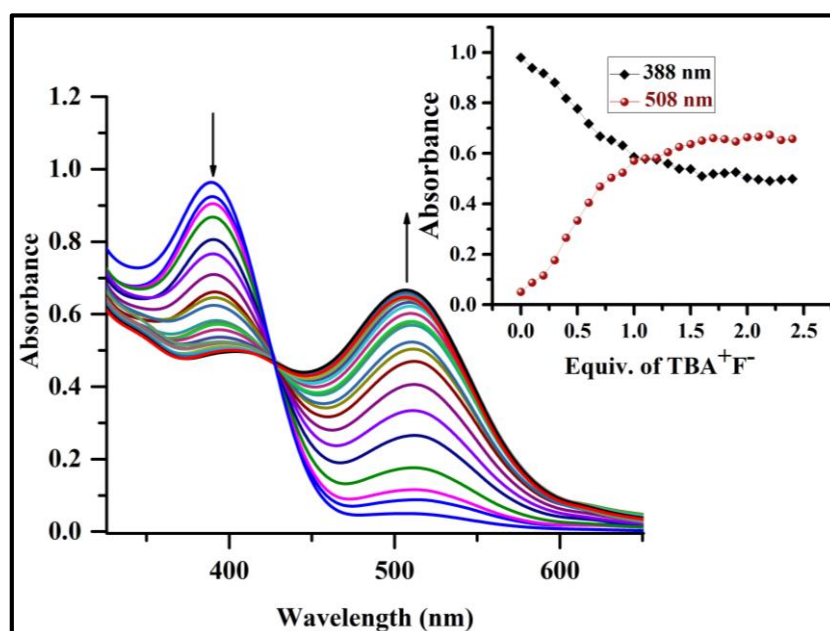
Fig. 2.31 UV-Vis titration spectra of receptor **L1R4** (4.5×10^{-5} M in DMSO) with incremental addition of TBA^+F^- (10^{-2} M in DMSO); Inset plot representing the variation of absorbance with increasing concentration of TBA^+F^-
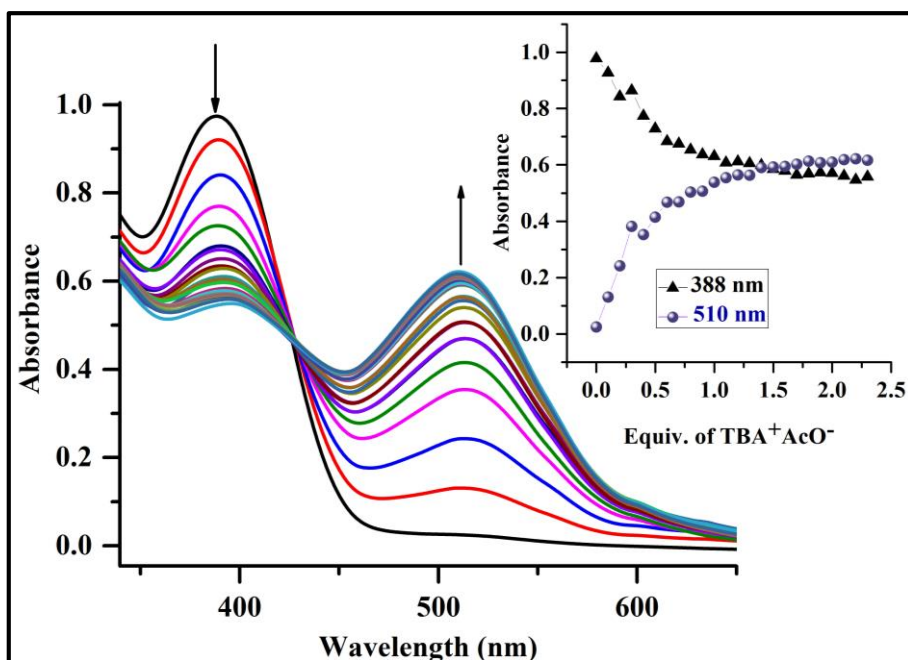
Fig. 2.32 UV-Vis titration spectra of receptor **L1R4** (4.5 $\times 10^{-5}$ M in DMSO) with incremental addition of TBA$^+$AcO$^-$ (10^{-2} M in DMSO); Inset plot representing the variation of absorbance with increasing concentration of TBA$^+$AcO$^-$
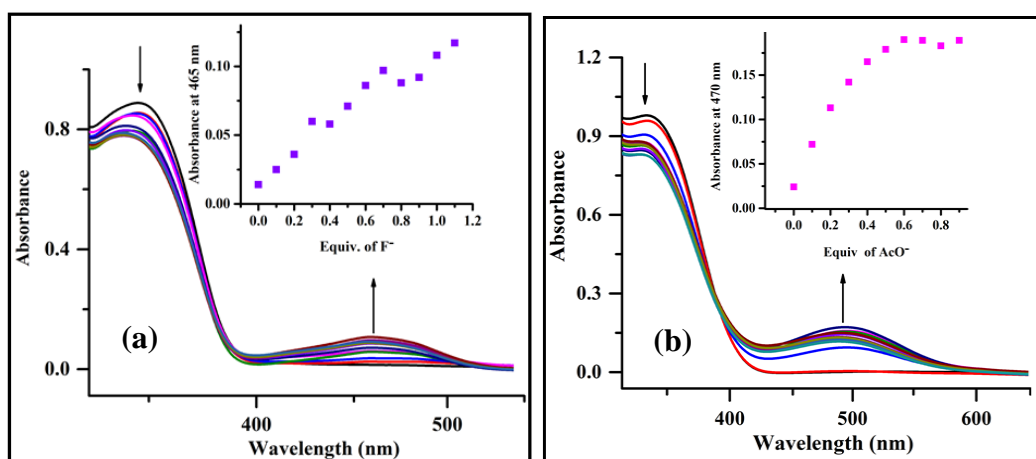
Fig. 2.33 UV-Vis titration spectra of receptor **L1R2** (4.5 $\times 10^{-5}$ M in DMSO) on gradual addition of (a) TBA$^+$F$^-$ (1$\times 10^{-2}$ M in DMSO); Inset showing isotherm at 465 nm and (b) TBA$^+$AcO$^-$ (1$\times 10^{-2}$ M in DMSO); Inset showing isotherm at 470 nm
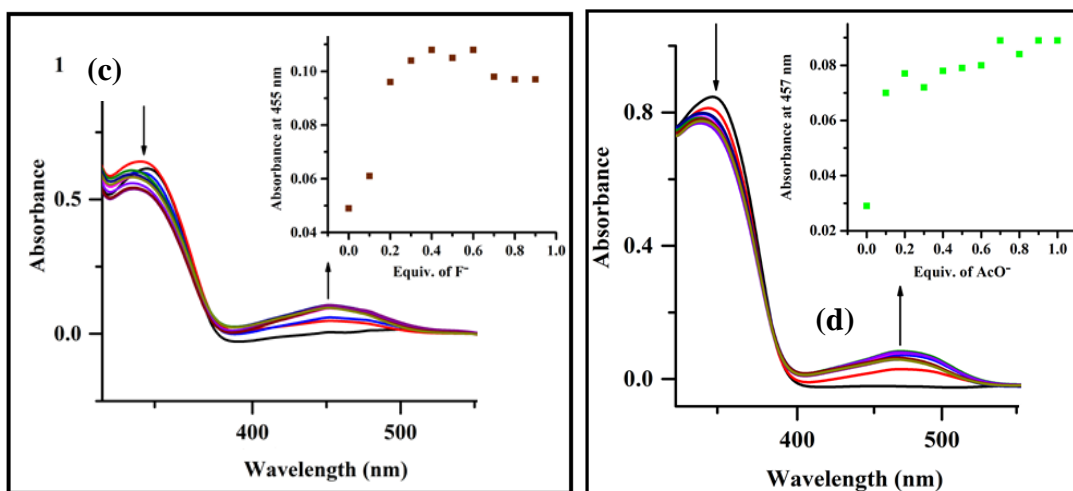
Fig. 2.34 UV-Vis titration spectra of receptor **L1R5** (4.5 ×10^{-5} M in DMSO) on gradual addition of (c) TBA^{+}F^{-} (1×10^{-2} M in DMSO); Inset showing isotherm at 455 nm (d) TBA^{+}AcO^{-} (1×10^{-2} M in DMSO); Inset showing isotherm at 457 nm

2.3.3 Change in absorption for the receptors L1R1-L1R4 in DMSO

L1R1 showed a massive bathochromic shift ($\Delta\lambda_{max}$) of 141 nm and 143 nm in the DMSO among all the receptors due to the stable intramolecular charge transfer transition (ICT) in the receptor **L1R1** on F^{-}/AcO^{-} binding.

The shift in absorption maxima ($\Delta\lambda_{max}$) after addition of 2 equiv. of F^{-} and AcO^{-} ions to the receptors **L1R1, L1R2, L1R4,** and **L1R5** (4.5 ×10^{-5} M) in the DMSO solutions is summarized in Table 2.1.

Table 2.1 Change in absorption ($\Delta\lambda_{max}$) of receptors **L1R1-L1R4** (4.5×10^{-5} M in DMSO solution) in the presence of F⁻ and AcO⁻ ions (2 equiv.)

Receptor[a]	λ_{max} (Receptor + TBA⁺F⁻)[b] nm	λ_{max} (Receptor + TBA⁺AcO⁻)[c] nm	$\Delta\lambda_{max}$ (Receptor + TBA⁺F⁻) nm	$\Delta\lambda_{max}$ (Receptor + TBA⁺AcO⁻) nm	Colour
L1R1	**545**	**547**	**141**	**143**	**Purple**
L1R2	465	470	95	100	Light pink
L1R3	308	308	0	0	Colourless
L1R4	507	510	119	122	Red
L1R5	455	457	95	97	Light yellow
L1R6	308	308	0	0	Colourless

[a] Absorption spectra were taken for receptors **L1R1-L1R4** at the concentration of (4.5×10^{-5} M in DMSO solution)

[b] TBA⁺F⁻ solution (2 equiv. in DMSO) was added to receptors **L1R1**-**L1R4** solution (DMSO)

[c] TBA⁺AcO⁻ solution (2 equiv. in DMSO) was added to receptors **L1R1**-**L1R4** solution (DMSO) DMSO)

2.3.4 Detection of inorganic anions using the receptors L1R1 and L1R4 in DMSO: H₂O (9:1 v/v)

The sodium salts of fluoride and acetate are major components in commercially available toothpaste, mouthwash, and vinegar. Therefore, the real-time applicability of the receptors **L1R1** and **L1R4** was explored with important inorganic anions such as Na⁺F⁻ and Na⁺AcO⁻ in the organo-aqueous medium DMSO: H₂O (9:1 v/v). As shown in Fig. 2.35, upon the addition of 2 equiv. of Na⁺F⁻ and Na⁺AcO⁻ (10^{-2} M in H₂O) to the receptors' **L1R1** and **L1R4** solutions (4.5×10^{-5} M), instant and noticeable colour change was observed from pale yellow to purple and from pale yellow to red, respectively.
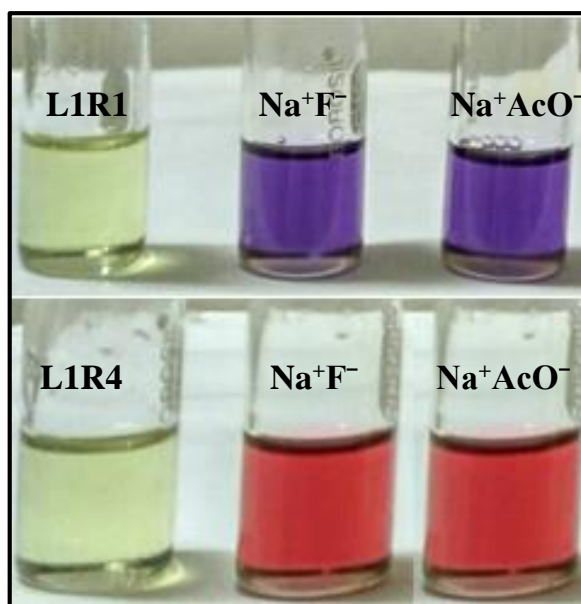
Fig. 2.35 Colour change of receptors **L1R1** and **L1R4** (4.5 ×10^{-5} M in DMSO) with the addition of 2 equiv. of Na$^+$F$^-$ and Na$^+$AcO$^-$ (10^{-2} M in distilled water) in DMSO: H$_2$O (9:1 v/v)

The titration experiment was carried out with the incremental addition of F$^-$ and AcO$^-$ ions to the receptor **L1R1** solution. The titration profile exhibited bathochromic shift ($\Delta\lambda_{max}$) of about 134 nm and 136 nm in comparison with the free receptor with the emergence of new bands at 538 nm and 540 nm as depicted in Fig. 2.36 and Fig. 2.37. Similarly, the titration studies conducted with the sequential addition of F$^-$ and AcO$^-$ ions as sodium salts to the receptor **L1R4** solution, resulted in bathochromic shift ($\Delta\lambda_{max}$) of 115 nm and 118 nm in comparison with the absorption band of the free receptor. The titration profile of **L1R1** and **L1R4** with the addition of the sodium salts of F$^-$ and AcO$^-$ ions is shown in Fig. 2.38 and Fig. 2.39. Interestingly, the presence of the p-nitro group in the receptor **L1R1** greatly enhanced the acidity of the active sites of the OH proton and thus, it strongly bonded with the anions even in the semi-aqueous medium. As shown in Fig. 2.40 and Fig. 2.41, the plotting of 1/[A-A$_0$] versus 1/[Anions] [Anions= F$^-$/AcO$^-$] showed good linear relationship indicating stable 1:1 stoichiometry between the receptors (**L1R1** and **L1R4)** and the active anions (TBA$^+$F$^-$, TBA$^+$AcO$^-$, Na$^+$F$^-$, and Na$^+$AcO$^-$) in the DMSO and the DMSO: H$_2$O (9:1 v/v)
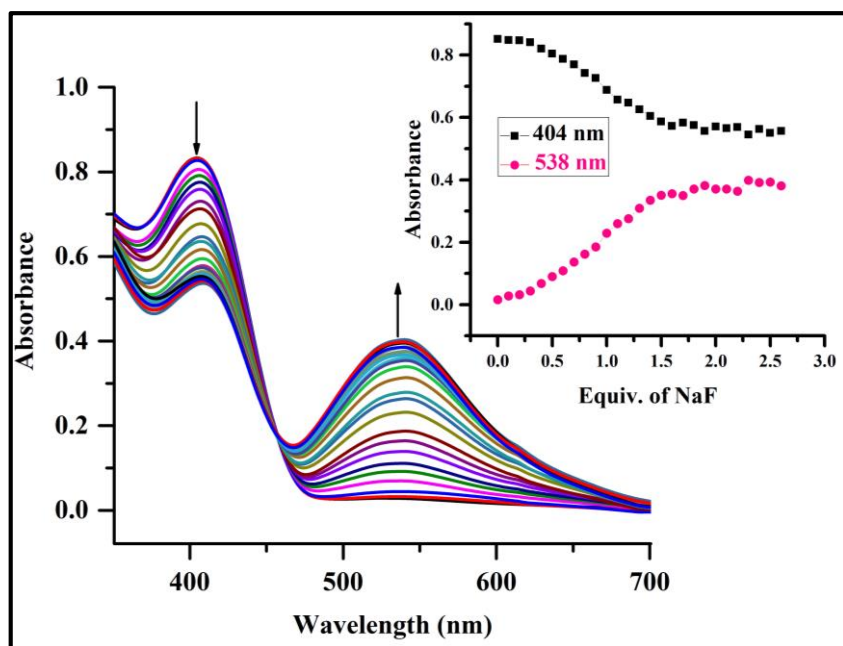
Fig. 2.36 UV-Vis titration spectra of receptor **L1R1** (4.5×10^{-5} M) with incremental addition of Na^+F^- (10^{-2} M in distilled water) in DMSO: H_2O (9:1 v/v); Inset plot representing the variation of absorbance with increasing concentration of Na^+F^-
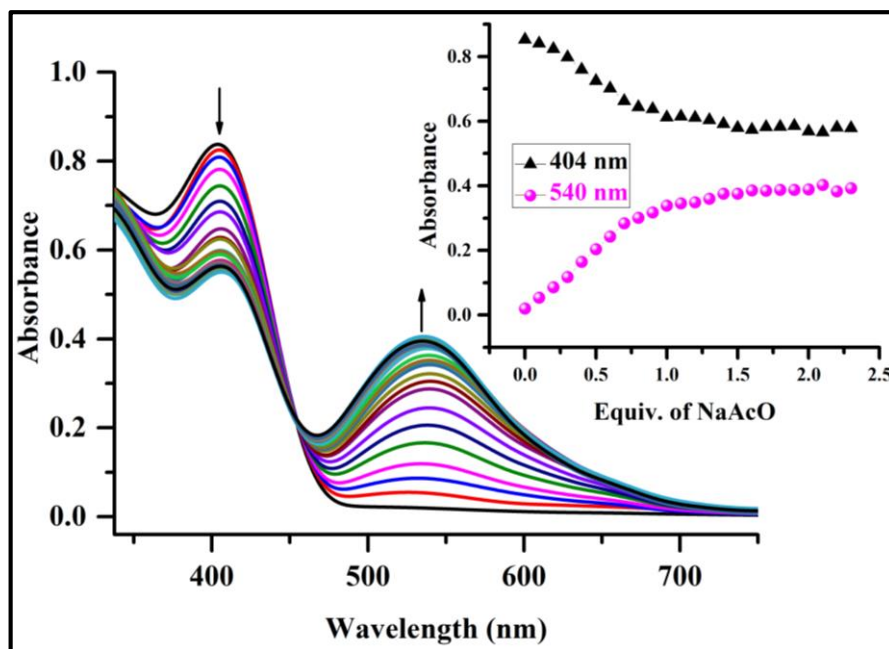
Fig. 2.37 UV-Vis titration spectra of receptor **L1R1** (4.5×10^{-5} M) with incremental addition of Na^+AcO^- (10^{-2} M in distilled water) in DMSO: H_2O (9:1 v/v); Inset plot representing the variation of absorbance with increasing concentration of Na^+AcO^-
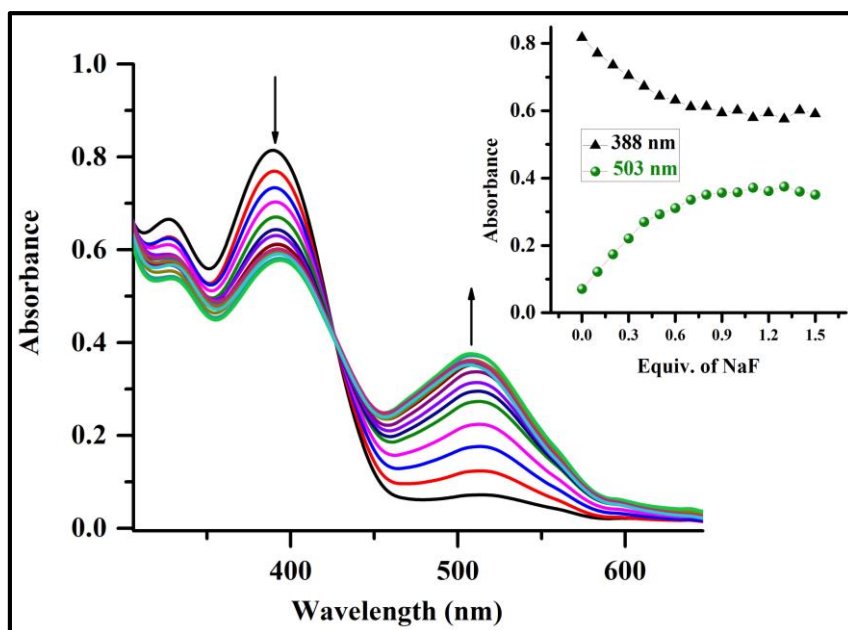
Fig. 2.38 UV-Vis titration spectra of receptor **L1R4** (4.5×10^{-5} M) with incremental addition of Na^+F^- (10^{-2} M in distilled water) in DMSO: H_2O (9:1 v/v); Inset plot representing the variation of absorbance with increasing concentration of Na^+F^-

Fig. 2.39 UV-Vis titration spectra of receptor **L1R4** (4.5×10^{-5} M) with incremental addition of Na^+AcO^- (10^{-2} M in distilled water) in DMSO: H_2O (9:1 v/v); Inset plot representing the variation of absorbance with increasing concentration of Na^+AcO^-

Equation	y = a + b*x			
Plot	L1R1+TBAF	L1R1+TBAAcO	L1R4+TBAF	L1R4+TBAAcO
Intercept	0.39608 ± 0.02174	0.0845 ± 0.01946	1.67022 ± 0.02836	0.57207 ± 0.03918
Slope	6.26266E-7 ± 1.30082E-8	2.20399E-6 ± 1.53312E-8	1.53262E-6 ± 2.18683E-8	5.35749E-7 ± 2.34423E-8
Residual Sum of Squares	0.03412	0.11364	0.21694	0.11079
Pearson's r	0.99764	0.99949	0.99797	0.98963
R-Square(COD)	0.99528	0.99898	0.99594	0.97937
Adj. R-Square	0.99485	0.99894	0.99574	0.9775
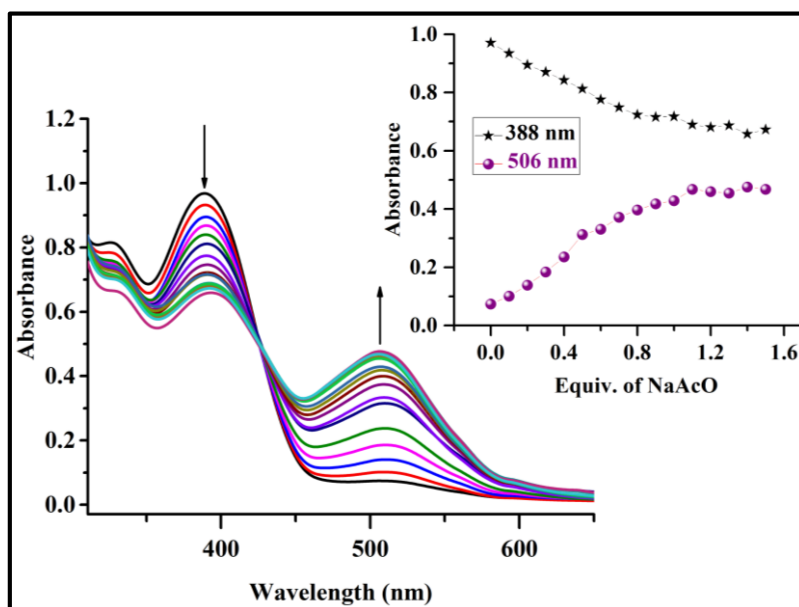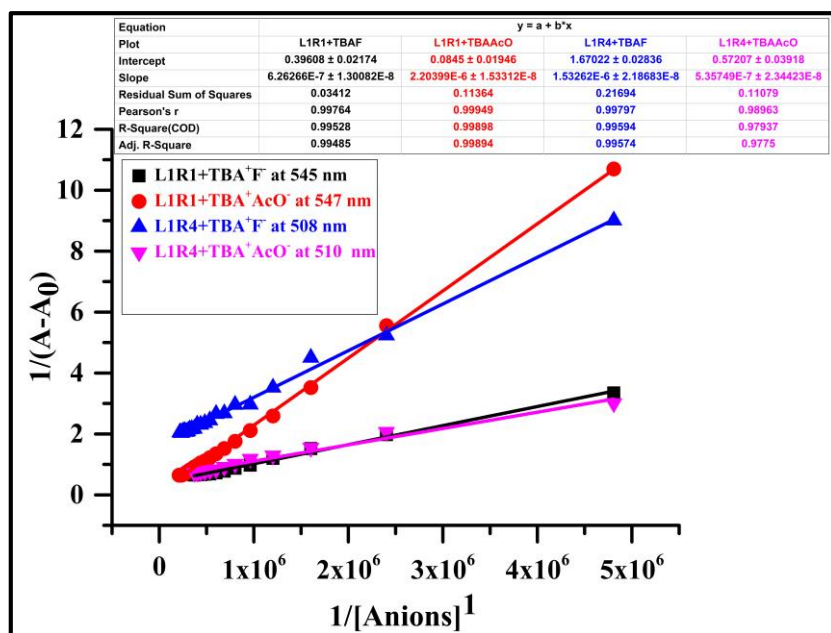
Fig. 2.40 B-H plot of receptors **L1R1** and **L1R4** with TBA^+ of F^- and AcO^- ions complex associated with the absorbance change at 545 nm, 547 nm, 508 nm and 510 nm in DMSO

Equation	y = a + b*x			
Plot	L1R1-NaF	L1R1-NaAcO	L1R4-NaF	L1R4-NaAcO
Intercept	1.03239 ± 0.14168	0.4583 ± 0.06327	0.09776 ± 0.08819	0.33444 ± 0.03468
Slope	5.31411E-6 ± 1.11644E-7	1.09858E-6 ± 4.65795E-8	2.80846E-6 ± 5.27647E-8	1.54522E-6 ± 1.91637E-8
Residual Sum of Squares	6.0264	0.85662	0.56131	0.05569
Pearson's r	0.9954	0.9842	0.99806	0.99931
R-Square(COD)	0.99082	0.96865	0.99613	0.99862
Adj. R-Square	0.99038	0.96691	0.99578	0.99846

Fig. 2.41 B-H plot of receptors **L1R1** and **L1R4** with Na^+ of F^- and AcO^- ions complex associated with the absorbance change at 538 nm, 540 nm, 503 nm and 506 nm in DMSO: H_2O (9:1 v/v)

2.3.5 Calculation of binding constant and detection limit from UV-Vis studies

The binding constant based on UV-Vis titration data was calculated using the Benesi-Hildebrand equation (Benesi and Hildebrand 1949) as given below (Eq. 2.1)

$$\frac{1}{(A-A_0)} = \frac{1}{(A_{max}-A_0)} + \frac{1}{K[X^-]^n (A_{max}-A_0)} ----- (Eq.\,2.1)$$

Where, A_0, A, and A_{max} are the absorption considered in the absence of anions, at intermediate and at concentration of saturation, K is the binding constant, $[X^-]$ is the concentration of anions, and *n* is the stoichiometric ratio.

The binding constant, detection limit, and binding ratio is given in Table 2.2.

Table 2.2 Binding constant and detection limit of receptors **L1R1, L1R2, L1R4,** and **L1R5** with active anions

Receptor +Anion	Medium	Binding constant (M^{-1})	Detection limit (ppm)
L1R1+TBA$^+$F$^-$	DMSO	7.4×10^4	2.8
L1R1+TBA$^+$AcO$^-$	DMSO	7.9×10^4	1.7
L1R2+TBA$^+$F$^-$	DMSO	2.1×10^2	12.3
L1R2+TBA$^+$AcO$^-$	DMSO	2.9×10^2	7.9
L1R4+TBA$^+$F$^-$	DMSO	5.0×10^4	5.2
L1R4+TBA$^+$AcO$^-$	DMSO	5.5×10^4	3.3
L1R5+TBA$^+$F$^-$	DMSO	1×10^2	15.4
L1R5+TBA$^+$AcO$^-$	DMSO	2.17×10^2	11.3
L1R1+ Na$^+$F$^-$	DMSO:H$_2$O (9:1 v/v)	6.6×10^3	0.35
L1R1+ Na$^+$AcO$^-$	DMSO:H$_2$O (9:1 v/v)	6.9×10^3	0.4
L1R4+ Na$^+$F$^-$	DMSO:H$_2$O (9:1 v/v)	2.2×10^3	3
L1R4+ Na$^+$AcO$^-$	DMSO:H$_2$O (9:1 v/v)	3.9×10^3	4.3

2.3.6   UV-Vis spectroscopic studies of receptor L1R1 in buffer solution

The anion is more pH sensitivity. Therefore, anion binding properties were a probe in buffer medium with receptor **L1R1** (4.5×10⁻ 5 M, DMSO: HEPES buffer; 9:1, v/v, pH 7.4). The receptor **L1R1** displayed an excellent affinity to AcO⁻ ion and showed a significant change in colour from pale yellow to pink as shown in Fig. 2.42.
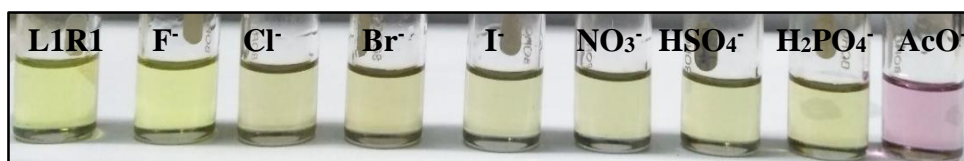
Fig. 2.42 Colour change of receptor **L1R1** (4.5×10^{-5} M, DMSO: HEPES buffer; 9:1, v/v, pH 7.4) after addition of 3 equiv. of the various anions in form of TBA salts

UV-Vis absorbance of the receptor was initially carried out in the presence of various interference anions, including (F⁻, Cl⁻ , Br⁻ , I⁻ , NO3 ⁻ , HSO₄⁻, H₂PO₄⁻ and AcO⁻ (1 × 10 $^{-2}$ M in DMSO) in form of TBA salts. Upon addition of 3 equiv. of aliquot anions, the receptor **L1R1** showed a significant red shift in the absorption band for AcO⁻ ion as shown in Fig. 2.43. In contrast with the addition of other anions, no significant shift in the absorption spectrum was observed.
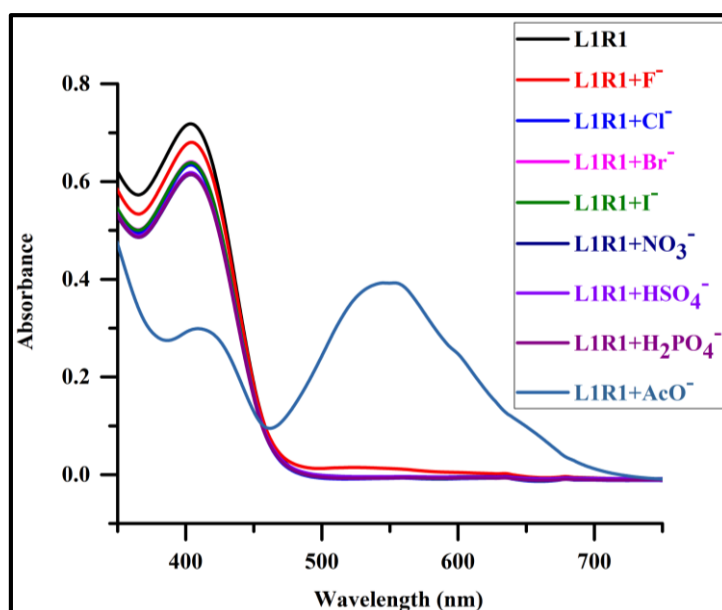
Fig. 2.43 UV-Vis absorption spectra change of receptor **L1R1** (4.5×10^{-5} M, DMSO: HEPES buffer; 9:1, v/v, pH 7.4) upon addition of 3 equiv. of TBA salts of anions

To further enlighten the nature of the interaction between receptor **L1R1** and AcO⁻ ion, UV-Vis titration studies were performed. Free receptor **L1R1** showed an intrinsic maximum absorption band at 404 nm attribute to the π π* transition. Upon successive addition of 0.1 equiv. of a standard solution of TABACO to receptor **L1R1** solution, the diminution in the intensity of absorption band at 404 nm and the parallel increase new band at 539 nm with a sharp isosbestic point at 453 nm, which indicate the one stable complex formation between receptor **L1R1**---AcO⁻ ion as given in Fig. 2.44. Bathochromic shift of 135 nm was noticed. This may be due to charge transfer between the anion bond -OH protons and the electron deficient NO2 group in the para position.
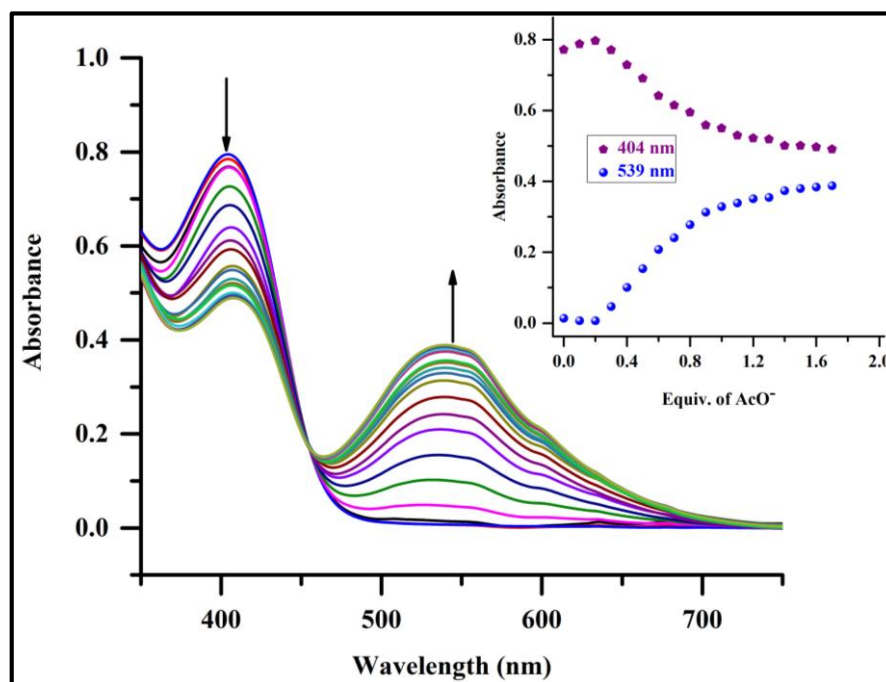
Fig.2.44 UV-Vis titration spectral of receptor **L1R1** (4.5×10^{-5} M, DMSO: HEPES buffer; 9:1, v/v, pH 7.4) upon step-wise addition of 0.1 equiv. of TBAAcO (1×10^{-2} M). Inset shows the binding isotherm at 539 nm.

2.3.7 Fluorescent anion titration studies

In addition to the UV-Vis titration experiments, fluorescence titration experiments were also conducted to evaluate the ability of the receptors **L1R1**, **L1R2**, **L1R4**, and **L1R5** (4.5×10^{-5} M in DMSO) as fluorescent anion sensors. Fluorescence

titration was performed for the receptor **L1R1** with the incremental addition of F⁻ and AcO⁻ ions. The fluorescence intensity gradually increased and showed good emission bands at 461 nm and 464 nm (λ_{exc}=410 nm) owing to strong interaction between the receptor and the active anions. Likewise, on titrating with F⁻ and AcO⁻ ions, **L1R2** displayed strong emission bands at 387 nm and 415 nm when excited at (λ_{exc}=350 nm). On the other hand, the receptors **L1R4** and **L1R5** exhibited emission bands at 433 nm and 437 nm (λ_{exc}= 373 nm), and at 365 nm and 370 nm (λ_{exc}=280 nm), respectively, when F⁻ and AcO⁻ ions were introduced sequentially. The fluorescence spectra are depicted in Fig. 2.45 (a and b), Fig. 2.46 (c and d), Fig. 2.47 (e and f), and Fig. 2.48 (g and h). Fluorescence enhancement may be due to intramolecular load transfer (ICT) between the-OH group and the-NO_2 group. Compared to all receptors, **L1R1** displayed a high increase in fluorescence due to the presence of the NO_2 group at para position. The data is summarized in Table 2.3 and clearly indicates that the receptor**s** selectively recognized F⁻ and AcO⁻ ions by the dual mode colorimetric and fluorometric methods in the DMSO.

Table 2.3 Fluorescence spectra data of receptors **L1R1, L1R2, L1R4,** and **L1R5** with the active anions in the DMSO

Sl.No	Receptor+Anions	λ excitation	λemission
1	**L1R1**+TBA⁺F⁻	410 nm	461 nm
2	**L1R1**+TBA⁺AcO⁻		464 nm
3	**L1R2**+TBA⁺F⁻	350 nm	387 nm
4	**L1R2**+TBA⁺AcO⁻		415 nm
5	**L1R4**+TBA⁺F⁻	373 nm	433 nm
6	**L1R4**+TBA⁺AcO⁻		437 nm
7	**L1R5**+TBA⁺F⁻	280 nm	365 nm
8	**L1R5**+TBA⁺AcO⁻		370 nm
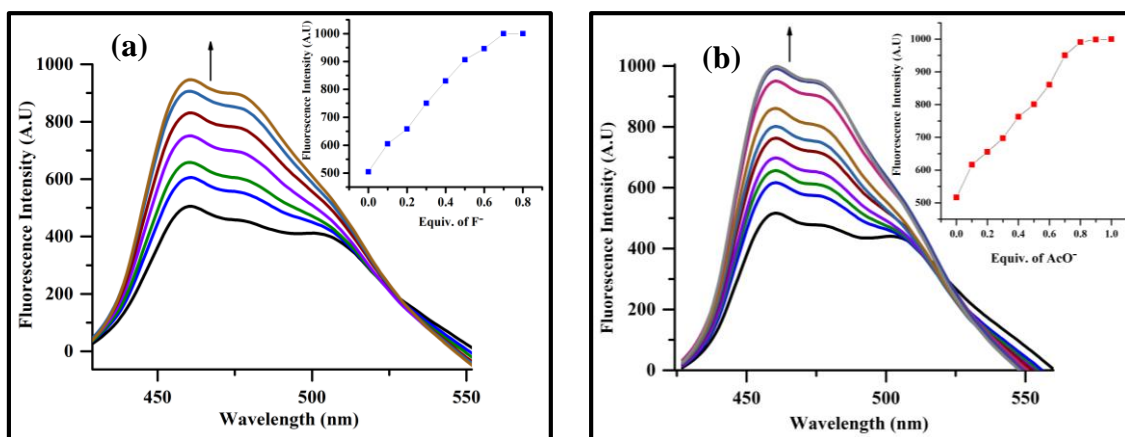
Fig. 2.45 Fluorescence spectra of **L1R1** (4.5 ×10^{-5} M) in DMSO with increasing concentration of (a) TBA$^+$F$^-$ ions (1 ×10^{-2} M); Inset plot representing equiv. addition of F$^-$ ion and (b) TBA$^+$AcO$^-$ ions (1 ×10^{-2} M)); Inset plot representing equiv. addition of AcO$^-$ ion
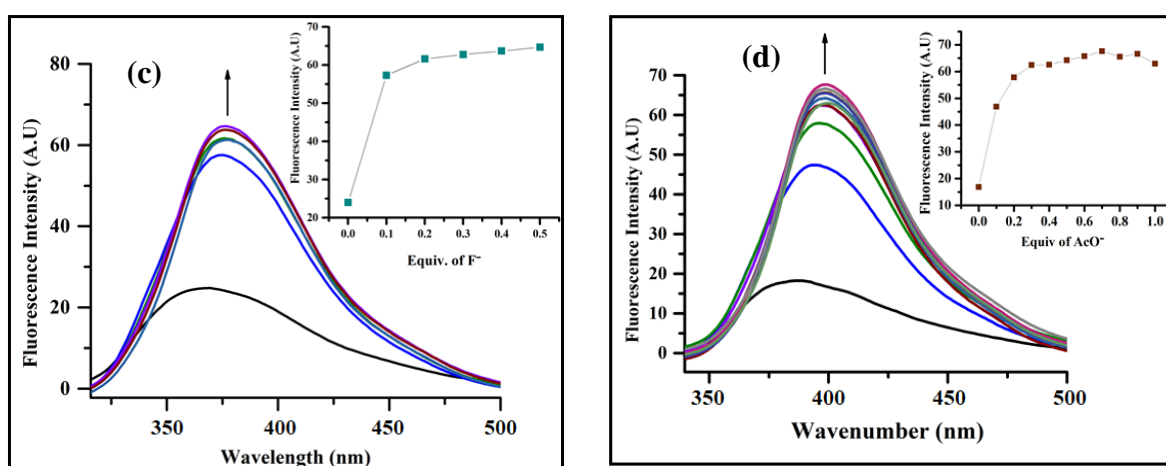
Fig. 2.46 Fluorescence spectra of **L1R2** (4.5 ×10^{-5} M) in DMSO with increasing concentration of (c) TBA$^+$F$^-$ ions (1 ×10^{-2} M); Inset plot representing equiv. addition of F$^-$ ion and (d) TBA$^+$AcO$^-$ ions (1 ×10^{-2} M); Inset plot representing equiv. addition of AcO$^-$ ion
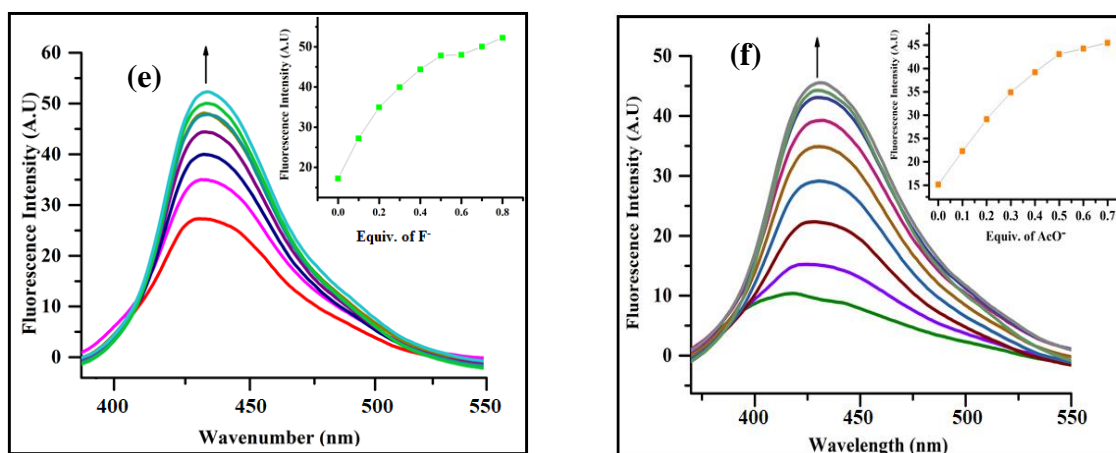
Fig. 2.47 Fluorescence spectra of **L1R4** (4.5 ×10^{-5} M) in DMSO with the increasing concentration of (e) TBA$^+$F$^-$ ions (1 ×10^{-2} M); Inset plot representing equiv. addition of F$^-$ ion and (f) TBA$^+$AcO$^-$ ions (1 ×10^{-2} M); Inset plot representing equiv. addition of AcO$^-$ ion
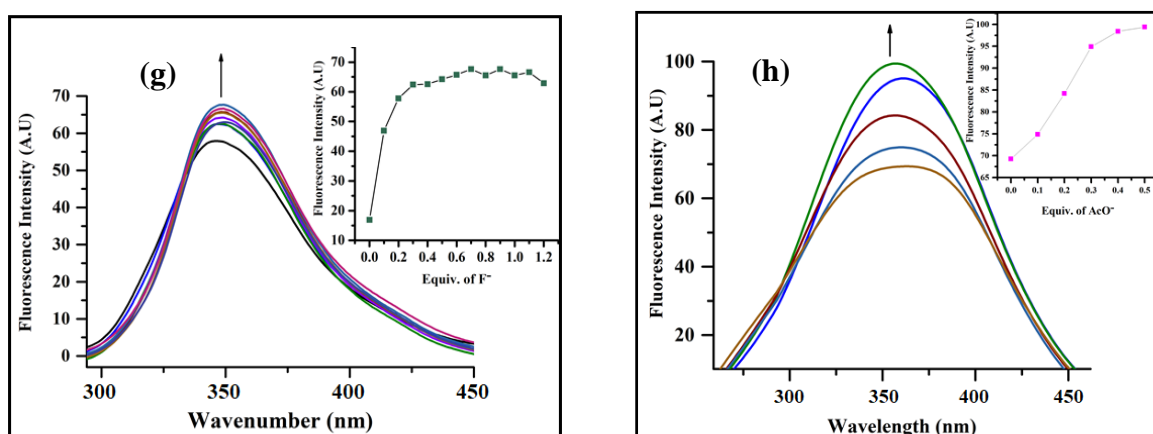
Fig. 2.48 Fluorescence spectra of **L1R5** (4.5 ×10^{-5} M) in DMSO with the increasing concentration of (g) TBA$^+$F$^-$ ions (1 ×10^{-2} M); Inset plot representing equiv. addition of F$^-$ ion and (h) TBA$^+$AcO$^-$ ions (1 ×10^{-2} M); Inset plot representing equiv. addition of AcO$^-$ ion

2.3.8 Solvent effect on electronic spectra

Based on the spectral position shifting and change in the nature of the UV-Vis spectral bands in solvents of different polarities, it was found that the receptor **L1R1** can act as a solvatochromic probe. Generally, the spectral shifts depend on the solute–solute and/or solute–solvent interaction at the molecular level through hydrogen bonding or extensive π-conjugation (Hadjmohammadi et al.2008; Homocianu 2011). The addition of 2

equiv. of AcO⁻ ion (1×10^{-2} M in DMSO) into the receptor **L1R1** induced colour change from pale yellow to pale yellow to purple, pink, dark blue, light purple, brown, blue, and lavender in different aprotic polar solvents such as DMSO, ACN, THF, Acetone, DCM, DMF, and 1,4-dioxane, respectively, as depicted in Fig. 2.49. The UV-Vis spectra recorded after adding 2 equiv. of AcO⁻ ion to the receptor **L1R1** of varying polarities resulted in new absorption bands with significant bathochromic shift (positive solvatochromis) as represented in Fig. 2.50. The shift in absorption maxima is given in Table 2.4. The shift in band indicated stable complex formation between the receptor **L1R1** and the AcO⁻ ion in different solvents. The bathochromic shift may be due to the different dipole moments in its ground and lower energy singlet excited state or change in hydrogen bonding strength in the different solvents (Berryman et al. 2008; Berryman and Johnson 2009; Chifotides et al. 2010).
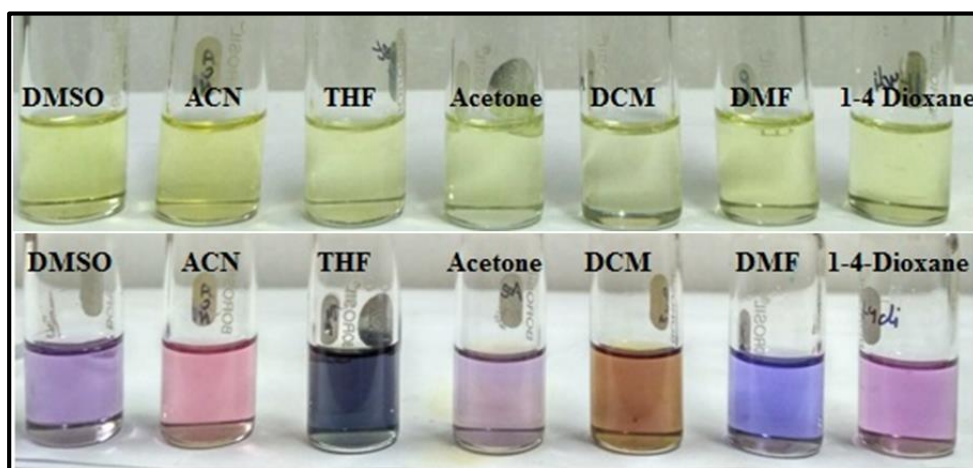
Fig. 2.49 Solvatochromism in receptor **L1R1** (4.5×10^{-5} M) upon adding 2 equiv. of AcO⁻ (1×10^{-2} M in DMSO) in different solvents
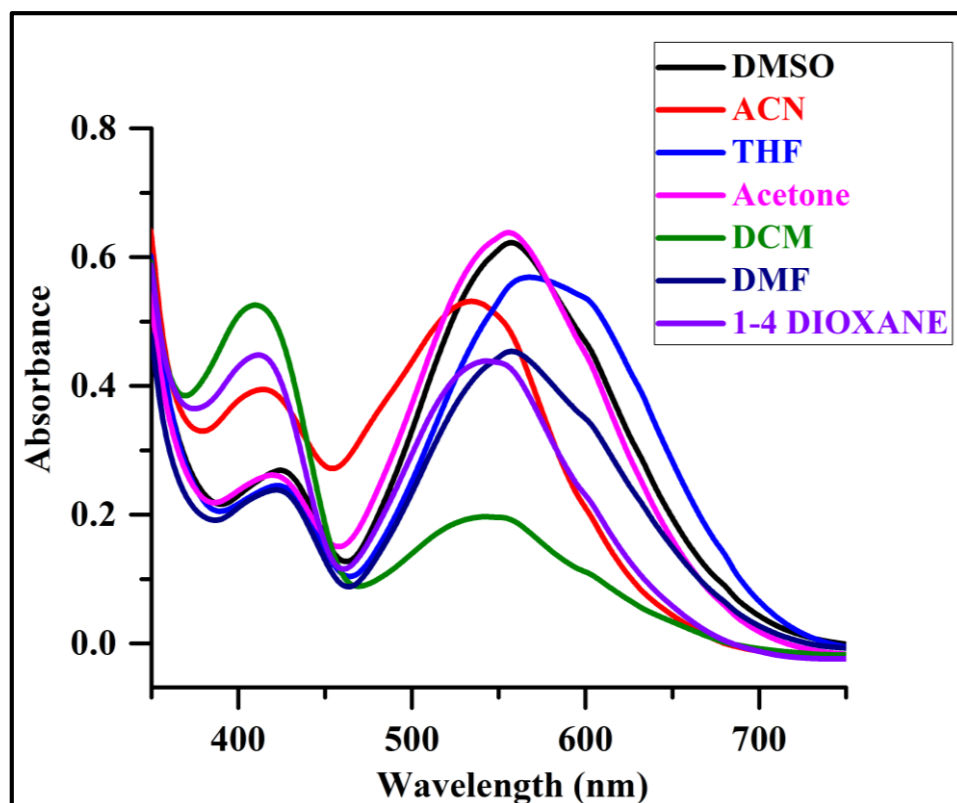
Fig. 2.50 UV-Vis absorption spectra of receptor **L1R1** (4.5×10 $^{-5}$ M) upon adding 2 equiv. of AcO$^-$ (1×10^{-2} M in DMSO) in different solvents

Table 2.4 Shift in absorption maxima ($\Delta\lambda_{red\ shift}$) of receptor **L1R1** in different polar aprotic solvents in the presence of 2 equiv. of AcO$^-$ ion

Receptor +Anions	Solvent	$\lambda_{red\ shift}$ (nm)	$\Delta\lambda_{red\ shift}$ (nm)	Colour Change
L1R1+ AcO$^-$	DMSO	557	153	purple
L1R1+ AcO$^-$	ACN	537	133	pink
L1R1+ AcO$^-$	THF	568	164	dark blue
L1R1+ AcO$^-$	Acetone	556	152	light purple
L1R1+ AcO$^-$	DCM	544	140	brown
L1R1+ AcO$^-$	DMF	555	151	blue
L1R1+ AcO$^-$	1-4 Dioxane	541	137	lavender

2.3.9 Real sample analysis

Encouraged by these results, it was decided to further explore the practical applicability of the receptor **L1R1** for the qualitative detection of F⁻ and AcO⁻ ions in seawater and commercially available product such as vinegar, mouthwash, and toothpaste, respectively. The toothpaste solution was prepared as 20 mg/ml in distilled water. When one drop of the toothpaste solution was added to the receptor **L1R1** (4.5×10^{-5} M) solution, a vivid colour change occured from pale yellow to purple.

Similarly, the introducion of 5 µl of vinegar into the receptor **L1R1** solution, altered the colour from pale yellow to purple. In addition, receptor **L1R1** showed colour change in the presence of mouthwash and seawater. The colour change observed is shown in Fig. 2.51.

Fig. 2.51 Colour change of the receptor **L1R1** (4.5×10^{-5} M) upon addition of vinegar, toothpaste, mouthwash, and seawater,

The UV-Vis absorption spectra recorded in the presence of vinegar, toothpaste, mouthwash, and seawater as shown in Fig. 2.52, yielded similar charge transfer band as observed in the case of TBA^+F^- and TBA^+AcO^- in the DMSO. Moreover, the selective detection of F⁻ and AcO⁻ ions in commercially available products has been presented in the form of a bar graph as shown in Fig. 2.53. Thus, the observed result confirm the qualitative detection of F⁻ and AcO⁻ ions in real samples, suggesting strong complex formation between the receptor **L1R1** and the F⁻/ AcO⁻ ions. Notably, the synthesized receptor **L1R1** can also be considered as a practical sensor for the qualitative detection of F⁻ and AcO⁻ ions in real samples like vinegar, mouthwash, and toothpaste prepared in aqueous media.
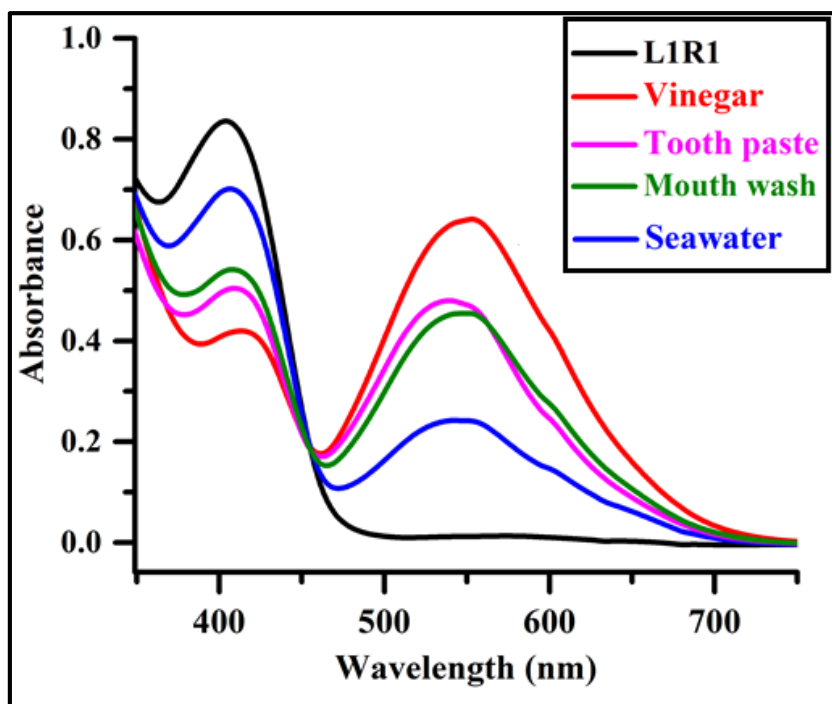
Fig. 2.52 UV-Vis absorption spectra of receptor **L1R1** (4.5×10^{-5} M) upon addition of a drop of vinegar, seawater, mouthwash, and toothpaste prepared in aqueous media
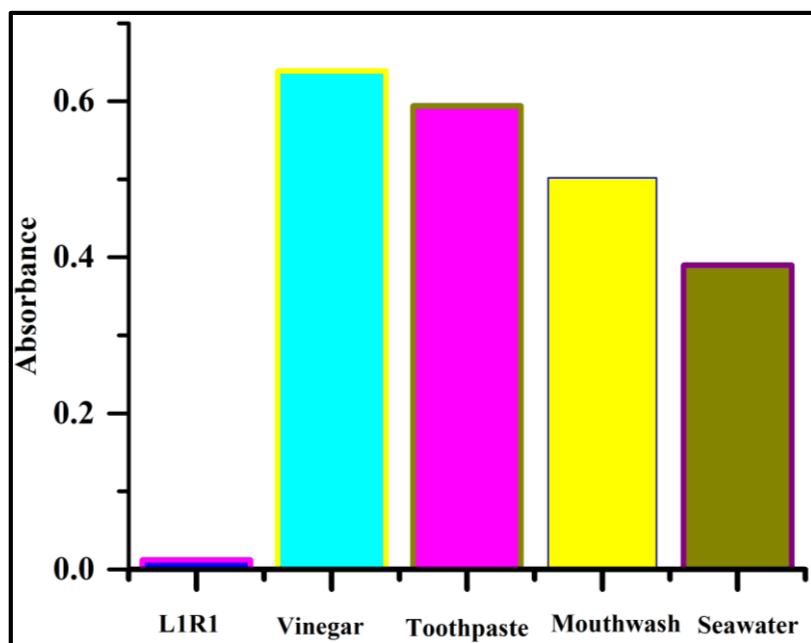
Fig. 2.53 Bar graph representation of receptor **L1R1** in the presence of real samples

2.3.10 Analytical application

In order to evaluate the practical applicability of the receptor **L1R1**, a test strip application was performed to detect the F^- and AcO^- ions. The test strip was prepared from (Whatman filter paper-40) by dipping it in to the receptor **L1R1** solution (4.5×10^{-5} M), and then drying it in a hot oven. Generally, protic solvents such as water and methanol interfere with the binding site and can cause disturbance in the interaction between the receptor and the anions.

Interestingly in the current study, on the addition of one drop of the sodium salts of F^- and AcO^- ions prepared in (10^{-2} M in H_2O) on to the test strip, the pale yellow colour changed to purple as represented in Fig. 2.54. The above experiment proves the feasible approach of the receptor **L1R1** as a test kit for the detection of F^- and AcO^- ions in an aqueous media.
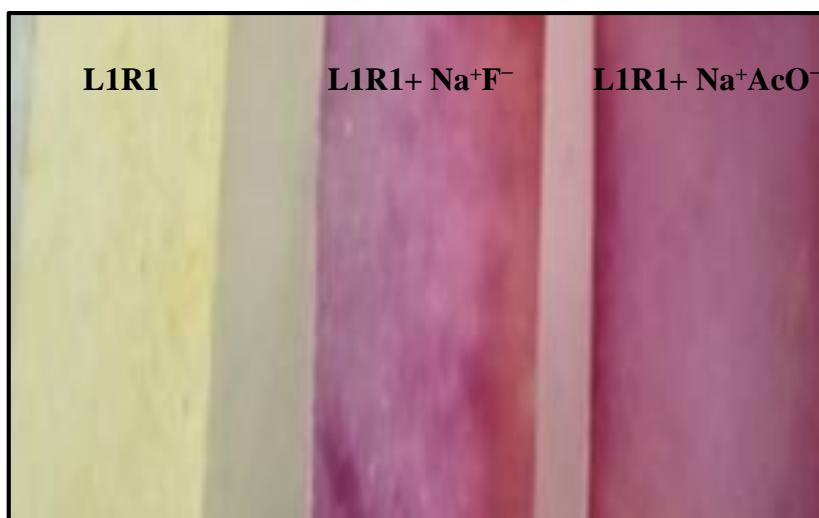
Fig. 2.54 Colour change of test paper of receptor **L1R1** (4.5×10^{-5} M) on addition of one drop of Na^+F^- and Na^+AcO^- (10^{-2} M in H_2O)

In an attempt to envisage the solid state sensing property by grinding equimolar mixture of the receptor **L1R1** with F^- and AcO^- ions, a colour change from pale yellow to black was observed as depicted in Fig. 2.55.
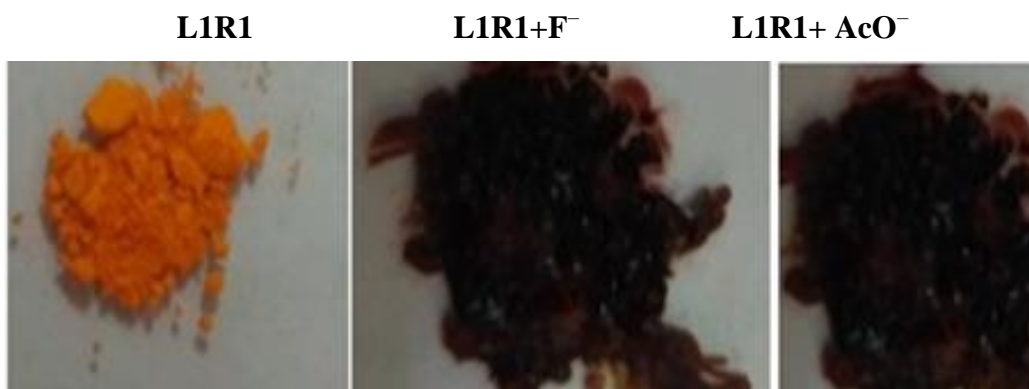
Fig. 2.55 Colour change of receptor **L1R1** (4.5×10^{-5} M) observed upon grinding 2 equiv. of F⁻ and AcO⁻ (10^{-2} M DMSO) ions

  The practical use of the receptor **L1R1** for the detection of F⁻ and AcO⁻ ions was further investigated using silica gel. The silica gel (60–120 mesh, 3 g) was first treated with the solution of the receptor **L1R1** (4.5×10^{-5} M in DMSO) and then dried in an oven to obtain a yellow coloured silica loaded with the receptor **L1R1**. The yellow colour turned to brown-red when the silica-loaded receptor **L1R1** was applied to the solution F⁻ and AcO⁻ (10^{-2} M DMSO) clearly reflecting the pactical utility of the receptor **L1R1** for the qualitative detection of F⁻ and AcO⁻ ions as represented in Fig. 2.56.

Silica   **L1R1+Silica** **L1R1+Silica+F⁻** **L1R1+Silica+AcO⁻**
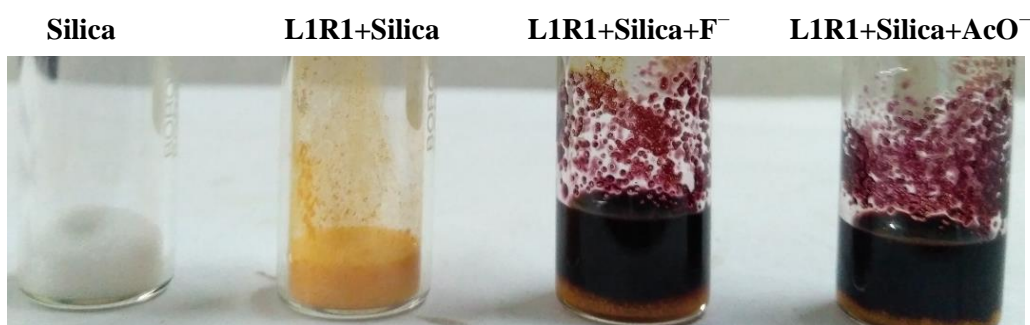
Fig. 2.56 Practical application of receptor **L1R1** (4.5×10^{-5} M in DMSO) for detection of F⁻ and AcO⁻ ions (1×10^{-2} M in DMSO) by the solid silica support method

2.3.11 ¹H NMR titration studies

  Based on the colorimetric, UV-Vis titration, and fluoresence titration experiments, it was found that the receptor **L1R1** was highly capable of sensing both the

basic F⁻ and AcO⁻ ions. To further investigate the nature of the interation between receptor **L1R1** and anions, ^{1}HNMR titration experiment was conducted in the DMSO-d_6 solvent in the absence and presence of the TBA[+] of F⁻ and AcO⁻ (1×10^{-2} M) ions. The ^{1}H-NMR spectrum of **L1R1** showed the presence of the -OH proton as a sharp singlet peak at 12.8 ppm. Upon addition of 0.5 equiv. of F⁻/AcO⁻ ions, the peak at 12.8 ppm exhibited downfield shift to **δ** 13.1 ppm and 13.3 ppm. The downfield shift specified the formation of a hydrogen bond between the receptor **L1R1** and the F⁻/AcO⁻ ions (Ghosh et al. 2016). However, at higher concentration of F⁻/AcO⁻ ions (1 equiv.), the proton signal for OH at **δ** 13.1 ppm and **δ** 13.3 ppm disappeared (Park et al. 2012) as shown in Fig. 2.57 and Fig 2.58. Moreover, the aromatic proton signals in **L1R1** underwent an upfield shift owing to the increase in electron density on the aromatic ring due to the deprotonation of the OH group. Thus, the proton NMR titration studies clearly favoured the OH----F⁻/AcO⁻ ion hydrogen bonding, followed by deprotonation of the receptor **L1R1**. On further addition of 2 equiv. F⁻/AcO⁻ ions, no chemical shift was observed, indicating 1:1 binding ratio between the receptor **L1R1** and the F⁻ /AcO⁻ ions as supported by the B-H plot.
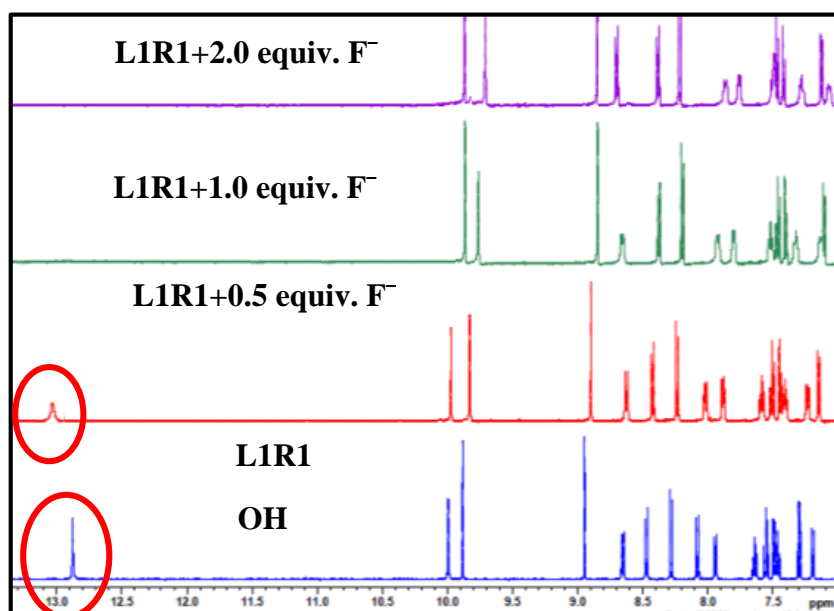
Fig. 2.57 ^{1}H-NMR titration spectra of receptor **L1R1** with incremental addition of TBA[+]F⁻ in DMSO-d_6
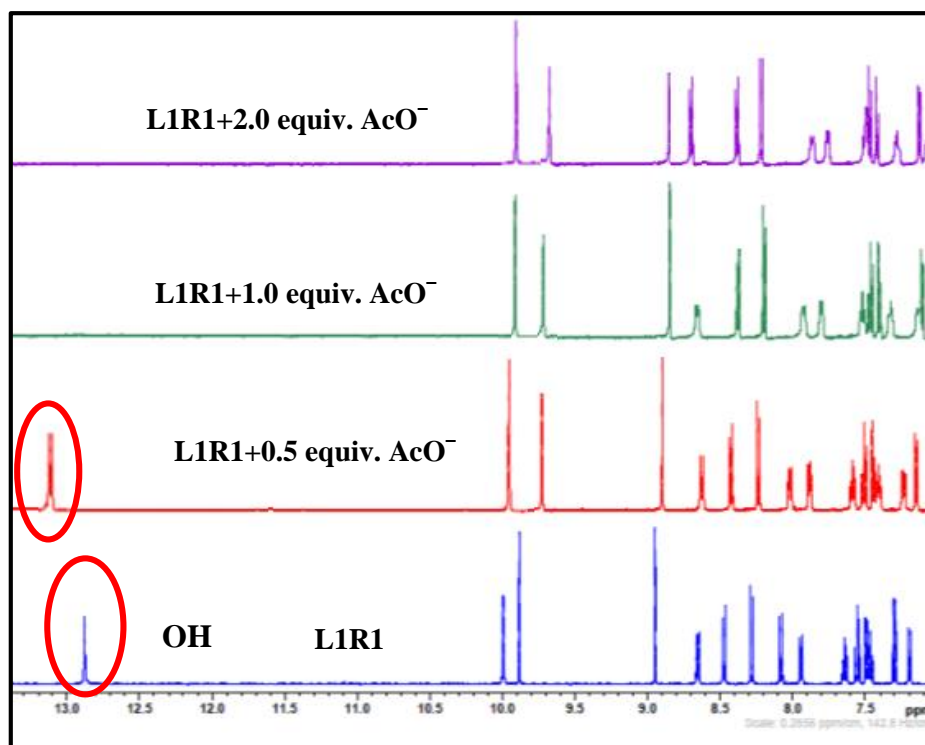
Fig. 2.58 ^{1}H-NMR titration spectra of receptor **L1R1** with incremental addition of TBA[+]AcO[−] in DMSO-d_6

2.3.12   Binding mechanism

The presence of the nitro group at the para position to the receptor **L1R1** is known to promote strong hydrogen bond interaction in the presence of anions. The ^{1}H-NMR studies of the receptor **L1R1** in the presence of anions confirmed the hyrogen bond, followed by the deprotonation of the naphthyl -OH functionality during the anion binding process. The occurrence of 1:1 binding ratio for the **L1R1** -anion complex revealed the successful binding of the anions to the naphthyl -OH fuctionality, following a deprotonation event. A charge separation in the receptor was induced resulting in ICT transition between the electron deficient NO_2 group at the p-position and the electron rich O[−] leading to colorimetric response. The binding mechanism is shown in Scheme 2.4.
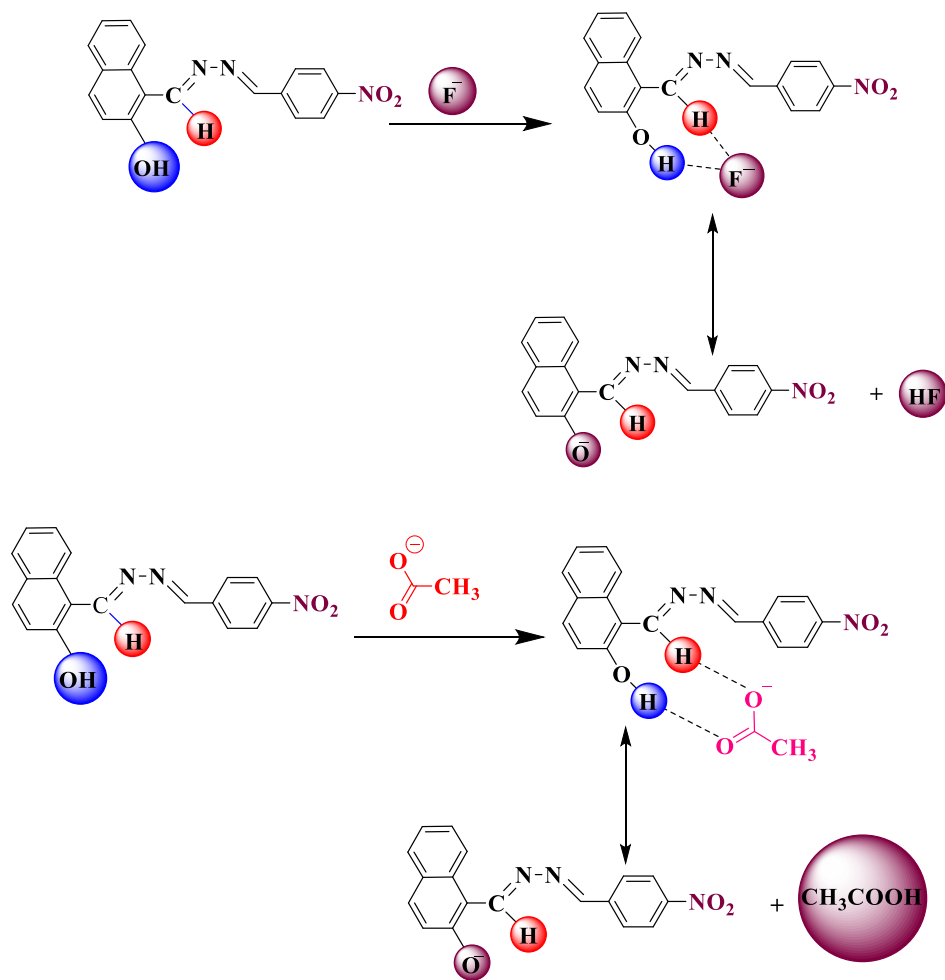
Scheme 2.4 Proposed binding mechanism of **L1R1** with F⁻ and CH₃COO⁻

2.3.13 DFT Calculations

The molecular modelling calculations of the receptors (**L1R1** and **L1R4**) in the absence and presence of the selective anions (F⁻ and AcO⁻) were performed by applying the B3LYP exchange-correlation functional and the basis set 6-31G* in the DMSO medium. The solvent effect on the model structure was applied by the conductor-like polarizable continuum model (CPCM) solvation model. All the calculations were done using the computational code Gaussian 09W (Royzen et al. 2006). The optimized structure of the receptors **L1R1 and L1R4** is shown in Fig. 2.59 with intramolecular hydrogen bond of lengths 1.693 and 1.713 Å. The nitro substitution at the ortho position of the **L1R4** resulted in a less planar structure compared with the **L1R1**, which possibly restricted the internal change transfer process. Also, the receptor **L1R1** was -9.68 kcal/mol energetically more

stable than **L1R4**. An analysis of the Mulliken's atomic charges indicates that the naphthol proton possessed maximum positive charge of 0.489 (**L1R1**) and 0.444 (**L1R4**) making possible the interaction with the incoming anions. Upon interaction with the anions, the O-H bond length of **L1R1** (1.004 Å) and **L1R4** (0.997 Å) increased to ~1.65 Å, proving that anionic analytes have the potential to form an internal hydrogen bond, and then to attract the naphthyl -OH towards itself. The complexation of **L1R1** with F⁻ and AcO⁻ resulted in the lowering of the interaction energy ($E_{int} = E_{complex}-E_{receptor}-E_{AcO-/F-}$) by -0.40 kcal/mol and -10.90 kcal/mol, indicating the affinity between the receptor and the anions along with the formation of a stable complex. Similar lowering in the interaction energy by -47.80 kcal/mol and -15.00 kcal/mol was noted when **L1R4** interacted with F⁻ and AcO⁻, respectively.
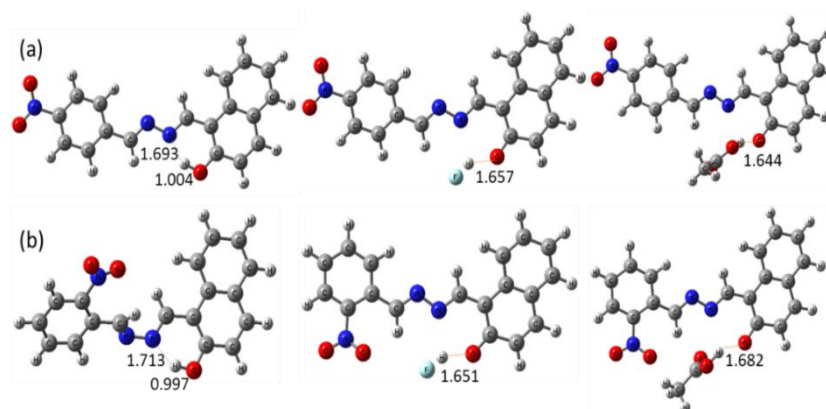
Fig. 2.59 Optimized structure of receptors (a) **L1R1**, and (b) **L1R4** and their complexes with F⁻ and AcO⁻ at B3LYP/6-31G* level in DMSO

As proposed, the possible intramolecular change transfer in the receptors upon interaction with the anions resulted in red shift in the absorption band in the visible region resulting in intense colour change, which could be visually detected. To complement the experimental evidence, the HOMO and LUMO diagrams of the receptors **L1R1** and **L1R4** was compared with their complexes formed with the F⁻ and AcO⁻ anions. As shown in Fig. 2.60, the electron density of the HOMO of **L1R1** was located mainly over the nitrophenol unit, but the LUMO electron density was distributed over the naphthol unit. Upon interaction with the anions F⁻ and AcO⁻, the HOMO electron density was observed at the naphthol unit, whereas the LUMO electron density at the nitrophenol unit. This observation supported possible intramolecular change transfer with the receptor **L1R1** upon interaction with the anions. Also, the

calculated band gap ΔE ($\Delta E = E_{LUMO} - E_{HOMO}$) of **L1R1** decreased from 0.10363 eV to 0.07682 eV and from to 0.10159 eV in the presence of F^- and AcO^-, respectively. Similarly, in the case of the receptor **L1R4**, the HOMO-LUMO energy gap was found to be $\Delta E = 0.10971$ before the binding decreased to 0.08098 eV and 0.07933 eV after complication with the F^- and AcO^- as illustrated in Fig. 2.61. The decrease in band gap due to ICT mechanism involved deprotonation of the OH proton due to the presence of the NO_2 group at the para position making the OH proton more acidic for easy deprotonation upon interaction with the anions.
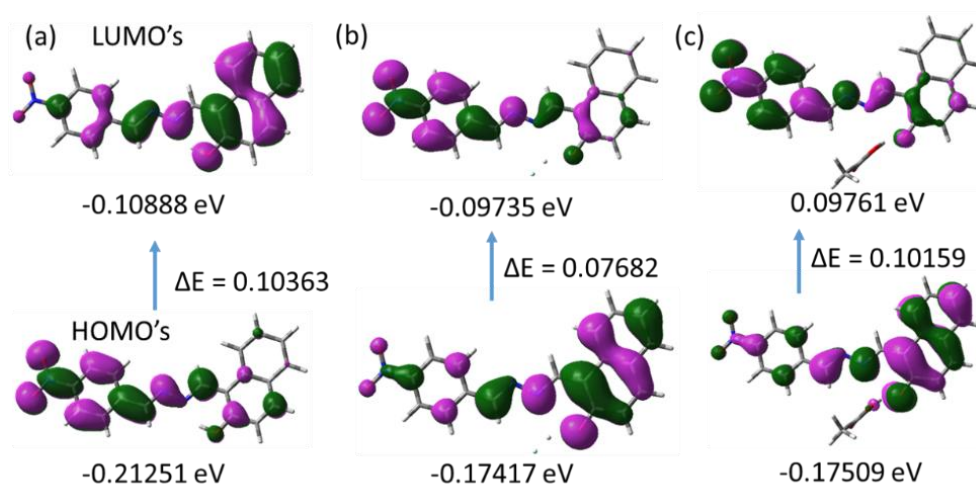
Fig. 2.60 HOMO and LUMO diagrams for (a) receptor **L1R1**, (b) receptor **L1R1**-F^-, and (c) receptor **L1R1**-AcO^- obtained by the B3LYP/6-31G* method
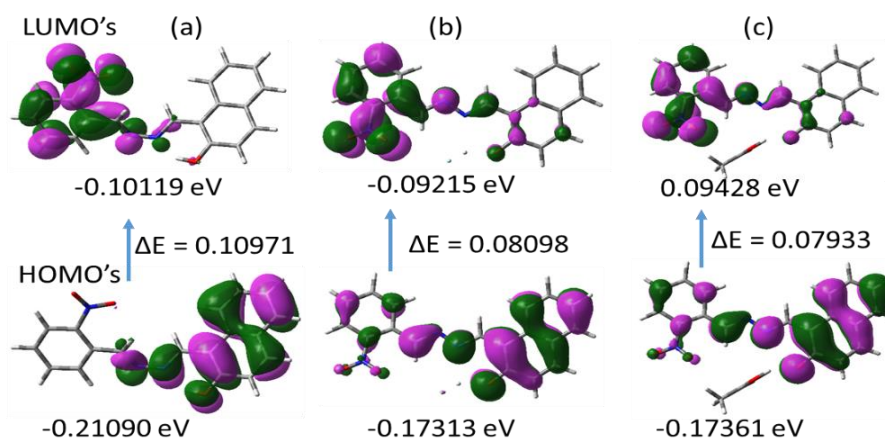
Fig. 2.61 HOMO and LUMO diagrams for (a) receptor **L1R4**, (b) receptor **L1R4**-F^-, and (c) receptor **L1R4**-AcO^- obtained by the B3LYP/6-31G* method

2.4　CONCLUSION

In conclusion, the present findings serve to illustrate the role of the positional substitution of the nitro functionality on anion binding and selectivity. The UV-Vis studies in the DMSO showed excellent selectivity of the receptor **L1R1** towards F⁻ and AcO⁻ ions with purple colouration and revealed sharp bathochromic shifts of 141 nm and 143 nm in the absorption maxima due to the presence of the electron-withdrawing effect of the NO_2 group at the para position, which strengthened the binding ability of the receptor with the anions. The binding constant was found to be 7.9×10^4 M^{-1} and 6.9×10^3 M^{-1} with detection limit of 1.7 ppm and 0.4 ppm for TBA^+AcO^- and Na^+AcO^-, respectively, reflecting the stability of the receptor **L1R1**-AcO⁻ complex in both the organic medium as well as in the organo-aqueous media. The ^{1}H-NMR titration and DFT calculation emphasized the hydrogen bond formation, followed by deprotonation of the OH proton. In the presence of the AcO⁻ ions, the receptor **L1R1** displayed unique solvatochromic properties in different polar aprotic solvents. In addition, the **L1R1** receptor showed itself to be capable of detecting F⁻ and AcO⁻ ions in sea water and real samples like toothpaste, vinegar, and mouthwash in an aqueous medium, thereby indicates the utility of the receptor in practical application. In the organic and aqueous media, test strip, and solid phase, the colorimetric response of the receptor **L1R1** to F⁻ and AcO⁻ ions signified its practical utility as a chemosensor.

CHAPTER 3

SUBSTITUENT EFFECT FOR COLORIMETRIC DETECTION OF BIOLOGICALLY AND ENVIRONMENTALLY RELEVANT ANIONS: INSIGHT IN REAL LIFE APPLICATION
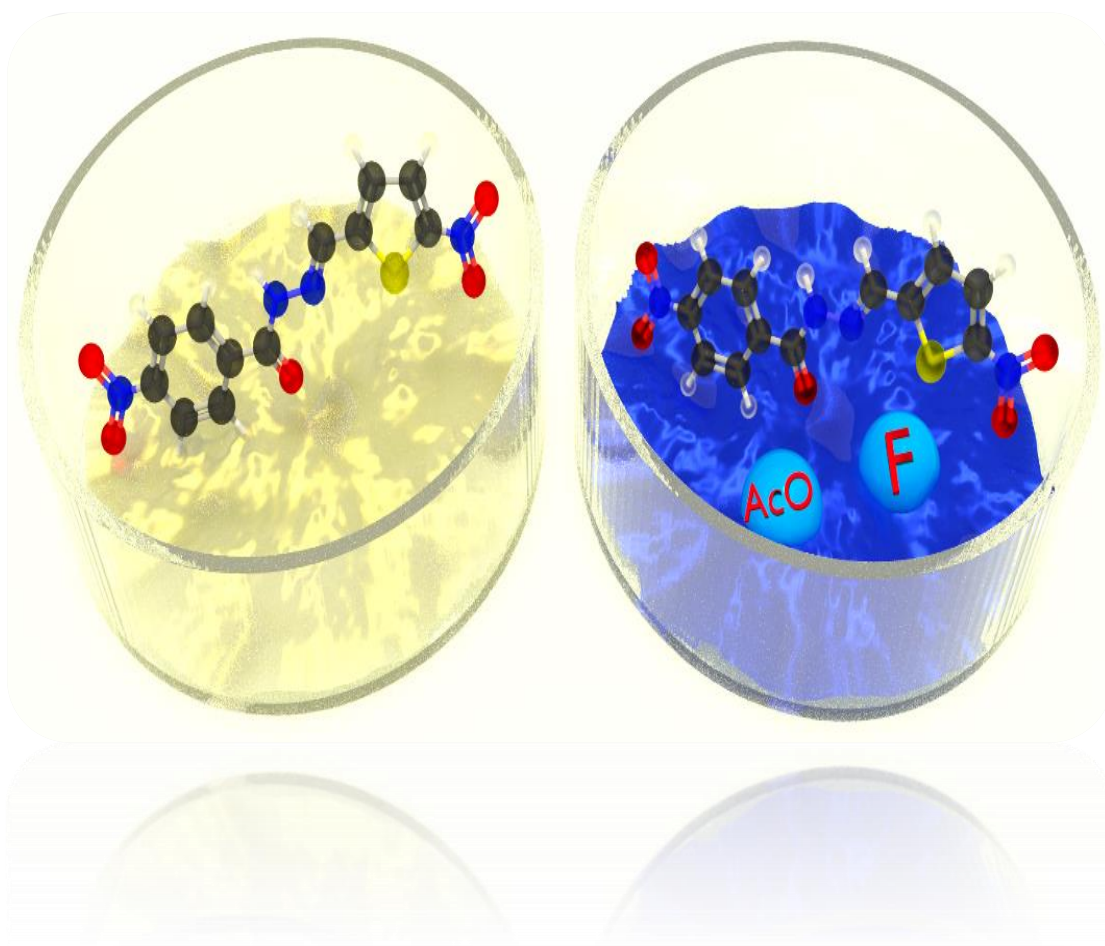
Abstract: *The chapter deals with the synthesis of different substituent hydrazide based receptors for the colorimetric detection of biologically important anions. The colorimetric anion sensing properties, detection mechanism, solvatochromic effect, and buffer studies of these receptors are studied in detail. The anion binding properties of the receptors are studied and confirmed by UV-Vis spectrophotometric, ^{1}H-NMR, and electrochemical studies. Further, fluoride ions in commercially available mouthwash is quantitatively analysed and its results presented.*

3.1   INTRODUCTION

The development of new organic receptors for the detection of anions and cations have received much interest in the last decade due to their major role in biology, environment, and chemistry (Fegade et al. 2013; Mallick et al. 2011). Anions are larger in size compared with cations, having different shapes and geometries, very small pH range, and lower hydration energies within a wide range of hydrophobicity (Keefe et al. 2000; Lee et al. 2005). Among various anions, the detection of biologically relevant fluoride, acetate, and phosphate have been the topic of intensive research due to their physiological effects. Fluoride plays a very important role due to its presence in daily life and is widely distributed in underground water, toothpaste, psychiatric drugs, and hypnotics (Zhang and Swager 2003). Fluoride ion is essential in dental health and osteoporosis treatment (Snowden and Anslyn 1999). However, when its content is more than 3-5 mg/L in drinking water (Ghosh et al. 2015), it may cause skeletal and dental fluorosis, bone disorder, liver and immune system disruption, osteoporosis, and osteoarthritis (Anuradha et al. 2000; Batista et al. 2007; Peng et al. 2005; Sharma et al. 2013). Acetate anions are essential for living organisms and are found in the form of acetyl coenzyme A, which aids in metabolic processes (Du et al. 2012). However, extensive subjection of humans to acetate ions may lead to prostate cancer (Sharma et al. 2014). Acetate ion has vivid applications in the form of inorganic sodium salts such as microbial growth control and in various food products like meat, fish, and poultry (Suganya et al. 2014). Meanwhile, the detection of phosphate ions is garnering immense interest due to its significant usage in chemotherapeutic and antiviral drugs. Additionally, phosphate plays a key role in insight transduction and energy storage of the biological system (Schumacher et al. 2007). Phosphate intake should be controlled

as excess intake can cause thyroid and parathyroid-related problems (Ogata et al. 2016). Arsenic (As) is considered to be the most dangerous toxic water pollutant and is harmful to living organisms (Cullen and Reimer 1989; Kalluri et al. 2009). The Agency for Toxic Substances and Disease Registry (ATSDR) and the Environmental Protection Agency (EPA) have mentioned that arsenic tops the list of hazardous elements (Edition 2011). According to the World Health Organization (WHO) and the U.S. Environmental Protection Agency (USEPA), the permissible limit of arsenic in drinking water should be 0.01 ppm (Yogarajah and Tsai 2015). Beyond an optimum amount, it can lead to serious health issues such as skin cancer, skin lesion, weight loss, loss of appetite, neutrotoxicity, cardiovascular disease, and diabetes (Mukherjee et al. 2005). In general, colorimetric chemosensor is composed of two fragments such as (1) anion-binding sites, and (2) signalling unit (chromophores) attached to the binding site. As anions bind to the binding site of the chemosensor, the signalling unit shows colour change in the anion detection phenomena (Zang and Jiang 2015). Moreover, various anion-binding functional groups are reported such as amide, urea, thiourea, pyrrole and imidazolium, and nitro moiety as signalling units (Dalapati et al. 2012; Gunnlaugsson et al. 2005; Saravanakumar et al. 2005). In the present paper, four new colorimetric receptors **L2R1-L2R4** with different substituents, including electron withdrawing (nitro moiety in **L2R1**), conjugated group (naphthyl in **L2R2**), and electron donating (methyl in **L2R3**) have been developed as shown in Scheme 3.1, to understand the substituent effects on the anion sensing process, including colour change, sensitivity, and selectivity. Among all the synthesized receptors **L2R2-L2R4**, only the receptor **L2R1** can selectively detect the sodium salts present in the form of F^-, AcO^-, AsO_2^- and AsO_4^{2-} in organo-aqueous media with much lower detection limit. This may be due to the presence of the $-NO_2$ functionality, which strengthens the binding ability of the host-guest.
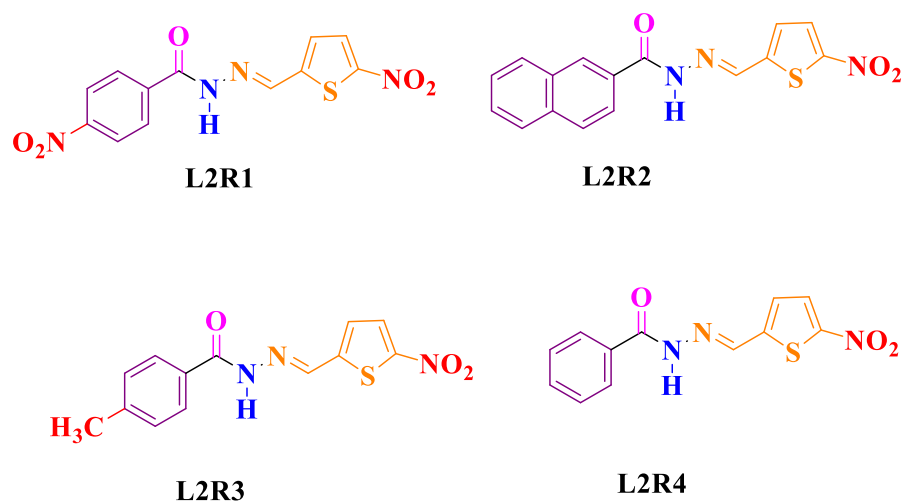
Scheme 3.1 Design of receptors **L2R1-L2R4**

3.2 EXPERIMENTAL SECTION

3.2.1 Materials

All chemicals were purchased from Sigma-Aldrich, Alfa Aesar or from Spectrochem and used without further purification. All solvents were procured from SD Fine, India with HPLC grade and used without further distillation.

3.2.2 Apparatus

The ^{1}H-NMR spectra were recorded on the Bruker, Avance (500 MHz) instrument using Tetramethylsilane (TMS) as an internal standard and DMSO-d_6 as the solvent. ^{13}C NMR spectra were recorded on Bruker Ascend (100 MHz) instrument using TMS as internal reference and DMSO-d_6. Resonance multiplicities are described as s (singlet), d (doublet), t (triplet) and m (multiplet). Infrared spectrum was recorded on Bruker Apex FTIR spectrometer. Mass-spectral data were obtained using a ESI-QToF (Waters-synapt G2S) high resolution mass spectrometer. The UV–Vis spectroscopy was performed with the analytikjena Specord S600 spectrometer in standard 3.0 mL quartz cells (2 optical windows) with 1 cm path length. A cyclic voltammogram was recorded on the Ivium electrochemical workstation (Vertex) at a scan rate of 50 mV with potential range 1.3 V to −1.3 V. All the reactions were continuously checked by the TLC on pre-coated silica gel 60 F_{254} plates. The melting point measurement was carried out on the Stuart – SMP3 melting point apparatus in open capillaries.

3.2.3 Preparation of analytical solutions for instrumental analysis

All the anion solutions in the form of TBA salts were prepared in the DMSO with a concentration of (1.0×10^{-2} M). The receptor solutions **L2R1**, **L2R2**, **L2R3**, and **L2R4** were prepared at concentration (2×10^{-5} M in the DMSO). The titration experiments were conducted by placing 2 ml of the respective receptor solutions in a quartz cuvette, and then adding the corresponding basic anions incrementally through a micro-pipette. The absorption spectra were reported after and before the anions were added. For the **L2R1** receptor, cyclic voltammetric experiments were performed with the sequential addition of acetate ions in which Tetrabutylammonium perchlorate was used as a supporting electrolyte.

3.2.4 Calculation of binding constant

The binding constant was calculated using (Eq. 3.1) (Benesi and Hildebrand 1948) as given below;

$$\frac{1}{(A-A_0)} = \frac{1}{(A_{max}-A_0)} + \frac{1}{K[X^-]^n \,(A_{max}-A_0)} \ldots\ldots\ldots \textbf{(Eq. 3.1)}$$

Where, A_0, A, and A_{max} are the absorption considered in the absence of anions, at intermediate and at concentration of saturation, K is the binding constant, $[X^-]$ is the concentration of anions, and n is the stoichiometric ratio.

3.2.5 Calculation of limit of detection (LOD)

The detection limit was evaluated on the basis of UV-Vis titration studies using (Eq. 3.2) (Kumar et al. 2018)

$$\textbf{LOD} = \frac{3 \times \sigma}{s} \ldots\ldots\ldots\ldots\ldots \textbf{(Eq. 3.2)}$$

Where, σ is the standard deviation of the calibration curve (SD) and s is the slope of the calibration curve.

3.2.6 Synthesis of receptors L2R1-L2R4

The receptors **L2R1**, **L2R2**, **L2R3**, and **L2R4** were synthesized by simple Schiff base condensation reaction between 5-nitrothiophene-2-carbaldehyde (0.17g, 1.10 mmol) with different functionalities, including 4-nitro-benzohydrazide (0.2g, 1.10

mmol)**,** 2-napto-hydrazide (0.1g, 0.53 mmol)**,** 4-methyl-benzohydrazide (0.1g, 0.66 mmol)**,** and benzo-hydrazide (0.1g, 0.73 mmol) as depicted in Scheme 3.2, and the reaction mixture was dissolved in 5 ml of methanol solution. To this, a catalytic amount 2-3 drops of acetic acid (CH$_3$CO$_2$H) was added and the mixture was refluxed at $60\,^\circ$C for 6 h. The final solid products were collected, filtered, and washed thoroughly with methanol. The final products were confirmed through TLC by the appearance of a single spot.
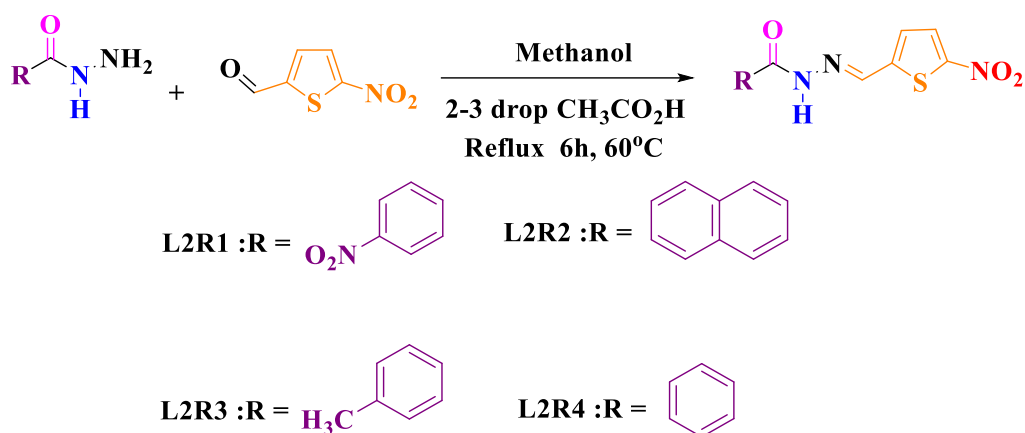
Scheme 3.2 Synthetic route of receptors **L2R1-L2R4**

3.2.7   Characterization data

The purity and structure of the receptors **L2R1**, **L2R2**, **L2R3**, and **L2R4** were confirmed by FT-IR, ^{1}H-NMR, ^{13}C-NMR, and mass spectroscopic methods. The characterization data has been compiled and given below

(E)-4-nitro-N'-((5-nitrothiophen-2-yl) methylene) benzohydrazide (L2R1)
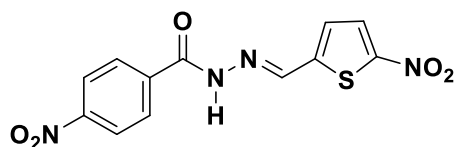
Data obtained for L2R1: Yield: 82%, Melting point: 230^{0}C, ^{1}H NMR (DMSO-d$_6$, 500 MHz, Me$_4$Si): δ_{ppm} 7.648 -7.637(d, 1H), 8.161-8.140 (m, 3H), 8.406 – 8.384 (d, 2H), 8.696 (s, 1H), 12.508 (s, 1H). ^{13}C NMR (DMSO-d$_6$, 100 MHz, Me$_4$Si): δ_{ppm}

162.29, 149.96, 146.70, 142.75, 138.98, 130.96, 130.70, 129.78, 128.92, 124.22, 124.03. FTIR (KBr pellet) (cm^{-1}): 3444 (N−H), 3114 (Ar-CH), 1673 (C=O), 1601 (HC=N), 1560 (C=C), 1526 (NO$_2$ stretch), 939 (C−H). Mass (ESI): m/z calculated for C$_{12}$H$_8$N$_4$O$_5$S = 320.02, Obtained: 321.0775 [M + H]$^+$

(E)-N'-((5-nitrothiophen-2-yl) methylene)-2-naphthohydrazide (L2R2)
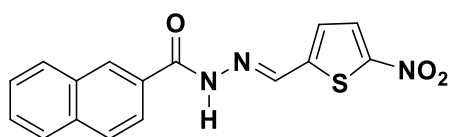
Data obtained for L2R2: Yield: 80%, Melting point: 262^{0}C, ^{1}H NMR (DMSO-d$_6$, 500 MHz, Me$_4$Si): δ$_{ppm}$ 7.647-7.595 (m, 4H), 7.795-7.778 (d, 1H), 8.050-8.028 (m, 1H), 8.159-8.117 (m, 2H), 8.229-8.206 (d,1H), 8.575 (s, 1H), 12.397 (s, 1H). ^{13}C NMR (DMSO-d$_6$, 100 MHz, Me$_4$Si): δ$_{ppm}$ 141.62, 131.00, 130.33, 128.91, 127.76, 126.63, 125.47. FTIR (KBr pellet) (cm^{-1}): 3450 (N−H), 2978 (Ar-CH), 1674 (C=O), 1530 (NO$_2$ stretch), 1568 (C=C), 1031 (C−H). Mass (ESI): m/z calculated for C$_{16}$H$_{11}$N$_3$O$_3$S = 325.05, Obtained: 326.1083 [M + H]$^+$

(E)-4-methyl-N'-((5-nitrothiophen-2-yl) methylene) benzohydrazide (L2R3)
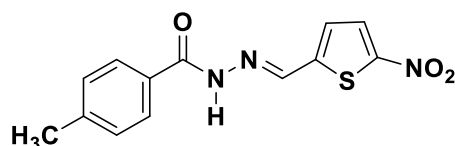
Data obtained for L2R3: Yield: 80%, Melting point: 241^{0}C, ^{1}H NMR (DMSO-d$_6$, 500 MHz, Me$_4$Si): δ$_{ppm}$ 2.405 (s, 3H), 7.379-7.359 (d, 2H), 7.601-7.591 (d, 1H), 7.850-7.832 (d, 2H), 8.160-8.150 (d, 1H), 8.705 (s, 1H), 12.182 (s, 1H). ^{13}C NMR (DMSO-d$_6$, 100 MHz, Me$_4$Si): δ$_{ppm}$ 147.35, 141.38, 131.01, 130.46, 130.00, 129.58, 128.26, 21.54. FTIR (KBr pellet) (cm^{-1}): 3418 (N−H), 3035 (Ar-CH), 1648 (C=O), 1584 (HC=N), 1495 (C=C), 1526 (NO$_2$ stretch), 1029 (C−H). Mass (ESI): m/z calculated for C$_{13}$H$_{11}$N$_3$O$_3$S = 289.05, Obtained: 290.1043 [M + H]$^+$

(E)-N'-((5-nitrothiophen-2-yl) methylene) benzohydrazide (L2R4)
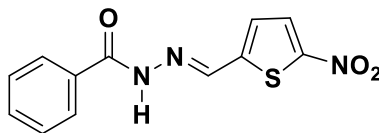
Data obtained for L2R4: Yield: 82%, Melting point: 250^0C, ^{1}H NMR (DMSO-d$_6$, 500 MHz, Me$_4$Si): δ_{ppm} 7.659-7.546 (m, 4H), 7.935-7.918 (d, 2H), 8.164-8.153 (d,1H), 8.709 (s, 1H), 12.254 (s, 1H). ^{13}C NMR (DMSO-d$_6$, 100 MHz, Me$_4$Si): δ_{ppm} 147.22, 133.36, 132.62, 131.00, 130.14, 129.07, 128.22. FTIR (KBr pellet) (cm^{-1}): 3258 (N−H), 3073 (Ar-CH), 1650 (C=O), 1599 (HC=N), 1495 (C=C), 1527 (NO$_2$ stretch), 1028 (C−H). Mass (ESI): m/z calculated for C$_{12}$H$_9$N$_3$O$_3$S = 275.04, Obtained: 276.0845 [M + H]$^+$

The representative spectrum of receptors **L2R1**, **L2R2**, **L2R3**, and **L2R4** is given below
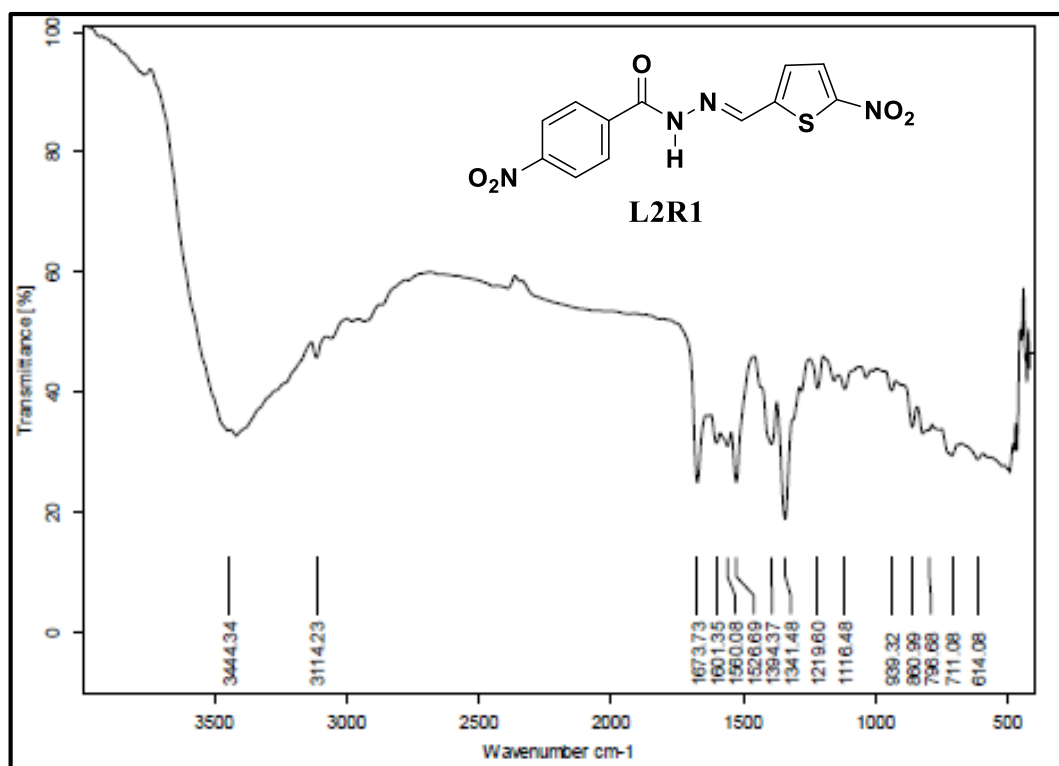
Fig. 3.1 FT-IR spectrum of **L2R1**
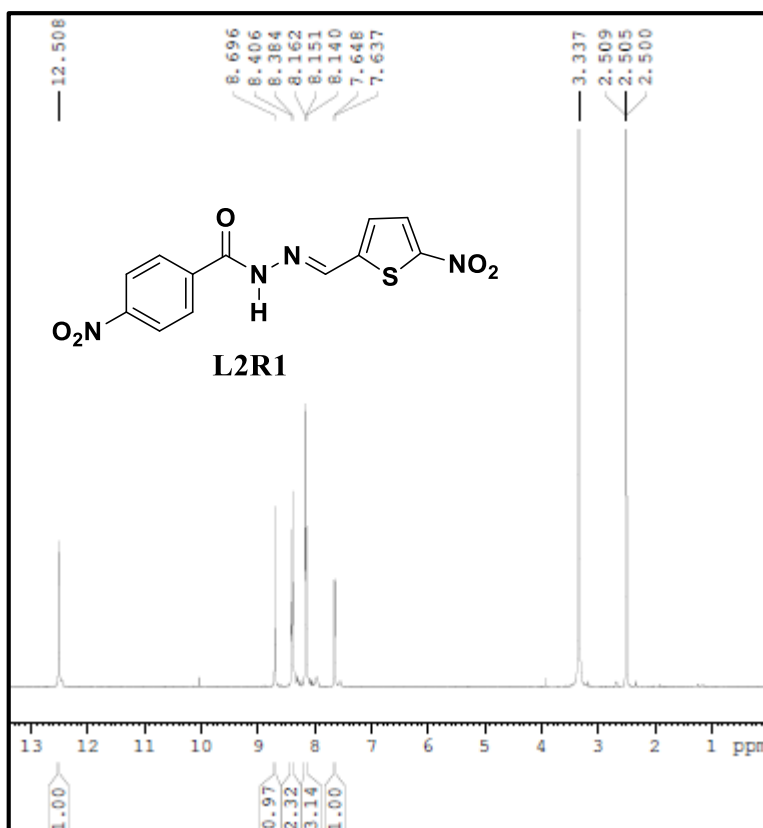
Fig. 3.2 ¹H-NMR spectrum of **L2R1**
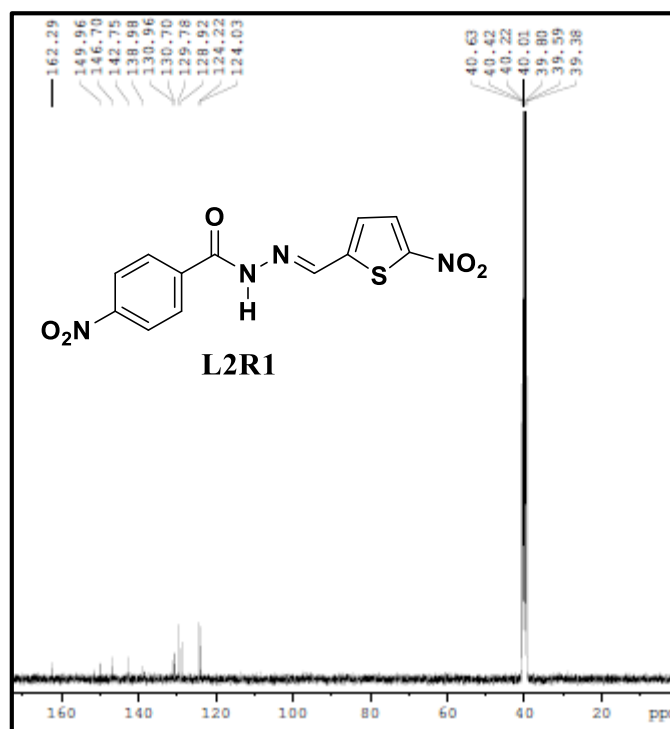
Fig. 3.3 ¹³C-NMR spectrum of receptor **L2R1**

Mass spectrum: L2R1

Exact Mass: 320.02

Mass obtained in the positive mode: 321.0775

Elemental composition: $C_{12}H_8N_4O_5S$

L2R1

322.0688

323.0734
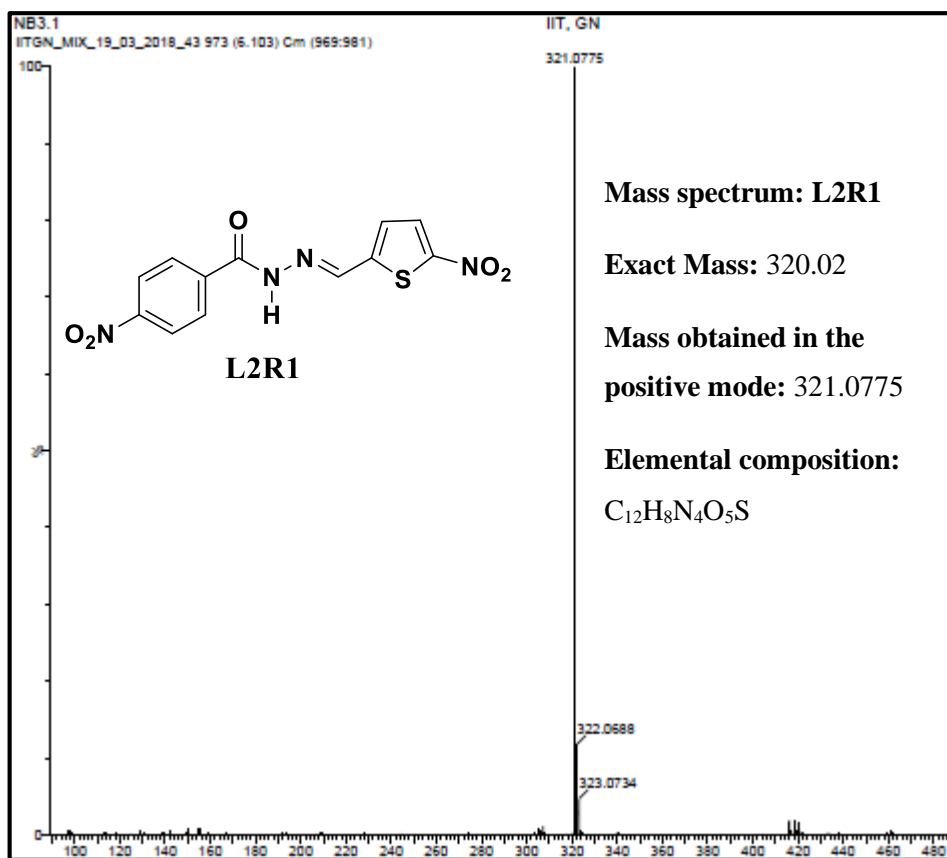
Fig. 3.4 ESI-MS spectrum of **L2R1**
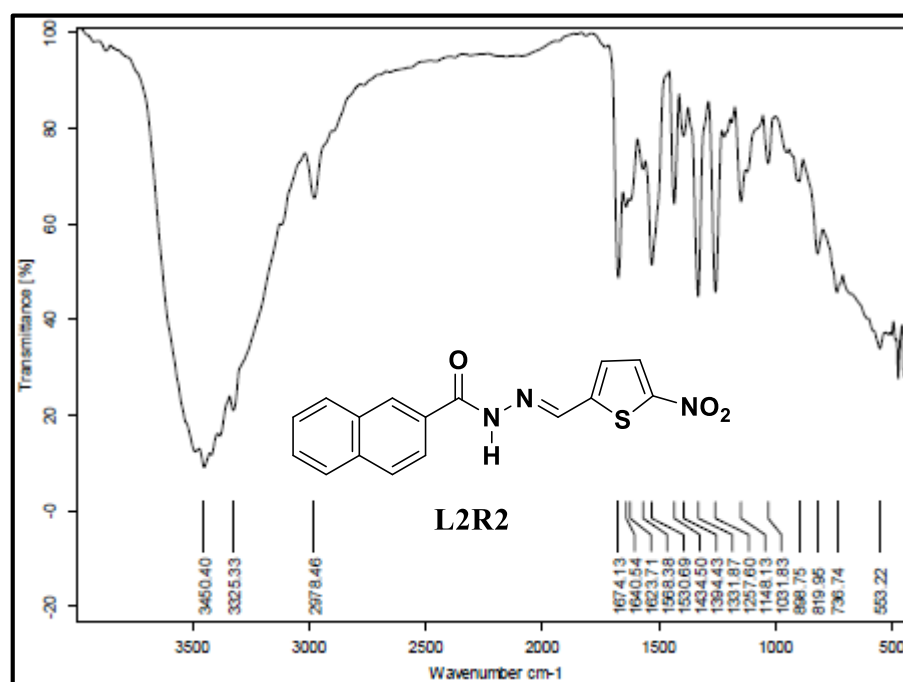
L2R2

Fig. 3.5 FT-IR spectrum of **L2R2**
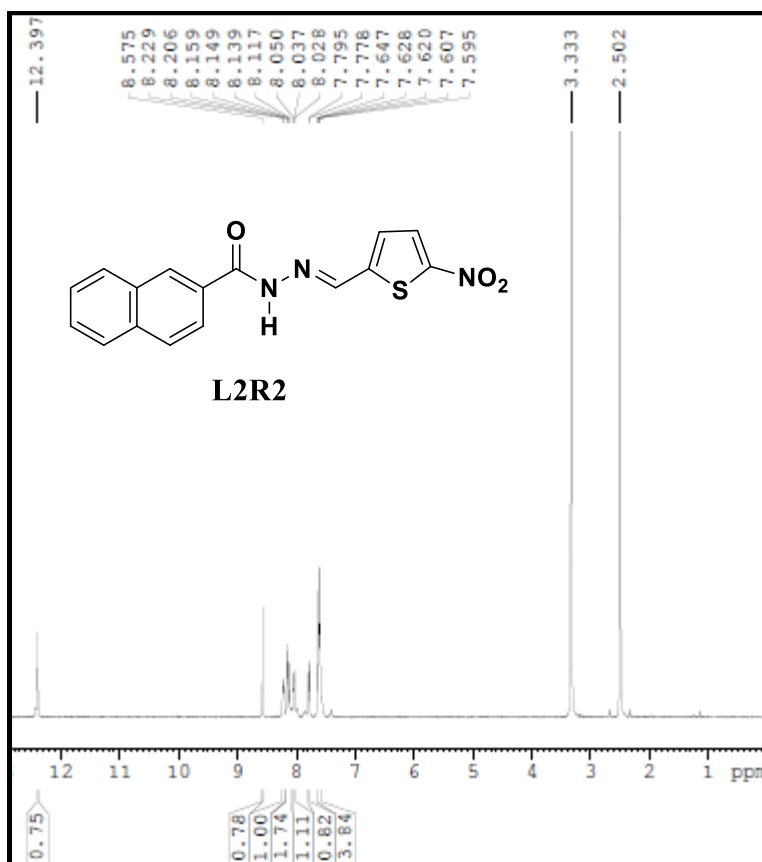
Fig. 3.6 ^{1}H-NMR spectrum of **L2R2**
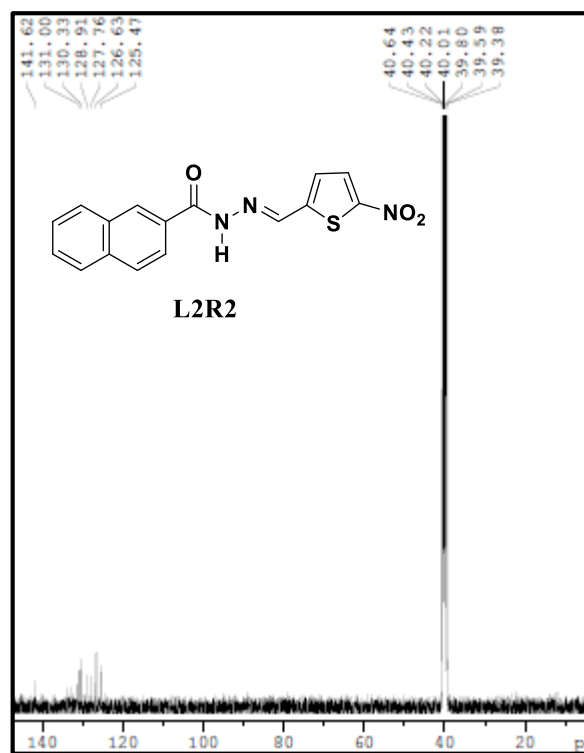
Fig. 3.7 ^{13}C-NMR spectrum of **L2R2**
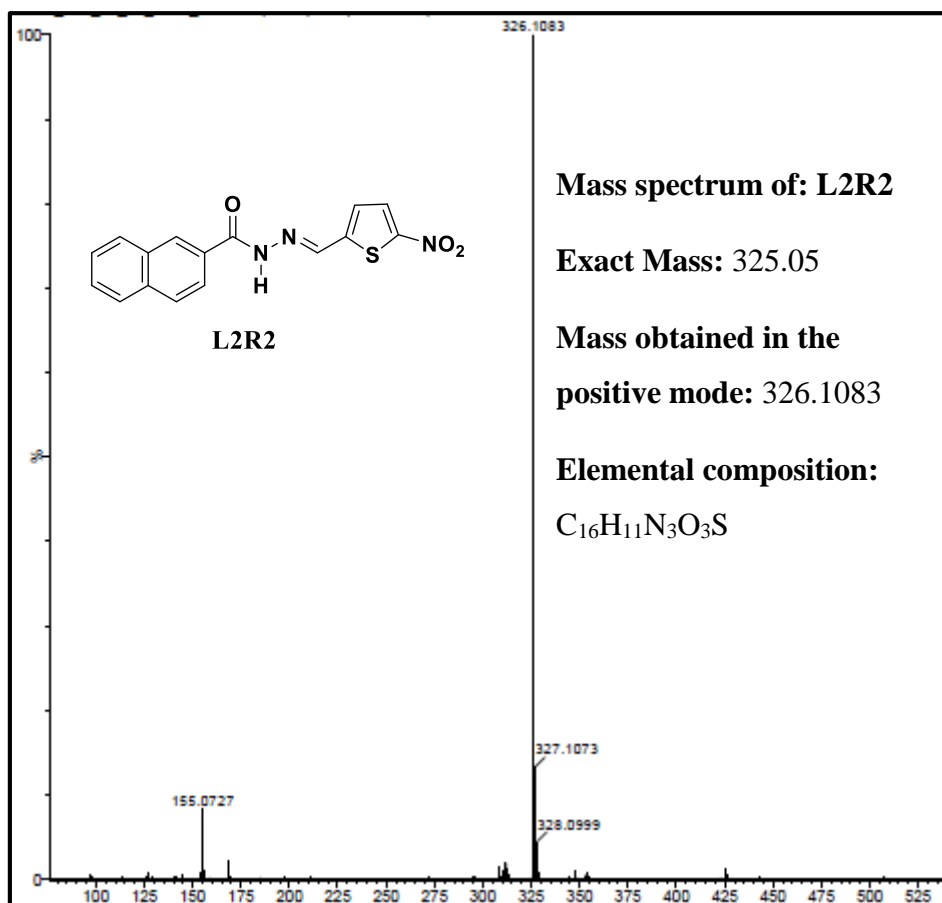
Fig. 3.8 ESI-MS spectrum of **L2R2**
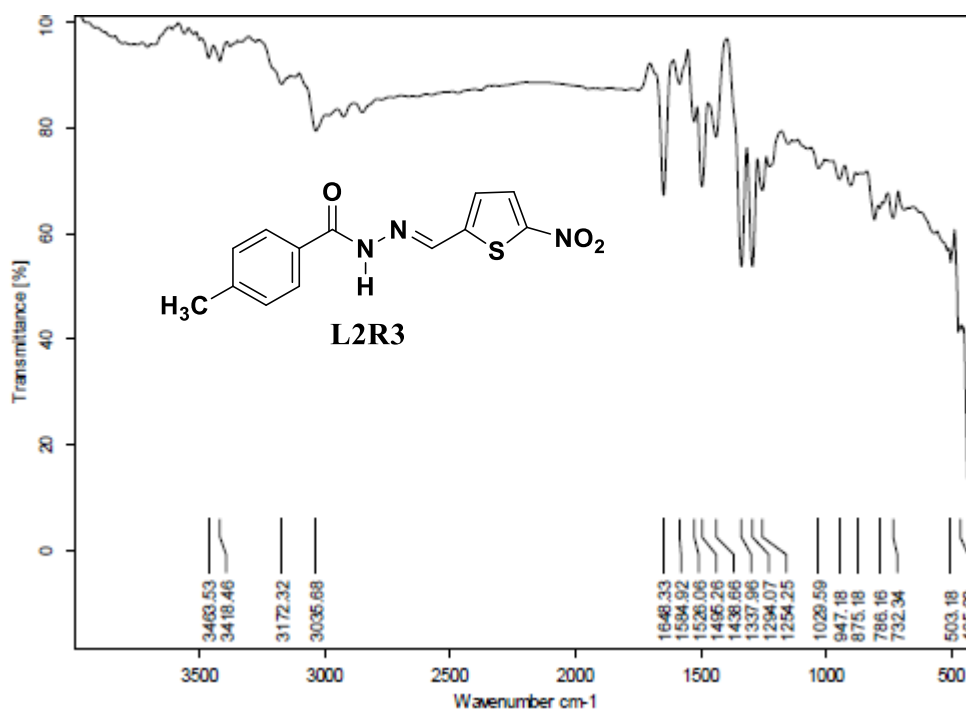
Fig. 3.9 FT-IR spectrum of **L2R3**

N.I.T.K Chemistry Department
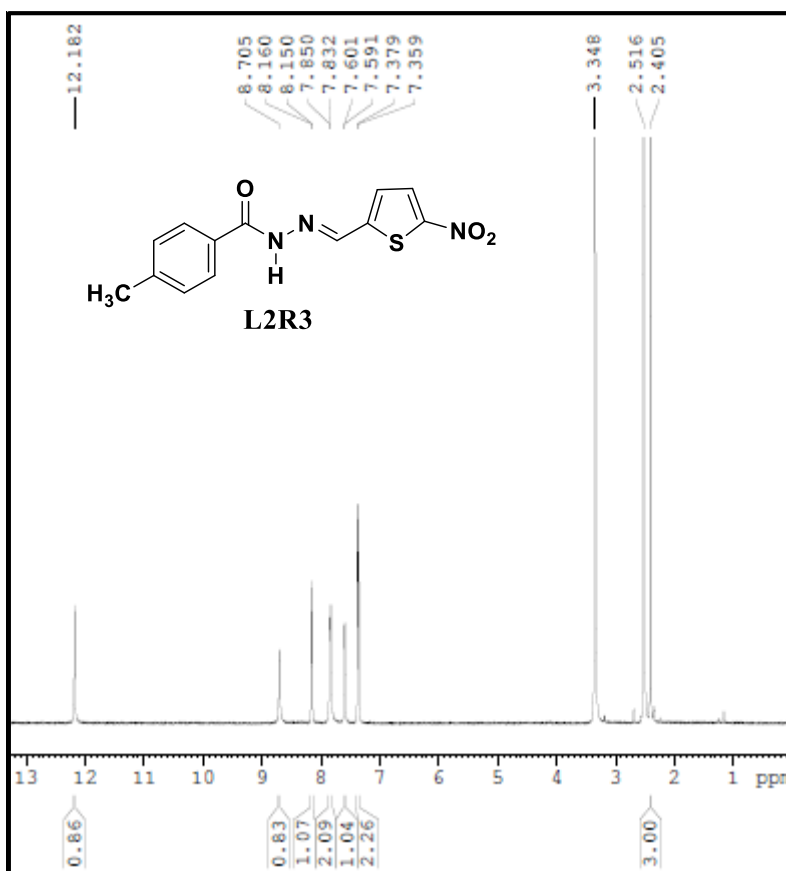
Fig. 3.10 ^{1}H-NMR spectrum of **L2R3**

Fig. 3.11 ^{13}C-NMR spectrum of **L2R3**

Mass spectrum: L2R3

Exact Mass: 289.05

Mass obtained in the positive mode: 290.1043

Elemental composition: $C_{13}H_{11}N_3O_3S$
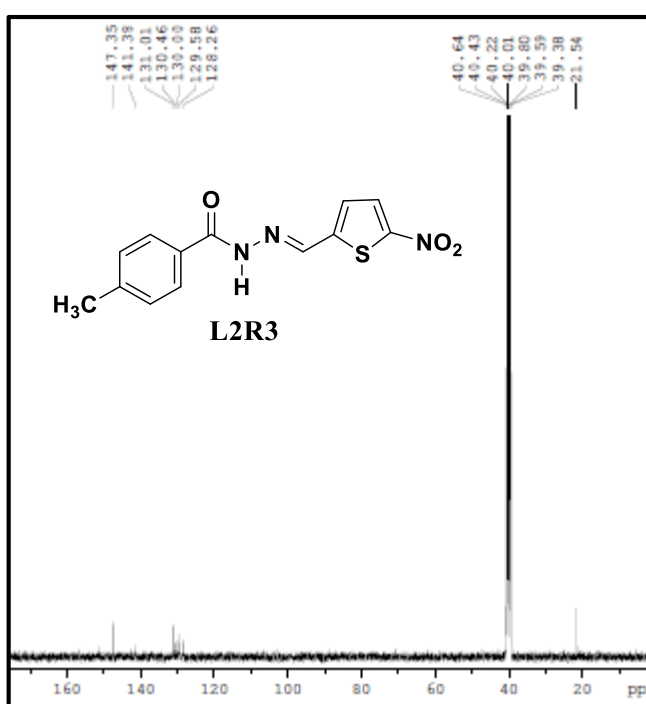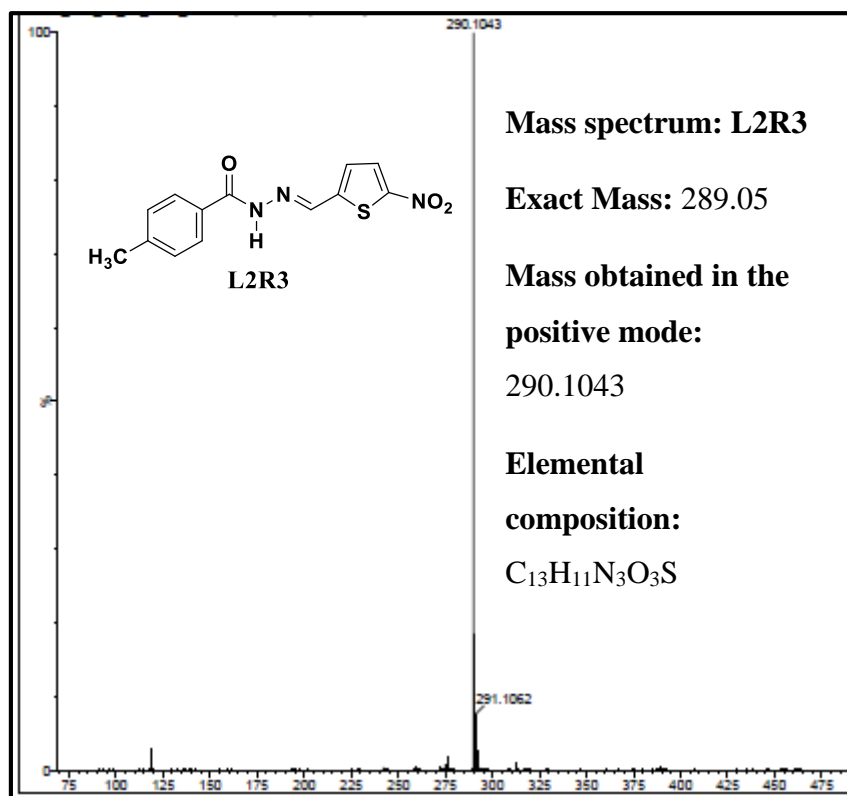
Fig. 3.12 ESI-MS spectrum of **L2R3**
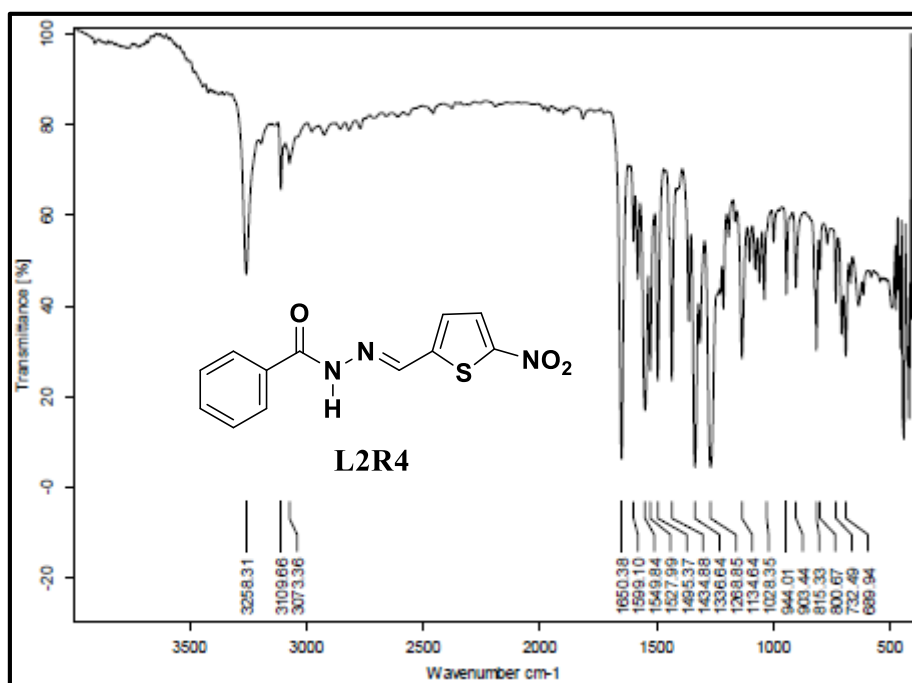
Fig. 3.13 FT-IR spectrum of **L2R4**
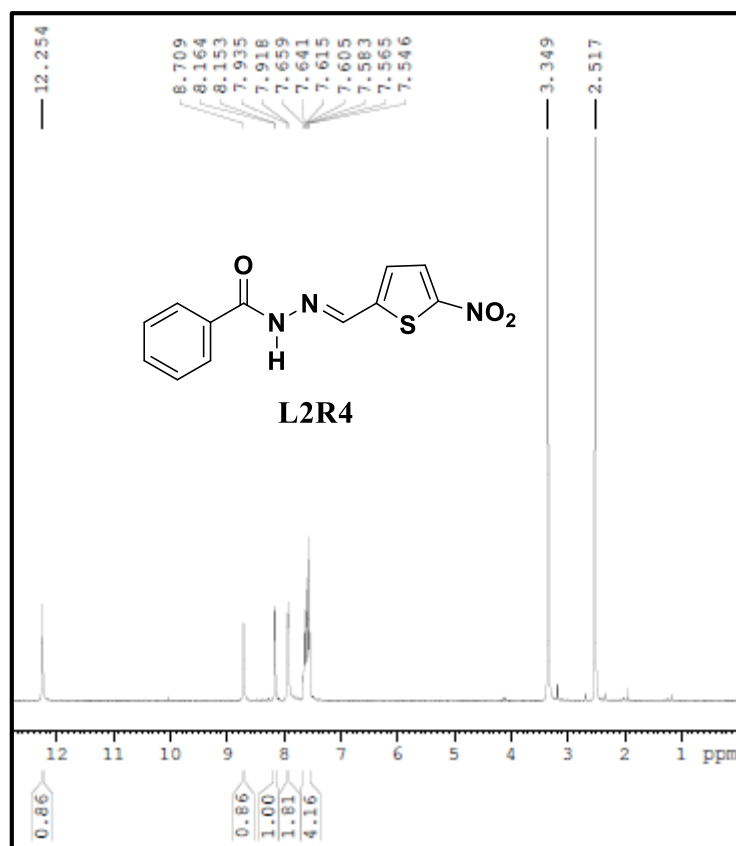
Fig. 3.14 ^{1}H-NMR spectrum of **L2R4**

Fig. 3.15 ^{13}C-NMR spectrum of **L2R4**

Mass spectrum: L2R4

Exact Mass: 275.04

Mass obtained in the positive mode: 276.0845

Elemental composition: $C_{12}H_9N_3O_3S$
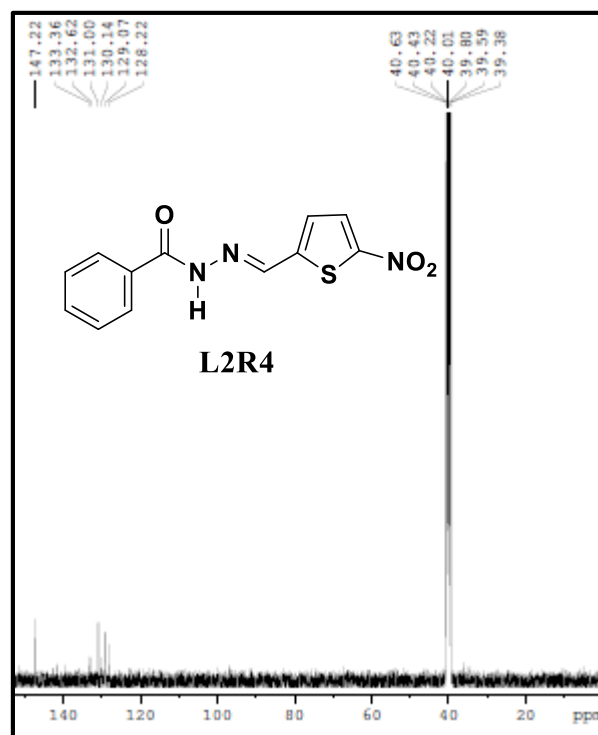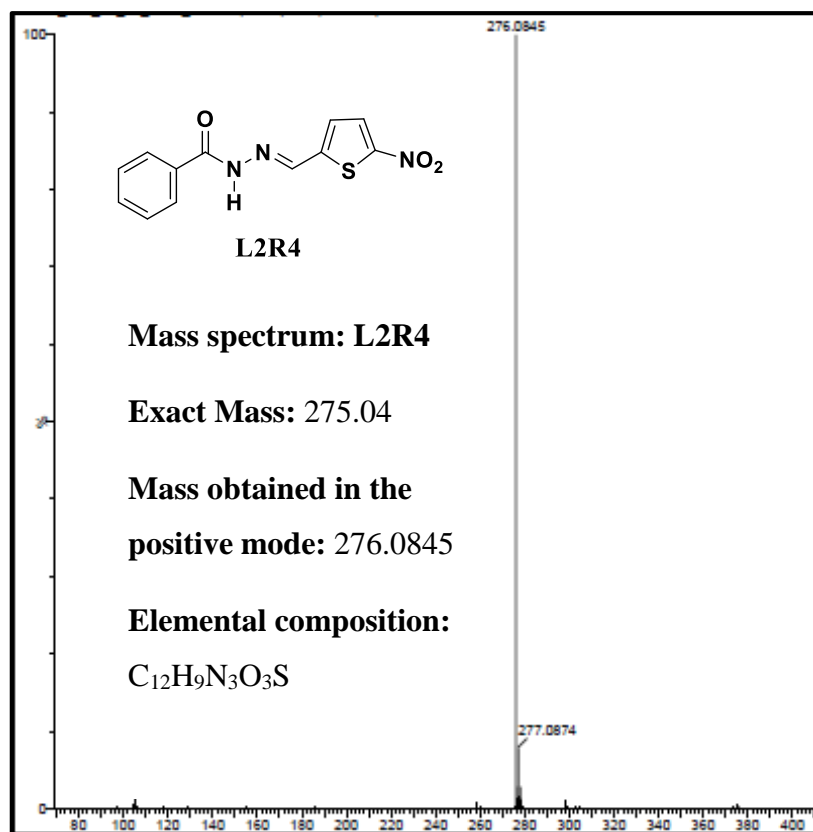
Fig. 3.16 ESI-MS spectrum of **L2R4**

3.3 RESULTS AND DISCUSSIONS

3.3.1 Anion sensing and comparative study

The colorimetric sensing ability was primarily investigated by adding different anions such as F^-, Cl^-, Br^-, I^-, NO_3^-, HSO_4^-, $H_2PO_4^-$, and AcO^- (1×10^{-2} M in the form of TBA as counteraction) in to the DMSO solution of the receptors **L2R1-L2R4**. Interestingly, the green colour solution of the receptor **L2R1** turned blue upon the addition of the relatively basic F^-, AcO^-, and $H_2PO_4^-$ ions as depicted in Fig. 3.17 (a). Whereas the receptors **L2R2, L2R3,** and **L2R4** showed colour change from pale yellow to purple, light violet and purple, respectively, only in the presence of the F^- and AcO^- ions as demonstrated in Fig. 3.17 (b, c, and d). The receptor **L2R1** showed intense colorimetric response due to the presence of NO_2 functionality. The change in colour was most probably due to hydrogen bond formation or deprotonation of the NH proton through anion interaction (Ghule et al. 2014). In contrast, other anions failed to cause any conspicuous colour change.
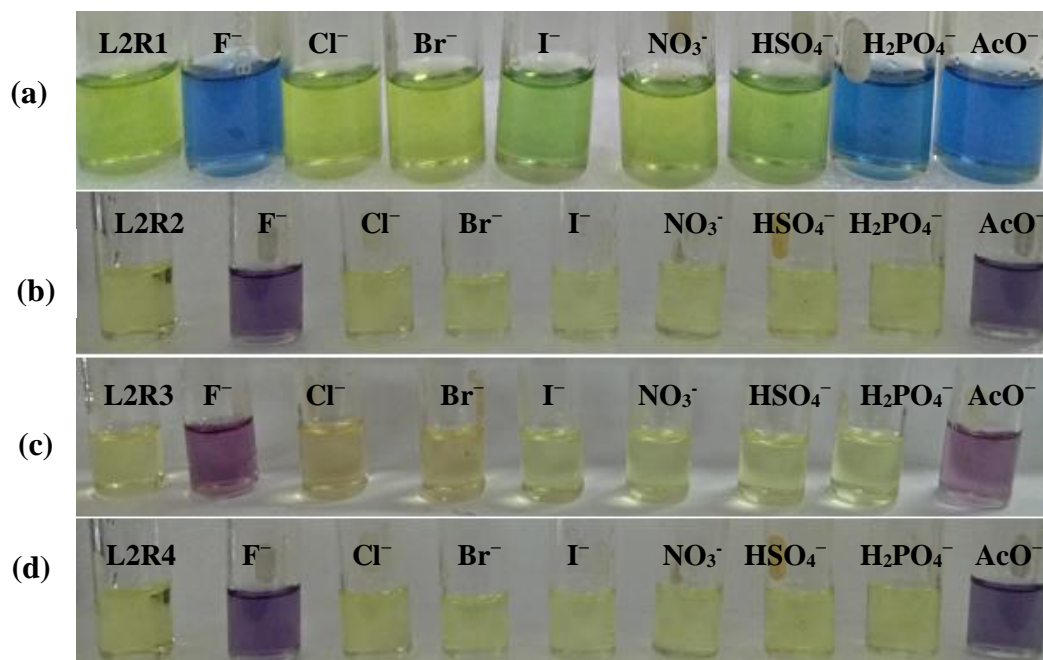
Fig. 3.17 Colorimetric screening of (a) **L2R1**, (b) **L2R2**, (c) **L2R3**, and (d) **L2R4** in $(2 \times 10^{-5}$ M in DMSO) with the presence of 2 equiv. of tetrabutylammonium salt $(1 \times 10^{-2}$ M in DMSO)

The UV-Vis absorption spectra were performed with the addition of the above-listed anions to the receptor solutions to support the colour change. As shown in Fig. 3.18 (a and b) and Fig. 3.19 (c and d), the receptor **L2R1** displayed a strong absorption band towards the F^-, AcO^- and $H_2PO_4^-$ ions, while the receptors **L2R2-L2R4** showed bathochromic shift only for the F^- and AcO^- ions.

Thus, the receptors **L2R1-L2R4** proved to be excellent colorimetric sensors for F^-, AcO^- and $H_2PO_4^-$ ions in the presence of other competing anions. However, no bathochromic shift was observed upon the addition of other anions.
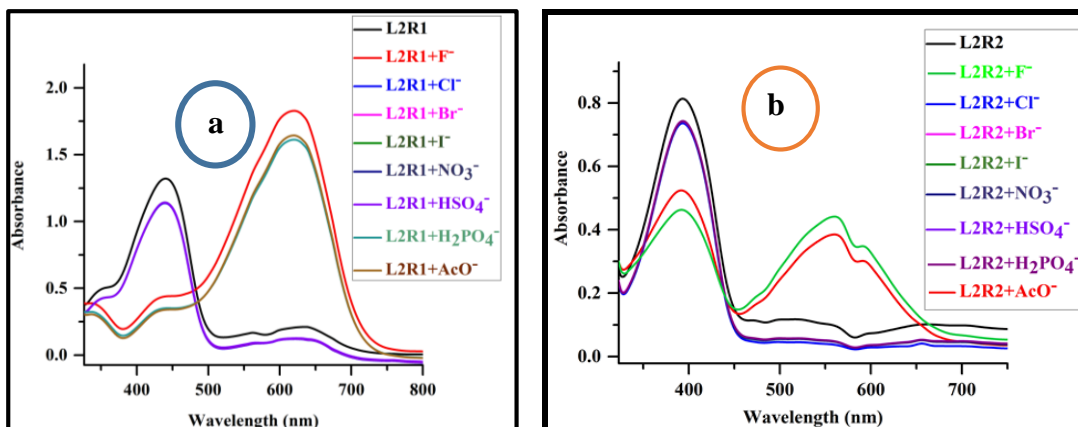
Fig. 3.18 UV-Vis spectral changes of the receptors (2×10^{-5} M in DMSO) (a) **L2R1** in the presence of 2 equiv. of different anions (1×10^{-2} M in DMSO) (b) **L2R2** in the presence of 2 equiv. of different anions (1×10^{-2} M in DMSO)
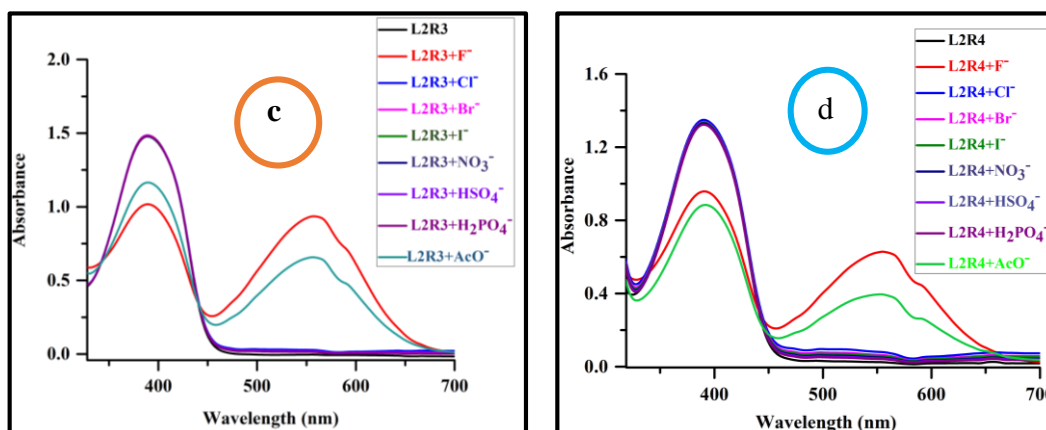
Fig. 3.19 UV-Vis spectral changes of receptors (2×10^{-5} M in DMSO) (c) **L2R3** in the presence of 2 equiv. of different anions (1×10^{-2} M in DMSO) (d) **L2R4** in the presence of 2 equiv. of different anions (1×10^{-2} M in DMSO)

3.3.2 Interference experiments

It can be seen from the above results that the receptors can identify the more basic F^- compared with AcO^- and $H_2PO_4^-$ ions over other competing anions. To further certify the excellent selectivity of the receptors **L2R1-L2R4**, interference experiments were carried out with the addition of 4 equiv. of anions such as Cl^-, Br^-, I^-, HSO_4^-, $H_2PO_4^-$, and AcO^- (1×10^{-2} M) to the DMSO solution of the receptors in the presence of 2 equiv. of F^- ion. The competitive anions had no obvious interference with the

detection of F⁻, but AcO⁻ showed little interference with the F⁻ ion due to similar basicity and surface charge density. However, the receptors **L2R2, L2R3,** and **L2R4** were unable to interact with the $H_2PO_4^-$ ion unlike the receptor **L2R1**. This might be due to the lower basicity of the $H_2PO_4^-$ ion compared with the F⁻ and AcO⁻ ions (Hijji et al. 2009).

In addition, the basic character of the anions in the DMSO followed the order $F^- > AcO^- > H_2PO_4^- > Cl^- > HSO_4^- > NO_3^- > Br^- > I^-$, which is generally in agreement with the Hofmeister series. This clearly suggests that in the DMSO, the basic nature of F⁻ is relatively higher than that of the AcO⁻ anion (Bordwell 1988; Gupta et al. 2017). The UV-Vis spectra and bar graph are represented in Fig. 3.20 (a and b), Fig. 3.21 (c and d), Fig. 3.22 (a and b), and Fig. 3.23 (a and b).
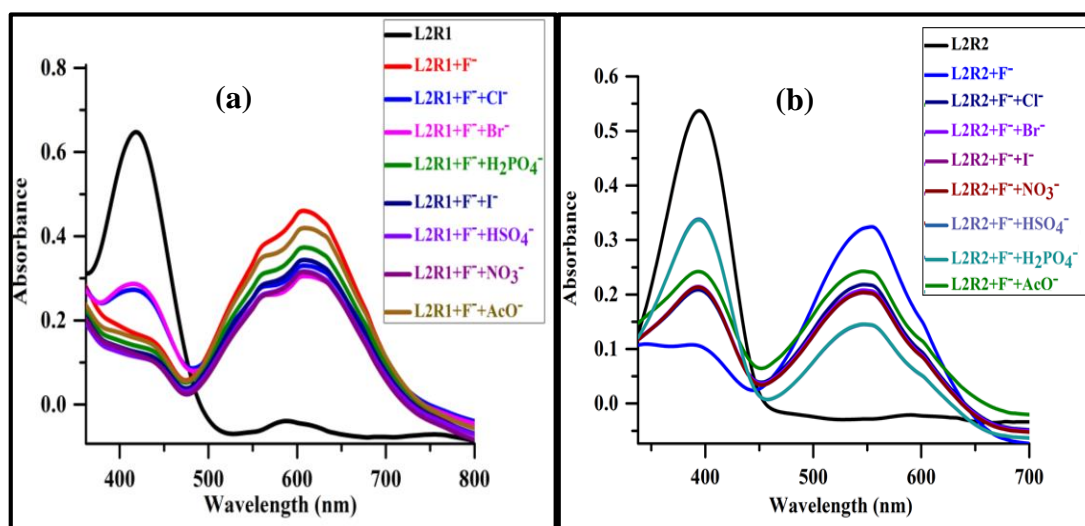
Fig. 3.20 UV-Vis absorption spectral changes of (a) **L2R1**-F⁻ (2 equiv.) with various interference anions (4 equiv.) in DMSO (b) **L2R2**-F⁻ (2 equiv.) with various interference anions (4 equiv.) in DMSO
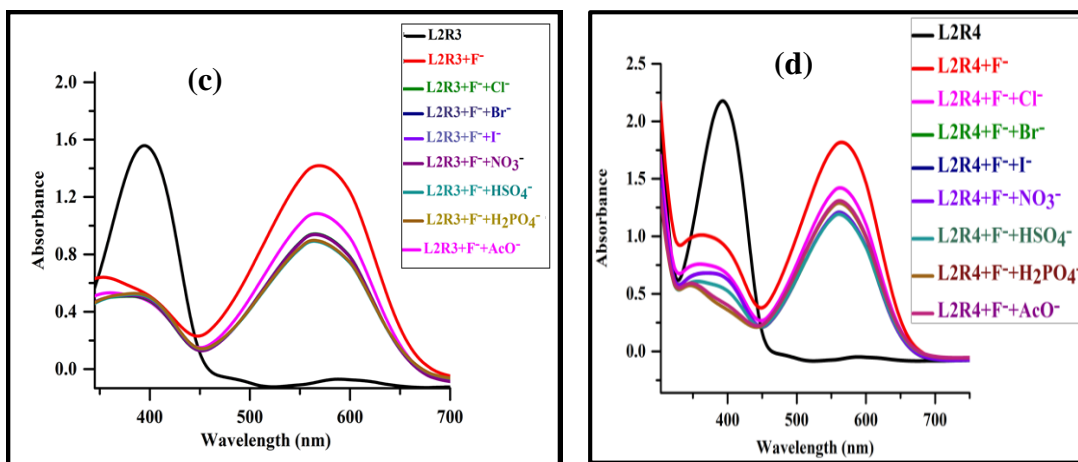
Fig. 3.21 UV-Vis absorption spectral changes of (c) **L2R3**-F⁻ (2 equiv.) with various interference anions (4 equiv.) in DMSO (d) **L2R4**-F⁻ (2 equiv.) with various interference anions (4 equiv.) in DMSO
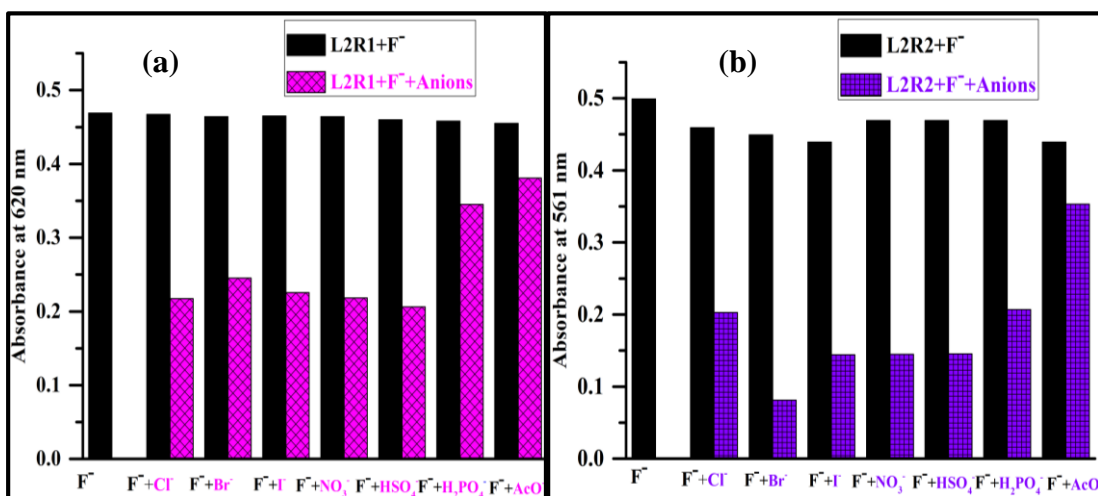
Fig. 3.22 Bar graph representation of interference response of (a) receptor **L2R1** towards 2 equiv. of F⁻ ion in the presence of 4 equiv. of other interference anions (black bar represents the addition of F⁻ ion to the solution and the purple bar represents the addition of other interference to the above solution (b) receptor **L2R2** towards 2 equiv. of F⁻ ion in the presence of 4 equiv. of other interference anions (black bar represents the addition of F⁻ ion to the solution and the blue bar represents the addition of other interference to the above solution
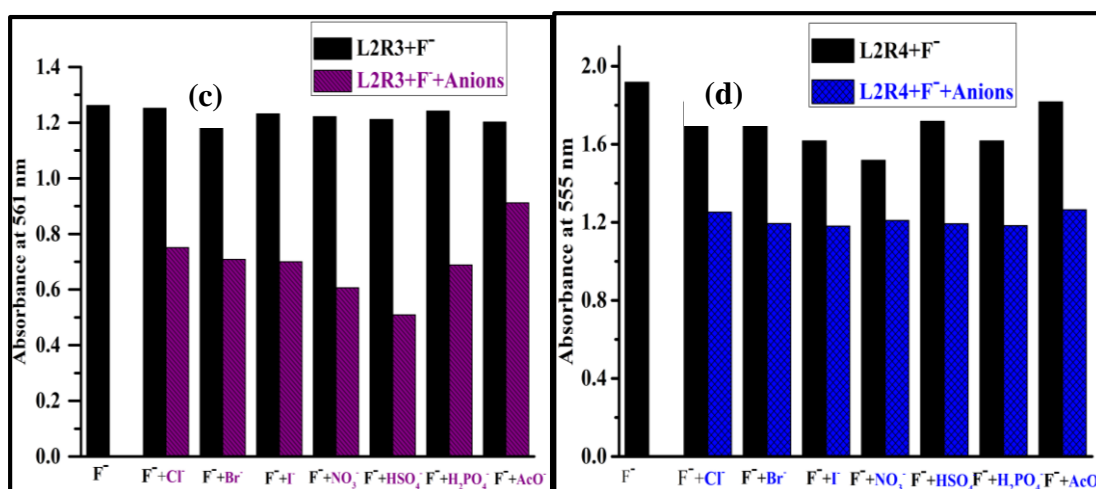
Fig. 3.23 Bar graph representation of interference response of (c) receptor **L2R3** towards 2 equiv. of F⁻ ion in the presence of 4 equiv. of other interference anions (black bar represents the addition of F⁻ ion to the solution and the violet bar represents the addition of other interference to the above solution (d) receptor **L2R4** towards 2 equiv. of F⁻ ion in the presence of 4 equiv. of other interference anions (black bar represents the addition of F⁻ ion to the solution and the blue bar represents the addition of other interference to the above solution

3.3.3 UV-Vis titration studies of receptors in DMSO

To gain deeper insight into the anion-binding affinity of the receptor **L2R1** with the F⁻, AcO⁻, and $H_2PO_4^-$ ions, the UV-Vis titration experiment was carried out in the DMSO as demonstrated in Fig. 3.24, Fig. 3.25, and Fig. 3.26. The free receptor **L2R1** exhibited an intense characteristic absorption band at 441 nm. Upon incremental addition of 0.1 equiv. of F⁻, AcO⁻, and $H_2PO_4^-$ ions to the DMSO solution of the receptor **L2R1,** the absorption band at 441 nm decreased greatly and new absorption bands appeared at 620 nm, 619 nm, and 617 nm. The titration spectra exhibited significant red shift by units of 179 nm, 178 nm, and 176 nm. The appearance of a new band at longer wavelength led to propose intramolecular charge transfer (ICT) between the electron-rich NH proton and the electron-deficient nitro moieties (Ashley et al. 2007; Murugesan et al. 2019). The presence of isosbestic points at 490 nm, 488 nm, and 487 nm represented the formation of a new complex in the system. The diminution of the band at 441 nm was a clear indication of the deprotonation of the NH proton

leading to dramatic colour change. Further to confirm the binding mode between the receptor **L2R1** and anions, UV-Vis titration was performed of **L2R1** with TBA$^+$OH$^-$ under conditions similar to those described for the other anions. The titration spectra are shown in Fig. 3.27. The spectral pattern was similar to that obtained on the addition of TBA$^+$F$^-$ or TBA$^+$AcO$^-$, confirming the deprotonation of the NH proton. The B-H plot for **L2R1**-F$^-$, **L2R1**-AcO$^-$, and **L2R1**-H$_2$PO$_4^-$ complexes revealed 1:1 binding ratio as represented in Fig. 3.28. Similarly, titration studies performed upon sequential addition of 0.1 equiv. of F$^-$ and AcO$^-$ ions to the receptors **L2R2-L2R4** solutions resulted in new absorption bands centred at 565 nm and 560 nm (**L2R2**), 561 nm and 556 nm (**L2R3**), and 555 nm and 554 nm (**L2R4**) in comparison with the absorption bands of the free receptors as shown in Fig.3.29, Fig. 3.30, Fig. 3.31, Fig. 3.32, Fig. 3.33, and Fig. 3.34. The B-H plot indicated the binding ratio of 1:1 for **L2R2**, **L2R3**, and **L2R4** with the F$^-$ and AcO$^-$ ions complex as represented in Fig. 3.35, Fig. 3.36, and Fig. 3.37. The bathochromic shift ($\Delta\lambda_{max}$) of the receptors **L2R1-L2R4** upon the addition of 2 equiv. of TBA$^+$F$^-$ and TBA$^+$AcO$^-$ in DMSO is summarized in Table 3.1.
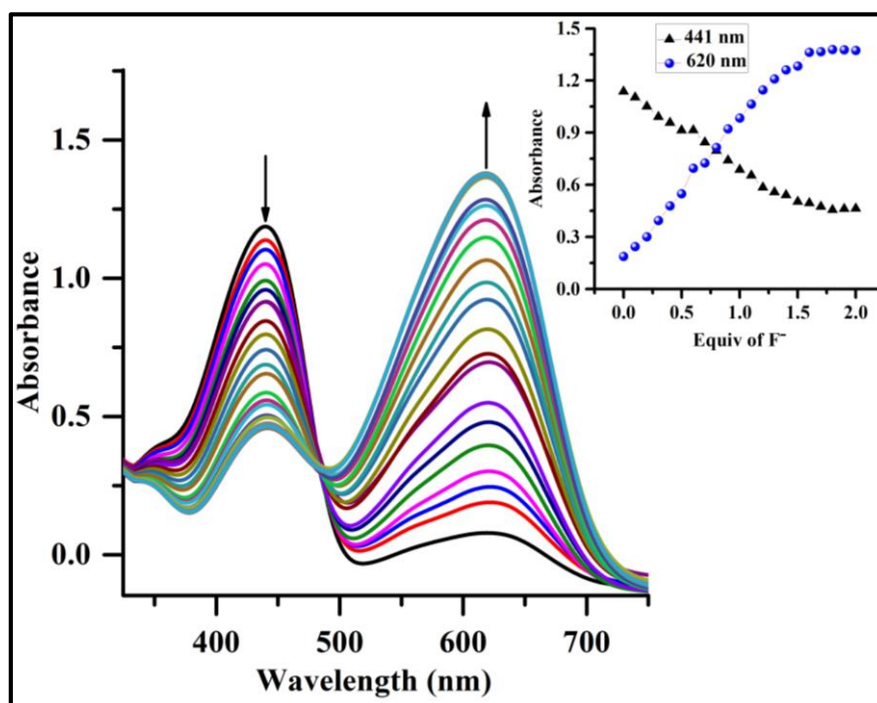
Fig. 3.24 UV-Vis titration spectra of receptor **L2R1** (2×10^{-5} M in DMSO) with the incremental addition of TBA$^+$F$^-$ (1×10^{-2} M in DMSO); Inset plot represents equiv. addition of F$^-$ and change in absorbance at 441 nm and 620 nm
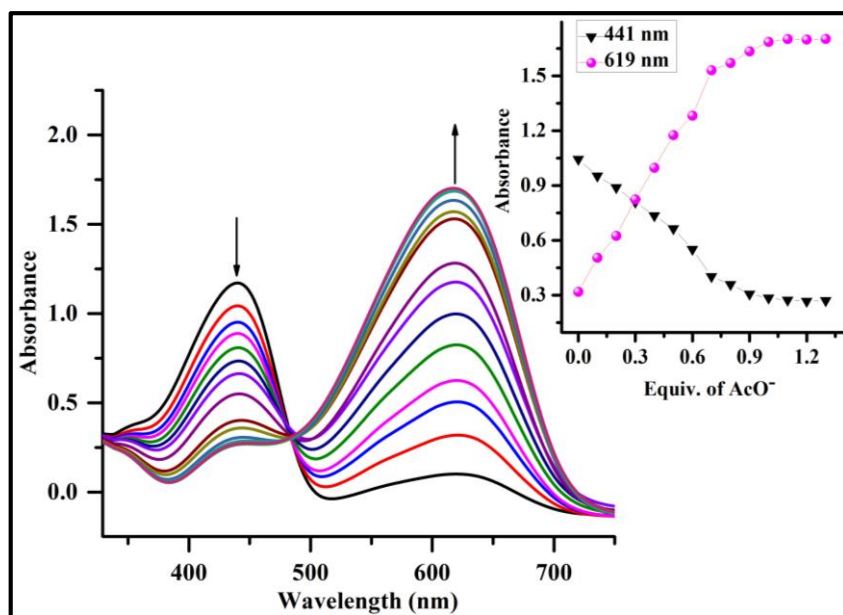
Fig. 3.25 UV-Vis titration spectra of receptor **L2R1** (2×10^{-5} M in DMSO) with the sequential addition of TBA^+AcO^- (1×10^{-2} M in DMSO); Inset plot represents the equiv. addition of AcO^- and change in absorbance at 441 nm and 619 nm
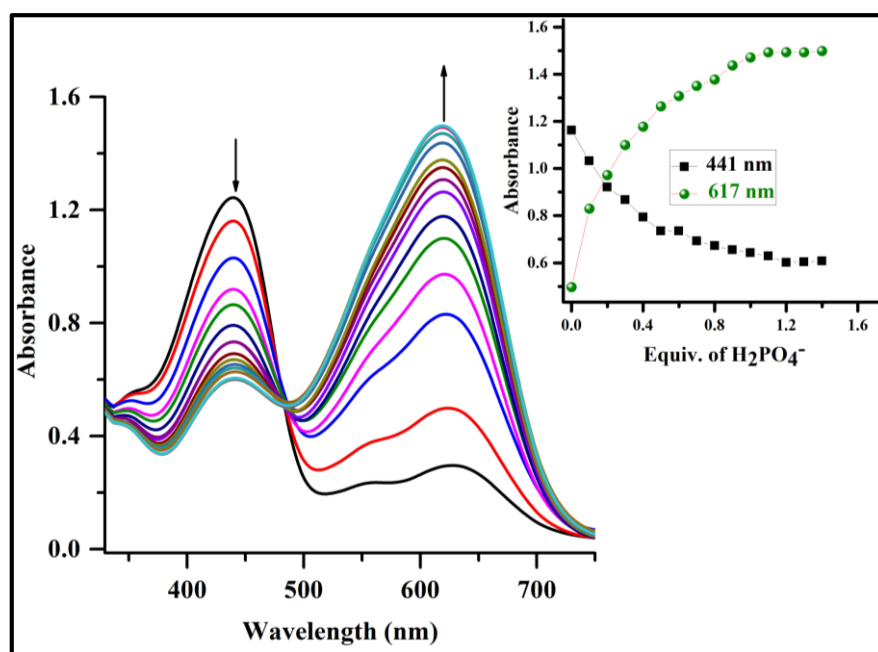
Fig. 3.26 UV-Vis titration spectra of receptor **L2R1** (2×10^{-5} M in DMSO) with sequential addition of $TBA^+H_2PO_4^-$ (1×10^{-2} M in DMSO); Inset plot represents the equiv. addition of $H_2PO_4^-$ and change in absorbance at 441 nm and 617 nm
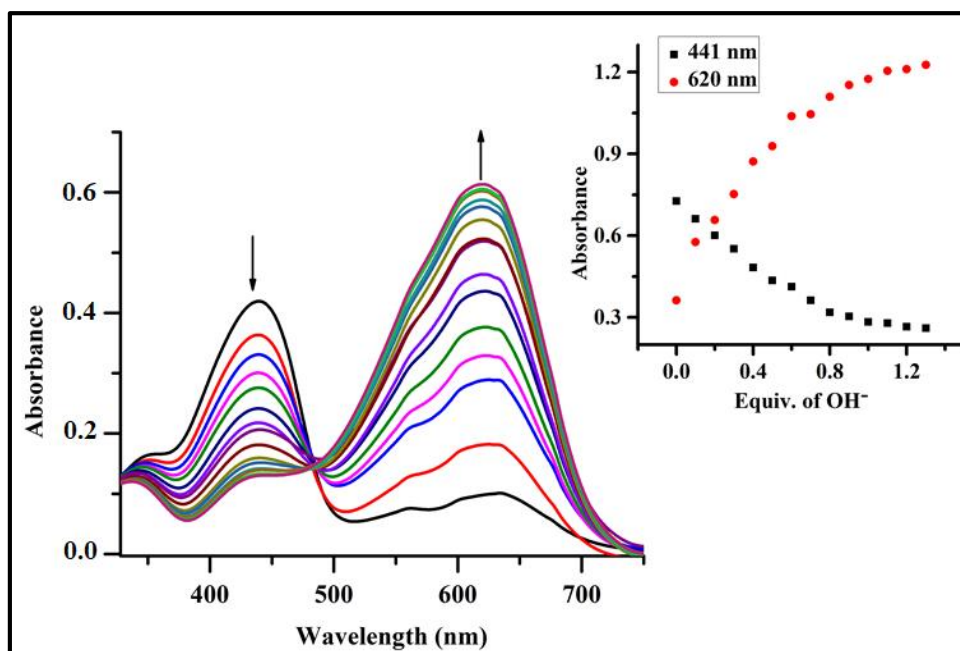
Fig. 3.27 UV-Vis titration spectra of receptor **L2R1** (2×10^{-5} M in DMSO) with incremental addition of TBA$^+$OH$^-$ (0-1.6 equiv.); 1×10^{-2} M in DMSO); Inset plot represents the equiv. addition of OH$^-$ and change in absorbance at 441 nm and 620 nm

Equation		y = a + b*x	
Plot	L2R1+TBAF	L2R1+TBAA	L2R1+TBAH$_2$PO$_4$
Intercept	0.04775 ± 0.02 78	0.05712 ± 0.02 306	0.28016 ± 0.00 669
Slope	2.39848E-4 ± 4.01576E-6	1.06184E-4 ± 3.07807E-6	3.28442E-5 ± 7.60007E-7
Residual Sum of Squares	0.01493	0.00545	0.00162
Pearson's r	0.99874	0.99707	0.99733
R-Square(CO D)	0.99748	0.99415	0.99467
Adj. R-Square	0.9972	0.99332	0.99414
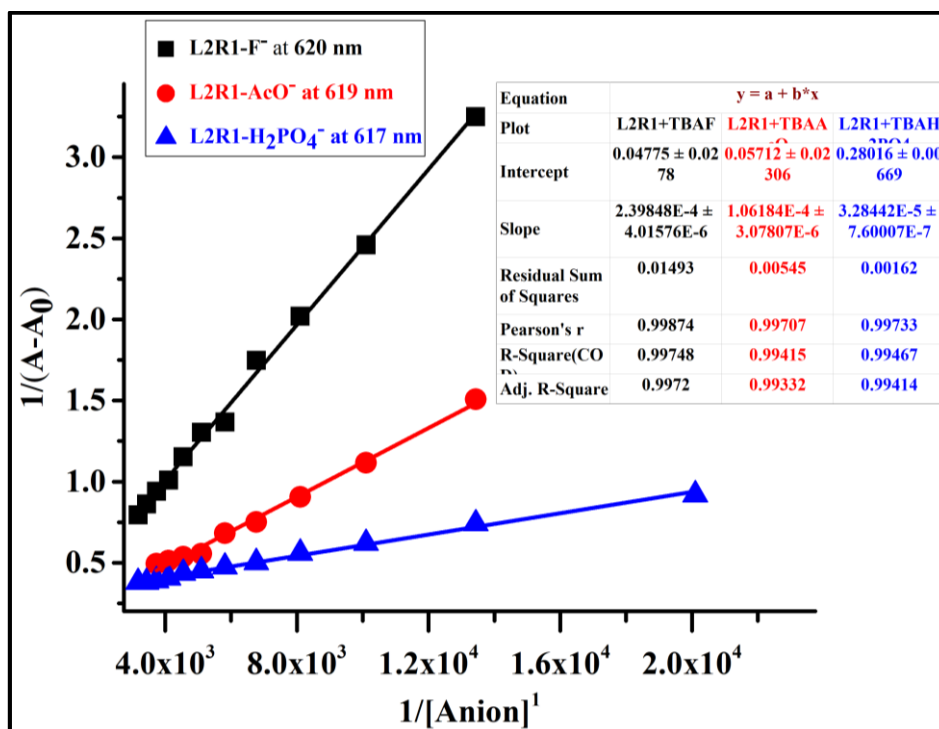
Fig. 3.28 B-H plot for 1:1 complex of **L2R1**-active anions
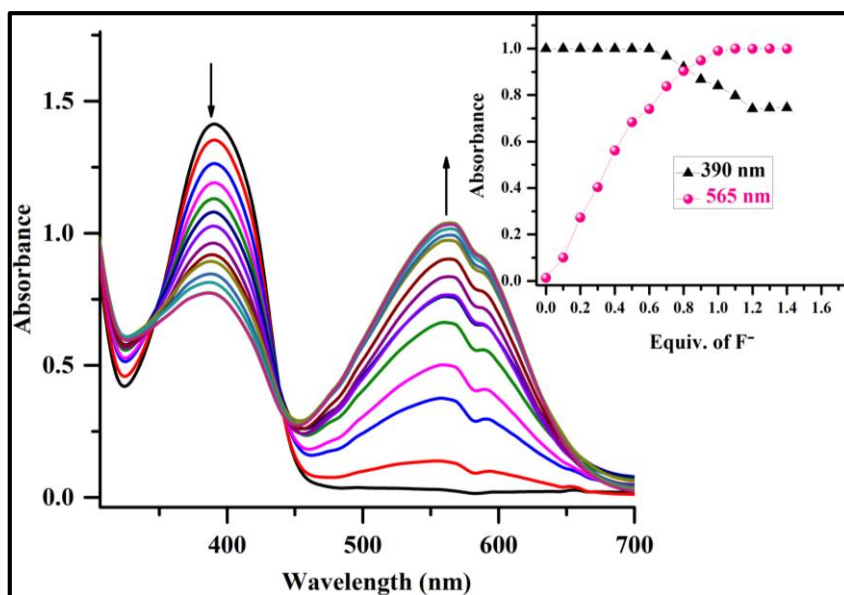
Fig. 3.29 UV-Vis titration spectra of receptor **L2R2** (2×10^{-5} M in DMSO) with incremental addition of TBA$^+$F$^-$ (1×10^{-2} M in DMSO); Inset plot represents the equiv. addition of F$^-$ and change in absorbance at 390 nm and 565 nm
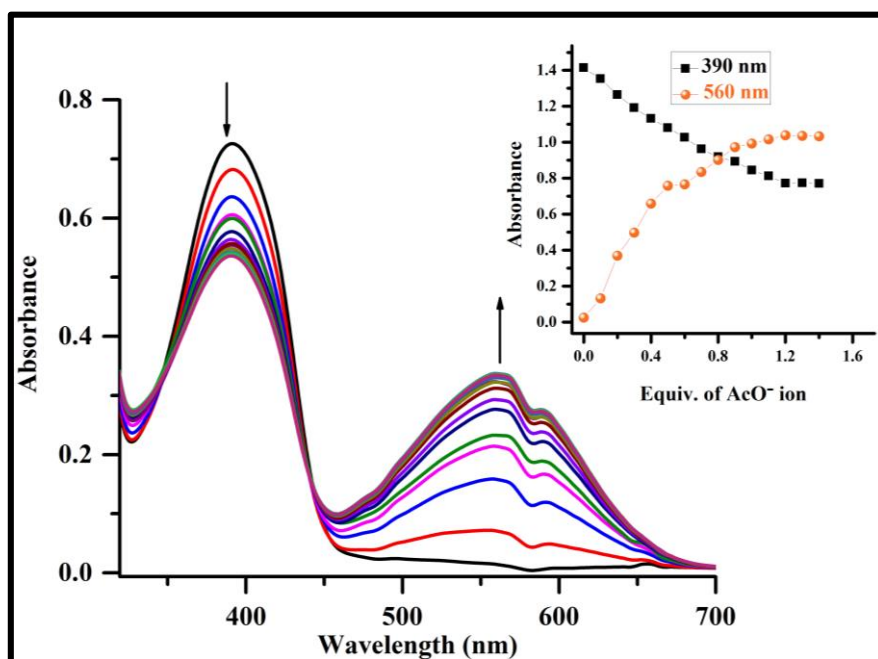
Fig. 3.30 UV-Vis titration spectra of receptor **L2R2** (2×10^{-5} M in DMSO) with incremental addition of TBA$^+$AcO$^-$ (1×10^{-2} M in DMSO); Inset plot represents the equiv. addition of AcO$^-$ and change in absorbance at 390 nm and 560 nm
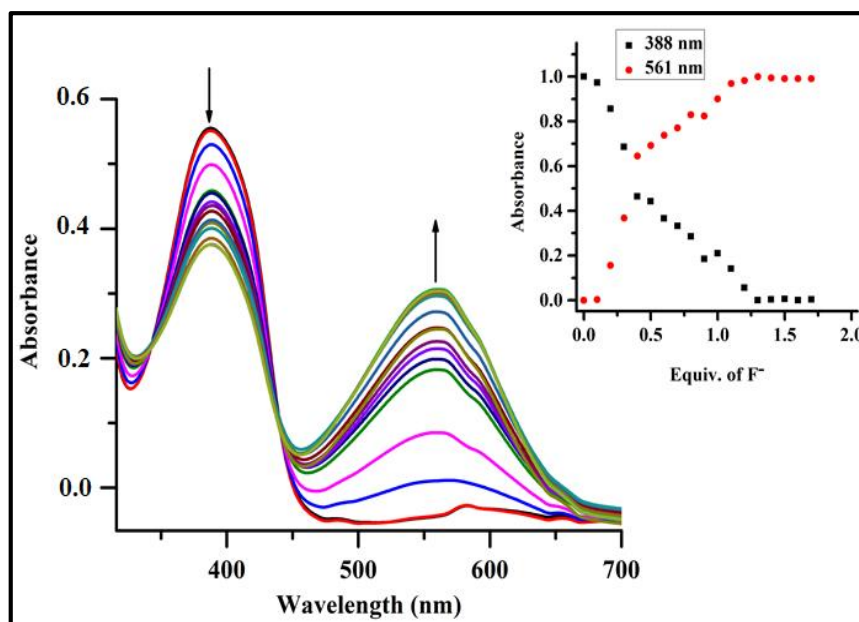
Fig. 3.31 UV-Vis titration spectra of receptor **L2R3** (2×10^{-5} M in DMSO) with increasing amounts TBA$^+$F$^-$ (1×10^{-2} M in DMSO); Inset plot represents the equiv. addition of F$^-$ and change in absorbance at 388 nm and 561 nm
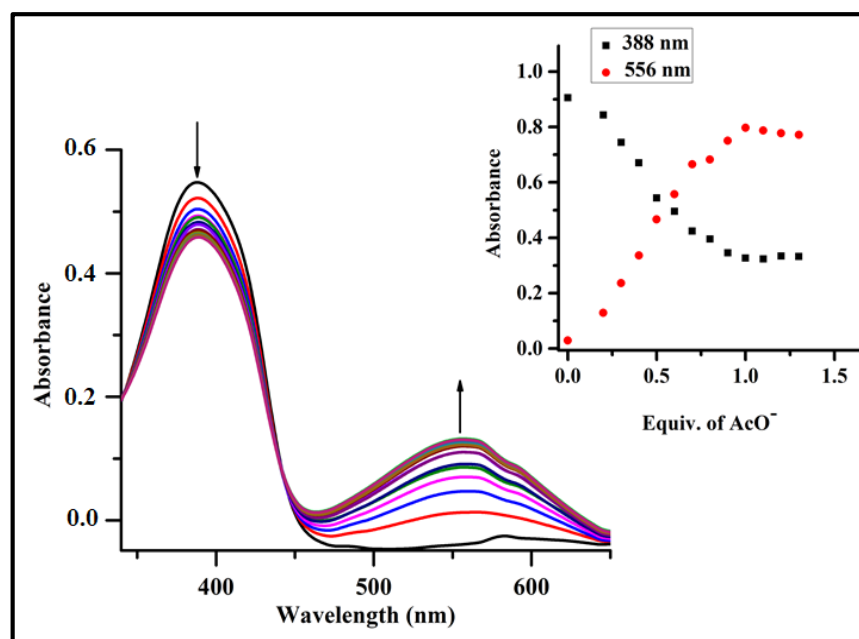
Fig. 3.32 UV-Vis titration spectra of receptor **L2R3** (2×10^{-5} M in DMSO) with increasing amounts TBA$^+$AcO$^-$ (1×10^{-2} M in DMSO); Inset plot represents the equiv. addition of AcO$^-$ and change in absorbance at 388 nm and 556 nm
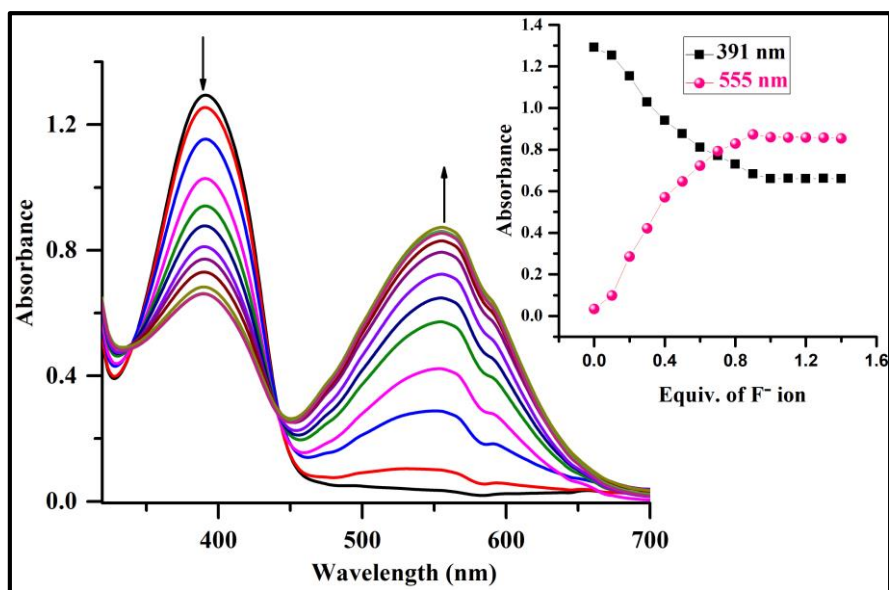
Fig. 3.33 UV-Vis titration spectra of receptor **L2R4** (2×10^{-5} M in DMSO) with increasing concentration of TBA$^+$F$^-$ (1×10^{-2} M in DMSO); Inset plot represents the equiv. addition of F$^-$ and change in absorbance at 391 nm and 555 nm
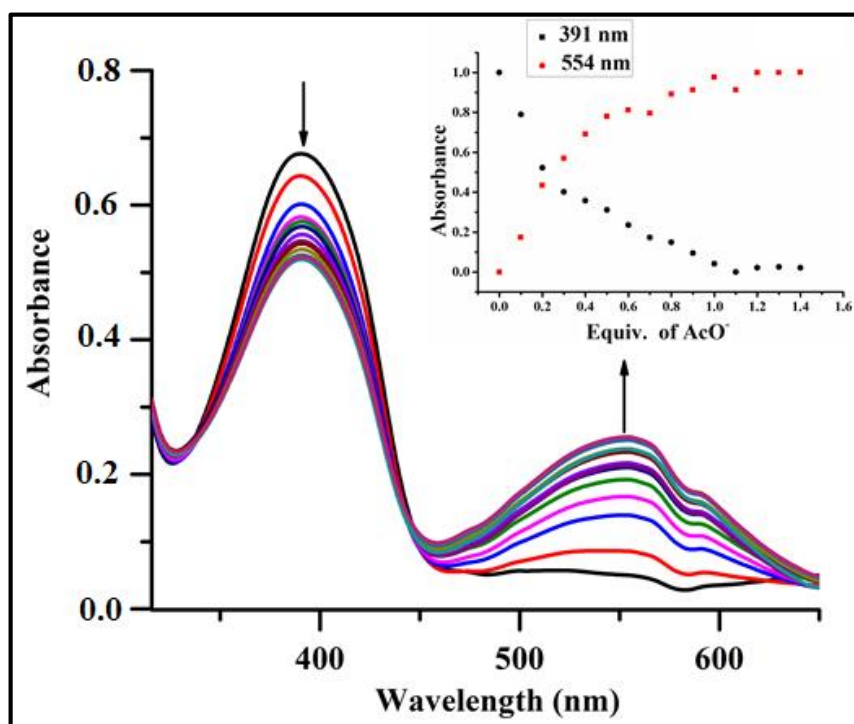
Fig. 3.34 UV-Vis titration spectra of receptor **L2R4** (2×10^{-5} M in DMSO) with increasing concentration of TBA$^+$AcO$^-$ (1×10^{-2} M in DMSO); Inset plot represents the equiv. addition of AcO$^-$ and change in absorbance at 391 nm and 554 nm
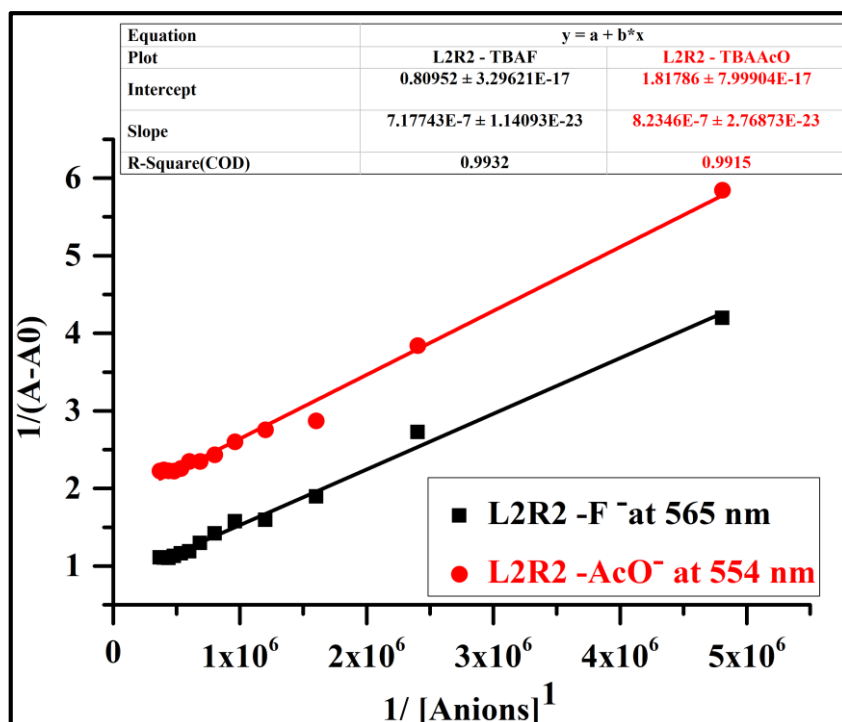
Fig. 3.35 B-H plot for 1:1 complex of **L2R2**-sensed anions
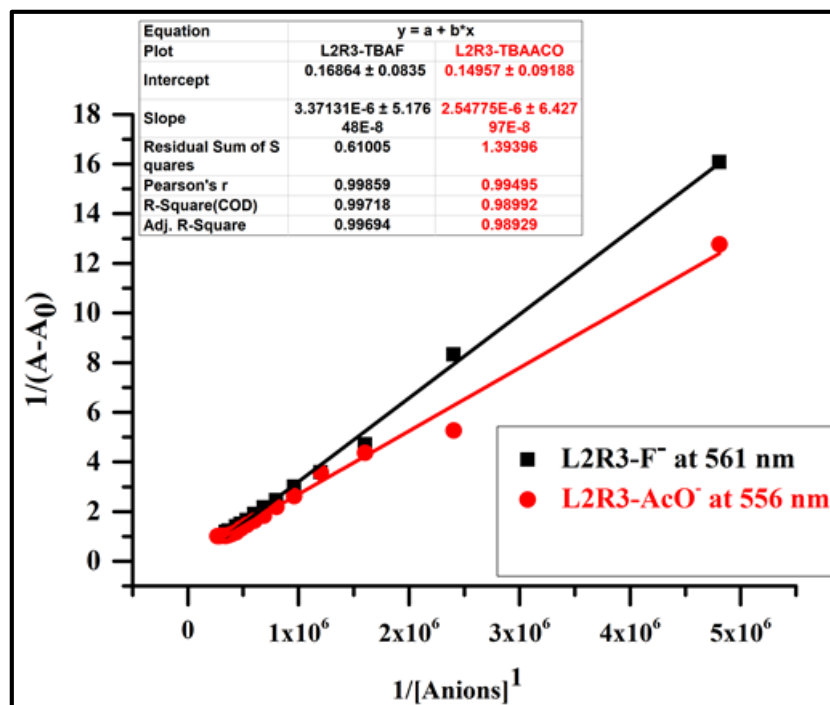
Fig. 3.36 B-H plot for 1:1 complex of **L2R3**-sensed anions
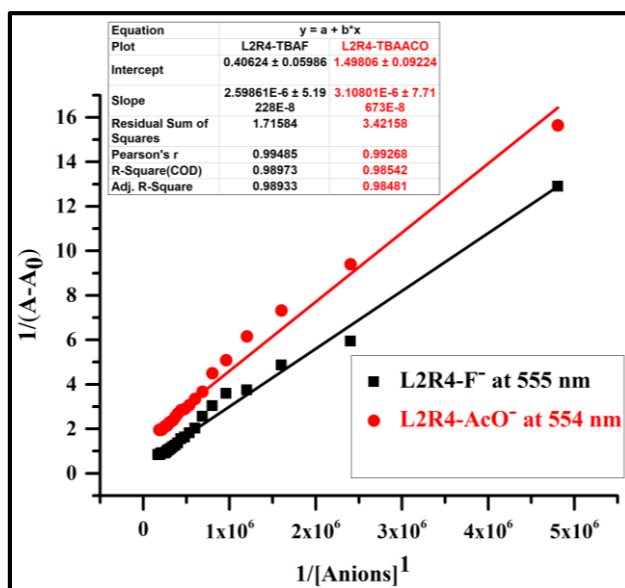
Fig. 3.37 B-H plot for 1:1 complex of **L2R4**-sensed anions

Table 3.1 Bathochromic shift in absorption band ($\Delta\lambda_{max}$) of the receptors **L2R1-L2R4** in DMSO in the presence of 2 equiv. TBA^+F^- and TBA^+AcO^- (1×10^{-2} M)

S.No.	Receptor+Anions	Medium	Bathochromic shift ($\Delta\lambda_{max}$) (nm)	Isosbestic point (nm)
1	**L2R1**+TBA^+F^-	DMSO	179	490
2	**L2R1**+ TBA^+AcO^-	DMSO	178	488
3	**L2R1**+ $TBA^+H_2PO_4^-$	DMSO	176	487
4	**L2R2**+ TBA^+F^-	DMSO	175	436
5	**L2R2**+ TBA^+AcO^-	DMSO	170	434
6	**L2R3**+ TBA^+F^-	DMSO	173	441
7	**L2R3**+ TBA^+AcO^-	DMSO	168	439
8	**L2R4**+ TBA^+F^-	DMSO	164	438
9	**L2R4**+ TBA^+AcO^-	DMSO	163	444

The observations in Table 3.1 show that the receptor **L2R1** had a high bathochromic shift ($\Delta\lambda_{max}$) compared with the other receptors **L2R2-L2R4** in the DMSO. This draws attention to the fact that only the **L2R1** receptor is more feasible for the ICT transition from anion-bound NH to an electron-deficient nitro group. The naphthyl group in the **L2R2** receptor had a conjunction effect, which resulted in a much

higher bathochromic shift compared with the electron-donating methyl group and phenyl ring with no substitution in the receptors **L2R3** and **L2R4.** However, the results above show that all the four **L2R1-L2R4** receptors have a good colorimetric response for the active anions, and yet the presence of the various substituent groups effectively modulated the colour and shift in the receptor absorption band.

3.3.4   UV–Vis titration of L2R1 with sodium salts in DMSO: H₂O (9:1 v/v)

Fluoride, acetate, arsenite, and arsenate are present in the form of sodium salt at the physiological level. Its deficiency or excess can lead to disorder in the ecosystem. In this regard, it is of more interest to develop sensors, which can detect F^-, AcO^-, AsO_2^-, and AsO_4^{2-} ions. The study was extended to detect F^-, AcO^-, AsO_2^-, and AsO_4^{2-} ions. Interestingly, the receptor **L2R1** (2×10^{-5} M) quickly and effectively sensed F^-, AcO^-, AsO_2^-, and AsO_4^{2-} (1×10^{-2} M, distilled H₂O) in the organo-aqueous medium DMSO: H₂O (9:1 v/v) by producing a colour change from pale yellow to blue. The titration studies conducted with the incremental addition of 0.1 equiv. of F^-, AcO^-, AsO_2^-, and AsO_4^{2-} as sodium salts to the measured quantity of the receptor **L2R1** solution (2×10^{-5} M) in DMSO: H₂O (9:1 v/v) showed the absorption peak at 441 nm shifted to longer wavelength at 615 nm, 617 nm, 613 nm, and 612 nm with bathochromic shift ($\Delta\lambda_{max}$) of 174 nm, 176 nm, 172 nm, and 171 nm. This bathochromic shift can be attributed to the charge transfer between the receptor **L2R1** and the added anions F^-, AcO^-, AsO_2^-, and AsO_4^{2-} with the highly acidic –NH unit of the receptor **L2R1**. The titration profile is represented in Fig.3.38, Fig. 3.39, Fig. 3.40, and Fig. 3.41. These spectral changes were also accompanied by the formation of single isosbestic points at 479 nm, 481 nm, 485 nm, and 483 nm indicating stable complex formation between the receptor **L2R1** and the corresponding anions (F^-, AcO^-, AsO_2^-, and AsO_4^{2-}). The above results can be attributed to the introduction of the electron-withdrawing NO₂ group into the backbone of the molecular receptor, thereby increasing the acidity of the N-H proton, enhancing its H-bond donor ability, and creating a stronger anion complex even in aqueous media (Ali et al. 2008). However, significantly less bathochromic shift was observed in the case of the organo-aqueous medium DMSO: H₂O (9:1 v/v) relative to DMSO, possibly due to the solvation of anions in water, which decreased its binding with the receptor (Kumar et al. 2008).
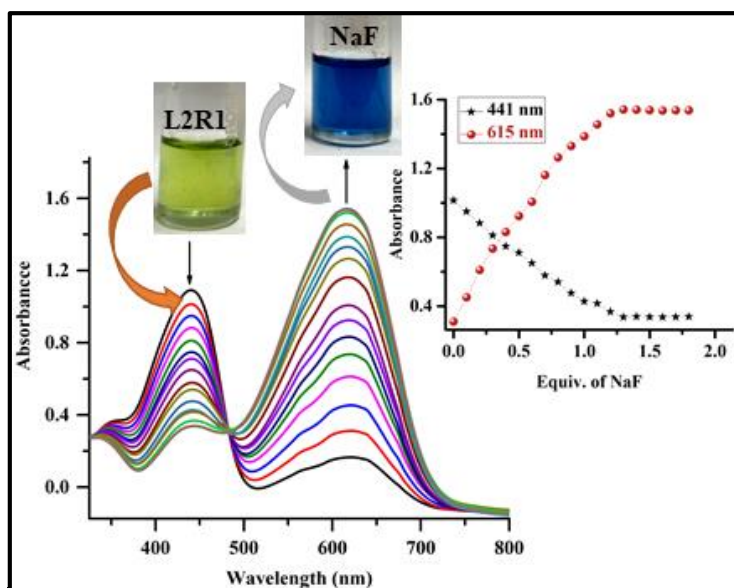
Fig. 3.38 UV-Vis titration spectra of receptor **L2R1** (2×10^{-5} M in DMSO) and colour change with the gradual addition of $Na^+ F^-$ (1×10^{-2} M in H_2O) in DMSO: H_2O (9:1 v/v); Inset plot represents the equiv. addition of $Na^+ F^-$ and change in absorbance at 441 nm and 615 nm
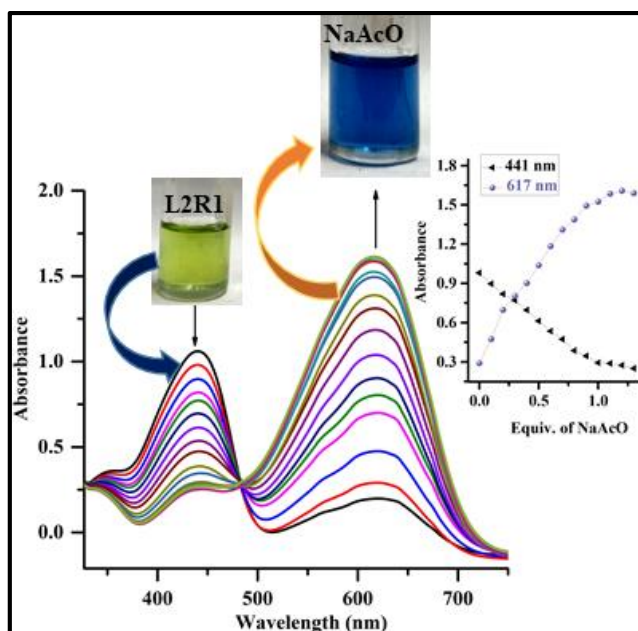
Fig. 3.39 UV-Vis titration spectra of receptor **L2R1** (2×10^{-5} M in DMSO) and colour change with the gradual addition of $Na^+ AcO^-$ (1×10^{-2} M in H_2O) in DMSO: H_2O (9:1 v/v); Inset plot represents the equiv. addition of Na^+AcO^- and change in absorbance at 441 nm and 617 nm
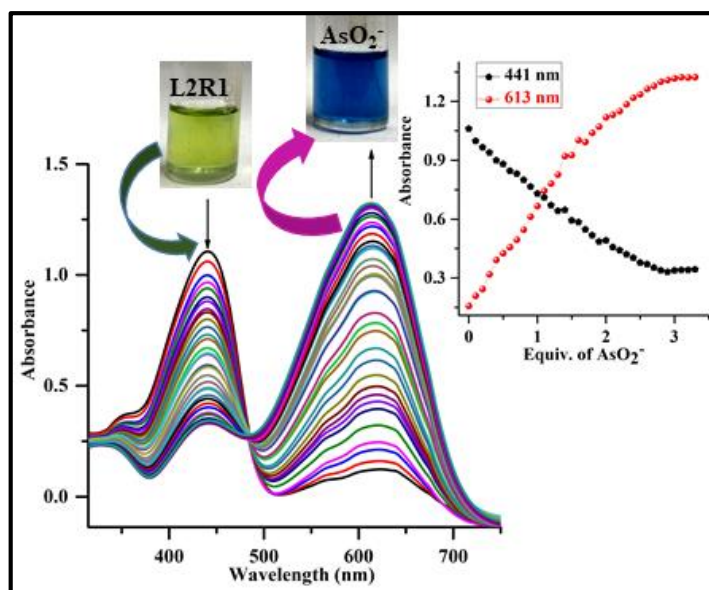
Fig. 3.40 UV-Vis titration spectra of receptor **L2R1** (2×10^{-5} M in DMSO) and colour change with the increasing concentration of AsO_2^- (1×10^{-2} M in H_2O) in DMSO: H_2O (9:1 v/v); Inset plot represents the equiv. addition of AsO_2^- and change in absorbance at 441 nm and 613 nm
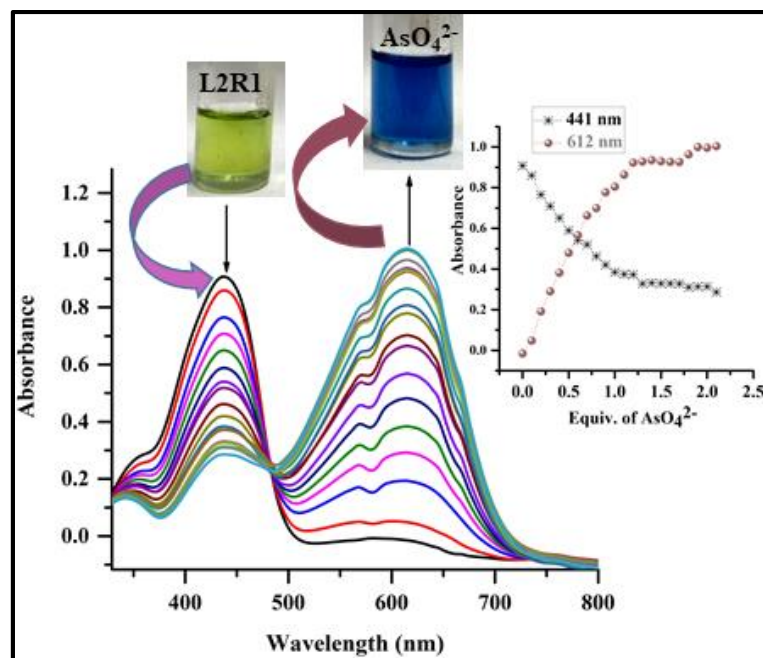
Fig. 3.41 UV-Vis titration spectra of receptor **L2R1** (2×10^{-5} M in DMSO) and colour change with the increasing concentration of AsO_4^{2-} (1×10^{-2} M in H_2O) in DMSO: H_2O (9:1 v/v); Inset plot represents the equiv. addition of AsO_4^{2-} and change in absorbance at 441 nm and 612 nm

Moreover, the Benesi–Hildebrand plot of $1/[A\ A_0]$ vs. $1/[Anion]^1$ [Anions= F^-, AcO^-, AsO_2^- and AsO_4^{2-}] for titration of **L2R1** with target anions provided a straight line as depicted in Fig. 3.42 in the DMSO: H_2O (9:1 v/v).

Equation		$y = a + b*x$		
Plot	L2R1-NaF	L2R1-NaAcO	L2R1-NaAsO2-	L2R1-NaAsO42-
Intercept	0.29775 ± 0.0355	0.37563 ± 0.05896	0.3957 ± 0.1032	0.66412 ± 0.02518
Slope	1.37712E-6 ± 2.4838 2E-8	1.0392E-6 ± 4.3411 9E-8	5.32376E-6 ± 9.409 5E-8	1.32385E-6 ± 1.9841 6E-8
Residual Sum of Squares	0.20813	0.74408	6.46895	0.19035
Pearson's r	0.99741	0.98465	0.9955	0.99765
R-Square(COD)	0.99482	0.96954	0.99102	0.9953
Adj. R-Square	0.9945	0.96785	0.99071	0.99508

Legend:
- ■ L2R1-NaF at 615 nm
- ● L2R1-NaAcO at 617 nm
- ▲ L2R1-NaAsO$_2^-$ at 613nm
- ▼ L2R1-NaAsO$_4^{2-}$ at 612 nm

Fig. 3.42 B-H plot for 1:1 complex of **L2R1** with sodium salts of F^-, AcO^-, AsO_2^-, and AsO_4^{2-} ions at selective wavelength of 615 nm, 617 nm, 613 nm and 612 nm in DMSO: H_2O (9:1 v/v)

The limit of detection (LOD) was calculated using a signal-noise ratio using the calibration curve between the absorbance of receptors-anion complex and the concentration of anions at selected wavelengths as depicted in Fig. 3.43, Fig. 3.44, Fig. 3.45, Fig. 3.46, and Fig. 3.47.

Equation	y = a + b*x		
Plot	L2R1-F-	L2R1-AcO-	L2R1-H2PO4-
Intercept	0.07222 ± 0.01005	0.13855 ± 0.02292	0.33438 ± 0.03217
Slope	3394.68823 ± 53.88852	6782.15049 ± 174.77262	7037.69168 ± 361.22081
Residual Sum of Squares	0.00465	0.01205	0.01108
Pearson's r	0.99849	0.99735	0.99348
R-Square(COD)	0.99699	0.99472	0.987
Adj. R-Square	0.99673	0.99405	0.9844

Legend:
- ■ L2R1-TBA$^+$F$^-$ at 620 nm
- ● L2R1-TBA$^+$AcO$^-$ at 619 nm
- ▲ L2R1-TBA$^+$H2PO$_4^-$ at 617 nm

Fig. 3.43 Calibration curve between absorbance of receptor **L2R1**-anion complex and concentration of anions at selected wavelength

Equation	y = a + b*x			
Plot	L2R1-Sodium fluoride	L2R1-Sodium acetate	L2R1-Arsenite	L2R1-Arsenate
Intercept	0.2141 ± 0.0197	0.22106 ± 0.025	0.1596 ± 0.0086	0.11669 ± 0.0132
Slope	4757.26096 ± 136.02993	5441.32681 ± 174.29251	2040.44085 ± 59.31136	17312.74012 ± 556.83677
Residual Sum of Squares	0.0109	0.01789	0.00207	0.00323
Pearson's r	0.99634	0.99541	0.99622	0.9964
R-Square(COD)	0.9927	0.99085	0.99245	0.99281
Adj. R-Square	0.99188	0.98983	0.99161	0.99178

Legend:
- ■ L2R1-Na$^+$F$^-$ at 615 nm
- ● L2R1-Na$^+$AcO$^-$ at 617 nm
- ▲ L2R1-Na$^+$AsO$_2^-$ at 613 nm
- ▼ L2R1-Na$^+$AsO$_4^{2-}$ at 612 nm

Fig. 3.44 Calibration curve between absorbance of receptor **L2R1**-anions complex and concentration of anions at selected wavelength

Equation	y = a + b*x	
Plot	L2R2- TBAF	L2R2- TBAAcO
Intercept	0.04797 ± 0.01851	0.06257 ± 0.01314
Slope	4910.42509 ± 207.810 83	3336.76089 ± 127.356 15
R-Square(COD)	0.99112	0.99134
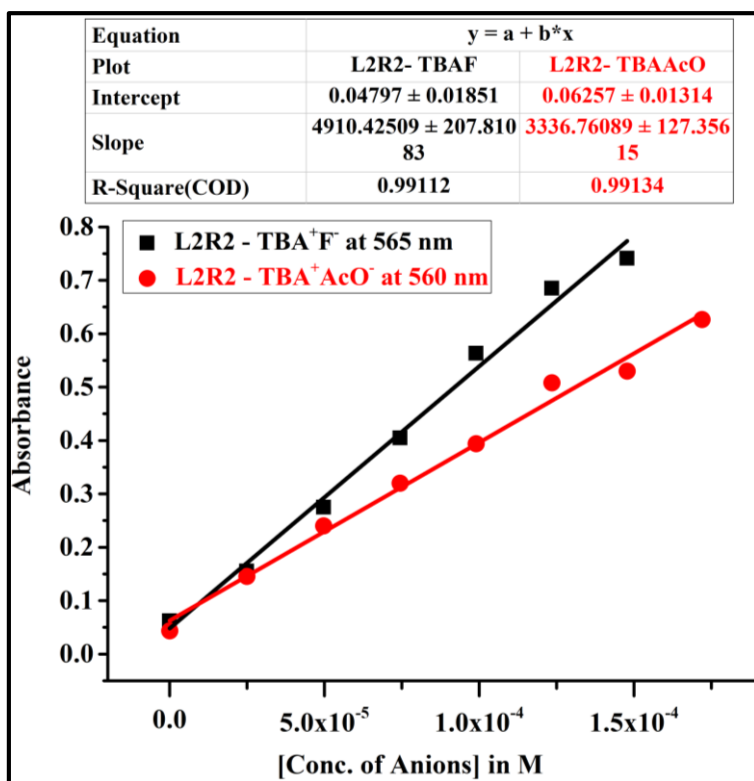
Fig. 3.45 Calibration curve between absorbance of receptor **L2R2**-anions complex and concentration of anions at selected wavelength

Equation	y = a + b*x	
Plot	L2R3-TBAF	L2R3-TBAAcO
Intercept	0.21677 ± 0.03034	0.05346 ± 0.01344
Slope	21388.34455 ± 1278.58987	2165.64779 ± 179.41254
Residual Sum of Squares	0.01703	0.00137
Pearson's r	0.98772	0.98655
R-Square(COD)	0.9756	0.97328
Adj. R-Square	0.97211	0.9666
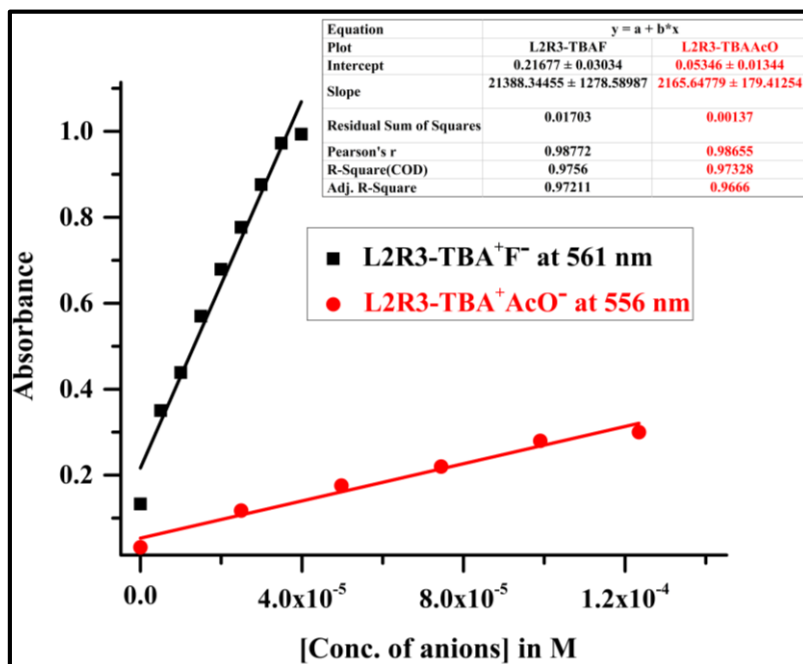
Fig. 3.46 Calibration curve between absorbance of receptor **L2R3**-anions complex and concentration of anions at selected wavelength

Equation	$y = a + b \cdot x$	
Plot	L2R4-TBAF	L2R4-TBAAcO
Intercept	0.06035 ± 0.01435	0.04165 ± 0.01562
Slope	4784.6923 ± 139.13427	5159.27828 ± 175.42727
Residual Sum of Squares	0.00294	0.00261
Pearson's r	0.99747	0.99712
R-Square(COD)	0.99495	0.99425
Adj. R-Square	0.99411	0.9931
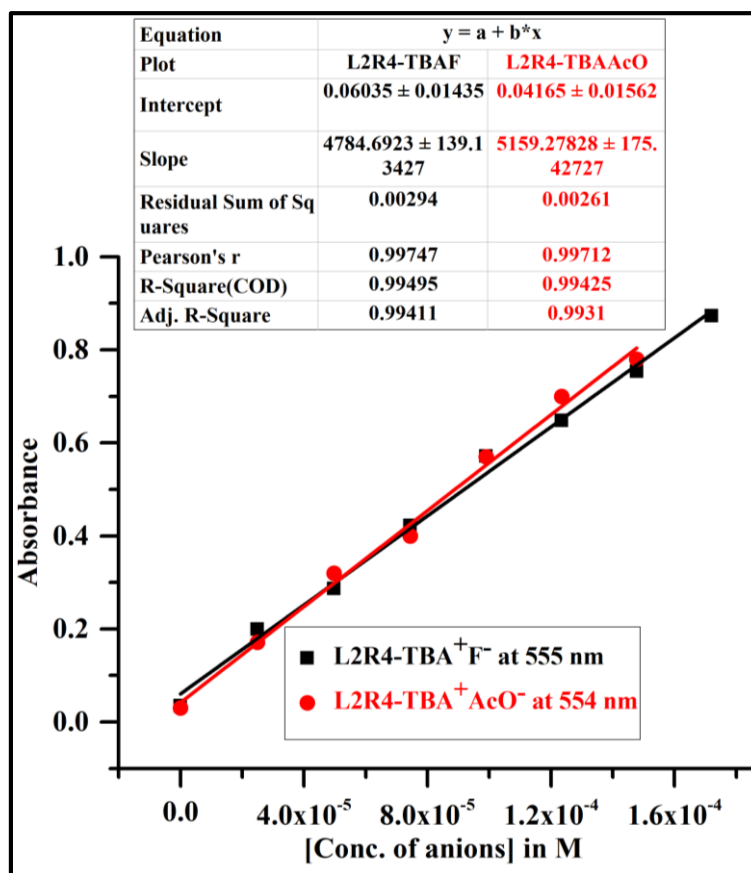
Fig. 3.47 Calibration curve between absorbance of receptor **L2R4**-anions complex and concentration of anions at selected wavelength

The binding constant and detection limit of the receptors-anion complex was observed to be in the order of **L2R1**>**L2R2**>**L2R3**>**L2R4.** The observed order indicated that the receptor **L2R1** with NO_2 substituent showed a relatively higher binding constant and detection limit than those with different substituent groups in the receptors **L2R2**, **L2R3,** and **L2R4**. Remarkably, the receptor **L2R1** could calorimetrically sense F⁻ ion in aqueous medium even at 0.392 ppm, far lower than the WHO guideline regarding F⁻ in drinking water (less than 1 ppm) (Fawell et al. 2001)**.** The corresponding binding constant and detection limit of receptors is presented in Table 3.2.

Table 3.2 Binding constant, medium, binding ratio, and limit of detection for receptors **L2R1-L2R4** with anions in DMSO and DMSO: H$_2$O, (9:1 v/v)

Receptor +anions	Medium	Binding constant (M^{-1})	Binding ratio	R^2	LOD (ppm)
L2R1+ TBA$^+$F$^-$	DMSO	5.01×10^6	1:1	0.99748	0.514
L2R1+ TBA$^+$AcO$^-$	DMSO	4.25×10^6	1:1	0.99415	0.725
L2R1+ TBA$^+$H$_2$PO$_4^-$	DMSO	3.12×10^6	1:1	0.99467	1.882
L2R2+ TBA$^+$F$^-$	DMSO	4.43×10^4	1:1	0.99328	2.33
L2R2+ TBA$^+$AcO$^-$	DMSO	4.03×10^4	1:1	0.99154	2.56
L2R3+ TBA$^+$F$^-$	DMSO	3.78×10^3	1:1	0.97633	3.76
L2R3+ TBA$^+$AcO$^-$	DMSO	3.30×10^3	1:1	0.9781	3.97
L2R4+ TBA$^+$F$^-$	DMSO	2.22×10^3	1:1	0.9925	4.32
L2R4+ TBA$^+$AcO$^-$	DMSO	1.45×10^3	1:1	0.99643	4.90
L2R1+Na$^+$F$^-$	DMSO:H$_2$O (9:1 v/v)	5.48×10^6	1:1	0.99482	0.392
L2R1+ Na$^+$AcO$^-$	DMSO:H$_2$O (9:1 v/v)	3.98×10^6	1:1	0.99108	0.823
L2R1+ Na$^+$AsO$_2^-$	DMSO:H$_2$O (9:1 v/v)	4.89×10^6	1:1	0.99102	0.643
L2R1+ Na$^+$AsO$_4^{2-}$	DMSO:H$_2$O (9:1 v/v)	4.22×10^6	1:1	0.9953	0.721

3.3.5 Role of pH in the selectivity of L2R1

In addition, the receptor **L2R1** anion binding properties were studied in the HEPES buffer (0.05 M, pH 7.35). The anion binding studies in the buffer medium with the receptor solution in DMSO/ HEPES (2×10^{-5}, 9:1 v/v, pH 7.35) exhibited excellent selectivity towards the AcO$^-$ ion with blue colouration. Fig. 3.48 and Fig. 3.49 clearly represent the selectivity of the receptor **L2R1** for AcO$^-$ ion over the other anions. The pre-organized structure, conformational stability, the basicity of the receptor, and the alkalescence of the anion can be accounted for the higher selectivity of the receptor **L2R1** towards the AcO$^-$ ion (Srikala et al. 2016). In contrast, the planar or triangular form of the AcO$^-$ ion is strongly linked to the protons-NH and CH (amine) embedded in the receptor **L2R1**. The titration spectra revealed the shift of the original absorption band from 441 nm to 611 nm. The bathochromic shifts of ($\Delta\lambda_{max}$=170 nm) was recorded upon the addition of AcO$^-$ with single isosbestic point at 481 nm indicating complex formation between **L2R1** and AcO$^-$ ion. The titration spectra are depicted in Fig. 3.50. Yet, unlike the receptor **L2R1**, **L2R2-L2R4** did not exhibit selective response

towards a particular anion in the presence of the HEPES buffer. These spectral changes show that the NH proton deprotonated upon interaction with the basic AcO⁻ ion at pH 7.35. The UV-Vis titration experiment was conducted with incremental addition of 0.1 equiv. of TBAOH to the solution of the receptor **L2R1**, showing similar spectral change supporting the deprotonation of the -NH proton in the buffer media at pH 7.35. The binding ratio was found to be 1:1 between the receptor **L2R**1- AcO⁻ ion indicating a one-step deprotonation process as shown in Fig. 3.51.
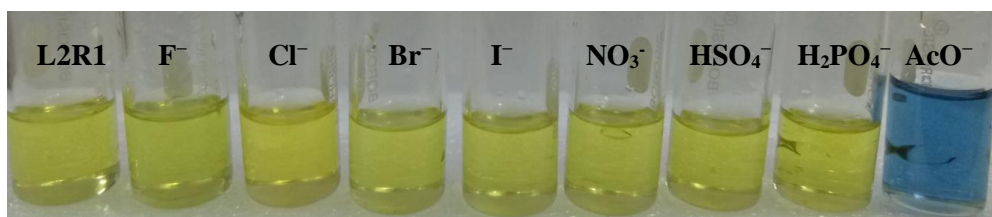
Fig. 3.48 Colour changes of the receptor **L2R1** (2×10^{-5} M, DMSO:HEPES buffer, 9:1 v/v, pH 7.35) with the addition of 3 equiv. of different tetrabutylammonium salt (1×10^{-2} M in DMSO)
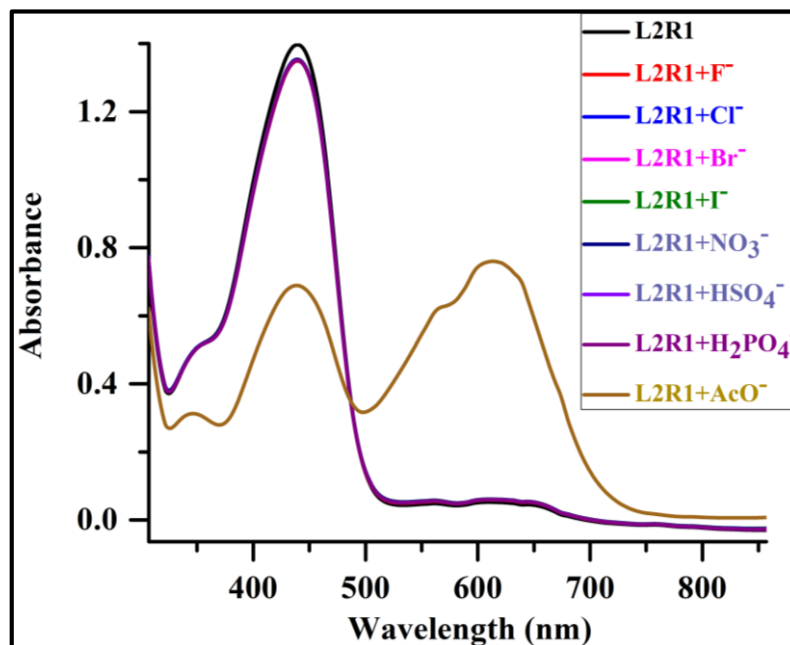
Fig. 3.49 UV-Vis spectra of receptor **L2R1** (2×10^{-5} M, DMSO:HEPES buffer, 9:1 v/v, pH 7.35) with the addition of 3 equiv. of tetrabutylammonium salt of various anions (1×10^{-2} M in DMSO)
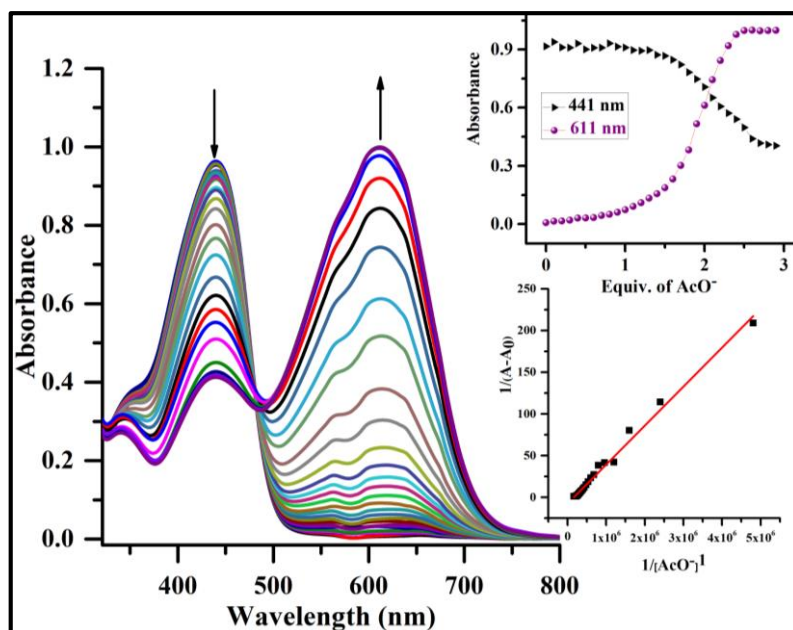
Fig. 3.50 UV-Vis titration spectra of **L2R1** (2×10^{-5} M in DMSO:HEPES buffer, 9:1 v/v, pH 7.35) with increasing amounts of TBA$^+$AcO$^-$ (1×10^{-2}M in DMSO); Inset plot representing the variation of absorbance with increasing concentration of AcO$^-$ ion and B-H plot for **L2R1**- AcO$^-$ complex
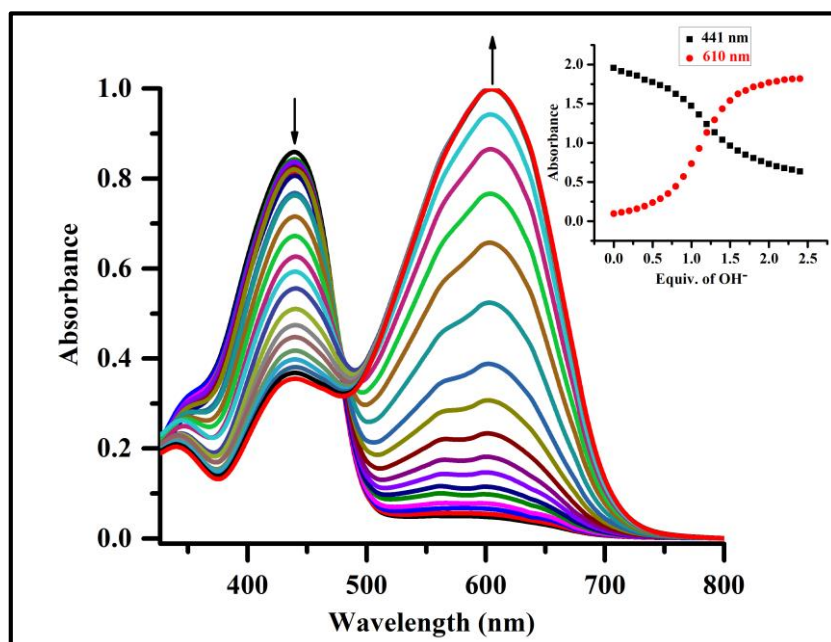
Fig. 3.51 UV-Vis titration spectra of **L2R1** (2×10^{-5} M in DMSO:HEPES buffer, 9:1 v/v, pH 7.35) with increasing amounts of TBA$^+$OH$^-$ (1×10^{-2} M in DMSO); Inset plot representing the variation of absorbance with increasing concentration of TBA$^+$OH$^-$

3.3.6 Solvatochromic behavioural studies of L2R1

The study was extended to investigated the solvent dependent charge transfer interaction in the presence of active anions. The addition of 2 equiv. of AcO⁻ to the receptor **L2R1** (2×10^{-5} M) induced optical signalling from pale yellow to blue, red, pink, orange, bright pink, and violet in various aprotic polar solvents such as DMSO, ACN, DCM, THF,1,4 –Dioxane, and acetone as demonstrated in Fig. 3.52. The UV-Vis spectra recorded with the addition of 2 equiv. of AcO⁻ to the receptor **L2R1** in solvents of varying polarities resulted in a new band with significant red shift as represented in Fig. 3.53. Among all the solvents, maximum shift in the absorption maxima was observed in the DMSO, followed by THF, and other aprotic solvents indicating the formation of a stable complex as shown in Table 3.3. Mechanistically, the occurrence of π-π* transitions in the receptor unit resulted in gradual increase of the dipole moment upon excitation. Concurrently, presence of polar solvent directed the stabilization of excited state more than the ground state. This reduced the separation between the two energy states which ensued in red shift of the absorption band. Magnitude of red shift was further influenced by the extent of variation of dipole moment in the excitation process. The occurrence of smaller magnitude of dipole moment in the ground state than in the excited state, led to a substantial shift of absorption band (termed as positive solvatochromism or bathochromic shift) (Hadjmohammadi et al. 2008; Marini et al. 2010; Saroj et al. 2011)
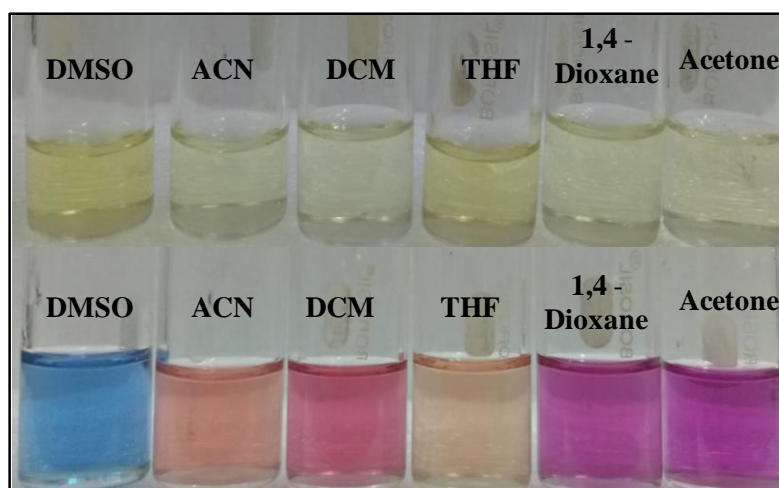
Fig. 3.52 Solvatochromis effect observed with the addition of 2 equiv. of AcO⁻ ion (1×10^{-2}M in DMSO) to the **L2R1** (2×10^{-5} M) solution in various polar aprotic solvents
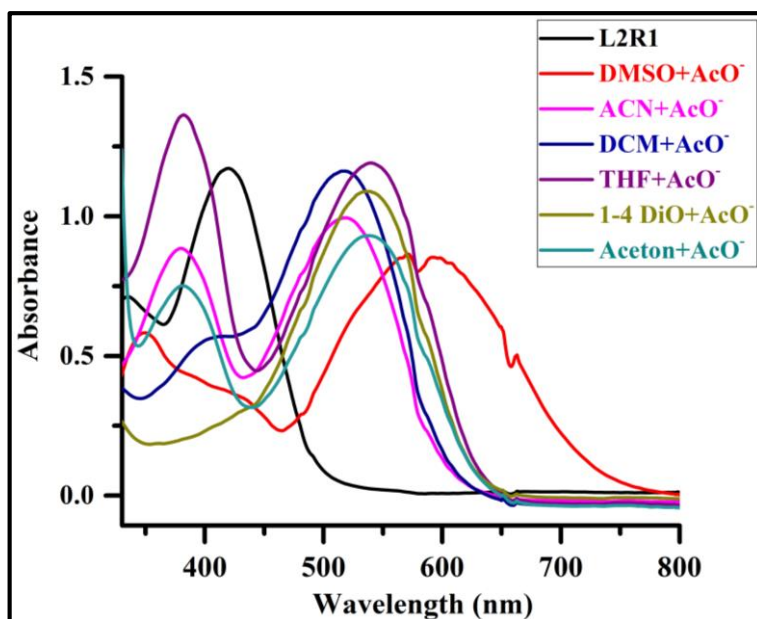
Fig. 3.53 Change in absorption spectra of **L2R1** (2×10^{-5} M) in the absence and presence of 2 equiv. of AcO$^-$ ion (1×10^{-2} M) in different aprotic solvents

Table 3.3 Change in the absorption band ($\Delta\lambda_{max}$) of receptor **L2R1** (2×10^{-5} M) in the presence of 2 equiv. of AcO$^-$ ion (1×10^{-2} M) in different aprotic solvents

Receptor L2R1 +Solvent	λ_{max}	$\Delta\lambda_{max}$
L2R1 +DMSO	610 nm	169 nm
L2R1 +ACN	515 nm	74 nm
L2R1 +DCM	512 nm	71 nm
L2R1 +THF	545 nm	104 nm
L2R1 +1-4 DIOX	535 nm	94 nm
L2R1 +ACETON	538 nm	97 nm

3.3.7 Cyclic voltammetry

The presence of NO$_2$, C=O, and –NH functionalities in the receptor **L2R1** created sufficient interest to investigate the impact of electrochemical reactions in the anion-binding process. The electrochemical responses of **L2R1** with AcO$^-$ were examined by cyclic voltammetry in acetonitrile medium using 0.01M

tetrabutylammonium perchlorate (TBAP) as the supporting electrolyte in the presence of three electrodes consisting of a platinized platinum (working), platinum wire (auxiliary), and saturated calomel (reference) electrodes. As shown in Fig. 3.54, the receptor **L2R1** displayed an oxidation peak at $+ 0.77$ V clearly indicating the role of $-$NH functionality in the oxidation process, and two reduction peaks at -0.85 V and -1.11 V corresponding to the reduction of keto (C=O) and nitro (NO$_2$) functionalities. With the gradual addition of AcO$^-$ ions, the oxidation peak showed a slight move to 0.81 V, and the reduction peak of NO$_2$ and keto functionality shifted to -0.82 V and -1.05 V suggesting the deprotonation of the –NH proton by the AcO$^-$ ion leaving the N$^-$ species behind (Pangannaya et al. 2018).
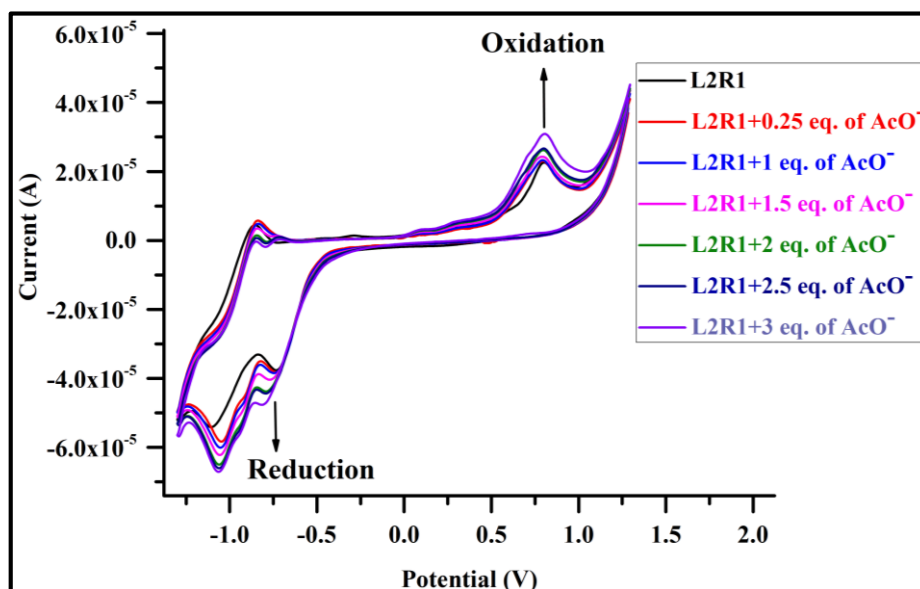
Fig. 3.54 Cyclic voltammogram of **L2R1** (4×10^{-5} M) with incremental addition of TBA$^+$AcO$^-$ ion (1×10^{-2} M in DMSO) in acetonitrile solution (0.25-3 equiv.)

3.3.8 ^{1}H NMR titration studies

To get insight into the binding mode of the interaction between **L2R1** and AcO$^-$ ion, ^{1}H NMR titration experiments were carried out in the DMSO- d$_6$. The free receptor **L2R1**, without the addition of anions, displayed an intense peak at 12.50 ppm indicating the N-H proton. Upon addition of 0.5 equiv. of AcO$^-$ ion, the peak at 12.50 ppm experienced a downfield shift along with broadening and decrease in intensity, and the peak at 8.69 ppm, corresponding to the imine C-H proton, exhibited an upfield shift as

illustrated in Fig. 3.55. The AcO⁻ ion initially formed a hydrogen bond with the –NH and the C-H protons. The upfield shift of the C-H proton was due to the increase in electron density on the aromatic ring upon interaction with the anions. Moreover, after the addition of 1 equiv. of AcO⁻ ion, the peak at 12.50 ppm vanished, suggesting deprotonation. This correlates with the fact that AcO⁻ ion induces deprotonation of the –NH proton. Further deprotonation was confirmed by the UV-Vis titration of **L2R1** with TBAOH. The results obtained from the ^{1}H-NMR titration experiments reflect the bifurcated hydrogen bond interaction of AcO⁻ with the -NH and C-H imine functionality, followed by deprotonation of the NH proton. This is likely due to the presence of the carbonyl group (C = O) adjacent to the NH proton and -NO$_2$ moiety at the para position of the phenyl ring, which makes the NH proton highly acidic and therefore, the **L2R1** is readily deprotonated in the presence of the basic AcO⁻ ion. This conclusion agrees well with that of (Evans et al. 2006) on the deprotonation of the highly acidic NH proton in the presence of AcO⁻ ion.
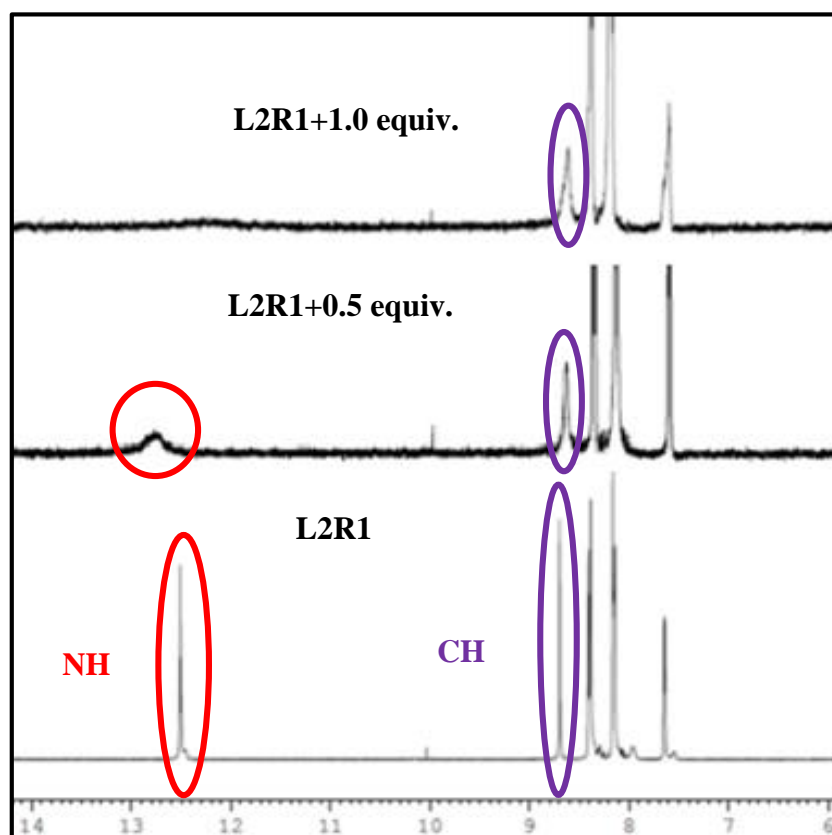
Fig. 3.55 ^{1}H-NMR titration spectra of **L2R1** in the absence and presence of different equiv. of TBA⁺AcO⁻ ion (0-1.0 equiv.) in DMSO- d$_6$

3.3.9 Binding mechanism

Based on the UV-Vis, Cyclic voltammetric, pH, and ^{1}H-NMR titration studies, the following binding mechanism was proposed. The addition of the strong basic AcO$^-$ ion initially led to bifurcated hydrogen bond interaction with NH and imine functionality with subsequent deprotonation of the NH proton. The deprotonation process often tends to increase the electron density by creating a charge separation in the receptor **L2R1** as seen in scheme 3.3. This facilitates ICT transition between the electron deficient NO$_2$ functionality at the para-position and the electron rich N$^-$ species resulting in optical colour change.
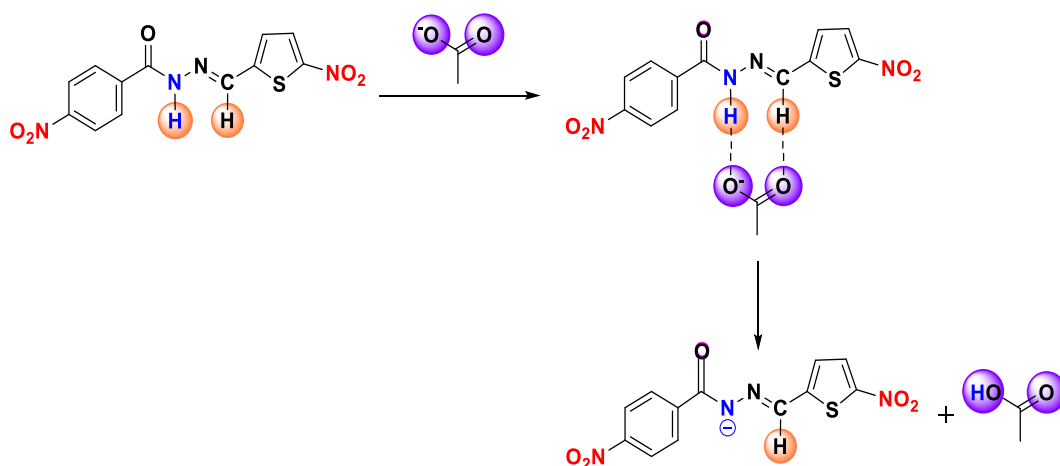
Scheme 3.3 Binding mode of **L2R1** with AcO$^-$ ion

3.3.10 Real-life application

The application of **L2R1** was demonstrated in real samples like toothpaste, mouthwash, and vinegar in aqueous medium. The toothpaste sample solution was prepared by adding 20 mg of commercially available toothpaste to 5 mL of distilled water, which was sonicated for 15 minutes. The mixture was then filtered. Upon addition of 1 drop of the toothpaste solution into 2 ml of the receptor solution, the colour of the solution changed from pale yellow to blue. Similar analysis was done using (2×10^{-5} M) of the receptor **L2R1** in DMSO and 5µl of commercially available vinegar solution. Like the toothpaste analysis, the introduction of 5µl vinegar altered the yellow colour of the receptor **L2R1** to blue as illustrated in Fig. 3.56. Thus, the observation

reflects the practical utility of the receptor **L2R1** in real- time samples by sensing F⁻ and AcO⁻ ions in aqueous mediums in toothpaste, mouthwash, vinegar, and seawater.

Fig. 3.56 Photograph of colour change of **L2R1** upon addition of one drop of commercially available products
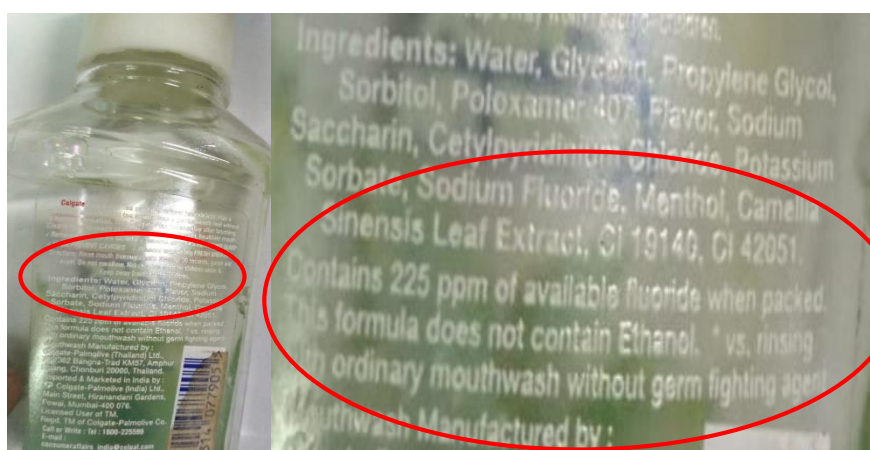
Fig. 3.57 Photograph of mouthwash contain 225 ppm of sodium fluoride

With the above results, the receptor **L2R1** was further utilized for the quantitative detection of F⁻ ion present in commercial mouthwash as illustrated in Fig. 3.57. For experimental studies, seawater was collected from the Arabian Sea (Latitude13°0'33.99", Longitude 74°47'17.23"). The amount of F⁻ ions in seawater/mouthwash was evaluated using a calibration curve, which was established by plotting absorbance *vs.* various standard concentration of Na^+F^- ion (1×10^{-2} M in distilled H_2O) as depicted in Fig. 3.58. A set of standard solution of Na^+F^- was prepared in a standard flask. The absorbance at 620 nm for each solution was recorded. The mouthwash sample was diluted by 50 times before analysis. Hence, the value obtained from the standard plot was multiplied by the proper dilution factor to calculate the

actual fluoride ion concentration in the mouthwash. The curve showed 1.59 ppm of F^- ions in seawater (215.5 ppm in mouthwash), which is comparable with the standard values (WHO Technical Report, 1994).
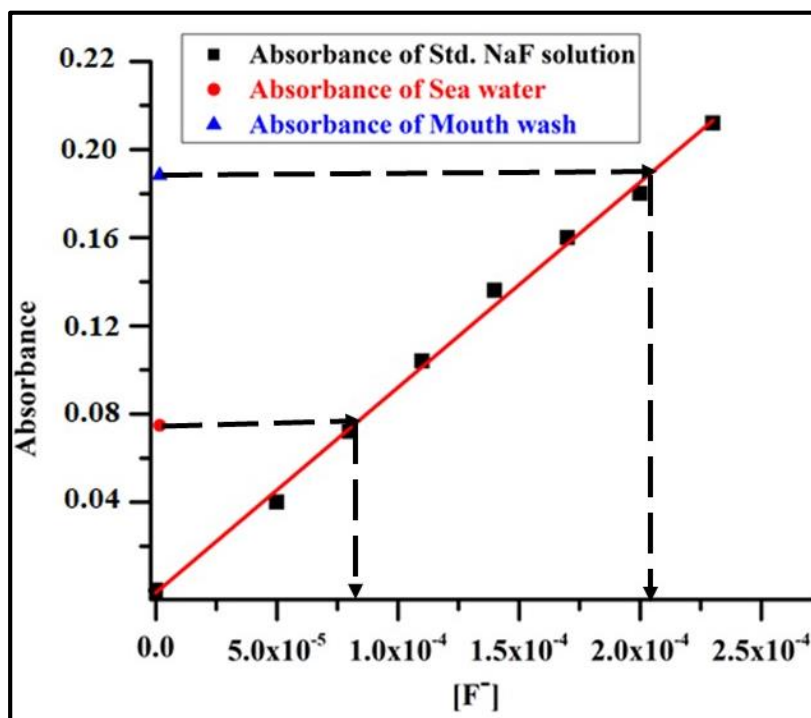
Fig. 3.58 Calibration curve for determination of F^- ion in seawater/mouthwash

3.3.11 Analytical application (Test strip)

To explore the practical implementation of the chemosensor, a test strip was prepared to check the practical application of **L2R1** by immersing (Whatman filter paper 42) into the DMSO solution of the receptor **L2R1** (2×10^{-5} M), followed by drying in a hot oven to determine the suitability of the "Dip-Stick" method for on-field detection of F^- and AsO_2^- ions. After complete drying, 0.5 equiv. and 1.0 equiv. of F^- and AsO_2^- ions was added to the coated test strip. Instantaneous colour change was observed from pale yellow to blue for the F^- and AsO_2^- ions as shown in Fig. 3.59. It was noted that as the concentration of F^- ion increased from 0.5 equiv. to 1.0 equiv., the colour of the test strip changed from light blue to dark blue. Thus, significant change in the colour of the paper strips clearly suggests the potential analytical application of the receptor **L2R1** for the detection of F^- ion in DMSO and AsO_2^- ion in aqueous medium.

| L2R1 | L2R1+F⁻ 0.5 equiv. | L2R1+F⁻ 1.0 equiv. | L2R1 | L2R1+AsO₂⁻ 0.5 equiv. | L2R1+AsO₂⁻ 1.0 equiv. |

Fig. 3.59 Colour changes observed on addition of 0.5 equiv. and 1.0 equiv. of F⁻ and AsO₂⁻ ions on test strip coated with **L2R**1 solution

3.4   CONCLUSION

In conclusion, a good yield of the four new receptors **L2R1-L2R4** was designed and synthesized with different substituents by simple condensation reaction. In the organic media, the receptor **L2R1** was found to be selective against F⁻, AcO⁻, and $H_2PO_4^-$ ions solely based on the following factors: (1) the receptor's intrinsic acidity due to the presence of two nitro substituents, and (2) the anion's basicity. In contrast, it was highly capable of sensing inorganic F⁻, AcO⁻, AsO_2^-, and AsO_4^{2-} in aqueous medium with lower detection limit of 0.392 ppm, 0.823 ppm, 0.643 ppm, and 0.721 ppm, highlighting the efficacy of the nitro group in fine tuning the colorimetric response of the receptor **L2R1** proves its utility as a chemosensor. The ^{1}H-NMR titration and cyclic voltammetric experiments confirmed the deprotonation of the NH proton suggesting that only one proton was transferred to the AcO⁻ ion supported by the B-H plot 1:1 binding ratio between **L2R1** and the AcO⁻ ion. The anion binding studies of the receptor **L2R1** in DMSO: HEPES buffer (9:1 v/v, pH 7.35) media exhibited selective detection of AcO⁻ ion with blue colouration. The receptor **L2R1** possess high selectivity for inorganic F⁻ ion with detection limit of 0.392 ppm in aqueous medium, which is much is much lower than the WHO permissible level (1 ppm) in drinking water. Additionally, **L2R1** proved itself a potential colorimetric chemosensor for qualitative and quantitative detection of fluoride ion in seawater and commercial mouthwash. Finally, it served as a practical colorimetric sensor in recognizing F⁻ and AsO_2^- ions using a test strip. To sum up, based on UV-Vis spectroscopic studies, ^{1}HNMR titration studies and electrochemical studies receptor **L2R1** could be regarded as efficient colorimetric chemosensors for anions.

CHAPTER 4

DESIGN AND SYNTHESIS NEW COLORIMETRIC RECEPTORS FOR NAKED-EYE DETECTION OF BIOLOGICALLY IMPORTANT FLUORIDE AND ACETATE ANIONS IN ORGANIC AND ARSENITE IN AQUEOUS MEDIUM BASED ON ICT MECHANISM: DFT STUDY AND TEST STRIP APPLICATION
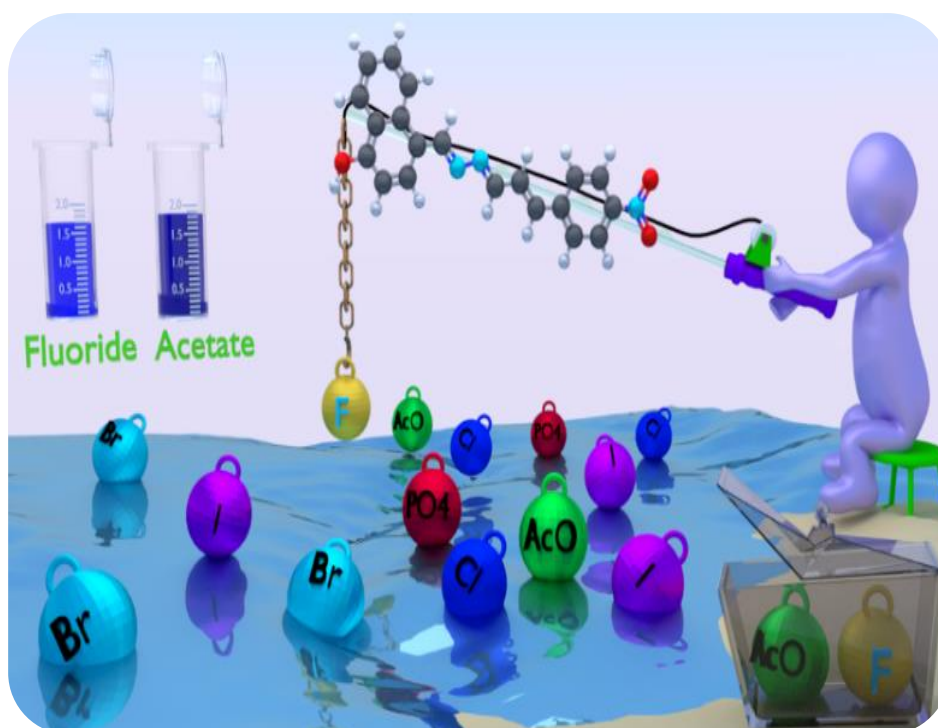
Abstract: *In this chapter, the design and syntheses of new receptors **L3R1**, **L3R2,** and **L3R3** is described and are characterized using standard spectroscopic techniques. The anion binding properties of the receptors are studied and confirmed by UV-Vis spectrophotometric, ^{1}H-NMR titration, and cyclic voltammetric studies. The plausible binding mechanism of the receptors towards active anion is proposed.*

4.1   INTRODUCTION

Colorimetric receptors with high selectivity, sensitivity, easy, and safe to handle have received significant attention and thus, a number of these have been reported for the detection of biologically important anions such as fluoride and acetate due to their physiological effects (Cho et al. 2005; Duke and Gunnlaugsson 2011; Jose et al. 2004; Piątek and Jurczak 2002; Ros-Lis et al. 2007; Sakai et al. 2012). Until recently, numerous receptors featuring binding site-signalling unit approach have been reported, most of which are restricted to working in organic solvents (Kubik 2010). Higher solvation energy of the anion in aqueous media results in restricted interaction between the host and the guest (Bencini et al. 2012; Huang et al. 2012; Wang et al. 2011). Therefore, there is need to strategically design receptors capable of detecting anions by surpassing the constraint of the aqueous media. Among all anions, arsenic (in the form of anions) is extremely toxic and lethal for living organisms. It exists in four oxidation states as As (V), As (III), As(0), and As (-3) in the environment (Hasegawa et al. 1999). In water, it mostly appears as oxyanions in both organic and inorganic forms (Sharma and Sohn 2009; Smedley and Kinniburgh 2002). The two inorganic forms of arsenic, viz., arsenite or As (III) and arsenate or As (V) are very toxic and can result in many adverse health effects such as dermatitis, and skin lungs, liver, bladder, and renal cancer (Hughes et al. 2011; Xu et al. 2018).

In the present work, three colorimetric receptors **L3R1**, **L3R2,** and **L3R3** have been designed and synthesized by the Schiff base condensation reaction. The synthesized receptors **L3R1** and **L3R2** have extended π-conjugation and -OH functionality in ortho- and para-positions. In particular, the nitro moiety and conjugate units in the receptors have been introduced as well-known chromophore units, which can enhance the chromogenic response of the receptors when reacting with anions

leading to a noticeable shift in the absorption band. Generally, the nature and position of the binding site and signalling unit play a key role in the chromogenic response of the anion detection process. Interestingly, the synthesized receptors can detect biologically important anions such as fluoride and acetate present in the form of TBA salts in organic (DMSO) and important inorganic salts such as NaF and NaAcO, and the most toxic arsenite in the organo-aqueous (DMSO: H_2O, 9:1 v/v) by naked eye with high selectivity, which should attract researchers to their importance in biological and environmental arenas. To elucidate the role of the -OH proton as a binding site for the sensing of anions, the receptor **L3R3** was synthesized without -OH functionality as shown in Scheme 4.1.
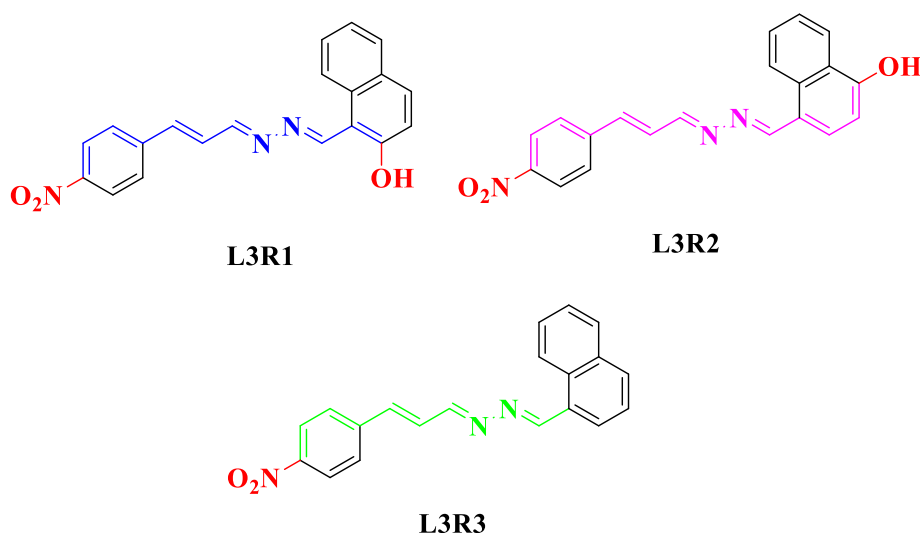
Scheme 4.1 Structural representation of receptors **L3R1**, **L3R2** and **L3R3**

4.2 EXPERIMENTAL SECTION

4.2.1 Material and methods

All the chemicals and tetrabutylammonium salts were purchased from Loba, Sigma-Aldrich and Alfa aesar and used without further purification. The ^{1}H-NMR spectra were recorded on the Bruker, Avance (400 MHz) instrument using Tetramethylsilane (TMS) as an internal standard and DMSO-d_6 as the solvent. ^{13}C NMR spectra were recorded on Bruker Ascend (125 MHz) instrument using TMS as internal reference and DMSO-d_6. Resonance multiplicities are described as s (singlet), d (doublet), t (triplet), and m (multiplet). The melting points were determined with the

Stuart-SMP3 melting-point apparatus in open capillaries. The infrared spectrum was recorded on the Bruker Apex FTIR spectrometer. The UV-Vis titration was performed in the Analytikejena Specord S600 in 3.00 ml quartz cells with 1 cm path length. The completion of the reaction was confirmed by checking with the TLC plates. Mass-spectral data was obtained using the ESI-QToF (Waters-synapt G2S) high-resolution mass spectrometer. Cyclic voltammogram was recorded on the Ivium electrochemical workstation (Vertex) at a scan rate of 20 mV/s with potential range of 1.0 V to −1.0 V.

4.2.2 Synthesis of intermediate S 4.1

The 4-nitrocinnamaldehyde (6.65 mmol) was treated with hydrazine hydrate (33.29 mmol) in the presence of ethanol and kept overnight at room temperature for stirring. The solid formed was filtered and washed with cooled ethanol, and dried to give a yellow colour intermediate product. The reaction is represented in Scheme 4.2.
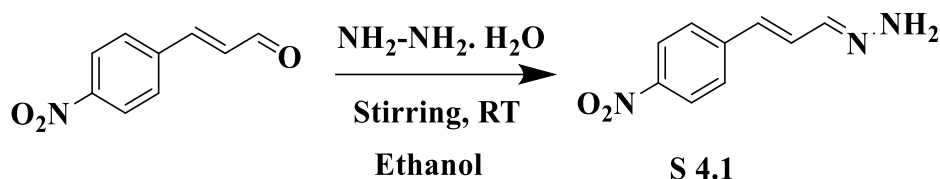
Scheme 4.2 Synthesis of intermediate **S 4.1**

4.2.3 Synthesis of the receptors L3R1, L3R2 and L3R3

The receptors **L3R1**, **L3R2**, and **L3R3** were synthesized by initiating a reaction between the intermediate **S 4.1** (0.75 mmol) and aldehyde substitutes such as 2-hydroxy-1-naphthaldehyde (1.5 mmol), 4-hydroxy-1-naphthaldehyde (1.5 mmol) and 1-naphthaldehyde (2.0 mmol) in methanol by adding 2-3 drops of acetic acid (CH_3CO_2H) as catalyst. The reaction mixture was refluxed at 60ºC for 6 h by continuous stirring. After completion of the reaction, the precipitate was filtered and washed several times with cold ethanol to obtain the desired products **L3R1, L3R2,** and **L3R3** as represented in Scheme 4.3.
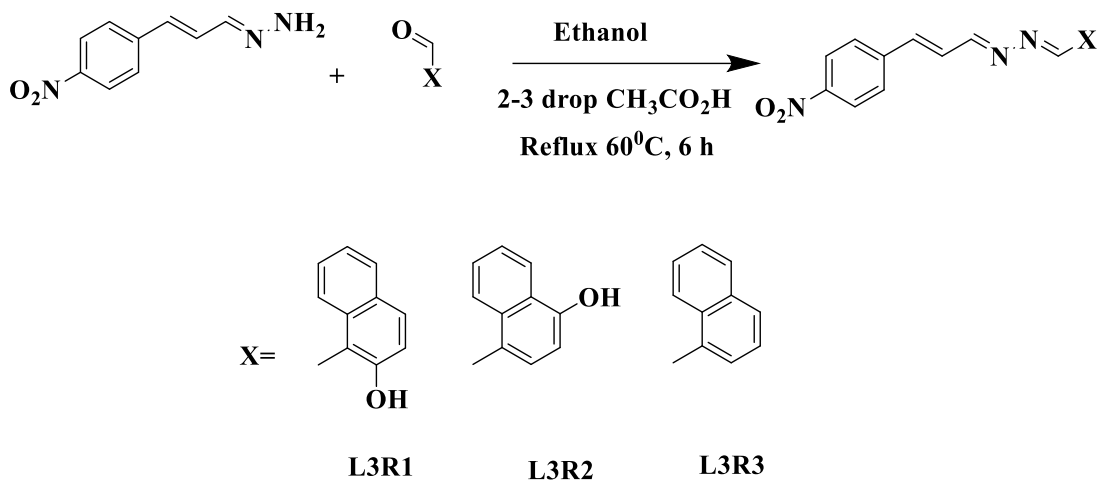
Scheme 4.3 Synthesis of the receptors **L3R1, L3R2** and **L3R3**

4.2.4   Calculation of binding constant based on UV-Vis titration data

Binding constant has been calculated using Benesi-Hildebrand equation (Benesi and Hildebrand 1948) as given below (Eq. 4.1).

$$\frac{1}{(A-A_0)} = \frac{1}{(A_{max}-A_0)} + \frac{1}{K[X^-]^n (A_{max}-A_0)} \ldots \ldots \ldots \ldots (Eq.\,4.1)$$

Where, A_0, A, and A_{max} are the absorption considered in the absence of anion, at intermediate and at concentration of saturation, respectively, K is the binding constant, $[X^-]$ is the concentration of the anion, and n is the stoichiometric ratio.

4.2.5   Calculation of LOD

The detection limit of the receptors **L3R1** and **L3R2** with the anions was calculated using equation (Eq. 4.2).

$$LOD = \frac{3 \times \sigma}{s} \ldots \ldots \ldots \ldots \ldots \ldots \ldots \ldots . (Eq.\,4.2)$$

Where, σ is the standard deviation of the calibration curve (SD), and s is the slope of the calibration curve.

4.2.6 Characterization data

The purity and structure of the intermediate **S 4.1** and receptors **L3R1, L3R2** and **L3R3** were confirmed by FT-IR, ^{1}H-NMR, ^{13}C-NMR, and mass spectroscopic methods. The characterization data has been compiled and given below.

(E)-((E)-3-(4-nitrophenyl)allylidene) hydrazine (S 4.1)
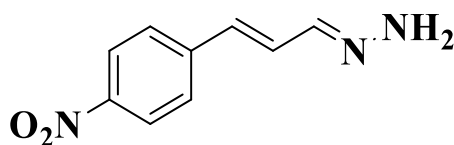
Data obtained for S 4.1: Yield: 80%. m.p: 200 ^{0}C. ^{1}H NMR (DMSO-d_6, 400 MHz, Me$_4$Si): δ_{ppm} 8.166-8.144 (d, 2H), 7.740-7.718 (d, 2H), 7.550-7.527 (d, 1H), 7.235 (s,2H) 7.136-7.073 (m, 1H), 6.721-6.681 (s, 1H). ^{13}C NMR (DMSO-d_6, 125 MHz, Me$_4$Si): δ_{ppm} 146.20, 144.68, 139.32, 132.75, 128.12, 127.27, 124.45. Mass (ESI): m/z calculated for $C_9H_9N_3O_2$: 191.07 Obtained: 192.0934 [M+H]$^+$. IR (KBr pellet) (cm^{-1}): 3317 (NH$_2$), 1328 (C=C), 1672 (CH=N), 736 (C-H), 1251 (NO$_2$) cm^{-1}.

1-((E)-(((1E,2E)-3-(4-nitrophenyl)allylidene)hydrazono)methyl)naphthalene-2-ol: (L3R1)
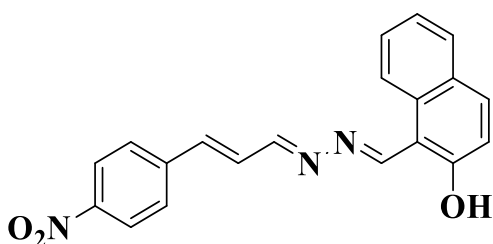
Data obtained for L3R1: Yield: 80%. m.p: 250 ^{0}C. ^{1}H NMR (DMSO-d_6, 400 MHz, Me$_4$Si): δ_{ppm} 13.051-12.895 (d,1H), 10.005-9.710 (d, 1H), 8.706-8.543 (m, 1H), 8.461-8.284 (m, 1H), 8.461-8.284 (m, 1H), 8.033-8.055 (m, 1H), 8.024-7.646 (m, 4H), 7.609-7.646 (m,1H), 7.646-7.596 (m, 1H), 7.304-7.452 (m, 2H), 7.244-7.281 (m, 1H). ^{13}C NMR (DMSO-d_6, 125 MHz, Me$_4$Si): δ_{ppm} 161.73, 160.53, 135.23, 129.40, 129.14, 128.49, 128.49, 128.34, 124.57, 124.32, 122.27, 119.37, 108.95. Mass (ESI): m/z

calculated for $C_{20}H_{15}N_3O_2$: 345.11 Obtained: 346.1548 [M+H]$^+$. IR (KBr pellet) (cm^{-1}): 3425 (OH), 2923 (C-H), 1602 (CH=N), 1385 (symmetrical NO_2), 1021 (N-N).

4-((E)-(((1E,2E)-3-(4-nitrophenyl)allylidene)hydrazono)methyl)naphthalene-1-ol: (L3R2)
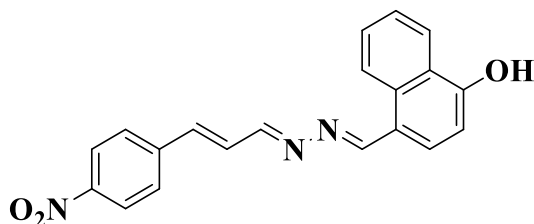
Data obtained for L3R2: Yield: 80%. m.p: 255 ^{0}C. ^{1}H NMR (DMSO-d$_6$, 400 MHz, Me$_4$Si): δ$_{ppm}$ 11.092 (s,1H), 9.181-8.621 (m, 1H), 8.601-8.266 (m, 1H), 8.250-8.244 (m, 1H), 7.963-7.924 (m, 1H), 7.684-7.648 (m, 3H), 7.584-7.546 (m, 3H), 7.502-7.462 (m,1H), 7.439-7.402 (m ,2H), 7.384-6.987 (m,1H). ^{13}C NMR (DMSO-d$_6$, 125 MHz, Me$_4$Si): δ$_{ppm}$ 168.49, 162.30, 157.80, 147.69, 142.75, 140.32, 134.23, 132.72, 130.37, 128.89, 128.56, 125.76, 125.20, 124.56, 123.19, 108.58. Mass (ESI): m/z calculated for $C_{20}H_{15}N_3O_2$: 345.11 Obtained: 346.1548 [M+H]$^+$. IR (KBr pellet) (cm^{-1}): 3426 (OH), 1126 (N-N), 1612 (CH=N), 1329 (symmetrical NO_2), 2925 (C-H), 1588-1512 (C=C).

(1E,2E)-1-(naphthalene-1-ylmethylene)-2-((E)-3-(4-nitrophenylallylidene) hydrazine (L3R3)
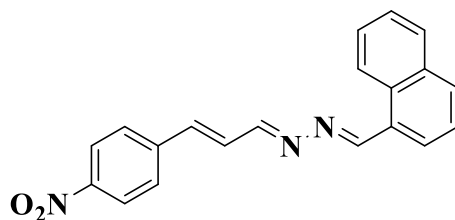
Data obtained for L3R3: Yield: 80%. m.p: 210 ^{0}C. ^{1}H NMR, (DMSO-d$_6$, 400 MHz, Me$_4$Si): δ$_{ppm}$ 9.447 (s,2H), 9.210-9.189 (d, 2H), 8.194-8.079 (m, 3H), 8.059-7.941 (m, 1H), 7.736-7.652 (m, 1H), 7.634-7.461 (m, 5H), 7.424-7.362 (m, 1H). ^{13}C NMR, (DMSO-d$_6$, 125 MHz, Me$_4$Si): δ$_{ppm}$ 163.51, 162.49, 162.43, 147.84, 142.54, 141.35, 134.06, 134.02, 132.61, 132.44, 131.14, 131.10, 130.90, 130.02, 129.70, 129.52,

129.31, 129.04, 128.13, 126.94, 126.02, 125.57, 125.32, 124.56. Mass (ESI): m/z calculated for $C_{20}H_{15}N_3O_2$: 329.12 Obtained: 330.1690 $[M+H]^+$. IR (KBR) (cm^{-1}): 2920-2852 (strong C-H stretch), 1710-1602 (CH=N), 1572 (C=C), 1364-1320 (symmetrical NO_2).

The representative spectrum of intermediate **(S 4.1)** and receptors **L3R1, L3R2** and **L3R3** is shown below
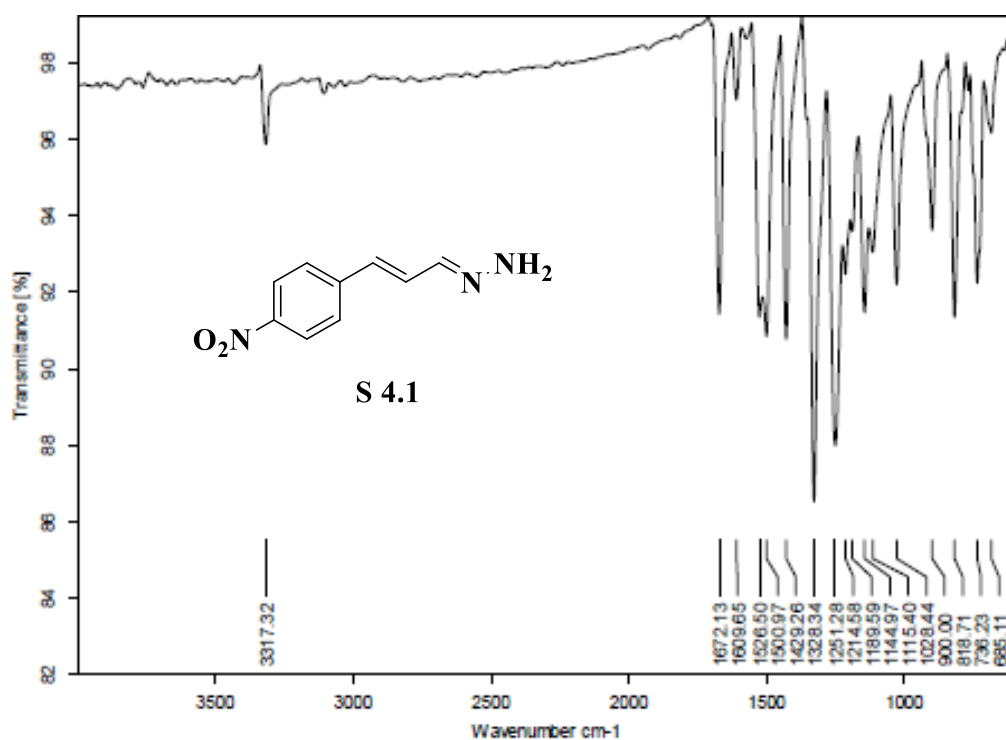
Fig. 4.1 FT-IR spectrum of intermediate **S 4.1**
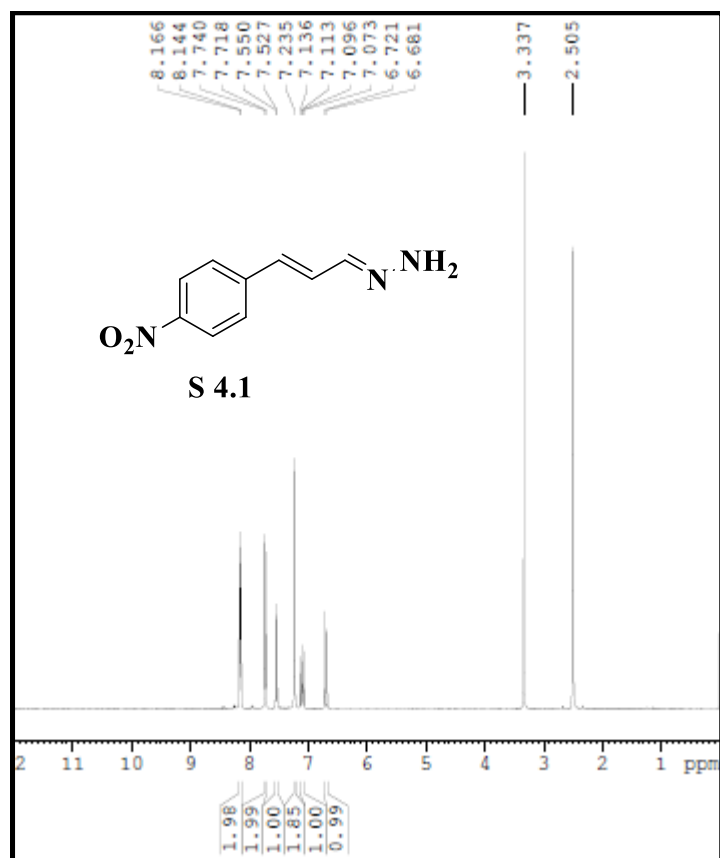
Fig. 4.2 ^{1}H-NMR spectrum of intermediate **S 4.1**

Fig. 4.3 ^{13}C-NMR spectrum of intermediate **S 4.1**

Mass spectrum of: S 4.1

Exact Mass: 191.07

Mass obtained in the positive mode: 192.0934

Elemental composition: $C_9H_9N_3O_2$
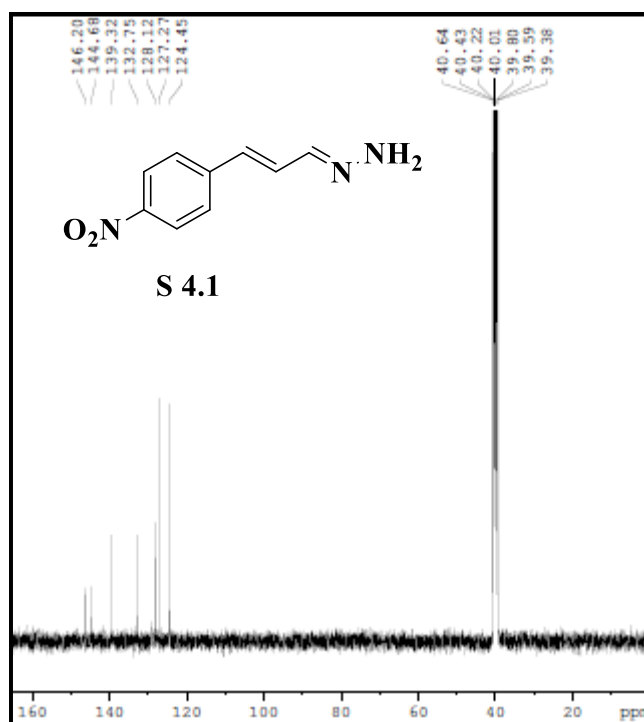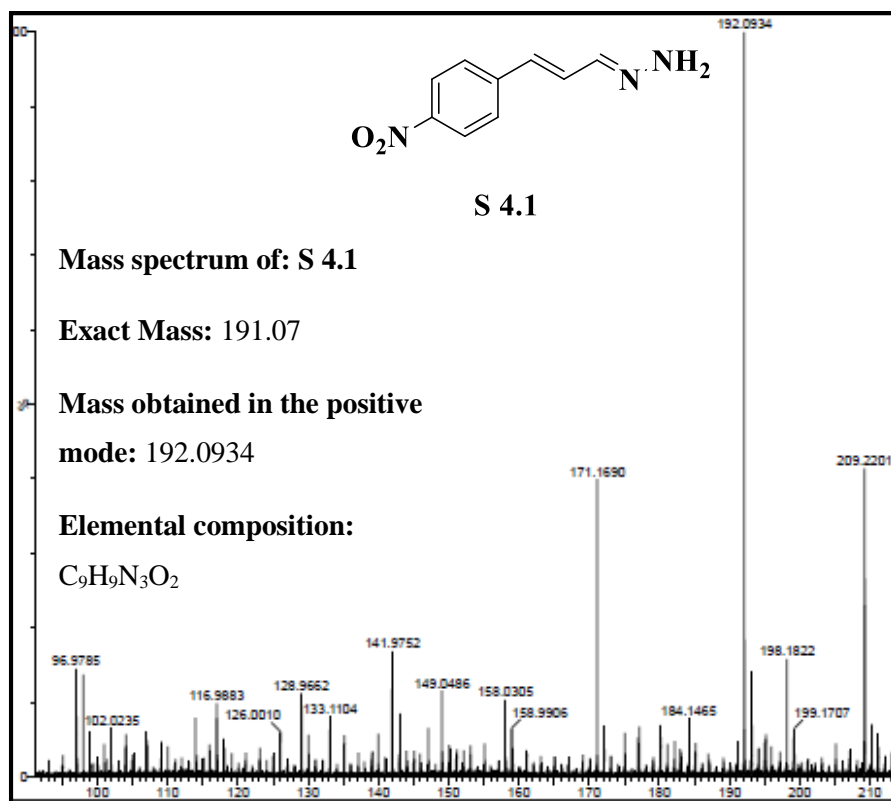
Fig 4.4 ESI-MS spectrum of receptor **S 4.1**
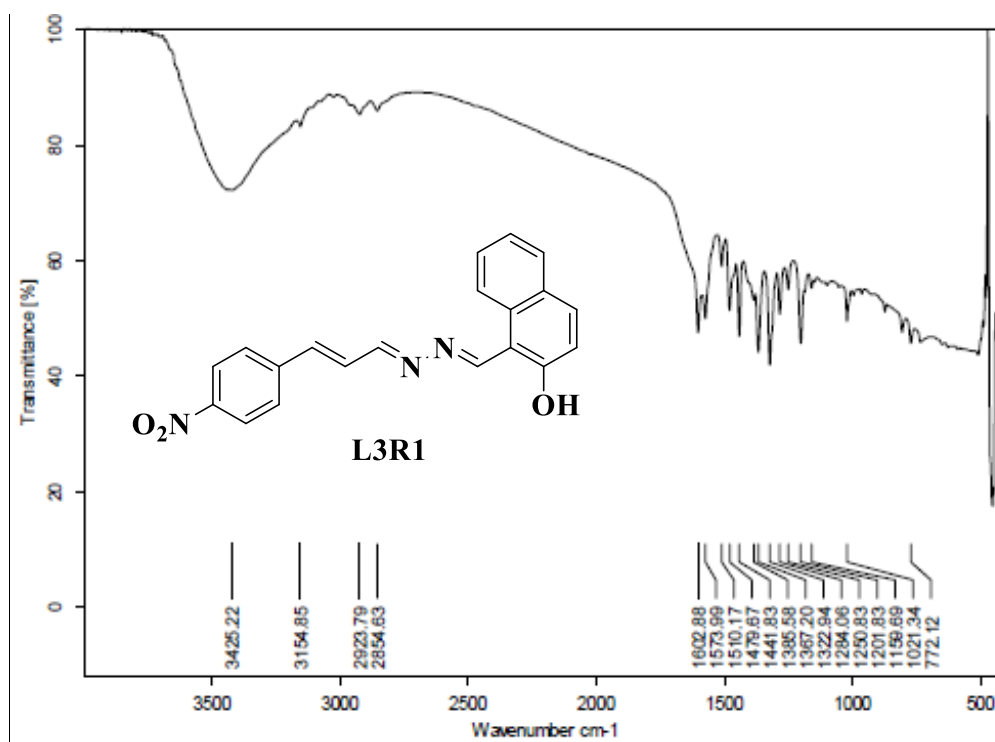
Fig 4.5 FT-IR spectrum of receptor **L3R1**
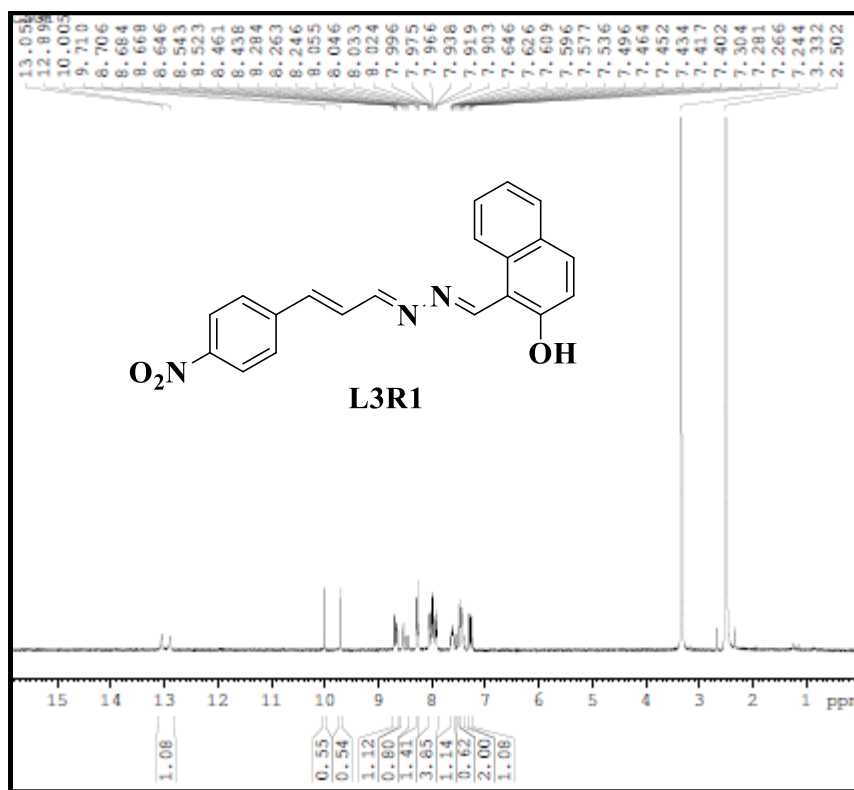
Fig. 4.6 ^{1}H-NMR spectrum of receptor **L3R1**

Fig. 4.7 ^{13}C-NMR spectrum of receptor **L3R1**

Mass spectrum: L3R1

Exact Mass: 345.11

Mass obtained in the positive mode: 346.1548

Elemental composition: $C_{20}H_{15}N_3O_3$
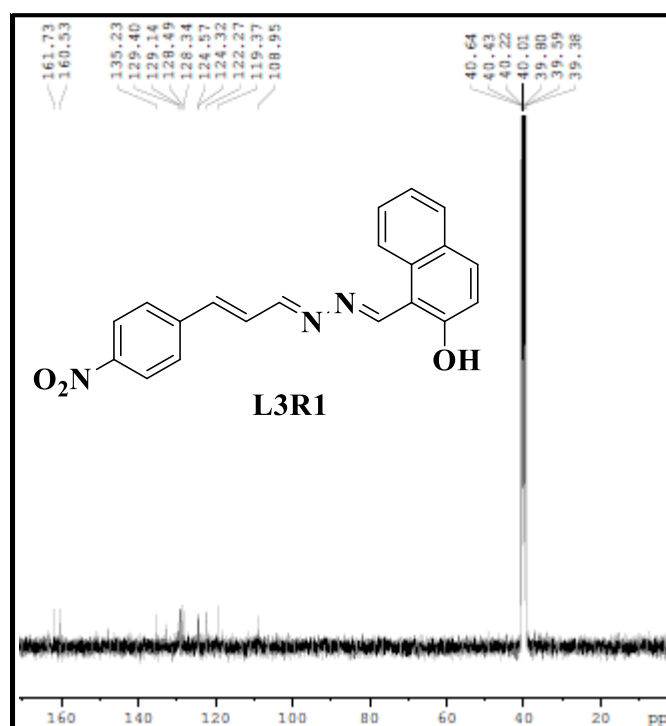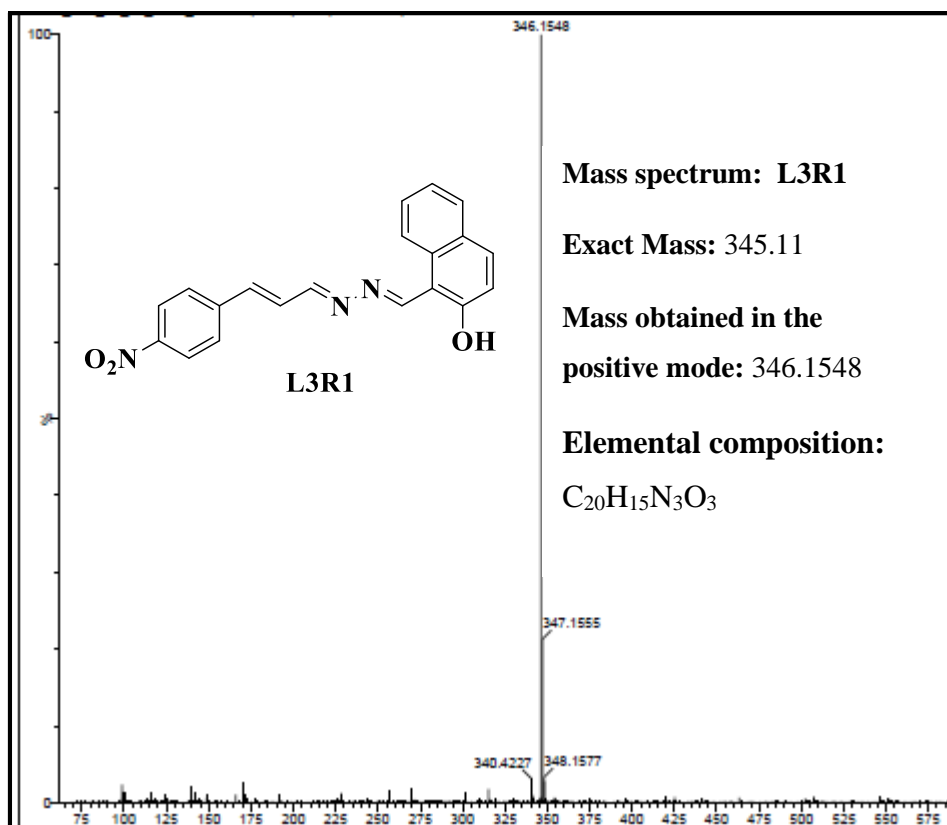
Fig. 4.8 ESI-MS spectrum of receptor **L3R1**
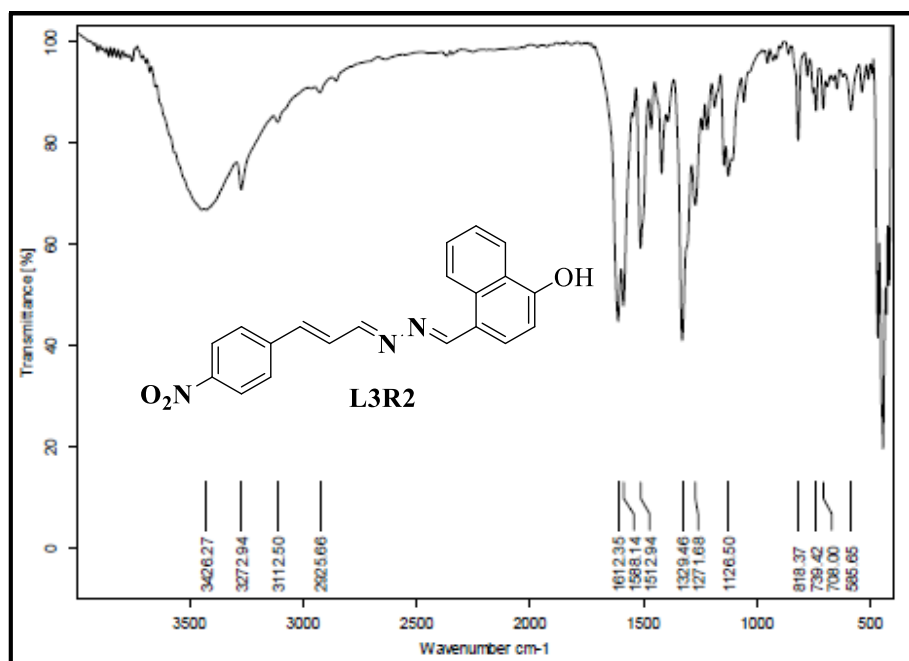
Fig. 4.9 FT-IR spectrum of receptor **L3R2**
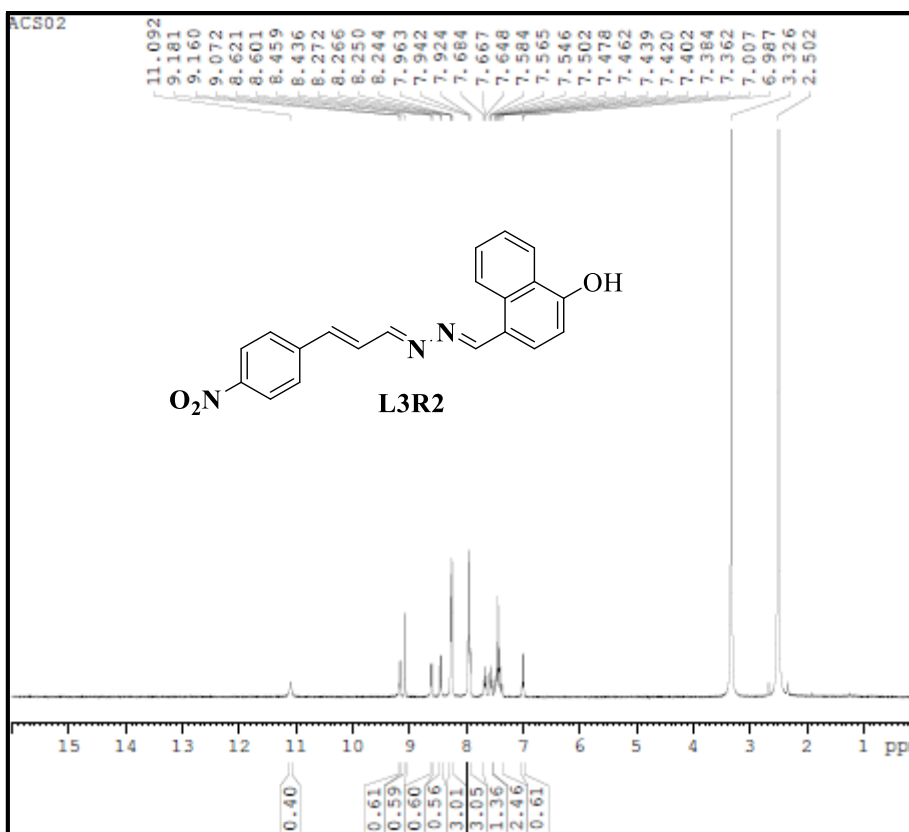
Fig. 4.10 ^{1}H-NMR spectra of receptor **L3R2**

Fig. 4.11 ^{13}C-NMR spectrum of receptor **L3R2**

Mass spectrum: L3R2

Exact Mass: 345.11

Mass obtained in the positive mode: 346.1548

Elemental composition: $C_{20}H_{15}N_3O_3$
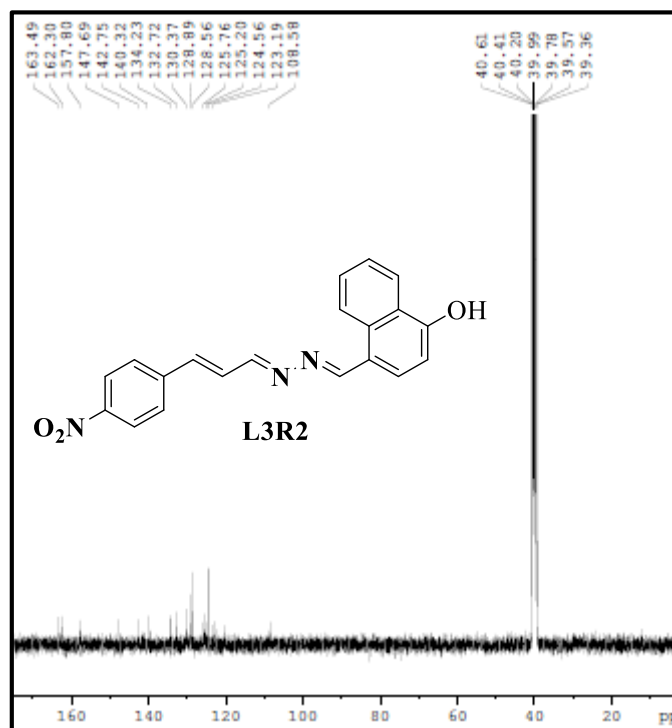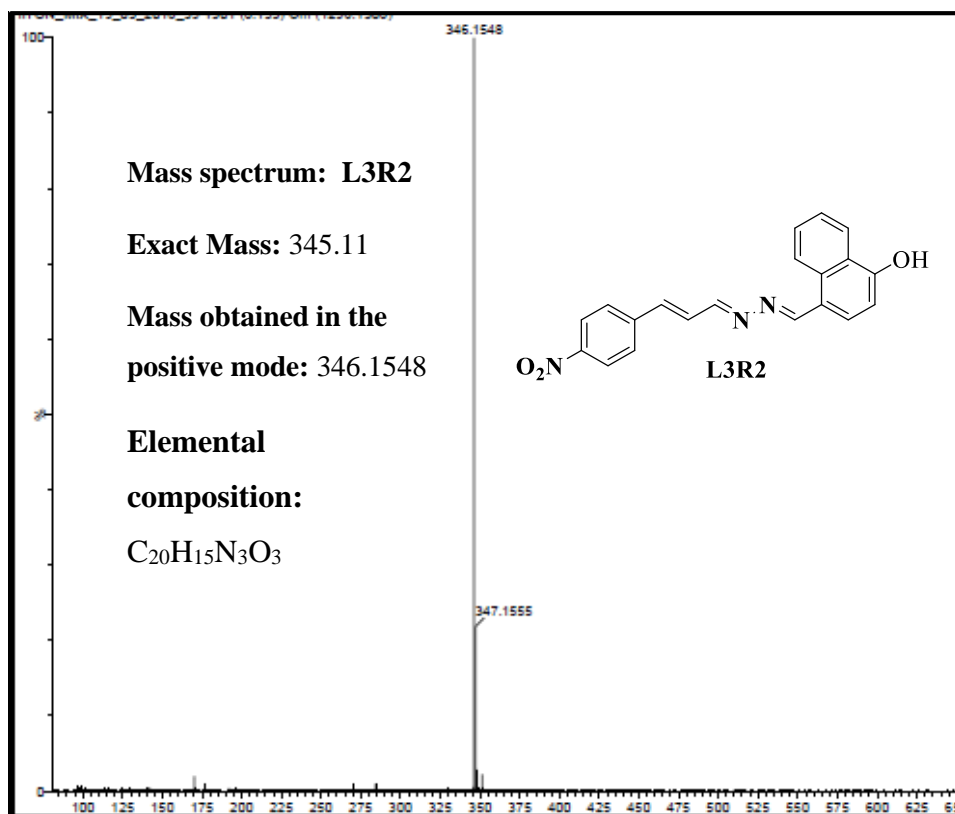
Fig. 4.12 ESI-MS spectrum of receptor **L3R2**
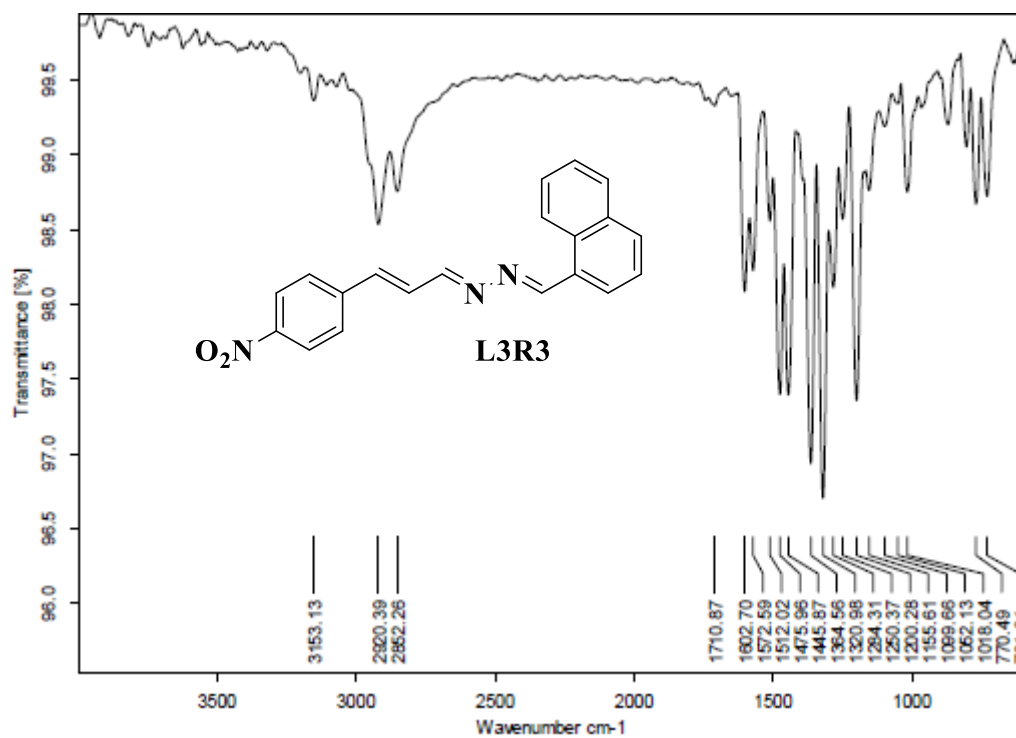
Fig. 4.13 FT-IR spectrum of receptor **L3R3**
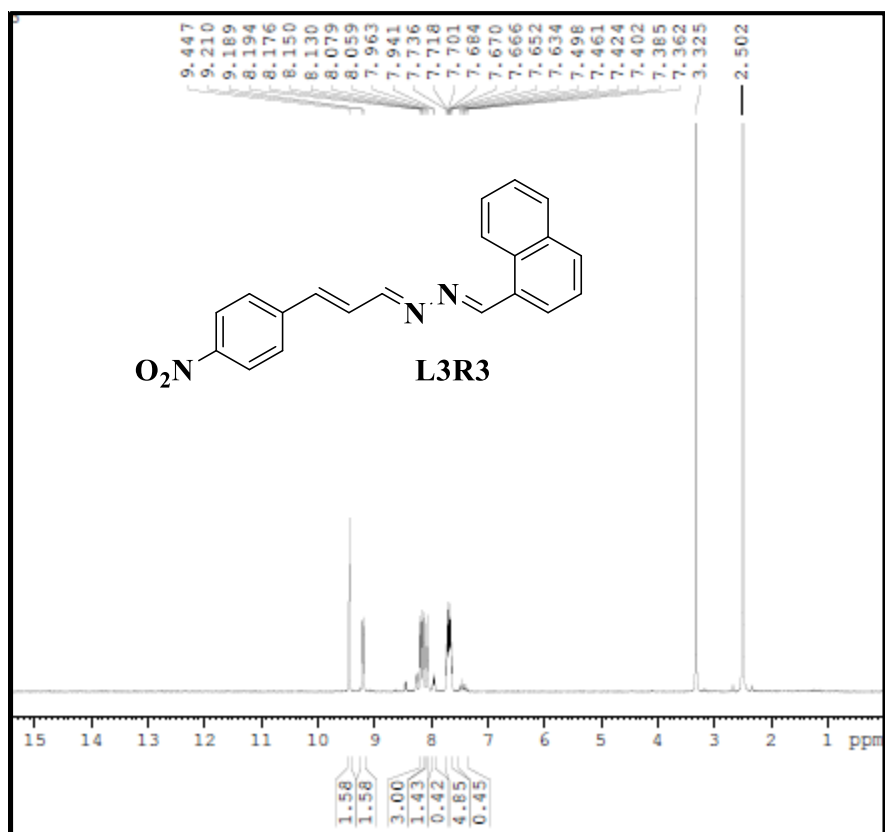
Fig. 4.14 ^{1}H-NMR spectrum of receptor **L3R3**

Fig. 4.15 ^{13}C-NMR spectrum of receptor **L3R3**

Mass spectrum: L3R3

Exact Mass: 329.12

Mass obtained in the positive mode: 330.1690

Elemental composition: $C_{20}H_{15}N_3O_2$
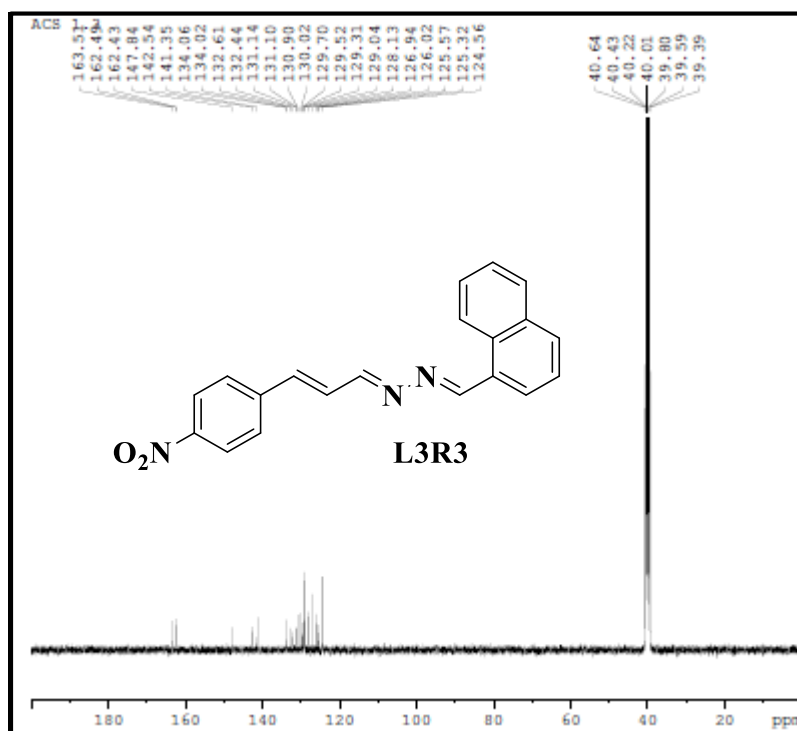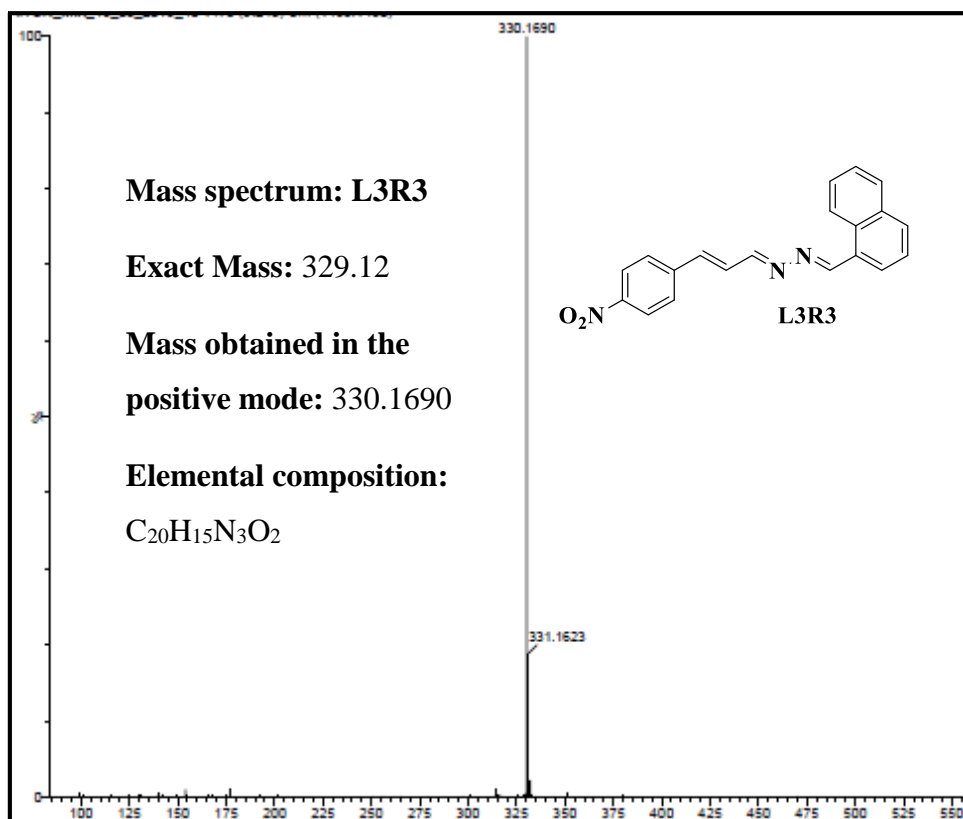
Fig. 4.16 ESI-MS spectrum of receptor **L3R3**

4.3 RESULTS AND DISCUSSION

4.3.1 Colorimetric detection of anions

Primarily, to 2 mL of test solutions of **L3R1** and **L3R2** in DMSO of concentration (1×10^{-5} M DMSO), 2 equiv. of tetrabutylammonium salts of anions such as F⁻, Cl⁻, Br⁻, I⁻, NO_3^-, $H_2SO_4^-$, $H_2PO_4^-$, AcO⁻ (1×10^{-2} M in DMSO) were added. **L3R1** and **L3R2** exhibited visual colorimetric response from pale yellow to purple and from pale yellow to blue towards F⁻ and AcO⁻ ions as illustrated in Fig. 4.17 and the corresponding UV-Vis spectra is shown in Fig. 4.18, Fig. 4.19 and Fig. 4.20. Only the F⁻ and AcO⁻ ions induced distinct spectral change, while the other tested anions failed to induce any spectral changes. On the other hand, due to the lack of an anion-binding -OH proton, **L3R3** did not show any change in either colour or UV-Vis spectra. This proves receptors **L3R1** and **L3R2** can serve as naked-eye colorimetric sensor for the detection of F⁻ and AcO⁻ ions.
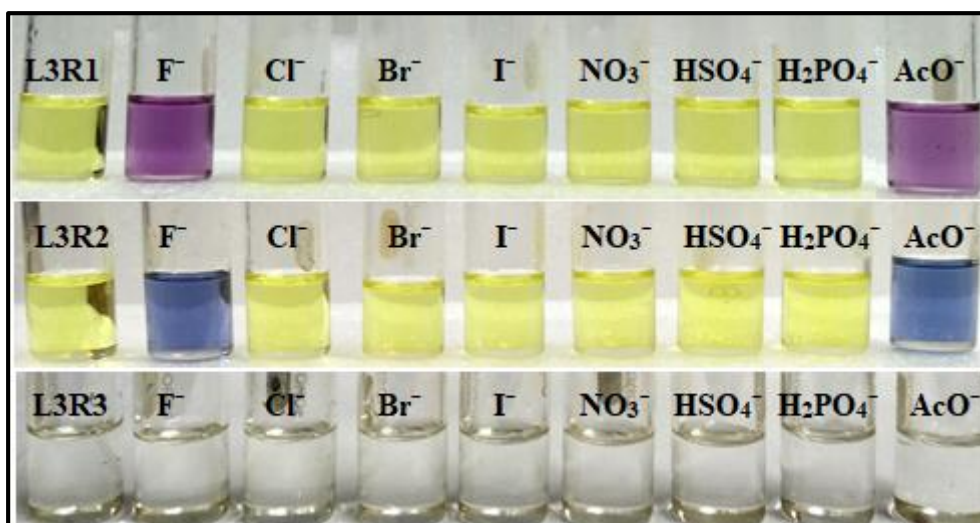
Fig. 4.17 Colour change seen for **L3R1-L3R3** (1×10^{-5} M DMSO) after addition of a series of TBA salts (1×10^{-2} M DMSO)
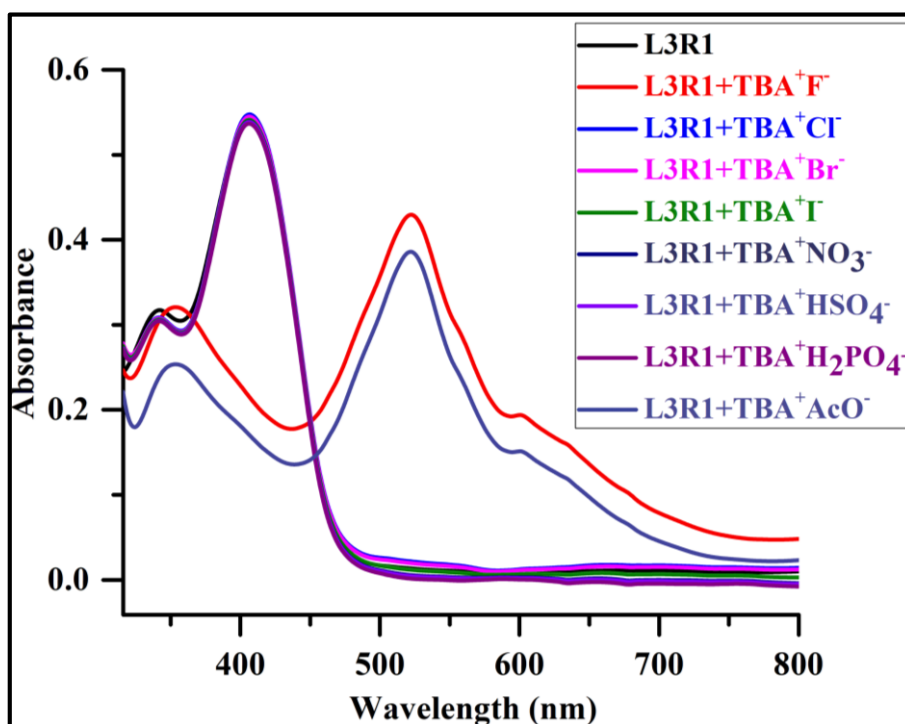
Fig. 4.18 UV-Vis spectral change of **L3R1** (1×10^{-5} M DMSO) after adding 2 equiv. of various anions as TBA salts (1×10^{-2} M DMSO)
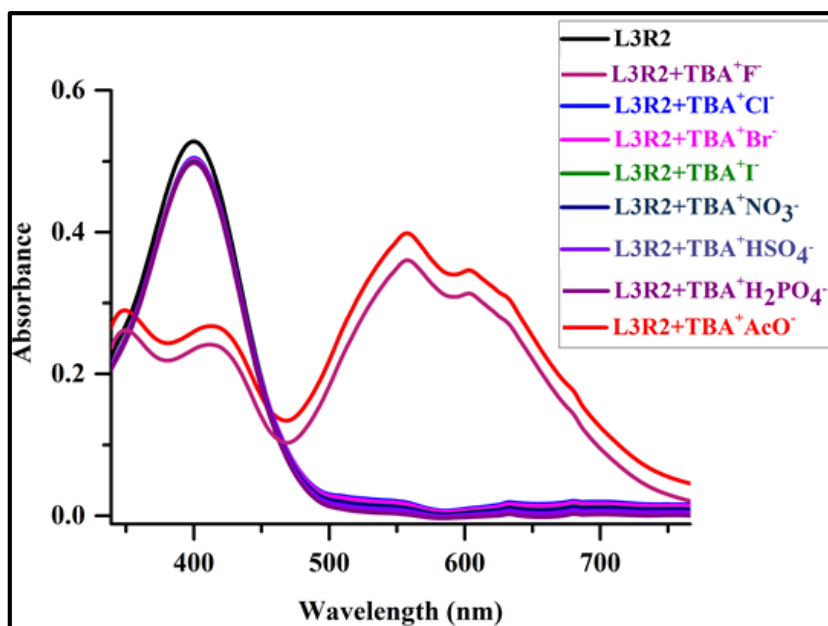
Fig. 4.19 UV-Vis spectral change of **L3R2** (1×10^{-5} M DMSO) after adding 2 equiv. of various anions as TBA$^+$ salts (1×10^{-2} M DMSO)
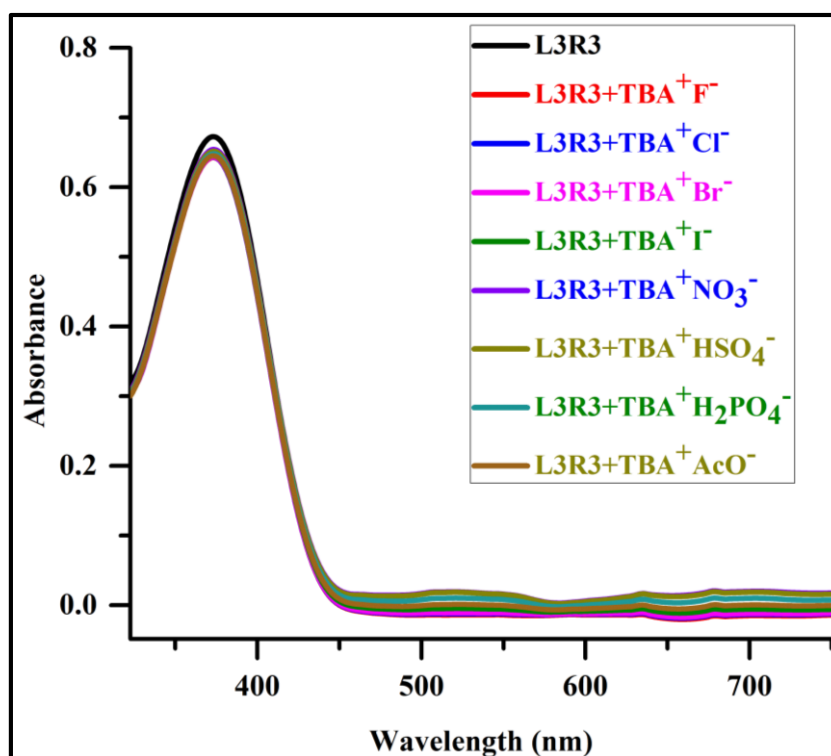
Fig. 4.20 UV-Vis spectral change of **L3R3** (1×10^{-5} M DMSO) after adding 2 equiv. of various anions as TBA$^+$ salts (1×10^{-2} M DMSO)

4.3.2 UV-Vis titration studies of the receptors L3R1 and L3R2 in DMSO

To further investigate the binding property of the -OH proton at the ortho-position of the receptor **L3R1** (1×10^{-5} M DMSO) with F$^-$ and AcO$^-$ ions, UV-Vis titration experiments were performed as portrayed in Fig. 4.21 and Fig. 4.22. The DMSO solution of the receptor **L3R1** was yellow due to the presence of a band at 407 nm. Upon incremental addition of 0.1 equiv. of F$^-$ and AcO$^-$ ions, this band progressively decreased, while new absorption bands at 521 nm ($\Delta\lambda_{max} = 114$ nm) and 518 nm ($\Delta\lambda_{max} = 111$ nm) increased with clear isosbestic points at 453 nm and at 451 nm correspondingly indicating the intramolecular charge transfer interaction within the receptor. The formation of this new visible band induced a change in colour from pale yellow to purple.

Similarly, titration for the receptor **L3R2** was conducted to figure out the role of the -OH proton in the anion binding process at the para-position. The UV-Vis spectrum of **L3R2**, exhibited maximum absorption band at around 398 nm, which was assigned to the π–π* transition of the chromophores. As the concentration of F$^-$ and AcO$^-$ ions increased from 0.1 equiv. to 2.0 equiv., the intensity of the absorption band at 398 nm decreased and new absorption bands at 557 nm and 560 nm gradually increased in the visible region as depicted in Fig. 4.23 and Fig. 4.24. At the same time, clear isosbestic points were observed at 460 nm and 462 nm, implying the conversion of the free receptor **L3R2** to a **L3R2**+F$^-$/ **L3R2**+AcO$^-$ complex.

Compared to the receptor **L3R1**, **L3R2** showed significant bathochromic shift ($\Delta\lambda_{max}$) of 159 nm and 162 nm when F$^-$ and AcO$^-$ ions were added. These experimental results clearly show that **L3R2** is more favourable towards the intramolecular charge transfer (ICT) between the anion-----OH units at the para- position and the electron deficient nitro moiety. The binding stoichiometry of the receptors **L3R1** and **L3R2** with the F$^-$ and AcO$^-$ ions was evaluated to be 1:2 and 1:1 as confirmed by the B-H plot depicted in Fig. 4.25 and Fig. 4.26.
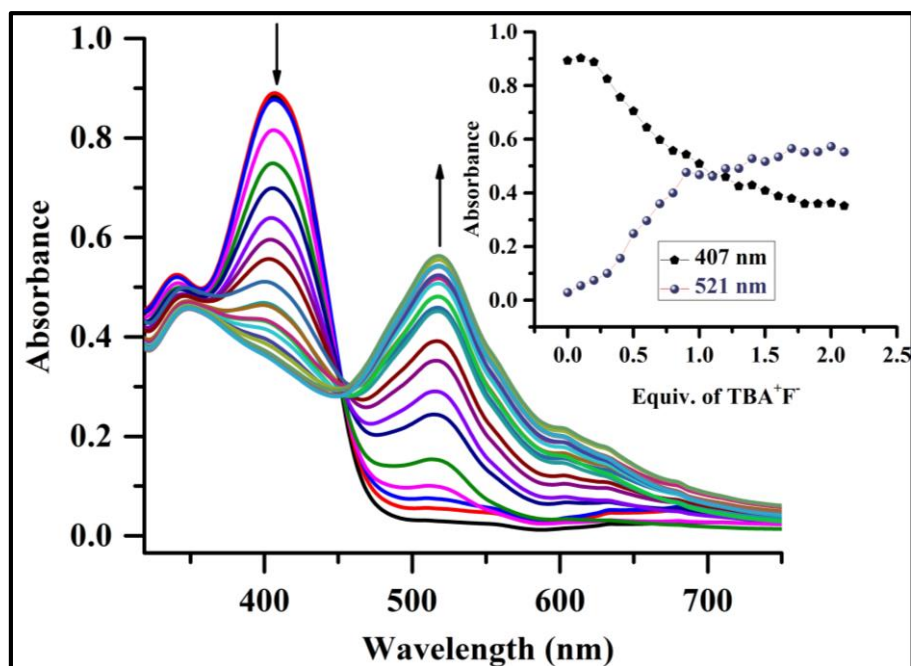
Fig. 4.21 UV-Vis absorption changes of **L3R1** (1×10^{-5} M in DMSO) upon sequential addition of TBA⁺F⁻ (1×10^{-2} M in DMSO); Inset attributed to the equiv. addition of TBA⁺F⁻ at particular wavelength of 407 nm and 521 nm
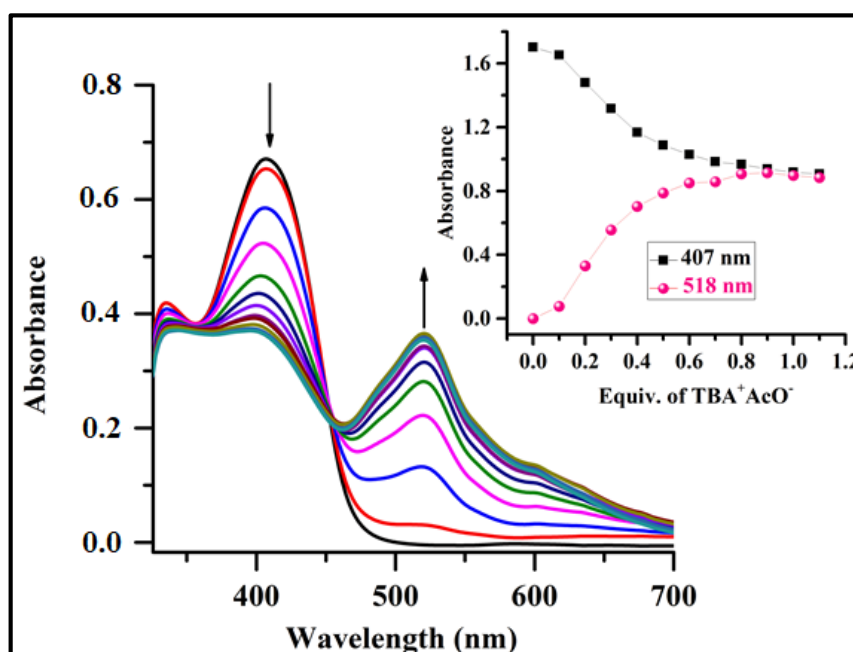
Fig. 4.22 UV-Vis absorption changes of **L3R1** (1×10^{-5} M in DMSO) upon sequential addition of TBA⁺AcO⁻ (1×10^{-2} M in DMSO); Inset attributed to the equiv. addition of TBA⁺AcO⁻ at particular wavelength of 407 nm and 518 nm
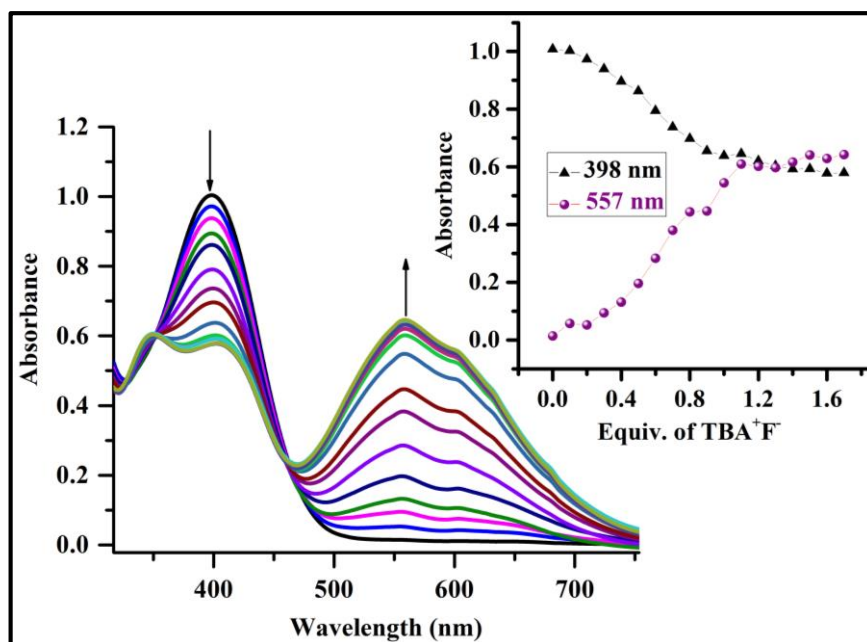
Fig. 4.23 UV-Vis absorption changes of **L3R2** (1×10^{-5} M in DMSO) upon sequential addition of TBA$^+$F$^-$ (1×10^{-2} M in DMSO); Inset attributed to the equiv. addition of TBA$^+$F$^-$ at particular wavelength 398 nm and 557 nm
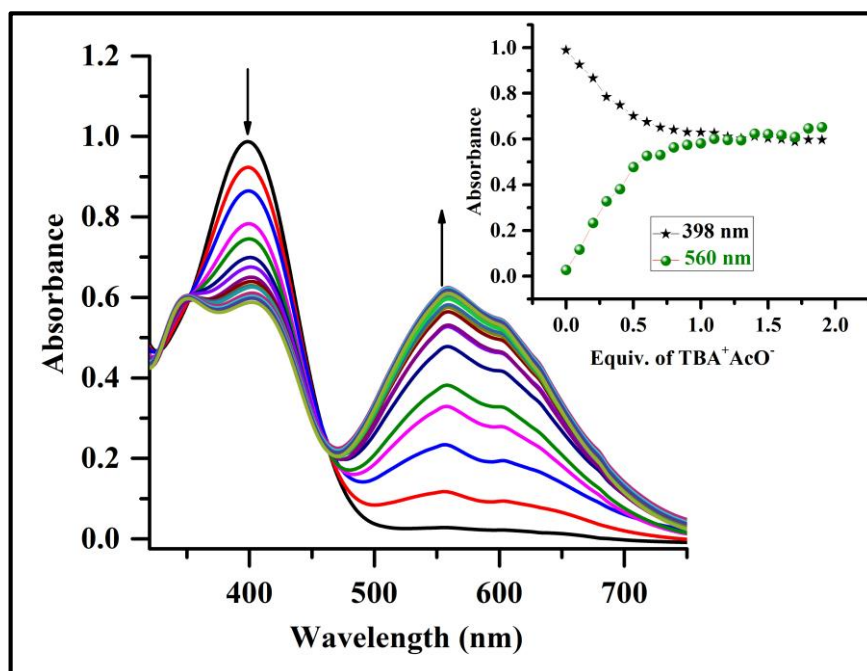
Fig. 4.24 UV-Vis absorption changes of **L3R2** (1×10^{-5} M in DMSO) upon sequential addition of TBA$^+$AcO$^-$ (1×10^{-2} M in DMSO); Inset attributed to the equiv. addition of TBA$^+$AcO$^-$ at particular wavelength 398 nm and 560 nm
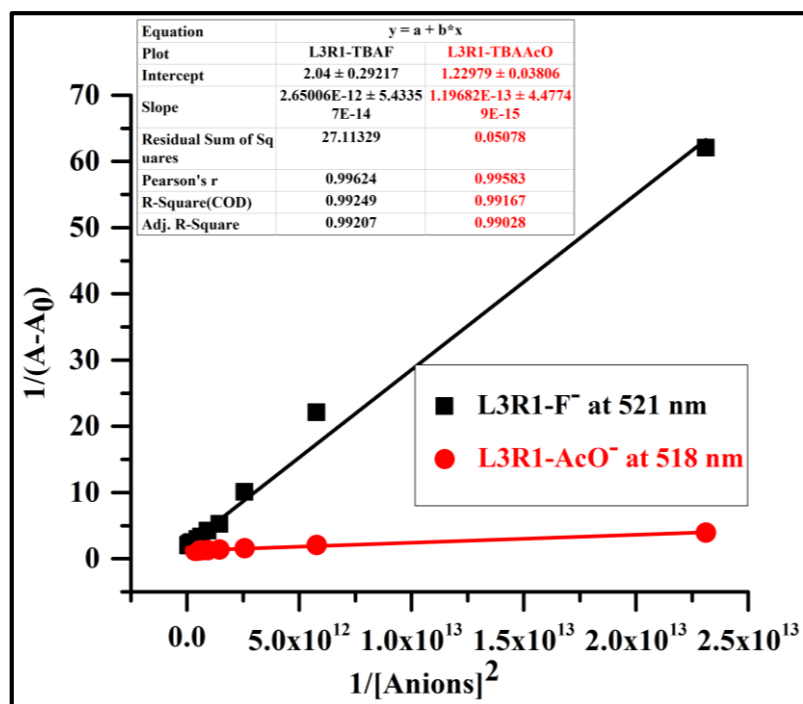
Fig. 4.25 B-H plot of the receptor **L3R1**-F⁻ and the **L3R1**-AcO⁻ complex at a selected wavelength of 521 nm and 518 nm in DMSO
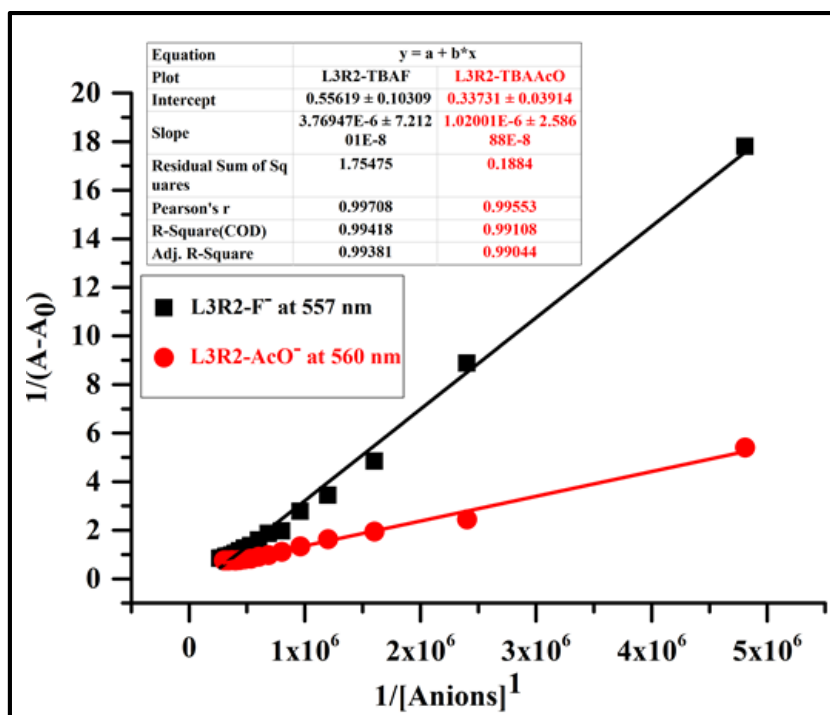
Fig. 4.26 B-H plot of the receptor **L3R2**-F⁻ and the **L3R2**-AcO⁻ complex at a selected wavelength of 557 nm and 560 nm in DMSO

4.3.3 UV-Vis titration study of receptors L3R1 and L3R2 using sodium salts in DMSO: H$_2$O (9:1 v/v)

The detection of anions in an aqueous medium is always challenging due to their high hydration free energy and solvent interference in the binding process. In this regard, in the present study, it was decided to check the binding and sensing ability of **L3R1** and **L3R2** in the organo-aqueous media DMSO: H$_2$O (9:1 v/v), towards different series of sodium salts such as F$^-$, Cl$^-$, Br$^-$, I$^-$, NO$_3^-$, HSO$_4^-$, H$_2$PO$_4^-$, AcO$^-$, and AsO$_2^-$ (1×10^{-2} M in distilled water). Interestingly, upon addition of 2 equiv. of different anions present in the form of sodium salts to the receptors **L3R1** and **L3R2** solution of concentration (1×10^{-5} M in DMSO: H$_2$O (v/v), only F$^-$, AcO$^-$, and AsO$_2^-$ induced incredible colour change from pale yellow to purple and from pale yellow to blue as presented in Fig. 4.27. The observed colour changes reflect the corresponding red shift in the absorption spectra as seen in Fig. 4.28 and Fig. 4.29. However, shift in the λ_{max} was not noticed with the addition of other anions involved in the present study.
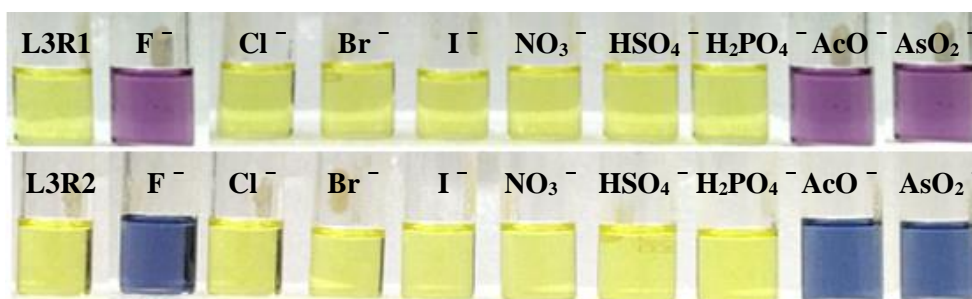
Fig. 4.27 Receptors **L3R1** and **L3R2** (1×10^{-5} M in DMSO) showing colour change upon addition of 2 equiv. of sodium salts (1×10^{-2} M in distilled water) in DMSO: H$_2$O (9:1 v/v)

As shown in Fig. 4.30, Fig. 4.31, and Fig. 4.32, with incremental addition of 0.1 equiv. of F$^-$, AcO$^-$, and AsO$_2^-$ ions, the maximum absorption band at 407 nm red shifted to the longer wavelength 516 nm, 513 nm, and 517 nm, respectively. Distinct single isosbestic points were observed at 451 nm, 449 nm, and 453 nm indicating the presence of two species such as **L3R1** and the complex of **L3R1** with the added anions of F$^-$, AcO$^-$, and AsO$_2^-$ in the DMSO: H$_2$O (9:1 v/v).

In order to elucidate the binding mechanism of F⁻, AcO⁻, and AsO₂⁻ ions with **L3R2**, UV–Vis titration experiments were performed wherein the band centred at 398 nm decreased in intensity with the gradual appearance of new red shift bands at 553 nm, 555 nm, and 565 nm, respectively. Meanwhile, single isosbestic points were observed at 458 nm, 460 nm, and 460 nm, indicating that the receptor **L3R2** interacted with the F⁻, AcO⁻, and AsO₂⁻ ions to produce a stable complex. The titration profiles are given in Fig. 4.33, Fig. 4.34, and Fig. 4.35. This reflects the ability of the receptors **L3R1** and **L3R2** to detect F⁻, AcO⁻, and AsO₂⁻ ions in an organo-aqueous medium. The B-H plot indicated a 1:2 and 1:1 binding interaction between the receptors **L3R1**/ **L3R2** and F⁻, AcO⁻, and AsO₂⁻ in (DMSO: H₂O 9:1 v/v) as represented in Fig. 4.36 and Fig. 4.37. The bathochromic shift ($\Delta\lambda_{max}$) of the receptors **L3R1** and **L3R2** upon addition of 2 equiv. of TBA salts of F⁻ and AcO⁻ in (DMSO) and the sodium salts of F⁻, AcO⁻ and AsO₂⁻ in the DMSO: H₂O (9:1 v/v) are summarized in Table 4.1.
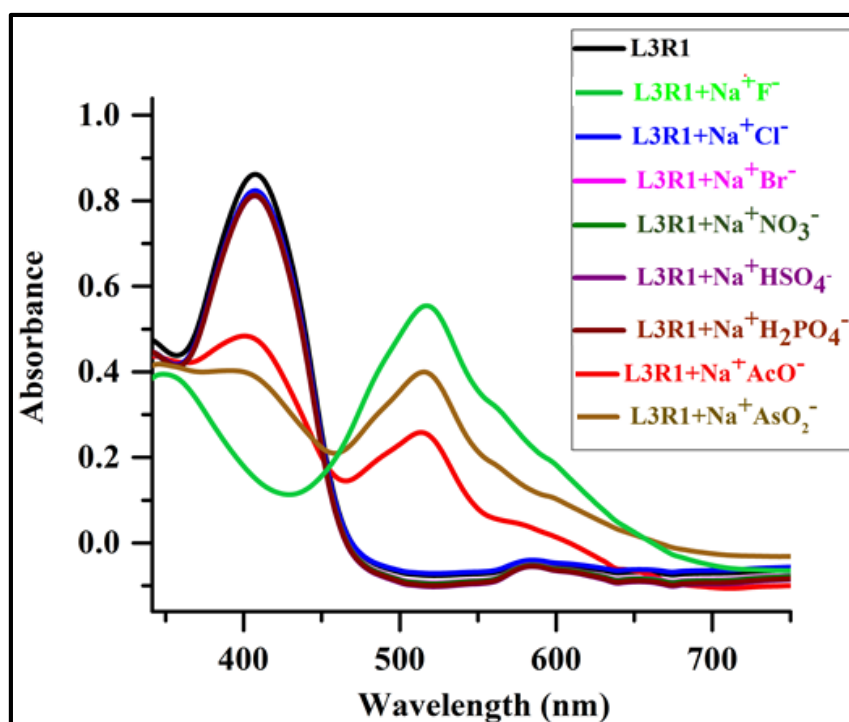
Fig. 4.28 UV-Vis spectral change of **L3R1** (1×10^{-5} M in DMSO) after adding 2 equiv. of Na⁺ salts (1×10^{-2} M in distilled water) in DMSO:H₂O (9:1 v/v)
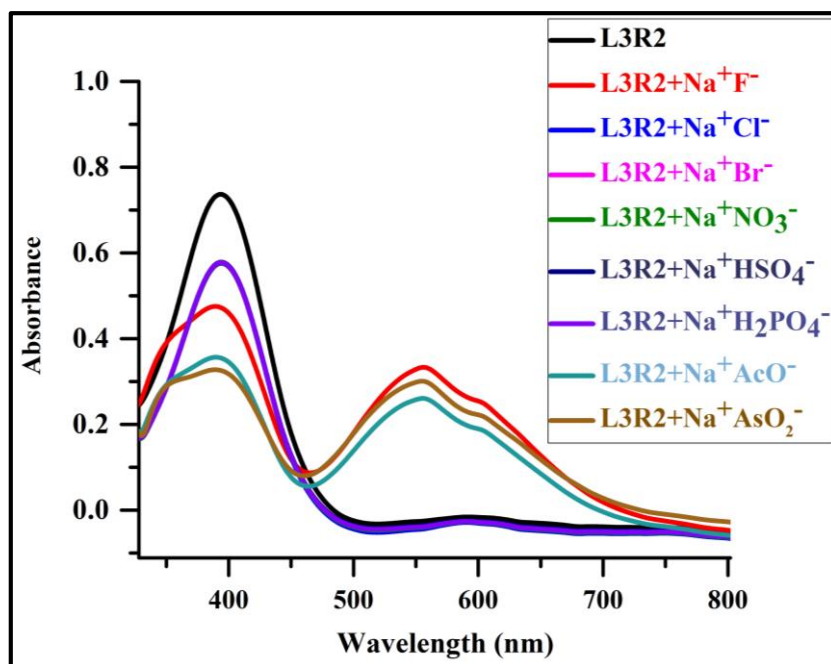
Fig. 4.29 UV-Vis spectral change of **L3R2** (1×10^{-5} M in DMSO) after adding 2 equiv. of Na^+ salts (1×10^{-2} M in distilled water) in DMSO:H_2O (9:1 v/v)
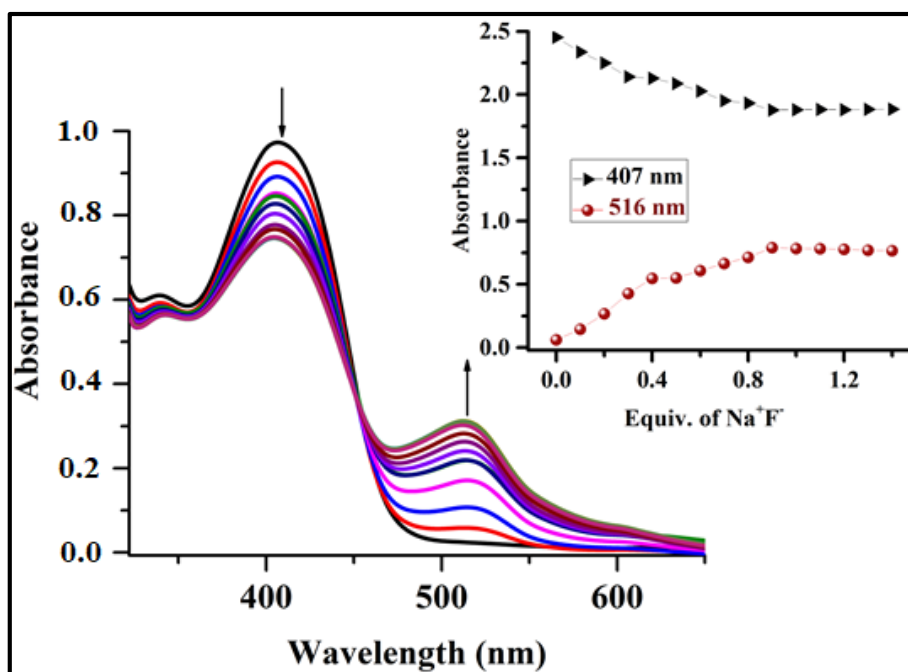
Fig. 4.30 UV-Vis spectral of **L3R1** (1×10^{-5} M in DMSO) with the increasing addition of Na^+F^- in the DMSO:H_2O (9:1 v/v); Inset attributed to the equiv. addition of Na^+F^- at particular wavelengths of 407 nm and 516 nm
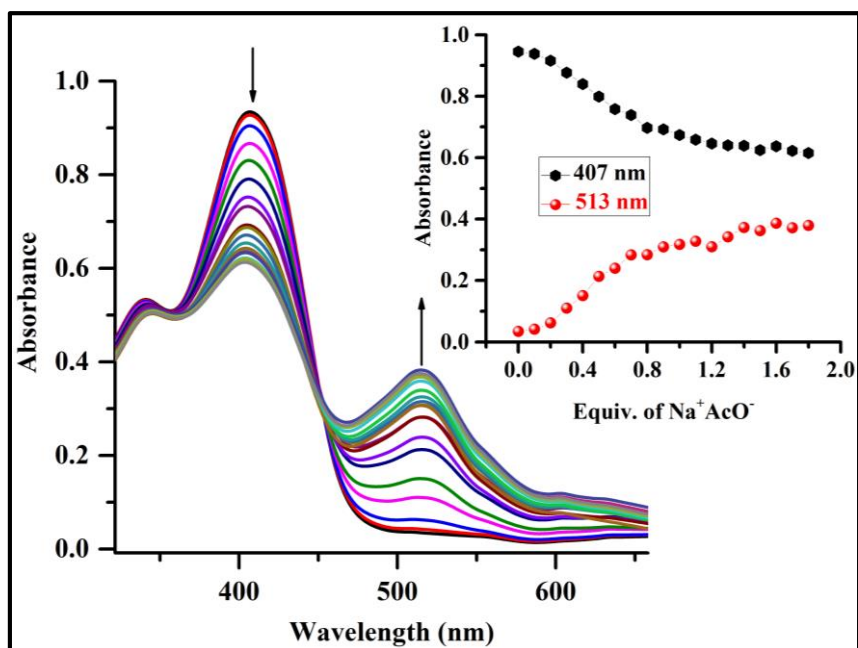
Fig. 4.31 UV-Vis spectral of **L3R1** (1×10^{-5} M in DMSO) with the increasing addition of Na$^+$AcO$^-$ in the DMSO:H$_2$O (9:1 v/v); Inset attributed to the equiv. addition of Na$^+$AcO$^-$ at particular wavelengths of 407 nm and 513 nm
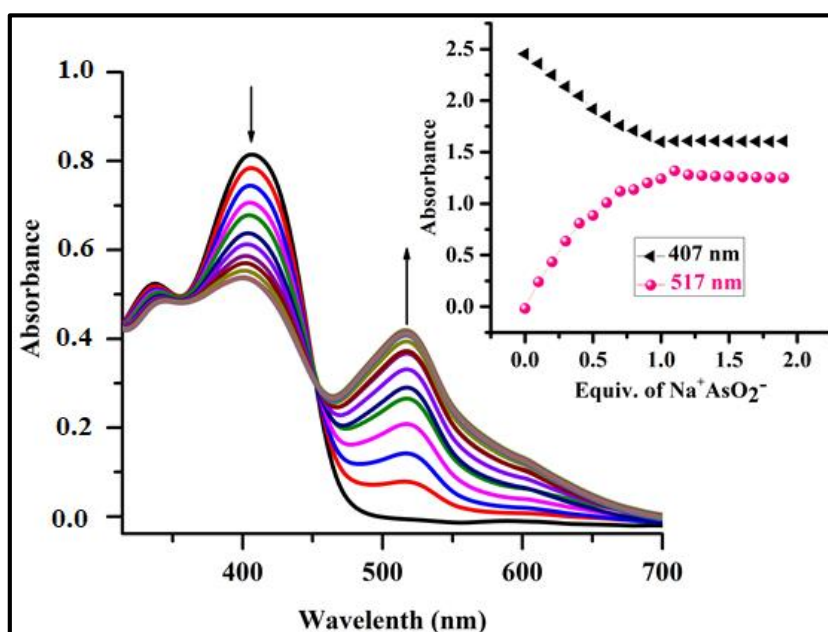
Fig. 4.32 UV-Vis spectral of **L3R1** (1×10^{-5} M in DMSO) with the increasing addition of Na$^+$AsO$_2^-$ in the DMSO:H$_2$O (9:1 v/v); Inset attributed to the equiv. addition of Na$^+$AsO$_2^-$ at particular wavelengths of 407 nm and 517 nm
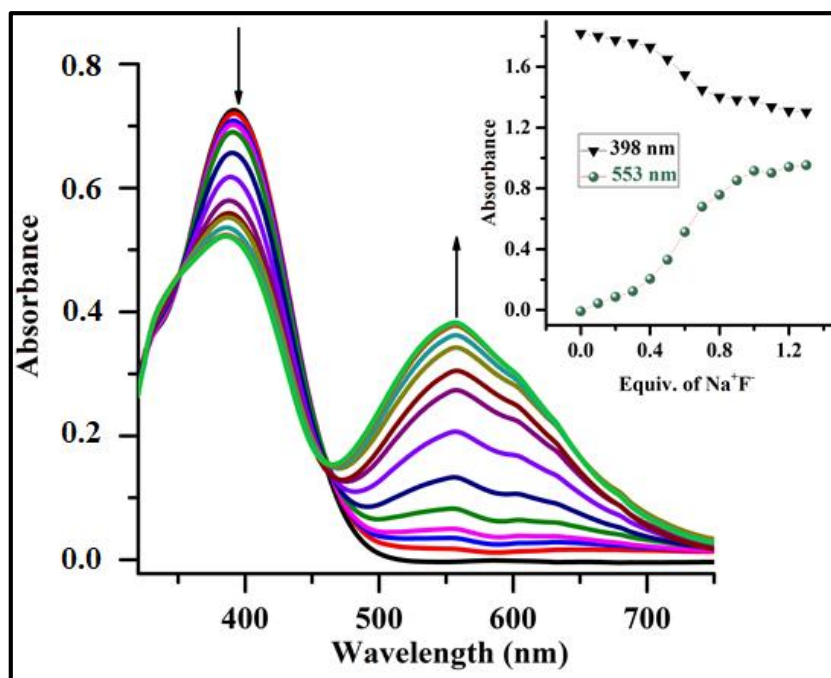
Fig. 4.33 UV-Vis spectral of **L3R2** (1×10^{-5} M in DMSO) with the increasing addition of Na^+F^- in the DMSO:H_2O (9:1 v/v); Inset attributed to the equiv. addition of Na^+F^- at particular wavelengths of 398 nm and 553 nm
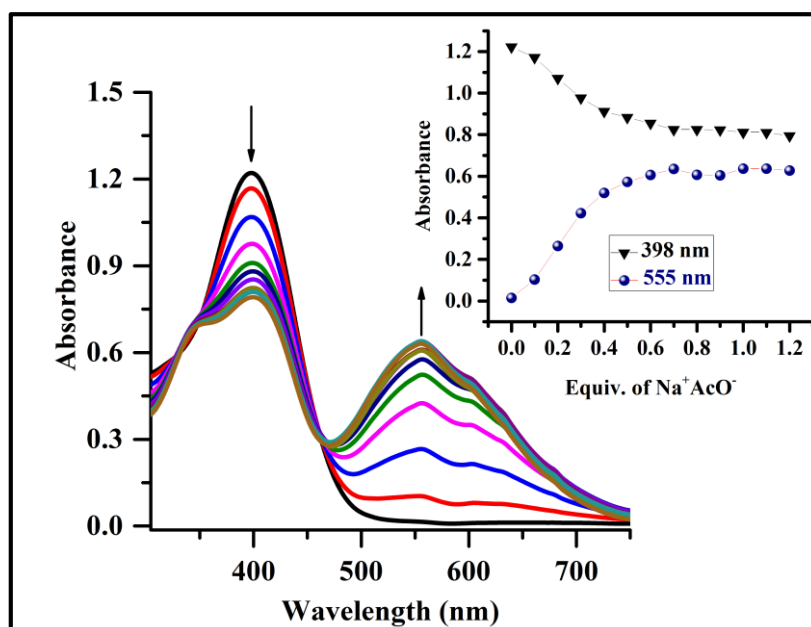
Fig. 4.34 UV-Vis spectral of **L3R2** (1×10^{-5} M in DMSO) with the increasing addition of Na^+AcO^- in the DMSO:H_2O (9:1 v/v); Inset attributed to the equiv. addition of Na^+AcO^- at particular wavelengths of 398 nm and 555 nm
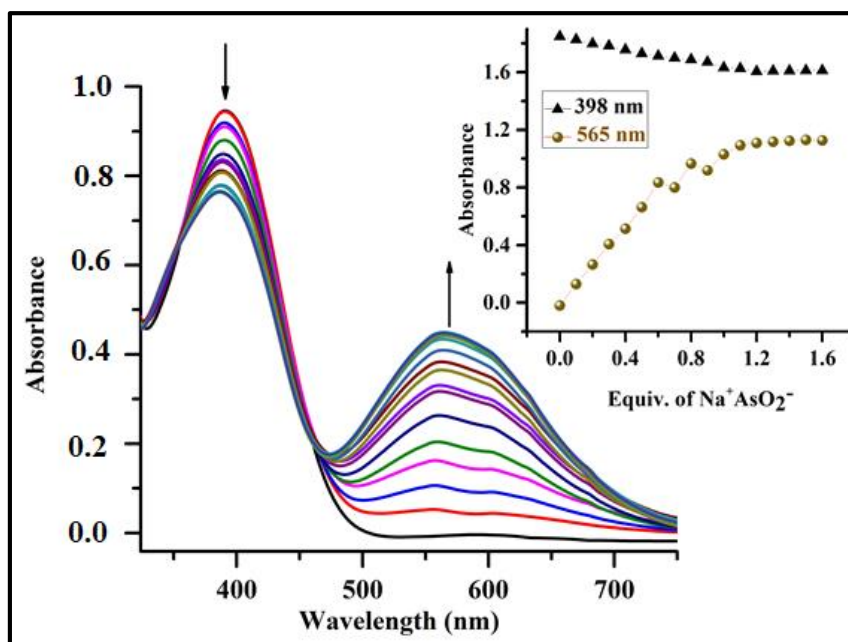
Fig. 4.35 UV-Vis spectral of **L3R2** (1×10^{-5} M in DMSO**)** with the increasing addition of $Na^+AsO_2^-$ in DMSO:H_2O (9:1 v/v); Inset attributed to the equiv. addition of $Na^+AsO_2^-$ at particular wavelengths of 398 nm and 565 nm
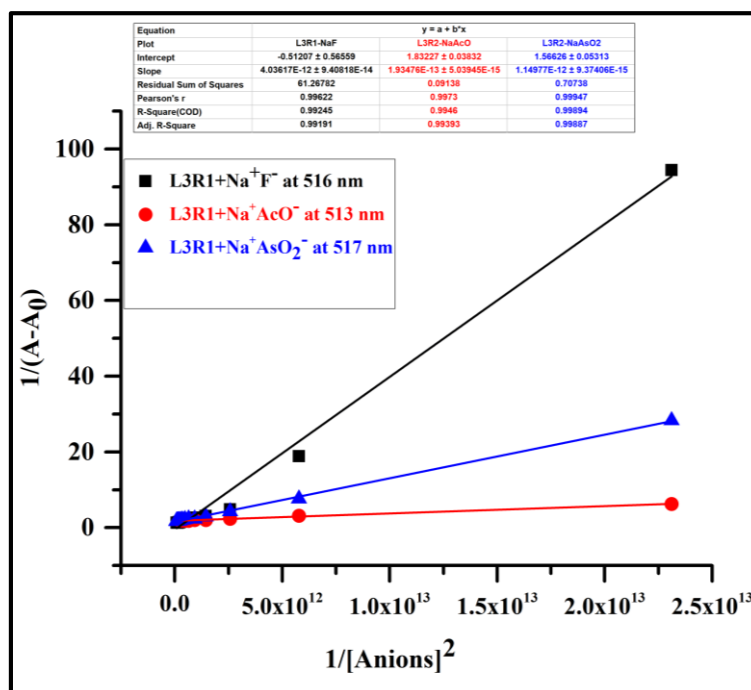
Fig. 4.36 B-H plot of the receptors **L3R1**-Na^+F^-, **L3R1**-Na^+AcO^-, and **L3R1**-$Na^+AsO_2^-$ complex at a selected wavelength of 516 nm, 513 nm, and 517 nm

---

Equation		y = a + b*x	
Plot	L3R2-NaF	L3R2-NaAcO	L3R2-NaAsO2
Intercept	1.3955 ± 0.22951	1.78599 ± 0.04185	0.37687 ± 0.0472
Slope	4.52955E-6 ± 1.32184E-7	8.34237E-7 ± 2.31273E-8	1.44332E-6 ± 3.30191E-8
Residual Sum of Squares	3.07938	0.08111	0.36782
Pearson's r	0.99577	0.99656	0.99584
R-Square(COD)	0.99156	0.99313	0.9917
Adj. R-Square	0.99071	0.99237	0.99118
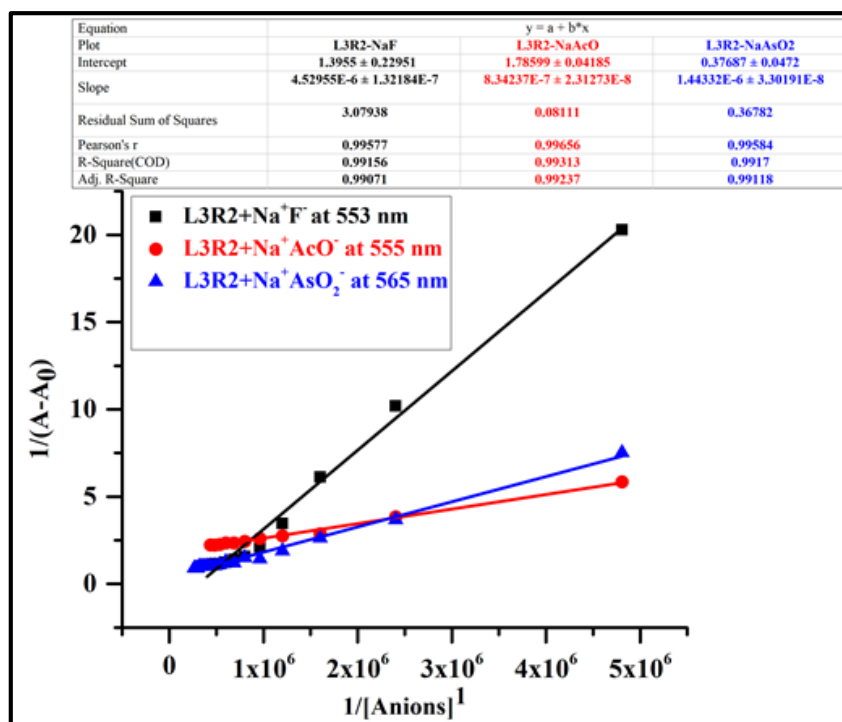
Fig. 4.37 B-H plot of receptor **L3R2**-Na^+F^-, **L3R2**-Na^+AcO^-, and **L3R2**-$Na^+AsO_2^-$ complex at a selected wavelength of 553 nm, 555 nm, 565 nm

Table 4.1 Bathochromic shift ($\Delta\lambda_{max}$) of the receptors **L3R1-L3R2** (1×10^{-5} M) in the presence of 2 equiv. of sensed anions in DMSO and DMSO: H_2O (9:1 v/v)

S.No	Receptor +anion	Medium	$\Delta\lambda_{max}$ nm
1	**L3R1**+TBA^+F^-	DMSO	114
2	**L3R1**+TBA^+AcO^-	DMSO	111
3	**L3R1**+ Na^+F^-	DMSO:H_2O (9:1 v/v)	109
4	**L3R1**+Na^+AcO^-	DMSO:H_2O (9:1 v/v)	106
5	**L3R1**+ $Na^+AsO_2^-$	DMSO:H_2O (9:1 v/v)	110
6	**L3R2**+TBA^+F^-	DMSO	159
7	**L3R2**+TBA^+AcO^-	DMSO	162
8	**L3R2**+ Na^+F^-	DMSO:H_2O (9:1 v/v)	155
9	**L3R2**+Na^+AcO^-	DMSO:H_2O (9:1 v/v)	157
10	**L3R2**+ $Na^+AsO_2^-$	DMSO:H_2O (9:1 v/v)	167

In a comparitive analysis of the anion sensing ability of the receptors **L3R1** and **L3R2**, the receptor **L3R2** induced a stable intramolecular charge transfer (ICT) from the donor (para-OH group) to the acceptor substituent ($-NO_2$ moiety) with an extended conjugate bond. As a result, the receptor **L3R2** displayed high bathochromic shift of 159 nm and 162 nm in the DMSO and of 155 nm, 157 nm, and 167 nm in the DMSO: H_2O (9:1 v / v).

The limit of detection was analysed for the receptors **L3R1** and **L3R2** in presence of anions and the graph obtained is depicted in Fig. 4.38, Fig. 4.39, Fig. 4.40, and Fig. 4.41. Binding constant, stoichiometric ratio and detection limit for receptors **L3R1** and **L3R2** with corresponding anions are given in Table 4.2.
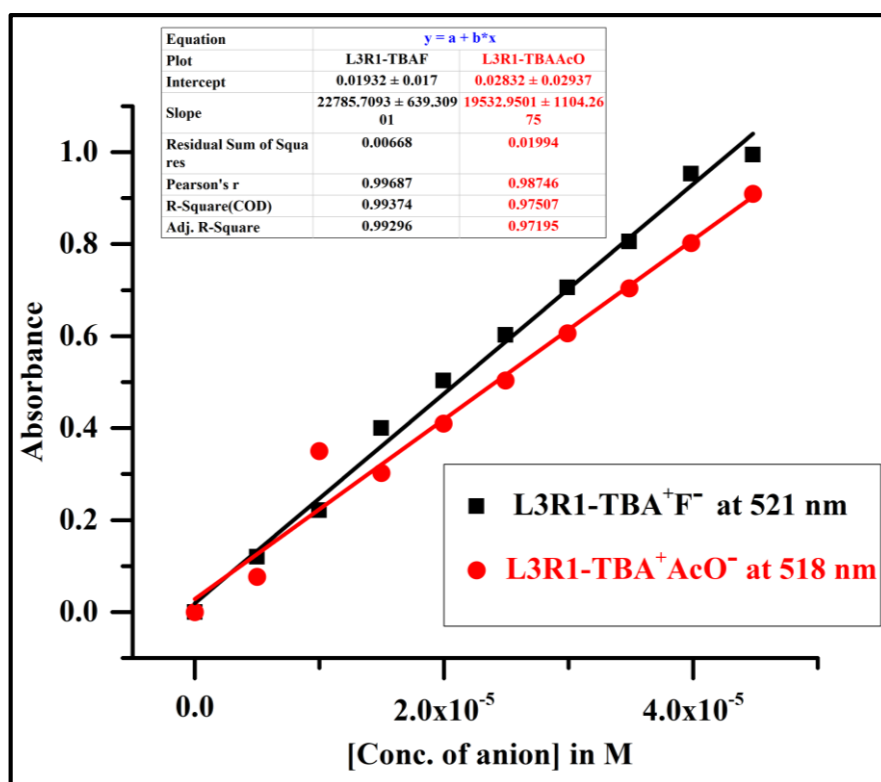
Fig. 4.38 Calibration curve between the absorbance of the receptor **L3R1**-anion complex and the concentration of anion at selected wavelengths
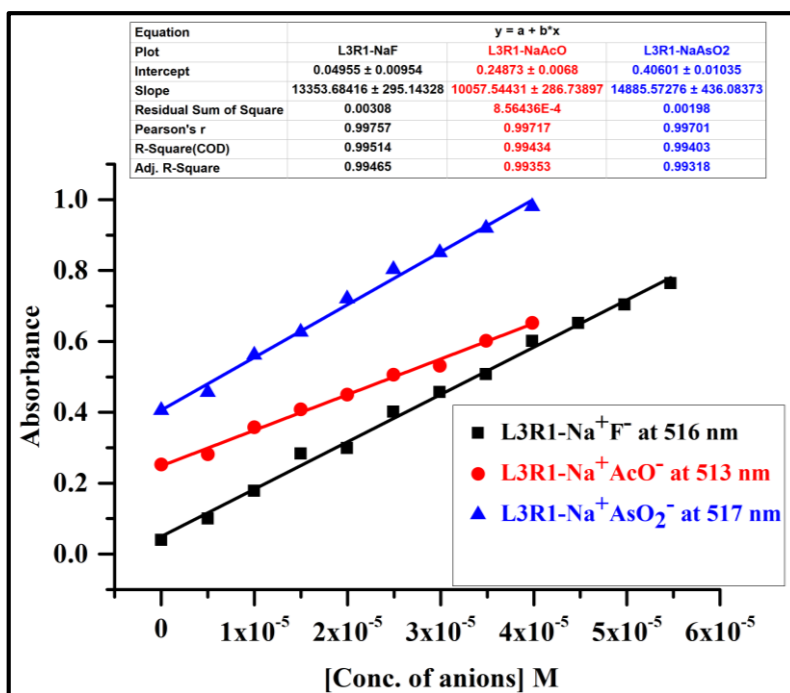
Fig. 4.39 Calibration curve between the absorbance of the receptor **L3R1**--anion complex and the concentration of the anion at selected wavelengths
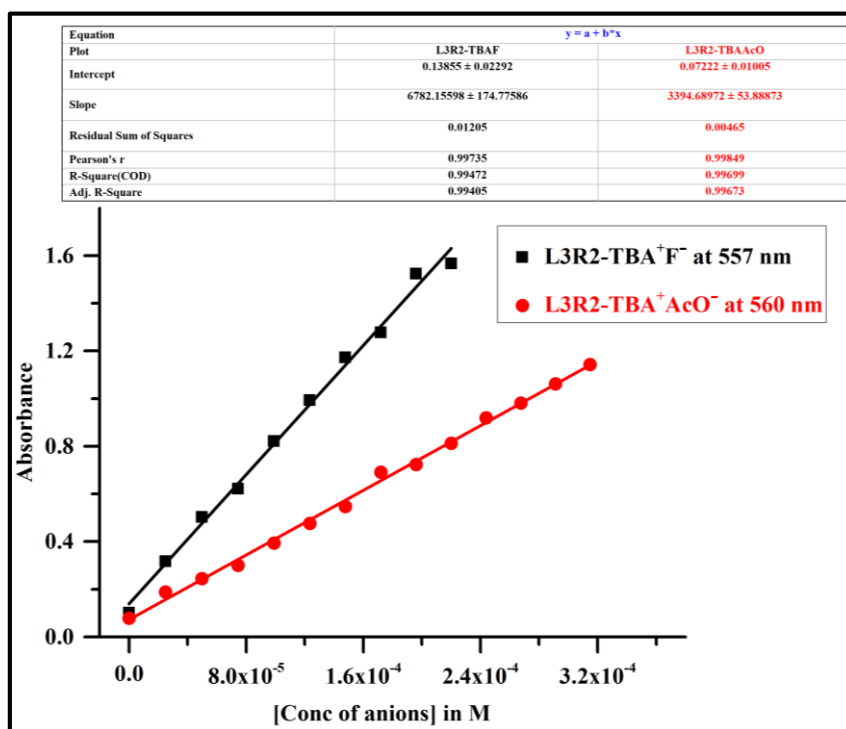
Fig. 4.40 Calibration curve between the absorbance of the receptor **L3R2**-anion complex and the concentration of the anion at selected wavelengths
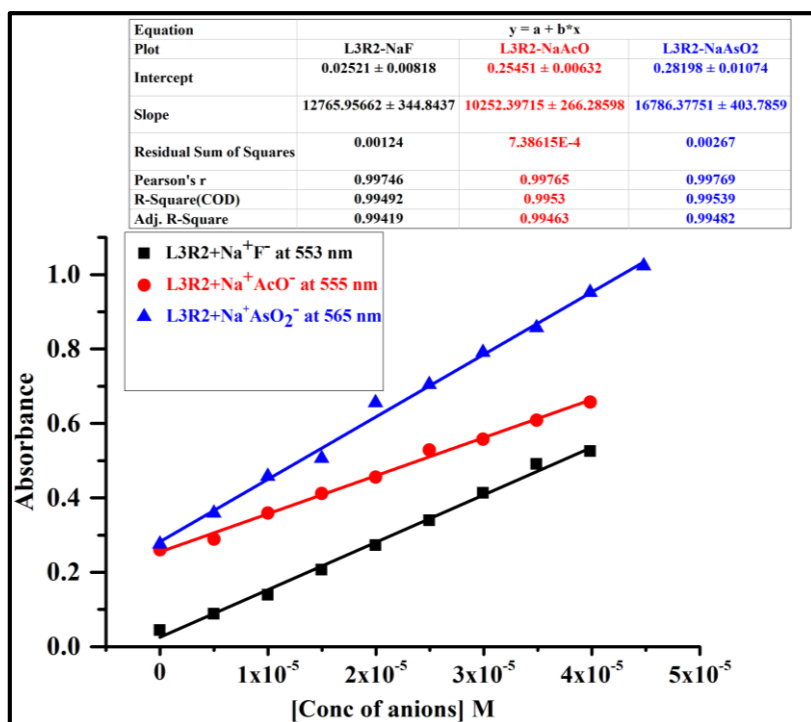
Fig. 4.41 Calibration curve between absorbance of receptor **L3R2**-anion complex and concentration of anion at selected wavelengths

Table 4.2 Calculated binding constant, LOD, and stoichiometry for receptors **L3R1** and **L3R2** with selective anions in DMSO and DMSO:H$_2$O (9:1 v/v)

Receptor	Medium	Binding Constant	LOD	Stoichiometry	R^2
L3R1+TBA$^+$F$^-$	DMSO	3.64×10^2 M^{-2}	6.10 µM (2.81 ppm)	1:2	0.9924
L3R1+TBA$^+$AcO$^-$	DMSO	4.32×10^2 M^{-2}	5.60 µM (1.90 ppm)	1:2	0.9916
L3R2+TBA$^+$F$^-$	DMSO	5.03×10^7 M^{-1}	4.93 µM (0.98 ppm)	1:1	0.9941
L3R2+TBA$^+$AcO$^-$	DMSO	7.03×10^7 M^{-1}	4.10 µM (0.74 ppm)	1:1	0.9910

L3R1+Na$^+$F$^-$	DMSO:H$_2$O (9:1 v/v)	7.39×10^3 M^{-2}	6.03 μM (2.56 ppm)	1:2	0.9921
L3R1+Na$^+$AcO$^-$	DMSO:H$_2$O (9:1 v/v)	6.44×10^3 M^{-2}	5.51 μM (1. 75 ppm)	1:2	0.9946
L3R1+Na$^+$AsO$_2^-$	DMSO:H$_2$O (9:1 v/v)	6.12×10^2 M^{-2}	4.70 μM (0.67 ppm)	1:2	0.9905
L3R2+Na$^+$F$^-$	DMSO:H$_2$O (9:1 v/v)	8.79×10^7 M^{-1}	4.01 μM (0.53 ppm)	1:1	0.9915
L3R2+Na$^+$AcO$^-$	DMSO:H$_2$O (9:1 v/v)	9.34×10^7 M^{-1}	3.09 μM (0.23 ppm)	1:1	0.9931
L3R2+Na$^+$AsO$_2^-$	DMSO:H$_2$O (9:1 v/v)	8.12×10^7 M^{-1}	2.19 μM (0.30 ppm)	1:1	0.9917

The binding ratio was obtained from the B-H plot. The detection limit of **L3R2** for the F$^-$ was found to be 0.98 ppm in the DMSO and 0.53 ppm in the DMSO: H$_2$O (9:1 v/v) reflect the stability of receptor-anion complex. The reason for the relatively higher detection limit can be ascribed to the solvent-anion interaction prevailing during the anion binding event.

4.3.4 Electrochemical studies

To further exploit the utility of **L3R1** and **L3R2**, cyclic voltammetric studies were conducted to gain insight in to their oxidation and reduction behaviour with incremental addition of AcO$^-$ ion to the solutions of **L3R1-L3R2** (1×10^{-5} M) in acetonitrile to understand the presence of the -NO$_2$ and -OH groups as well their nature of interaction with the anions. In the absence of the AcO$^-$ ion, **L3R1** and **L3R2** showed oxidation peaks at 0.56 V and 0.6 V corresponding to the OH proton and reduction peaks at -0.77 V and -0.69 V assigned to the -NO$_2$ group. On sequential addition of AcO$^-$ ions to the **L3R1** solution, not much shift was observed between **L3R1** and the AcO$^-$ ion as

depicted in Fig. 4.42. On the other hand, with the sequential addition of AcO⁻ ion into **L3R2**, the oxidation peak at 0.6 V shifted to 0.65 V, which was attributed to the deprotonation of the OH group by the AcO⁻ ion leaving behind a negative charge on oxygen (O⁻) as depicted in Fig. 4.43. The reduction peak of the NO_2 group at -0.69 V shifted to -0.66 V indicating direct participation of the redox activity in the anion binding phenomena (Sharma et al. 2015). The subsequent shift of the oxidation and reduction peak is a clear indication of the occurrence of a complex electrochemical process during the interaction.
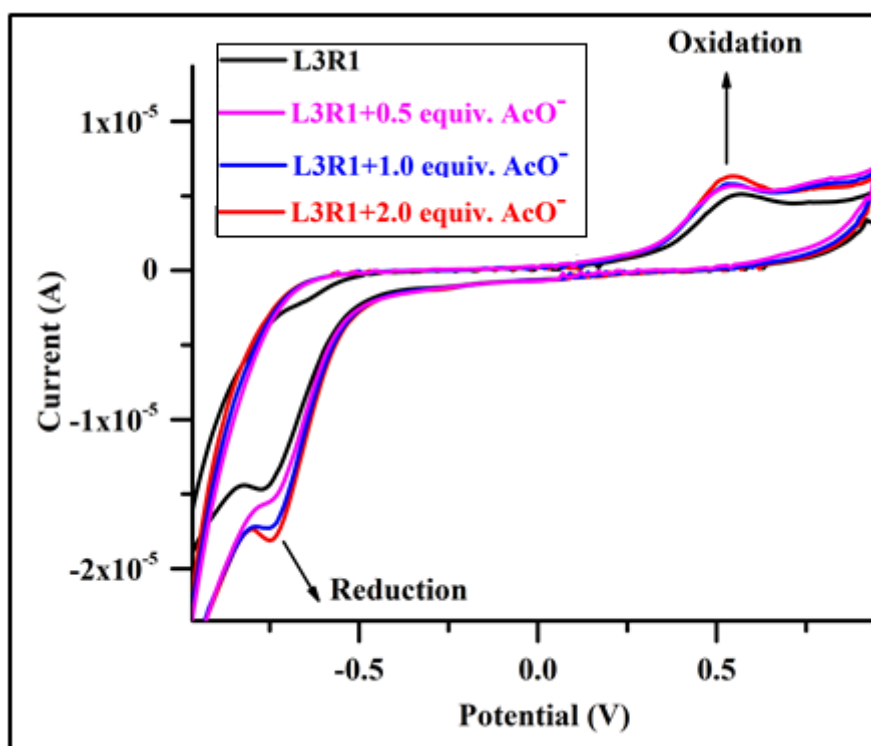
Fig. 4.42 Cyclic voltammogram of the receptor **L3R1** (1×10^{-5} M) in acetonitrile with the incremental addition (0.5 equiv.-2.0 equiv.) of TBA⁺AcO⁻ (1×10^{-2} M in DMSO)
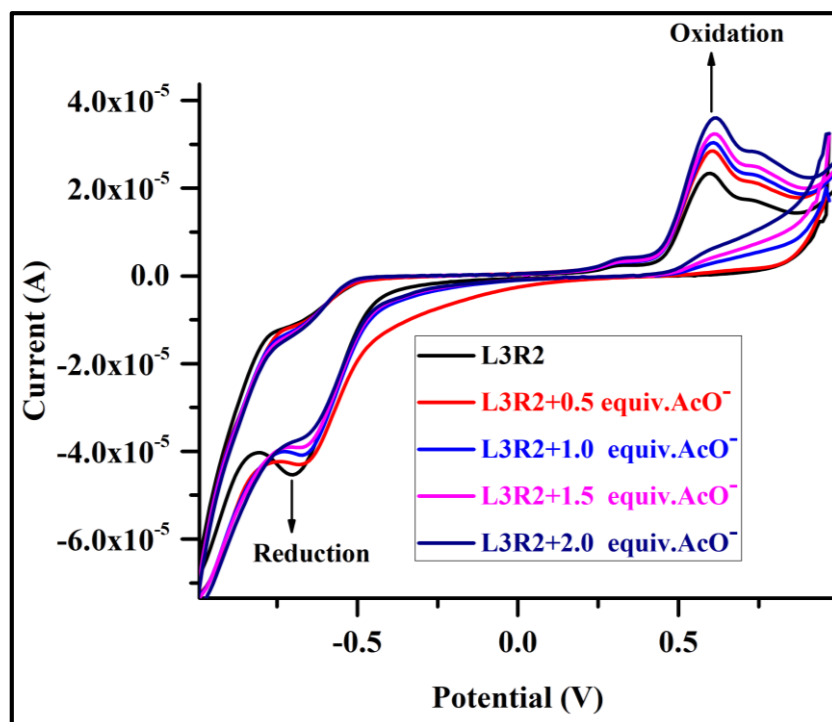
Fig. 4.43 Cyclic voltammogram of the receptor **L3R2** (1×10^{-5} M) in acetonitrile with the incremental addition of (0.5 equiv.-2.0 equiv.) TBA$^+$AcO$^-$ (1×10^{-2} M in DMSO)

4.3.5   Solvatochromism studies

Solvatochromism explains the change in the electronic spectra of a receptor when dissolved in different solvent media, and is related to the change in the electronic structure of the subjected molecules caused by the variation of the solvent polarity, especially hydrogen bonding strength (or) change in the dipole moment in the ground and lower energy singlet excited state, which results in substantial shift in the absorption band (termed as positive solvatochromism) with increasing solvent polarity (Arabahmadi et al. 2014; Dey and Das 2011). Notably, **L3R2** showed solvatochromic behaviour upon addition of 2 equiv. of AcO$^-$ ion to the solution prepared by different solvents such as DMSO, ACN, THF, Acetone, DCM, and 1-4 Dioxane as it produced visible colour change from pale yellow to deep blue, violet, light blue, green, light green, and brown, respectively, as depicted in Fig. 4.44. Further, the UV-Vis absorption spectra were recorded for **L3R2** in the presence of different polar aprotic solvents. It exhibited a strong absorption band in the 542 nm-624 nm range as depicted in Fig. 4.45. The new absorption bands at higher wavelengths are due to the ICT mechanism

between the electron donor (para-OH group) and the electron acceptor groups (-NO$_2$ moiety). Moreover, **L3R2** possesses a typical D-π-A type structural motif, which is responsible for good solvatochromism in different solvents. The bathochromic shift in different aprotic polar solvents is illustrated in Table 4.3.

Fig. 4.44 Solvatochromic effect upon addition of 2 equiv. AcO$^-$ (1×10^{-2} M in DMSO) to the **L3R2** (1×10^{-5} M) solution in various solvents with different polarities
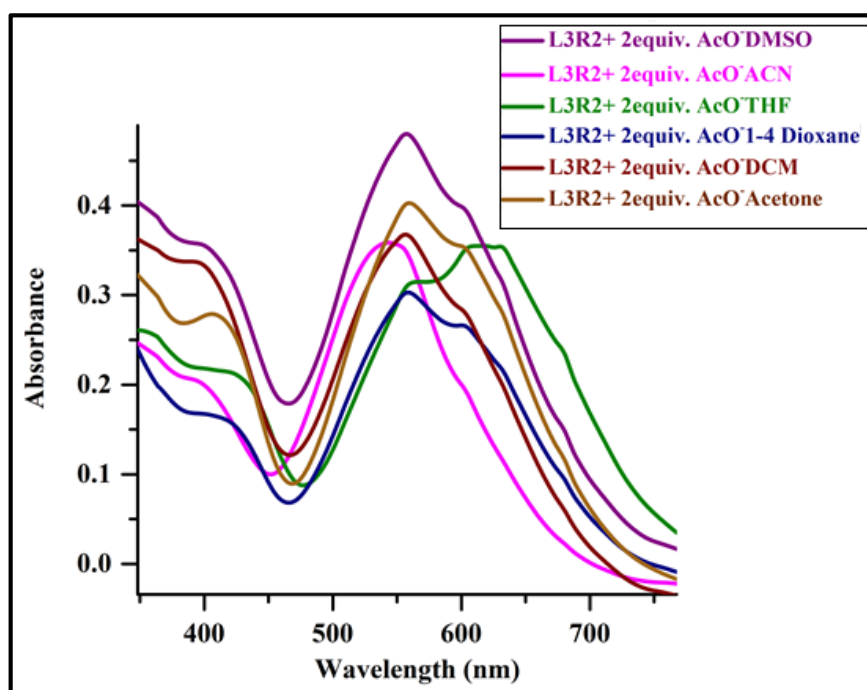
Fig. 4.45 UV-visible absorption spectra of **L3R2** (1×10^{-5} M) in different polar aprotic solvents upon addition 2 equiv. AcO$^-$ (1×10^{-2} M in DMSO)

Table 4.3 Bathochromic shift ($\Delta\lambda_{max}$) in absorption band of **L3R2** in different solvent upon addition of 2 equiv. TBA$^+$AcO$^-$ (1×10^{-2} M in DMSO)

Receptor+Anions	Solvent	$\Delta\lambda_{max}$ (nm)
L3R2+AcO$^-$	THF	624
L3R2+AcO$^-$	DMSO	560
L3R2+AcO$^-$	Acetone	557
L3R2+AcO$^-$	DCM	553
L3R2+AcO$^-$	1-4 Dioxane	550
L3R2+AcO$^-$	ACN	542

4.3.6 ^{1}HNMR titration studies

^{1}H-NMR titration experiments were conducted to further investigate the interaction of **L3R2** with F$^-$/AcO$^-$ in DMSO-d_6. The ^{1}H-NMR spectrum of the free receptor **L3R2,** without the addition of anions, showed one singlet peak at 10.3 ppm assigned to the phenol -OH proton as mentioned in Fig. 4.46. However, the signal at 10.3 ppm assigned to the -OH proton disappeared after the addition of 0.5 equiv of F$^-$ ion, suggesting the formation of a hydrogen bond between the -OH of the receptor **L3R2** and the F$^-$ ion, followed by the deprotonation process (Lee et al. 2001). Further, with the addition of the 1.0 equiv. of the F$^-$ ion, the aromatic proton signals in **L3R2** underwent an upfield shift indicating the presence of through-bond effect, which tends to increase the electron density on the aromatic ring.

Surprisingly, no upfield shift was observed when 2 equiv. of the anions was added. This phenomenon reflects the 1:1 stoichiometry between **L3R2** and the F$^-$ ion, which was confirmed by the B-H plot. Hence, it clearly proves that the F$^-$ ion acts as a base and gives rise to deprotonation upon interaction with the OH proton of the receptor **L3R2**. In addition, the change in colour of the receptor **L3R2** from pale yellow to blue is due to the deprotonation of the –OH group resulting in a negative charge of the oxygen atom (O$^-$). Hence, the detection process, followed by deprotonation mechanism, but no signal for HF$_2^-$ was observed in the ^{1}H-NMR spectrum. This may be due to the fact that

HF_2^- is not suitable in a highly polar solvent like DMSO (Li et al. 2018; Wang et al. 2014). The ^{1}H-NMR titration of **L3R2** with the AcO⁻ ions also exhibited similar behaviour as shown by the F⁻ ion and demonstrated in Fig. 4.47.
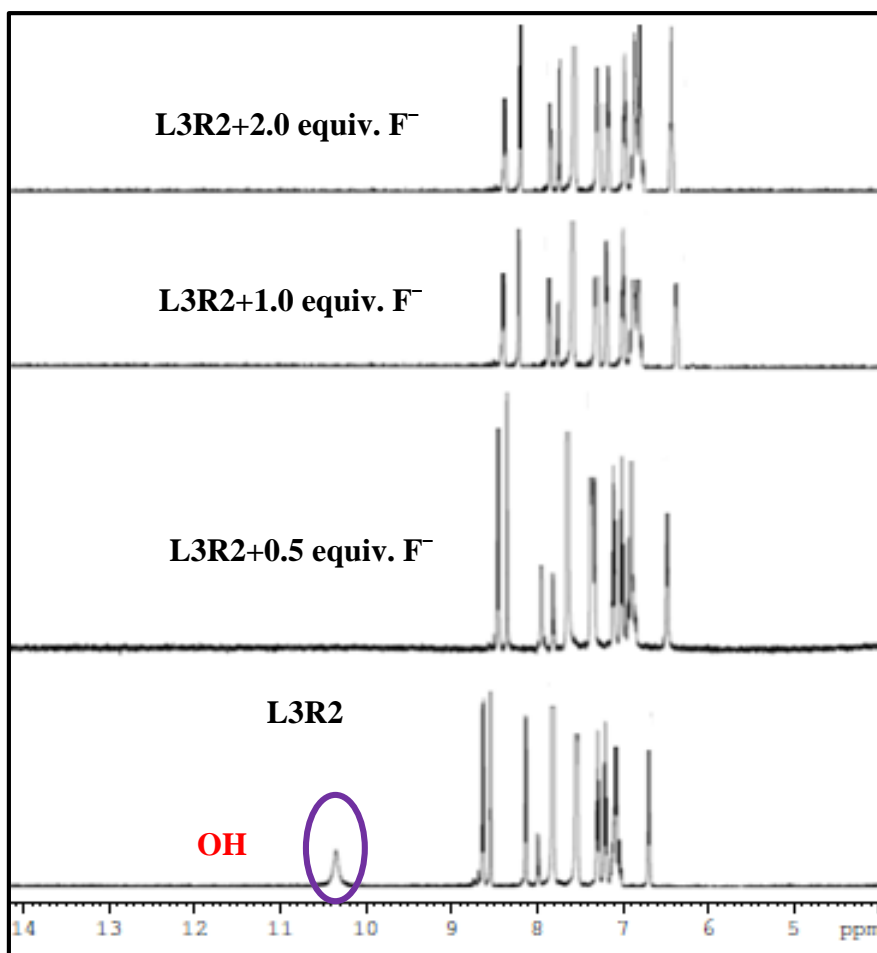
Fig. 4.46 ^{1}H-NMR spectrum of **L3R2** in DMSO-d_6 with sequential addition of TBA⁺F⁻
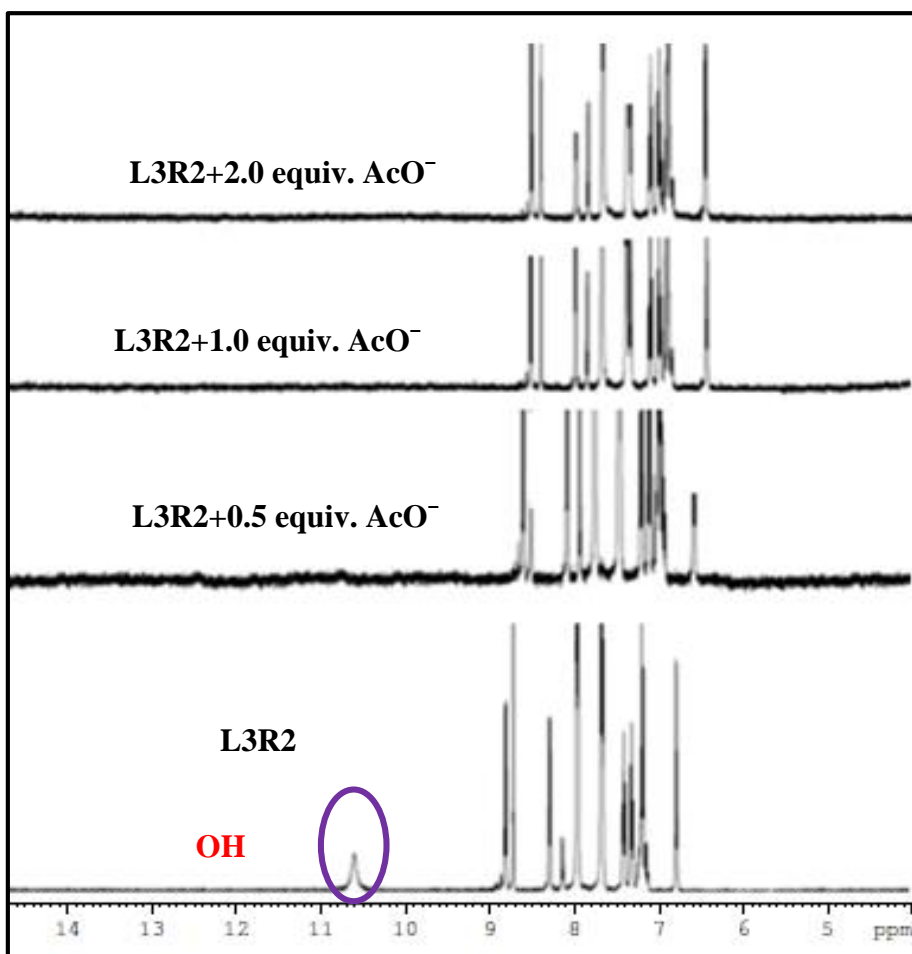
Fig. 4.47 ¹H-NMR spectrum of **L3R2** in DMSO-d$_6$ with sequential addition of TBA⁺AcO⁻

In order to verify the deprotonation process during the anion complexation with the receptor **L3R2**, the UV-Vis titration experiment of the receptor **L3R2** was performed. The titration profile afforded similar spectral pattern and colour change as observed for other basic anions TBA⁺F⁻ and TBA⁺AcO⁻, suggesting deprotonation of the OH⁻ proton. The OH⁻ induced spectral change of the receptor **L3R2** is shown in Fig.4.48.
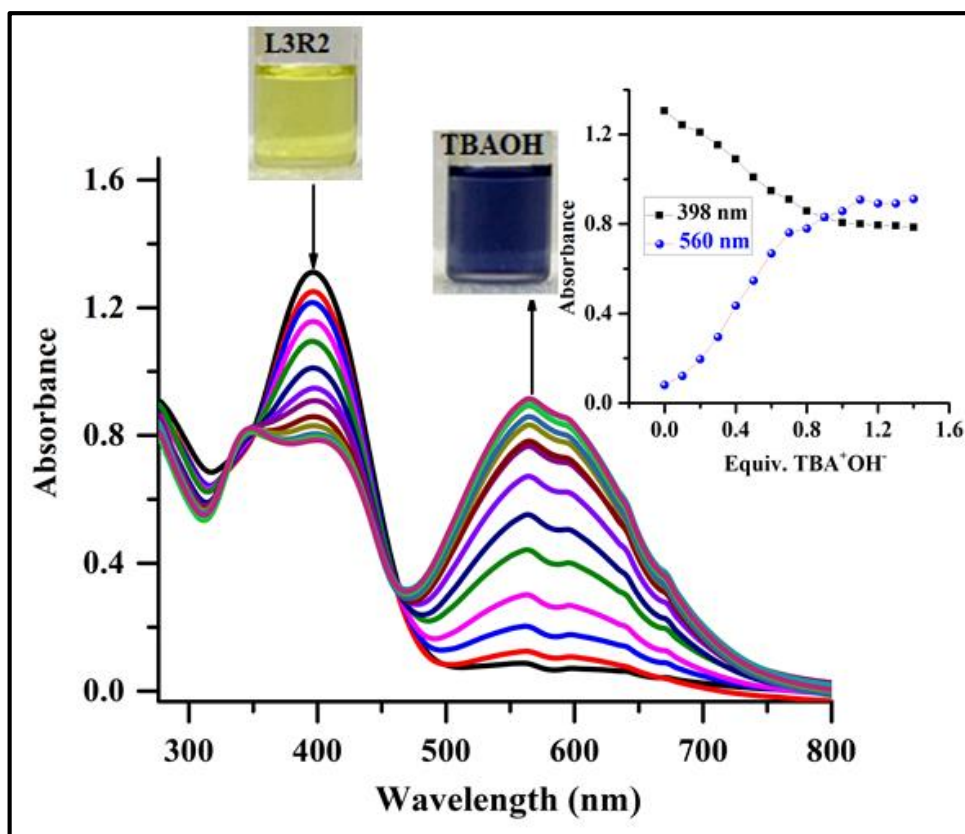
Fig. 4.48 UV-Vis titration spectra of receptor **L3R2** (1×10^{-5} M in DMSO) with incremental addition of TBA$^+$OH$^-$ (1×10^{-2} M in DMSO); Inset plot representing binding isotherm at 398 nm and 560 nm

4.3.7 Binding mechanism

The electrochemical studies and ^{1}H-NMR titration of the receptor **L3R2** in the presence of anions confirmed the deprotonation of the OH functionality during the anion binding process. The occurrence of the 1:1 binding ratio of the **L3R2**-anion complex revealed the successful binding of the anions to the OH functionality at the para-position, following the deprotonation event, and as a result, the electron density over the deprotonated receptor **L3R2** increased. Thus, the charge separation in the receptor was introduced, which resulted in ICT transition between the electron deficient NO_2 group and the electron rich -O$^-$, resulting in a visible colour change The binding mechanism is shown in Scheme 4.4.
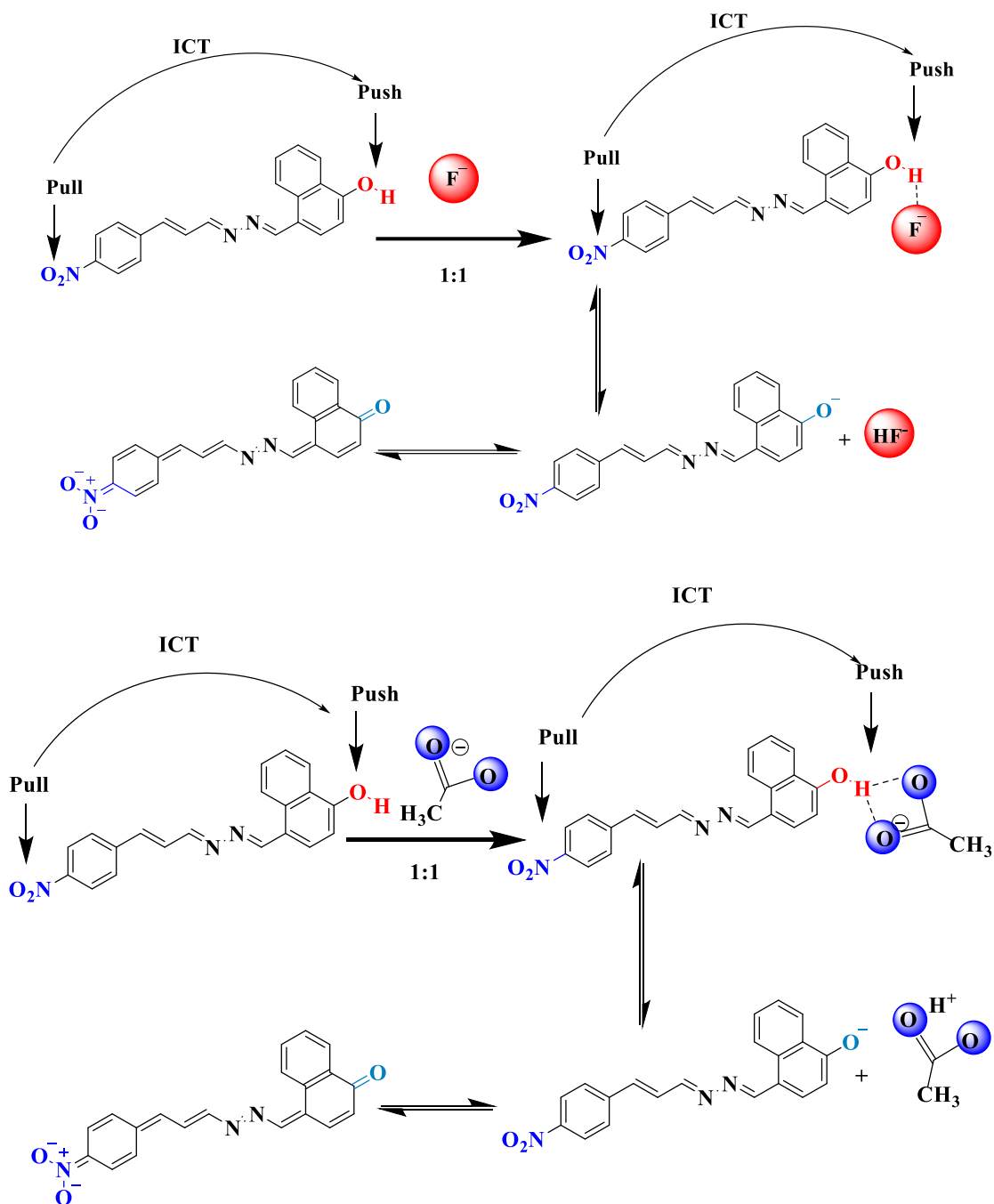
Scheme 4.4 Proposed binding mode of receptor **L3R2** with anion in the solution

4.3.8 Colorimetric test-kits

To check for practical application, test kits were utilized to sense F^- and AsO_2^- ions. As shown in Fig. 4.49, test strips were prepared by immersing filter papers into a solution of the receptor **L3R2** (1×10^{-5} M in DMSO) and then drying them in air. The test

strips coated with **L3R2** were utilized to sense F⁻ and AsO₂⁻ ion. When F⁻ and AsO₂⁻ ions were added on to the test kit, a remarkable colour change was observed from pale yellow to blue under natural light. Therefore, test kits coated with the chemosensor **L3R2** solution would be convenient for detecting F⁻ and AsO₂⁻ ions. These results show that the chemosensor **L3R2** could be a valuable practical sensor for sensing biologically important F⁻ in an organic medium and toxic AsO₂⁻ in an aqueous medium.

L3R2   **L3R2+TBA⁺F⁻**   **L3R2+ Na⁺AsO₂⁻**
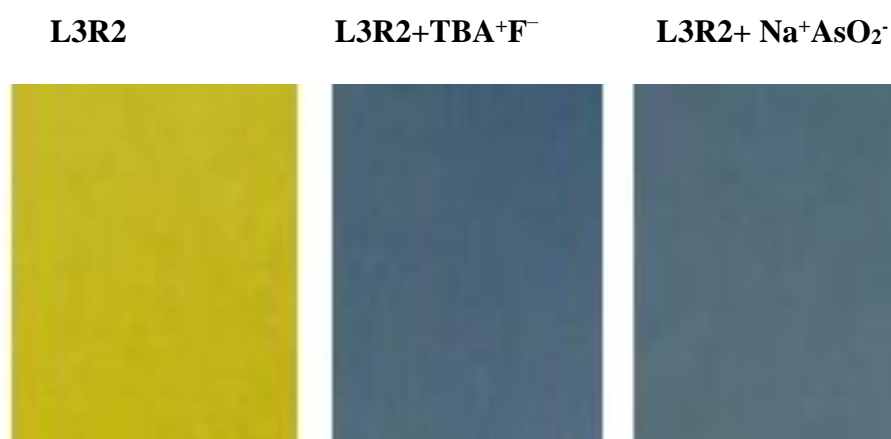
Fig. 4.49 Test strip application of **L3R2** for sensing TBA⁺F⁻ (1×10^{-2} M in DMSO) and NaAsO₂⁻ (1×10^{-2} M distilled H_2O)

4.3.9   Real-application of receptors L3R1 and L3R2

The detection of the sodium salts of anions by the receptors is necessary as it plays an important role in practical application. Sodium fluoride and sodium acetate are essential ingredients of toothpaste, mouthwash, and vinegar. With this in view, it was aimed to check the anion sensing ability in aqueous medium using sodium acetate and sodium fluoride. Surprisingly, upon adding one drop of toothpaste, mouthwash, vinegar and seawater prepared in an aqueous medium to the receptor **L3R1** and **L3R2** solutions (1×10^{-5} M in DMSO), a sharp change in colour from pale yellow to purple and from pale yellow to blue was observed as shown in Fig. 4.50. The UV-Vis spectral of the receptors **L3R1** and **L3R2** in the presence of vinegar, toothpaste, mouthwash, and seawater yielded similar charge transfer band as observed in the case of standard TBA⁺F⁻ and TBA⁺AcO⁻ ions as depicted in Fig. 4.51 and Fig. 4.52.
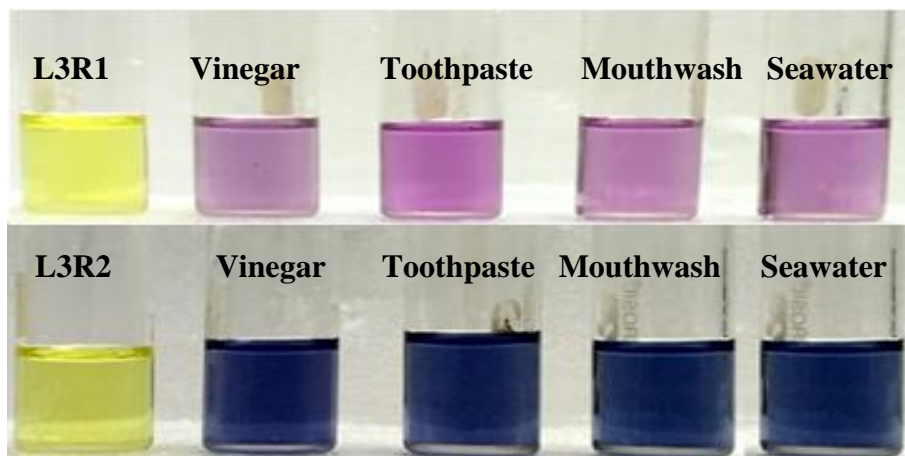
Fig. 4.50 Colour change of the receptors **L3R1** and **L3R2** (1×10^{-5} M in DMSO) upon the addition of a drop of vinegar, toothpaste, mouthwash, and seawater prepared in distilled water
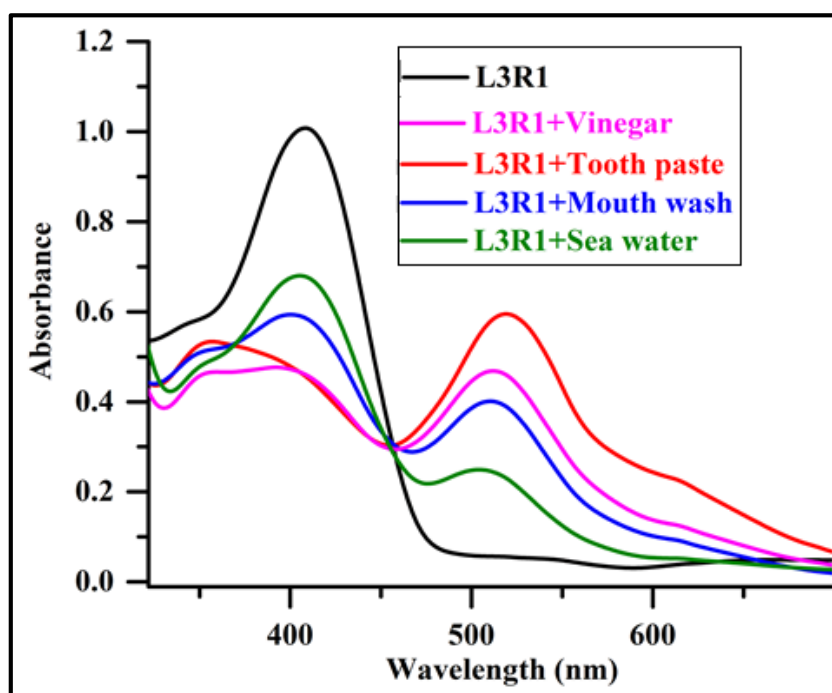
Fig. 4.51 UV-Vis spectra of **L3R1** (1×10^{-5} M in DMSO) upon the addition of a drop of vinegar, toothpaste, mouthwash, and seawater prepared in distilled water
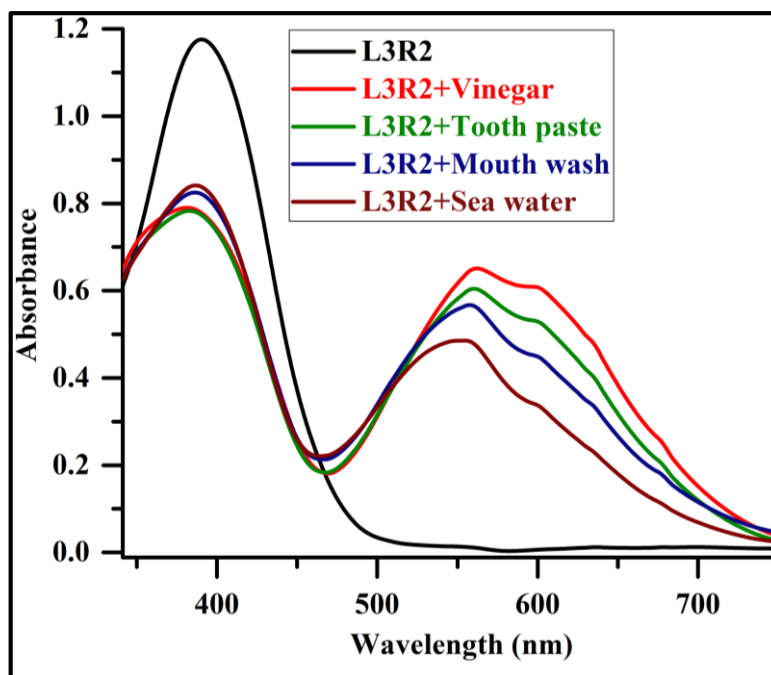
Fig. 4.52 UV-Vis spectra of **L3R2** (1×10^{-5} M in DMSO) upon the addition of a drop of vinegar, toothpaste, mouthwash, and seawater prepared in distilled water

4.3.10 DFT studies

Theoretical investigations of the colorimetric responses of the receptors towards F^- and AcO^- ions were carried out to corroborate with the experimental results supporting the binding mechanism. The geometrical and electronic properties of the molecules and the complex were performed using the Gaussian 09 package (Gaussian09 2009 p. 09). Ground state geometry optimizations and excited state electronic transitions for all the receptors and complexes were carried out initially in the gas phase, followed by geometry optimization in the solvent phase. To achieve this, the Gaussian inbuilt, IEF-PCM solvent model was employed, wherein the dimethylsulfoxide solvent was chosen for all the ground and excited state calculations.

The ground state calculations were performed with DFT B3LYP (Becke three parameters hybrid functional with Lee-Yang-Perdew correlation functionals) (Lee et al. 1988; Zhao and Truhlar 2008) with the 6-311+G(d,p) basis set (Hariharan and Pople 1973; Hehre et al. 1972), and the excited state calculations were carried out with TDDFT using the same functional and basis set.

The receptor **L3R1** had its HOMO distributed over the complete structure, while the LUMO was highly localized on the cinnamaldehyde and the NH-NH linkage as shown in Fig. 4.53 and Fig. 4.54. Though the receptor created complexity with the F⁻ and AcO⁻ ions, the HOMO and LUMO distribution remained nearly consistent. The present observations signify that the receptor **L3R1** does not favour intra-molecular charge transfer (ICT) due to similar electronic distribution before and after the binding. The receptor **L3R2** had its HOMO majorly distributed on the naphthalene moiety with the LUMO localized only on the cinnamaldehyde and the NH-NH linkage. Such distribution can better support the ICT in the system. Similar to **L3R1**, no changes in electronic distribution was observed upon complexation. The **L3R2** receptor complexed with the F⁻ and AcO⁻ ions, and the HOMO and HOMO-1 localized on the naphthyl unit consisting of the OH proton as the binding site, whereas the LUMO and LUMO+1 were localized on the conjugated unit and on the nitro group as depicted in Fig. 4.55 and Fig 4.56.

The experimental UV-Vis titration with the F⁻ and AcO⁻ ions was in good agreement with the red shift in the absorption spectra. The observed experimental UV-Vis titration results relate the red shift to the band gap reduction upon complexation with the F⁻ and AcO⁻ ions. The HOMO and LUMO energy gap of **L3R1** was 2.613 eV, and this energy gap before and after binding with F⁻ and AcO⁻ ions reduced to 2.401 eV and 1.744 eV, respectively. The receptor **L3R2** possessing an energy gap of 2.718 eV upon binding with F⁻ and AcO⁻ ions reduced to 1.989 eV and 1.668 eV, respectively. Hence, based on the experimental results, it can be concluded that **L3R2** can be considered favourable for ICT transition in comparison with **L3R1**.
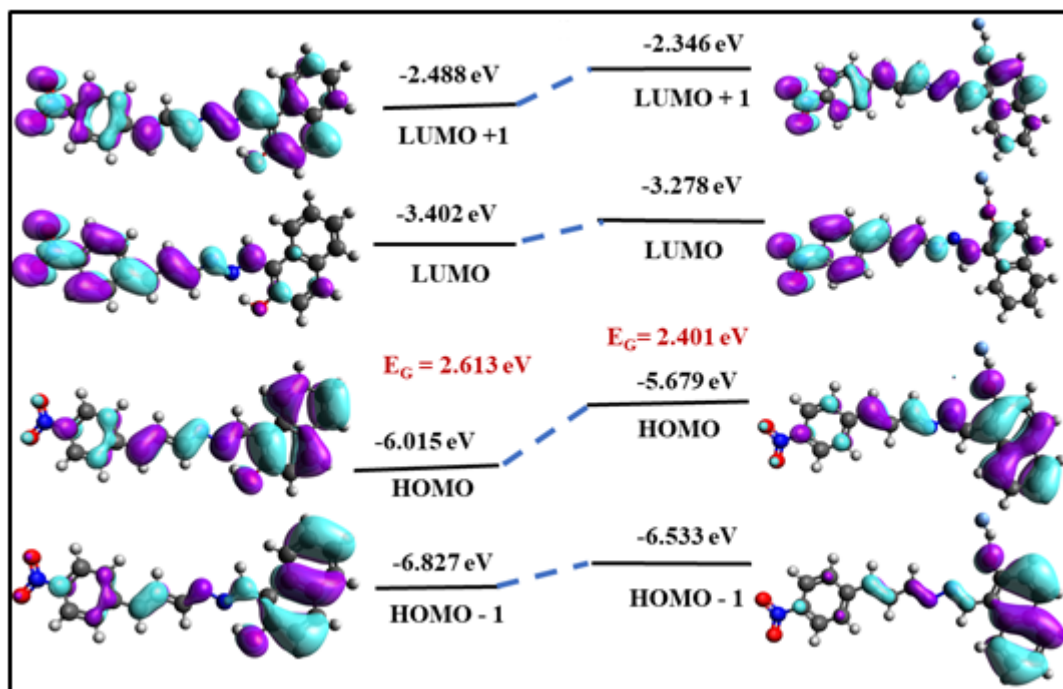
Fig. 4.53 Energy levels diagrams of **L3R1** and complex formation with F⁻ ion obtained by 6-31 + G (d,p)
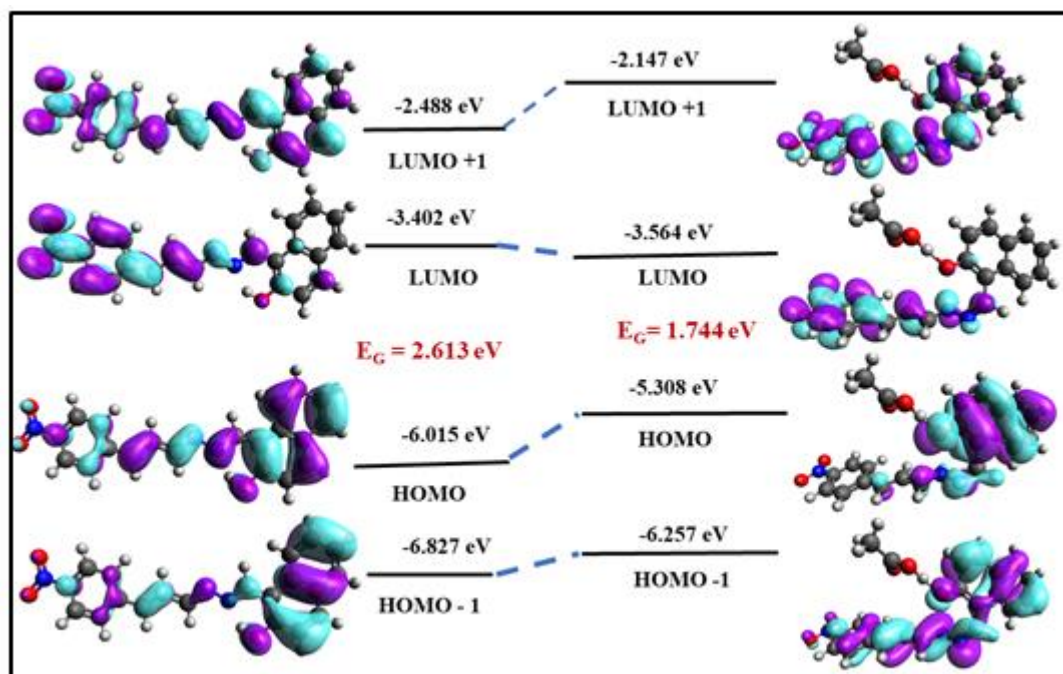
Fig. 4.54 Energy levels diagrams of **L3R1** and complex formation with AcO⁻ ion obtained by 6-31 + G (d,p)
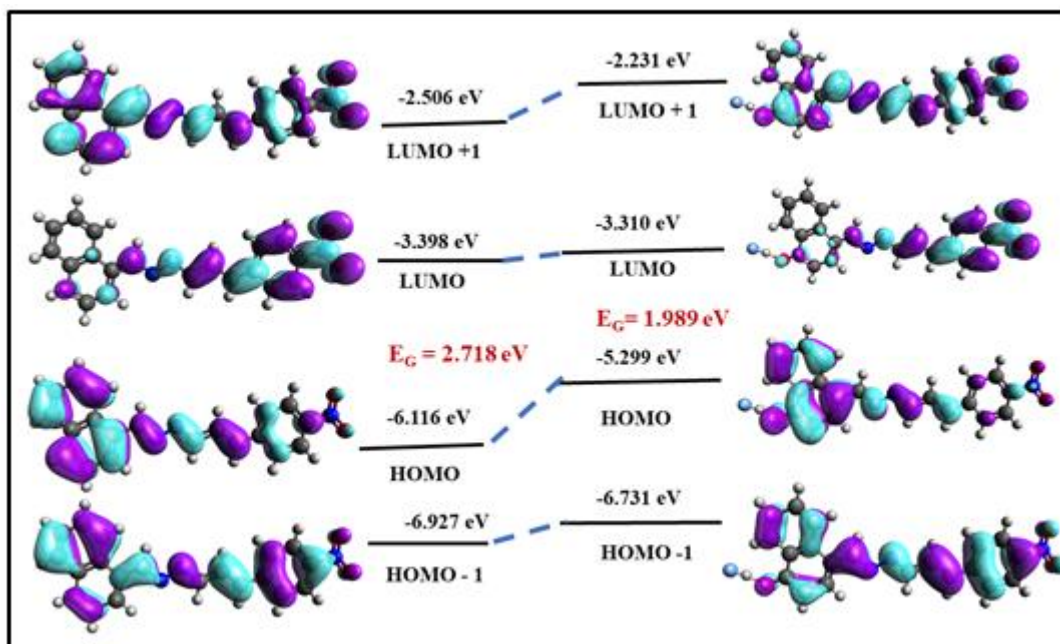
Fig. 4.55 Energy levels diagrams of **L3R2** and complex formation with F⁻ ion obtained by 6-311+G (d,p)
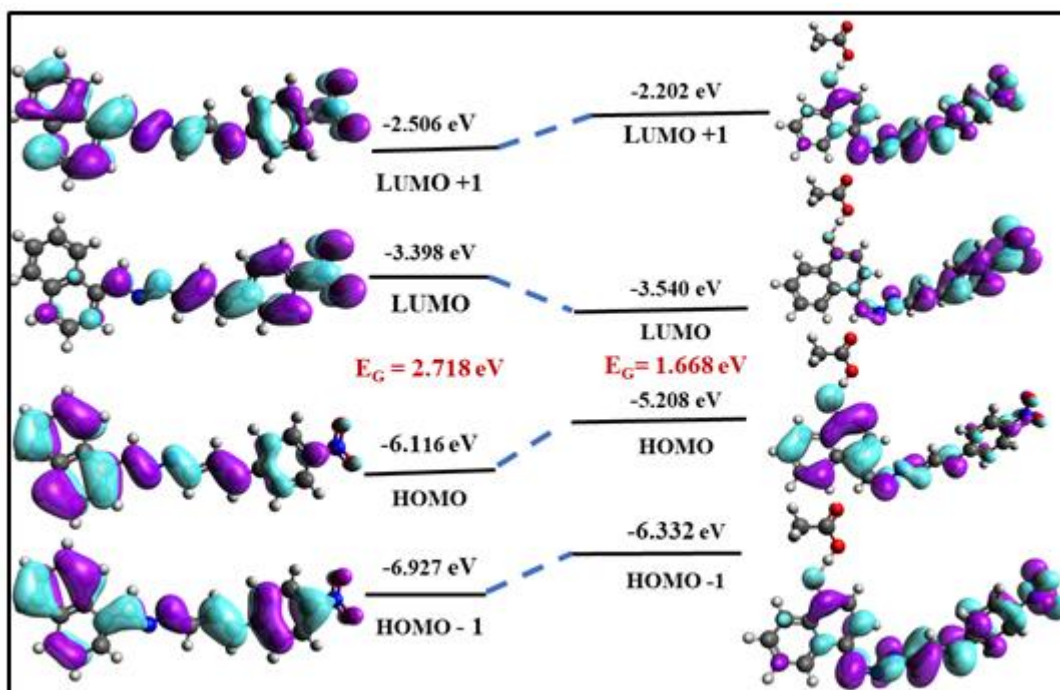
Fig. 4.56 Energy levels diagrams of **L3R2** and complex formation with AcO⁻ ion obtained by 6-311+G (d,p)

The molecular orbital energy level of the receptors **L3R1** and **L3R2** and their complex with F⁻ and AcO⁻ ions are summarized in Table 4.4.

Table 4.4 Molecular orbital energy of the receptors **L3R1** and **L3R2** and their complex with the sensed anions

Receptor	HOMO-1 eV	HOMO eV	LUMO eV	LUMO+1 eV	E$_G$ eV
L3R1	-6.827	-6.015	-3.402	-2.488	2.613
L3R2	-6.927	-6.116	-3.398	-2.506	2.718
Receptor+Complex	HOMO-1 eV	HOMO eV	LUMO eV	LUMO+1 eV	E$_G$ eV
L3R1+F⁻	-6.533	-5.679	-3.278	-2.346	2.401
L3R1+AcO⁻	-6.257	-5308	-3.564	-2.147	1.744
L3R2+F⁻	-6.731	-5.299	-3.310	-2.231	1.989
L3R1+ AcO⁻	-6.332	-5.208	-3.540	-2.202	1.668

From this observation, it can be concluded that **L3R2** is energetically more favourable for electronic transition in comparison with **L3R1** due to the lower energy gap between the HOMO and LUMO complexes with the sensed anions.

Further, the TD-DFT calculation was recorded to understand the shift in the UV-Vis absorbance spectra of the free receptors **L3R1** and **L3R2** and their complex with the F⁻ and AcO⁻ ions. The blank receptor **L3R1** without the addition of anion, displayed maximum absorption band at 533 nm, and upon addition of F⁻ and AcO⁻ ions exhibited a shift in the absorption band from 533 nm to 85l nm and 609 nm as illustrated in Fig. 4.57. Similarly, the receptor **L3R2** exhibited an absorption maximum at 507 nm after complexation with the anions and displayed a redshift at 694 nm and 869 nm as depicted in Fig. 4.58. The experimental and theoretical wavelength shift after complexation with anions is reported in Table 4.5. The results rationalize that the receptor **L3R2** showed maximum redshift compared with the receptor **L3R1** for the F⁻ and AcO⁻ ions and agreed well with the experimental results.
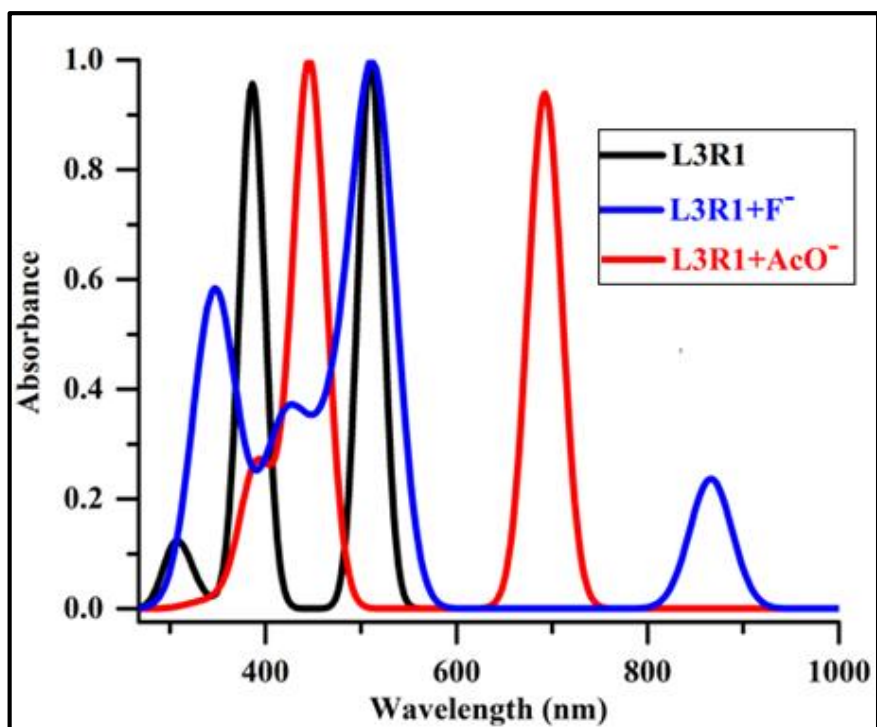
Fig. 4.57 UV-Vis absorption spectra of **L3R1** and complexation with corresponding anions calculated using TD-DFT calculation
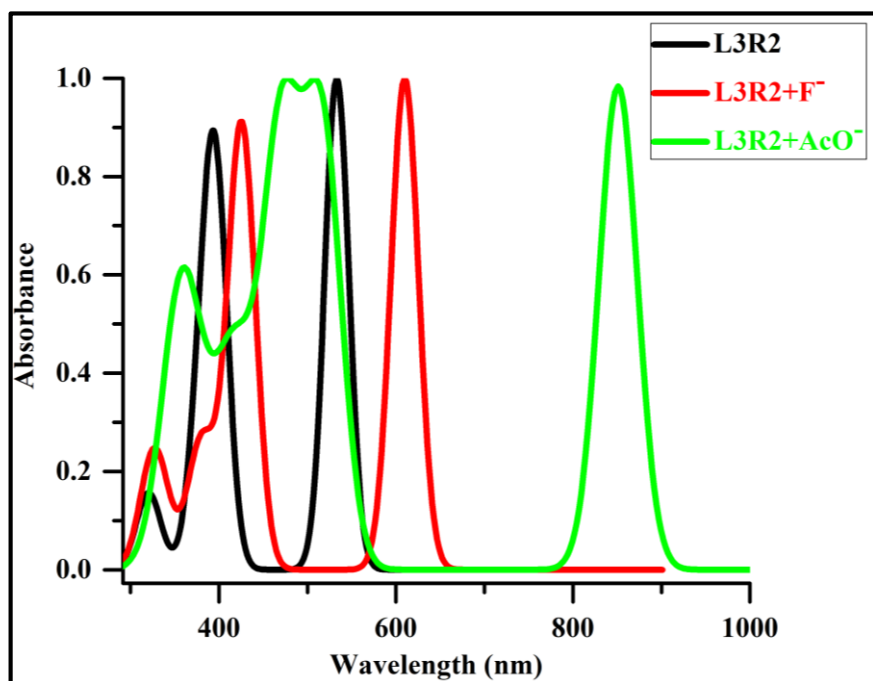
Fig. 4.58 UV-Vis absorption spectra of **L3R2** and complexation with corresponding anions calculated using TD-DFT calculation

Table 4.5 Theoretical and Experimental shift of **L3R1** and **L3R2** upon binding with F⁻ and AcO⁻ ions

S.No	Receptor+ Anions	TD-DFT (nm)	Experimental (nm)
1	**L3R1**+F⁻	318	114
2	**L3R1**+AcO⁻	76	111
3	**L3R2**+F⁻	187	159
4	**L3R2**+AcO⁻	362	162

4.4   CONCLUSIONS

Three new anion receptors **L3R1**, **L3R2,** and **L3R3** exhibiting positional substitution effects of the OH proton was developed, synthesized, and characterized. The colorimetric and UV-Vis results revealed that among all the tested anions, only F⁻ and AcO⁻ ions induced strong binding ability with the OH proton of the receptors **L3R1** and **L3R2** in the DMSO with substantial colour change from pale yellow to purple and from pale yellow to blue. The receptor **L3R2** was successfully applied to the detection of Na^+F^-, Na^+AcO^-, and $Na^+AsO_2^-$ in the organic-aqueous mixture DMSO: H_2O (9:1 v/v) with higher binding constant of 8.79×10^7 M⁻¹, 9.34×10^7 M⁻¹, and 8.12×10^7 M⁻¹ compared with **L3R1** owing to the presence of the -OH group at the para- position, suggesting stable receptor-anion complexation in the organo-aqueous media. The binding modes of the receptor **L3R2** with the two analytes (F⁻ and AcO⁻ ions) were proposed to be 1:1 based on the B-H plot, which also supported the proposed mechanism. For analytical application, a test strip of the receptor **L3R2** was used to detect the TBA^+F^- and $NaAsO_2^-$ ion. Additionally, the practical use of the chemosensors **L3R1** and **L3R2** was exploited to determine the presence of F⁻ and AcO⁻ ions in toothpaste, mouthwash, vinegar, and seawater, which revealed their practical utility as real-time sensors. The ^{1}H-NMR titration and cyclic voltammetric studies supported the deprotonation of the -OH proton in the anion-binding mechanism. Furthermore, the DFT studies supported the proposed binding mechanism and experimental data of **L3R1** and **L3R2** with F⁻ and AcO⁻ ions.

CHAPTER 5

CHEMOSENSOR BASED ON HYDRAZINYL PYRIDINE FOR SELECTIVE DETECTION OF F⁻ ION IN ORGANIC MEDIA AND CO₃²⁻ IONS IN AQUEOUS MEDIA: DESIGN, SYNTHESIS, CHARACTERIZATION AND PRACTICAL APPLICATION
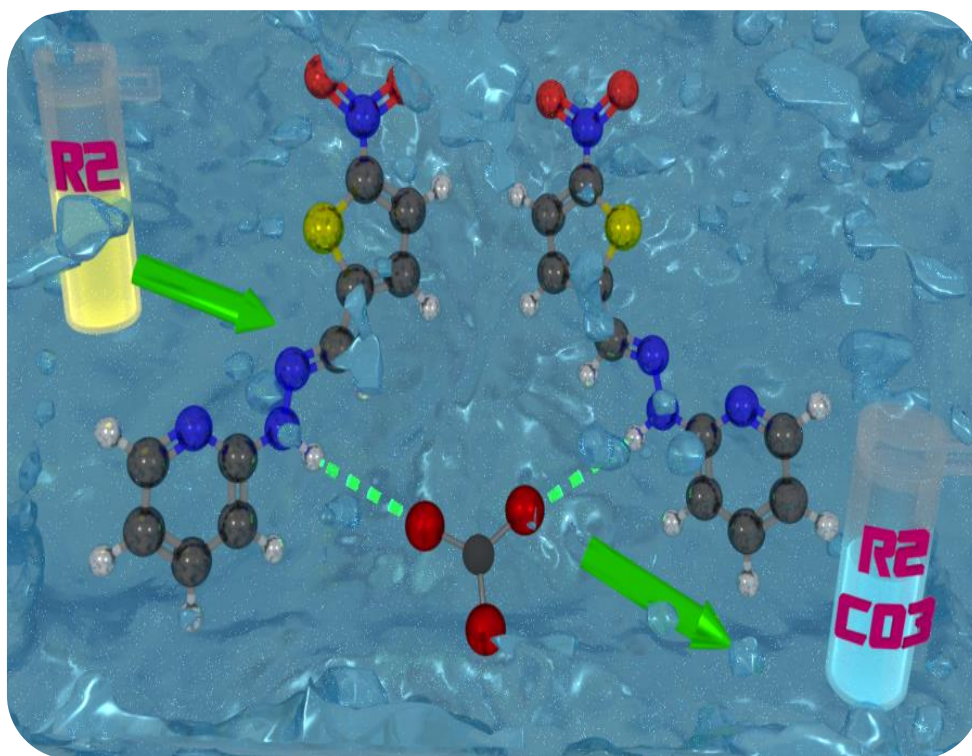
Abstract: In this chapter, the design, synthesis, and characterization of two organic receptors is described. The applicability of the receptors in the colorimetric detection of anions is discussed in detail through UV-Vis spectrophotometric, ^{1}H-NMR titration studies, and electrochemical studies supported by DFT studies. The binding mechanism of the receptors towards active anions is included.

5.1   INTRODUCTION

Anions play a crucial role in the biological field, the medical system (Martinez-Manez and Sancenón 2003; Matthews and Beer 2005), chemical sciences (Hijji et al. 2009; Joo et al. 2007), and environmental science (Beer et al. 1997; Schmidtchen and Berger 1997). Since two decades, various effects have been employed to design and synthesize organic receptors for the detection of biologically important anion species (Han et al. 2007; Zhang et al. 2010). The detection of biotic anions such as F^-, AcO^-, and $H_2PO_4^-$ are of special interest due to their significant role in biological phenomena such as protein synthesis, hormone transportation, remineralization of tooth, etc. (Gunnlaugsson et al. 2006). Among the various anions, the detection of F^- ion is of particular importance. Its use in dental care creams and in the treatment of osteoporosis makes it an interesting target of study (Pramanik et al. 2018; Wang et al. 2016). However, excess of F^- ions in the human body can cause severe health hazards such as fluorosis, skin diseases, nerve diseases, kidney problems, urolithiasis, acute gastric, and even cancer (Reclaru and Meyer 1998). Generally, its detection is of priority, but AcO^- also plays an important role in several biological phenomena and in numerous metabolic processes (Kumar et al. 2018; Zhang et al. 2009). Very few colorimetric chemosensors are available to detect oxyanions such as acetate, bicarbonate, and carbonate due to their similar basicity and high energy of hydration that opposes the forces of recognition (Marcus 1991). Although CO_3^{2-} ions are equally important as the other anions, there is only a handful of literature available for its detection (Han et al. 2010; Hennrich et al. 2001). Carbonate compounds are extensively used in the manufacture of glass, rayon, rubber, plastic, paper, printing ink, and cosmetics, while carbonates are important candidates for electric vehicles and in hybrid electric vehicle power sources, wherein vinylene carbonate is used as an additive electrolyte for rechargeable Li-ion batteries(Aurbach et al. 2004; Ghorai et al. 2016; Tas 2009;

Zougagh et al. 2005). Furthermore, it plays a vital role in agriculture planting, soil science (Choi et al. 2002), hydrology (Morris et al. 2010), and geology (Jain et al. 2006). Despite these wide applications in different processes, carbonate ion is toxic in high doses. Its strong caustic impact on the gastrointestinal tract may result in severe abdominal pain, nausea, diarrhoea, collapse, and even death (Liu et al. 1999). Numerous analytical methods have been developed for the detection of carbonates such as the Fourier transform infrared (FT-IR) spectroscopy (Little and Wentzell 1995), passive acoustic emission (Amundson et al. 1988; Yao et al. 1989), gas chromatography (Tsukada et al. 1990), pH-ion-sensitive field-effect transistor as a sensitive element (Lee et al. 2000; Shin et al. 1996), and ion selective electrode (Lee et al. 2005; Martinez-Manez and Sancenón 2003). Colorimetric anion sensors are basically made up of two parts, namely, the anion binding sites and the chromophore subunit that can indicate the binding event through an optical signal (Nishiyabu and Anzenbacher 2006; Patil et al. 2018). The ICT mechanism is the best signalling unit in which electronic transition takes place through the push-pull reaction from the electron donor to the electron acceptor moiety, and can give spectroscopic and/or colour change that allows it to serve as a colorimetric sensor for target anions (Li et al. 2010). Many chemosensors were synthesized to detect these anions, but most of them interfere with each other such as F^- and AcO^- ions due to their similar basicity and surface charge density (Beer and Gale 2001; Gale 2001; Nishiyabu and Anzenbacher 2005). In view of these specifications, two new colorimetric chemosensors **L4R1** (X = O) and **L4R2** (X = S) with different heterocyclic rings containing sulfur and oxygen atoms were developed and synthesized in this research paper in combination with the N-H group as a binding site and the NO_2 group as a signalling unit as shown in Scheme 5.1. The receptor **L4R1** showed high selectivity towards F^- ion in the DMSO over the other interference anions. Moreover, in the DMSO, receptor **L4R2** could discriminate between F^- and AcO^- ions based on distinct change in colour from pale yellow to aqua and from pale yellow to green. The introduction of electron-withdrawing nitro groups to **L4R1** and **L4R2**, which leads to the increase in the acidity of the NH proton, has a positive effect on the affinity and selectivity of the receptors towards the anions. However, in an aqueous environment, the receptors **L4R1** and **L4R2** are highly capable of detecting CO_3^{2-} ions.

L4R1, X=O
L4R2, X=S
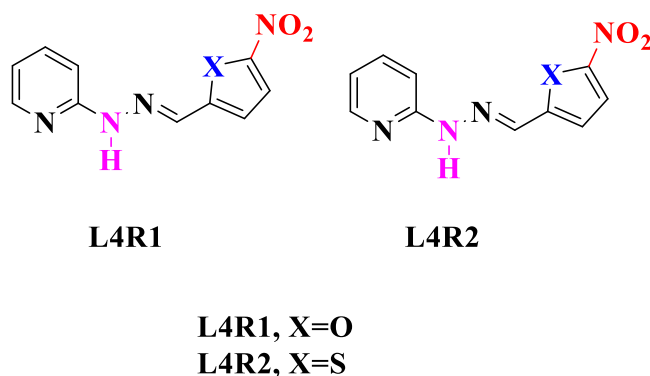
Scheme 5.1 Structure of receptors **L4R1** and **L4R2**

5.2 EXPERIMENTAL SECTION

5.2.1 Materials and methods

All the chemicals used in the present study were procured from Sigma-Aldrich, Alfa Aesar or Spectrochem and used without further purification. All the solvents were purchased from SD Fine, India, and were of HPLC grade and used without further distillation. The ^{1}H-NMR samples were recorded on Bruker Avance (400 MHz) instrument using Tetramethylsilane (TMS) as internal reference and the DMSO-d_6 as the solvent. ^{13}C NMR spectra were recorded on Bruker Ascend (125 MHz) instrument using TMS as internal reference and DMSO-d_6 as solvent. Resonance multiplicities are explained as s (singlet), d (doublet), t (triplet), and m (multiplet). The ESI-MS data was obtained using an ESI-QToF (Waters-synapt G2S) high resolution mass spectrometer. The melting points were measured on the stuart-SMP3 melting-point apparatus in open capillaries. The infrared spectra were recorded on the Bruker alpha FT-IR spectrometer. The UV-Vis spectroscopy was performed with the Analytike jena Specord S600 spectrometer in standard 3.00 ml quartz cells with 1 cm path length. The completion of the reaction was confirmed by checking with the TLC plates. Cyclic voltammogram was recorded on the Ivium electrochemical workstation (Vertex) at a scan rate of 20 mV/s and potential range of -1.5 V to 1.5 V. Density Functional Theory (DFT) simulation has been performed on the receptor molecule using GAUSSIAN 09 package. A close shell Becke-Lee-Yang-Parr hybrid exchange-correlation three-parameter functional (B3LYP) along with 6-311++G(d) basis set were used in the simulation to drive a complete geometry optimization for isolated receptor and its

complex formation with anions. Berny's optimization algorithm was used to fully optimize the molecular geometry, which involve redundant internal coordinates. To confirm the convergence to the minima on the potential energy surface, the harmonic vibrational wavenumber were calculated using analytic second derivative and properly scale down to control the systematic error caused by incompleteness of the basis set. In a second step, the time dependent DFT (TD-DFT) method were used considering the same B3LYP exchange-correlation functional with 6-311+G (d,p) basis set to obtain the UV-Vis absorption spectra of free and complex receptor.

5.2.2   Synthesis of receptors L4R1 and L4R2

The receptors **L4R1** and **L4R2** were synthesized by reacting 2-hydrazinyl pyridine (6.65 mmol) with different aldehyde such as 5-nitrofuran-2-carbaldehyde (0.75 mmol) and 5-nitro thiophene-2-carbalehyde (1.5 mmol) in methanol and by adding 2-3 drops of acetic acid (CH_3CO_2H) as catalyst. The reaction mixture is refluxed at 60ºC for 6 h by continuous stirring. After completion of the reaction as monitored in the TLC, the precipitate was filter washed several times with cold methanol to obtain the desired products, **L4R1** and **L4R2** as represented in Scheme 5.2.
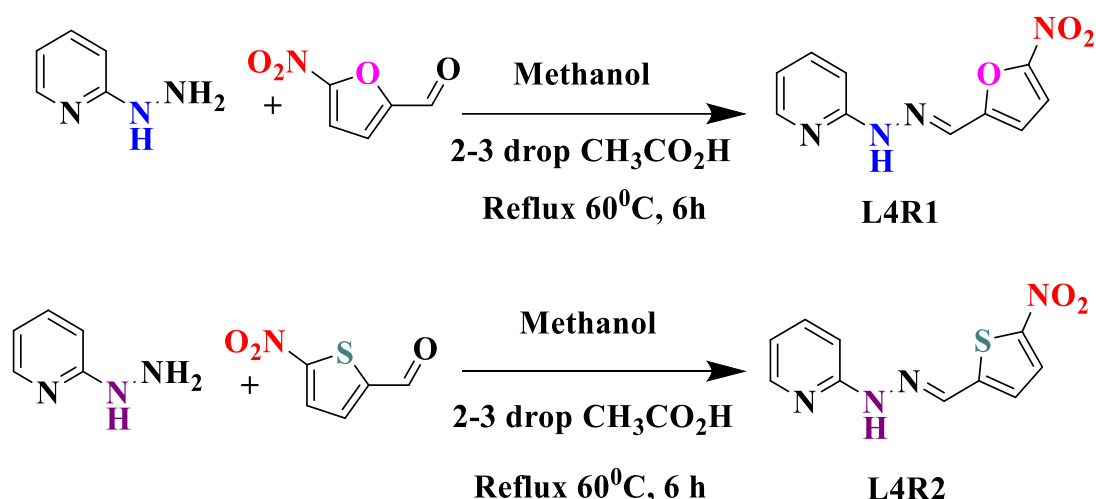
Scheme 5.2 Synthesis of the receptors **L4R1** and **L4R2**

5.2.3   Characterization data

The purity and structure of the receptors **L4R1,** and **L4R2** were confirmed by FT-IR, ^{1}H-NMR, ^{13}C-NMR, and mass spectroscopic methods. The characterization data has been compiled and given below.

(E)-2-(2-(5-nitrofuran-2-yl) methylene) hydrazinyl) pyridine (L4R1)
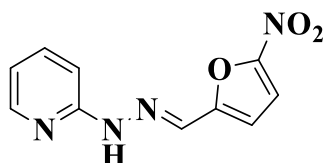
Data obtained for receptor L4R1: Yield: 80%. m.p.: 200 ^{0}C. ^{1}H NMR (DMSO-d$_6$, 400 MHz, Me$_4$Si): δ_{ppm} 11.541 (s, 1H), 8.186-8.172 (m, 1H), 7.958 (d, J=8Hz, 1H), 7.792 (d, J=7.5 Hz, 1H), 7.738-7.694 (m, 1H), 7.264 (d, J= 6.5Hz, 1H),7.104-7.094 (d, J=5Hz, 1H), 6.901-6.868 (m, 1H). ^{13}C NMR (DMSO-d$_6$, 125 MHz, Me$_4$Si): δ_{ppm} 156.49, 154.10, 151.65, 148.42, 138.78, 126.85, 116.94, 116.03, 112.43, 112.37, 107.33. IR (KBr pellet) (cm^{-1}): 3257 (NH), 1259 (C-O), 1539 (C=C), 1643 (C=N), 1367 (NO$_2$). Mass (ESI): m/z calculated for C$_{10}$H$_8$N$_4$O$_3$: 232.20 Obtained: 233.1134 [M+H$^+$].

(E)-2-(2-(5-nitrothiophen-2-yl) methylene) hydrazinyl) pyridine (L4R2)
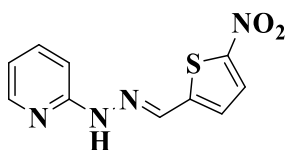
Data obtained for receptor L4R2: Yield: 84%. m.p.: 260 ^{0}C. ^{1}H NMR (DMSO-d$_6$, 400 MHz, Me$_4$Si): δ_{ppm} 11.519 (s, 1H), 8.173-8.164 (d, J=3.6 Hz, 2H), 8.085-8.074 (d, J=4.4 Hz, 1H), 7.732-7.688 (s, 1H), 7.367 (d, J=6.4 Hz, 1H), 7.232 (d, J=8.4 Hz, 1H), 6.893-6.863 (m, 1 H). ^{13}C NMR (DMSO-d$_6$, 125 MHz, Me$_4$Si): δ_{ppm} 156.43, 149.50, 149.23, 148.44, 148.39, 138.80, 132.25, 132.20, 131.47, 126.81, 126.78, 116.93, 116.85, 107.24. IR (KBr pellet) (cm^{-1}): 3422 (NH), 1336 (NO$_2$), 2963 (C-H), 2872 (C-H), 1620 (CH=N), 1594 (C=C), 843 (C-S). Mass (ESI): m/z calculated for C$_{10}$H$_8$N$_4$O$_2$S: 248.26 Obtained: 249.0938 [M+H$^+$].

The representative spectrum of receptors **L4R1** and **L4R2** is given below
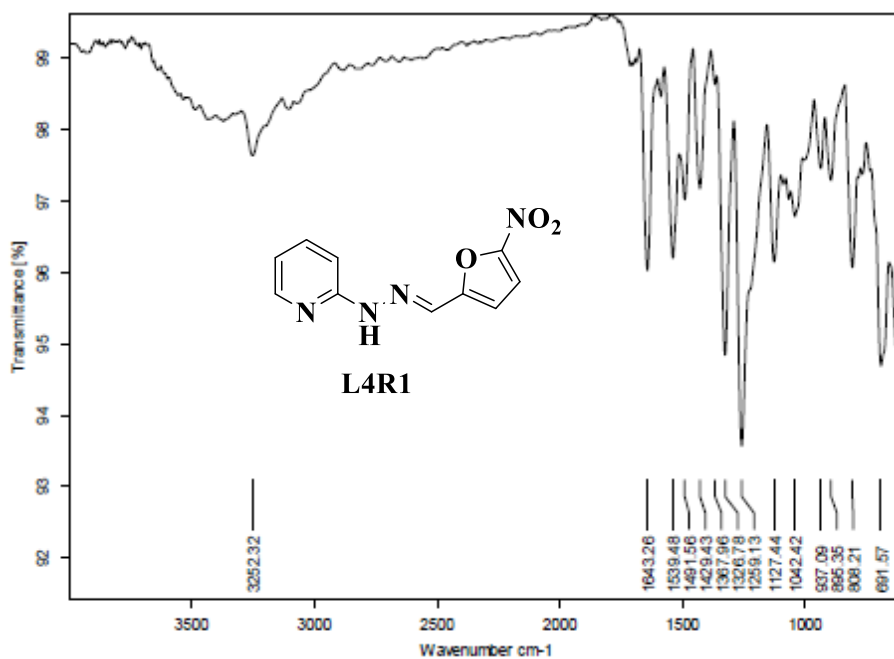
Fig. 5.1 FT-IR spectrum of **L4R1**
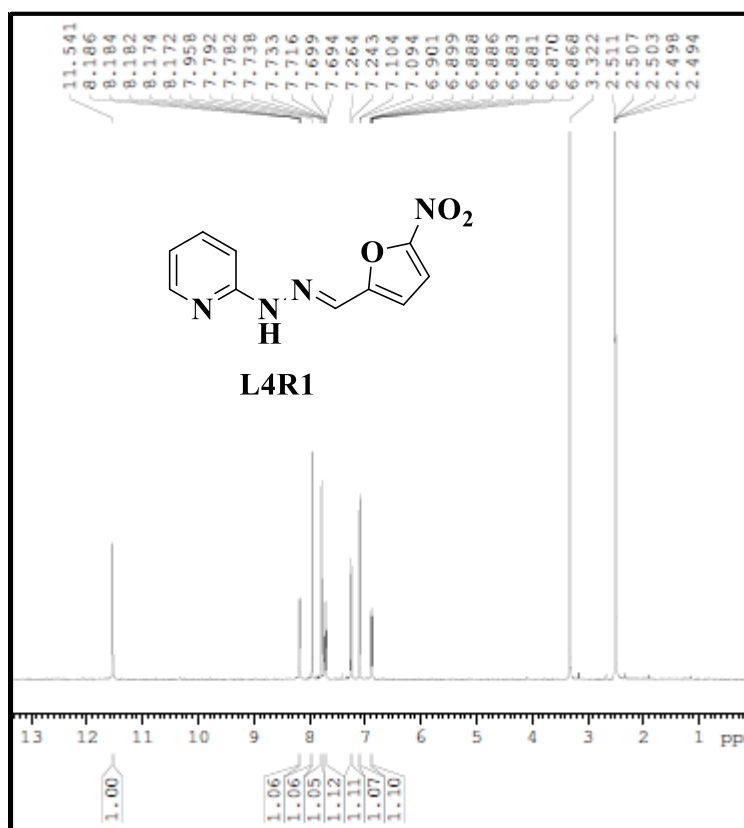
Fig. 5.2 ^{1}H-NMR spectrum of **L4R1**

Fig. 5.3 ^{13}C-NMR spectrum of **L4R1**

Mass spectrum: L4R1

Exact Mass: 232.06

Mass obtained in the positive mode: 233.1134

Elemental composition: $C_{10}H_8N_4O_3$
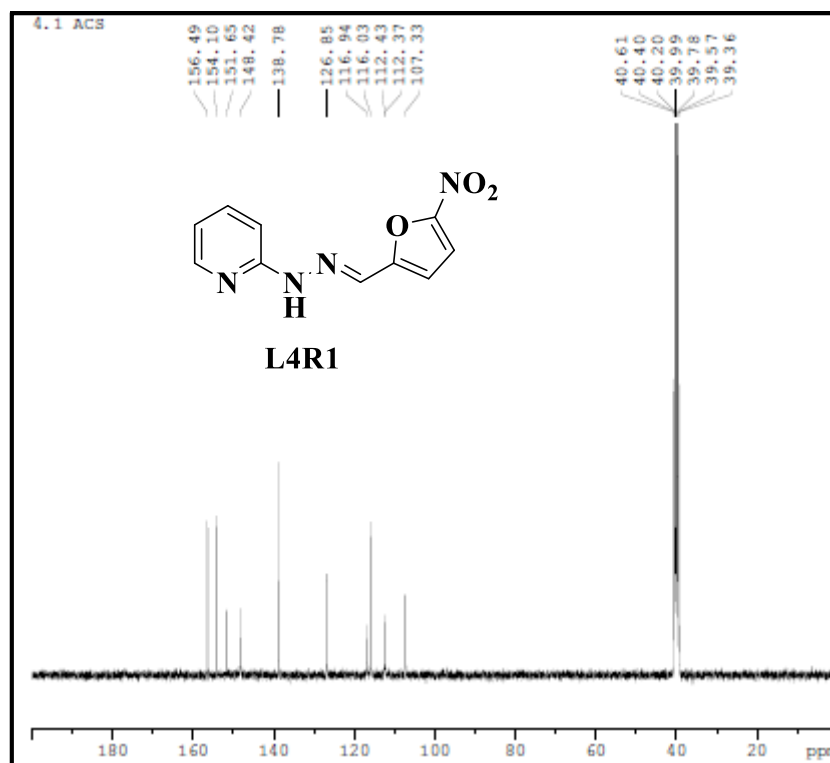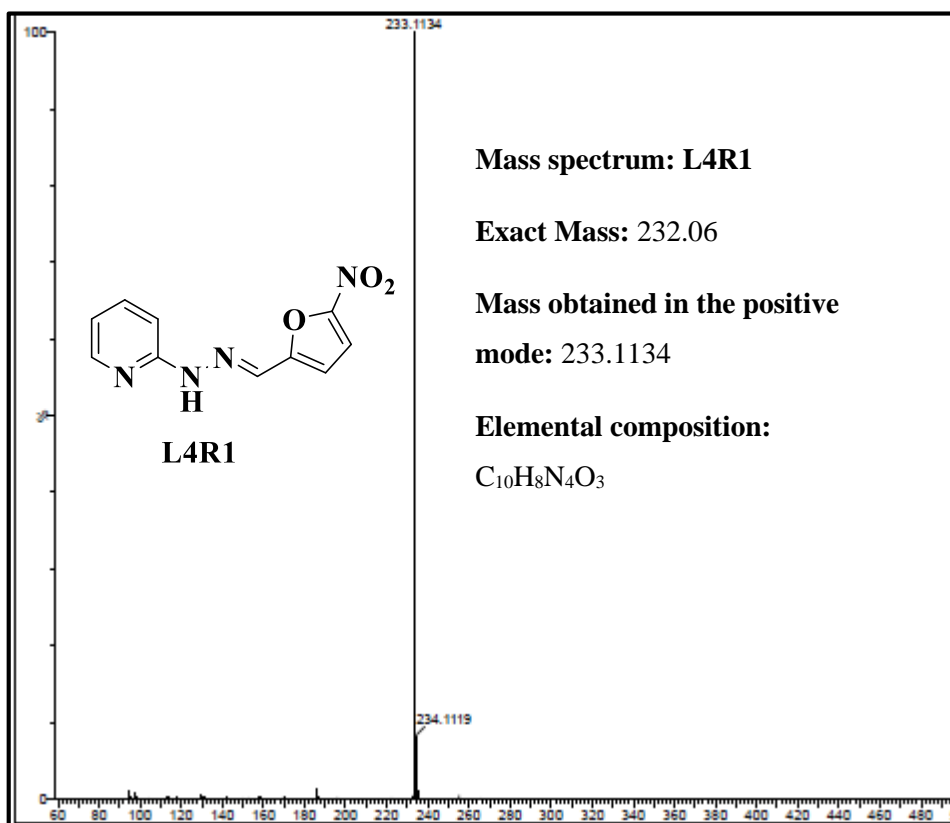
Fig. 5.4 ESI-MS spectrum of **L4R1**
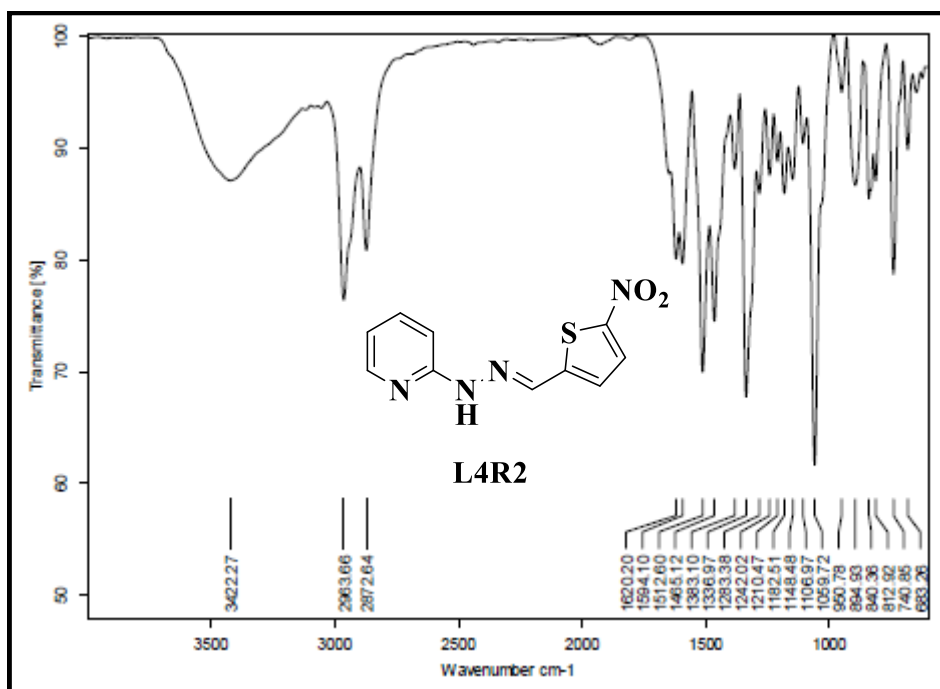
Fig. 5.5 FT-IR Spectrum of **L4R2**
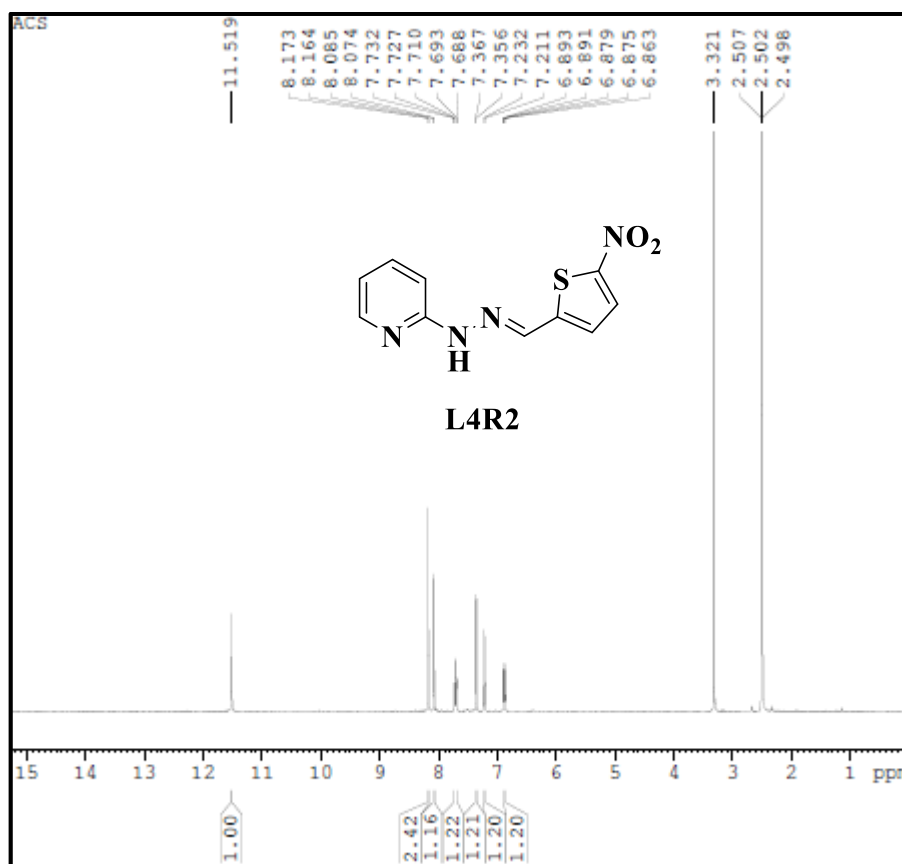
Fig. 5.6 ^{1}H-NMR spectrum of **L4R2**

Fig. 5.7 ^{13}C-NMR spectrum of **L4R2**

Mass spectrum: L4R2

Exact Mass: 248.04

Mass obtained in the positive mode: 249.0938

Elemental composition: $C_{10}H_8N_4O_2S$
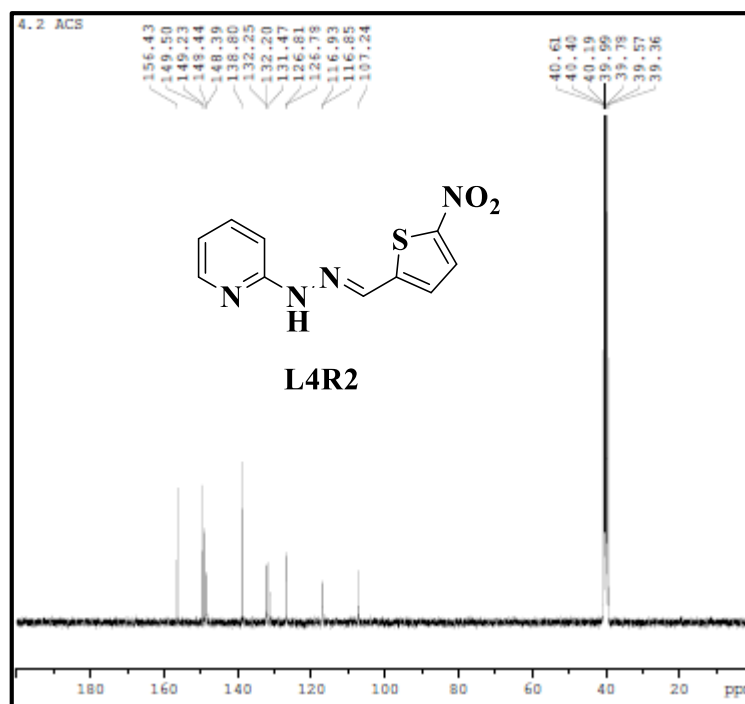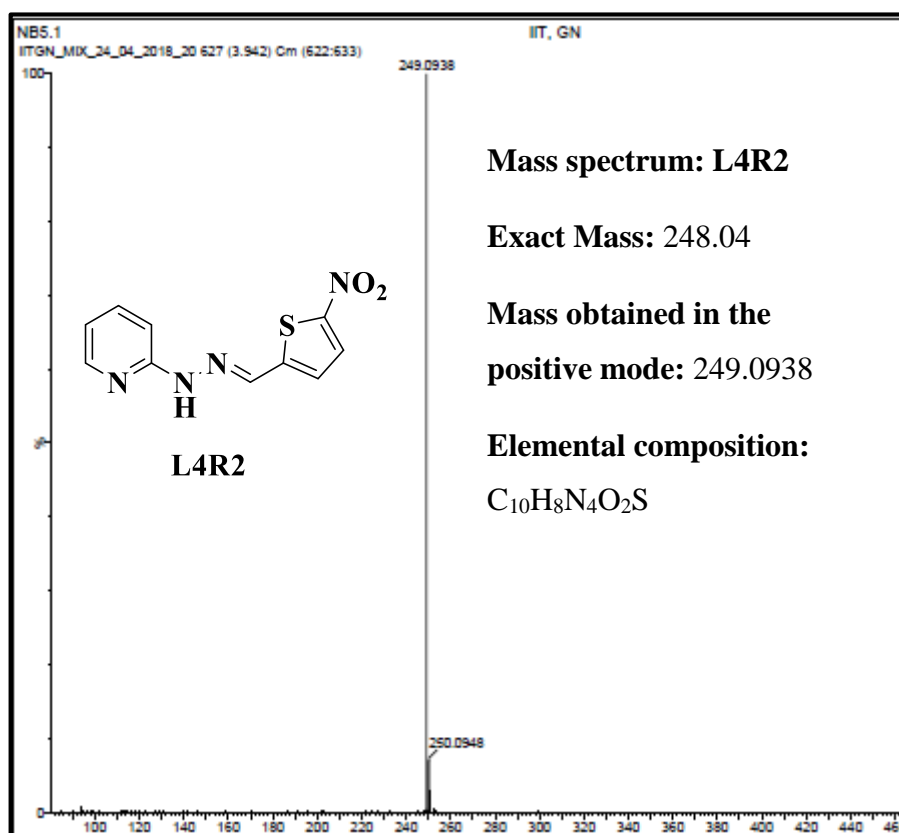
Fig. 5.8 ESI-MS spectrum of **L4R2**

5.3   RESULT AND DISCUSSION

5.3.1   Colorimetric detection of anions

A significant feature of the receptors **L4R1** and **L4R2** is their specific selectivity towards a particular anion over other interference anions, and therefore, the colorimetric and UV-Vis spectra are performed in the DMSO. In the colorimetric experiment, the receptors **L4R1** and **L4R2** (1×10^{-4} M in DMSO) are treated against different TBA salts like F^-, Cl^-, Br^-, I^-, NO_3^-, HSO_4^-, $H_2PO_4^-$, and AcO^- (1×10^{-2} M in DMSO). Spontaneous and visually detectable colour change is observed only when the receptors **L4R1** and **L4R2** reacted with F^- and AcO^- ions owing to high basicity (Arslan et al. 2017). As is known, AcO^- is the main interference ion with F^- due to their similar basicity and surface charge density, and thus, it is difficult to distinguish between them. In the present study, the receptor **L4R1** only responded to the most electronegative F^- ion by significant colour change from pale yellow to aqua, whereas the receptor **L4R2** successfully discriminated between F^- and AcO^- anions with distinct colour change from pale yellow to aqua and green. On the other hand, the remaining anions showed no colour change in the same condition as shown in Fig. 5.9. The observed colour changes exhibited by these receptors may be due to the formation of strong hydrogen bonds or the deprotonation of the NH group on interaction with F^- and AcO^- ions. These hydrogen bonds or deprotonations affect the electronic properties of the chromophore, resulting in colour change along with new charge-transfer interaction between the anion-bound NH group and the electron deficient nitro group (Manivannan et al. 2015).

Fig. 5.9 Colour change of the receptors **L4R1** and **L4R2** (1×10^{-4} M in DMSO) with the addition of 2 equiv. of various tetrabutylammonium salts (1×10^{-2} M in DMSO)

5.3.2 Comparative and interference studies

The UV-Vis experiment was conducted to investigate selectivity and high sensitivity towards basic F^- ions over other competitive anions in order to correlate the naked-eye observational study. As shown in Fig. 5.10 and Fig. 5.11, the UV-Vis spectra response of **L4R1** appeared to be highly selective for F^- ion, whereas in the case of receptor **L4R2,** a significant bathochromic shift was observed for both F^- and AcO^- ions. Under similar conditions, no obvious change in the UV-Vis absorption was observed when equal amounts of other tested tetrabutyl ammonium salts (TBA) were added. Conversely, it was worth noting that the intensity of the absorption band for AcO^- ion was much less compared with the F^- ion. This reflects the high selectivity of the receptors **L4R1** and **L4R2** towards F^- ions over the other interference anions in the DMSO, which can be ascribed to anion basicity and hydration energy. The interference of other anions for the detection of F^- was also investigated by recording the UV-Vis spectra of **L4R1** and **L4R2** upon addition of 2 equiv. of F^- and 4 equiv. of other anions. It may be noted that no significant interference from any other anions was observed as depicted in Fig. 5.12 and Fig. 5.13. The bar graph representation in Fig. 5.14 and Fig. 5.15 confirmed the excellent selectivity of **L4R1** and **L4R2** for F^- ion over other related anions in the DMSO.
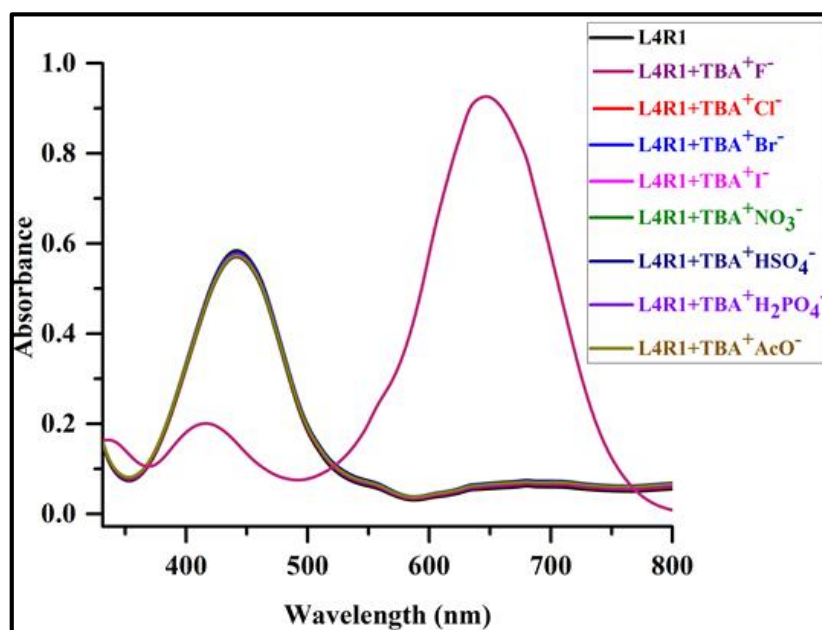
Fig. 5.10 Comparative study carried out for **L4R1** (1×10^{-4} M in DMSO) in the presence of different series of TBA salts (1×10^{-2} M in DMSO)
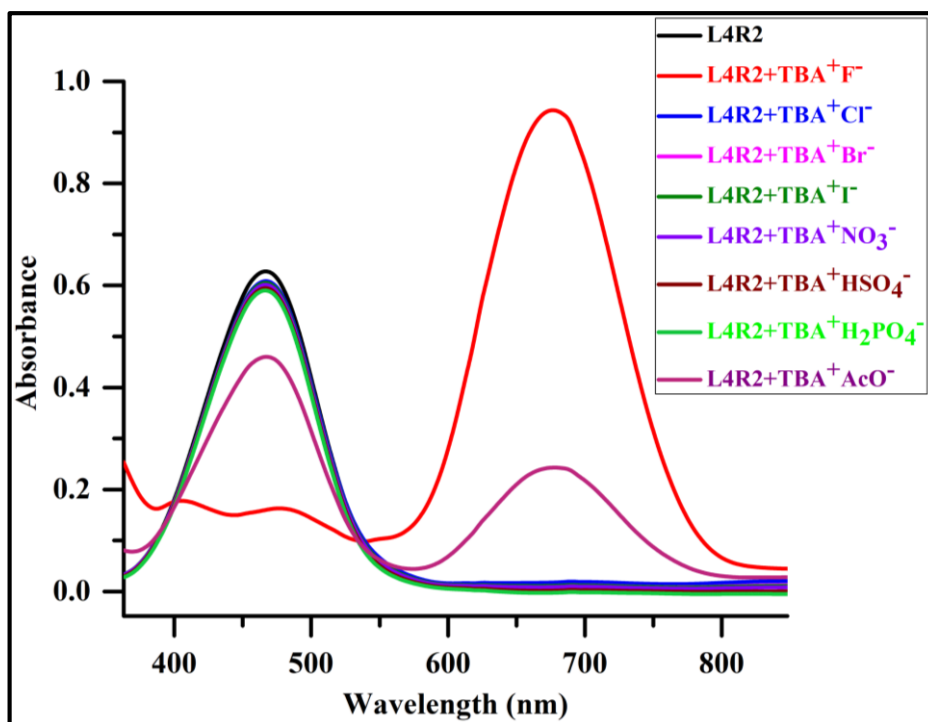
Fig. 5.11 Comparative study carried out for **L4R2** (1×10^{-4} M in DMSO) in the presence of different series of TBA salts (1×10^{-2} M in DMSO)
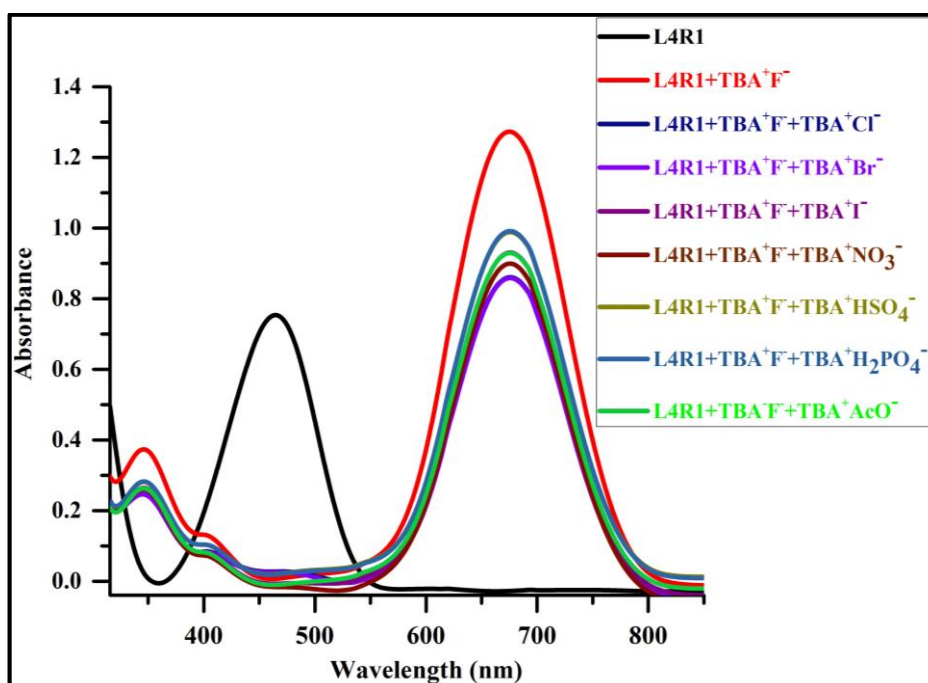
Fig. 5.12 UV-Vis absorption spectral changes of **L4R1**-F$^-$ (2 equiv.) with other interference anions (4 equiv.) in DMSO
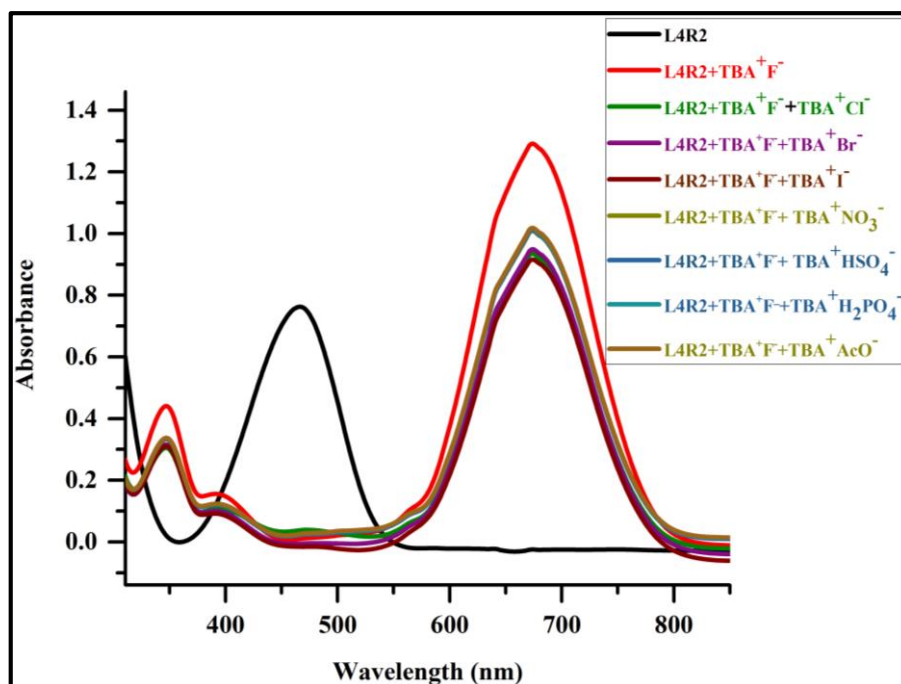
Fig. 5.13 UV-Vis absorption spectral changes of **L4R2**-F⁻ (2 equiv.) with other interference anions (4 equiv.) in DMSO
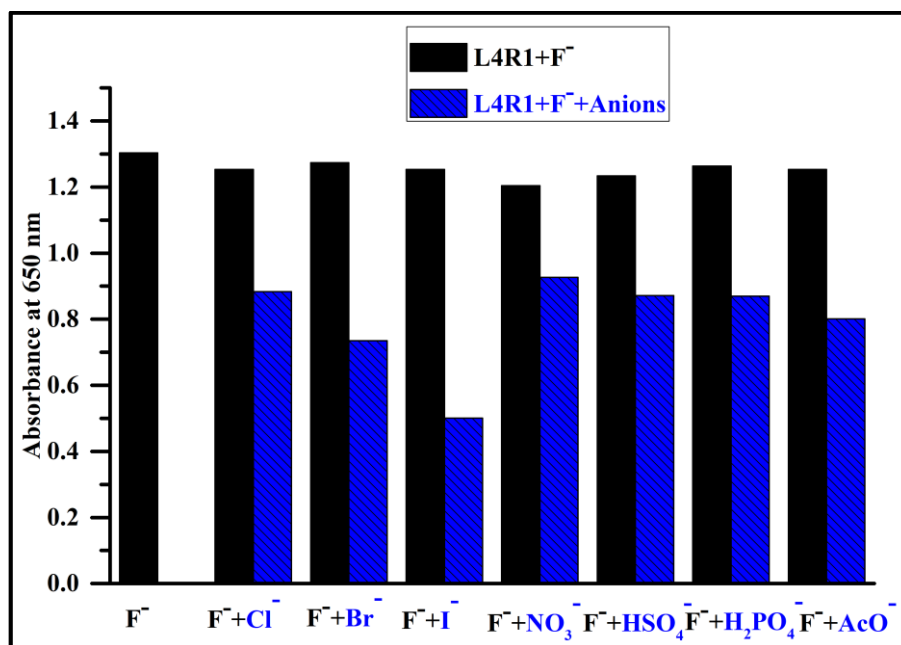
Fig. 5.14 Bar graph representation of interference response of receptor **L4R1** towards 2 equiv. of F⁻ ion in the presence of 4 equiv. of other interference anions (black bar represents the addition of F⁻ ion to the solution and the blue bar represents the addition of other interference anions to the above solution)
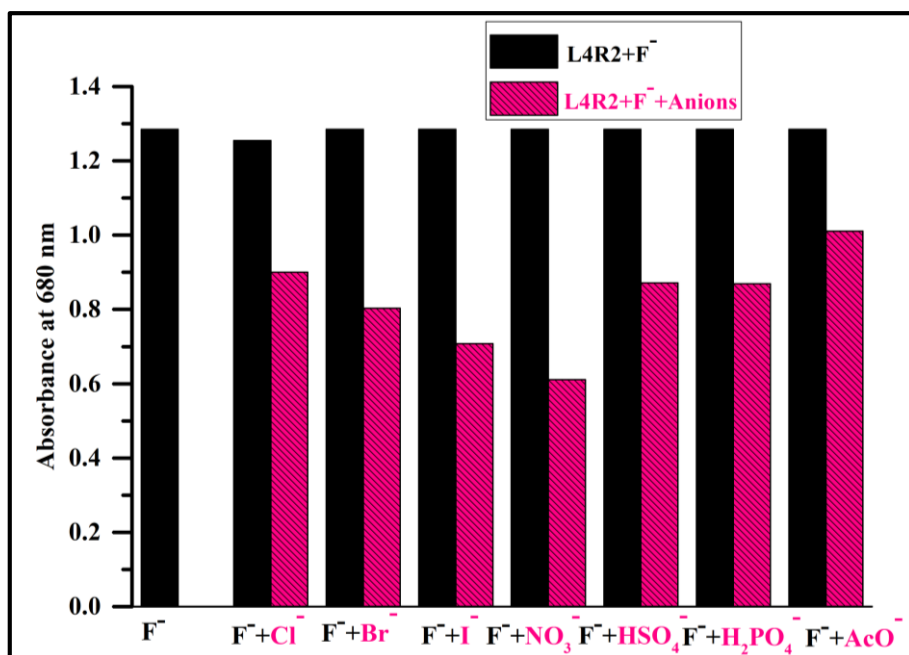
Fig. 5.15 Bar graph representation of interference response of receptor **L4R2** towards 2 equiv. of F⁻ ion in the presence of 4 equiv. of other interference anions (black bar represents the addition of F⁻ ion to the solution and the pink bar represents the addition of other interference anions to the above solution)

5.3.3   UV-Vis titration studies of L4R1 and L4R2 with anions in DMSO

To obtain a quantitative assessment of the receptor **L4R1**, the UV-Vis titration experiment was carried out by adding a standard solution of the TBA⁺F⁻ to the receptor **L4R1** solution in the DMSO. As depicted in Fig.5.16, the free receptor **L4R1** in the DMSO, without the addition of anion, displayed a characteristic absorption band at 442 nm, which was attributed to the $\pi \rightarrow \pi^*$ transition of the nitro chromophore moiety (Wang et al. 2018). Upon incremental addition of 0.1 equiv. of F⁻ ions, the intensity of the absorption band at 442 nm decreased, and a new band at 650 nm increased accompanied with dramatic colour change from pale yellow to aqua. The excellent selectivity of the receptor **L4R1** for the F⁻ ion was attributed to its unique properties such high charge density, small ionic radius (1.3 A˚), and hard Lewis base (Shao et al. 2008). The UV-Vis titration of the receptor **L4R1** with F⁻ ions yielded a single isosbestic point at 504 nm with a bathochromic shift ($\Delta\lambda_{max}$) of 208 nm, indicating equilibrium between **L4R1** and F⁻ ions. Fig. 5.17 and Fig. 5.18 shows the changes in

the UV–Vis spectra of the receptor **L4R2** at a concentration of (1×10^{-4} M in DMSO) upon addition of F⁻ and AcO⁻ ions. The free receptor **L4R2** is dominated by strong absorption bands at 465 nm and 450 nm. Upon incremental addition of 0.1 equiv. of F⁻ and AcO⁻ ions to **L4R2**, the band at 465 nm and 450 nm progressively decreased, while a new band at about 680 nm and 657 nm appeared and the intensity increased gradually. There is distinct colour change of the receptor solution from pale yellow to aqua and from pale yellow to green in the presence of F⁻ and AcO⁻ ions. The colour change with significant bathochromic shift ($\Delta\lambda_{max}$) of about 215 nm and 207 nm can be attributed to the strong interaction between the receptor and the targeted anions (Chen et al. 2017). The presence of isosbestic points at 530 nm and 516 nm in the absorption spectra indicate formation of a single component upon complexation between receptor **L4R2** and anions (F⁻ and AcO⁻) in DMSO. To ensure that the detection process follows deprotonation and not complex formation, receptors **L4R1** and **L4R2** was titrated with TBA hydroxide as represented in Fig. 5.19 and Fig. 5.20. The titration profiles afforded similar spectral pattern and same colour change as observed for basic anions F⁻ and AcO⁻. This confirms that the deprotonation of NH proton is responsible for the colorimetric change and not complex formation.
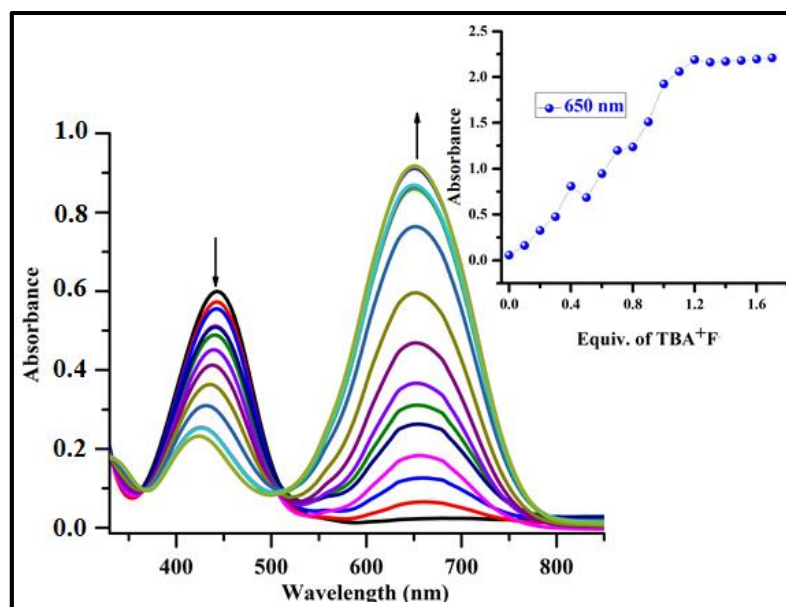
Fig. 5.16 Change in UV-Vis absorption spectra of **L4R1** (1×10^{-4} M in DMSO) in DMSO solution upon sequential addition of TBA⁺F⁻ (1×10^{-2} M in DMSO); Insert attributed to equiv. addition of TBA⁺F⁻ at particular wavelength of 650 nm
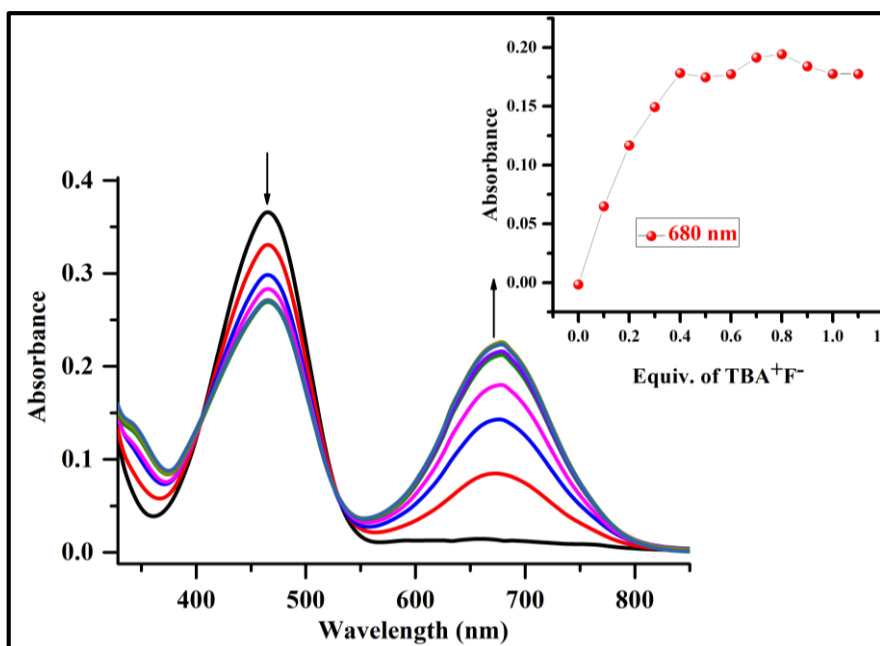
Fig. 5.17 Change in UV-Vis absorption spectrum of **L4R2** (1×10^{-4} M in DMSO) in DMSO solution upon sequential addition of TBA$^+$F$^-$ (1×10^{-2} M in DMSO); Inset attributed to equiv. addition of TBA$^+$F$^-$ at particular wavelength of 680 nm
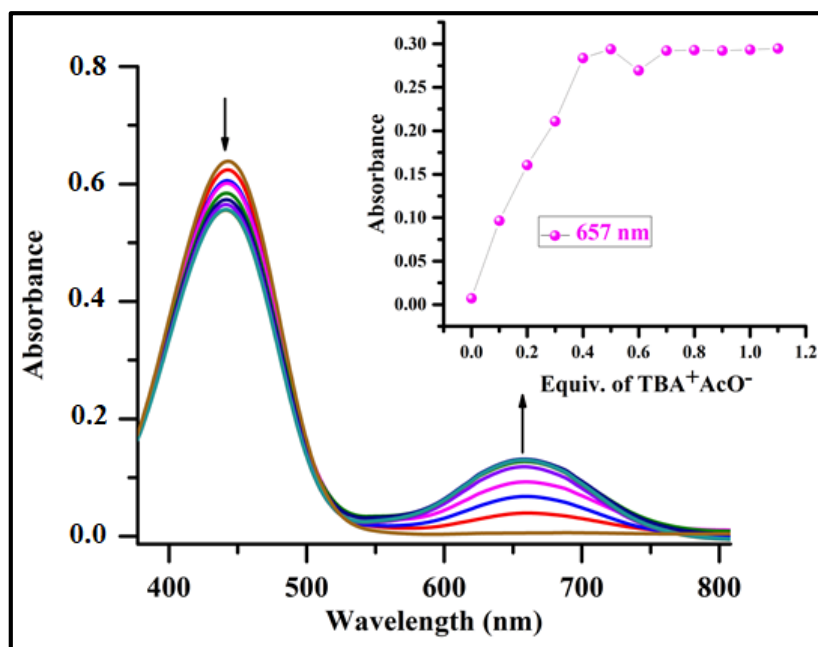
Fig. 5.18 Change in UV-Vis absorption spectrum of **L4R2** (1×10^{-4} M in DMSO) solution upon sequential addition of TBA$^+$AcO$^-$ (1×10^{-2} M in DMSO); Inset attributed to equiv. addition of TBA$^+$AcO$^-$ at particular wavelength of 657 nm
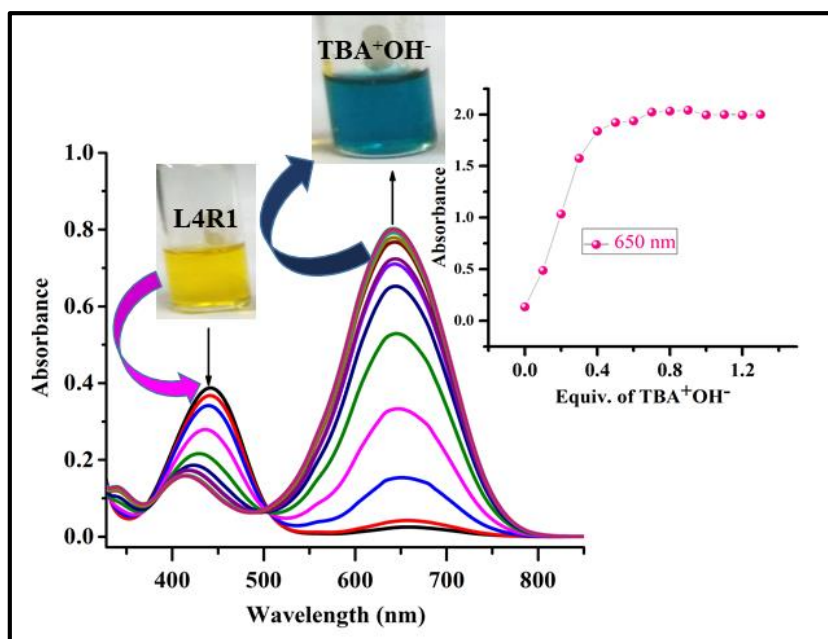
Fig. 5.19 UV-Vis titration spectra of receptor **L4R1** (1×10^{-4} M in DMSO) solution upon sequential addition of TBA$^+$OH$^-$ (1×10^{-2} M in DMSO); Inset attributed to equiv. addition of TBA$^+$OH$^-$ at particular wavelength of 650 nm
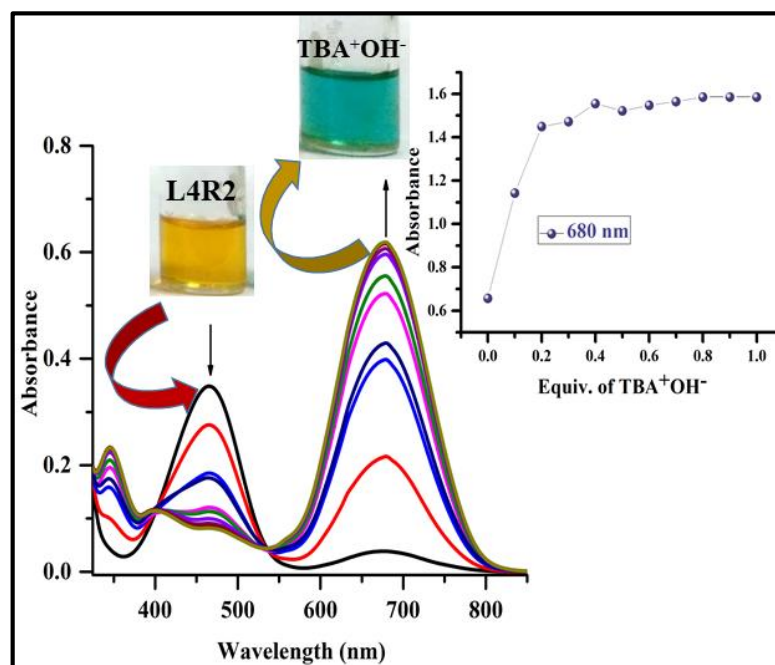
Fig. 5.20 UV-Vis titration spectra of receptor **L4R2** (1×10^{-4} M in DMSO) solution upon sequential addition of TBA$^+$OH$^-$ (1×10^{-2} M in DMSO); Inset attributed to equiv. addition of TBA$^+$OH$^-$ at particular wavelength of 680 nm

5.3.4   UV-Vis titration studies of L4R1 and L4R2 with CO_3^{2-} in DMSO: H_2O (9:1 v/v)

The binding ability of the receptors **L4R1** and **L4R2** (1×10^{-4} M in DMSO) towards different series of sodium salts including F^-, Cl^-, Br^-, $H_2PO_4^-$, HSO_4^{2-}, HCO_3^-, HSO_4^-, NO_3^-, AcO^-, and CO_3^{2-} (1×10^{-2} M in H_2O) was studied by the naked-eye colorimetric experiments and the UV-Vis spectroscopy technique. As shown in Fig. 5.21, the receptors **L4R1** and **L4R2** solutions showed distinct colour change from pale yellow to aqua upon the addition of 2 equiv. of CO_3^{2-} ions. This was most likely due to the presence of the electron withdrawing chromogenic nitro group, which enhanced the acidity of the –NH proton making it highly capable of competing with water molecules in an aqueous medium for CO_3^{2-} ion detection. On the other hand, the colour remained unchanged after the addition of the other chosen sodium salts, which meant a weak interaction with the receptors. Consequently, in DMSO: H_2O (9:1 v/v), CO_3^{2-} strongly bonded with the NH proton resulting in a strong complex formation NH-- CO_3^{2-}.
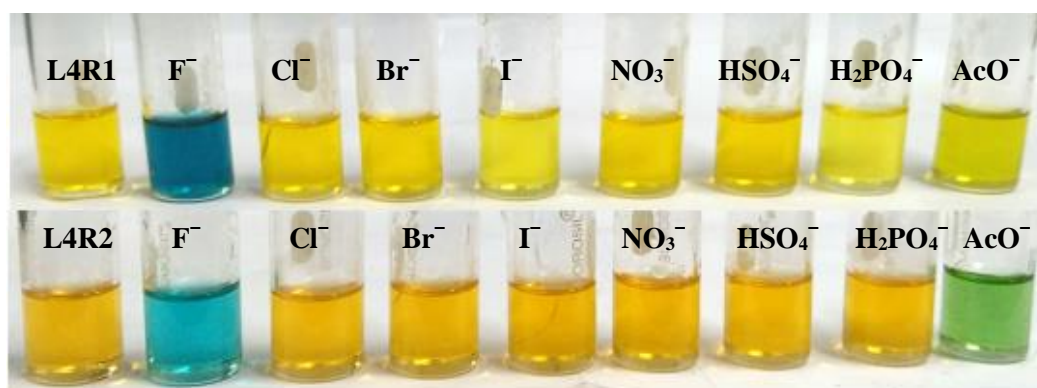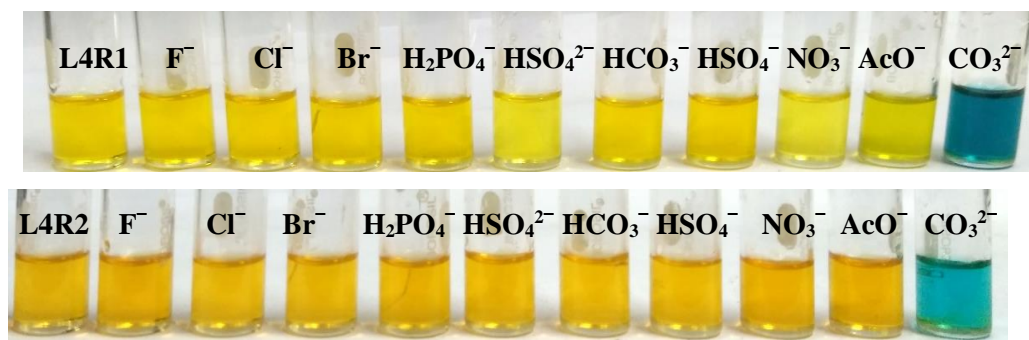

Fig. 5.21 Colour change of the receptors **L4R1** and **L4R2** (1×10^{-4} M in DMSO) with the addition of 1 equiv. of various sodium salts (1×10^{-2}M in H_2O) in DMSO: H_2O (9:1 v/v)

5.3.5   Competitive studies

To further verify the selectivity of **L4R1** and **L4R2** towards CO_3^{2-} ions among all the other anions, a comparative experiment was conducted through the UV-Vis absorption spectroscopy in DMSO: H_2O (9:1 v/v). Upon the addition of 2 equiv. of various anions in the form of sodium salts to solutions of **L4R1** and **L4R2**, a sharp shift in the UV-Vis absorption band was observed only for the CO_3^{2-} ions as illustrated in Fig. 5.22 and Fig. 5.23.
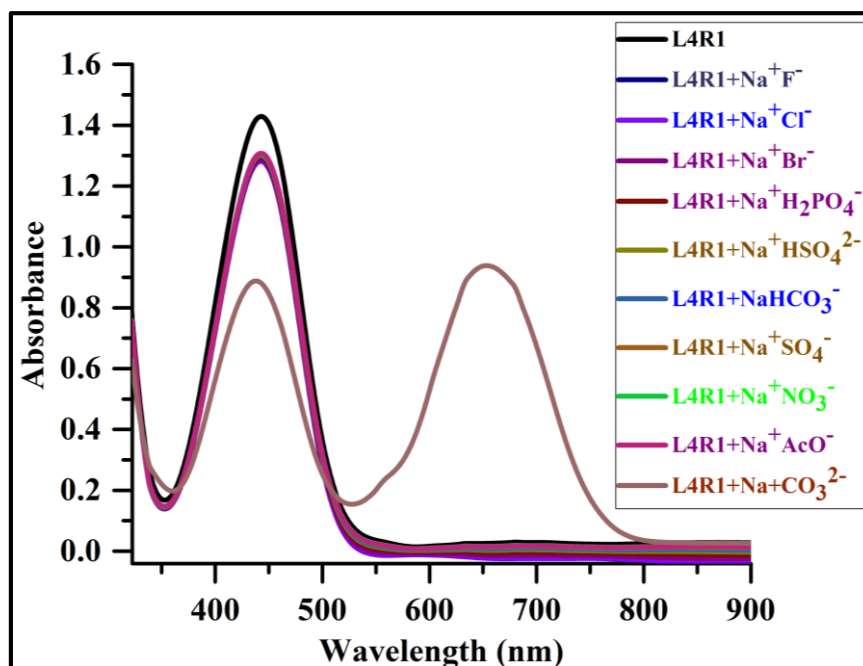
Fig. 5.22 A comparative study carried out for **L4R1** (1×10^{-4} M in DMSO) in the presence of various sodium salts (1×10^{-2}M in H$_2$O) in DMSO: H$_2$O (9:1 v/v)
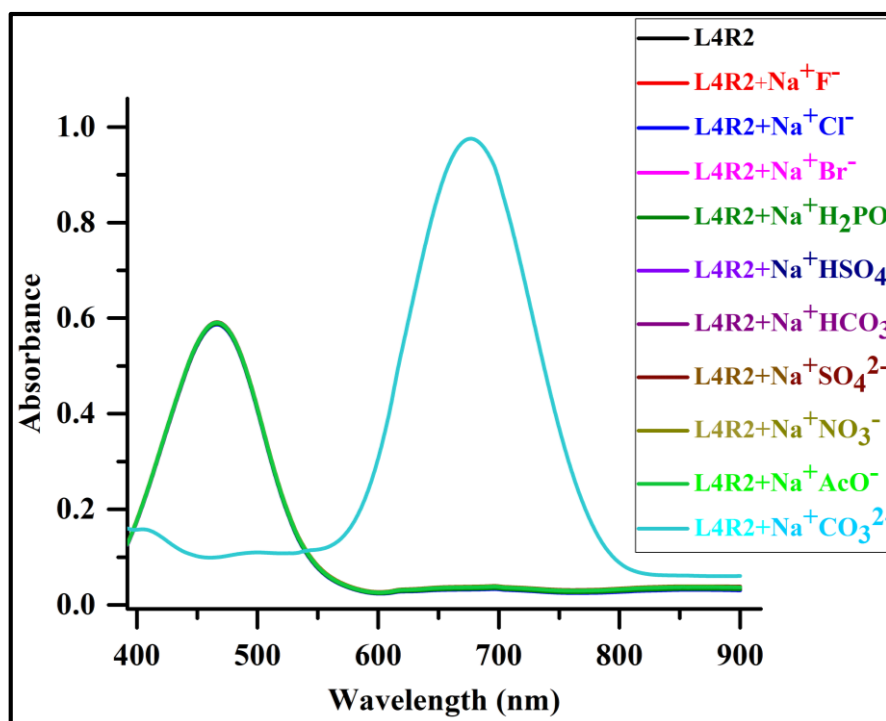
Fig. 5.23 A comparative study carried out for **L4R2** (1×10^{-4} M in DMSO) in the presence of various sodium salts (1×10^{-2}M in H$_2$O) in DMSO: H$_2$O (9:1 v/v)

In order to investigate the interference of other anions in the detection process, UV-Vis absorption study was performed with the addition of 2 equiv. of CO_3^{2-} ion to the receptors **L4R1** and **L4R2** solutions containing 4 equiv. of other anions as shown in Fig. 5.24 and Fig. 5.25. The UV-Vis spectra displayed a significant red shift with a new band centred at 644 nm and 675 nm. The spectral pattern was similar to that obtained on the addition of CO_3^{2-} ions to the free receptors **L4R1** and **L4R2**. Thus, the receptors **L4R1** and **L4R2** is found to be selective in the detection of CO_3^{2-} ions in mixed media as represented in the form of a bar graph as shown in Fig. 5.26 and Fig. 5.27.
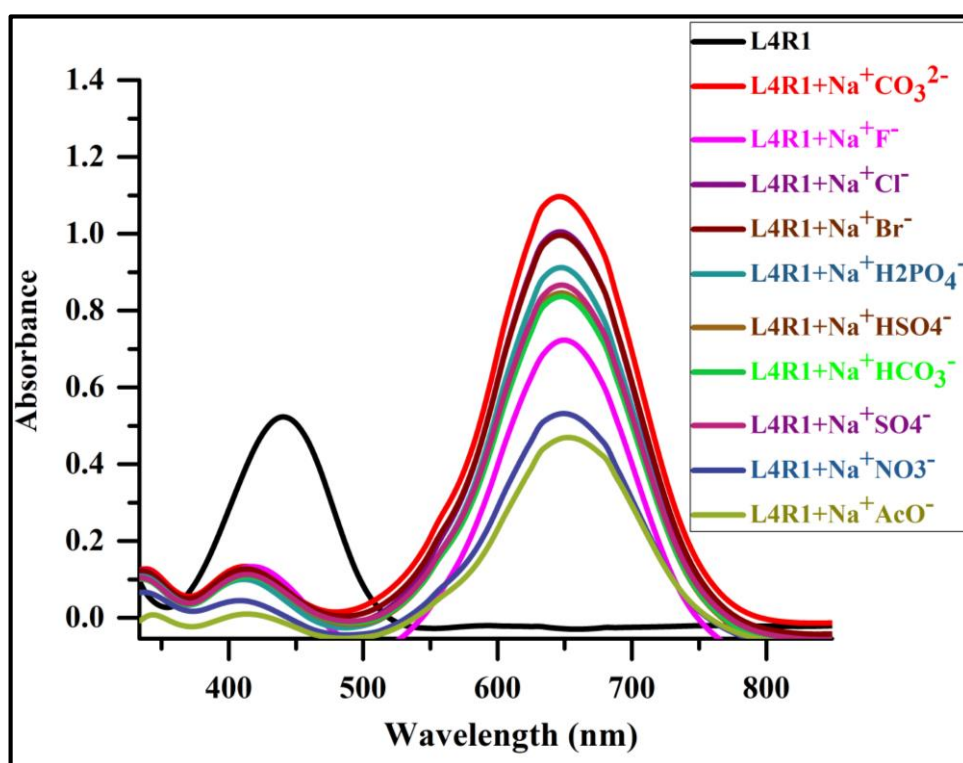
Fig. 5.24 UV-Vis absorption spectral changes of **L4R1**-CO_3^{2-} (2 equiv.) with various interference anions (4 equiv.) in in DMSO: H_2O (9:1 v/v)
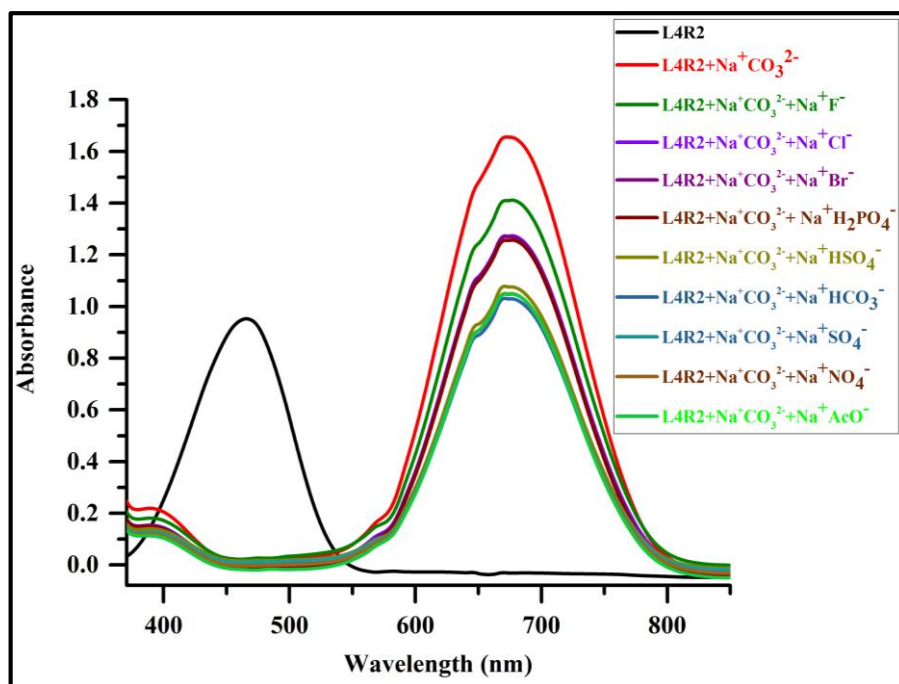
Fig. 5.25 UV-Vis absorption spectral changes of **L4R2**-CO_3^{2-} (2 equiv.) with various interference anions (4 equiv.) in DMSO: H_2O (9:1 v/v)
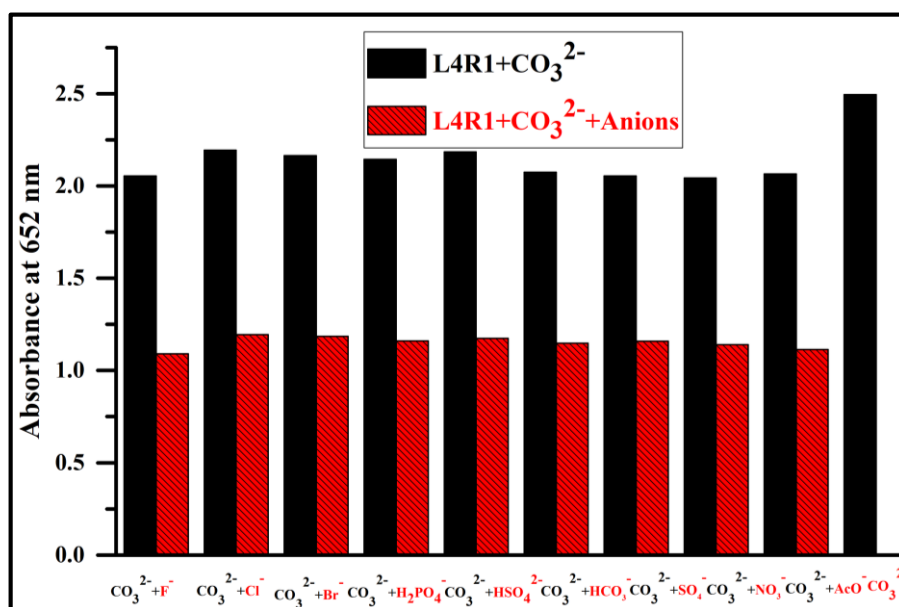
Fig. 5.26 Bar graph representation of interference response of receptor **L4R1** towards 2 equiv. of CO_3^{2-} ion in the presence of 4 equiv. of other interference anions (black bar represents the addition of CO_3^{2-} ion to the solution and the red bar represents the addition of other interference to the above solution)
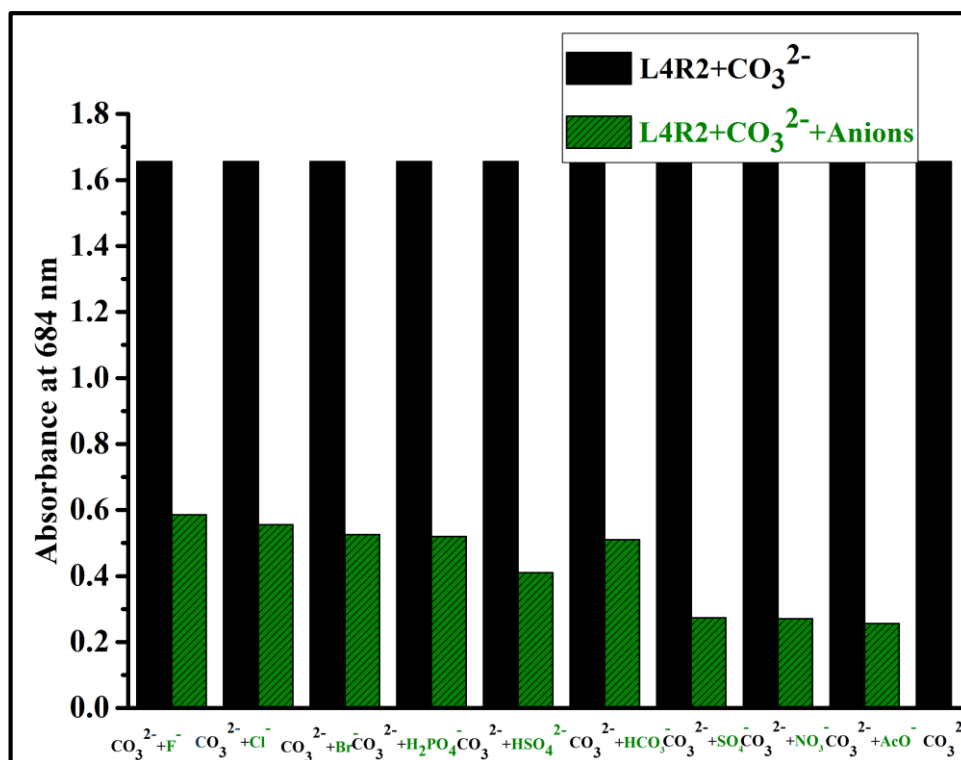
Fig. 5.27 Bar graph representation of interference response of receptor **L4R2** towards 2 equiv. of CO_3^{2-} ion in the presence of 4 equiv. of other interference anions (black bar represents the addition of CO_3^{2-} ion to the solution and the green bar represents the addition of other interference to the above solution)

As displayed in Fig. 5.28 and Fig. 5.29, the free receptors **L4R1** and **L4R2** showed a strong absorption band centred at 442 nm and 465 in DMSO: H_2O (9:1 v/v). Upon incremental addition of CO_3^{2-} ions to the **L4R1** and **L4R2** solutions, the maximum absorption band at 442 nm and 465 nm gradually reduced, and concomitantly new absorption bands appeared at 652 nm and 684 nm with bathochromic shift of ($\Delta\lambda_{max}$) 210 nm and 219 nm. In addition, a well-defined isosbestic point was observed at 506 nm and 503 nm confirming the complex formation between the receptors **L4R1/L4R2** and the CO_3^{2-} ions.
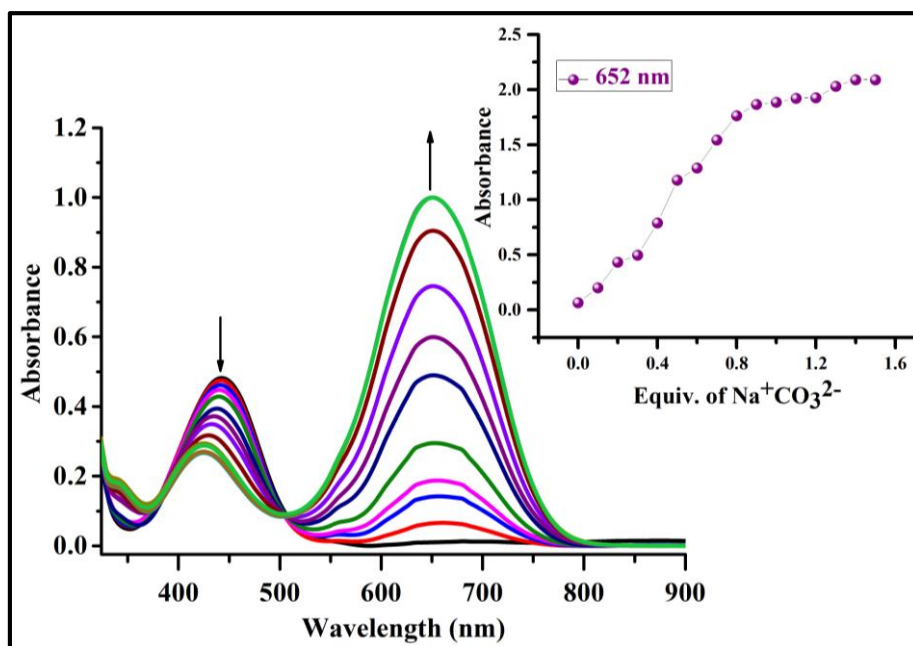
Fig. 5.28 UV-Vis titration spectra of receptor **L4R1** (1×10^{-4} M in DMSO) with the incremental addition of $Na^+CO_3^{2-}$ in DMSO: H_2O (9:1 v/v); Inset plot representing the variation of absorbance with concentration of CO_3^{2-}ion at 652 nm
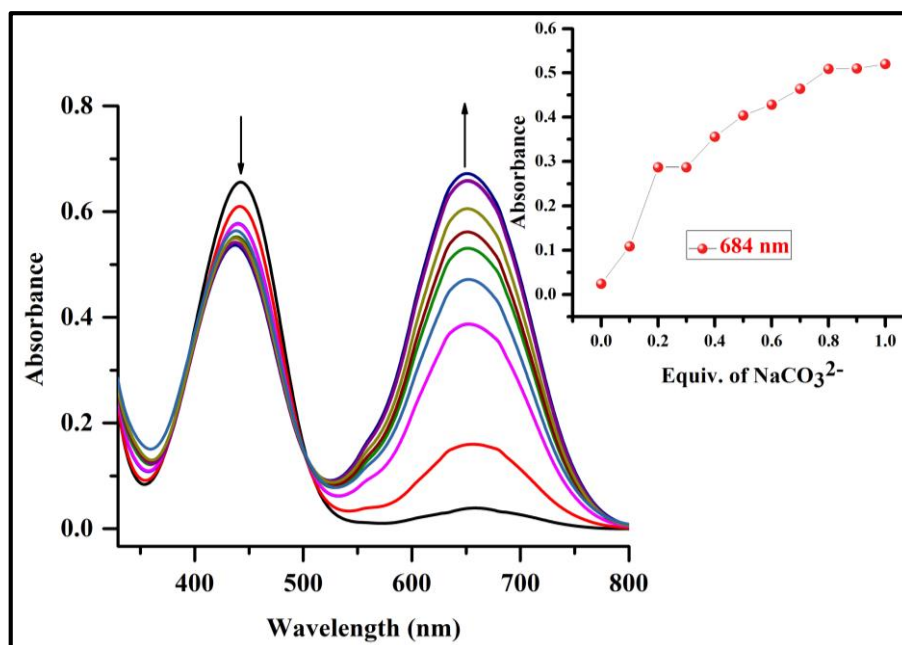
Fig. 5.29 UV-Vis titration spectra of receptor **L4R2** (1×10^{-4} M in DMSO) with the incremental addition of $Na^+CO_3^{2-}$ in DMSO: H_2O (9:1 v/v); Inset plot representing the variation of absorbance with concentration of CO_3^{2-}ion at 684 nm

5.3.6 Determination of binding constant and limit of detection

Based on the UV-Vis titration studies, the binding constant and binding stoichiometries of the complex were evaluated using the Benesi-Hildebrand equation (Benesi and Hildebrand 1948) as given in (Eq. 5.1)

$$\frac{1}{(A-A_0)} = \frac{1}{(A_{max}-A_0)} + \frac{1}{K[X^-]^n (A_{max}-A_0)} \dots\dots\dots\dots (Eq.\,5.1)$$

Where, A_0, A, and A_{max} are the absorption considered in the absence of anion, at intermediate and at concentration of saturation, respectively, K is the binding constant, $[X^-]$ is the concentration of the anion, and n is the stoichiometric ratio.

The plot of $1/(A-A_0)$ *vs.* $1/[A^-]^2$ ($A^-=F^-$, AcO^-, CO_3^{2-}) showed good linearity resulting in 1:2 binding ratio of the receptors **L4R1** and **L4R2** with aforementioned anions F^- and AcO^- as illustrated in Fig. 5.30 and Fig. 5.31. Furthermore, the definite stoichiometric ratio between receptors and CO_3^{2-} ion was determined to be 2:1 from UV-Vis spectral changes with the help of the Benesi–Hildebrand equation in DMSO: H_2O (9:1 v/v) as depicted in Fig. 5.32.

The limit of detection was analyzed using (Eq. 5.2) for the receptors **L4R1** and **L4R2** in the presence of the target anions and the graph is represented in Fig. 5.33, Fig. 5.34, and Fig. 5.35.

$$LOD = \frac{3 \times \sigma}{s} \dots\dots\dots\dots\dots\dots\dots. (Eq.\,5.2)$$

Where, σ is the standard deviation of the calibration curve (SD), and s is the slope of the calibration curve. The binding constant, stoichiometry, and limit of detection of the receptors **L4R1** and **L4R2** with corresponding anions is summarized in Table 5.1.
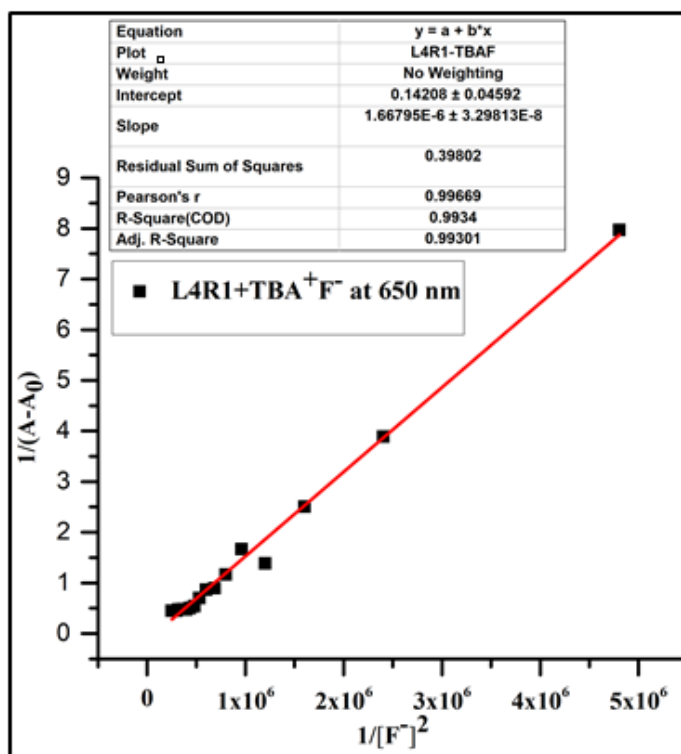
Fig. 5.30 B-H plot for **L4R1-** TBA$^+$F$^-$ complex at selective wavelength of 650 nm in DMSO
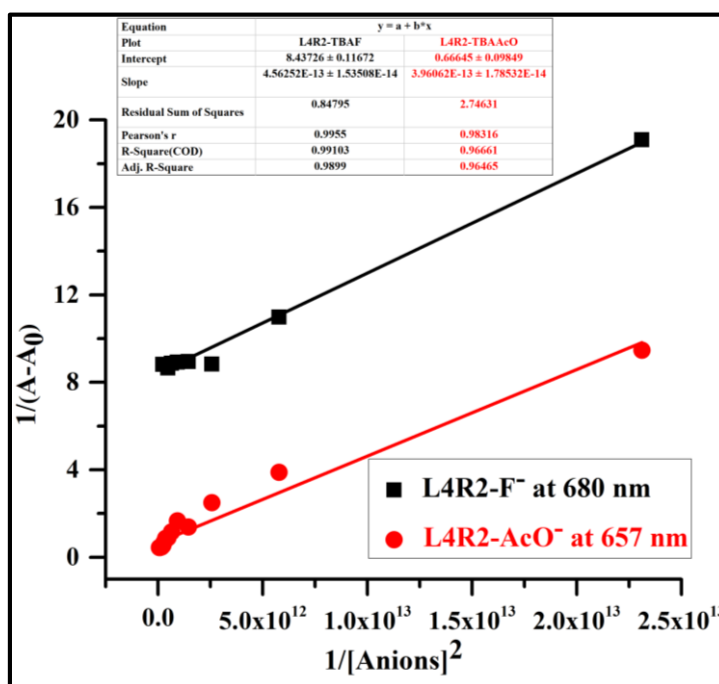
Fig. 5.31 B-H plot for **L4R2-**TBA$^+$F$^-$ and **L4R2-**TBA$^+$AcO$^-$ complex at selective wavelength of 680 nm and 657 nm in DMSO
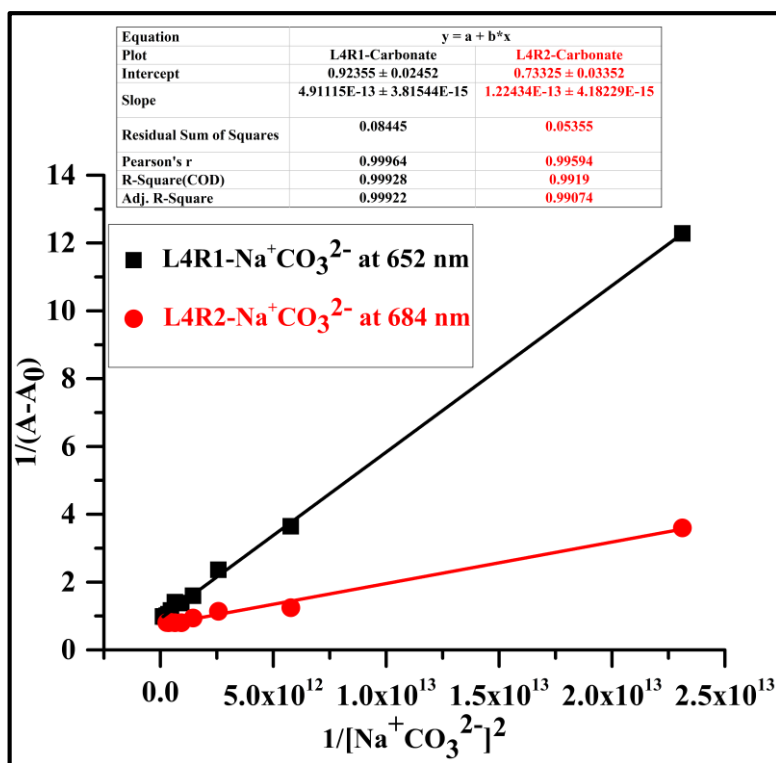
Fig. 5.32 B-H plot for **L4R1-**$Na^+CO_3^{2-}$ and **L4R2-** $Na^+CO_3^{2-}$ complex at selective wavelength of 652 nm and 684 nm in DMSO: H_2O (9:1 v/v)
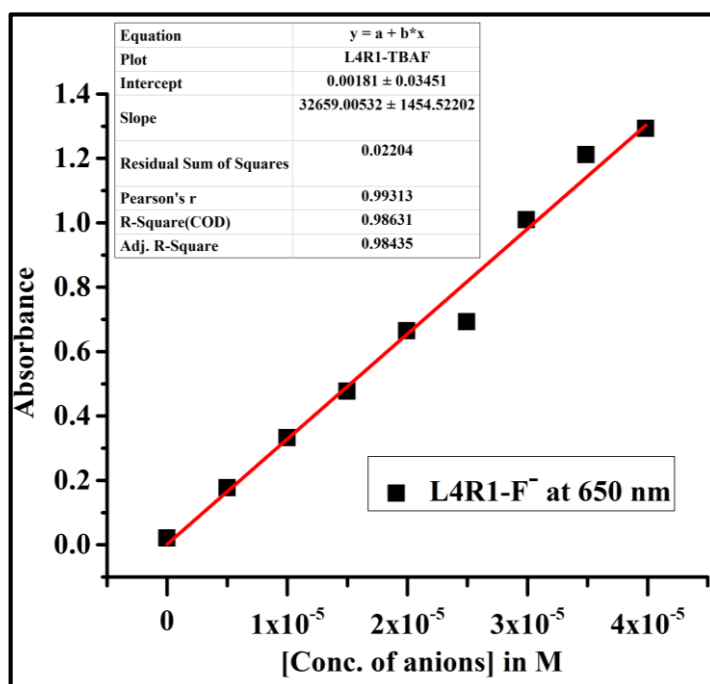
Fig. 5.33 Calibration curve between absorbance of receptor **L4R1-**anion complex and concentration of anion at selected wavelength of 650 nm
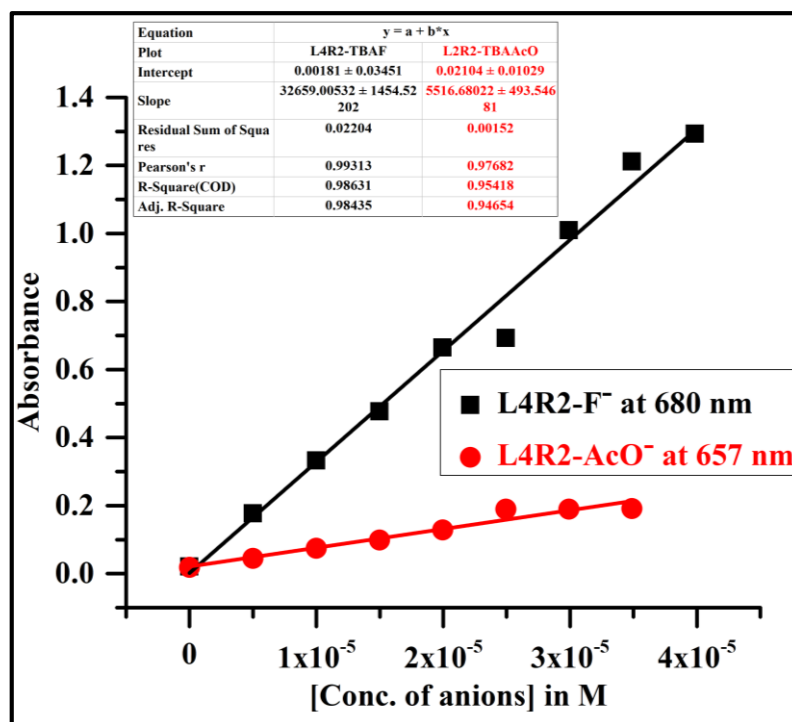
Fig. 5.34 Calibration curve between absorbance of receptor **L4R2**-anion complex and concentration of anion at selected wavelengths of 680 nm and 657 nm
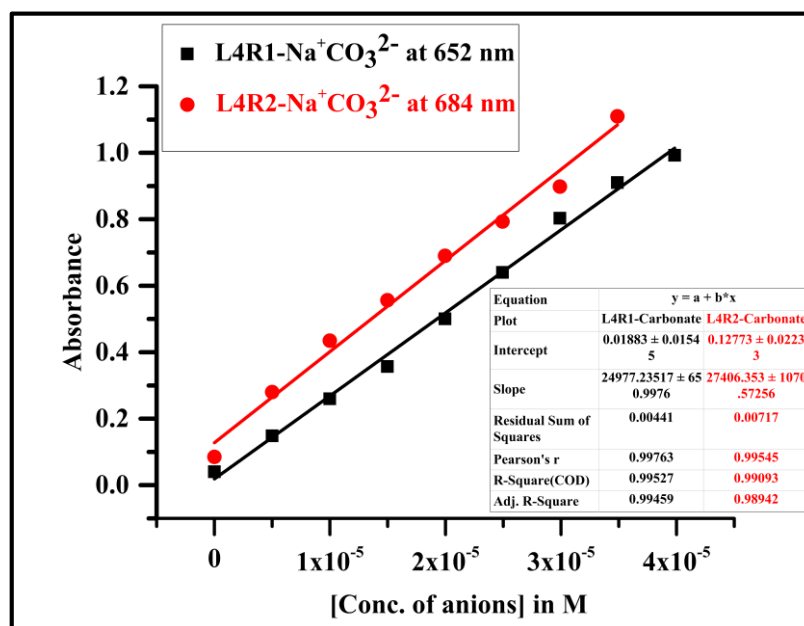
Fig. 5.35 Calibration curve between absorbance of receptors-anion complex and concentration of anion at selected wavelengths of 652 nm and 684 nm in DMSO: H_2O (9:1 v/v)

Table 5.1 Binding constant, binding ratio and detection limit of receptor **L4R1** and **L4R2** with various anions

Receptor	Media	Binding-constant (M^{-2})	Limit of detection (ppm)	Stoichiometry	Complex $\Delta\lambda_{max}$ (nm)
L4R1+F⁻	DMSO	2.3×10^4	0.9	1:2	208
L4R2+F⁻	DMSO	8.57×10^4	0.74	1:2	215
L4R2+AcO⁻	DMSO	1.3×10^3	1.7	1:2	207
L4R1+CO_3^{2-}	DMSO: H₂O (9:1 v/v)	2.79×10^4	0.51	2:1	210
L4R2+CO_3^{2-}	DMSO: H₂O (9:1 v/v)	8.72×10^4	0.47	2:1	219

The receptors **L4R1** and **L4R2** reported high binding constant and detection limit towards CO_3^{2-} ions, indicating strong interaction with CO_3^{2-} ions in DMSO: H₂O (9:1 v/v). The receptors effectively combated the solvent interference in the presence of Na⁺ counter ion implying a binding ratio of 2:1 of the receptors with the CO_3^{2-} ions.

5.3.7 Electrochemical study

The binding process of the receptors **L4R1** and **L4R2** (2.5×10^{-4} M in DMSO) with the CO_3^{2-} ions (1×10^{-2} M in H₂O) was further elucidated by the cyclic voltammetry experiment to understand the presence of electroactive groups such as -NO₂ and -NH as well as their nature of interaction in the absence and presence of the CO_3^{2-} ions. The cyclic voltammetry experiment was carried out with three-electrode cells consisting of platinized platinum (working), platinum wire (auxiliary), and saturated calomel (reference) electrode. The experiments were performed in the DMSO using 0.01 M tetrabutylammonium perchlorate (TBAP) as the supporting electrolyte. In the absence of anions, **L4R1** displayed an anodic peak at +0.17 V due to the oxidation of the –NH group and a cathodic peak at -0.8V due to the reduction of the nitro group. A significant change in the cyclic voltammetry was observed upon the addition of increasing amounts of CO_3^{2-} ions into the **L4R1** solution

as shown in Fig. 5.36. The anodic peak at +0.17 V shifted to 0.34 V, and the cathode peak at -0.8 V moved to -0.75 V.

Similarly, the free receptor **L4R2** without the addition of CO_3^{2-} ions exhibited an anodic peak at +0.11 V and a cathodic peak at -0.83 V. Successive addition of CO_3^{2-} ions to **L4R2** resulted in an increase in intensity of the original oxidation peak with shift to +0.17 V towards the positive side attributed to the NH proton formed a strong complex with the CO_3^{2-} ions, and the cathodic peak at -0.83 V shifted to -0.77 V as described in Fig. 5.37. From the CV results as displayed in Table 5.2, it can be concluded that upon the addition of CO_3^{2-} ions, both the receptors **L4R1** and **L4R2** showed maximum anodic peak shift towards the positive site, and the reduction peak shifted less, probably owing to the increase in electron density over the complex through strong hydrogen bonding between the NH proton and the CO_3^{2-} ions (Kaifer and Gómez-Kaifer 2008). The UV-Vis titration experiment and the CV studies strongly support the hydrogen bonding between the receptors **L4R1** and **L4R2** and the CO_3^{2-} ions.
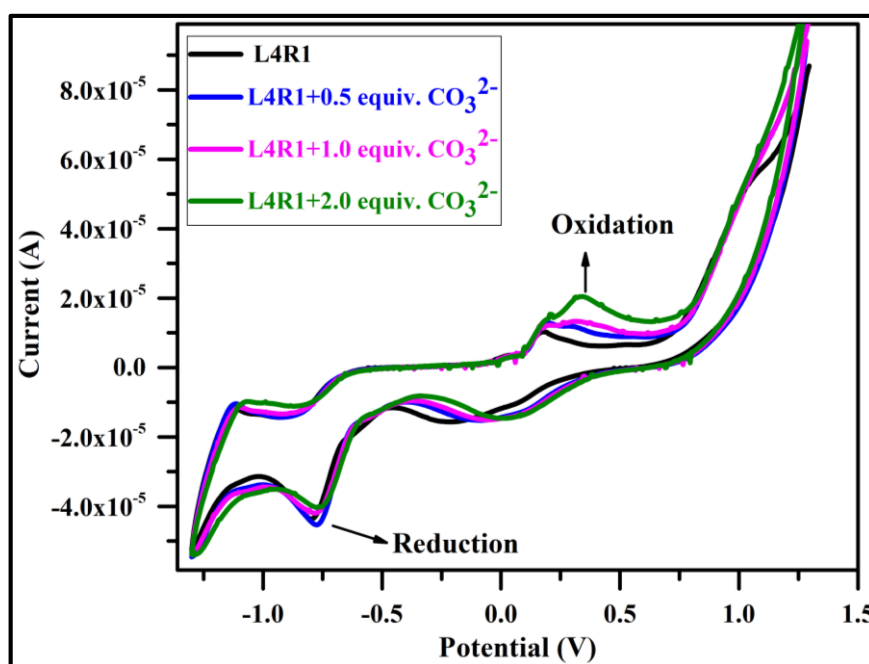
Fig. 5.36 Cyclic voltammogram of receptor **L4R1** (2.5×10^{-4} M in DMSO) with the incremental addition of $Na^+CO_3^{2-}$ (1×10^{-2} M in H_2O)
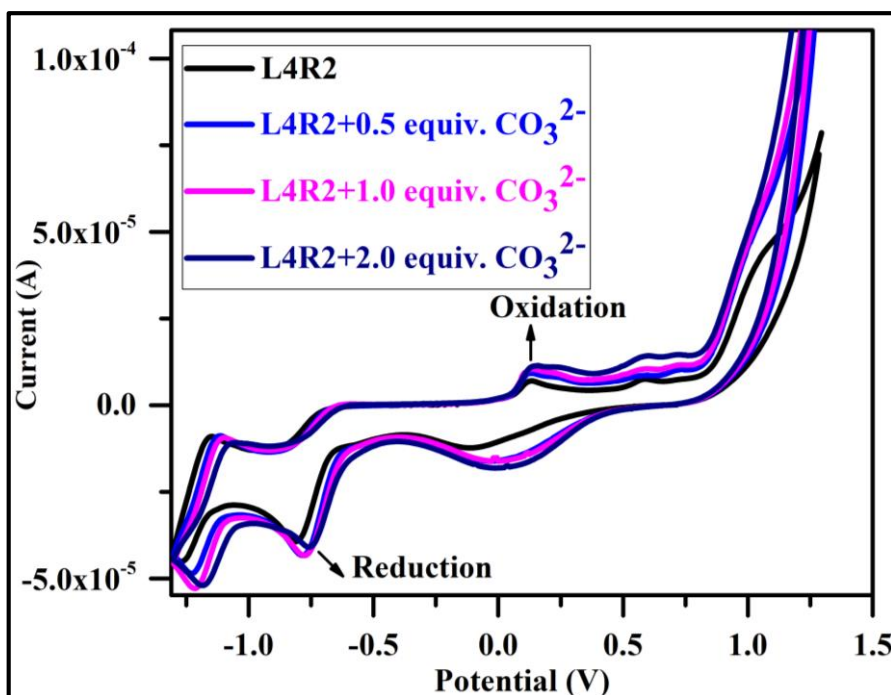
Fig. 5.37 Cyclic voltammogram of receptor **L4R2** (2.5 $\times 10^{-4}$ M in DMSO) with the incremental addition of $Na^+CO_3^{2-}$ (1 $\times 10^{-2}$ M in H_2O)

Table 5.2 Oxidation and reduction peaks of receptors and their complexes with anions

Receptors	Oxidation (V)	Reduction (V)
L4R1	+0.17	-0.8
L4R1+ CO_3^{2-}	+0.34	-0.75
L4R2	+0.11	-0.83
L4R2+ CO_3^{2-}	+0.17	-0.77

5.3.8 FT-IR spectroscopy of L4R1 and L4R2 with CO_3^{2-} ion

Infrared spectroscopic studies were conducted to investigate the receptors' **L4R1** and **L4R2** (1×10^{-4} M in DMSO) binding mechanism with CO_3^{2-} using KBr. As seen in Fig. 5.38 (a and b), the free receptors **L4R1** and **L4R2** in the absence of anions, exhibited sharp peaks at 3462 cm^{-1} and 3428 cm^{-1} reflecting the NH stretching vibration. After the addition of 2 equiv. of CO_3^{2-} ions, the peaks at 3462 cm^{-1} and 3428 cm^{-1} shifted to 3436 cm^{-1} and 3438 cm^{-1}. In the meantime, not much significant change was observed regarding the other

peaks in the spectra. From these results, it can be concluded that the basicity of CO_3^{2-} ions is not enough to deprotonate the NH proton, thereby creating a strong hydrogen bonding complex with the NH proton of the receptors **L4R1** and **L4R2** (Thimaradka et al. 2018).
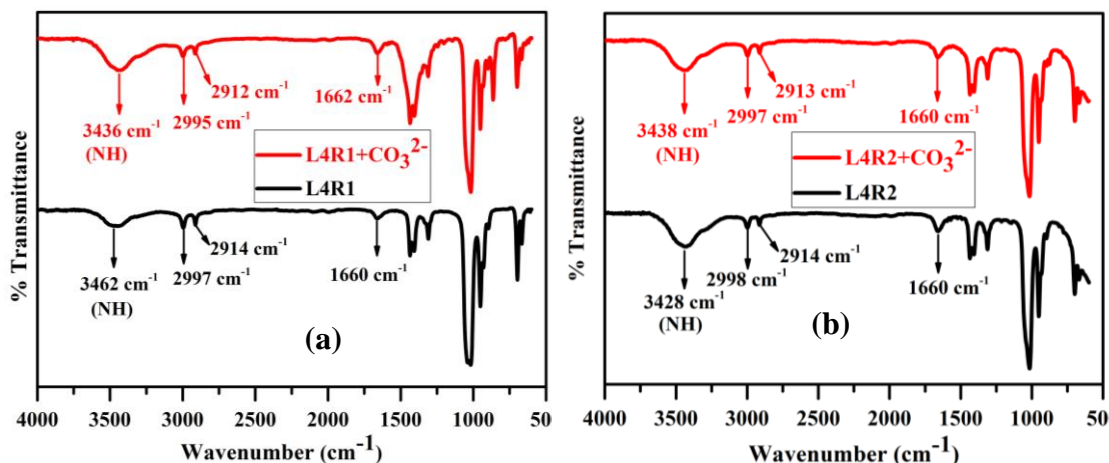
Fig. 5.38 IR spectrum of (a) free receptors **L4R1** (1×10^{-4} M in DMSO) with incremental addition of CO_3^{2-} ions (1×10^{-2} M in H$_2$O), and (b) free receptors **L4R2** (1×10^{-4} M in DMSO) with sequential addition of with CO_3^{2-} ions (1×10^{-2} M in H$_2$O)

5.3.9 ^{1}H-NMR titration studies

In order to validate the proposed binding mechanism between the receptors **L4R1** and **L4R2** and the active anions (F$^-$ and CO_3^{2-}), ^{1}H-NMR titration was performed in the DMSO-d$_6$. In the absence of anions, the free receptors **L4R1** and **L4R2** showed NH proton signal at 11.8 ppm and 11.6 ppm, respectively, as depicted in Fig. 5.39 and Fig. 5.40. Upon addition of 1 equiv. of F$^-$ ion to the receptor **L4R1** solution, the signal at 11.8 ppm experienced a downfield shift to 12.3 ppm, and simultaneously the intensity of the peak decreased owing to strong hydrogen bonding between the N-H proton and the F$^-$ ion. As the concentration of the F$^-$ ion increased to 2 equiv., the N-H proton signal at 12.3 ppm disappeared suggesting deprotonation. This may be due to the small ionic size (1.3 Å) and high electronegativity (4.1) of F$^-$ ion, which makes the NH proton to deprotonate. In addition, the signals corresponding to the imine and aromatic protons shifted upfield with the addition of the F$^-$ ion, possibly due to the increase in charge density and deprotonation of the NH proton.
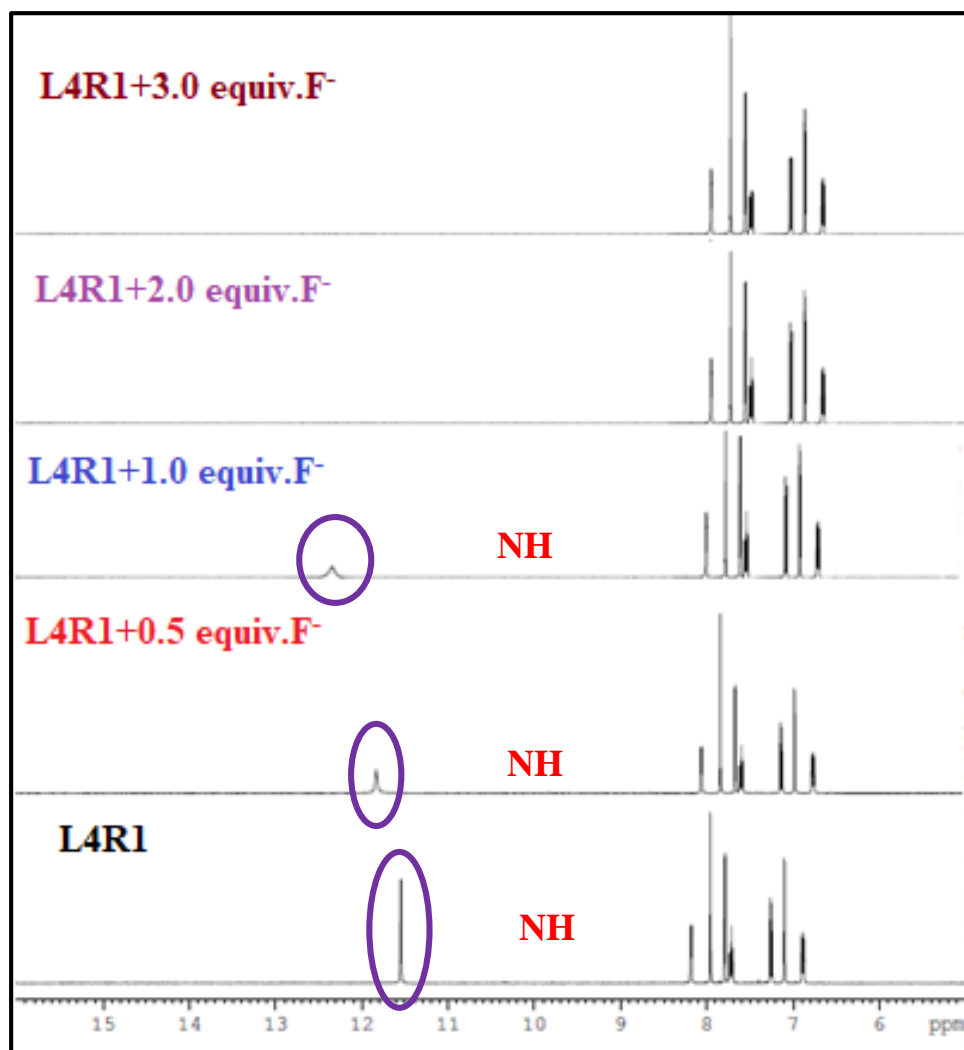
Fig. 5.39 ^{1}HNMR titration spectra of **L4R1** upon progressive addition of TBA$^+$F$^-$ in DMSO-d$_6$

Similarly, with the addition of 0.5 equiv. of F$^-$ to the receptor **L4R2** solution, the N-H proton experienced a downfield shift from 11.6 ppm to 12.1 ppm. Further, with the addition of 1 equiv. of F$^-$ ion, the NH proton signal at 12.1 ppm disappeared, indicating deprotonation of the NH proton. Therefore, the NH group acted as an electron donor and the nitro moiety as an electron acceptor forming ICT transition. Notably, no further chemical upfield shift was observed upon the addition of 3 equiv. of F$^-$ ions to the solution of **L4R1** and **L4R2**. This phenomenon reflected the 1:2 binding model for **L4R1** and **L4R2** to the F$^-$ ion in agreement with the B-H plot. As a result, the proton ^{1}H-NMR studies clearly favoured the H-bonding interaction between

the NH proton and the F⁻ ion, as increased concentration of the F⁻ ion led to deprotonation of N-H leaving behind electron-rich N⁻ species.
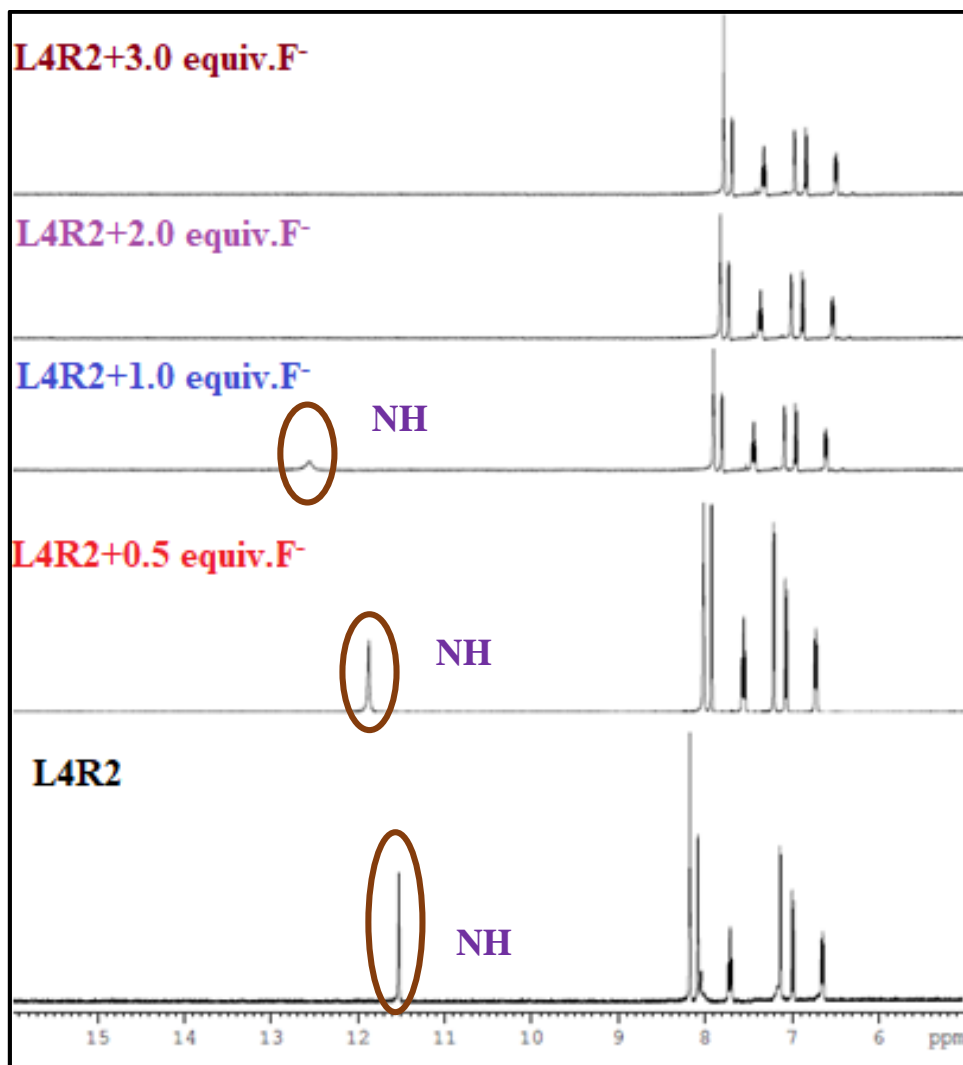
Fig. 5.40 ^{1}HNMR titration spectra of **L4R2** upon progressive addition of TBA$^+$F$^-$ in DMSO-d$_6$

On the other hand, ^{1}H-NMR titration was carried out in the DMSO-d$_6$ between the receptors **L4R1** and **L4R2** and CO$_3^{2-}$ ion as shown in Fig. 5.41 and Fig. 5.42. Without adding CO$_3^{2-}$ ion, the receptors **L4R1** and **L4R2** displayed a strong signal at 11.8 ppm and 11.6 ppm for the NH proton. After adding (0.5 equiv. to 2.0 equiv.) CO$_3^{2-}$ ion, the NH signal underwent a downfield shift from 11.8 ppm to 12.0 ppm. Similarly, in the case of **L4R2**, the NH proton experienced a downfield shift from 11.6 ppm to 12.0 ppm. The downfield shift indicated hydrogen bonding between the NH proton of

the receptors **L4R1/L4R2** and the CO_3^{2-} ion (NH---CO_3^{2-}). In addition, there was no appearance of any new peak or chemical shift in the aromatic region, suggesting that the basicity of the CO_3^{2-}ion was not sufficient to deprotonate the NH proton even after the addition of the 2 equiv., although it caused a bathochromic shift in the absorption spectra due to 2:1 complex formation (Pérez-Casas and Yatsimirsky 2008; Zapata et al. 2008).
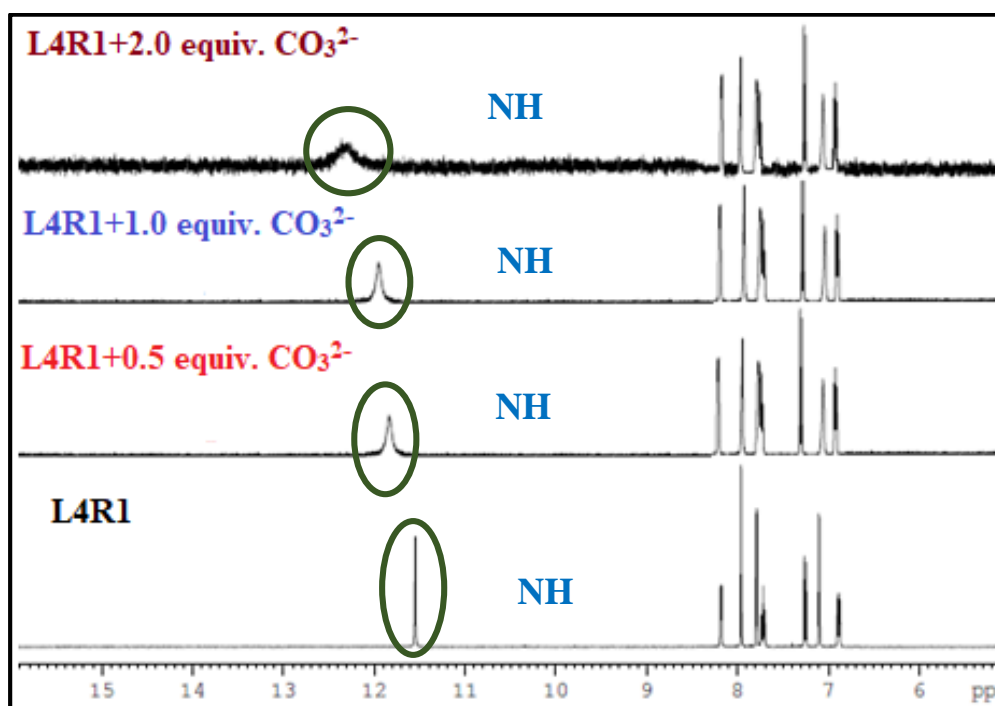
Fig 5.41 ^{1}HNMR titration spectra of **L4R1** upon progressive addition of CO_3^{2-} ion in DMSO-d_6
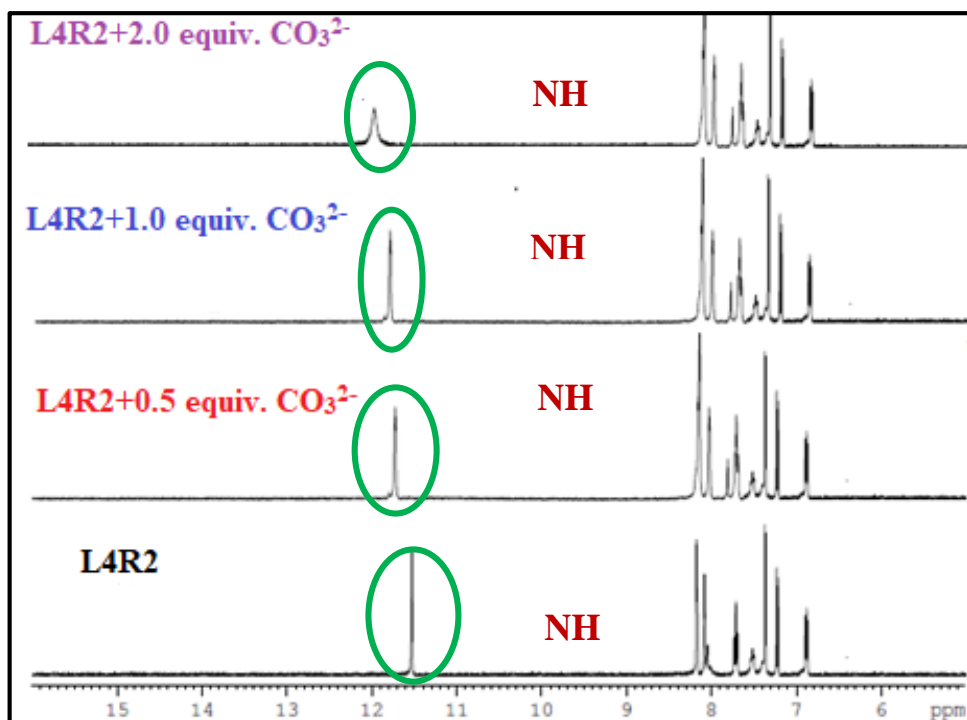
Fig. 5.42 ^{1}HNMR titration spectra of **L4R2** upon progressive addition of CO_3^{2-} ion in DMSO-d_6

5.3.10 Anion binding studies by mass spectrometry

Mass spectral analysis was used to investigate the binding mechanism between the receptors and the target anions. The mass spectrum showed characteristic peak at [m/z: 231.05, calcd: 231.15] and [m/z: 247.01, calcd: 247.00] corresponding to the receptors (**L4R1**---N^- + H-F^-) and (**L4R2**---N^- + H-F^-) deprotonated by 2 equiv. of F^- ion as illustrated in Fig. 5.43 and Fig. 5.44. Similarly, the positive-ion mass spectrum of the receptors **L4R1** and **L4R2** upon addition of 2 equiv. CO_3^{2-} ions displayed characteristic peak **L4R1**-CO_3^{2-} [m/z: 524.41, calcd: 525.05] and **L4R2**-CO_3^{2-} [m/z: 556.53, calcd: 557.00] confirming 2:1 bonding mode between the receptor and the CO_3^{2-} ions as illustrated in Fig. 5.45 and Fig. 5.46.
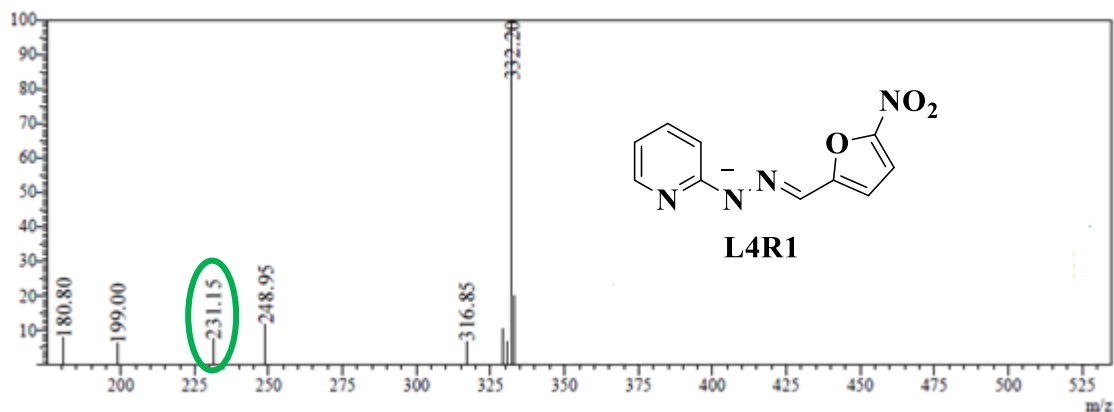
Fig. 5.43 LC-MS spectrum of **L4R1+F⁻**
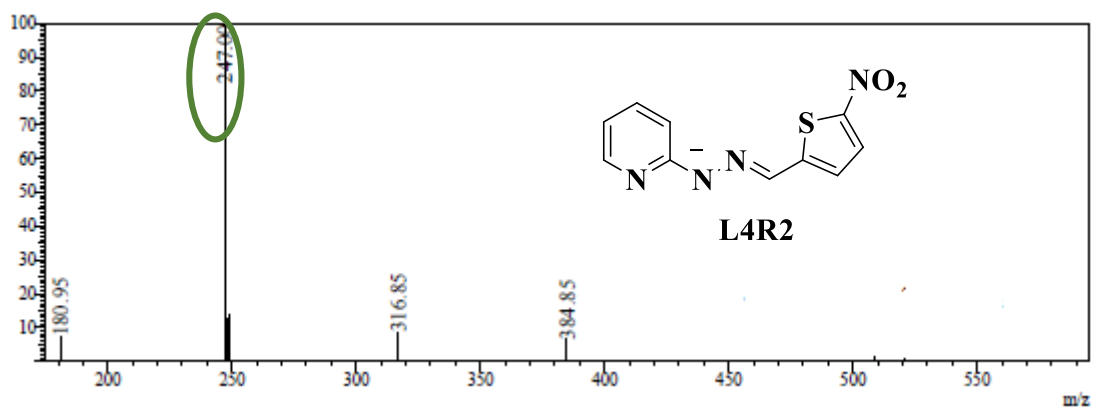
Fig. 5.44 LC-MS spectrum of **L4R2+F⁻**
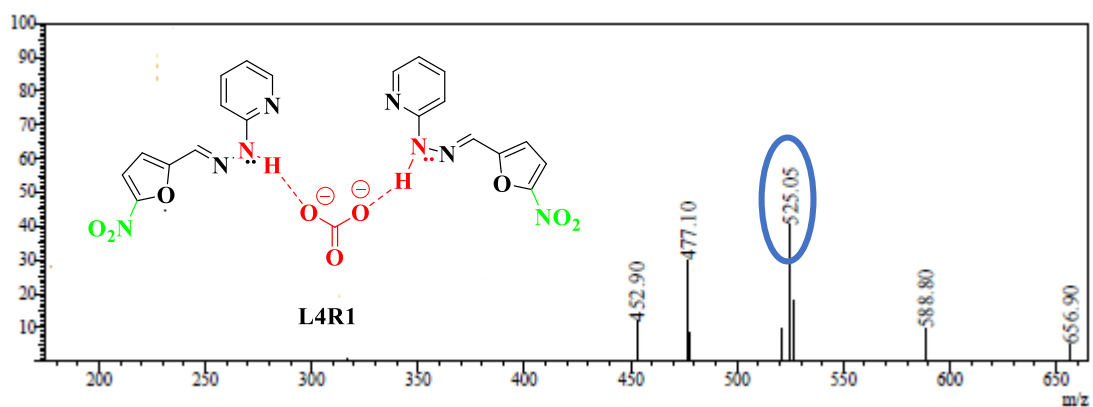
Fig. 5.45 LC-MS spectrum of **L4R1+CO₃²⁻**
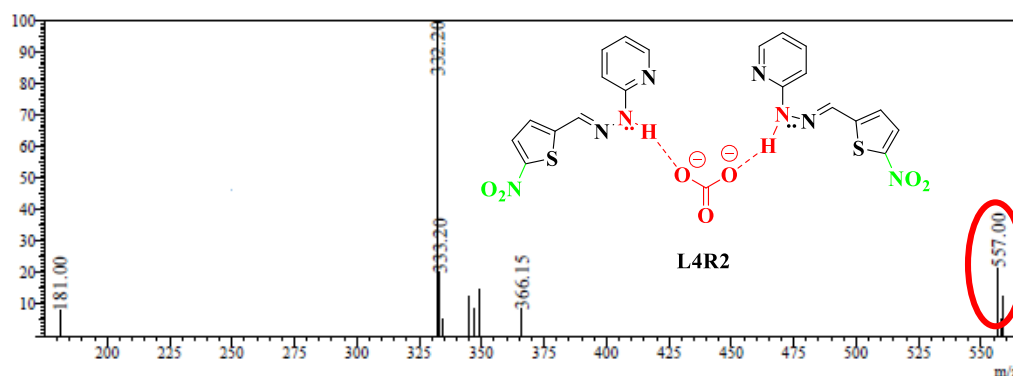
Fig. 5.46 LC-MS spectrum of **L4R2+CO₃²⁻**

5.3.11 Binding mechanism

The proposed anion detection mechanism in the solution is shown in Scheme 5.3 and Scheme 5.4. The detection of anions using the receptors **L4R1** and **L4R2** is a two-step process based on the results of the UV-Vis, ^{1}H-NMR titration, mass analysis, and stoichiometric studies. At first, the F⁻ ion binds to the receptor through hydrogen bonding and thus, a 1:1 adduct is generated to form a hydrogen bonding NH---F⁻ complex. The second F⁻ ion causes the deprotonation of the NH proton in the receptors **L4R1** and **L4R2** resulting in increased electron density over the complex system, and leaving behind N⁻ species. This induces a charge separation in the molecule and hence, intramolecular charge transfer (ICT) interaction increases between the electron deficient NO₂ group and the electron rich N⁻ resulting in colorimetric response.
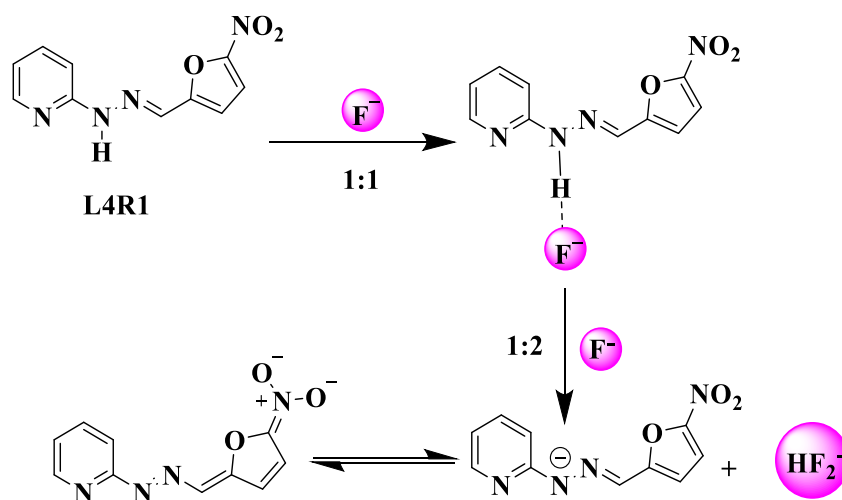
Scheme 5.3 Proposed binding approach of **L4R1** with F⁻
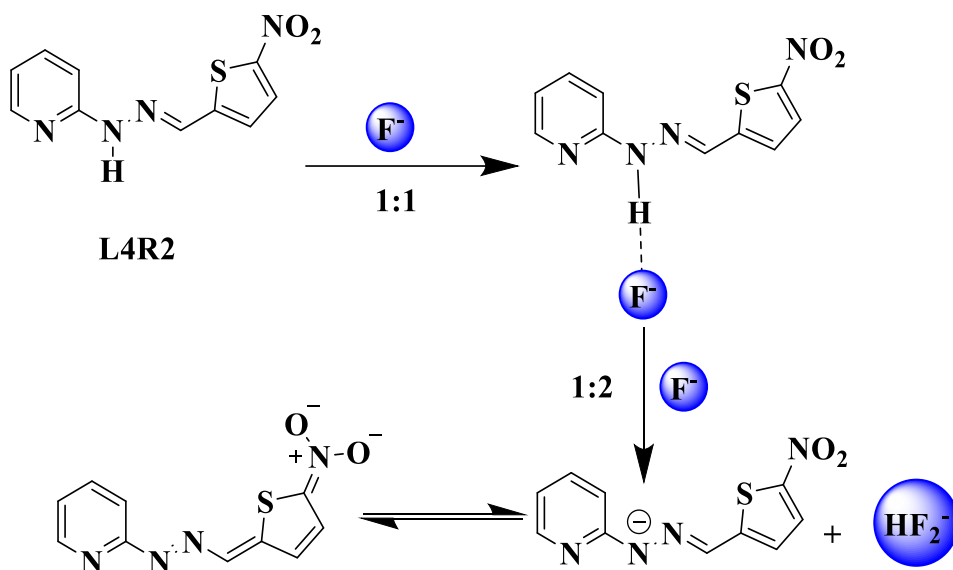
Scheme 5.4 Proposed binding approach of **L4R2** with F⁻

Based on the UV-Vis titration, FT-IR spectral studies, electrochemical study, ¹H-NMR titration studies, and mass analysis, the proposed binding mechanism of the receptors **L4R1** and **L4R2** with CO_3^{2-} ions is shown in Scheme 5.5. The phenomenon of 2:1 binding ratio for the receptors and the carbonate complex indicates the successful binding of the receptors to the carbonate ion by strong hydrogen bonding.
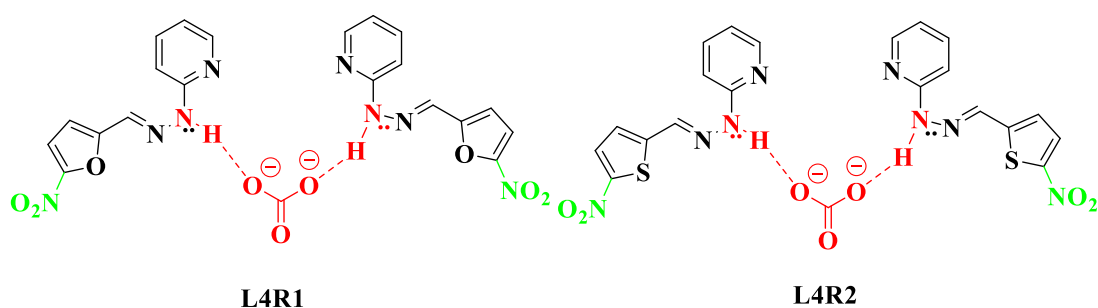
Scheme 5.5 Binding mechanism of receptors **L4R1** and **L4R2** with CO_3^{2-} ions

5.3.12 Practical application using a test strip

To investigate the practical application of the receptors **L4R1** and **L4R2**, test strips were prepared by immersing the filter papers into the DMSO solutions of **L4R1**

and **L4R2** (1×10^{-4} M in DMSO) and drying them in a hot oven at 60˚C. The test strips, loaded or coated with **L4R1** and **L4R2**, were further utilized to detect the anions. As shown in Fig 5.47, when F⁻ was added to the test strip **L4R1**, it elicited vital colour change from pale yellow to blue. Similarly, on the addition of F⁻ and AcO⁻ ions to the test strip **L4R2**, prompt colour change was observed from dark red to blue and green as represented in Fig. 5.48. These results show that **L4R1** and **L4R2** are excellent, fast, and convenient practical colorimetric tools for detecting biologically important anions like F⁻ and AcO⁻.

L4R1   **L4R1+TBA⁺F⁻**
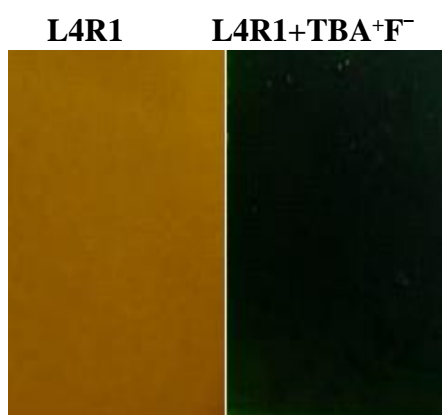
Fig. 5.47 Photograph of test strip of free receptor **L4R1** and color change after addition of F⁻ solution on coated test strip **L4R1**

L4R2   **L4R2+ TBA⁺F⁻**   **L4R2+ TBA⁺AcO⁻**
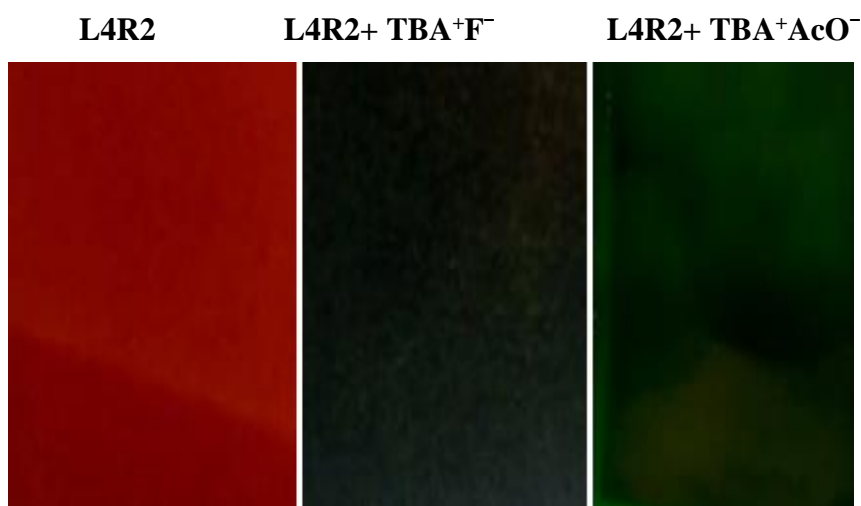
Fig. 5.48 Photograph of test strip of free receptor **L4R2** and color change after addition of F⁻ and AcO⁻ solution on coated test strip **L4R2**

In the same process, the detection of CO_3^{2-} ions was investigated by using a test strip. When the test strip coated with **L4R1** and **L4R2** was immersed in the aqueous solution of CO_3^{2-} (1×10^{-2} M in H_2O), a clear colour change was observed from pale yellow to blue that could be visually viewed as depicted in Fig. 5.49. The development of such a test strip for the sensing of anions is extremely attractive in field measurement because it does not require any additional instrument. This result emphasizes that **L4R1** and **L4R2** are highly selective for CO_3^{2-} ion.
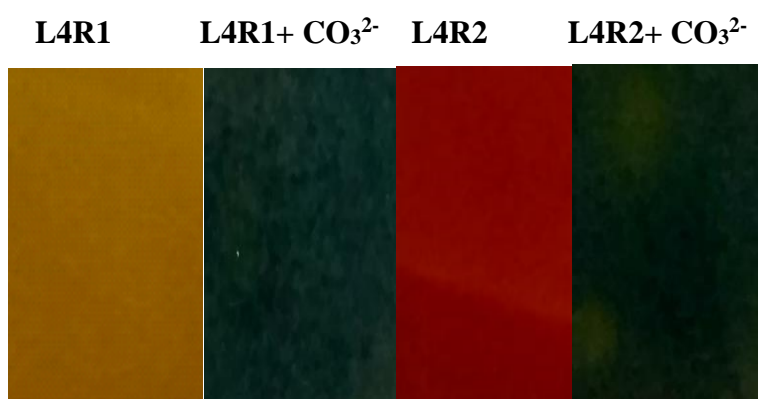
Fig. 5.49 Photograph of test strip of receptors **L4R1** and **L4R2** upon addition of 2 equiv. of CO_3^{2-} on coated test strip

5.3.13 DFT studies

The experimental results clearly indicate that **L4R1** shows high selectivity and sensitivity towards the F^- ions in the presence of other tested anions. To better understand the influence of F^- ions on the UV-Vis spectra of the receptor, DFT studies were performed. All the calculations for ground state optimization and excited state electronic transitions were carried out using the Gaussian 09 package (Gaussian09 2009). DFT with B3LYP (Becke three parameters hybrid functional with Lee-Yang-Perdew correlation functionals) (Lee et al. 1988; Miehlich et al. 1989) with the 6–311+G(d,p) (Hariharan and Pople 1973; Hehre et al. 1972) basis set were used for all the ground state calculations, while the excited state calculations were carried out with the TD-DFT with the same basis set used for the ground state. Initially, the ground state optimization was performed in the gas phase, followed by the solvent phase. The effect of solvation on the energy was attributed to the receptors, and to further correlate the

experimentally observed absorption spectra, solvent phase optimization for both the ground and excited states was carried out. To accomplish this, self-consistent reaction field using the conductor polarizable continuum model (SCRF-CPCM) (Tomasi and Persico 1994) was employed, wherein dimethylsulfoxide was chosen as the solvent medium. The TD-DFT calculations were carried out to estimate the first 6 singlet vertical transition energies and to determine the oscillator strength pertaining to such transitions. The molecular orbitals for both the receptor and the anion bound complex were visualized with the Avogadro software (Hanwell et al. 2012). Fig. 5.50 shows the electronic orbital distribution of the occupied and unoccupied states of both the receptor **L4R1** and the complex **L4R1**+F⁻ along with their energy values. The bathochromic shift observed in the experimental absorption spectrum of **L4R1** upon binding with F⁻ ion effectively signified reduction in band gap of the system, caused mainly due to variation in the energy values of HOMO and LUMO. The value of HOMO of the bare receptor **L4R1** was observed as 6.070 eV and that of LUMO as 3.316 eV with energy gap value of ~2.754 eV, and this energy gap value upon complex formation was further reduced to ~2.267 eV. The HOMO+1 of the complex resulted in an electronic cloud, mainly localized on the pyridine moiety and the imine linkage, whereas that of the HOMO and LUMO was observed to be evenly distributed over the nitro group on the furfural and pyridine moiety. Such observed effects highly support the strong binding nature of the anions with the -NH proton, forming a push-pull effect between the electron donor and the electron acceptor moieties upon complexation. Further, similar theoretical calculations were carried out to arrive at the optimized structure of **L4R2** and its complexes, and to interpret the observed spectroscopic response of **L4R2** towards F⁻ and AcO⁻ ions. As shown in Fig. 5.51 and Fig. 5.52, the energy gap between the HOMO and LUMO of the free receptor **L4R2** is around ~2.666 eV. Upon addition of F⁻ and AcO⁻ ions, the energy gap reduces to ~2.171 eV and to ~2.232 eV in correlation with the red shift observed for the absorption peak in the UV-Vis spectra in line with the exhibited colorimetric colour change. The HOMO and LUMO of the receptor **L4R2** were mainly distributed on the pyridine moiety possessing the -NH group, whereas the complexation with the F⁻ and AcO⁻ ions altered the HOMO and LUMO that got localized on the nitro moiety emphasizing the electron donor capability of the -NH group with the same nitro moiety as the electron acceptor.
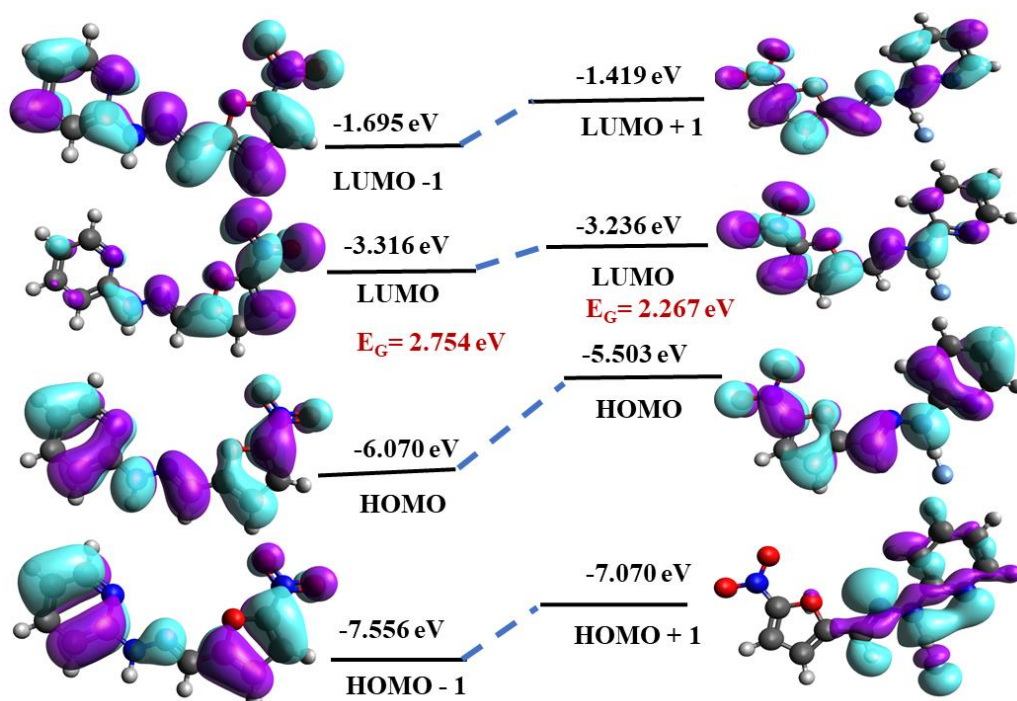
Fig. 5.50 Optimized molecular orbital of receptor **L4R1** before and after addition of F⁻ ion with energy levels of 6-31+G(d,p)
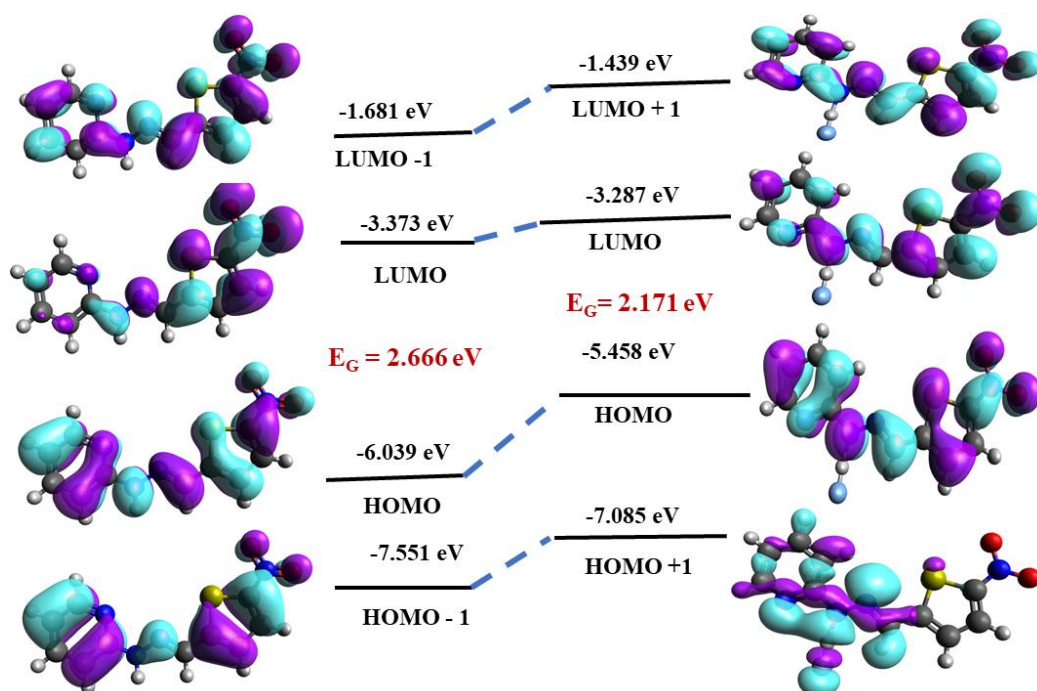
Fig. 5.51 Optimized molecular orbital of receptor **L4R2** before and after addition of F⁻ ion with energy levels of 6-31+G(d,p)
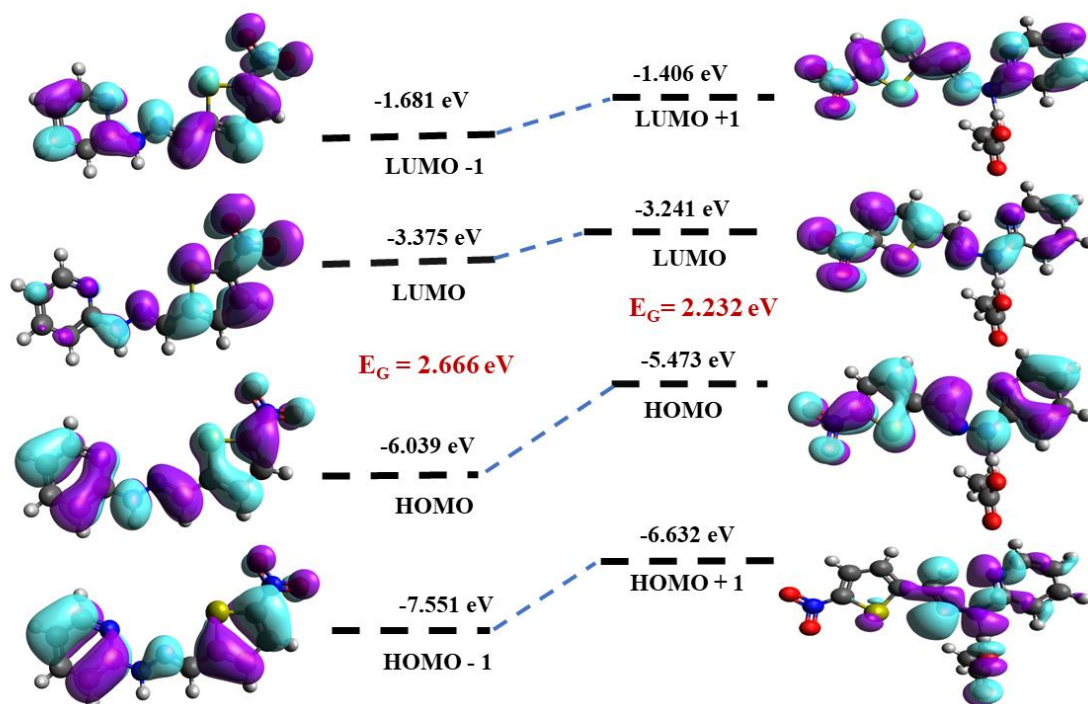
Fig. 5.52 Optimized molecular orbital of receptor **L4R2** before and after addition of AcO⁻ ion with the energy levels of 6-31+G(d,p)

Further theoretical calculations were performed in order to investigate the nature of the ICT and to evaluate the spectral behaviour of **L4R1** upon complexation with the CO_3^{2-} ions. The HOMO and LUMO values of the free receptor **L4R1** was found to be 6.070 eV and 3.316 eV with energy gap value of ~2.754 eV. After binding with CO_3^{2-} ions, the energy gap greatly reduced from ~2.754 eV to ~2.194 eV resulting in strong complex formation. The HOMO+1 of the complex is completely localized on the carbonate moiety, and in the case of HOMO and LUMO, the electronic densities were localized on the carbonate ions, and one among the receptor **L4R2** confirmed the 2:1 binding between the receptor and the CO_3^{2-} ions as illustrated in Fig. 5.53. Similarly, the receptor **L4R2** showed HOMO and LUMO of value 6.039 eV and 3.373 eV, respectively, with energy gap value of ~2.666 eV as depicted in Fig. 5.54. These values further shifted upon complexation to 5.498 eV and 3.234 eV, respectively, for HOMO and LUMO in the presence of CO_3^{2-} ions. The energy gap reduced from ~2.666 eV to ~2.264 eV due to complex formation. Thus, on binding with CO_3^{-2} ions, the HOMO+1 gets distributed on one of the receptors, whereas in the case of HOMO and LUMO, the electronic distribution is localized on the carbonate ions and the receptors.

Consequently, this result reflects strong complex formation between the -NH proton and the carbonate ions with binding ratio of 2:1. The theoretical predictions on the binding ratio clearly support the experimental results derived from the B-H plot. Further, the theoretical predictions of the energy gap of **L4R2** are lesser in comparison with that of **L4R1**. This implies that the binding is stronger in **L4R2** in comparison with **L4R1**. This correlates with the experimental UV-Vis titration studies, wherein there was a large redshift observed in **L4R2** in comparison with **L4R1** upon interaction with the anions.
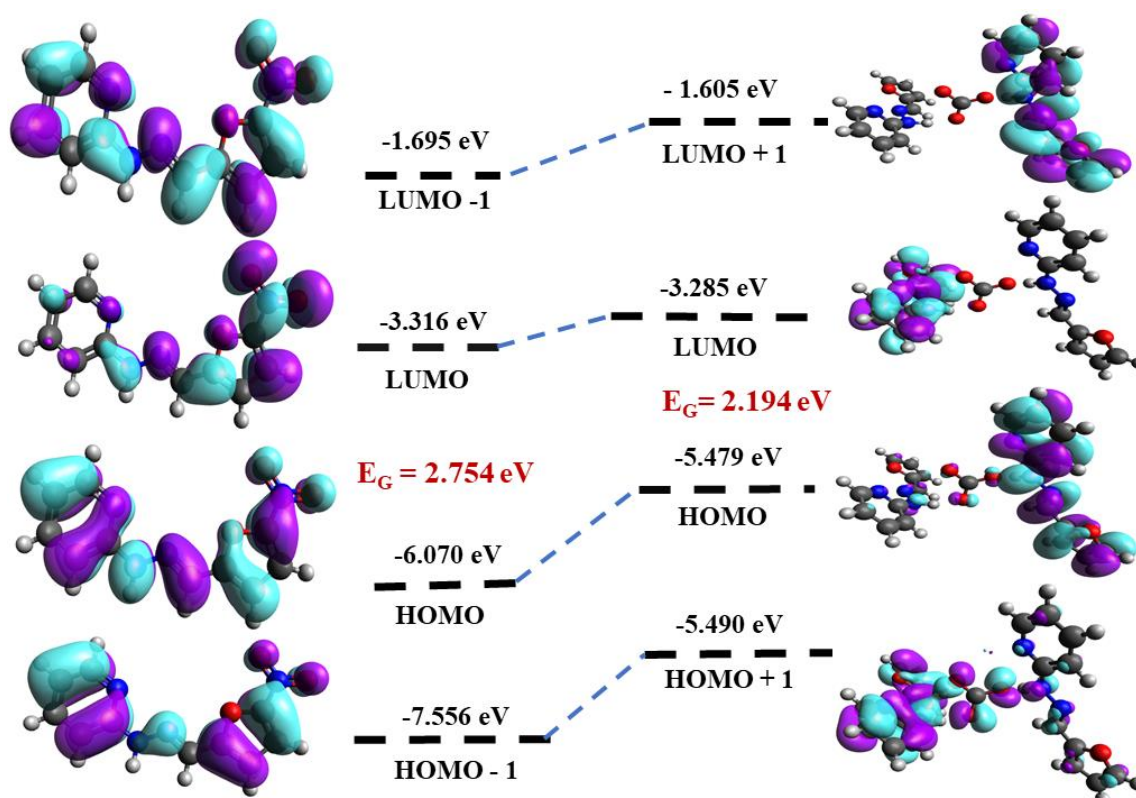
Fig. 5.53 Optimized molecular orbital of receptor **L4R1** before and after addition of CO_3^{2-} ion with energy levels of 6-31+G (d,p)
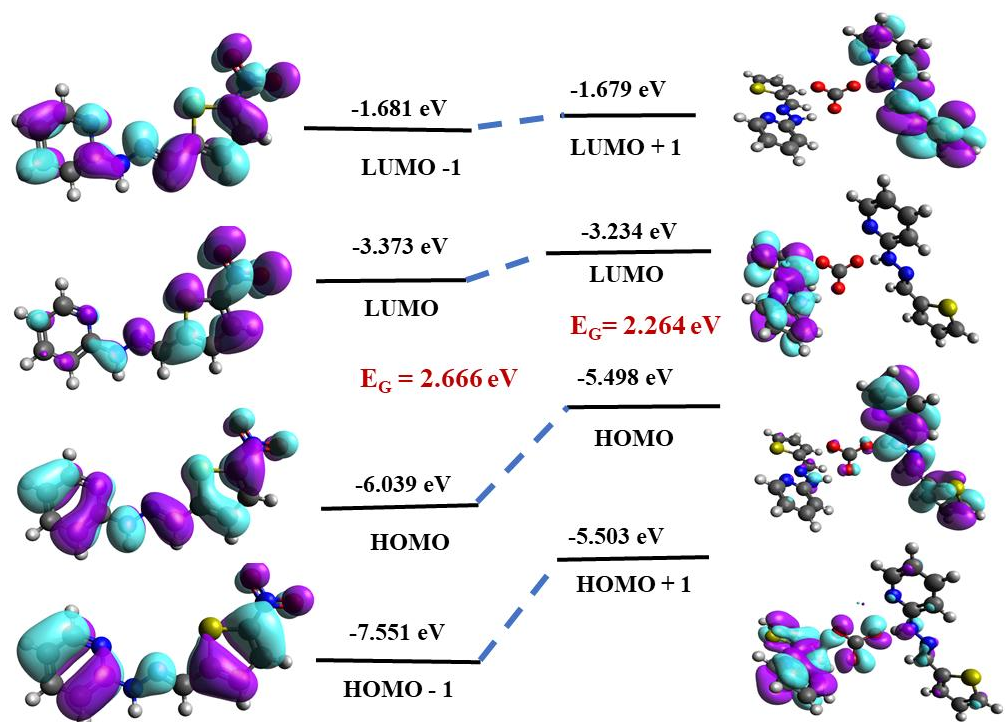
Fig. 5.54 Optimized molecular orbital of receptor **L4R2** before and after addition of CO_3^{2-} ion with energy levels of 6-31+G (d,p)

The molecular orbital energy level of the receptors **L4R1** and **L4R2** and their complexes with F^-, AcO^-, and CO_3^{2-} ions are summarized in Table 5.3.

Table 5.3 Molecular orbital energy of receptors **L4R1** and **L4R2** and their complexes with sensed anions

Receptor	HOMO-1 eV	HOMO eV	LUMO eV	LUMO-1 eV	E_G eV
L4R1	-7.556	-6.070	-3.316	-1.695	2.754
L4R2	-7.551	-6.039	-3.373	-1.681	2.666
Receptor+ Complex	HOMO+1 eV	HOMO eV	LUMO eV	LUMO+1 eV	E_G eV
L4R1+F^-	-7.070	-5.503	-3.236	-1.419	2.267
L4R2+F^-	-7.085	-5.458	-3.287	-1.439	2.171
L4R2+AcO^-	-6.632	-5.473	-3.241	-1.406	2.232
L4R1+ CO_3^{2-}	-5.490	-5.479	-3.285	-1.605	2.194
L4R2+ CO_3^{2-}	-5.503	-5.498	-3.234	-1.679	2.264

The optimized structure of the receptors and their complexes was further calculated by TD-DFT to understand the nature of absorbance and shift in wavelength, before and after binding with the anions. The TD-DFT results of the receptors **L4R1** and **L4R2**, and their complexes with the corresponding anions are shown in Fig. 5.55, Fig. 5.56 (a, b) and Fig. 5.57 (c, d). Moreover, the theoretical and experimental redshift observed for the receptors **L4R1** and **L4R2** after complexation with F^-, AcO^-, and CO_3^{2-} ions is summarized in Table 5.4.

Table 5.4 Theoretical and experimental shift in transition energy of receptors upon complexation

S.No	Receptor +Anions	Theoretical $\Delta\lambda_{max}$ (nm)	Experimental $\Delta\lambda_{max}$ (nm)
1	**L4R1**+F^-	55	208
2	**L4R2**+F^-	64	215
3	**L4R2**+AcO^-	60	194
4	**L4R1**+CO_3^{2-}	121	210
5	**L4R2**+ CO_3^{2-}	188	219

The receptor **L4R1** showed absorption maxima at 488 nm theoretically, and upon complexation with F^- shifted to 544 nm and 618 nm for the CO_3^{2-} ions. Similarly, **L4R2** showed absorption maxima at 507 nm, and upon complexation with F^-, AcO^-, and CO_3^{2-} ions, this λ_{max} shifted to 571 nm, 567 nm, and 695 nm differing by units of 64 nm, 60 nm, and 188 nm, respectively. Hence, it can be concluded that the red shift observed for the CO_3^{2-} ion complex with **L4R2** is a potent receptor for the detection of CO_3^{2-} ions in an aqueous medium. The theoretical shift observed in the absorption spectrum for CO_3^{2-} ions for both the receptors is in good agreement with the experimental details.
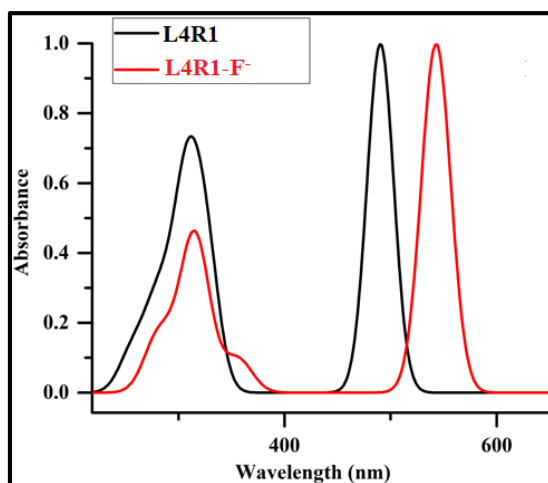
Fig. 5.55 TD-DFT derived UV-Vis spectra of **L4R1** and **L4R1**+F⁻ complex
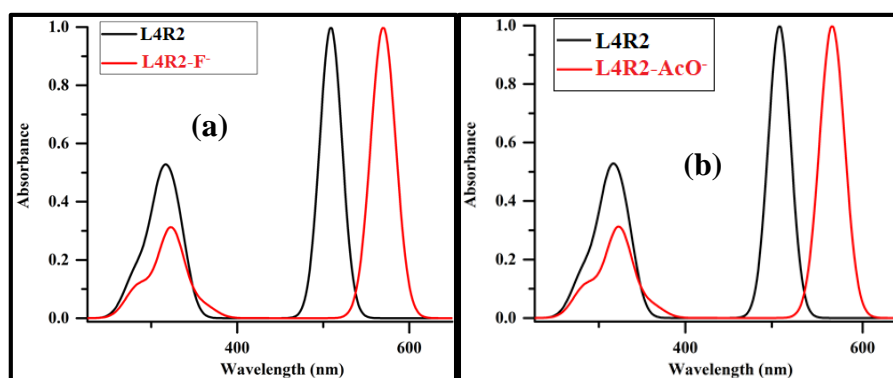
Fig. 5.56 TD-DFT derived UV-Vis spectra of (a) **L4R2** and **L4R2**+F⁻ complex, and (b) **L4R2** and **L4R2**+AcO⁻ complex
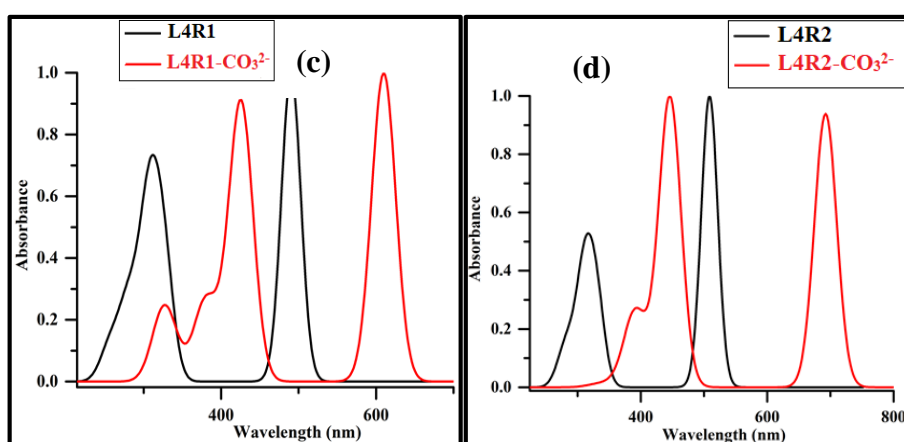
Fig. 5.57 TD-DFT derived UV-Vis spectra of (c) **L4R1** and **L4R1**+CO_3^{2-} complex (d) **L4R2** and **L4R2**+ CO_3^{2-} complex

5.4 CONCLUSION

In conclusion, the anion sensing ability of the two receptors **L4R1** and **L4R2** was investigated via naked-eye, UV-Vis, ^{1}H-NMR titration, and electrochemical and computational studies. **L4R1** showed high selectivity for F$^-$ ions, whereas **L4R2** efficiently distinguished between F$^-$ and AcO$^-$ ions by displaying distinct colour change from pale yellow to aqua and green in the presence of various competitive anions in the DMSO. The UV-Vis titration studies indicated a strong binding of F$^-$ with the receptors **L4R1** and **L4R2**, giving a binding constant of 2.3×10^4 M^{-2} and 8.57×10^4 M^{-2}, respectively. In addition, the ^{1}H-NMR titration and mass spectral data suggested 1:2 binding ratio between the receptors **L4R1** and **L4R2** and the F$^-$ ion confirming the deprotonation process involved in the binding mechanism. There are several advantages associated with the receptors **L4R1** and **L4R2** for CO$_3^{2-}$ ions detection such as (i) a simple synthesis of the receptors **L4R1** and **L4R2**; (ii) high selectivity over other competing sodium salts in the aqueous DMSO: H$_2$O (9:1 v/v); and (iii) practical application of **L4R1** and **L4R2** by using the test strip. Therefore, the receptors **L4R1** and **L4R2** can be constituted as simple and inexpensive chemosensors for the detection of CO$_3^{2-}$ ions in the aqueous DMSO: H$_2$O (9:1 v/v). In addition, the DFT and TD-DFT studies supported the experimental data and the proposed sensing mechanism.

CHAPTER 6

DESIGN AND SYNTHESIS OF MALONOHYDRAZIDE BASED COLORIMETRIC RECEPTORS FOR DISCRIMINATION OF MALEATE OVER FUMARATE AND DETECTION OF F^-, ACO^- AND AsO_2^- IONS
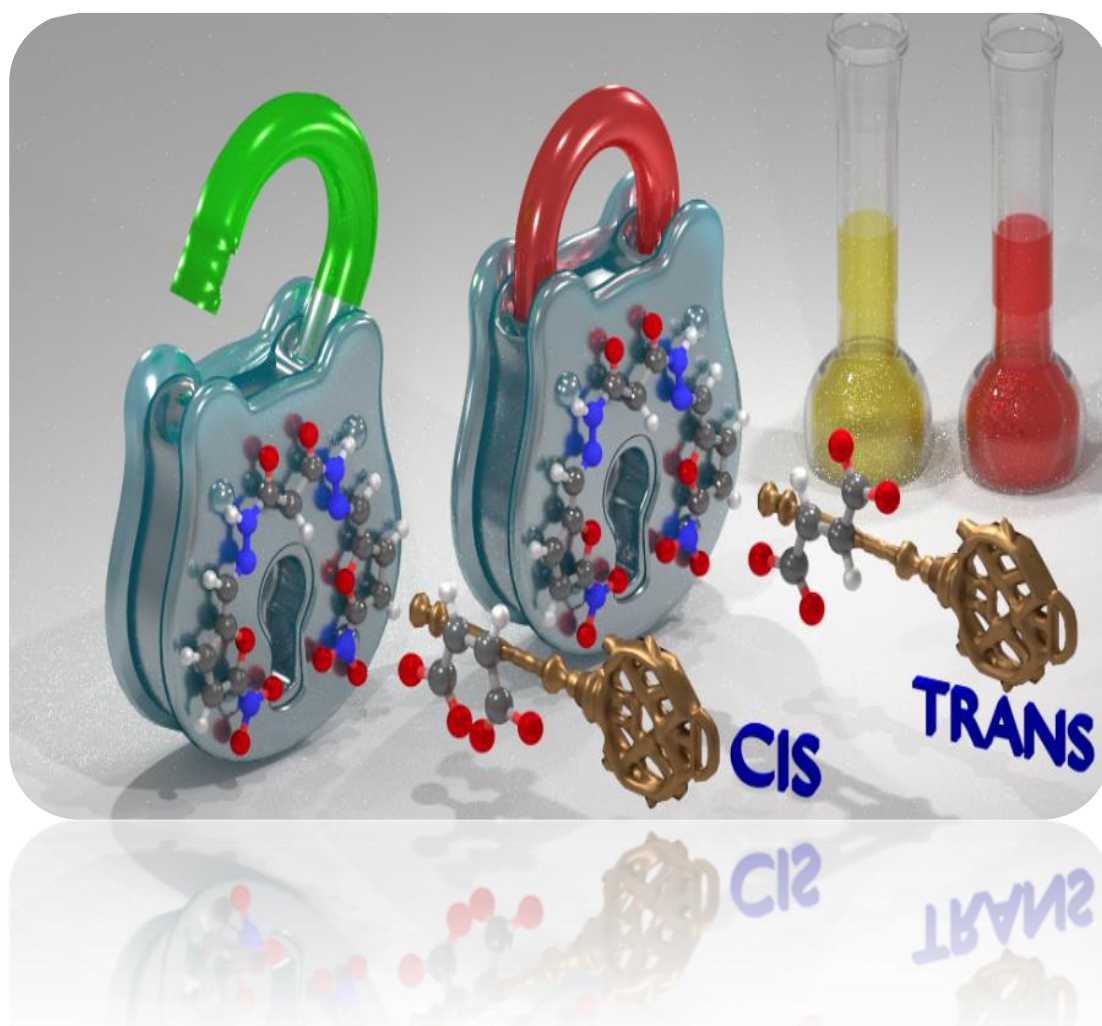
Abstract: In this chapter, the design, syntheses, and characterization of new malonohydrazide Schiff's base derivatives as colorimetric receptors for discriminative detection of maleate ion over fumarate ion is discussed in detail. The colorimetric anion sensing properties and detection mechanism of these receptors are incorporated. In addition, the receptors are studied for colorimetric detection of other biologically important anions such as fluoride and acetate. The binding model of the receptors with fluoride and maleate ions is proposed on the basis of UV-Vis spectral studies supported by DFT studies.

6.1   INTRODUCTION

Anion sensing via synthetic organic receptor is a field of interest in supramolecular chemistry because of its importance in chemical and biological systems (Li et al. 2004; Marcotte et al. 2003; Zhang and Jin 2012). Majority of the receptors follow the binding methodology for the detection of anions. The receptors designed via this methodology comprises of two parts, *viz.*, signalling unit and the binding site, which are attached together with a covalent linker. Upon binding of the anions to the binding site, the physical properties of the receptor changes and is transformed to optical changes by the signalling unit. In this methodology, the binding take place via non-covalent interaction, generally hydrogen bond formation, which makes this detection methodology reversible (Duke et al. 2008; Evans et al. 2006; Jiang et al. 2009; Nie et al. 2004; Wu et al. 2004). Based on this methodology, substantial efforts have been made by researchers to establish new receptors that are capable of detecting anions (Su et al. 2010; Villamil-Ramos and Yatsimirsky 2011). However, majority of these efforts was restricted to the detection of inorganic anions (Jin et al. 2013; Jose et al. 2005; Sun et al. 2013; Wu et al. 2012), mainly fluoride (Ajayakumar et al. 2013; Cametti and Rissanen 2013; Duke et al. 2010; Dydio et al. 2011; Guo et al. 2012; Li et al. 2010; Ren et al. 2011; Sharma et al. 2013; Zhao et al. 2012) and cyanide(Kumari et al. 2011; Lin et al. 2012; Niu et al. 2008; Odago et al. 2010; Park et al. 2011; Shiraishi et al. 2009; Xu et al. 2010). Along with inorganic anion detection, efforts were also been made to develop receptors for the colorimetric detection of organic molecules (Ghosh and Majumdar 2013; Lawrence et al. 2012; Mohadesi and Taher 2007). Among the widespread organic molecules, the detection of dicarboxylates ions attains

substantial prominence due to its vital applications in various metabolic and biological processes (El-Sherif 2010; Nisbet et al. 2009; Shin et al. 2011; Xu et al. 2012). Therefore, few receptors have been reported for the selective detection of dicarboxylates (Ghosh et al. 2010; Gunnlaugsson et al. 2002; Jadhav and Schmidtchen 2006; Kral et al. 1995; Lavigne and Anslyn 1999; Liu et al. 2005; Raker and Glass 2002; Zhao et al. 2004). However, among dicarboxylates, the colorimetric discrimination of geometrically isomeric dicarboxylates such as cis-maleate ion and trans-fumarate ion as shown in Scheme 6.1, are important due to their different biological behaviours (Eiam-Ong et al. 1995; Gougoux et al. 1976). Trans-fumarate is generated in the kerb's cycle, whereas maleate is a well-known inhibitor of this cycle. Moreover, excess intake of maleate is found to be detrimental to the kidneys and can cause several kidney diseases (Costero et al. 2006; Stepiński et al. 1984). In spite of this wide application of dicarboxylates, only scant receptors have been reported so far to differentiate the geometric isomers due to their similar chemical and physical properties (Sancenón et al. 2003; Yen and Ho 2006). Among the other biologically important anions, the colorimetric detection of fluoride and acetate ions play an imperative role in a broad range of chemical and biological systems, and sometimes they are of environmental concern (Beer and Gale 2001; Bianchi et al. 1997; Cametti and Rissanen 2013; Kirk 1991; Sessler et al. 2006). For example, fluoride draws special attention due to its various applications in health, medicine, environmental science, and also in the purification of drinking water (Esteban-Gomez et al. 2005; Evans et al. 2006; Han et al. 2007; Jose et al. 2004; Sessler et al. 2006; Yoo et al. 2008). On the other hand, carboxylates are of immense interest due to their biochemical behaviours in enzymes and antibodies and also as crucial components of various biological processes (Fitzmaurice et al. 2002; Wang et al. 2011). Coming to arsenic toxicity, they have many adverse effects on human and the environment if they reach 0.01 ppm as defined by the EPA. Arsenic can cause skin cancer, damage to the lung, liver, DNA, and infertility when it exceeds its limit (Chauhan et al. 2017; Saha et al. 2017; Tchounwou et al. 2012). Among the two forms of arsenic, As^{3+} is more dangerous than As^{5+} due to its high coordinating ability with sulfhydryl groups of biomolecules. To the best of knowledge, two new colorimetric chemosensors, **L5R1** and **L5R2** have been developed and synthesized as shown in Scheme 6.2, having NH group as the binding site and

connected with a methyl spacer for colorimetric discrimination of maleate ion over fumarate ion. These binding sites are separated by a spacer, to make the molecule more flexible. In addition, the receptors **L5R1** and **L5R2** are capable of sensing biologically important fluoride and acetate ions with low detection limit.
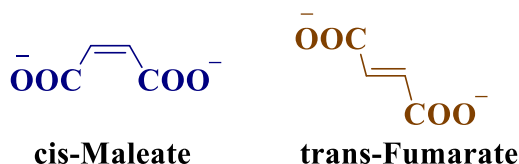
Scheme 6.1 Example of dicarboxylates
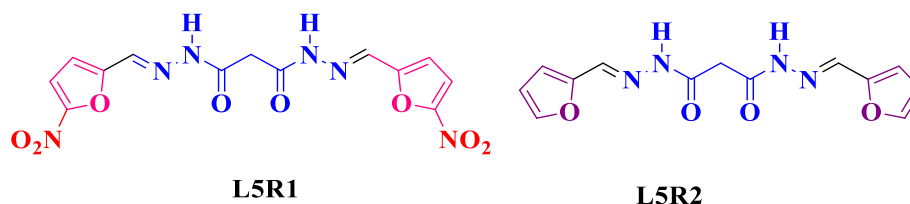
Scheme 6.2 Schematic design of receptors **L5R1** and **L5R2**

6.2   EXPERIMENTAL SECTION

6.2.1   Materials and methods

All the chemicals used in the present study were procured from Sigma-Aldrich. All the solvents purchased from SD Fine, India, were of HPLC grade and used without further distillation. Thin-layer chromatography was performed using Merck TLC Silica Gel F254 plates. The melting point was measured on the Stuart SMP3 melting-pont apparatus in open capillaries. Infrared spectra were recorded on the Bruker alpha FTIR spectrometer. ^{1}H NMR were recorded on Bruker Ascent (400 MHz) instrument using TMS as internal reference and DMSO-d$_6$ as the solvent. ^{13}C NMR spectra were recorded on Bruker Ascend (100 MHz) instrument using TMS as internal reference and DMSO-d$_6$ as solvent. Resonance multiplicities are described as s (singlet), d (doublet), t (triplet), and m (mutiplet). Mass spectrum was recorded on Bruker Daltonics ESI Q TOF. The UV-Vis titration was carried out using the Jasco-V-670 spectrophotometer in 3.00 ml quartz cuvette of 1 cm path length. The fluorescence study was recorded in the JASCO-FP-6200 Spectrometer. Cyclic voltammogram was recorded on IVIUM electrochemical workstation (Vertex) at a scan rate of 20 mV/s with the potential

range −3 V to 3 V. Density Functional Theory (DFT) simulation has been performed on the receptor molecule using GAUSSIAN 09 package. A close shell Becke-Lee-Yang-Parr hybrid exchange-correlation three-parameter functional (B3LYP) along with 6-311++G(d) basis set were used in the simulation to drive a complete geometry optimization for isolated receptor and its complex formation with anions. Berny's optimization algorithm was used to fully optimize the molecular geometry, which involve redundant internal coordinates. To confirm the convergence to the minima on the potential energy surface, the harmonic vibrational wavenumber were calculated using analytic second derivative and properly scale down to control the systematic error caused by incompleteness of the basis set. In a second step, the time dependent DFT (TD-DFT) method were used considering the same B3LYP exchange-correlation functional with 6-311+G (d,p) basis set to obtain the UV-Vis absorption spectra of free and complex receptor.

6.2.2   Calculation of binding constant

Binding constant has been calculated using Benesi-Hildebrand equation (Benesi and Hildebrand 1948) as given below in (Eq. 6.1)

$$\frac{1}{(A-A_0)} = \frac{1}{(A_{max}-A_0)} + \frac{1}{K[X^-]^n (A_{max}-A_0)} \ldots\ldots\ldots (Eq.\ 6.1)$$

Where, A_0, A, and A_{max} are the absorption considered in the absence of anion, at intermediate and at concentration of saturation, respectively, K is the binding constant, $[X^-]$ is the concentration of the anion, and n is the stoichiometric ratio.

6.2.3   Calculation of limit of detection (LOD)

The detection limit of the receptors **L5R1 and L5R2** with the anions was calculated by using (Eq. 6.2)

$$LOD = \frac{3 \times \sigma}{s} \ldots\ldots\ldots\ldots (Eq.\ 6.2)$$

Where, σ is the standard deviation of the calibration curve (SD) and s is the slope of the calibration curve.

6.2.4 Synthesis of intermediate malonohydrazide (S 6.1)

Diethylmalonate (0.16g, 1mmol) and hydrazine hydrate (0.10g, 2mmol) were refluxed at 50°C for 2 h under solvent-free conditions. The progress of the reaction was monitored by TLC. Finally, a good yield of the white coloured product was obtained (Tayade et al. 2014).

.
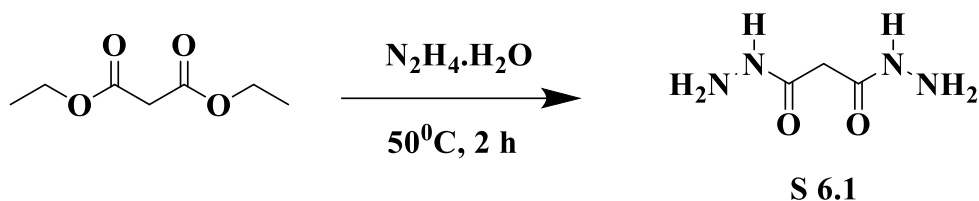
Scheme 6.3 Synthesis of intermediate **S 6.1**

6.2.5 Synthesis of receptor (L5R1) N'', N'³-bis((E)-(5-nitrofuran-2-yl)methylene) malonohydrazide

Malonohydrazide **S 6.1** (0.75g, 1mmol) and 5-nitrofuran-2-carbaldehyde (1.514g, 2mmol) was refluxed in 5 mL methanol at 50˚C for 5h in the presence of acetic acid (CH_3CO_2H) as the catalyst. The formation of the product was confirmed through TLC by the generation of a single spot indicative of the disappearance of the starting materials. After cooling to room temperature, the reaction mixture was filtered and washed with methanol to obtain the pure product **L5R1** as shown in Scheme 6.4.
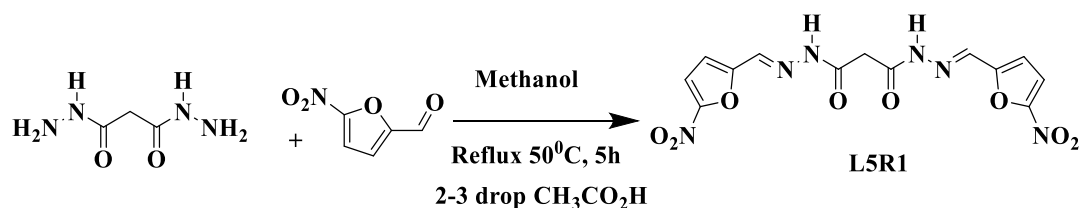
Scheme 6.4 Synthesis of receptor **L5R1**

6.2.6 Synthesis of receptor (L5R2) N'',N'³-bis((E)-furan-2-yl)methylene) malonohydrazide

Malonohydrazide **S 6.1** (0.75g, 1mmol) and furan-2-carbaldehyde (0.756g, 2mmol) was refluxed in 5 mL methanol at 50˚C for 5h in the presence of acetic acid

(CH₃CO₂H) as the catalyst. The formation of the product was confirmed through TLC by the generation of a single spot indicative of the disappearance of the starting materials. After cooling to room temperature, the reaction mixture was filtered and washed with methanol to obtain the pure product **L5R2** as shown in Scheme 6.5.
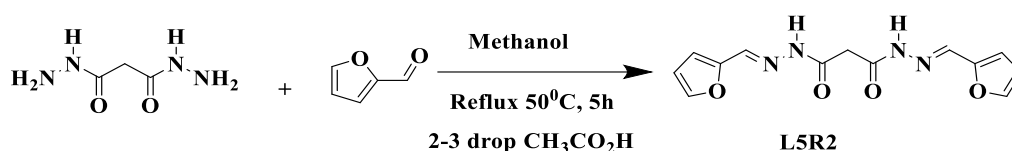
Scheme 6.5 Synthesis of receptor **L5R2**

6.2.7 General method for preparation of tetrabutylammonium salts

About 1.0 M tetrabutylammonium hydroxide solution prepared in (2.0 equiv.) methanol 5 mL was added to a stirred solution of the corresponding dicarboxylic acid (2.5 mmol) in dry methanol (5 mL). The resulting mixture was stirred for 2 h at room temperature. The solvent was evaporated under reduced pressure and dried over P_2O_5 to obtain the final product of the desired dicarboxylic acid, and the salts were immediately used for further application (Tseng et al. 2007).

6.2.8 Stoichiometric ratio determination using Job plot method

A Job plot is used to determine binding stoichiometry. In this method, the total molar concentration of anion and receptor are kept constant. However, the mole fraction of both is continuously varied. The UV-Vis absorbance was measured for each fraction. This absorbance was plotted against the mole fractions of the two components. The maximum absorbance on the plot corresponds to the stoichiometry of the two species.

6.2.9 Characterization data

The purity and structure of the intermediate **S 6.1** and receptors **L5R1,** and **L5R2** were confirmed by FT-IR, ^{1}H-NMR, ^{13}C-NMR, and mass spectroscopic methods. The characterization data has been compiled and given below.
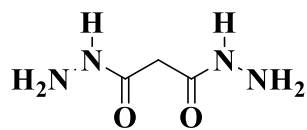
Data obtained for intermediate S 6.1: Yield: 80%. m.p.: 160 ^{0}C. IR (ATR) (cm^{-1}): 1591 (C=O), 3209 (N-H), 1639 (C=N) cm^{-1}. ^{1}H NMR (DMSO-d$_6$, 400 MHz, Me$_4$Si): δ_{ppm} 9.061 (s, 2H), 4.441-4.041 (s, 4H), 2.900 (s, 2H). Mass (ESI): m/z calculated for C$_3$H$_8$N$_4$O$_2$: 132.06 Obtained: 133.00 [M+H]$^+$.
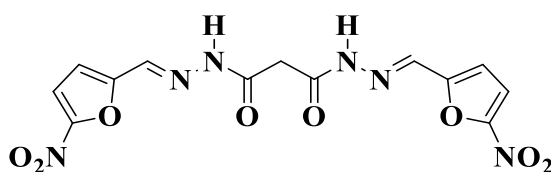
(N'', N'3-bis ((E)-(5-nitrofuran-2-yl)methylene)malonohydrazide (L5R1) : Yield: 80%. m.p: 350°C. IR (ATR) (cm^{-1}): 3199 (N-H), 3056 (N-H), 1644 (C=N), 1340 (NO$_2$), 1588 (C=O). ^{1}H NMR (DMSO-d$_6$, 400 MHz, Me$_4$Si): δ_{ppm} 12.040-11.910 (triplet, 2H), 8.174-7.796 (s,1H), 7.787-7.759 (s,1H), 7.261-7.227 (s,2H), 7.217-7.159 (m,2H), 3.969 (s, 1H), 3.675 (s,1H). ^{13}C NMR (DMSO-d$_6$, 100 MHz, Me$_4$Si): δ_{ppm} 153.998, 144.371, 137.641, 136.757, 134.567, 130.060, 129.024, 128.794, 128.036, 126.970, 122.891, 116.725. Mass (ESI): m/z calculated for C$_{13}$H$_{10}$N$_6$O$_8$: 378.06 Obtained: 379.05 [M+H]$^+$.
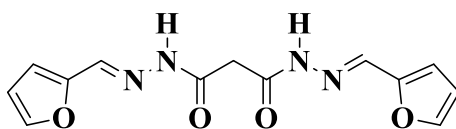
(N'', N'3-bis ((E)-furan-2-yl)methylene)malonohydrazide (L5R2): Yield: 80%. m.p: 320°C. IR (ATR) (cm^{-1}): 3437 (N-H), 2997 (C-H), 2917 (C-H), 1649 (CH=N). ^{1}H NMR (DMSO-d$_6$, 400 MHz, Me$_4$Si): δ_{ppm} 11.548-11.403 (triplet, 2H), 8.085-8.079 (s,1H), 7.875-7.757 (triplet, 3H), 6.908-6.828 (triplet, 2H), 6.622-6.589 (doublet, 2H), 3.859 (s, 1H), 3.562 (s, 1H). ^{13}C NMR (DMSO-d$_6$, 100 MHz, Me$_4$Si): δ_{ppm} δ 153.989, 144.304, 139.346, 137.164, 136.195, 129.826, 129.626, 128.733, 128.620, 127.942, 127.109, 126.447, 123.097, 116.152, 72.726. Mass (ESI): m/z calculated for C$_{13}$H$_{12}$N$_4$O$_4$: 288.09 Obtained: 288.30.

The representative spectrum of intermediate **S 6.1** and receptors **L5R2** and **L5R2** is given below
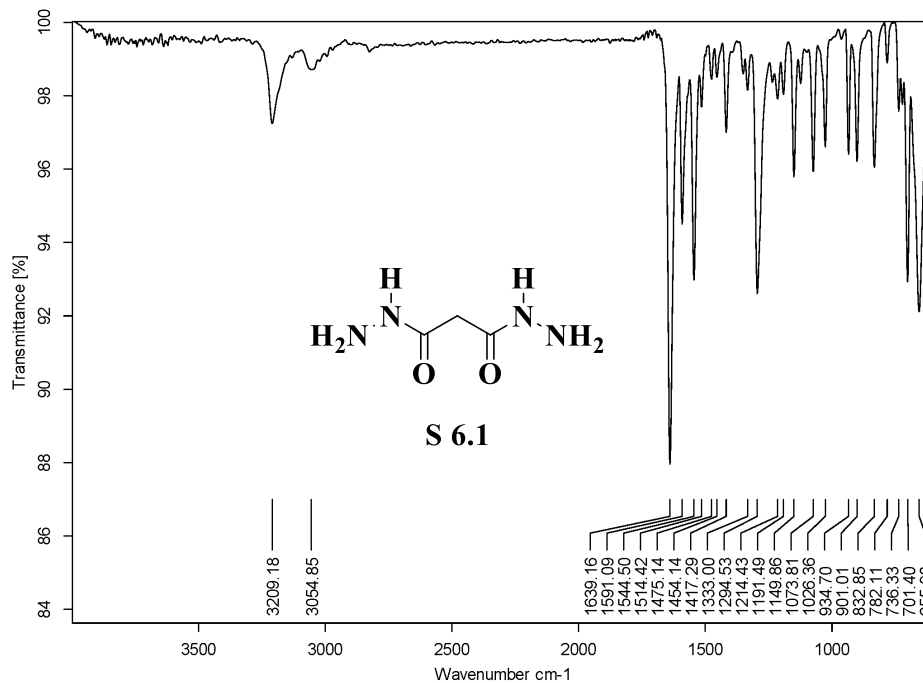
Fig. 6.1 FT-IR spectrum of **S 6.1**
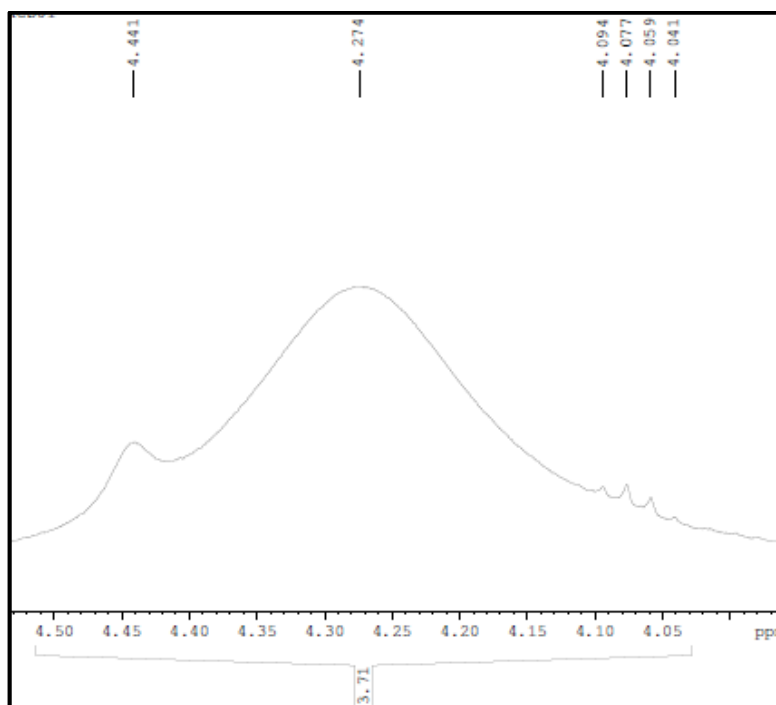
Fig. 6.2 Expanded aromatic region of **S 6.1**
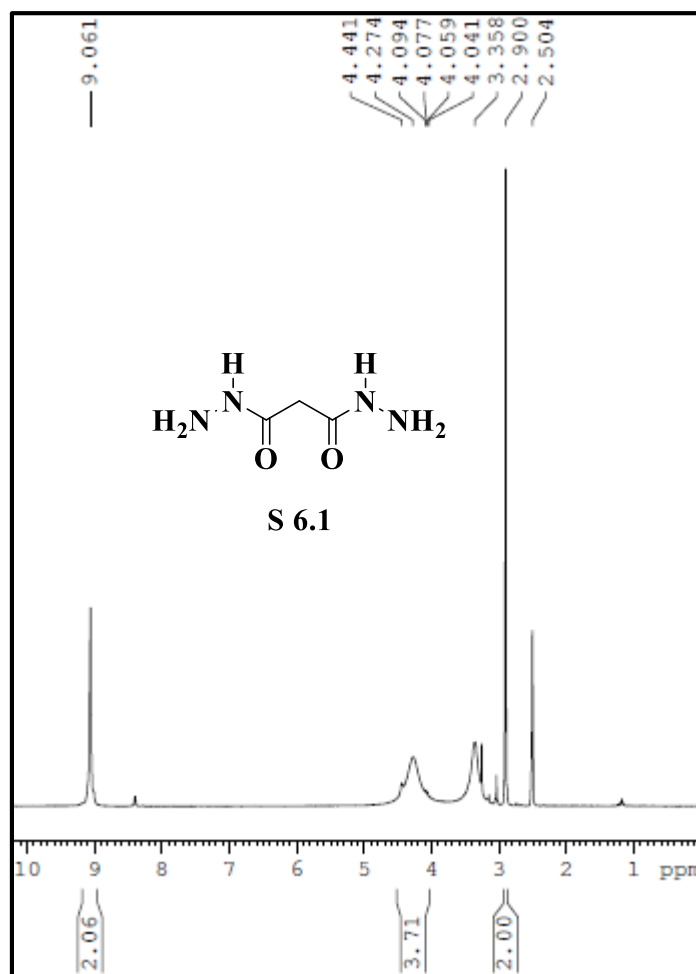
Fig. 6.3 ^{1}H-NMR spectrum of **S 6.1**

Mass spectrum: S 6.1

Exact Mass: 132.06

Mass obtained in the positive mode: 133.00

Elemental composition: $C_3H_8N_4O_2$
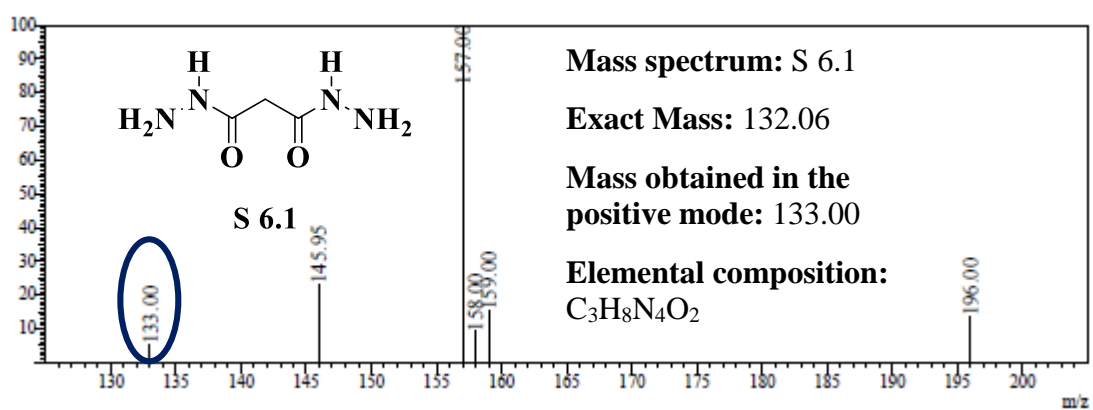
Fig. 6.4 Mass spectrum of **S 6.1**
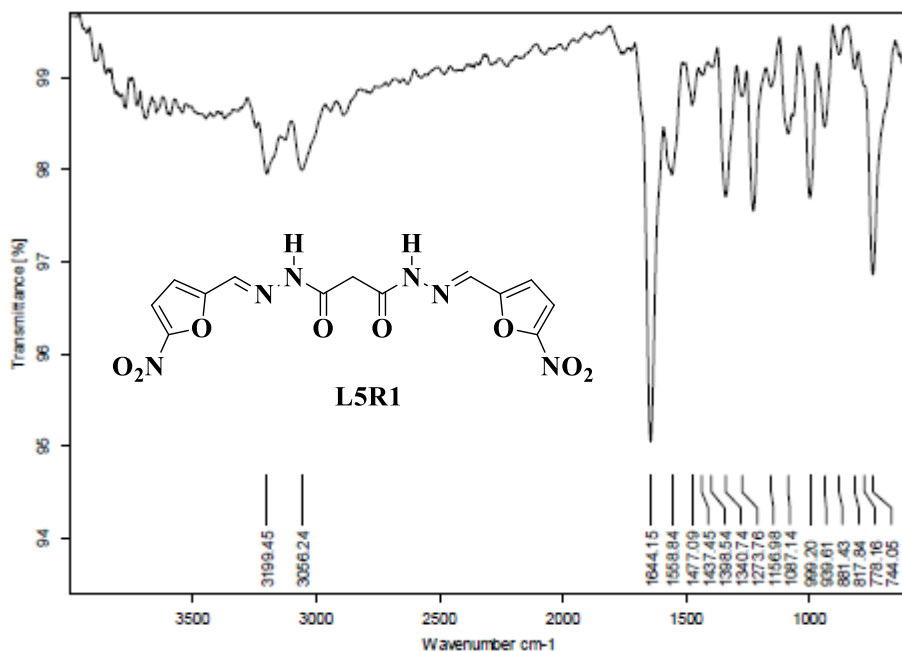
Fig. 6.5 FT-IR spectrum of receptor **L5R1**
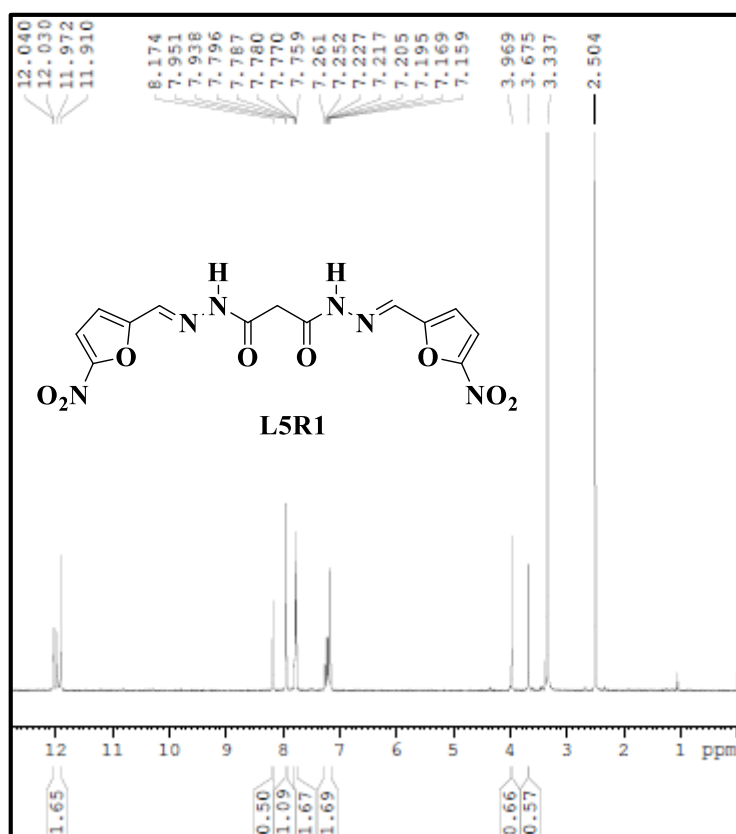
Fig. 6.6 ^{1}H-NMR spectrum of receptor **L5R1**

Fig. 6.7 ^{13}C-NMR spectrum of receptor **L5R1**

Exact Mass: 378.06

Mass obtained in the positive mode: 379.05

Elemental composition: $C_{13}H_{10}N_6O_8$
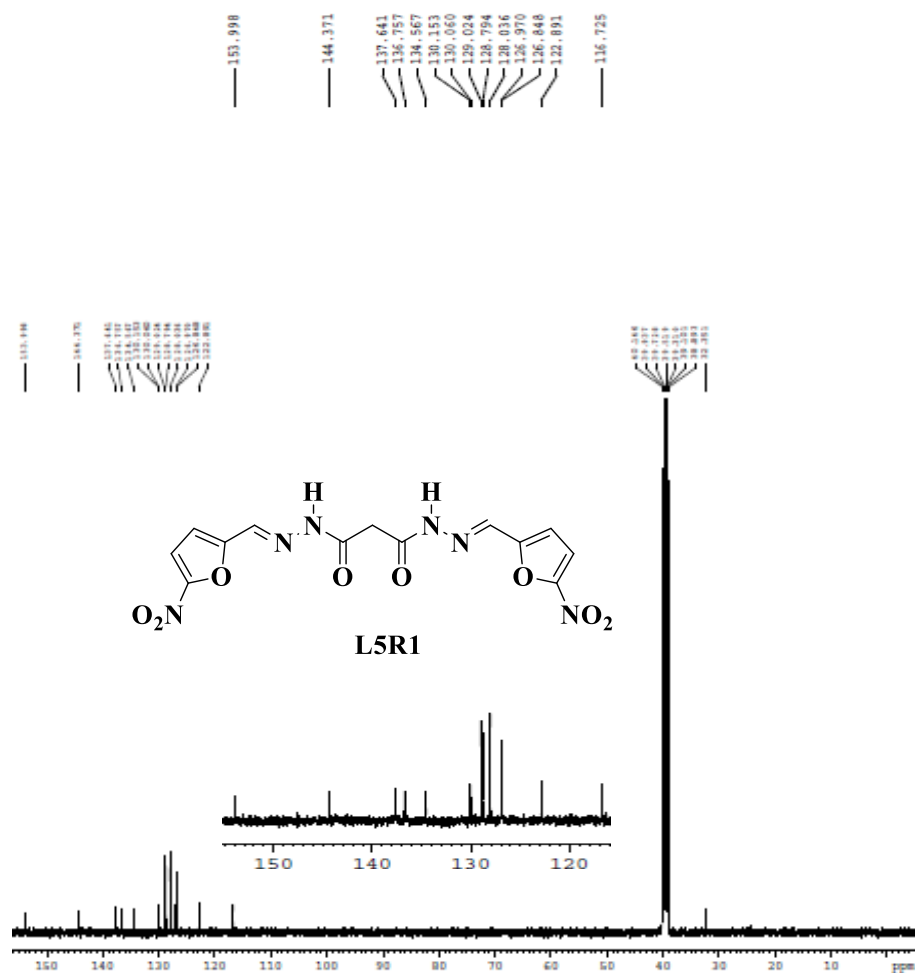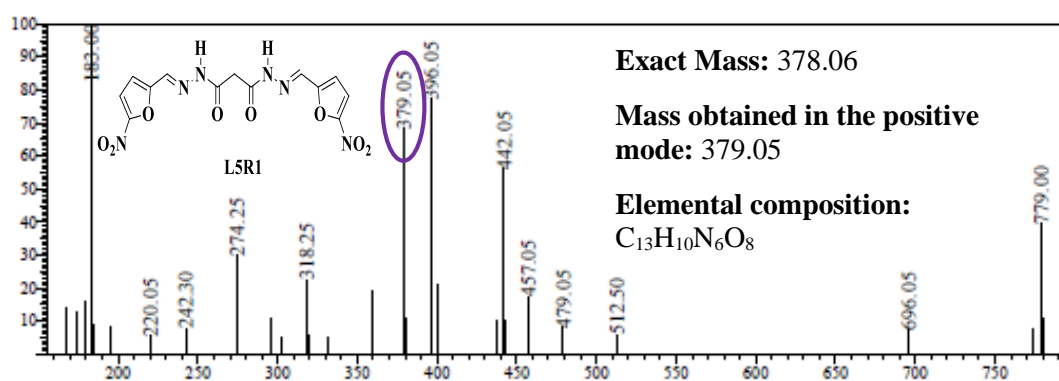
Fig. 6.8 Mass spectrum of receptor **L5R1**

Fig. 6.9 FT-IR spectrum of receptor **L5R2**

Exact Mass: 288.09

Mass obtained in the positive mode: 288.30

Elemental composition: $C_{13}H_{12}N_4O_4$
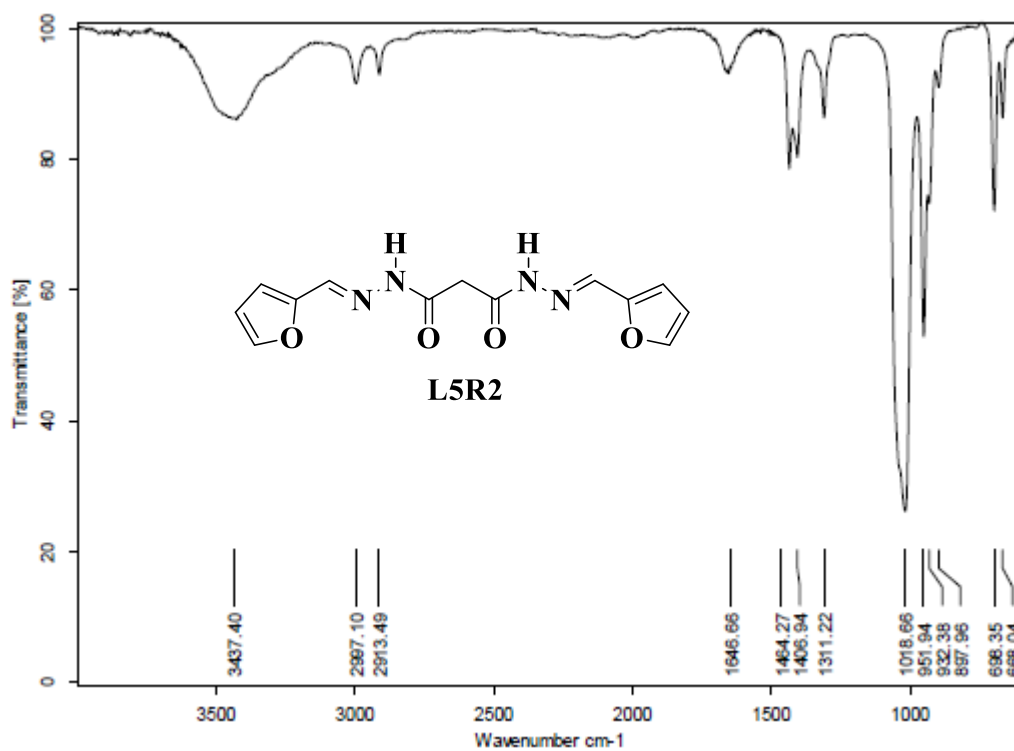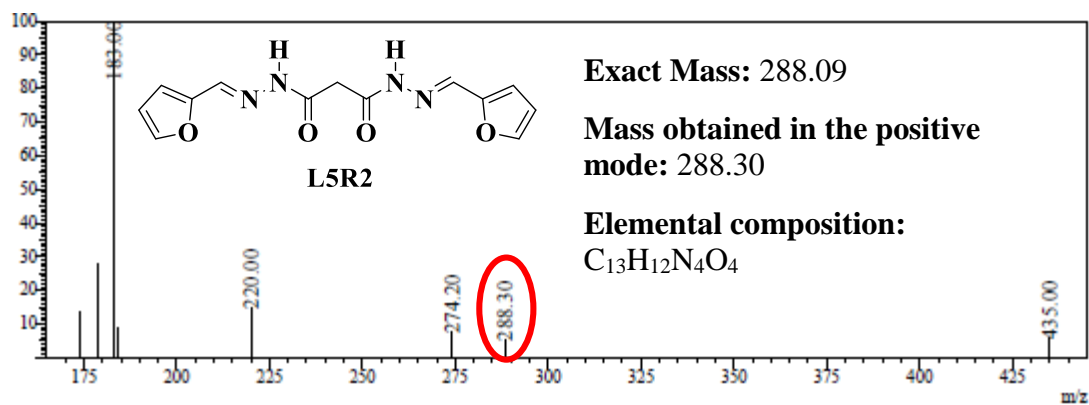
Fig. 6.10 Mass spectrum of receptor **L5R2**
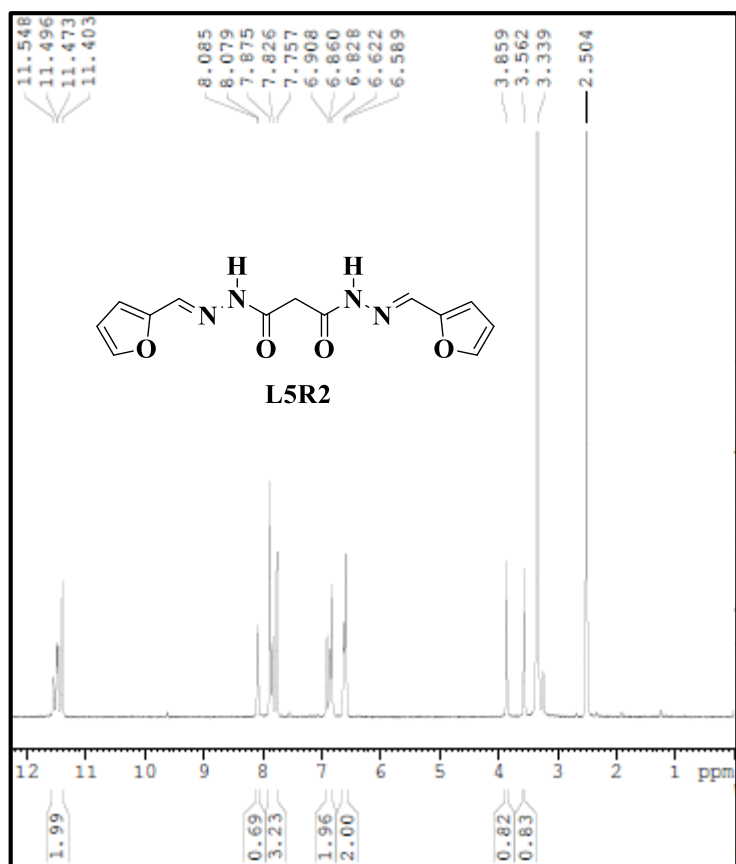
Fig. 6.11 ^{1}H-NMR spectrum of receptor **L5R2**
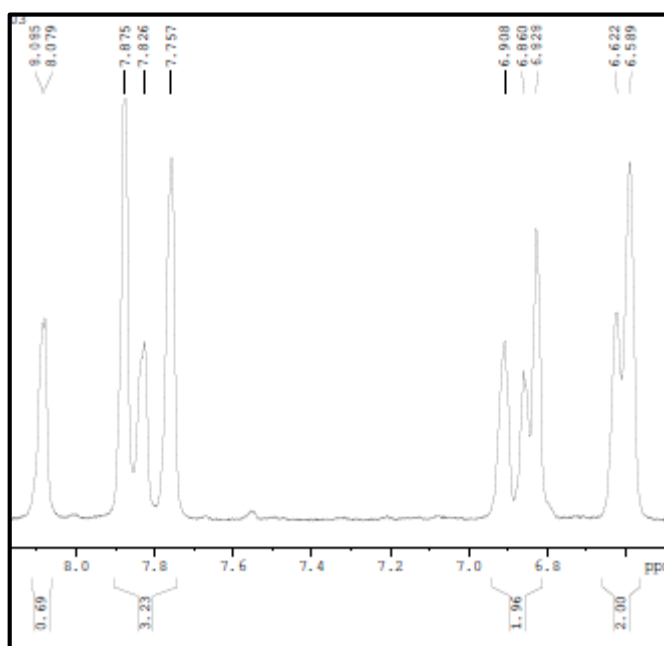
Fig. 6.12 Expended aromatic region of receptor **L5R2**
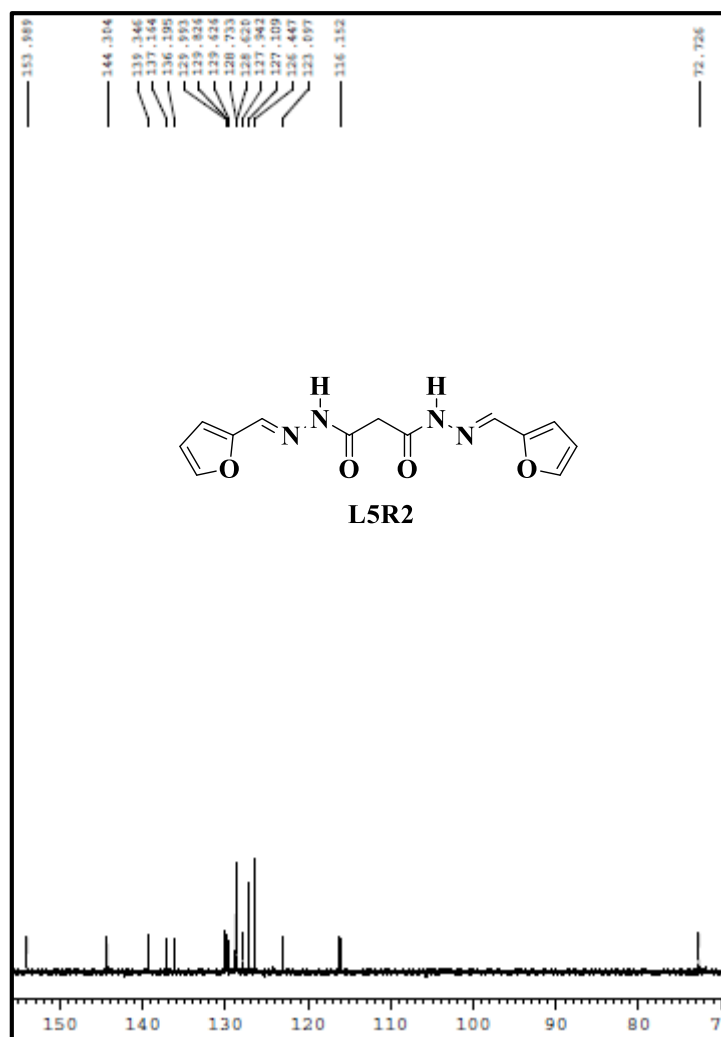
Fig. 6.13 ^{13}C-NMR spectrum of receptor **L5R2**

6.3 RESULT AND DISCUSSION

6.3.1 Colorimetric detection of anions

The anion binding ability of the receptors **L5R1** and **L5R2** (2×10^{-5} M in DMSO) was evaluated visually by adding 2 equiv. of different anions such as F$^-$, Cl$^-$, Br$^-$, I$^-$, NO$_3^-$, HSO$_4^-$, H$_2$PO$_4^-$, and AcO$^-$ (1×10^{-2} M) in the form of tetrabutylammonium salts in the DMSO solution of the receptors. Notably, **L5R1** and **L5R2** exhibited colorimetric response toward F$^-$ and AcO$^-$ ions via vivid colour change from pale yellow to magenta and red as shown in Fig. 6.14. In order to evaluate the selectivity of the receptors **L5R1** and **L5R2** towards F$^-$ and AcO$^-$ ions, a comparative experiment was conducted by observing change in the absorption band. As shown in Fig. 6.15 and Fig. 6.16, only the F$^-$ and AcO$^-$ ions induced instantaneous red shift in the absorption maxima, while the

other anions did not cause any change in absorption. These results indicate that the receptors **L5R1** and **L5R2** showed excellent selectivity for F⁻ and AcO⁻ ions in the presence of other anions in DMSO.
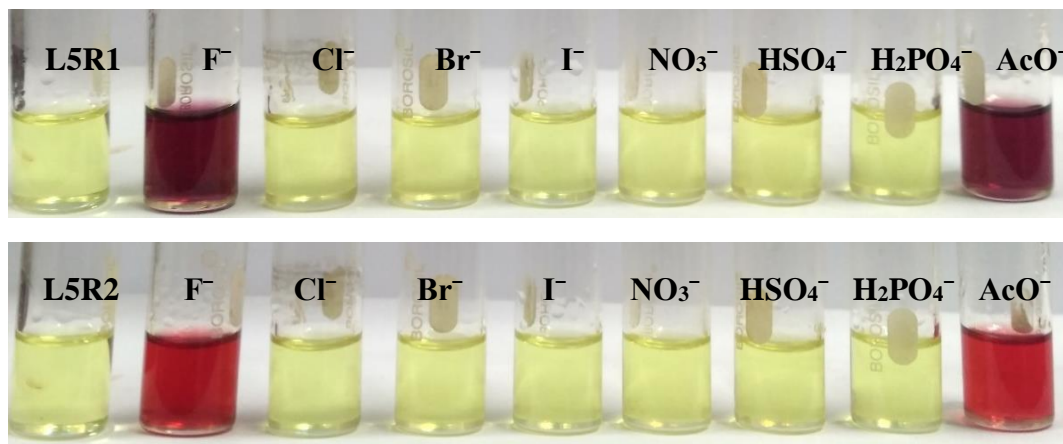
Fig. 6.14 Colour change of receptors **L5R1** and **L5R2** (2×10^{-5} M in DMSO) in the presence of 2 equiv. of series of anions in the form of tetrabutylammonium salts (1×10^{-2} M in DMSO)
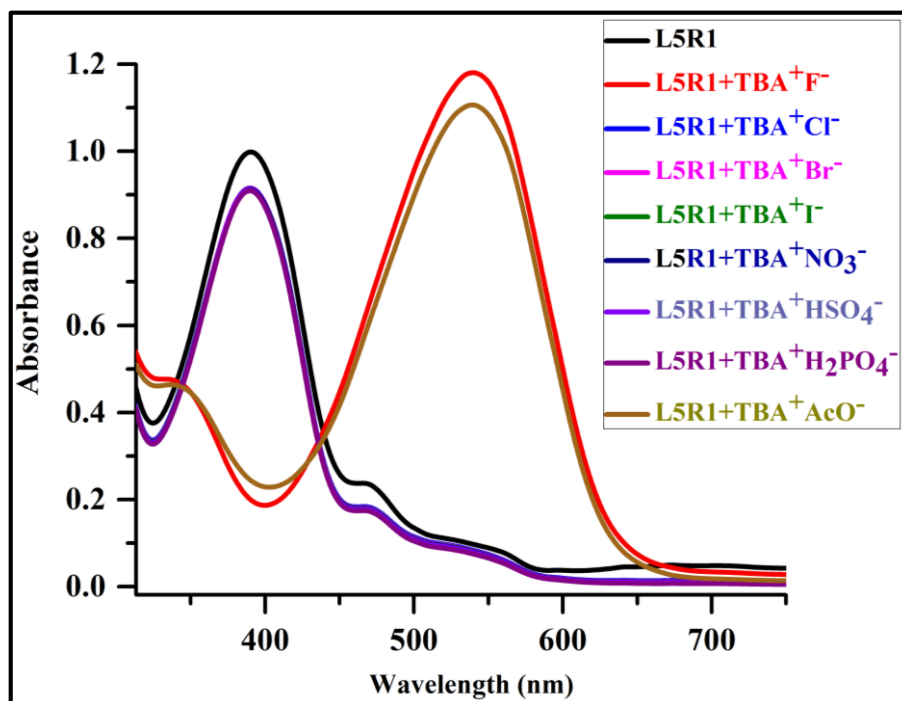
Fig. 6.15 UV-Vis absorption spectra of **L5R1** (2×10^{-5} M in DMSO) upon addition of 2 equiv. of various anions as TBA salts (1×10^{-2} M in DMSO)
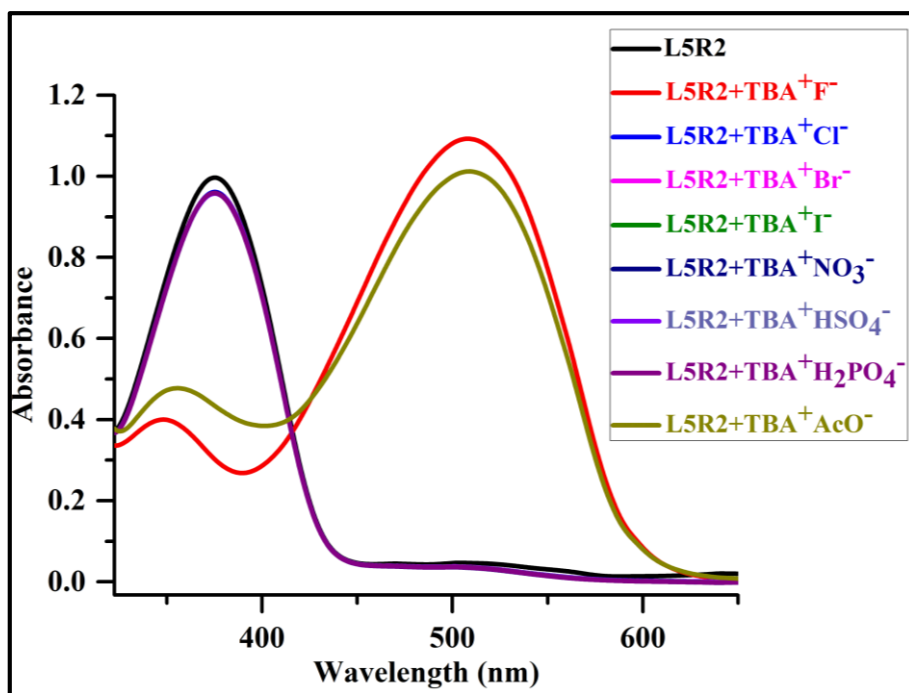
Fig. 6.16 UV-Vis absorption spectra of **L5R2** (2×10^{-5} M in DMSO) upon addition of 2 equiv. of various anions as TBA salts (1×10^{-2} M in DMSO)

6.3.2   UV-Vis titration studies of receptors L5R1 and L5R2 in DMSO

To understand the nature of the receptor-anion interaction, a UV-Vis titration experiment was performed by incremental addition of 0.1 equiv. of TBA^+F^- and TBA^+AcO^- to **L5R1** (2×10^{-5} M in DMSO). The constant incremental addition of TBA^+F^- and TBA^+AcO^- resulted in a steady decrease in intensity of the absorbance band at 389 nm. Meanwhile, a new absorption band appeared at 536 nm and 533 nm with a clear isosbestic points at 434 nm and 430 nm suggesting the formation of only one UV-Vis active species. This bathochromic shift of 147 nm and 144 nm was attributed to the intramolecular charge transfer (ICT) process between the anion-bond NH unit and the electron-deficient -NO_2 group as shown in Fig. 6.17 and Fig. 6.18. The presence of the NO_2 chromophore at the para- position with respect to the NH group led to an intense colorimetric change (Cho et al. 2005). The binding stoichiometry of **L5R1** with F^- and AcO^- ions was evaluated to be 1:2 as confirmed by the Job plot and the B-H plot analysis as depicted in Fig. 6.19 and Fig. 6.20.
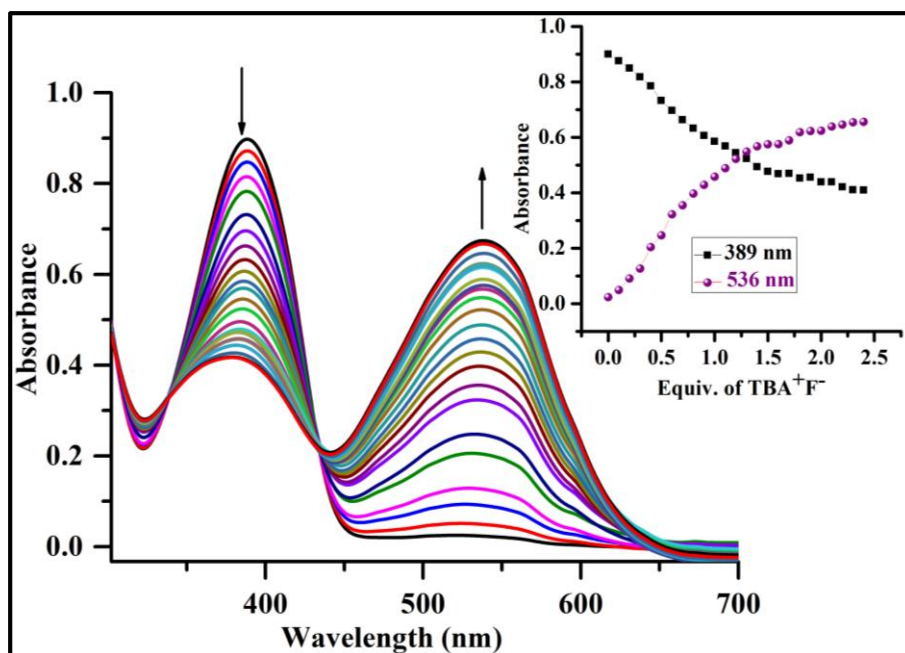
Fig. 6.17 UV-Vis titration spectra of receptor **L5R1** (2×10^{-5} M in DMSO) with incremental addition of TBA$^+$F$^-$ (1×10^{-2} M in DMSO); Inset plot representing absorption isotherm at 389 nm and 536 nm
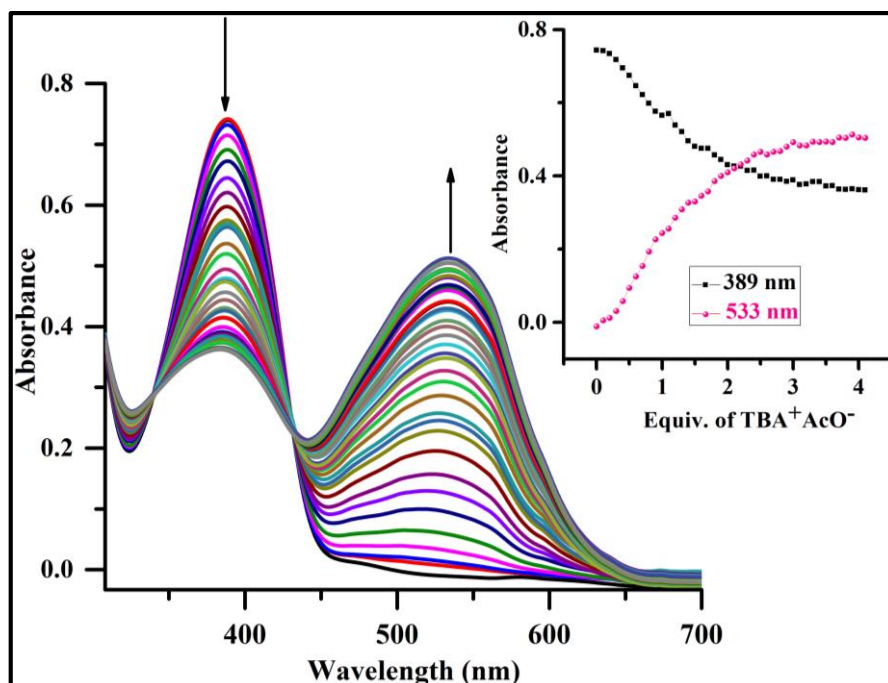
Fig. 6.18 UV-Vis titration spectra of receptor **L5R1** (2×10^{-5} M in DMSO) with incremental addition of TBA$^+$AcO$^-$ (1×10^{-2} M in DMSO); Inset plot representing absorption isotherm at 389 nm and 533 nm
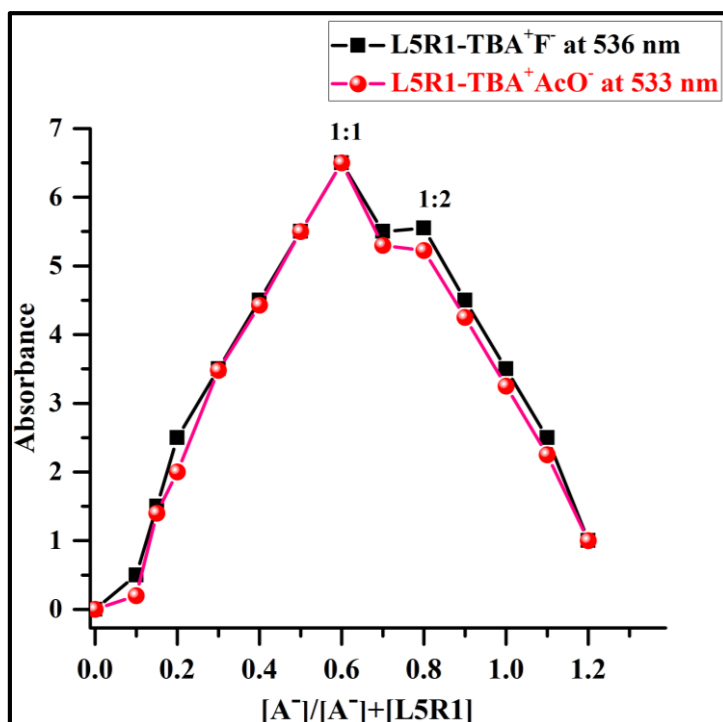
Fig. 6.19 Job plot at 536 nm and 533 nm which indicates 1:2 complexation ratio between **L5R1** and anion
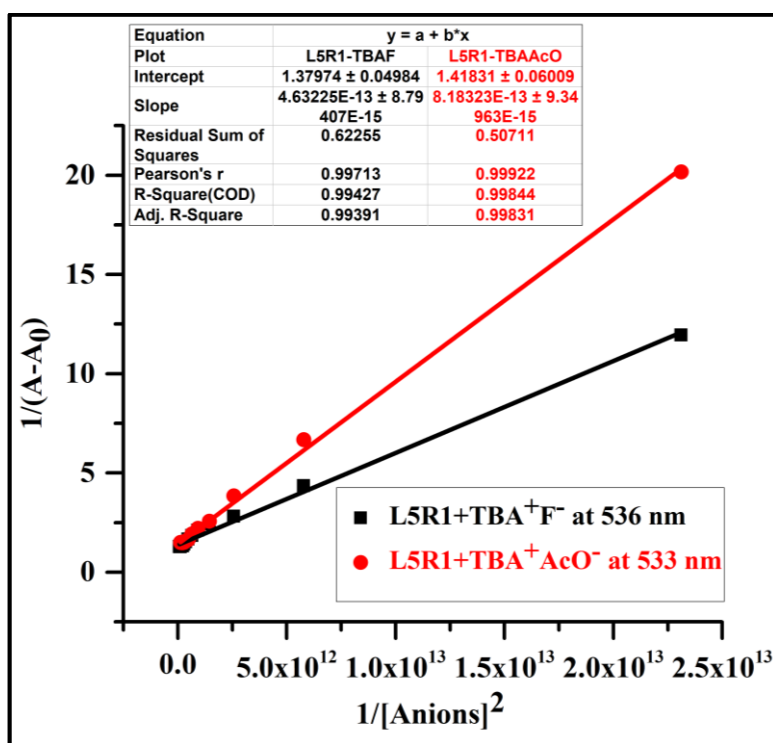
Fig. 6.20 B-H plot of receptor **L5R1** with anions at a selective wavelengths of 536 nm and 533 nm

Further, UV-Vis titration experiment for the receptor **L5R2** with TBA$^+$F$^-$ and TBA$^+$AcO$^-$ was carried out in the DMSO. The UV-Vis spectrum of the receptor **L5R2** exhibited a strong absorption band at around 380 nm. With the incremental addition of 0.1 equiv. of TBA$^+$F$^-$ and TBA$^+$AcO$^-$, the colour of the DMSO solution of the receptor **L5R2** dramatically changed from pale yellow to orange, accompanied by a new intense absorption band centred at about 513 nm and 510 nm in the UV-Vis spectrum as shown in Fig. 6.21 and Fig. 6.22. At the same time, clear isosbestic points were observed at 402 nm and 408 nm, implying the conversion of the free receptor **L5R2** to a **L5R2**+F$^-$ and **L5R2**+AcO$^-$ complex. The Job plot and B-H plot indicated a 1:1 binding interaction between receptor the **L4R2** and the anion (Anion=F$^-$ and AcO$^-$) complexes as depicted in Fig. 6.23 and Fig. 6.24.
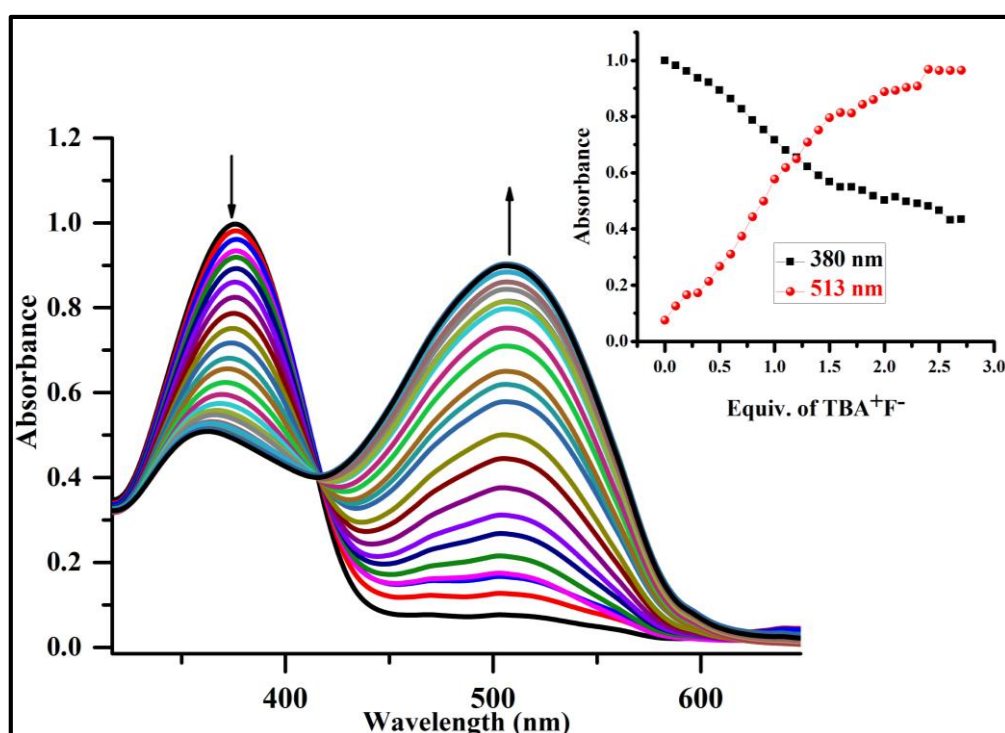
Fig. 6.21 UV-Vis titration spectra of receptors **L5R2** (2×10^{-5} M in DMSO) with the incremental addition of TBA$^+$F$^-$ (1×10^{-2} M in DMSO); Inset plot representing the absorption isotherm at 380 nm and 513 nm
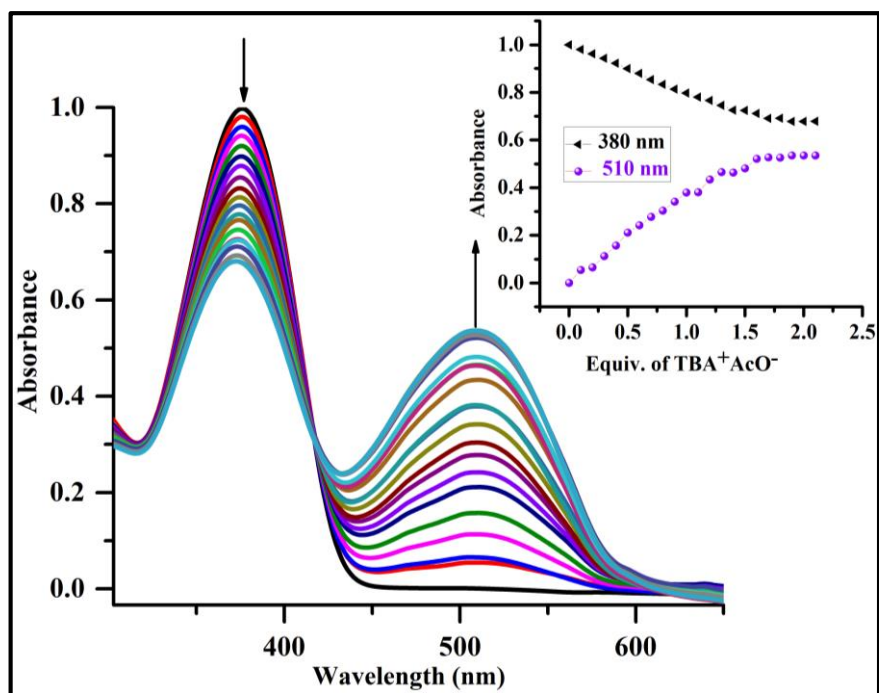
Fig. 6.22 UV-Vis titration spectra of receptors **L5R2** (2×10^{-5} M in DMSO) with the incremental addition of TBA⁺AcO⁻ (1×10^{-2} M in DMSO); Inset plot representing the absorption isotherm at 380 nm and 510 nm
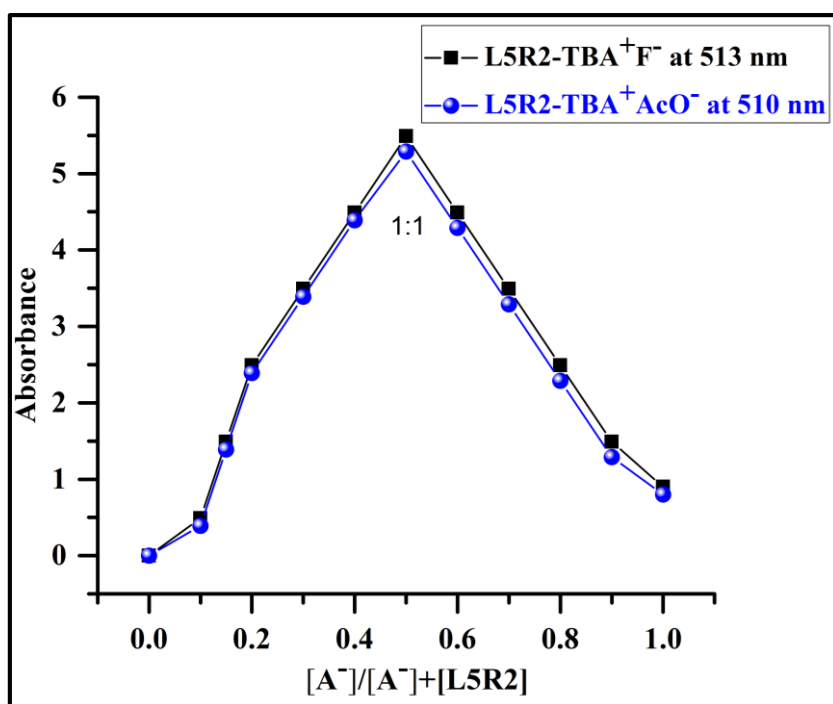
Fig. 6.23 Job plot at 513 nm and 510 nm which indicates 1:1 complexation ratio between **L5R2** and anion

Equation		$y = a + b*x$
Plot	L5R2+TBAF	L5R2+TBAAcO
Intercept	0.45972 ± 0.13416	0.28108 ± 0.12072
Slope	6.22004E-6 ± 1.14319E	5.33437E-6 ± 9.10115E
Residual Sum of Squa	7.9121	3.51264
Pearson's r	0.9958	0.99725
R-Square(COD)	0.99163	0.9945
Adj. R-Square	0.99129	0.99421

- ■ L5R2+TBA$^+$F$^-$ at 513 nm
- ● L5R2+TBA$^+$AcO$^-$ at 510 nm
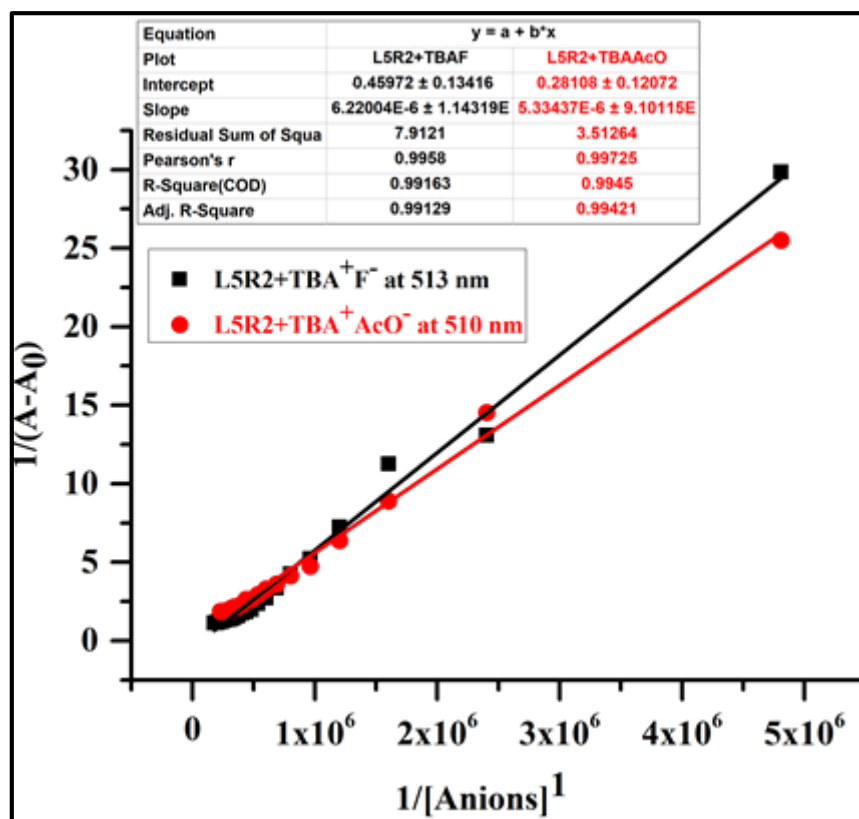
Fig. 6.24 B-H plot for 1:1 complex of **L5R2**-TBA$^+$F$^-$ and **L5R2**-TBA$^+$AcO$^-$ at selective wavelength 513 nm and 510 nm

6.3.3   Colorimetric detection of sodium salts in aqueous DMSO: H_2O (9:1 v/v)

From the viewpoint of the practical applications of anion sensors, it is crucial that the receptors can be operational in water-containing media. Indeed, water is a highly competitive solvent and interferes in the sensing process of anions by mediating interaction between partners. Consequently, anions are strongly solvated and interactions between targeted anions and molecular sensors are drastically attenuated (Huang et al. 2013; Kubik 2010). This is the reason why the direct sensing of inorganic anions in water constitutes to be quite a difficult task. However, this hindrance could be overcome by utilizing the sensor decorated with electron withdrawing moieties (NO_2 substituents) to recognize anions with high affinity.

Interestingly, with the addition of F$^-$, AcO$^-$, and AsO_2^- (1×10^{-2} M in H_2O) to the receptor **L5R1** and **L5R2** solutions (2×10^{-5} M in DMSO), the colour of the solutions changed from light yellow to magenta and red in the organo-aqueous medium DMSO:

H$_2$O (9:1 v/v) as given in Fig.6.25. To explore the applicability of sensors in an aqueous environment, further UV-Vis spectrophotometric titrations were performed in DMSO: H$_2$O (9:1 v/v) solutions with the incremental addition of 0.1 equiv. of Na$^+$F$^-$, Na$^+$AcO$^-$, and NaAsO$_2^-$ as their sodium salt to **L5R1** and **L5R2** solutions, the change in absorption maximum reflected comparison with the titration profile obtained by the addition of the TBA salts of F$^-$ and AcO$^-$ to the DMSO. However, titration of **L5R1** and **L5R2** with anions afforded spectral and colour changes similar to those observed in organic (DMSO) media.

The titration profile is represented in Fig. 6.26, Fig. 6.27, Fig. 6.28, Fig. 6.29, Fig. 6.30, and Fig. 6.31. This proved the practical utility of the receptors **L5R1** and **L5R2** in the semi-aqueous medium DMSO: H$_2$O (9:1 v/v). Furthermore, the definite stoichiometric ratio between receptors and aforementioned anions was determined to be 1:2 and 1:1 from UV-Vis spectral changes with the help of the Benesi–Hildebrand method and also Job plot experiments in the DMSO: H$_2$O (9:1 v/v) as depicted in Fig. 6.32, Fig. 6.33, Fig. 6.34 and 6.35. The bathochromic shift ($\Delta\lambda_{max}$) for the receptors **L5R1** and **L5R2** after the addition of active anions in DMSO and DMSO: H$_2$O (9:1 v/v) is summarized in Table 6.1.
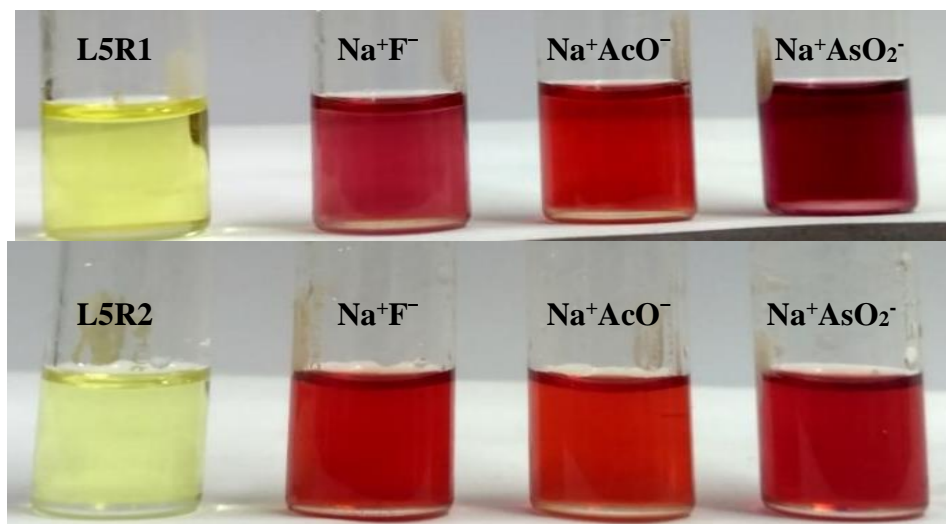
Fig. 6.25 Colour change of receptors **L5R1** and **L5R2** (2×10^{-5} M in DMSO) in the presence of 2 equiv. of sodium salts of F$^-$, AcO$^-$, and AsO$_2^-$ (1×10^{-2} M in H$_2$O) in DMSO: H$_2$O (9:1 v/v)
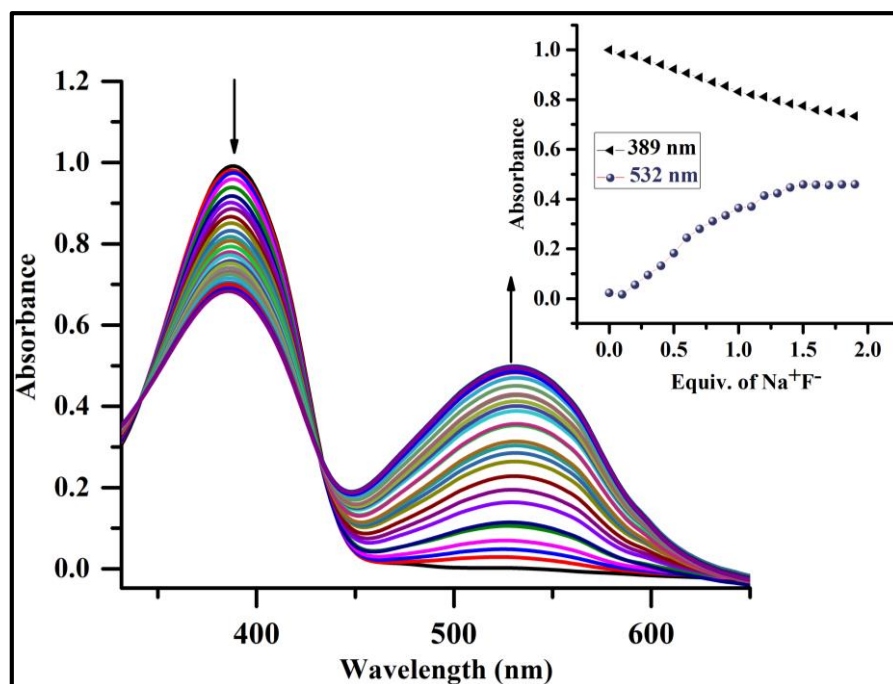
Fig. 6.26 UV-Vis titration spectra of receptor **L5R1** (2×10^{-5} M in DMSO) with the incremental addition of Na^+F^- (1×10^{-2} M in H_2O) in DMSO: H_2O (9:1 v/v); Inset plot representing absorption isotherm at 389 nm and 532 nm
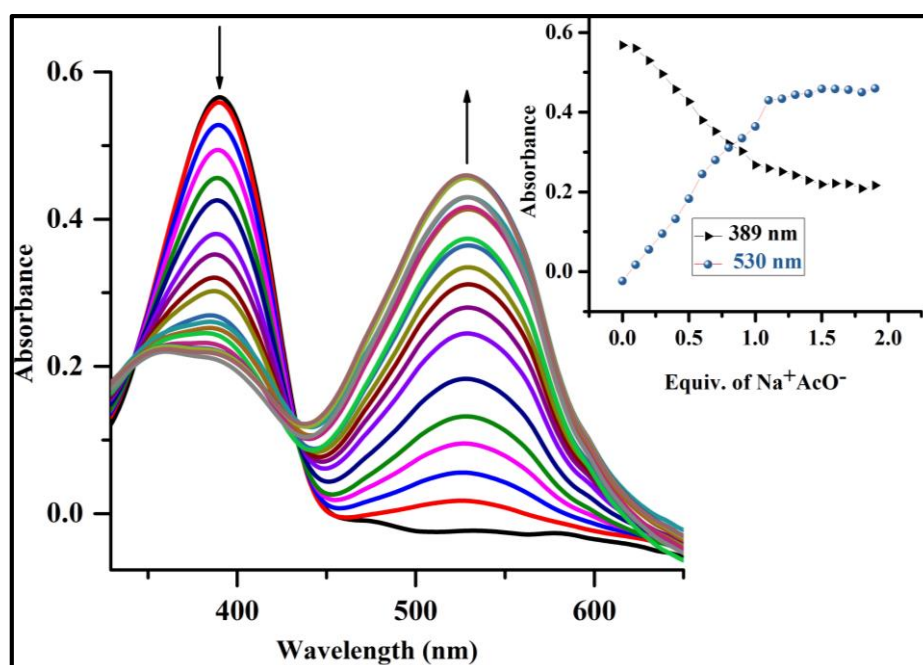
Fig. 6.27 UV-Vis titration spectra of receptor **L5R1** (2×10^{-5} M in DMSO) with the incremental addition of Na^+AcO^- (1×10^{-2} M in H_2O) in DMSO: H_2O (9:1 v/v); Inset plot representing absorption isotherm at 389 nm and 530 nm
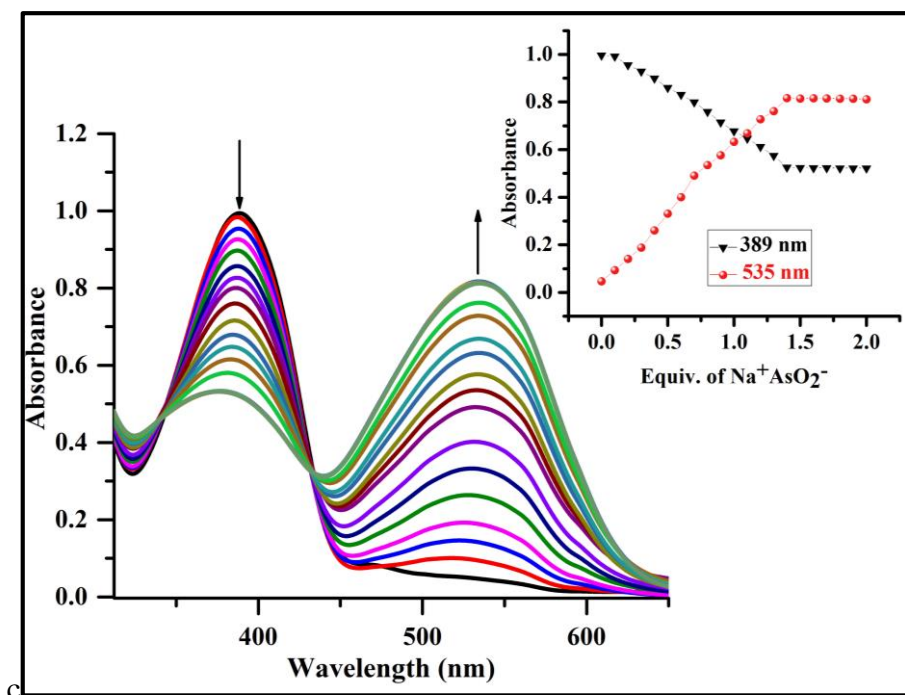
Fig. 6.28 UV-Vis titration spectra of receptor **L5R1** (2×10^{-5} M in DMSO) with the incremental addition of $Na^+AsO_2^-$ (1×10^{-2} M in H_2O) in DMSO: H_2O (9:1 v/v); Inset plot representing absorption isotherm at 389 nm and 535 nm
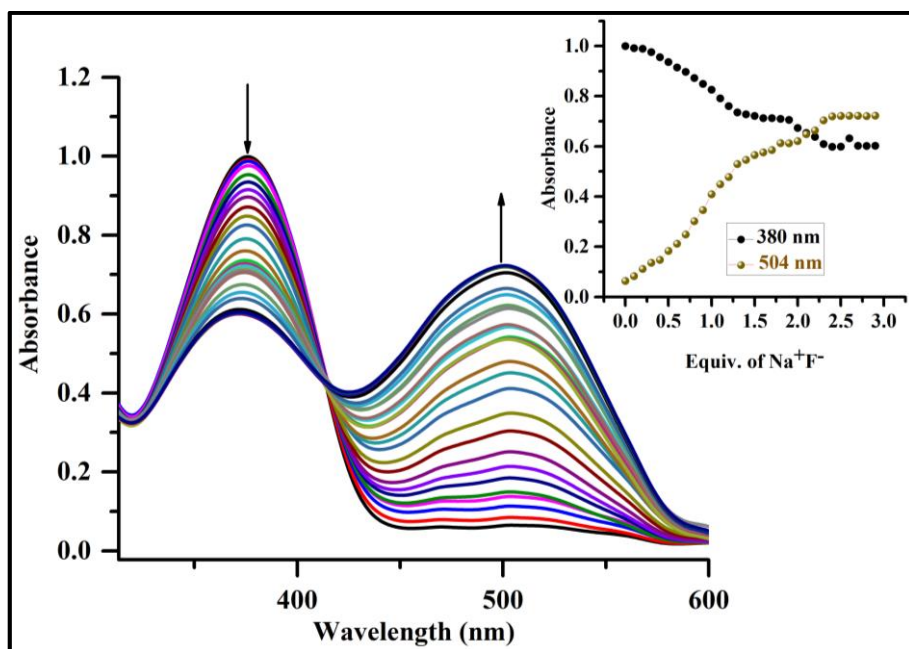
Fig. 6.29 UV-Vis titration spectra of receptor **L5R2** (2×10^{-5} M in DMSO) with the incremental addition of Na^+F^- (1×10^{-2} M in H_2O) in DMSO: H_2O (9:1 v/v); Inset plot representing absorption isotherm at 380 nm and 504 nm
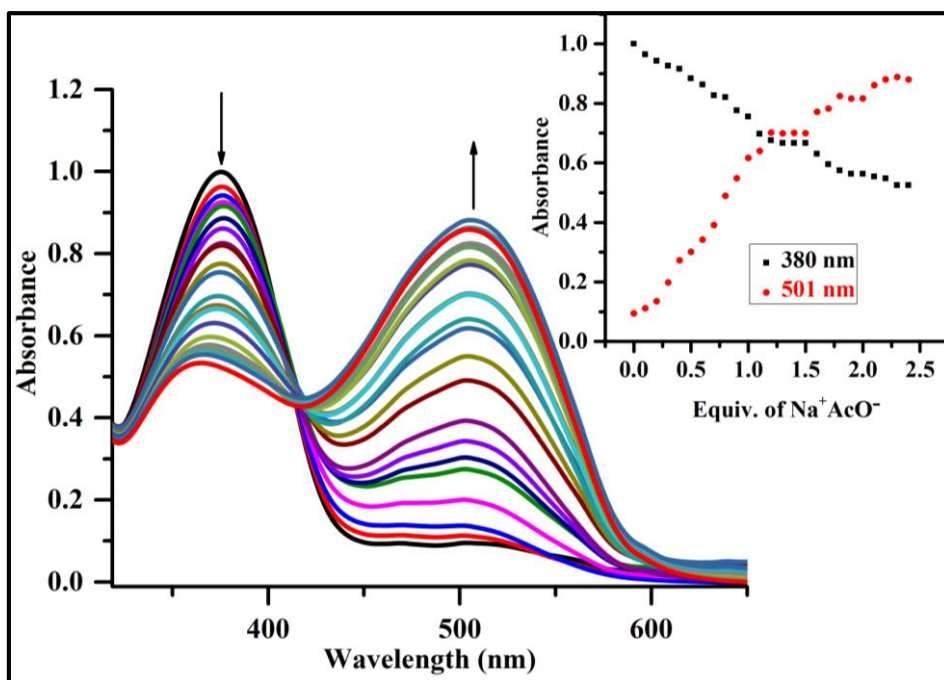
Fig. 6.30 UV-Vis titration spectra of receptor **L5R2** (2×10^{-5} M in DMSO) with the incremental addition of Na^+AcO^- (1×10^{-2} M in H_2O) in DMSO: H_2O (9:1 v/v); Inset plot representing absorption isotherm at 380 nm and 501 nm
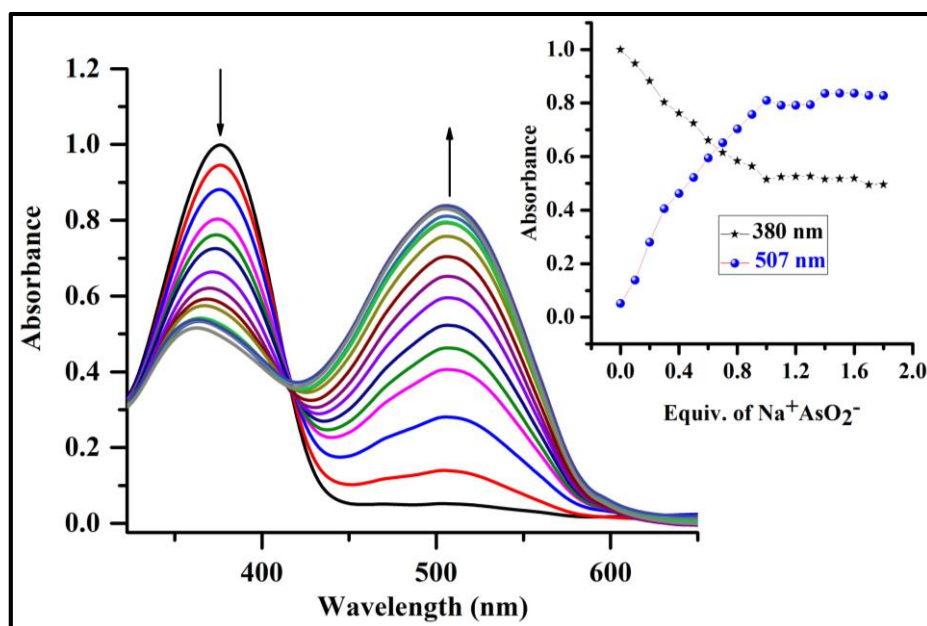
Fig. 6.31 UV-Vis titration spectra of receptor **L5R2** (2×10^{-5} M in DMSO) with the incremental addition of $Na^+AsO_2^-$ (1×10^{-2} M in H_2O) in DMSO: H_2O (9:1 v/v); Inset plot representing absorption isotherm at 380 nm and 507 nm
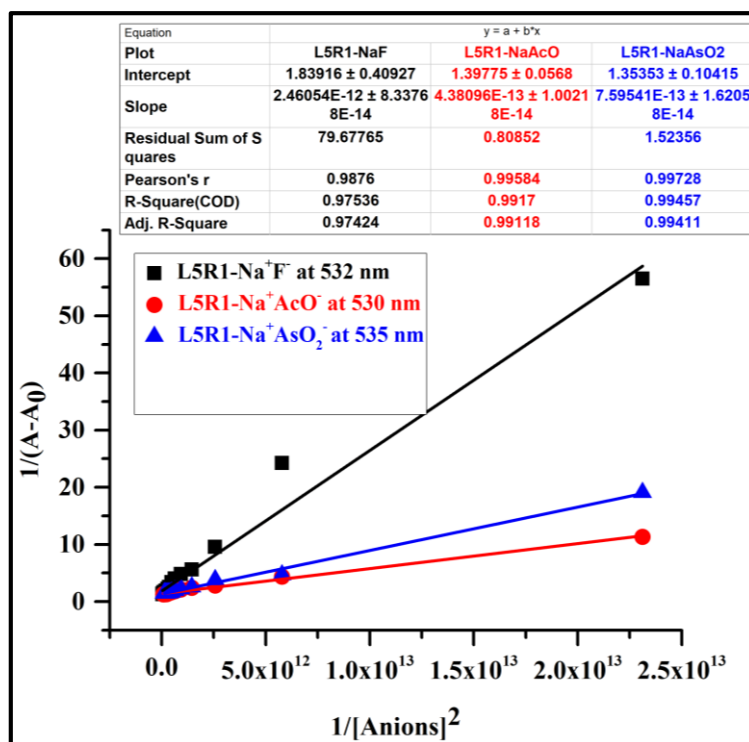
Fig. 6.32 B-H plot of receptor **L5R1** binding with F^-, AcO^-, and AsO_2^- associated with absorbance change at 532 nm, 530 nm, and 535 nm in DMSO: H_2O (9:1 v/v)
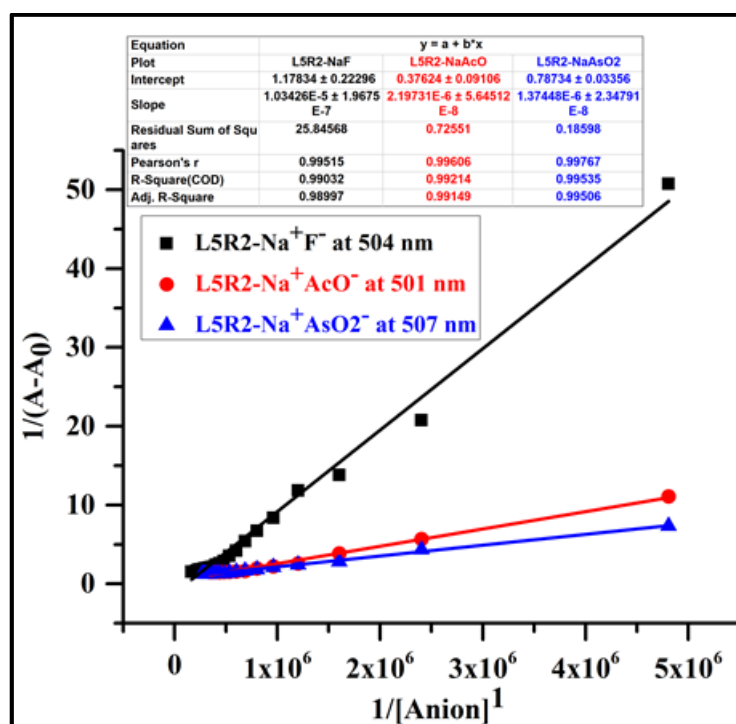
Fig. 6.33 B-H plot for **L5R2**-Na^+F^-, **L5R2**-Na^+AcO^- and **L5R2**-$Na^+AsO_2^-$ complex in at 504 nm, 501 nm and 507 nm in DMSO: H_2O (9:1 v/v)
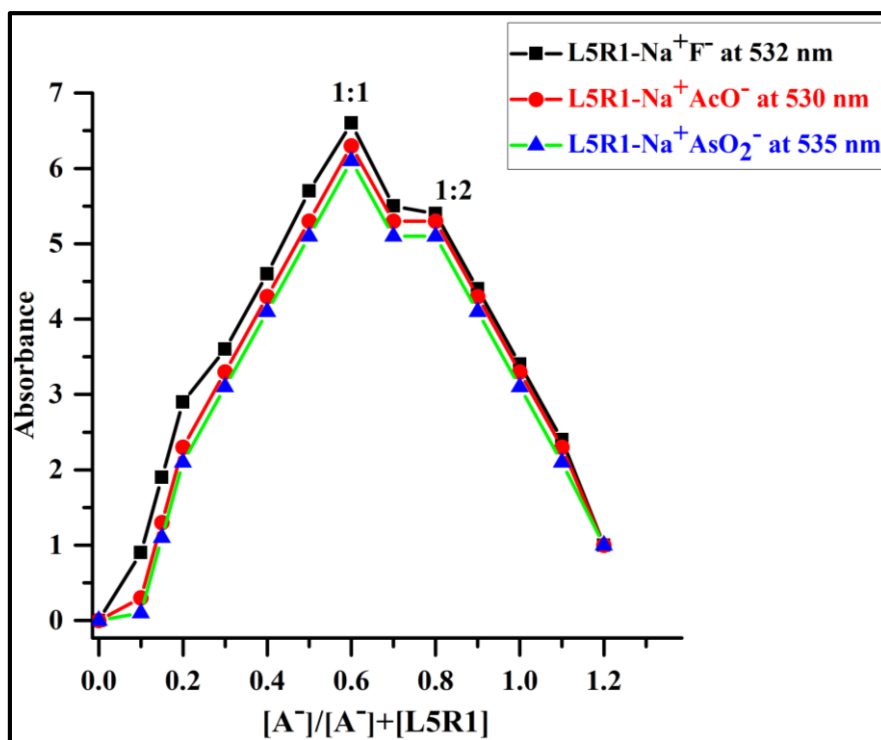
Fig. 6.34 Job plot at 532 nm, 530 nm, and 535 nm which indicates 1:2 complexation ratio between **L5R1** and target anion
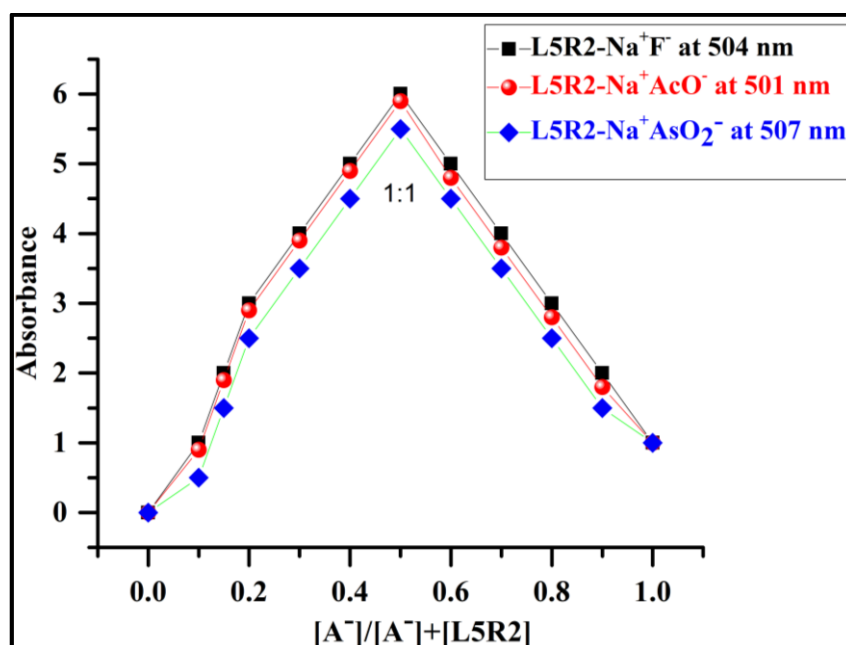
Fig. 6.35 Job plot at 504 nm, 501 nm, and 507 nm which indicates 1:2 complexation ratio between **L5R2** and target anion

Table 6.1 Bathochromic shift ($\Delta\lambda_{max}$) of receptors **L5R1** and **L5R2** (2×10^{-5} M) in the presence of active anions (1×10^{-2} M) in DMSO and DMSO: H_2O (9:1 v/v)

S.No	Receptor +anion	Medium	$\Delta\lambda_{max}$ nm
1	**L5R1**+TBA$^+$F$^-$	DMSO	147
2	**L5R1**+TBA$^+$AcO$^-$	DMSO	144
3	**L5R1**+ Na$^+$F$^-$	DMSO:H_2O (9:1 v/v)	143
4	**L5R1**+Na$^+$AcO$^-$	DMSO:H_2O (9:1 v/v)	141
5	**L5R1**+ Na$^+$AsO$_2$$^-$	DMSO:H_2O (9:1 v/v)	146
6	**L5R2**+TBA$^+$F$^-$	DMSO	133
7	**L5R2**+TBA$^+$AcO$^-$	DMSO	130
8	**L5R2**+ Na$^+$F$^-$	DMSO:H_2O (9:1 v/v)	124
9	**L5R2**+Na$^+$AcO$^-$	DMSO:H_2O (9:1 v/v)	121
10	**L5R2**+ Na$^+$AsO$_2$$^-$	DMSO:H_2O (9:1 v/v)	127

In general, the NO_2 substituted receptor **L5R1** showed large bathochromic shift ($\Delta\lambda_{max}$) of about 147 nm and 144 nm in the DMSO, and 143 nm, 141 nm, and 146 nm, in the case of DMSO: H_2O (9:1 v/v) when compared to the receptor **L5R2** due to the presence of the strong electron withdrawing NO_2 group substituent. As a result of a significant increase in the intramolecular charge transfer transition (ICT) in **L5R1** compared to **L5R2**, a more effective push-pull trend between the NH and NO_2 groups was observed.

6.3.4 Fluorescent titration of receptors L5R1 and L5R2

The complexation studies of the receptors **L5R1** and **L5R2** (2×10^{-5} M in DMSO) with TBA$^+$F$^-$ and TBA$^+$AcO$^-$ ions were also carried out by fluorescence titration. The fluorescence spectra are depicted in Fig. 6.36, Fig. 6.37, Fig. 6.38, and Fig. 6.39. The fluorescence spectra of the free receptors **L5R1** and **L5R2** in the DMSO were recorded with excitation at 470 nm and 450 nm. Upon sequential addition of F$^-$ and AcO$^-$ ions to the solutions of **L5R1** and **L5R2**, remarkable fluorescence enhancement was observed at 558 nm, 554 nm, 518 nm, and 512 nm. The fluorescence spectral data

of the receptors and the receptors+anions complexes is collected in Table 6.2. Interestingly, **L5R1** showed good fluorescence sensing ability compared with the receptor **L5R2** due to ICT transition from the donor (NH moiety) to the acceptor (NO_2 group) (Hou et al. 2014; Sivakumar et al. 2010).

Table 6.2 Fluorescence spectral data for the receptors **L5R1** and **L5R2** with F^- and AcO^- ions in DMSO

Sl.No	Receptor+Anions	λ_{ex} (nm)	λ_{em} (nm)	Stock shift
1	**L5R1**+F^-	470 nm	558 nm	**88 nm**
2	**L5R1**+AcO^-	470 nm	554 nm	**84 nm**
3	**L5R2**+F^-	450 nm	518 nm	68 nm
4	**L5R2**+AcO^-	450 nm	512 nm	62 nm
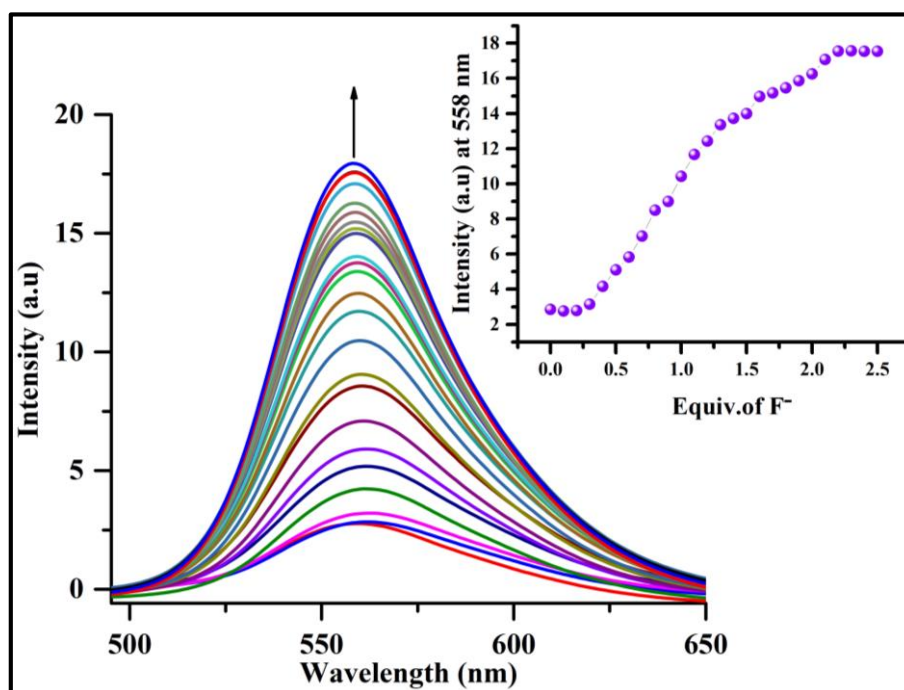
Fig. 6.36 Fluorescence titration spectra of **L5R1** (2×10^{-5} M in DMSO) upon sequential addition of TBA^+F^- ion (λ_{ex},470 nm, $\lambda_{em,}$ 558 nm) in the DMSO; Inset showing variation as a function of the equiv. of F^- at $\lambda_{em,}$ 558 nm
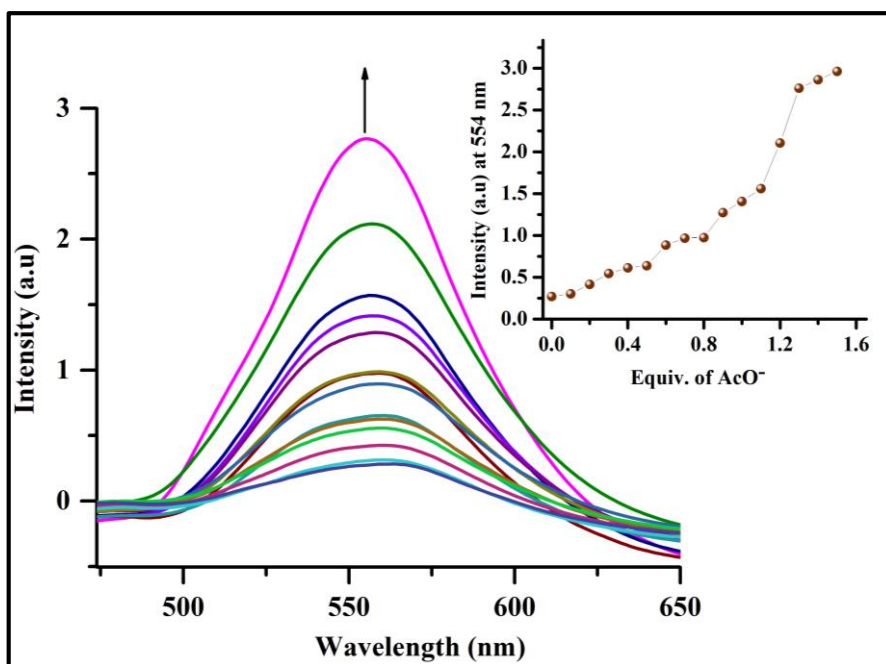
Fig. 6.37 Fluorescence titration spectra of **L5R1** upon sequential addition of TBA$^+$AcO$^-$ ion (λ_{ex},470 nm, $\lambda_{em,}$ 554 nm) in DMSO; Inset showing variation as a function of the equiv. of AcO$^-$ at $\lambda_{em,}$ 554 nm
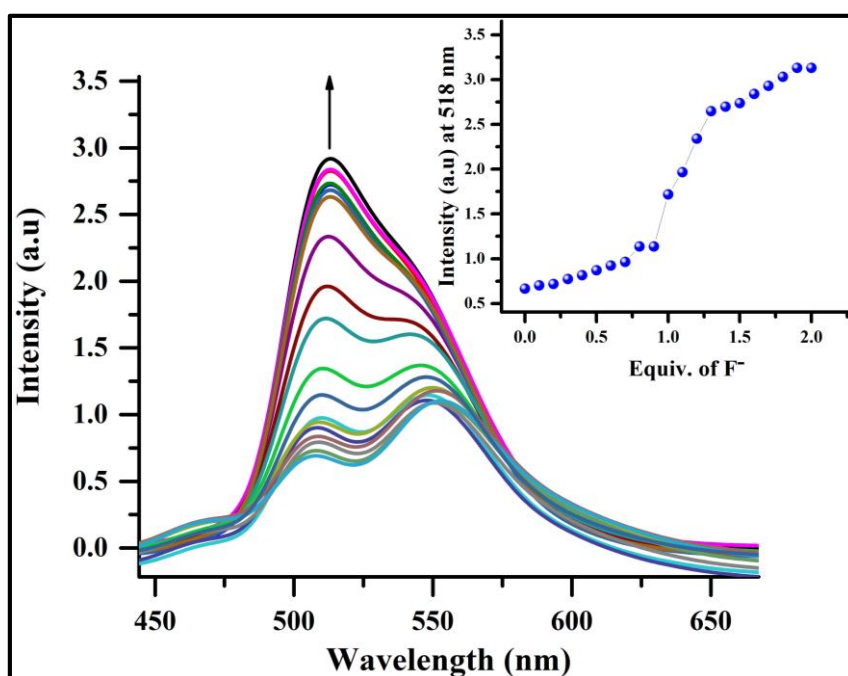
Fig. 6.38 Fluorescence titration spectra of **L5R2** (2×10^{-5} M in DMSO) upon sequential addition of TBA$^+$F$^-$ ion (λ_{ex},450 nm, $\lambda_{em,}$ 518 nm) in DMSO; Inset showing variation as a function of the equiv. of F$^-$ at $\lambda_{em,}$ 518 nm
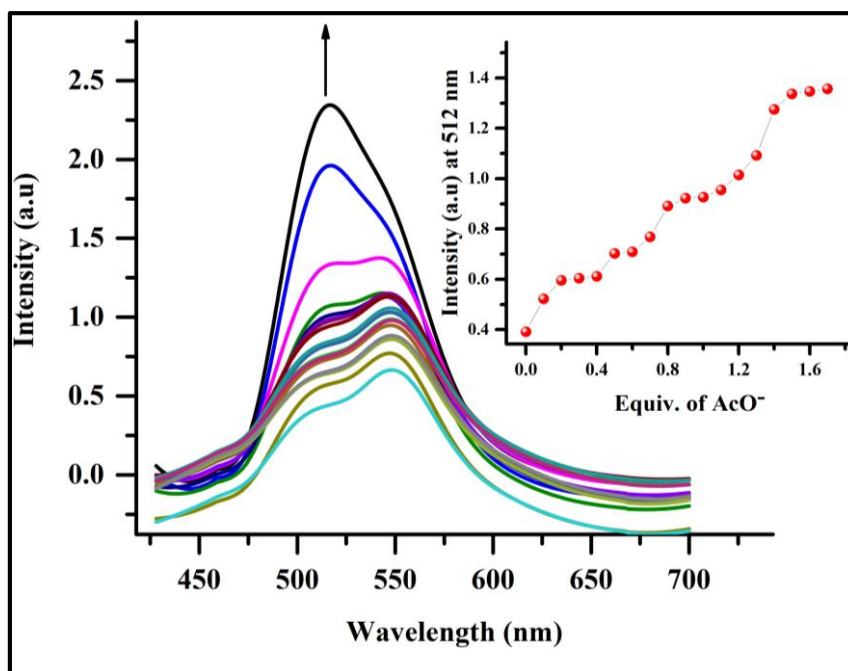
Fig. 6.39 Fluorescence titration spectra of **L5R2** upon sequential addition of TBA⁺AcO⁻ ion (λ_{ex}, 450 nm, $\lambda_{em,}$ 512 nm) in DMSO; Inset showing variation as a function of the equiv. of TBA⁺AcO⁻ at $\lambda_{em,}$ 512 nm

6.3.5 Cyclic voltammetry

The presence of NO_2 and NH groups in the receptor **L5R1** (2×10^{-5} M in ACN) drove the need to investigate the impact of electrochemical reaction in the anion binding mechanism. Cyclic voltammetric studies were carried out with incremental addition of F⁻ and AcO⁻ ions to the solution of **L5R1**. The free receptor in the absence of anions exhibited an oxidation peak at 0.45 V corresponding to the NH moiety and a reduction peak at -1.08 V relating to the NO_2 group. Upon sequential addition of F⁻ ion, the oxidation peak at 0.45 V shifted to 1.18 V, and the reduction peak at -1.08 V moved to -0.84 V as illustrated in Fig 6.40. Similarly, on incremental addition of the AcO⁻ ions to **L5R1**, the oxidation peak switched to 1.22 V and the reduction peak moved to -0.82 V from the original oxidation and reduction peak as depicted in Fig. 6.41. The shift in oxidation peak upon the addition of anions reflects the deprotonation of the NH group (Pangannaya et al. 2018). The band gap values of the free receptor **L5R1** and the **L5R1-**anions complex obtained using Eq. 6.3 is summarized in Table 6.3.

$$I_p = -(E_{ox}+4.4) \text{ eV}\text{-----------}(1)$$

$$E_a = -(E_{red}+4.4) \text{ eV}\text{-----------}(2)$$

$$E_g = E_a - I_p\text{-------------}Eq. 6.3$$

Table 6.3 Band gap values obtained from receptors **L5R1** and their complexes with anions

Receptors	Oxidation (V)	Reduction (V)	Bandgap (eV)
L5R1	0.45	-1.08	1.53
L5R1+F$^-$	1.18	-0.84	2.02
L5R1+AcO$^-$	1.22	-0.82	2.04
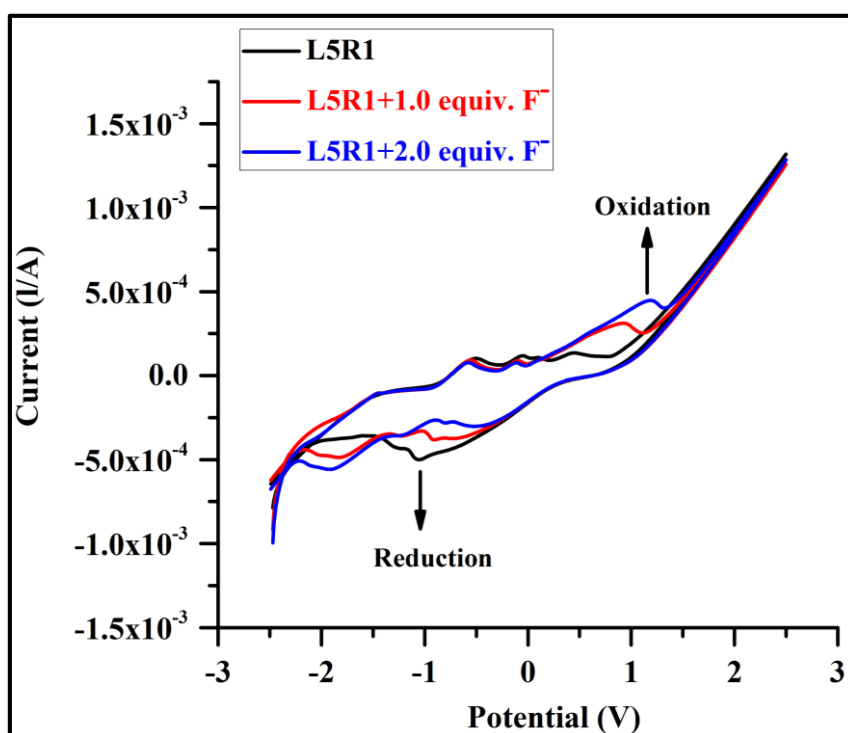
Fig. 6.40 Cyclic voltammetric of receptor **L5R1** (2×10^{-5} M in ACN) with sequential addition of F$^-$ ion (1.0-2.0 equiv.)
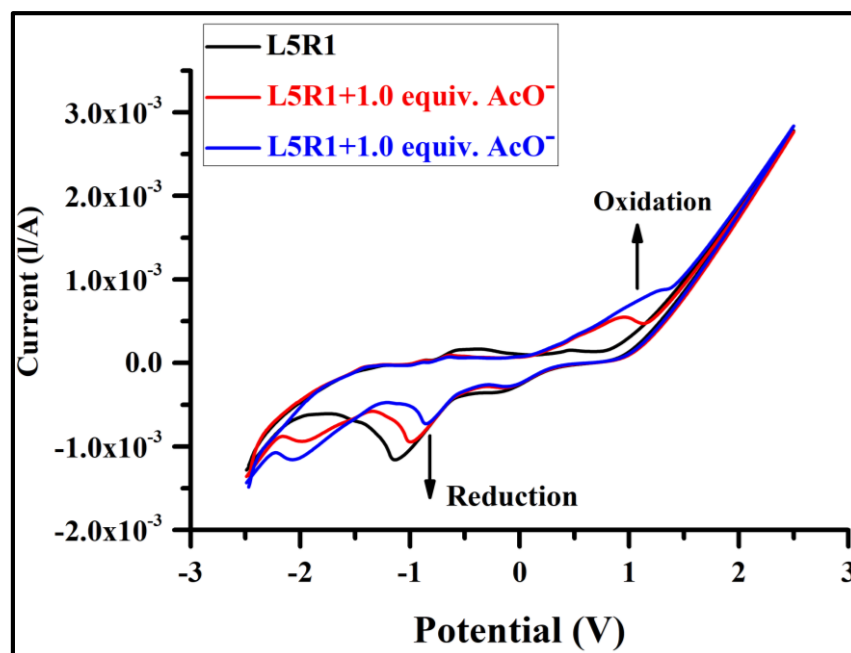
Fig. 6.41 Cyclic voltammetric of receptor **L5R1** ($2{\times}10^{-5}$ M in ACN) with sequential addition of AcO⁻ ion (1.0-2.0 equiv.)

6.3.6 Colorimetric discrimination of isomeric dicarboxylates

The DMSO solution of the receptors **L5R1** and **L5R2** ($2{\times}10^{-5}$ M in DMSO) was tested for colorimetric discrimination of maleate ion and fumarate ion present in the form of TBA salts. Upon adding 2 equiv. maleate ion and fumarate ion to the **L5R1** and **L5R2** solutions, substantial colour changes from pale yellow to wine red and orange were observed only in the presence of maleate ion, while fumarate ion did not produce any colour change as depicted in Fig. 6.42 and Fig. 6.43.

Fig. 6.42 Colour change observed upon addition of 2 equiv. of maleate ion and fumarate ion ($1{\times}10^{-2}$ M in DMSO) to the receptor **L5R1** solution ($2{\times}10^{-5}$ M in DMSO)
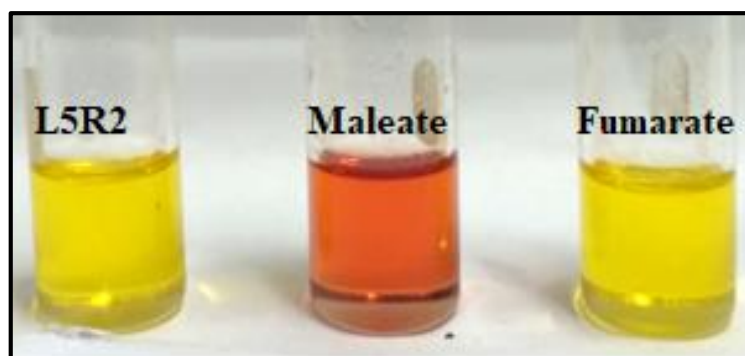
Fig. 6.43 Colour change observed upon addition of 2 equiv. of maleate ion and fumarate ion (1×10^{-2} M in DMSO) to the receptor **L5R2** solution (2×10^{-5} M in DMSO)

6.3.7 Competitive studies

Additionally, the isomeric selectivity of the receptors **L5R1** and **L5R2** (2×10^{-5} M in DMSO) with maleate ion and fumarate ion (1×10^{-2} M) in the DMSO was investigated by UV-Vis spectroscopy. Upon the addition of maleate ion and fumarate ion to **L5R1** and **L5R2** solutions, a prominent change in the UV-Vis spectrum was observed. However, no change was observed with the addition of fumarate ion as shown in Fig. 6.44 and Fig. 6.45. The receptors **L5R1** and **L5R2** displayed high selectivity for maleate ion over fumarate ion.

This may be because maleate ion is more basic in nature (pk_{a1}: 5.0, pk_{a2}: 18.8 in DMSO) than fumarate ion (pk_{a1}: 9.0, pk_{a2}: 11.0 in DMSO) (Choi et al. 2002). Thus, the confirmed maleate ion bonded strongly with the acidic NH protons, which resulted in quick colour change and a bathochromic shift in the absorption band after the addition.
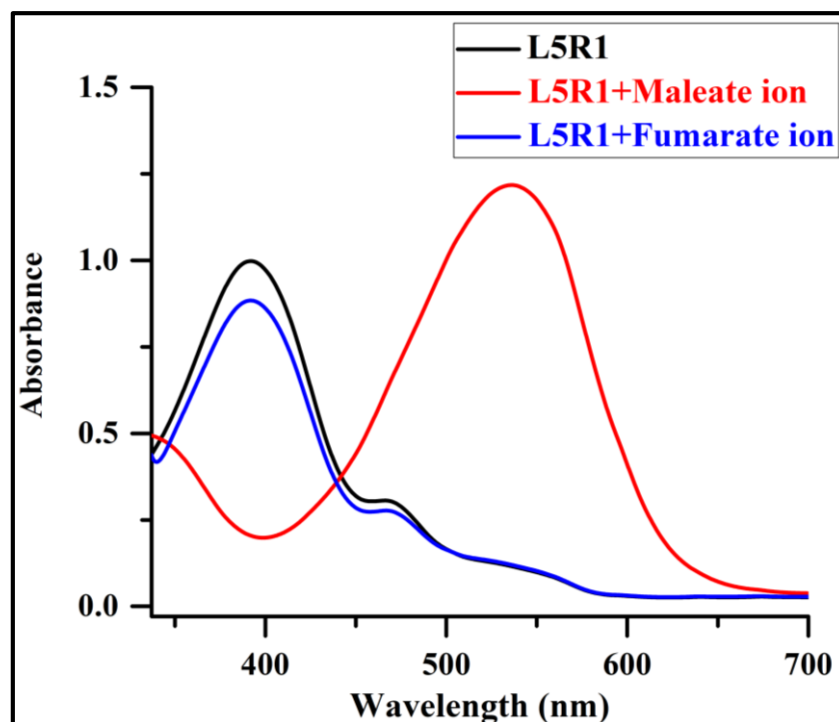
Fig. 6.44 UV-Vis spectra of **L5R1** (2×10^{-5} M in DMSO) with the addition of 2 equiv. of maleate ion and fumarate ion (1×10^{-2} M in DMSO)
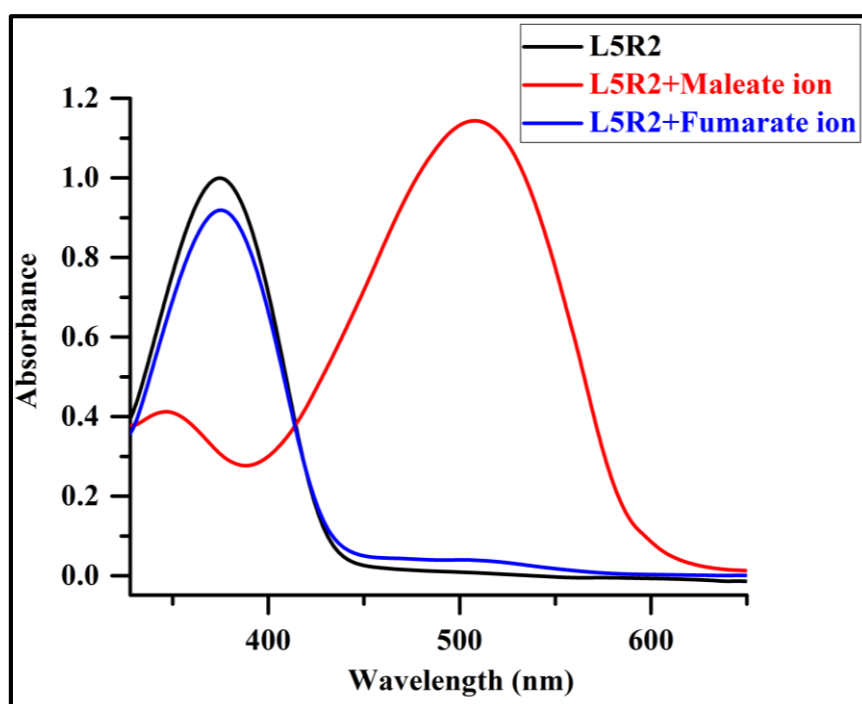
Fig. 6.45 UV-Vis spectra of **L5R2** (2×10^{-5} M in DMSO) with the addition of 2 equiv. of maleate ion and fumarate ion (1×10^{-2} M in DMSO)

6.3.8 UV-Vis titration studies of receptors L5R1 and L5R2 with maleate ion

In order to understand the nature of the interaction between the receptors **L5R1** and **L5R2** and the maleate ion, the UV-Vis titration experiment was carried as represented in Fig. 6.46 and Fig. 6.47. The titration profile exhibited significant bathochromic shift ($\Delta\lambda_{max}$) of 139 nm and 121 nm in comparison with the free receptors with the emergence of a new band at longer wavelength at 528 nm and 501 nm, and a subsequent decrease in the band at 389 nm and 380 nm. The bathochromic shift with clear isosbestic points at 434 nm and 420 nm revealed intermolecular hydrogen bonding complex between the maleate ion and the –NH proton of the receptors **L5R1** and **L5R2** (Sancenón et al. 2003; Yen and Ho 2006).

In addition, the presence of the two carbonyl groups and the -NO_2 groups adjacent to the –NH binding units made the NH proton highly acidic, and as a result, the maleate ion strongly bonded with **L5R1** compared with **L5R2**, which lacked the NO_2 group. As a matter of fact, the receptor **L5R1** showed a more intense change in colour (from pale yellow to wine red) with maximum bathochromic shift than **L5R2** (from pale yellow to orange) when binding with maleate ion. The analysis of the B-H plot showed a 1:1 stoichiometry for the receptors and the maleate ion complex as depicted in Fig. 6.48. In the Job plot, maximum was achieved at a 0.5 mole ratio of the receptors, which also confirmed 1:1 binding stoichiometry between the receptors and the maleate ion as mentioned in Fig. 6.49.

The calibration of the detection limit of anions (Anions= TBA^+F^-, TBA^+AcO^-, Na^+F^-, Na^+AcO^-, $Na^+AsO_2^-$) vs. absorbance of receptors-anions complex at selective wavelengths is depicted in Fig. 6.50, Fig. 6.51, Fig. 6.52, Fig. 6.53, and Fig. 6.54.
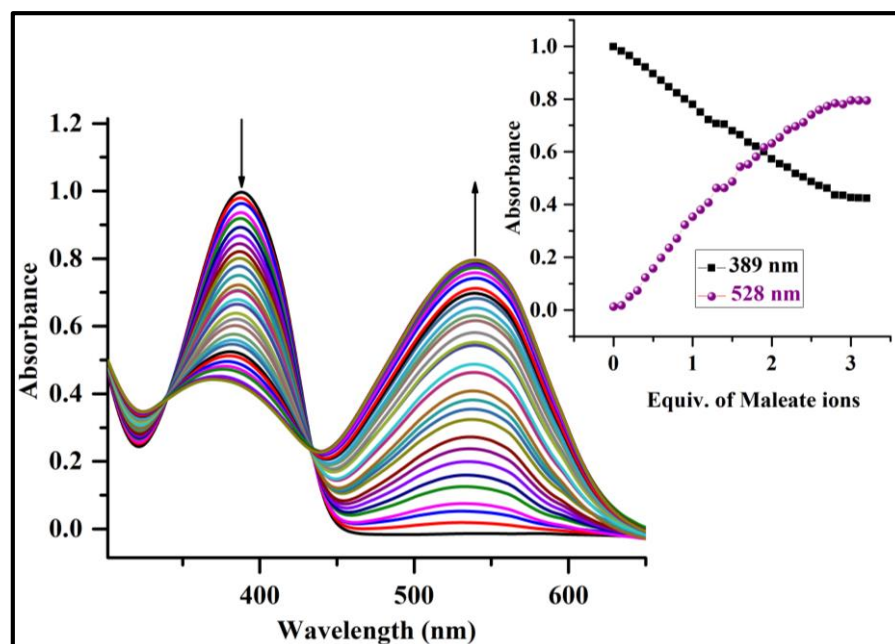
Fig. 6.46 UV-Vis titration of receptor the **L5R1** (2×10^{-5} M in DMSO) with standard solution of maleate ion (1×10^{-2} M in DMSO); Inset plot representing the variation of absorbance with increasing concentration of maleate ion
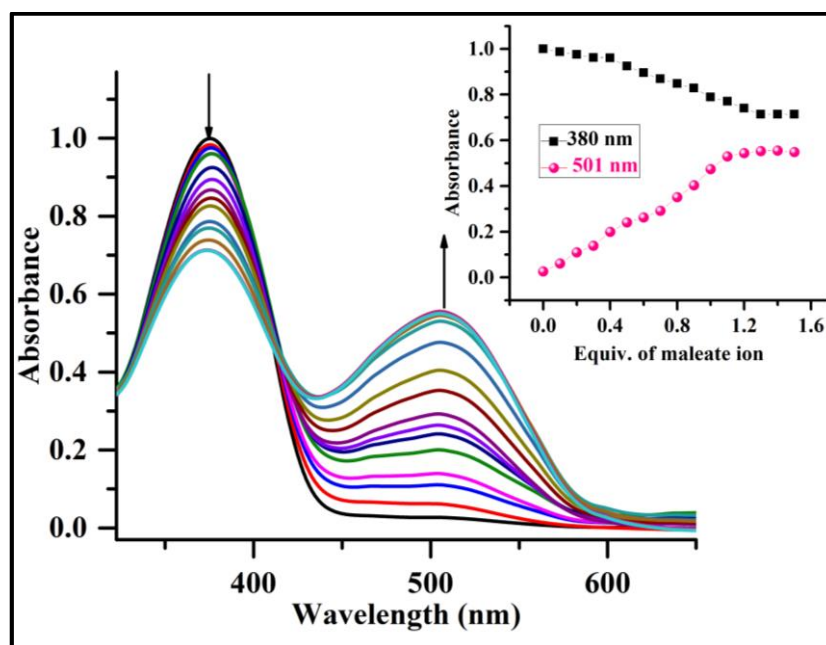
Fig. 6.47 UV-Vis titration of the receptor **L5R2** (2×10^{-5} M in DMSO) with standard solution of maleate ion (1×10^{-2} M in DMSO); Inset plot representing the variation of absorbance with increasing concentration of maleate ion
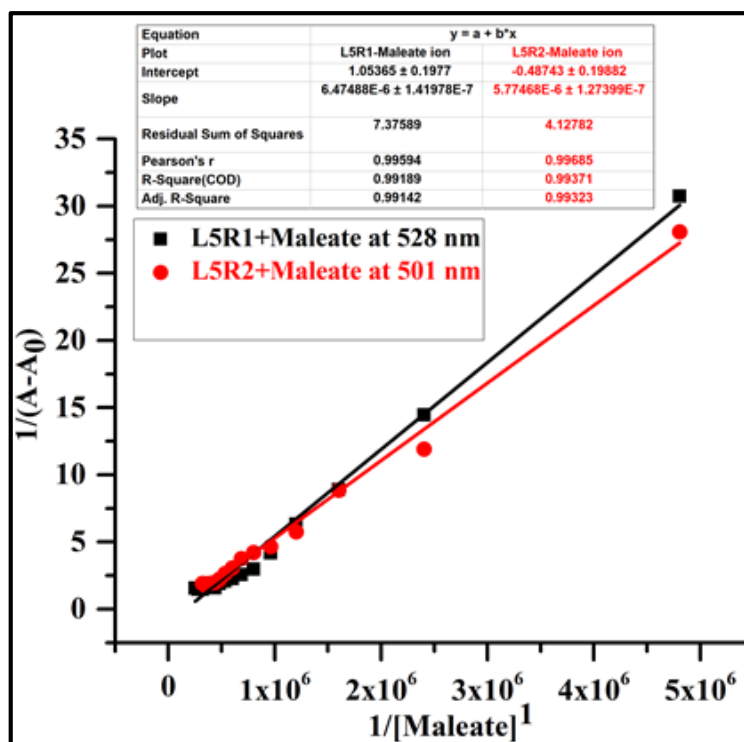
Fig. 6.48 B-H plot of receptors **L5R1** and **L5R2** binding with maleate ion associated with absorbance change at 528 nm and 501 nm
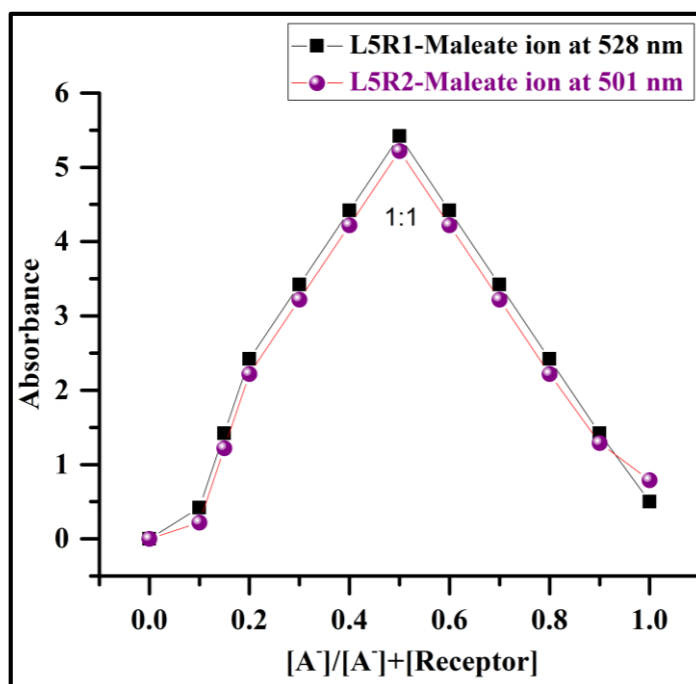
Fig. 6.49 Job plot at 528 nm and 501 nm which indicates 1:1 complexation ratio between receptors and maleate ion
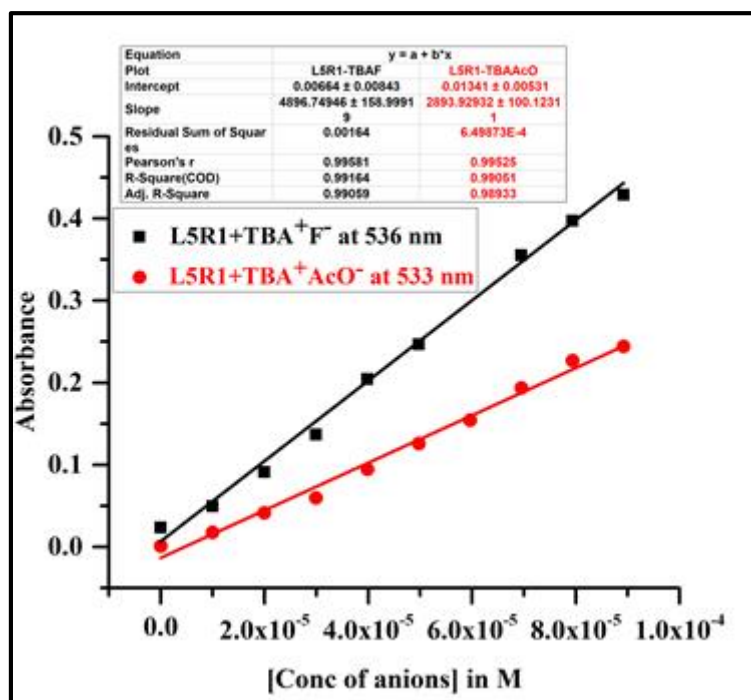
Fig. 6.50 Linear calibration curve between concentration of TBA salts of F⁻ and AcO⁻ ions and absorbance of the receptor **L5R1**+F⁻ and **L5R1**+AcO⁻ complex monitored at specific wavelengths
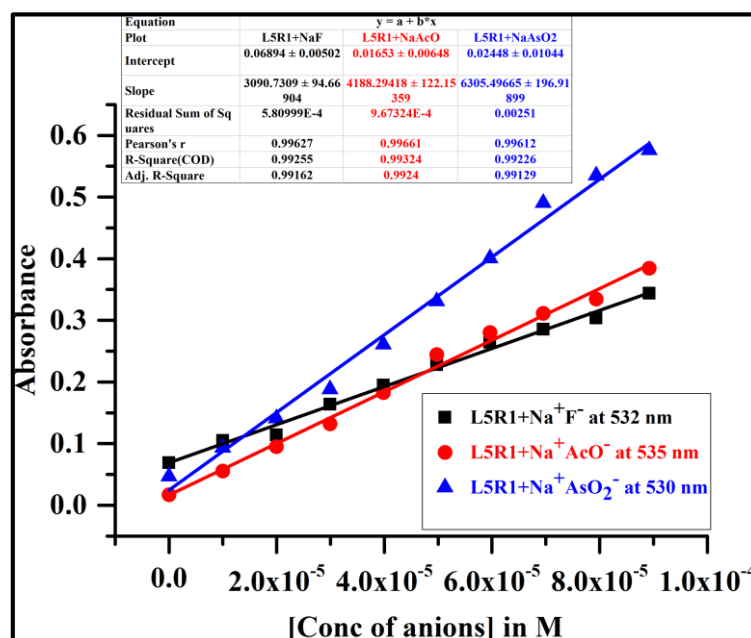
Fig. 6.51 Linear calibration curve between concentration of sodium salts (N⁺aF, Na⁺AcO⁻, and Na⁺AsO₂⁻) and absorbance of the receptors **L5R1**+Na⁺F⁻, **L5R1**+Na⁺AcO⁻, and **L5R1**+ Na⁺AsO₂⁻ complex monitored at specific wavelengths
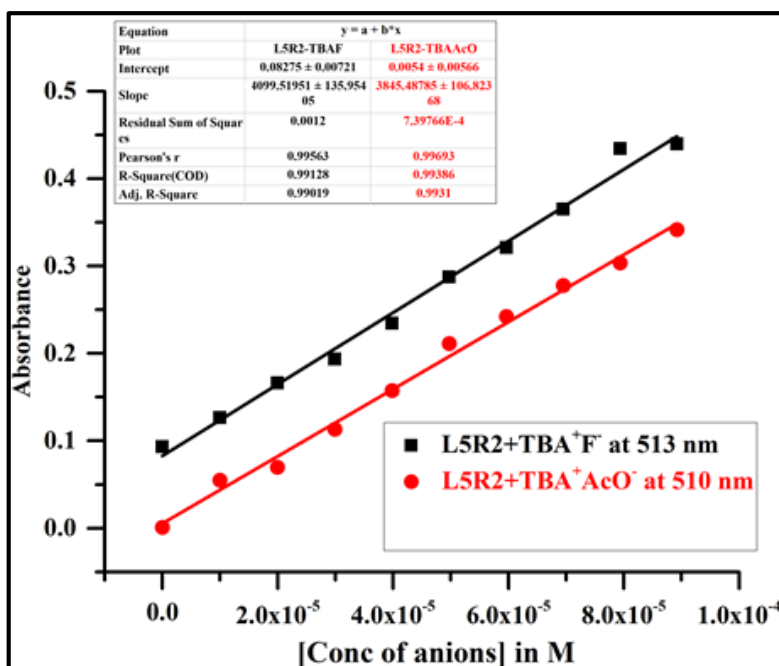
Fig. 6.52 Linear calibration curve between concentration of TBA salts of F⁻ and AcO⁻ ions and absorbance of receptors **L5R2**+F⁻, and **L5R2**+AcO⁻ complex, monitored at specific wavelength
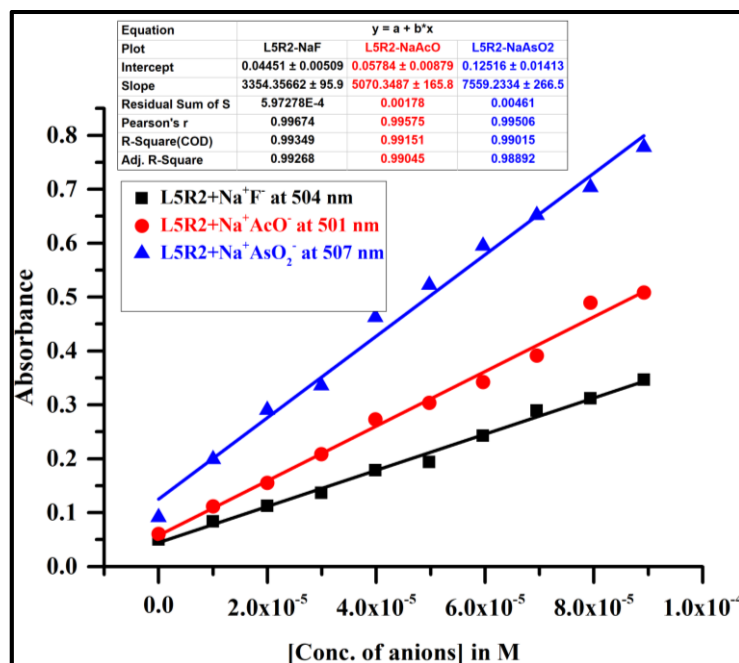
Fig. 6.53 Linear calibration curve between concentration of sodium salts (Na⁺F⁻, Na⁺AcO, and Na⁺AsO₂⁻) and absorbance of the receptors **L5R2**+Na⁺F⁻, **L5R2**+Na⁺AcO⁻, and **L5R2**+ Na⁺AsO₂⁻ complex monitored at specific wavelengths

Equation		$y = a + b \cdot x$	
Plot		L5R1-Maleate	L5R2+Maleate
Intercept		0.00792 ± 0.00569	0.02433 ± 0.0063
Slope		3458.9349 ± 107.40 582	4125.66419 ± 118.9 085
Residual Sum of Squares		$7.47851E{-}4$	$9.16612E{-}4$
Pearson's r		0.99617	0.99669
R-Square(COD)		0.99235	0.9934
Adj. R-Square		0.99139	0.99257

■ L5R1+Maleate at 528 nm
● L5R2+Maleate at 501 nm
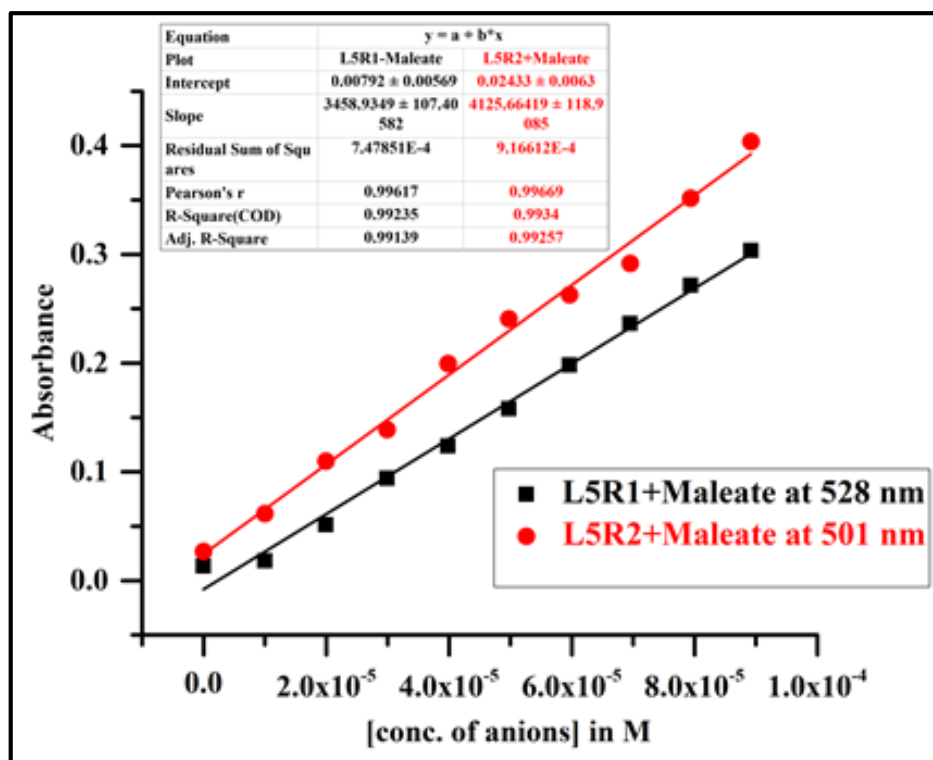
Fig. 6.54 Linear calibration curve between concentration of maleate and absorbance of the receptors **L5R1**+maleate and **L5R2**+maleate complex monitored at specific wavelengths

The receptor **L5R1** showed a higher binding constant of about $8.4 \times 10^{-5}\,M^{-2}$ and $5.1 \times 10^{-5}\,M^{-2}$ for the F^- and AcO^- ions in the DMSO, and $6.2 \times 10^{-5}\,M^{-2}$, $5.9 \times 10^{-5}\,M^{-2}$, and $6.9 \times 10^{-5}\,M^{-2}$ for F^-, AcO^- and AsO_2^- in (DMSO: H_2O, 9:1; v/v) than the receptor **L5R2** due to the presence of the two nitro groups in **L5R1**, which increased the acidity of the -NH protons and enhanced its hydrogen bonding ability, resulting in a strong binding with active anions in organic as well as organo-aqueous medium. The binding ratio, binding constant, and detection limit are given in Table 6.4.

Table 6.4 Binding constant, limit of detection, stoichiometric, and R^2 for **L5R1** and **L5R2** with various anions

S.No.	Receptor$_+$ anions	Medium	Binding constant (K)	LOD ppm	Stoichiometry	R^2
1	**L5R1**+TBA$^+$F$^-$	DMSO	8.4×10^5 M^{-2}	0.160	1:2	0.99011
2	**L5R1**+TBA$^+$AcO$^-$	DMSO	5.1×10^5 M^{-2}	0.185	1:2	0.98949
3	**L5R2**+TBA$^+$F$^-$	DMSO	4.7×10^5 M^{-1}	0.231	1:1	0.99163
4	**L5R2**+TBA$^+$AcO$^-$	DMSO	4.3×10^5 M^{-1}	0.371	1:1	0.9945
5	**L5R1**+Na$^+$F$^-$	(DMSO: H$_2$O, 9:1 v/v)	6.2×10^5 M^{-2}	0.181	1:2	0.99046
6	**L5R1**+Na$^+$AcO$^-$	(DMSO: H$_2$O, 9:1 v/v)	5.9×10^5 M^{-2}	0.197	1:2	0.99372
7	**L5R1**+Na$^+$AsO$_2^-$	(DMSO: H$_2$O, 9:1 v/v).	6.9×10^5 M^{-2}	0.154	1:2	0.99552
8	**L5R2**+Na$^+$F$^-$	(DMSO: H$_2$O, 9:1 v/v).	3.4×10^5 M^{-1}	1.81	1:1	0.99032
9	**L5R2**+Na$^+$AcO$^-$	(DMSO: H$_2$O, 9:1 v/v).	2.3×10^5 M^{-1}	1.93	1:1	0.99214
10	**L5R2**+Na$^+$AsO$_2^-$	(DMSO: H$_2$O, 9:1 v/v).	3.8×10^5 M^{-1}	0.99	1:1	0.99535
11	**L5R1**+maleate ion	DMSO	8.8×10^5 M^{-1}	0.154	1:1	0.99189
12	**L5R2**+maleate ion	DMSO	7.8×10^5 M^{-1}	0.19	1:1	0.99371

6.3.9 ^{1}H-NMR titration studies

The binding mode of **L5R1** with TBA$^+$F$^-$ was examined by ^{1}H-NMR in the DMSO-d$_6$. The free receptor **L5R1,** without the addition of the anions, exhibited a triplet signal at 12 ppm, which was assigned to the NH proton as shown in Fig. 6.55. When 0.25-0.5 equiv. of F$^-$ was added to the solution, the intensity of the -NH peak of the receptor **L5R1** at 12 ppm displayed a broad singlet and a downfield shift from 12 ppm to 12.3 ppm indicating the formation of the hydrogen bonding N-H----F$^-$. Meanwhile, with the gradual increase in F$^-$ concentration to (1.0 equiv.), the signal at 12.3 ppm disappeared, which can be attributed to the deprotonation of the -NH proton. In addition, the signals corresponding to the imine and aromatic protons shifted slightly upfield with the addition of the F$^-$ ion as electron density increases due to deprotonation (Zhang et al. 2009). Therefore, hydrogen bonding occurs in -NH and F$^-$ binding mode, followed by deprotonation suggesting 1:2 binding between the NH proton and the F$^-$ ion.

Similarly, ^{1}H-NMR titrations were performed in order to determine the mechanism of interaction of **L5R1** with the maleate ion as shown in Fig. 6.56. With the addition of maleate ion (0.25 equiv-2 equiv.) to **L5R1** in the DMSO-d6, the peak corresponding to the NH proton as a triplet experiences downshift and the intensity of the peak reduces, signifying strong intermolecular hydrogen bond complex (Trivedi 2014). In addition, other aromatic protons do not change confirming the sensing process involving hydrogen bonding, instead of the deprotonation between **L5R1** and the maleate ion.
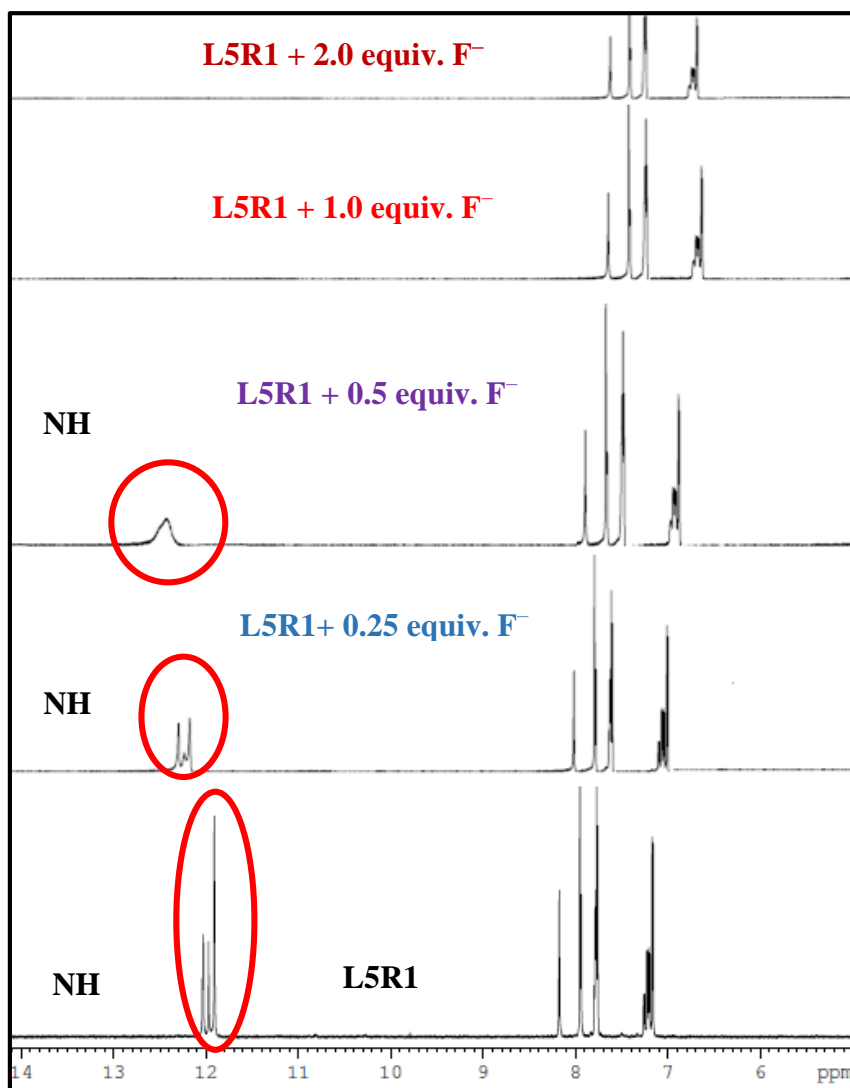
Fig. 6.55 [^1]HNMR titration of **L5R1** recorded in the DMSO-d_6 upon sequential addition of F$^-$ ion
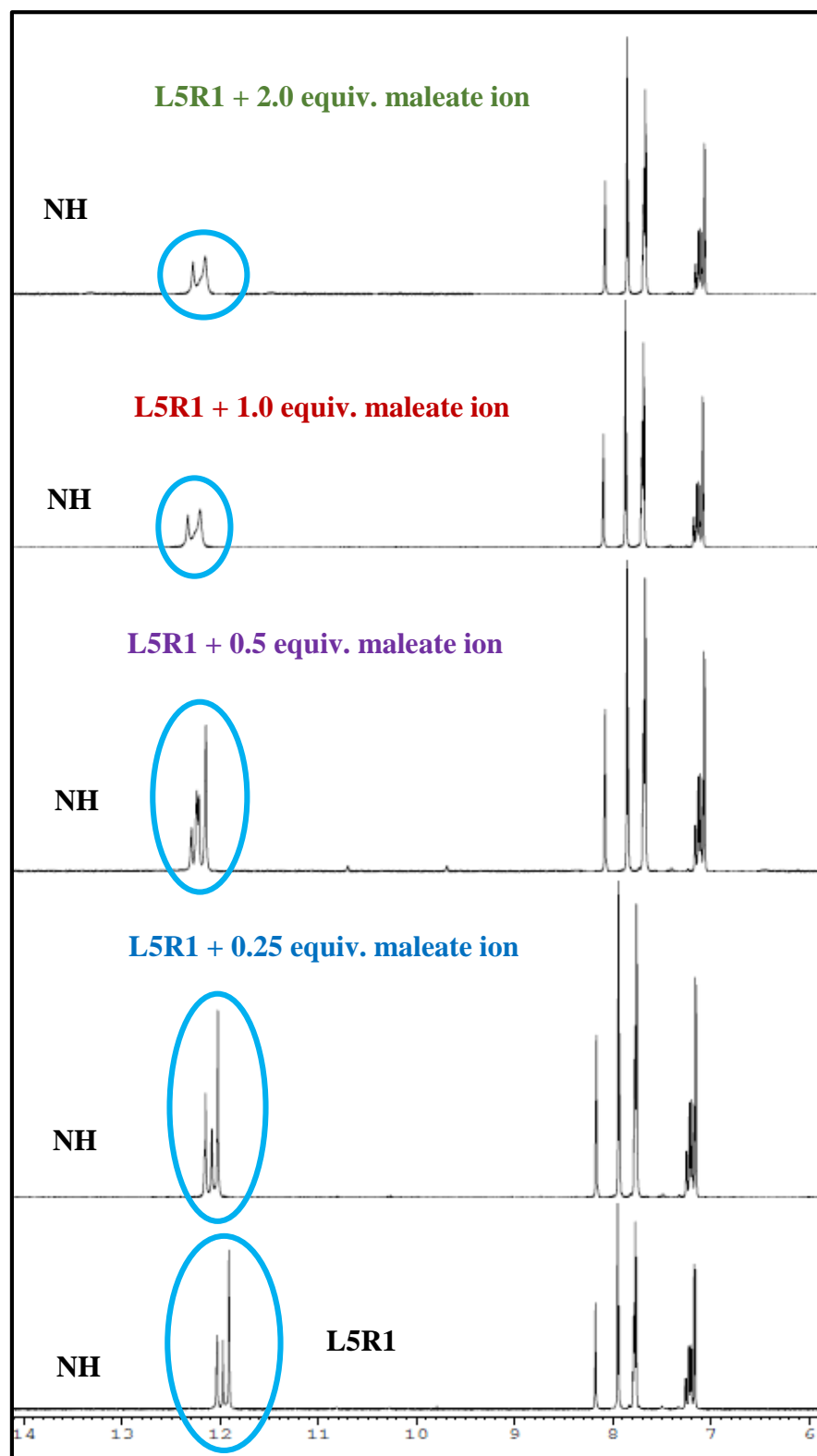
Fig. 6.56 ^{1}HNMR titration of **L5R1** recorded in the DMSO-d_6 upon sequential addition of maleate ion

6.3.10 Binding mechanism

Based on the results obtained from UV-Vis titrations, CV studies, ^{1}H-NMR titration, job plot and B-H plot, a possible binding model between the receptor **L5R1** and F$^-$ ion was proposed in Scheme 6.6. At first, the F$^-$ ion bonded through hydrogen bonding to the NH protons of the receptor **L5R1,** which resulted in 1:1 adduct and NH----F$^-$ complex formation. Further, the second F$^-$ ion induced deprotonation of the NH proton in the receptor **L5R1**, leaving behind N$^-$ rich species due to the push-pull effect of the ICT transition from the donor (NH group) to the acceptor (NO$_2$ moiety) within the receptor, which reflected the 1:2 binding stoichiometry between **L5R1** and the F$^-$ ion. As a result, a two- step binding mechanism was observed.
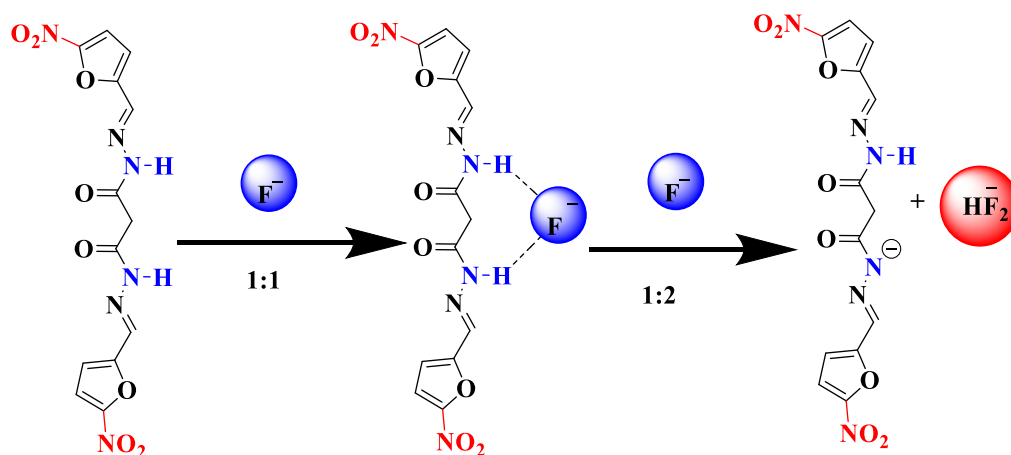
Scheme 6.6 Binding mode of **L5R1** with F$^-$ ion

As shown in Scheme 6.7 (a), the maleate ion with its cis conformation fits perfectly into the NH protons of the receptor **L5R1** and induces strong complex formation due to strong intermolecular hydrogen bond, instead of deprotonation. The isomeric discrimination of the maleate *vs.* fumarate ion by **L5R1** can be associated with receptor orientation. The orientation of the receptors changes with the conformation of the incoming guest (maleate ion) stereochemistry. The cis conformation of the maleate ion easily fits with the NH proton of the receptors and forms a hydrogen bonded complex structure as shown in Scheme 6.7 (b). However, the fumarate ion does not exactly fit with the NH group of the receptor because of its trans conformation.
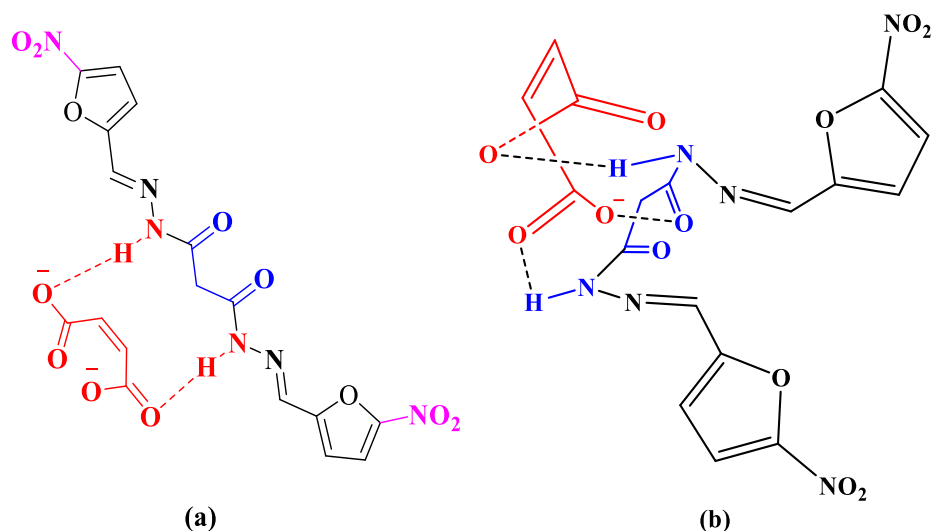
Scheme 6.7 Binding mode of (a) **L5R1** with maleate ion, and (b) orientation change of receptor **L5R1** with maleate ion

6.3.11 Analytical application

6.3.11.1 Fluoride detection in toothpaste solution

With the aim to investigate the real-time application of the receptors **L5R1** and **L5R2** as chemosensors, an attempt was made to qualitatively detect F^- ions in commercially available toothpaste. For this, a toothpaste sample was prepared by dissolving 100 mg in 10 ml of water. Upon adding 2 equiv. of toothpaste solution into the **L5R1** and **L5R2** solutions, a significant colour change from pale yellow to wine-red and pale yellow to orange-red was observed due to complexation between the receptors and F^- ion as illustrated in Fig. 6.57. Further, the UV-Vis titration was also recorded to measure the change in absorption pattern. The absorption bands at 389 nm and 380 nm red-shifted to 532 nm and 503 nm upon incremental addition of the analyte solution to the receptors **L5R1** and **L5R2** (2×10^{-5} M) in the DMSO as depicted in Fig. 6.58 and Fig. 6.59. Thus, the results clearly indicate the capability of the receptors **L5R1** and **L5R2** to detect F^- ion in toothpaste. The detection limit (LOD) ($3\sigma/s$) of the receptors **L5R1** and **L5R2** to detect F^- ion was calculated to be 0.48 ppm and 0.53 ppm, respectively, as shown in Fig. 6.60.
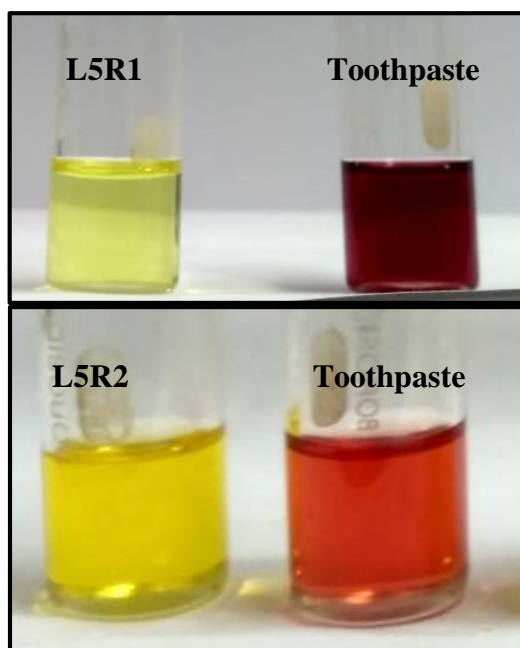
Fig. 6.57 Colour change observed upon addition of 2 equiv. of toothpaste solution containing F⁻ ion into the solutions of **L5R1** and **L5R2** in the DMSO
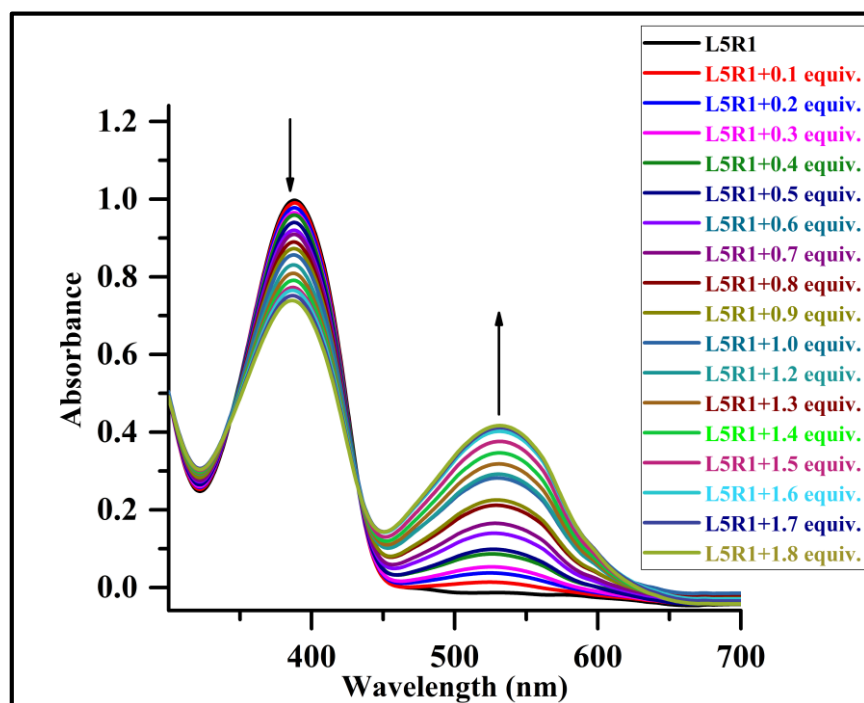
Fig. 6.58 UV-vis titration spectra of receptor **L5R1** (2×10^{-5} M in DMSO) with incremental addition of F⁻ ion; Inset showing equiv. addition of F⁻ ion in toothpaste solution

Fig. 6.59 UV-vis titration spectra of receptor **L5R2** (2×10^{-5} M in DMSO) with incremental addition of F$^-$ ion; Inset showing equiv. addition of F$^-$ ion in toothpaste solution

Equation	y = a + b*x	
Plot	L5R1-Toothpaste	L5R2+Toothpaste
Intercept	0.2268 ± 0.02646	0.15813 ± 0.01709
Slope	17221.71172 ± 499.18899	10073.69991 ± 322.38552
Residual Sum of Squares	0.01615	0.00674
Pearson's r	0.99666	0.99593
R-Square(COD)	0.99332	0.99187
Adj. R-Square	0.99249	0.99086
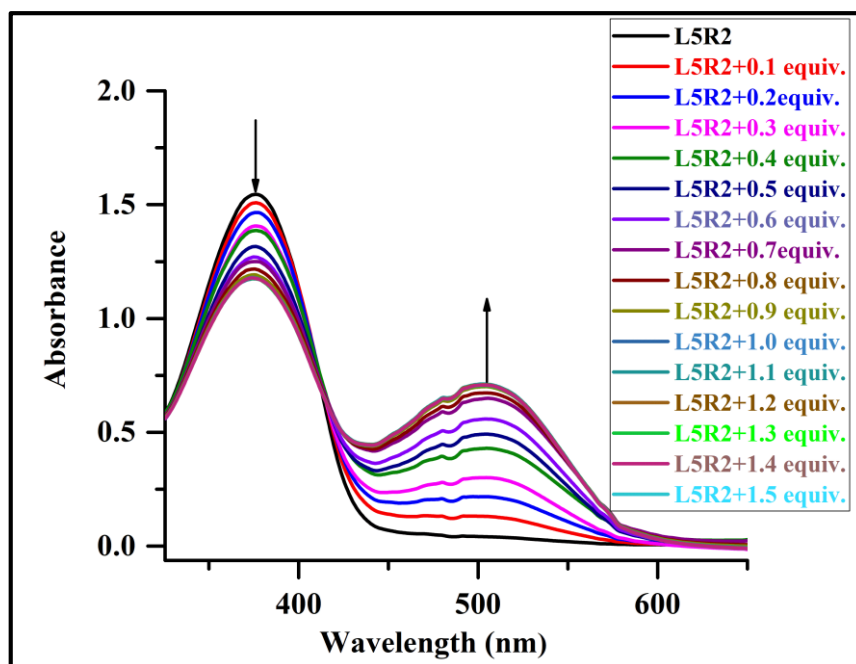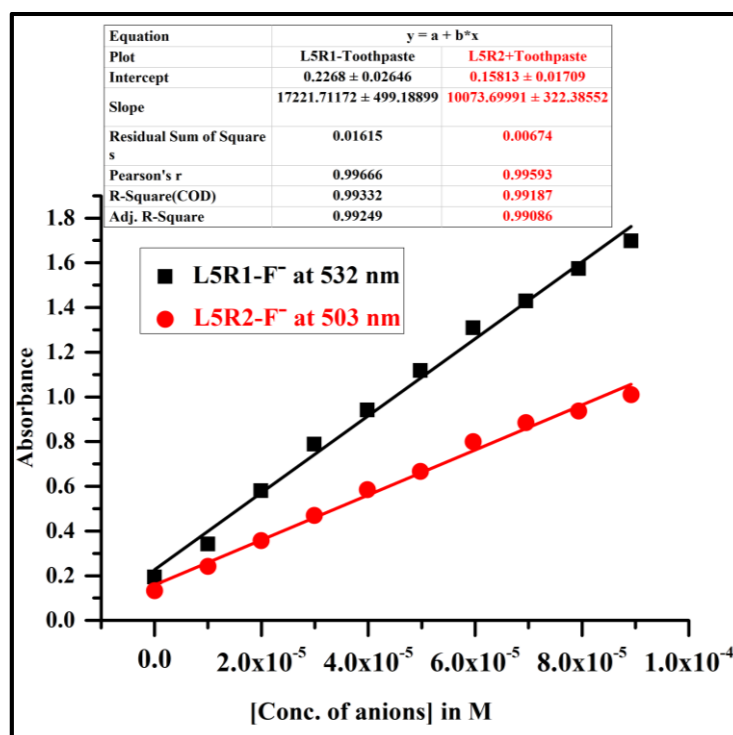
Fig. 6.60 Calibration curve of absorbance of receptors **L5R1** and **L5R2** anion complex v/s concentration of F$^-$ ion presents in toothpaste solution

6.3.11.2   Test kits for detection of maleate ion

To explore the practical application of the receptors **L5R1** and **L5R2**, an attempt was made to analyze the maleate ion using a test kite (paper strip).The test strips were prepared by soaking cut filter paper in the **L5R1** and **L5R2** solutions (2×10^{-5} M) in DMSO and then drying the strips in an air oven maintained at 50^{0}C. After drying, they were immersed in a solution of maleate ion prepared (1×10^{-2} M) in DMSO. As shown in Fig. 6.61, the colour of the paper strips changed from pale yellow to red-pink and orange, which was visible to the naked eye. The significant change in colour of the paper strips clearly suggests the potential analytical application of the receptors for the detection of maleate ion.
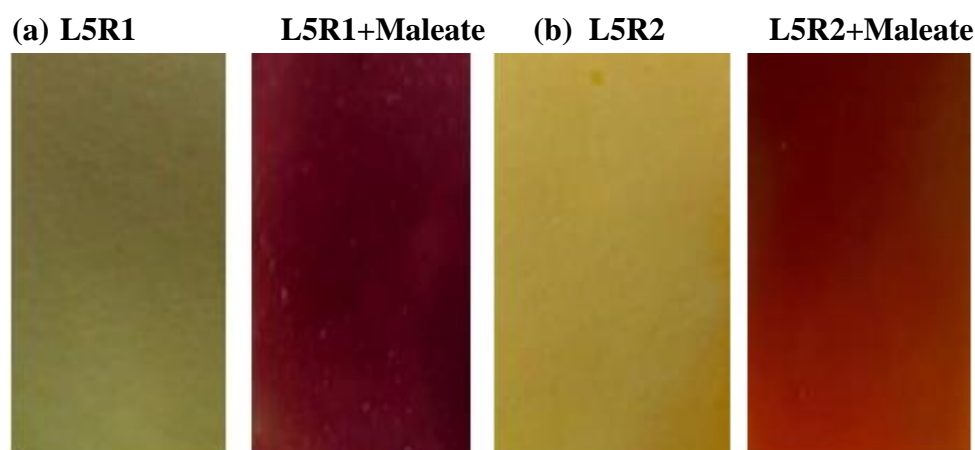
Fig. 6.61 Photograph of the test strips with the receptors (a) **L5R1,** and (b) **L5R2** for recognition of maleate ion in DMSO

6.3.12   DFT studies

In order to better understand the nature of the ionic interaction of the receptors with the anions and to support a few of the experimental evidences, computational studies were performed using the Gaussian 09 software (Frisch et al. 2009; Gaussian 2003; Frisch et al. 2004). The structures were initially optimized under gas phase, followed by the solvent phase. The ground state optimization of the systems was carried out using the B3LYP (Becke three parameters hybrid functional with Lee-Yang-Perdew correlation functionals) with 6–31+G(d,p) for the bare receptors and anion complexes. The excited state calculations were carried out with TD-DFT/B3LYP functional and the

same basis set was used for the ground state calculations (Lee et al. 1988; Jain et al. 2006). Geometry optimizations involving self-consistence field convergence were restricted to a minimum threshold energy of 10^{-6}. It was followed by frequency calculations to validate the optimized structure corresponding to a global minima on the potential energy surface. The solvent effect on the energy parameters of the receptors and complexes was also studied using the self-consistent reaction field based on the polarizable continuum model (PCM) (Cossi et al. 1994) using the integral equation formalism variant (IEFPCM) (Berryman et al. 2008; Cances et al. 1997). On par with the experimental conditions, dimethylsulfoxide was employed as a solvent medium for all the computational calculations. The excited state calculations were carried out on both the receptors and the complexes to better understand the nature of the electronic transitions in the system. The excited state yielding six lowest-lying excited state transitions were computed in the solvent medium.

6.3.12.1 Receptor L5R1 with F⁻ and AcO⁻ ions

The receptor **L5R1** had its HOMO majorly distributed on one of the furfuraldehyde moiety, and a few traces of the HOMO was seen on the other arm of the receptor containing furfuraldehyde. HOMO-1 possesses a closer energy value with that of HOMO and exhibits exact distribution opposite to that of HOMO. LUMO has its distribution on the imine linkage and majorly on the carbonyl group. The energy bandgap of the bare receptor showed a value of 3.365 eV, which upon binding with the fluoride ion came down to 2.846 eV as illustrated in Fig. 6.62. The electronic orbital distribution of the F⁻ ion bound complex showed a disimilar trend to that of the unbound receptor. The charge transfer in the system was prominent between the HOMO and LUMO orbitals transferring between the furfuraldehyde group on both the arms of the central carbonyl core. A few traces of the electronic distribution was found around the fluoride ion at the HOMO-1 level and a good amount of orbital distribution was observed at the HOMO-2 level. The receptor bound acetate similarly exhibited a good charge transfer mechanism between the furfuraldehyde on either side of the carbonyl group as shown in Fig. 6.63. The two highest occupied levels and the two lowest unoccupied levels of the complex did not show their distributions on theAcO⁻ ions. However, the lower occupied level had its electronic density distributed majorly on the

acetate ion. The energy bandgap value of the receptor bound complex showed a value of 3.047 eV in comparison with that of the receptor with 3.365 eV.
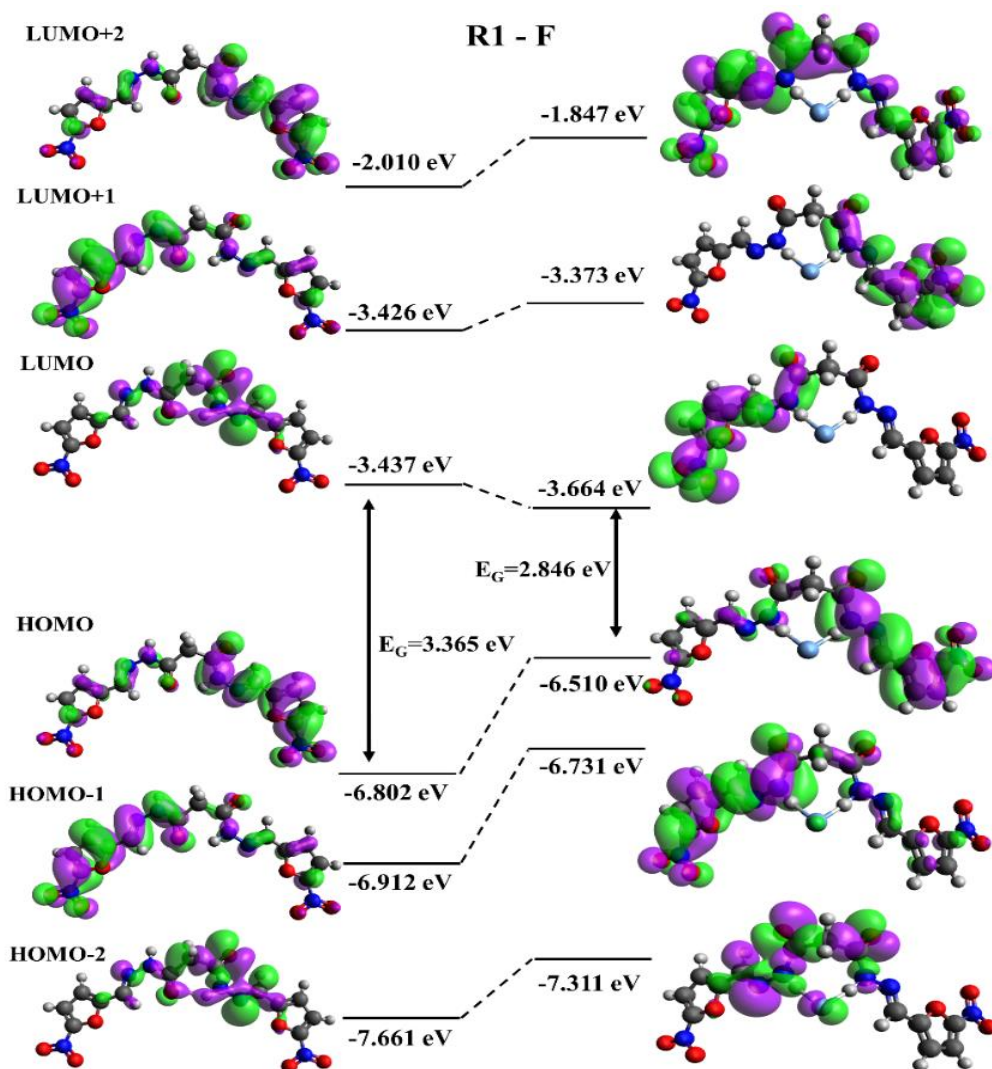
Fig. 6.62 Optimized molecular orbital of receptor **L5R1**, before and after addition of F⁻ ion with energy levels of 6-31+G (d,p)
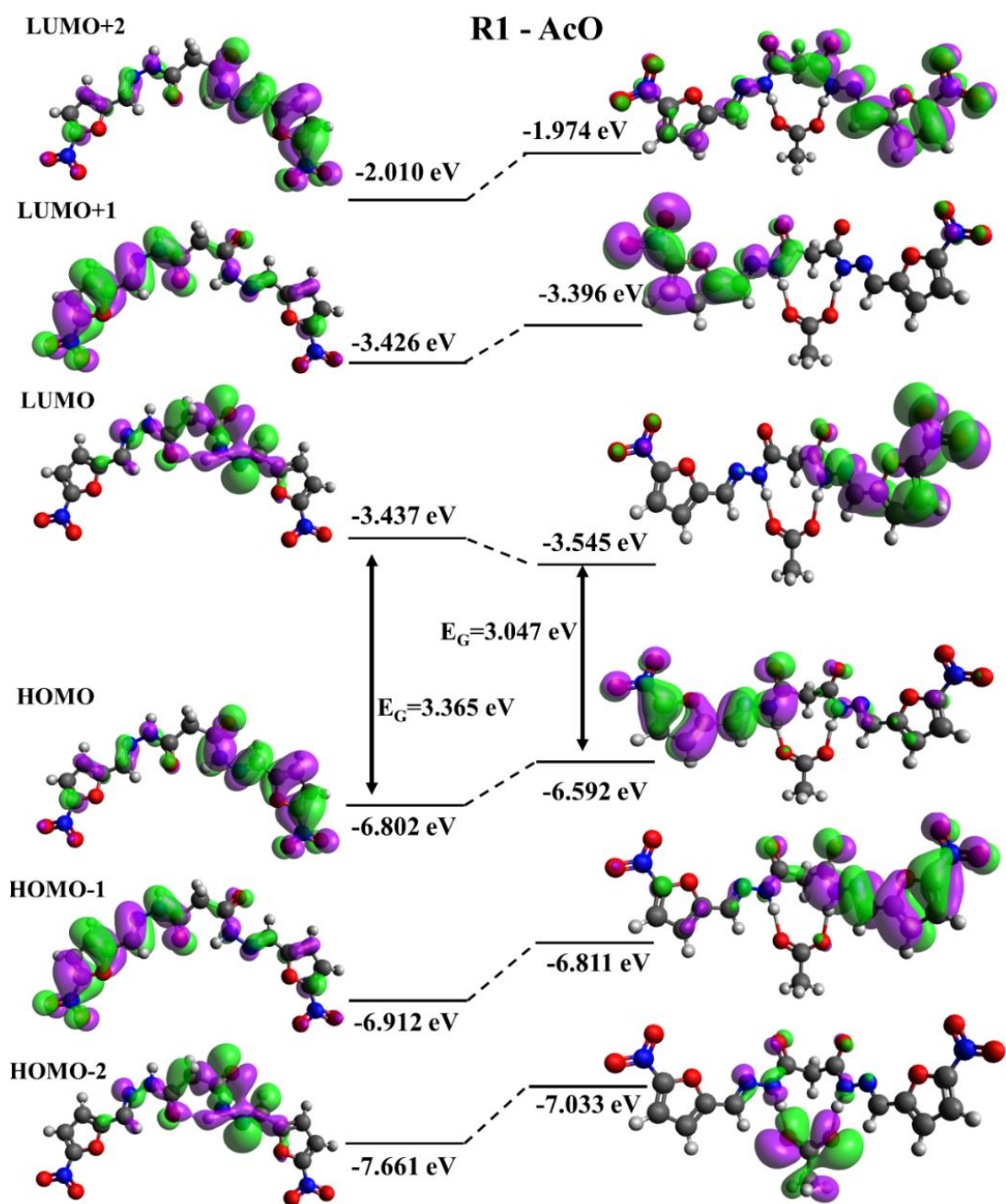
Fig. 6.63 Optimized molecular orbital of receptor **L5R1**, before and after addition of

AcO‾ ion with energy levels of 6-31+G (d,p)

6.3.12.2 Receptor L5R2 with F⁻ and AcO⁻ ions

The receptor **L5R2** exhibited a similar trend in the occupied electronic distribution as that of the receptor **L5R1**, wherein the absence of the NO_2 group did not influence the altering the orbital distribution of the system. However, the distribution of the electronic density in the LUMO orbital was highly concentrated on one of the furfuraldehyde and imine linkage. Such type of orbital distribution is brought about by the effect of F⁻ ion upon complexation. The energy band gap value of the receptor **L5R2** turned out to be 4.179 eV, and with that of the complexation exhibited a value of 4.01 eV as illustrated in Fig.6.64. The electronic orbital distribution of the F⁻ bound complex showed a disimilar trend as that of the unbound receptor. Herein, the distribution of the orbitals in the HOMO level was mainly on one of the furfuraldehyde group and few minor traces of distribution was observed on other furfuraldehyde groups, and a similar trend was observed for the LUMO orbital as well. Such distributions were carried forward for higher LUMO orbitals and lower HOMO orbitals as observed from the energy distribution. The introduction of the NO_2 group into the receptor **L5R1** played no major role in altering the electronic orbital distributions of the system. Similar electronic orbital distributions were observed for the AcO⁻ bound receptor **L5R2** as depicted in Fig. 6.65.
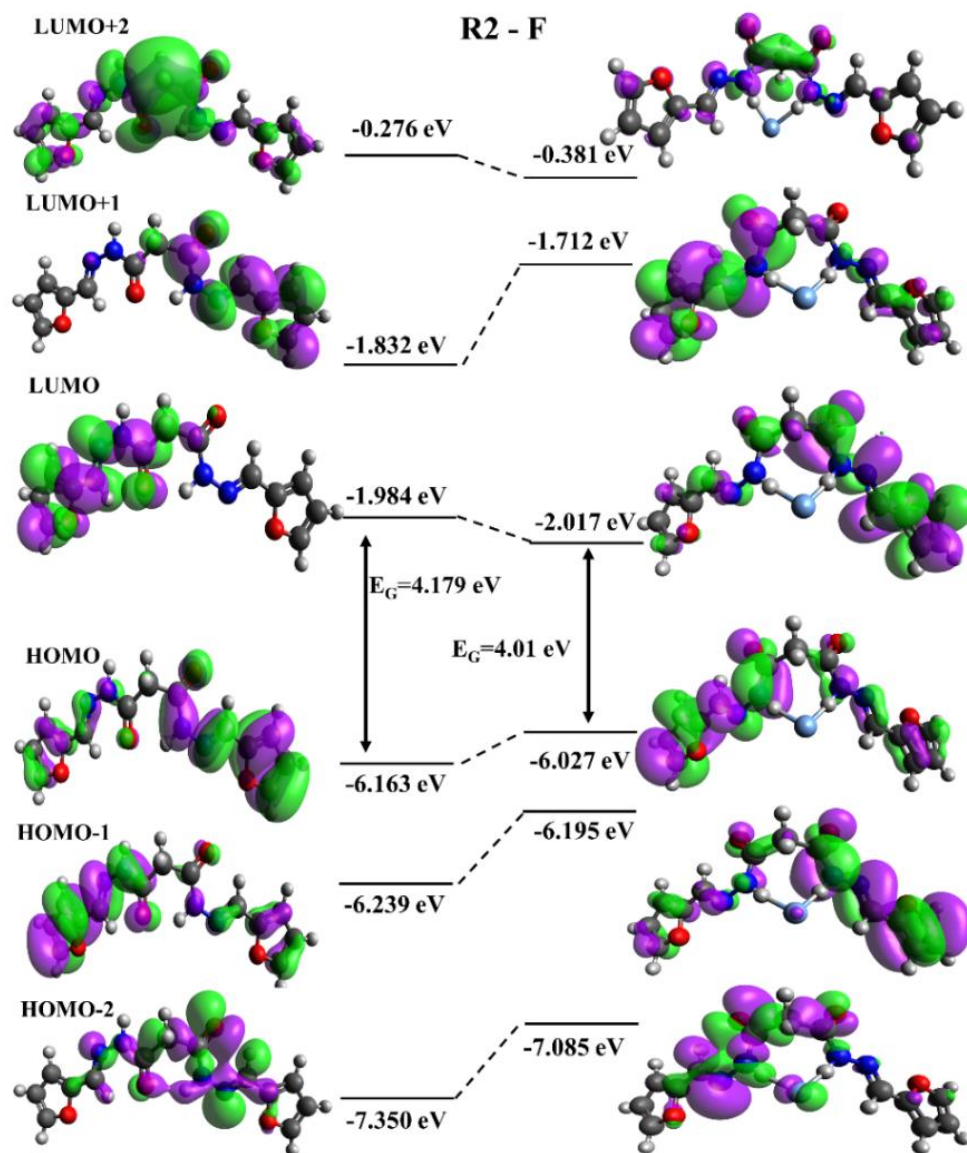
Fig. 6.64 Optimized molecular orbital of receptor **L5R2**, before and after addition of F⁻ ion with energy levels of 6-31+G (d,p)
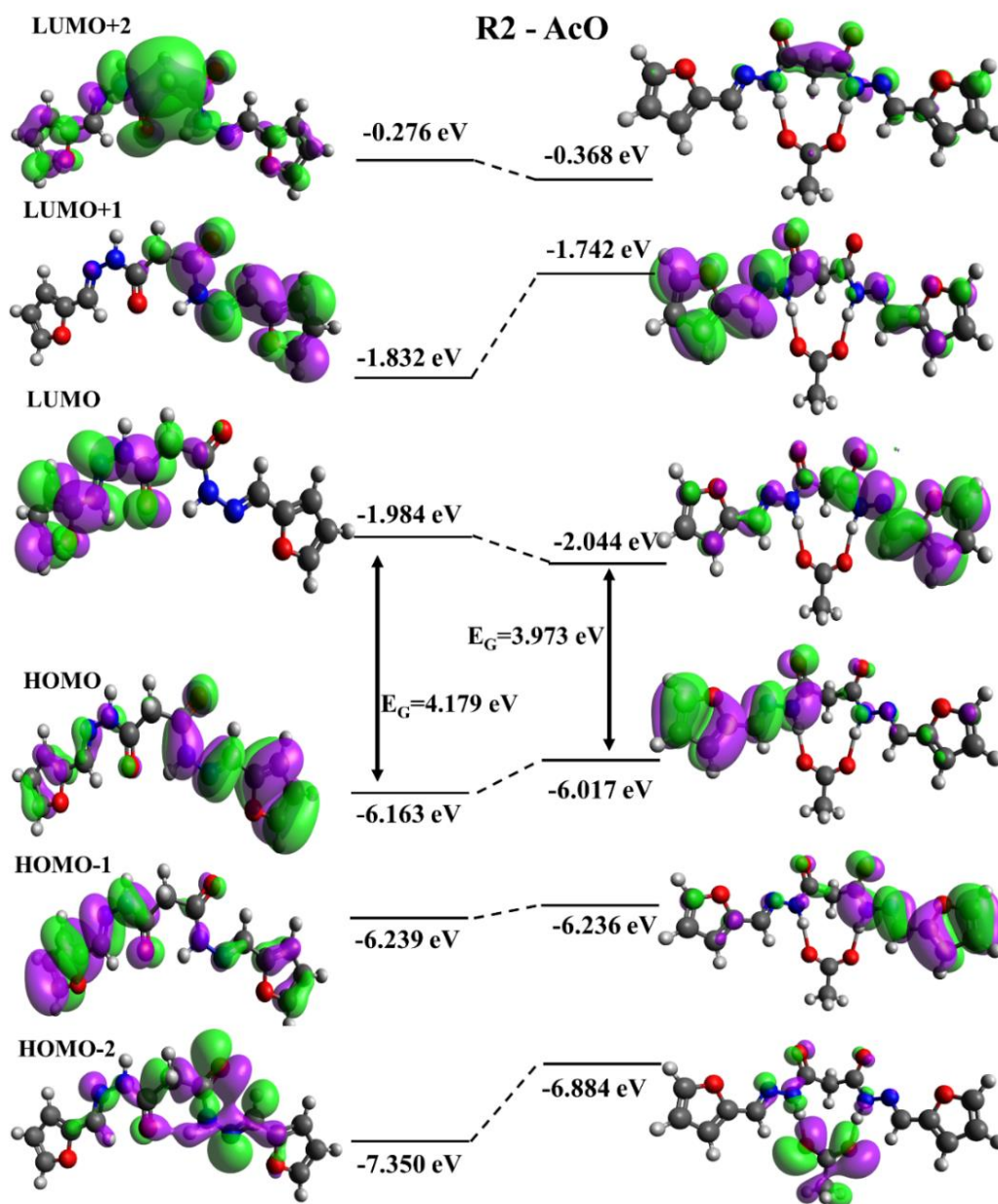
Fig. 6.65 Optimized molecular orbital of receptor **L5R2**, before and after addition of AcO⁻ ion with energy levels of 6-31+G (d,p)

6.3.12.3 Receptors L5R1 and L5R2 with maleate ion

The receptors were designed to bind primely with maleate ion, and in effect **L5R1** with the presence of the NO_2 group efficiently bonded with maleate ion. The electronic distribution of the receptor-bound maleate ion is shown in Fig. 6.66 and Fig. 6.67. In comparison with that of F⁻ and AcO⁻ ions, maleate ion majorly influences the electronic orbitals of the receptors. The HOMO and LUMO orbitals of the receptor

L5R1 exhibited complete delocalization of the electronic orbitals on the entire molecular network. The nature of electronic transition brought about by such distribution would be of the π-π* type. The HOMO-1 and LUMO+1 orbitals of the molecular system exhibited similar distribution patterns as that of the HOMO and LUMO orbitals. There were no traces of distribution found on the maleate ion in the **L5R1** bound complex. However, **L5R2**, devoid of the NO_2 group in its structure exhibited a special distribution. The HOMO orbital of the system was majorly distributed in the entire molecular network, whereas LUMO was majorly concentrated on the maleate ion. Such type of distribution gives rise to charge transfer in the system. The electronic bandgap energy level of the receptor **L5R1** bound maleate ion was exhibited as 3.277 eV, and that of the receptor **L5R2** was exhibited as 3.514 eV.
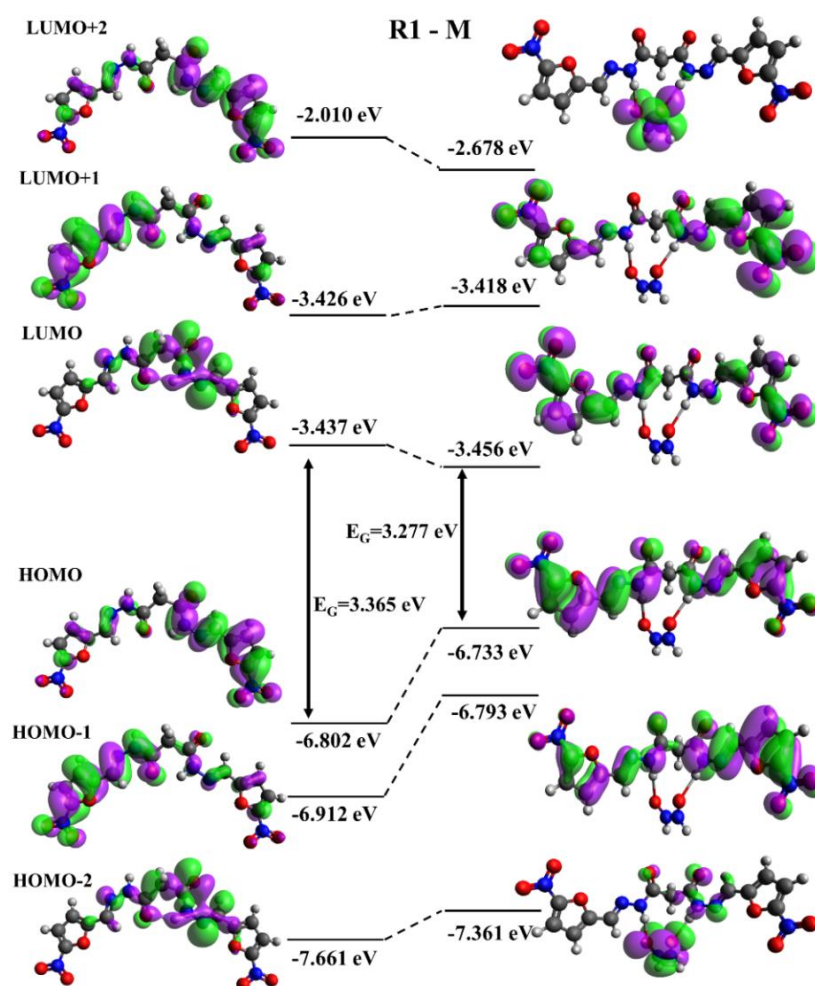
Fig. 6.66 Optimized molecular orbital of receptor **L5R1,** before and after addition of maleate ion with energy levels of 6-31+G(d,p)

LUMO+2

R2 - M

-0.276 eV

-1.770 eV

LUMO+1

-1.832 eV

-1.925 eV

LUMO

-1.984 eV

-2.607 eV

E_G=4.179 eV

E_G=3.514 eV

HOMO

-6.163 eV

-6.121 eV

HOMO-1

-6.239 eV

-6.172 eV

HOMO-2

-7.350 eV

-7.225 eV
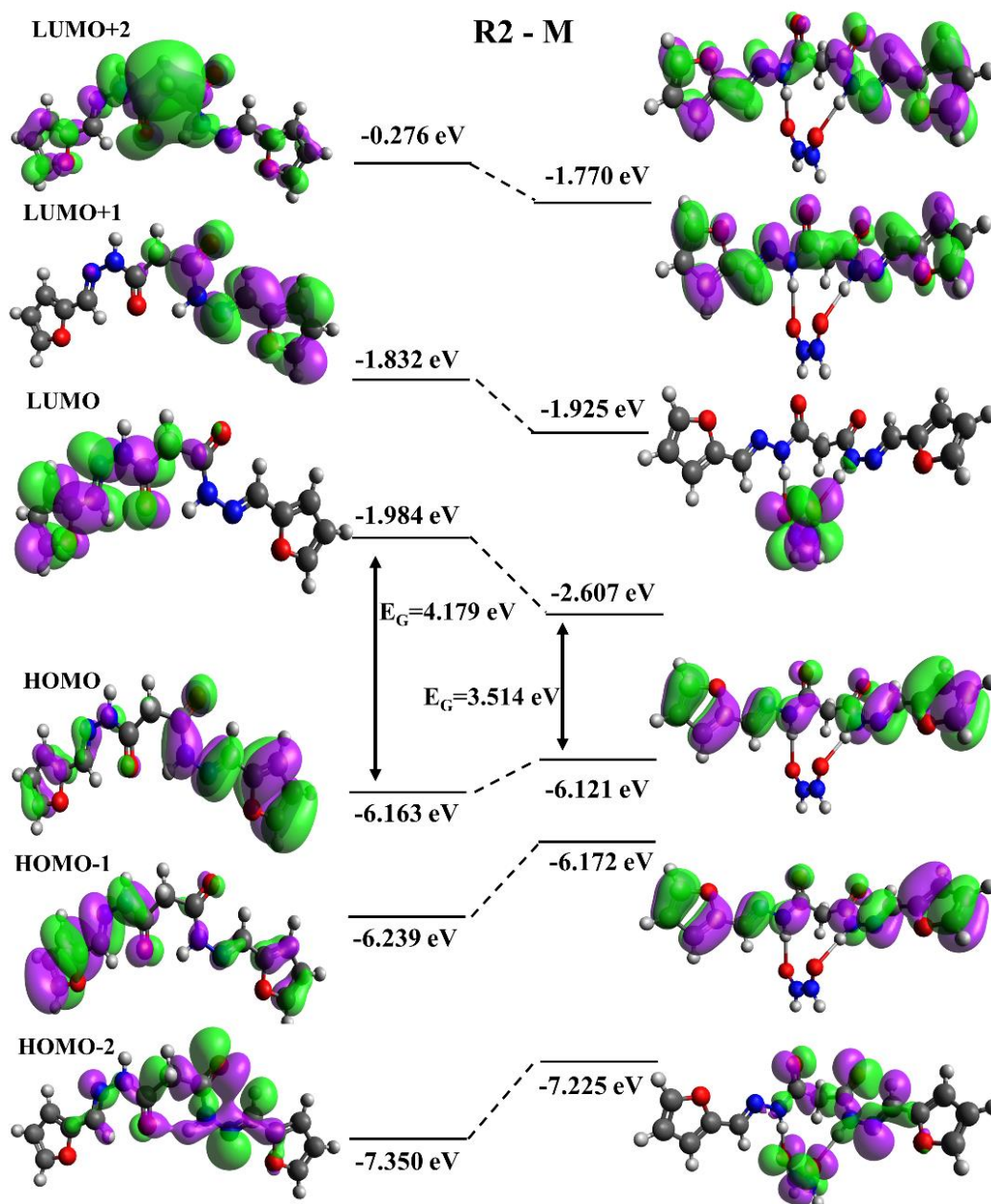
Fig. 6.67 Optimized molecular orbital of receptor **L5R2,** before and after addition of maleate ion with energy levels of 6-31+G (d,p)

The molecular orbital energy level of the receptors **L5R1** and **L5R2** and their complexes with F⁻, AcO⁻, and maleate ions is summarized in Table 6.5.

Table 6.5. Molecular orbital energy of receptors **L5R1** and **L5R2** and their complexes with sensed anions

Receptor	HOMO	LUMO	$\Delta E = E_{LUMO} - E_{HOMO}$
L5R1	-6.802 eV	-3.437 eV	3.365 eV
L5R2	-6.163 eV	-1.984 eV	4.179 eV
Receptor+Complex	HOMO	LUMO	$\Delta E = E_{LUMO} - E_{HOMO}$
L5R1+F⁻	-6.510 eV	-3..664 eV	2.846 eV
L5R1+AcO⁻	-6.592 eV	-3.545 eV	3.047 eV
L5R1+Maleate	-6.733 eV	-3.456 eV	3.277 eV
L5R2+F⁻	-6.027 eV	-2.017 eV	4.01 eV
L5R2+ AcO⁻	-6.017 eV	-2.044 eV	3.973 eV
L5R2+ Maleate	-6.121 eV	-2.607 eV	3.514 eV

6.4 CONCLUSION

To conclude, new receptors **L5R1** and **L5R2** were designed and synthesized for the colorimetric discrimination of the maleate ion over fumarate ion. The receptors **L5R1** and **L5R2** with NH groups as binding sites showed significant colour change from pale yellow to magenta and from pale yellow to red only with the addition of maleate ion, whereas the fumarate ion failed to show any colour change with both the receptors, and resulted in bathochromic shift of 139 nm and 121 nm in the UV-Vis spectra. This shift was due to the strong intermolecular hydrogen bond complex between the receptors and the maleate ion. The binding of the maleate ion to the receptor was through hydrogen bonding, which was confirmed by ^{1}H-NMR titration. In addition, the receptors **L5R1** and **L5R2** showed remarkable colorimetric response to biologically important anions F⁻ and AcO⁻ in the DMSO and inorganic F⁻, AcO⁻, and AsO_2^- in the organo-aqueous (DMSO: H_2O; 9:1 v/v). Lower detection limit of 0.181 ppm, 0.197 ppm, and 0.154 ppm was achieved for Na^+F^-, Na^+AcO^-, and $Na^+AsO_2^-$, respectively, with the receptor **L5R1** proving its utility as an excellent chemosensor in an organo-aqueous medium. The receptor **L5R1** exhibited excellent fluorescence

enhancement with the addition of F^- and AcO^- ions owing ICT transition from the donor (NH) group to the acceptor (NO_2) moiety. Colorimetric test paper for maleate ion was prepared and could be used to detect maleate ion by naked eye with the advantages of rapidness, and good selectivity. In addition, the receptors **L5R1** and **L5R2** can also be considered as a practical sensor for qualitative and quantitative detection of fluoride ion in toothpaste conveniently even at 0.48 ppm and 0.53 ppm in aqueous media. Receptors serve as powerful colorimetric sensor for F^- with promising potential in practical applications. The TD-DFT studies provided full support for the anion binding mechanism by illustrating that the lower energy gap between HOMO and LUMO was responsible for the corresponding change in colour and redshift in the absorption band.

CHAPTER 7

SPECTROSCOPIC STUDIES OF COLORIMETRIC RECEPTORS FOR DETECTION OF BIOLOGICALLY IMPORTANT INORGANIC F⁻, ACO⁻ AND H₂PO₄⁻ ANIONS IN ORGANO-AQUEOUS MEDIUM: REAL-LIFE APPLICATION
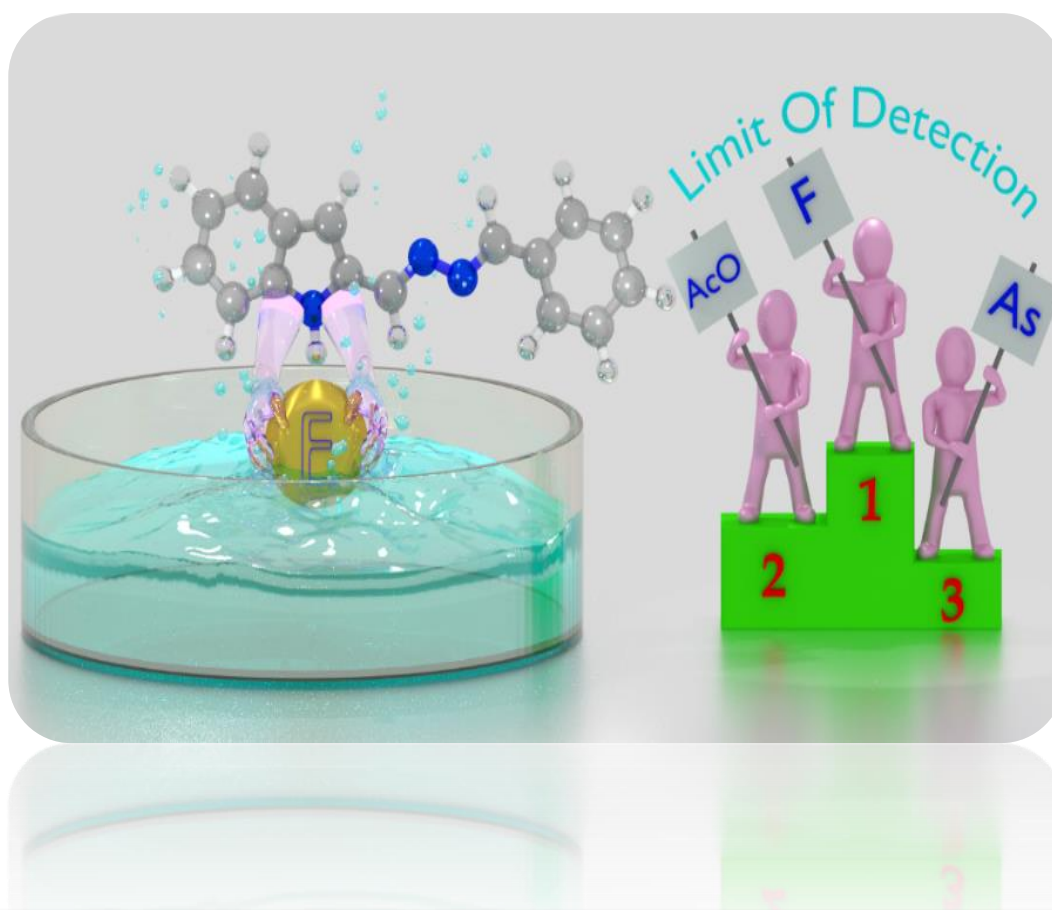
Abstract: In this chapter, the design, synthesis, and characterization of new receptors is described. The applicability of the receptors in the colorimetric detection of multi anions in both organic and organo-aqueous *media is discussed in detail through UV-Vis, ^{1}H-NMR titration studies, and electrochemical techniques. The binding mechanism of the receptors towards active anions is included*

7.1 INTRODUCTION

Anions receptor chemistry has gained unique attention among supramolecular chemists in light of its role in biology and the environment (Martinez-Manez and Sancenón 2003; Steed 2010)**.** Design-based synthetic artificial receptors that can recognize and sense anions through visible, electrochemical, and optical response are of special interest owing to the low cost and simple instrumentation required (Gholivand et al. 2007; Mohadesi and Taher 2007)**.** Moreover, there is need to develop a single molecular probe to detect multiple analytes in various environments. The literature survey has shown that synthetic receptors usually involve two subunits, a receptor and an optical signalling chromophore. These synthesized receptors are made-up of amide (Kim et al. 2008)**,** pyrrole (Ghosh and Maiya 2004), urea (Jose et al. 2007; Quinlan et al. 2007), thiourea (Evans et al. 2006; Jose et al. 2004), and imidazole (Zapata et al. 2008) subunits, which are known to promote fluoride, acetate, and phosphate ion binding through hydrogen-bond interaction or N-H deprotonation events. Recently, neutral-anion receptor system based on heterocyclic derivatives such as pyrrole, indole, etc., which possess relatively acidic proton, have been extensively studied (Cho et al. 2005; Esteban-Gomez et al. 2005; Jose et al. 2004; Vázquez et al. 2004)**.** Chemosensors containing nitrophenyl (Dey et al. 2012), quinone (Kodlady et al. 2019; San-José et al. 2010), nitronaphthalene urea (Li et al. 2018), azo-dye (Li et al. 2019)**,** and tripodal receptor as signalling units have been reported. The covalent linking of an optical signalling chromophoric fragment leads to visually observable color change assigned to conformational change in the receptor or the change transfer process. Among the wide range of anions present in the Hofmeister series of anions, fluoride (F$^-$), acetate (AcO$^-$), and phosphate (H$_2$PO$_4$$^-$) have gained attention for their significant role in physiological applications (Guo et al. 2018; Gupta et al. 2014; Hu et al. 2015; Jiang et al. 2016; Jo et al. 2015; Shang et al. 2018; Suganya et al. 2015; Wu

et al. 2017). Thus, as part of ongoing research on anion recognition, two organic receptors **L6R2** and **L6R3** bearing the -NH group as the anion binding site and the NO_2 group as the signalling unit were designed and synthesized. The presence of imine linkages in the receptors provided extended conjuncture and nitro functionality as a signalling unit eventually increasing colorimetric sensitivity towards organic anions like TBA^+F^-, TBA^+AcO^-, and $TBA^+H_2PO_4^-$, and inorganic anions such as Na^+F^-, Na^+AcO^-, $Na^+H_2PO_4^-$, and $Na^+AsO_2^-$ in both organic and organo-aqueous media.

L6R1 **L6R2** **L6R3**

7.2   EXPERIMENTAL SECTION

7.2.1 Materials and methods

All the chemicals used in the present study were purchased from Sigma- Aldrich, and Alfa Aesar and were used without further purification. All the solvents procured from SD Fine, India, were of HPLC grade and used without further distillation. The UV –Vis spectroscopy was carried out with the Analytikjena Specord S600 spectrometer in standard 3.0 mL quartz cell with 1cm path length. Infrared spectrum was recorded on Bruker Apex FTIR spectrometer. All the reactions were monitored by TLC on pre-coated silica gel 60 F254 plates. The ^{1}H-NMR samples were recorded on Bruker Avance (400 MHz) instrument using Tetramethylsilane (TMS) as internal reference and the DMSO-d_6 as the solvent. ^{13}C NMR spectra were recorded on Bruker Ascend (125 MHz) instrument using TMS as internal reference and DMSO-d_6 as solvent. Resonance multiplicities are explained as s (singlet), d (doublet), t (triplet), and m (multiplet). The mass spectra were recorded on Waters Micromass Q-Tofmicro spectrometer with ESI source. The elemental analysis for carbon, nitrogen, and oxygen was carried out using an Oxford instrument elemental analyzer. Cyclic voltammogram was recorded on

IVIUM electrochemical workstation (Vertex) at a scan rate of 20 mV/s with the potential range −1.5 V to 1.5 V.

7.2.2 Calculations for binding constants from UV-Vis studies

The binding constant was calculated using (Eq. 7.1) (Benesi and Hildebrand 1948) as given below;

$$\frac{1}{(A-A_0)} = \frac{1}{(A_{max}-A_0)} + \frac{1}{K[X^-]^n (A_{max}-A_0)} \dots\dots\dots\dots \textit{(Eq. 7.1)}$$

Where, A_0, A, and A_{max} are the absorption considered in the absence of anion, at intermediate and at concentration of saturation, respectively, K is the binding constant, $[X^-]$ is the concentration of the anion, and n is the stoichiometric ratio.

7.2.3 Calculation of limit of detection (LOD)

The detection limit of the receptors with the anions was calculated by using (Eq. 7.2)

$$LOD = \frac{3 \times \sigma}{s} \dots\dots\dots\dots\dots (Eq. 7.2)$$

Where, σ is the standard deviation of the calibration curve (SD) and s is the slope of the calibration curve.

7.2.4 Synthesis of intermediate (E)-1-(hydrazonomethyl) naphthalene-2-o1 (S 7.1)

A mixture of 2-Hydroxy-1-naphthaldehyde (0.344 g, 2 mmol) and hydrazine hydrate (3 mL, 3 mmol) was dissolved in 5 mL ethanol. The reaction mixture was kept for stirring overnight at room temperature. The yellow color solid product was collected by filtration and washed with cold ethanol to obtain the target intermediate (S 7.1).
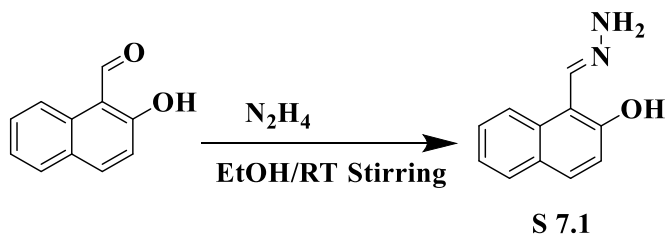
Scheme 7.1 Synthesis of intermediate **S 7.1**

7.2.5 Synthesis of receptor 2-((Z)-(((E)-(2-hydroxynaphthalen-1yl) methylene) hydrazono) methyl) quinoline-8-ol (L6R1)

Intermediate **S 7.1** (0.374 g, 2 mmol) and 8-Hydroxy-quinoline-2-carbaldehyde (0.346 g, 2 mmol) was dissolved in 5 mL methanol, to which 2–3 drops of acetic acid (CH$_3$CO$_2$H) was added and the reaction mixture was refluxed at 60 °C for 5 h as shown in (Scheme 7.2). The yellow solid precipitate was collected by filtration and washed with cold methanol to obtain the final product. The formation of the product was confirmed by TLC by the generation of a single spot indicating the absence of the starting material.
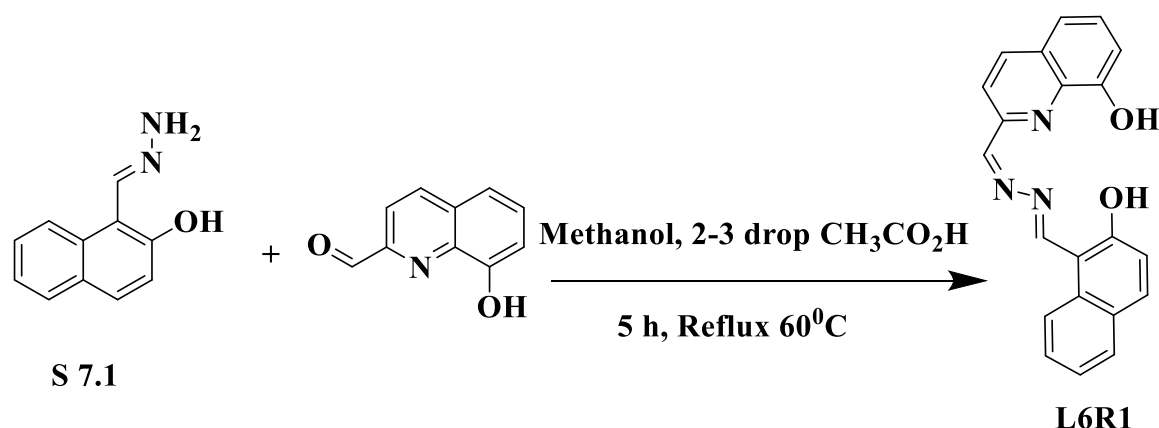
Scheme 7.2 Synthesis of receptor **L6R1**

7.2.6 Synthesis of receptor 2-((E)-(((E)-4- nitrobenzylidene)hydrazono)methyl)-1H-indole (L6R2)

(E)-(4-nitrobenylidene)hydrazine (66.25mg, 1.323mmol) and indole-2-carboxaldehyde (192.11mg, 1.323mmol) were mixed in 5 mL methanol. A drop of acetic acid (CH$_3$CO$_2$H) was added and the reaction mixture was refluxed at 60^{0}C for 5 h. The formation of the product was checked through TLC by the generation of a single spot indicating the disappearance of the starting materials. After cooling to room temperature, the red coloured solid product was collected by filtration and washed with methanol and dried to obtain the pure product **(L6R2)** as seen in (Scheme 7.3).
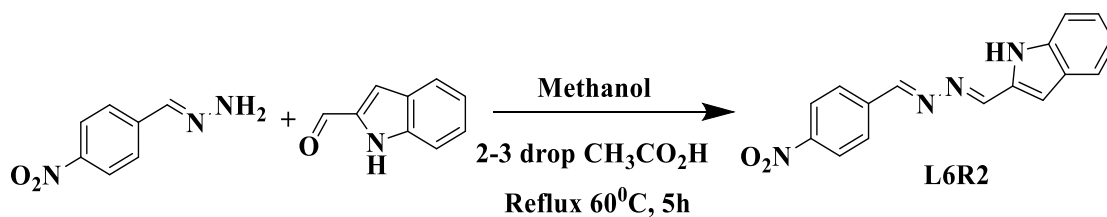
Scheme 7.3 Synthesis of receptor **L6R2**

7.2.7 Synthesis of receptor 2-((E)-(((E)-4-nitrobenzylidene)hydrazono)methyl)-1H-pyrrole (L6R3)

A mixture of (E)-(4-nitrobenylidene) hydrazine (66.25 mg, 1.323mmol) and pyrrole-2-carboxyladehyde (125.86 mg, 1.323 mmol) was mixed in 5 mL methanol. About (2-3) drops of acetic acid (CH_3CO_2H) was added and the reaction mixture was refluxed at 60^0C for 5 h. The formation of the product was checked through TLC by the generation of a single spot indicating the disappearance of the starting materials. After cooling to room temperature, the solid yellow-coloured product was collected by filtration and washed with methanol and dried to obtain the pure product (**L6R3**) as illustrated in (Scheme 7.4).
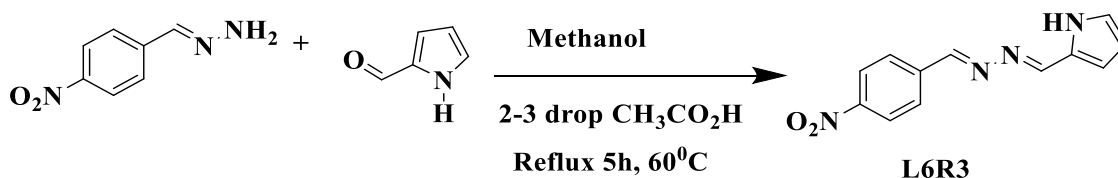
Scheme 7.4 Synthesis of receptor **L6R3**

7.2.8 Characterization data

The purity and structure of the intermediate **S 7.1** and receptors **L6R1, L6R2** and **L6R3** were confirmed by FT-IR, ^{1}H-NMR, ^{13}C-NMR, and mass spectroscopic and elemental analysis. The characterization data has been compiled and given below.

Data obtained for S 7.1: Yield 89%., m.p. $200^{\circ}C$. FT-IR (KBr pellet) (cm^{-1}): 3428 (OH), 2998-2914 (NH_2), 1660 (C=N), 1436 (C=C). ^{1}H NMR (DMSO-d_6, 400 MHz, Me_4Si): δ_{ppm} 12.822 (s,1H), 8.881 (s,1H), 8.114-8.096 (d,1H), 7.848-7.832 (d,1H), 7.771-7.754 (d,1H), 7.539-7.508 (t,1H), 7.368-7.338 (m,1H), 7.151-7.132 (d,1H),

6.997 (s,2H).^{13}C NMR (DMSO-d$_6$, 125 MHz, Me$_4$Si): δ_{ppm} 156.60, 140.30, 131.33, 130.17, 129.19, 128.20, 127.34, 123.44, 120.92, 119.07, 110.07. Mass (ESI): m/z calculated for C$_{11}$H$_{10}$N$_2$O:186.08 Obtained: 187.1473 [M+H]$^+$

Data obtained for receptor L6R1: Yield 80%, m.p. 280°C. FT-IR (KBr pellet) (cm^{-1}): 3381 (OH), 1590 (CH=N), 1509 (C=C), 1098 (N-N). ^{1}H NMR (DMSO-d$_6$, 400 MHz, Me$_4$Si): δ_{ppm} 12.908 (s,1H), 9.986 (s,1H), 9.880 (s,1H), 8.950 (s,1H), 8.659-8.642 (d,1H), 8.482-8.465 (d,1H), 8.292-8.275 (d,1H), 8.090-8.072 (d,1H), 7.951-7.935 (d,1H), 7.657-7.626 (t,1H), 7.573-7.542 (t,2H), 7.500-7.467 (t,1H), 7.452-7.291 (t,1H), 7.204-7.189 (d,1H). ^{13}C NMR (DMSO-d$_6$, 125 MHz, Me$_4$Si): δ_{ppm} 163.33, 162.10, 161.14, 154.22, 151.06, 138.94, 137.35, 135.82, 132.77, 129.76, 129.68, 129.46, 128.77, 128.36, 124.41, 122.19, 119.26, 119.15, 118.31, 112.72, 108.88. Mass (ESI): m/z calculated for C$_{21}$H$_{15}$N$_3$O$_2$: 341.37. Obtained: 342.1293 [M+H]$^+$.

Data obtained for receptor L6R2: Yield=90%, m.p=306°C , ^{1}H NMR (DMSO-d$_6$, 400 MHz, Me$_4$Si): δ_{ppm} 6.715-6.712 (d, 1H, Ar-H), 7.130-7.125 (d, 1H, Ar-H), 7.741-7.644 (m, 3H, Ar-H), 7.935 (s,1H, Ar-H), 8.081-8.064 (d,1H, -CH), 8.151-8.135 (d, 1H, Ar-H), 8.194-8.180 (d,1H, CH), 8.514 (s, 1H, Ar-H),9.192-9.175 (d, 1H, Ar-H), 9.443(s, 1H, NH). ^{13}C NMR (DMSO-d$_6$, 125 MHz, Me$_4$Si): δ_{ppm} 162.37, 150.91, 149.56, 141.09, 134.05, 132.44, 130.79, 129.66, 129.28, 128.12, 126.96, 126.05, 125.49, 117.84, 113.14. FT-IR (KBr pellet) (cm^{-1}): 3441 (N-H stretch), 3309 (Ar-CH stretch), 1614 (C=N stretch), 1510-1534 (C=C stretch), 1586 (N-O stretch), 1339-1315 (N-O stretch), 1126 (C-H stretch), 1079 (N=N stretch); Mass (ESI): m/z calculated for C$_{16}$H$_{12}$N$_4$O$_2$=292.1036, Obtained=293.1036 [M+H]$^+$; Anal. Calcd for C$_{16}$H$_{12}$N$_4$O$_2$: C, 65.75; N, 19.17; O, 10.95. Found: C, 63.53; N, 18.86; O, 9.91.

Data obtained for receptor L6R3: Yield=90%, m.p. =242°C. ^{1}H NMR (DMSO-d$_6$, 400 MHz, Me$_4$Si): δ_{ppm} 7.740-7.643(m, 4H, Ar-H), 7.935(s, 1H, Ar-H), 8.080-8.064 (d, 1H, Ar-H), 8.193-8.135 (m, 2H, CH), 9.192-9.175 (d, 1H, Ar-H), 9.442 (s,1H, NH). ^{13}C NMR (DMSO-d$_6$, 125 MHz, Me$_4$Si): δ_{ppm} 162.38, 150.91, 149.56, 147.09, 134.05, 132.44, 131.13, 130.79, 129.66, 129.28, 128.13, 126.96, 126.05, 125.49, 117.84, 113.14. FT-IR (KBr pellet) (cm^{-1}): 3415 (N-H stretch), 3231 (Ar-CH stretch), 1618 (CH=N stretch), 1518 (C=C stretch), 1583 (N-O stretch), 1365-1309 (N-O stretch), 1092 (N=N stretch); Mass (ESI): m/z value calculated for C$_{12}$H$_{10}$N$_4$O$_2$=242.0882,

Obtained=243.0882 [M+H] $^+$; Anal. Calcd for $C_{16}H_{10}N_4O_2$: C, 59.50; N, 23.13; O, 13.21. Found: C, 57.53; N, 22.86; O, 12.91.

The representative spectra of synthesized intermediate **(S 7.1)** and receptors **L6R1, L6R2** and **L6R3** have been given below
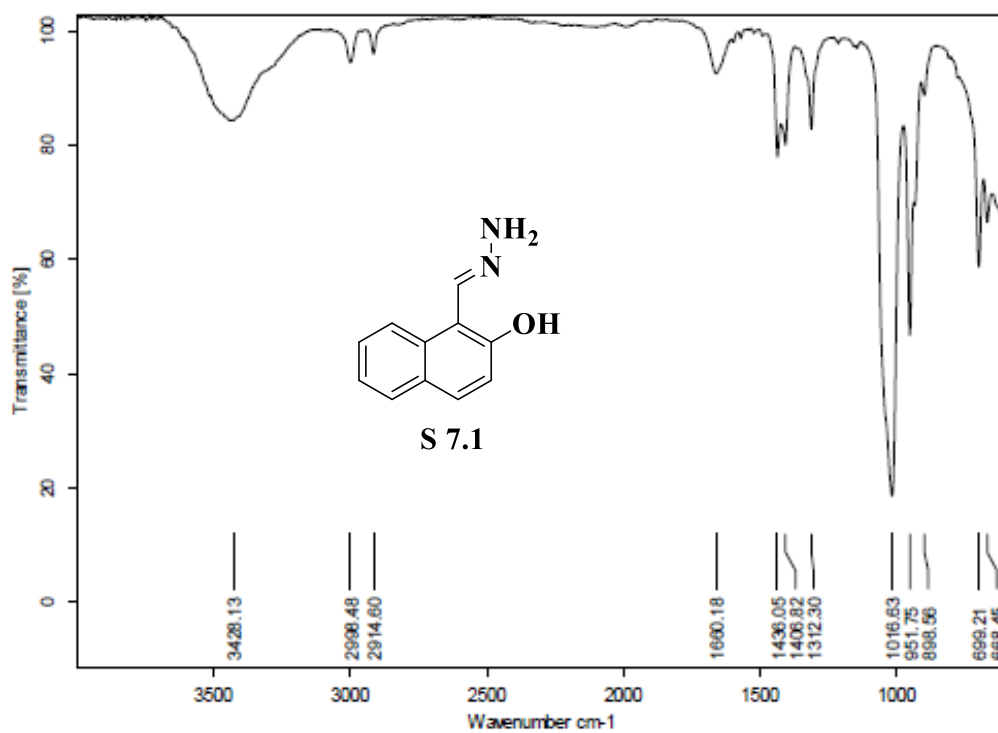
Fig. 7.1 FT-IR spectrum of intermediate **S 7.1**
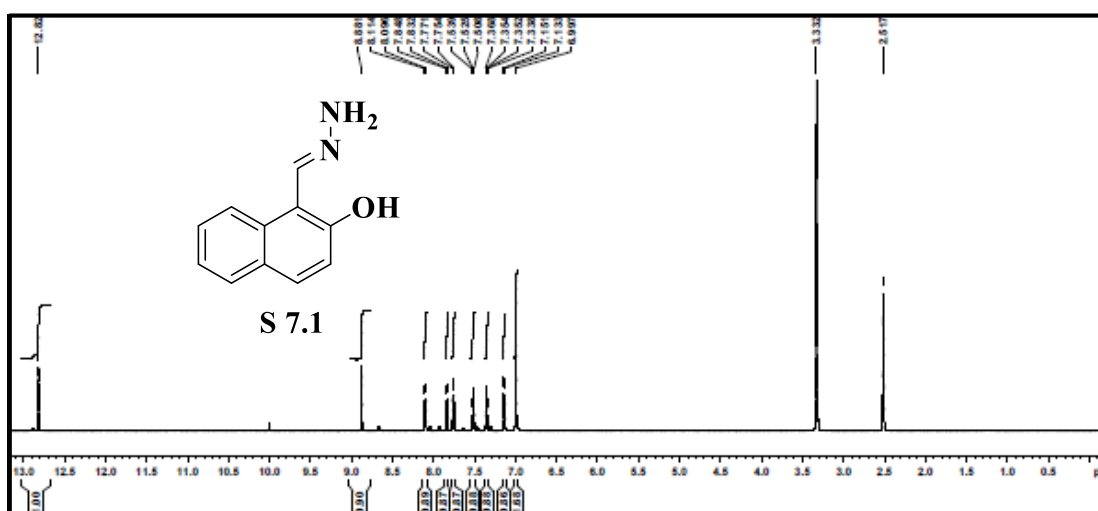
Fig. 7.2 ^{1}H NMR spectrum of intermediate **S 7.1**
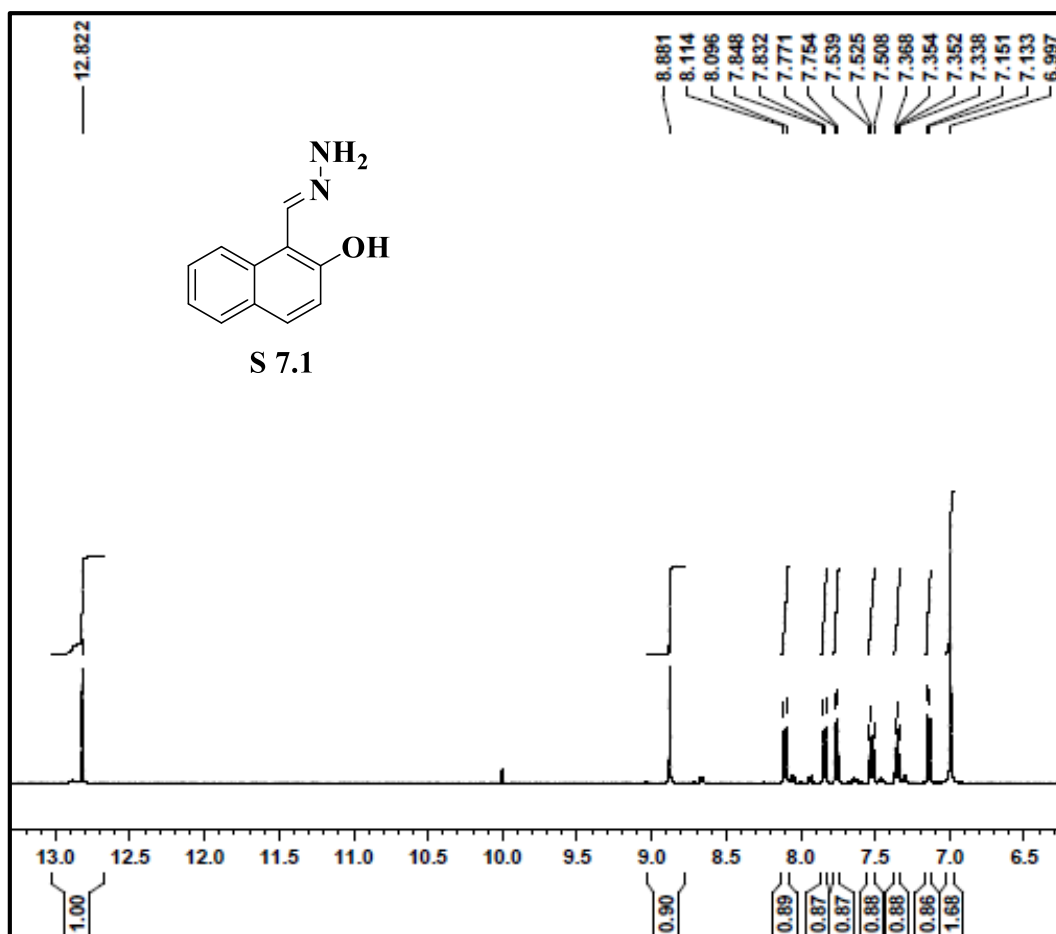
Fig. 7.3 Extended aromatic region of intermediate **S 7.1**

Fig. 7.4 ^{13}C-NMR spectrum of intermediate **S 7.1**

Mass spectrum: S 7.1

Exact Mass: 186.08

Mass obtained in the positive mode: 187.1473

Elemental composition: $C_{11}H_{10}N_2O$
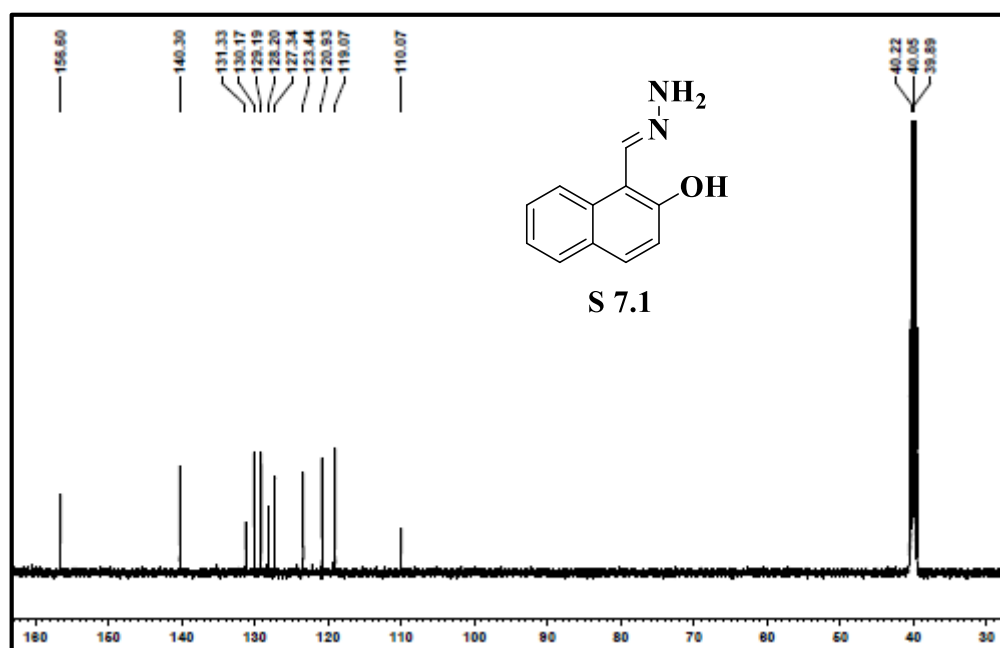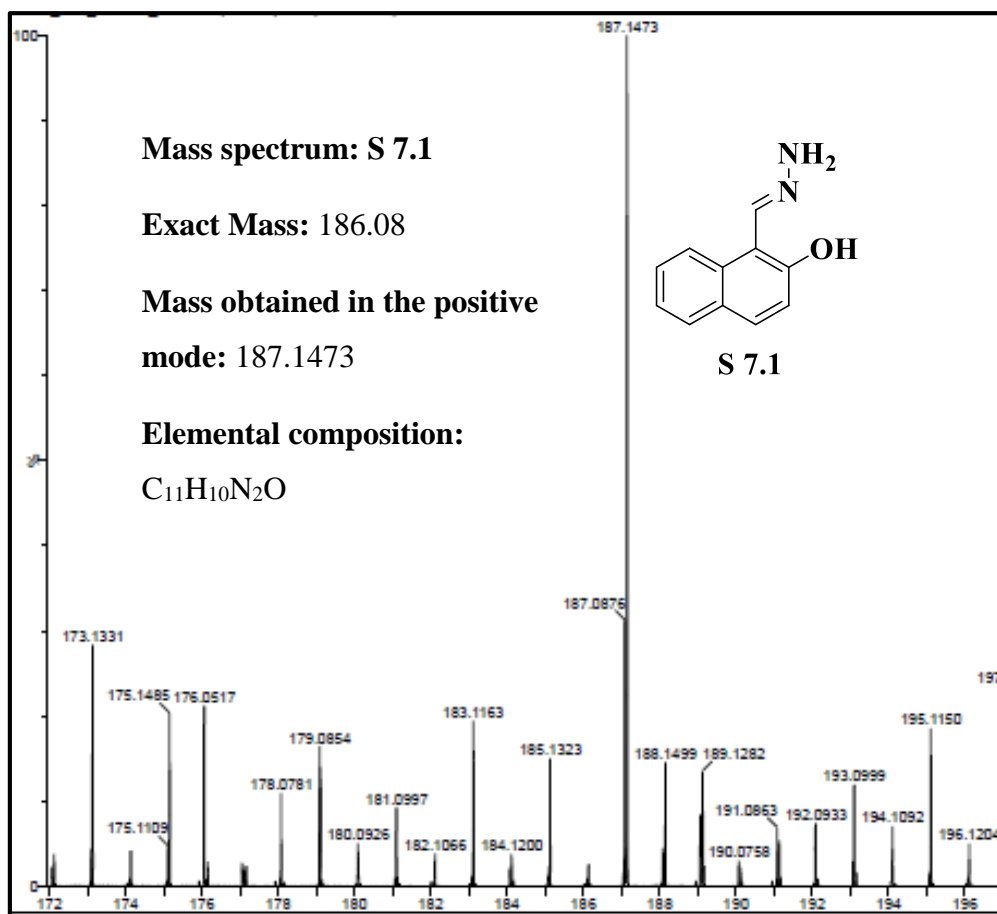
Fig. 7.5 ESI-MS spectrum of intermediate **S 7.1**
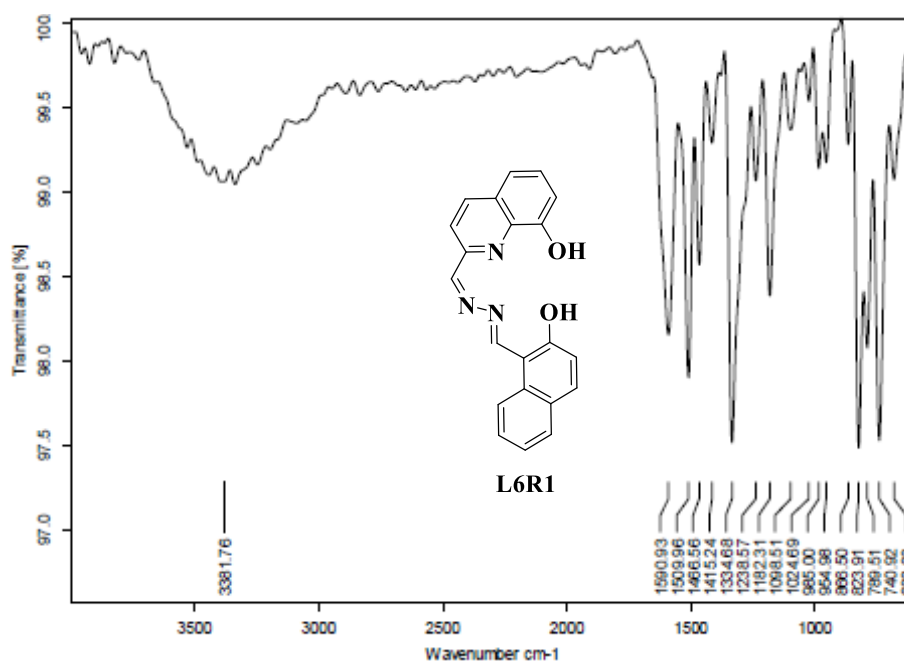
Fig. 7.6 FT-IR spectrum of receptor **L6R1**
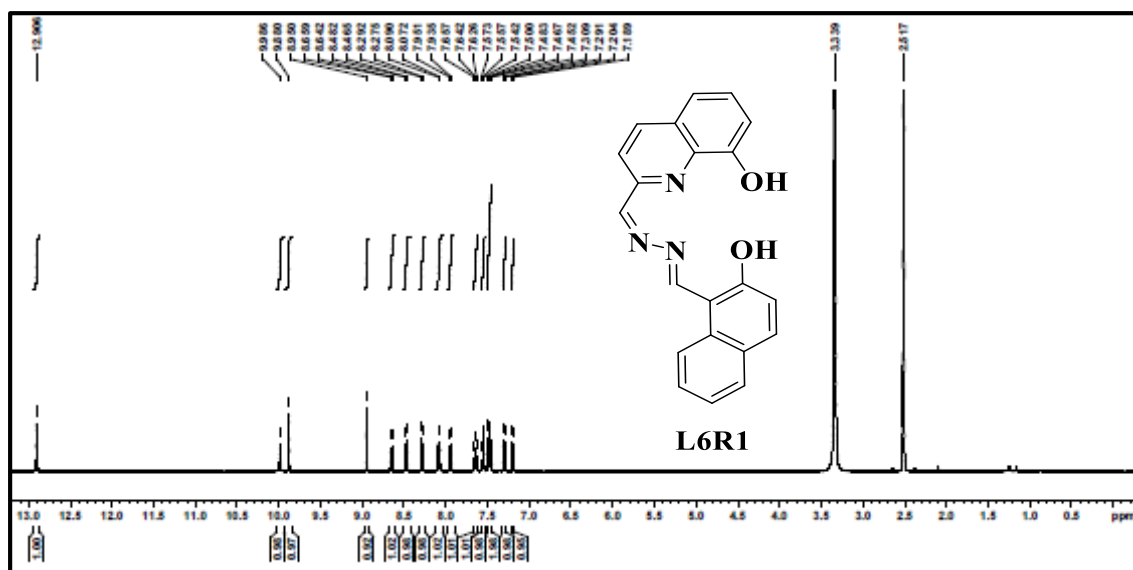
Fig. 7.7 ^{1}H-NMR spectrum of receptor **L6R1**
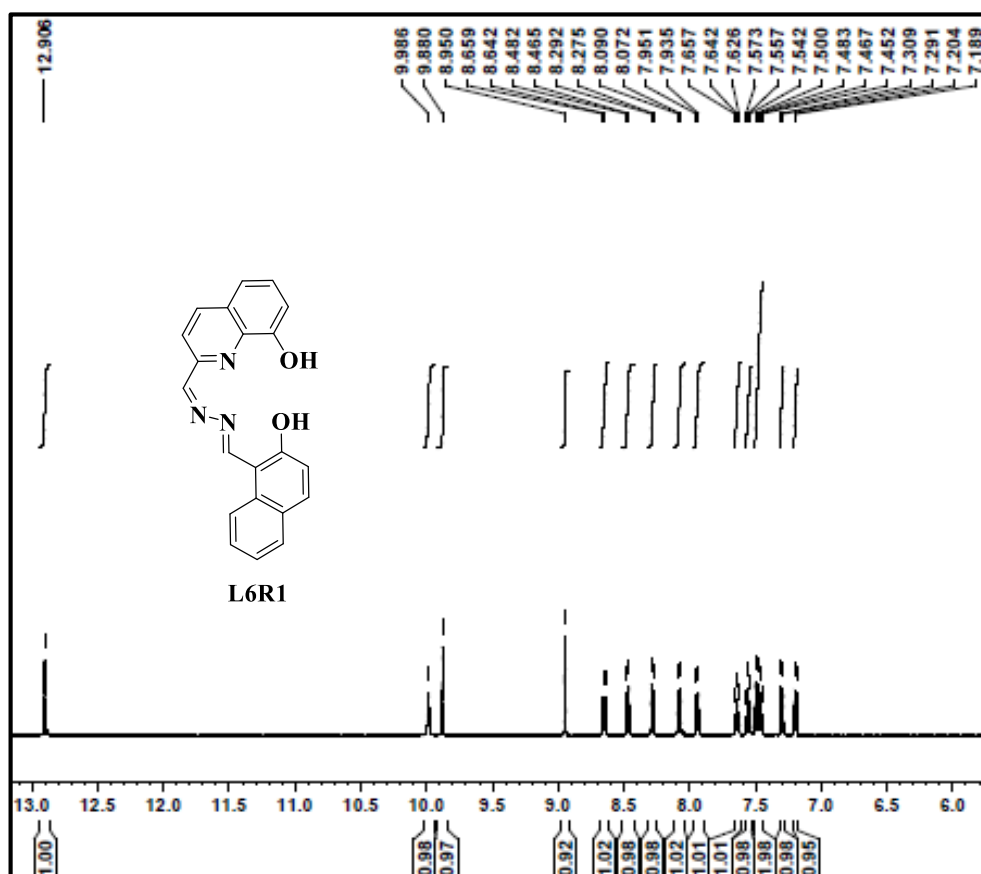
Fig. 7.8 Extended aromatic region of receptor **L6R1**

Fig. 7.9 ^{13}C-NMR spectrum of receptor **L6R1**

Mass spectrum: L6R1

Exact Mass: 341.37

Mass obtained in the positive mode: 342.1293

Elemental composition: $C_{21}H_{15}N_3O_2$
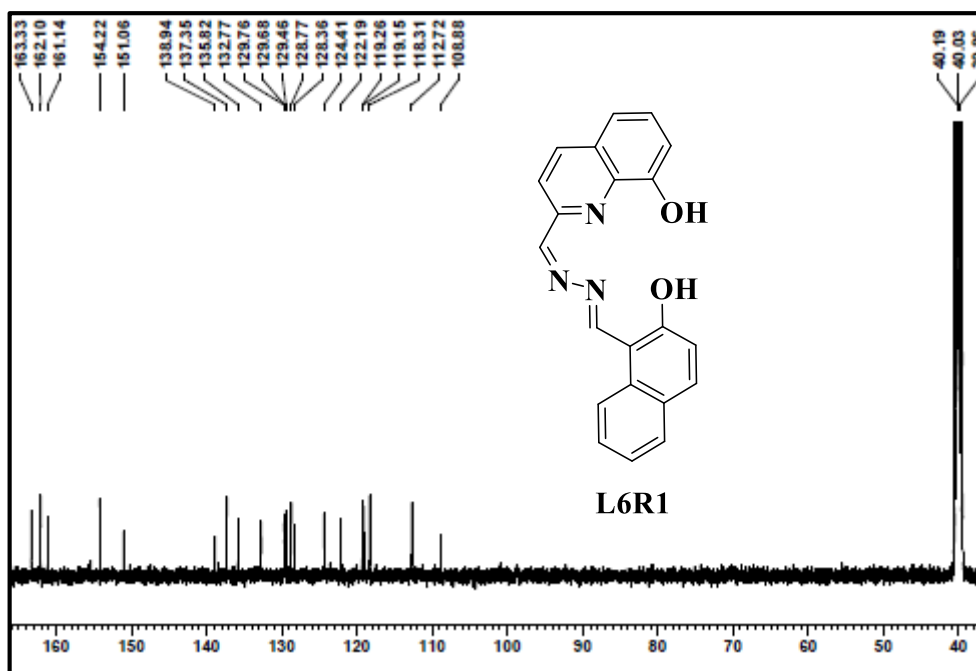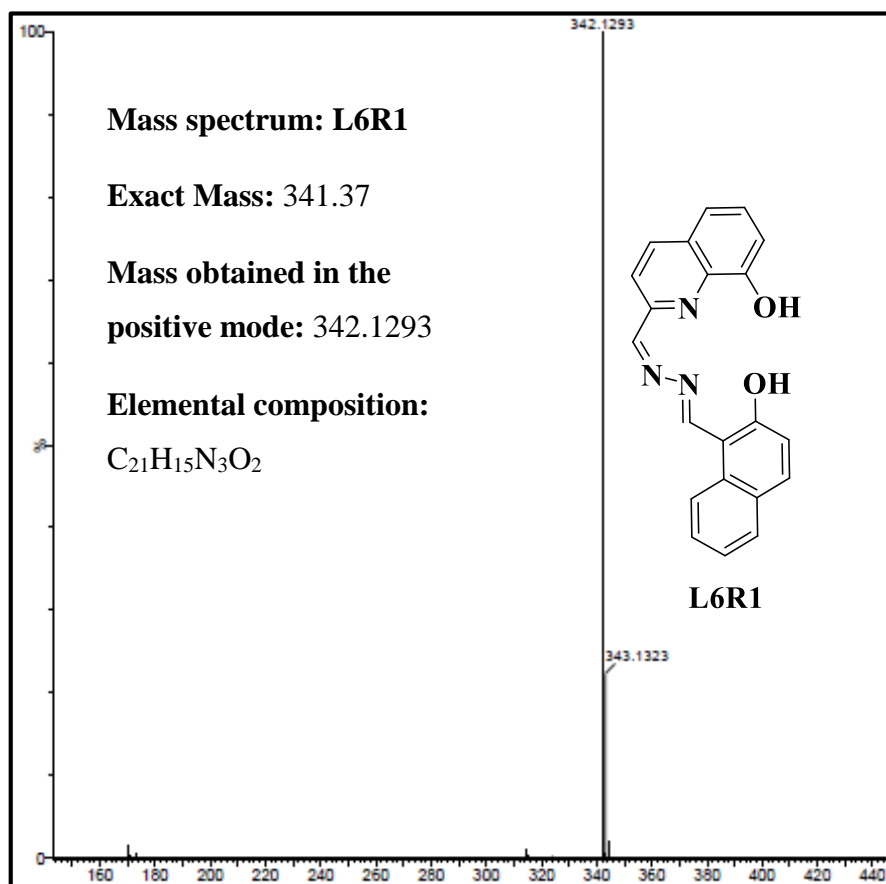
Fig. 7.10 ESI-MS spectrum of receptor **L6R1**
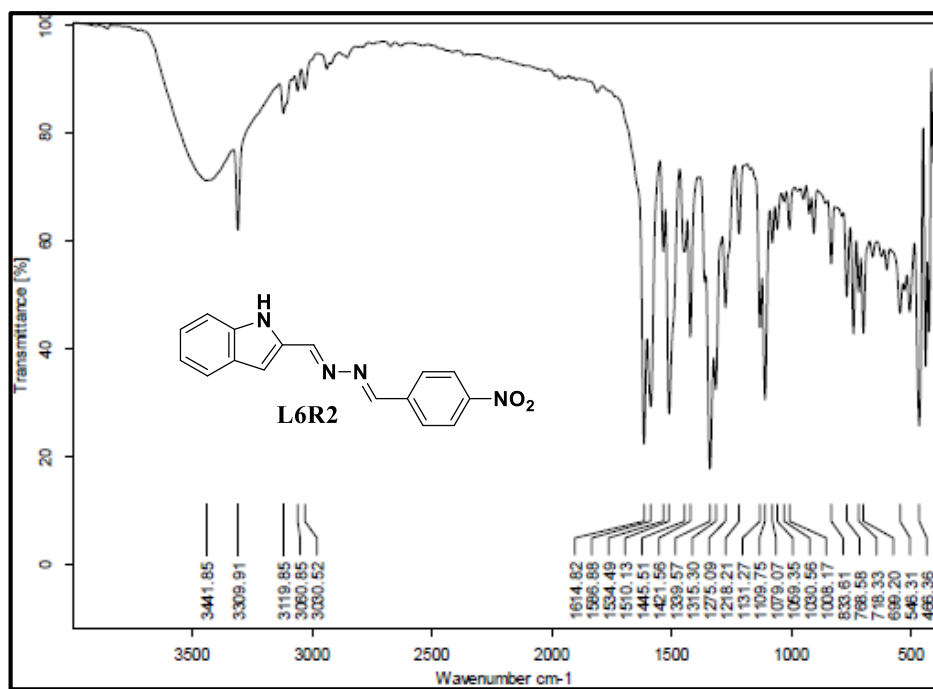
Fig. 7.11 FT-IR spectrum of receptor **L6R2**
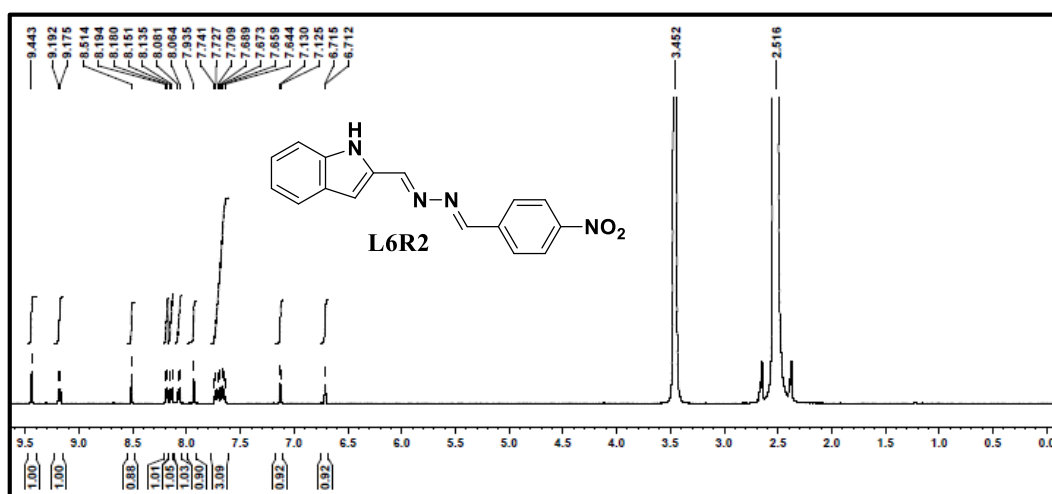
Fig. 7.12 ^{1}H-NMR spectrum of receptor **L6R2**
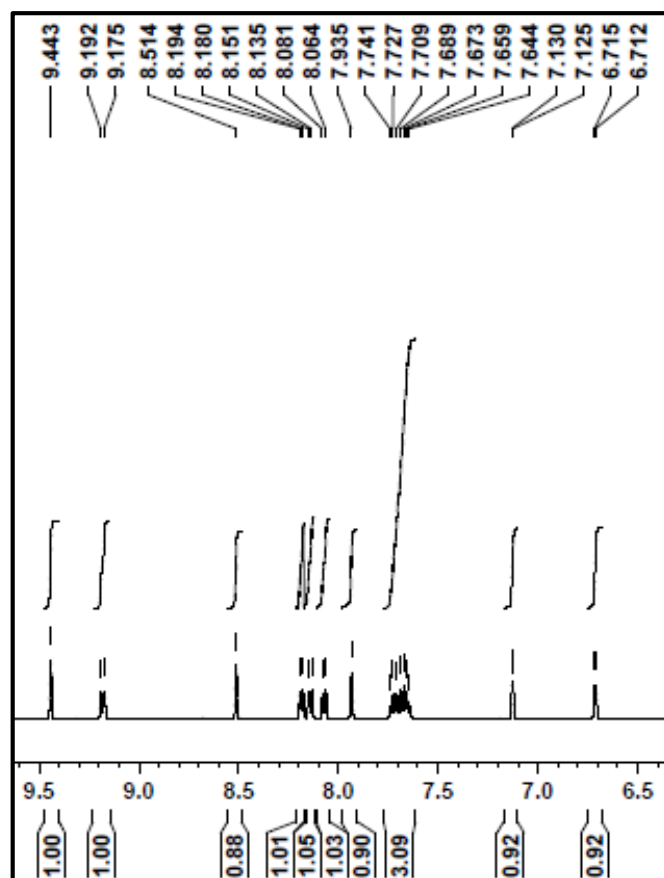
Fig. 7.13 Extended aromatic region of receptor **L6R2**

L6R2

Fig. 7.14 ^{13}C-NMR spectrum of receptor **L6R2**

Mass spectrum: L6R2

Exact Mass: 292.10

Mass obtained in the positive mode: 293.1036
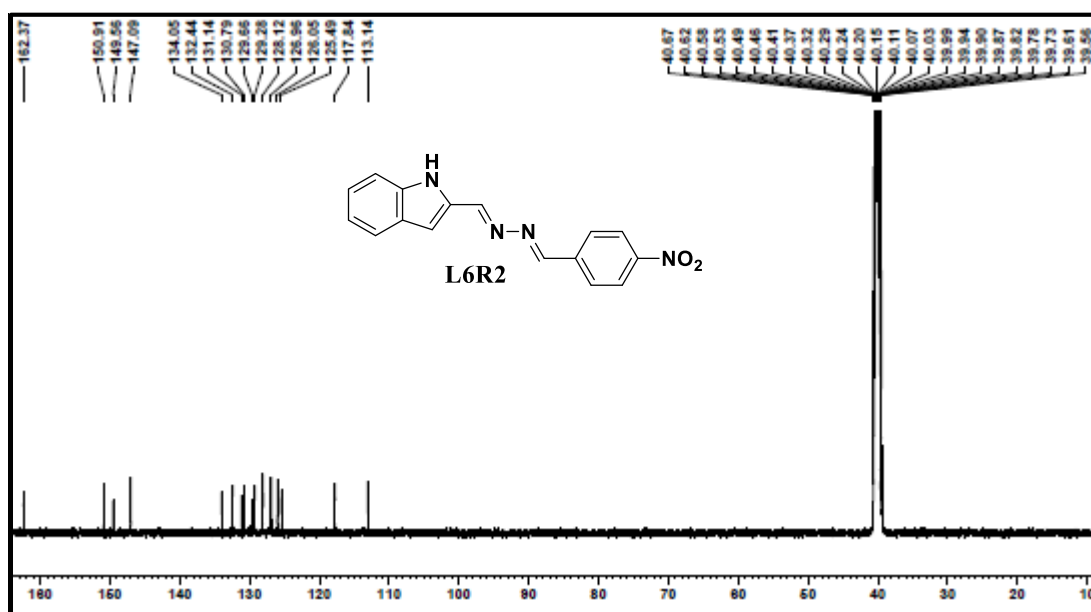
Elemental composition: $C_{16}H_{12}N_4O_2$
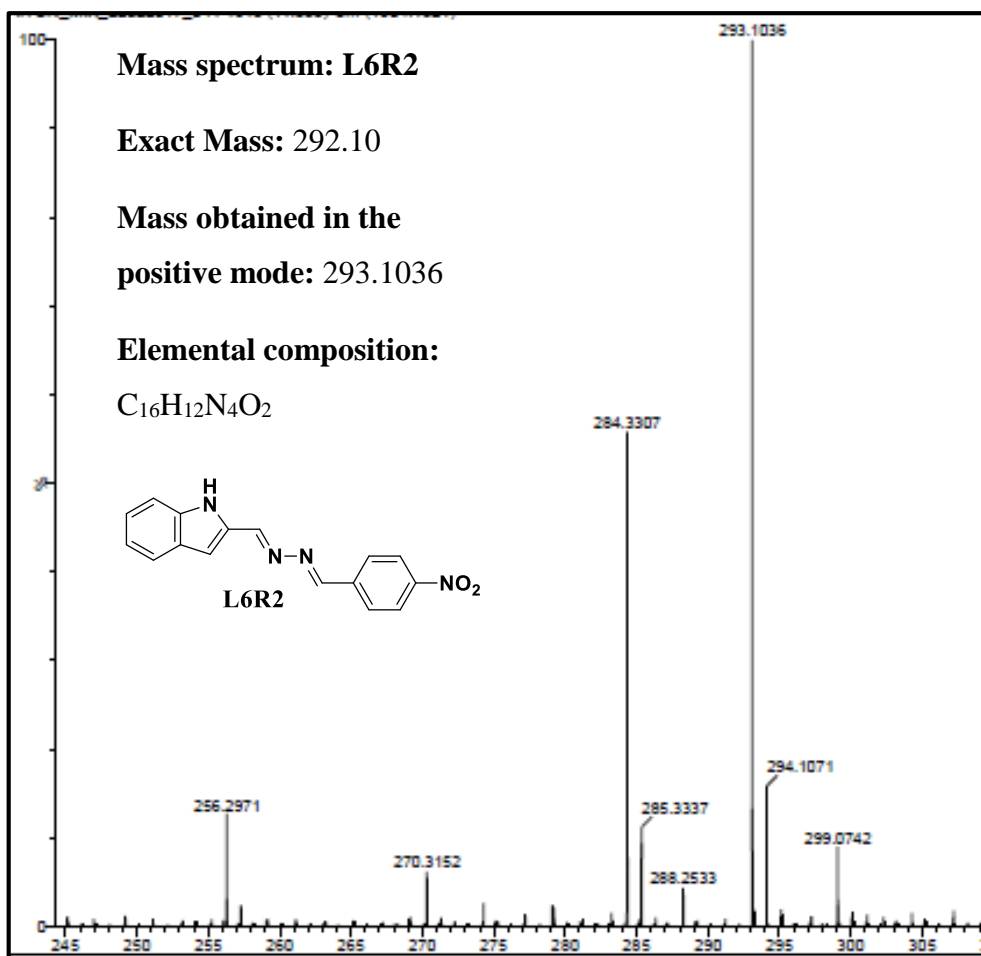
Fig. 7.15 ESI-MS spectrum of **L6R2**
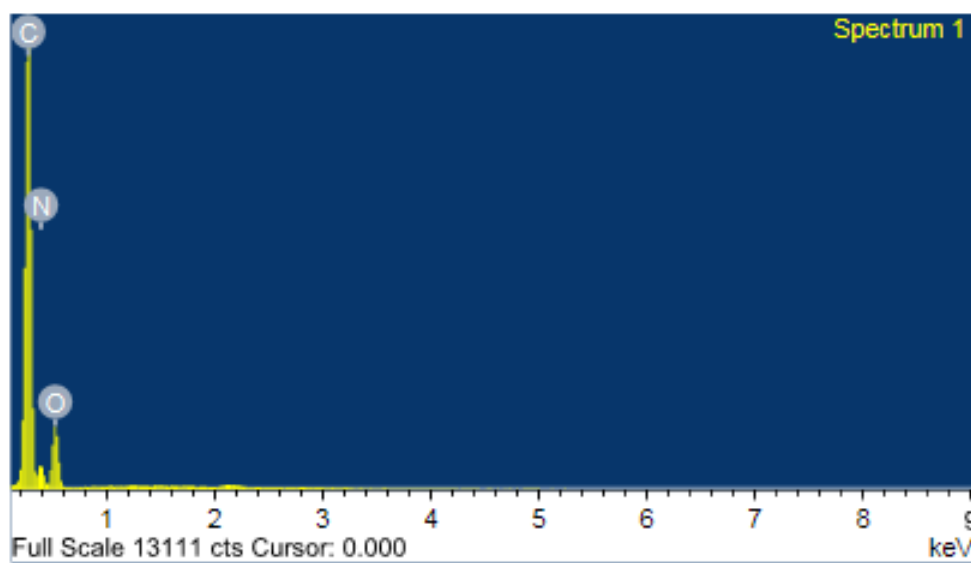
Fig. 7.16 Elemental analysis of receptor **L6R2**
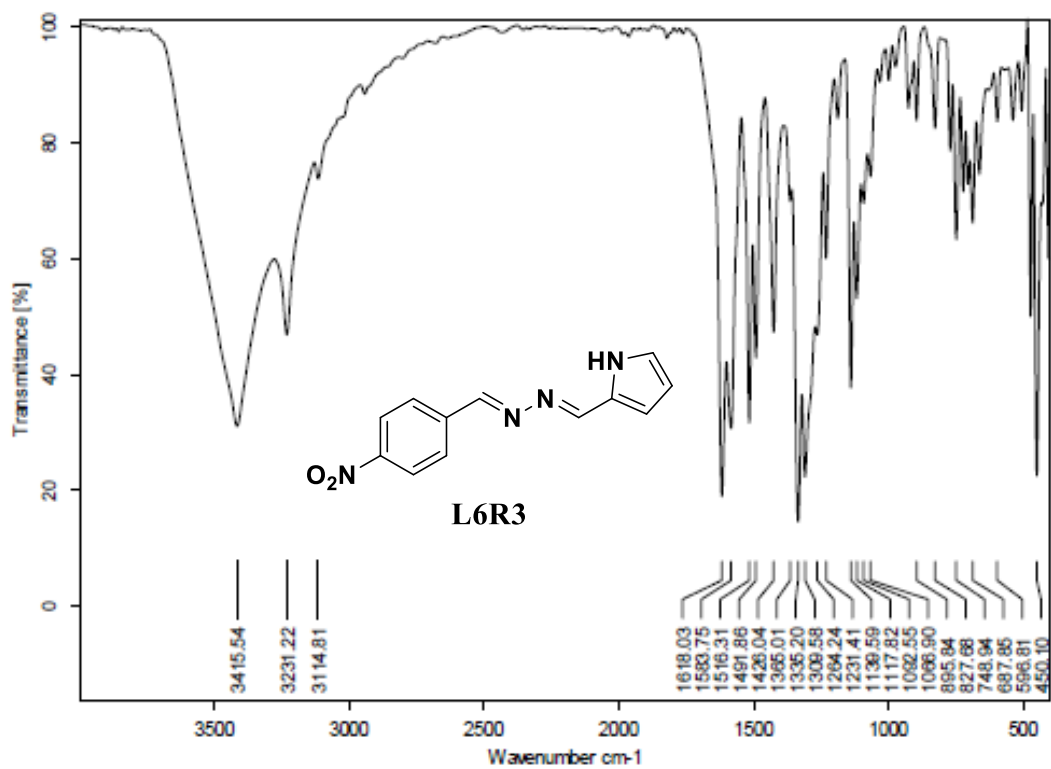
Fig. 7.17 FT-IR spectrum of receptor **L6R3**
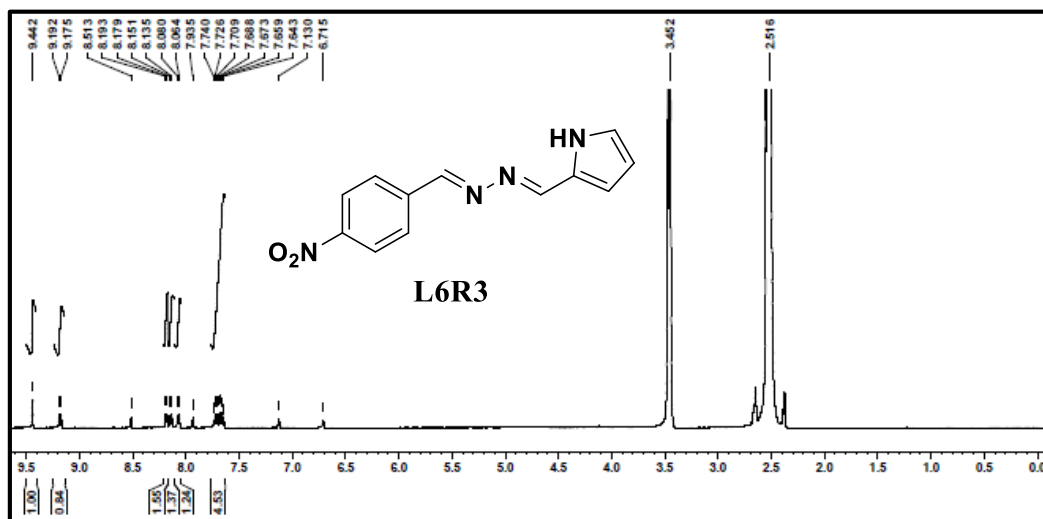
Fig. 7.18 ^{1}H-NMR spectrum of receptor **L6R3**
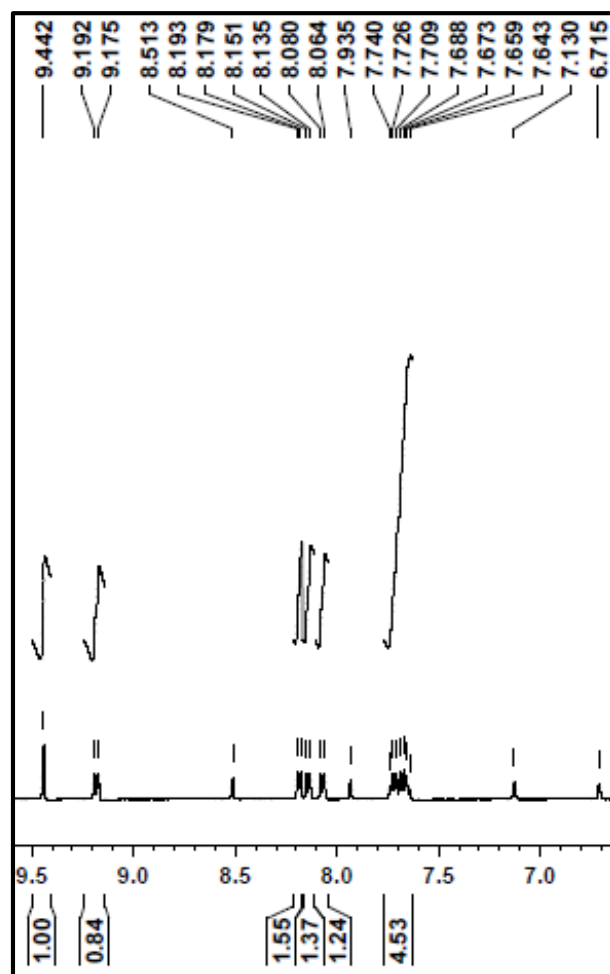
Fig. 7.19 Expanded aromatic region of receptor **L6R3**
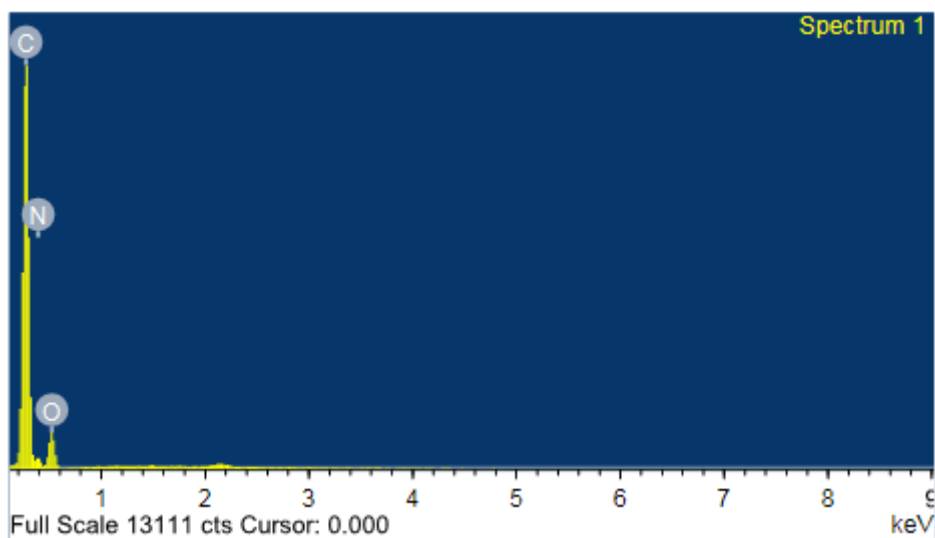
Fig. 7.20 Elemental analysis of receptor **L6R3**

Fig. 7.21 ^{13}C-NMR spectrum of receptor **L6R3**

Mass spectrum: L6R3

Exact Mass: 242.08

Mass obtained in the positive mode: 243.0882

Elemental composition:

$C_{21}H_{15}N_3O_2$
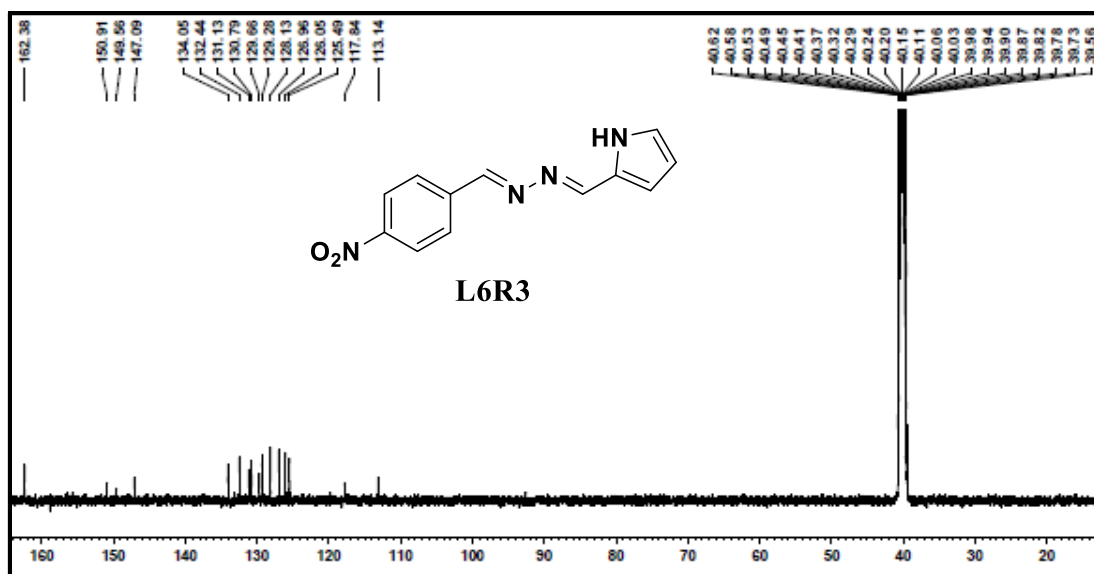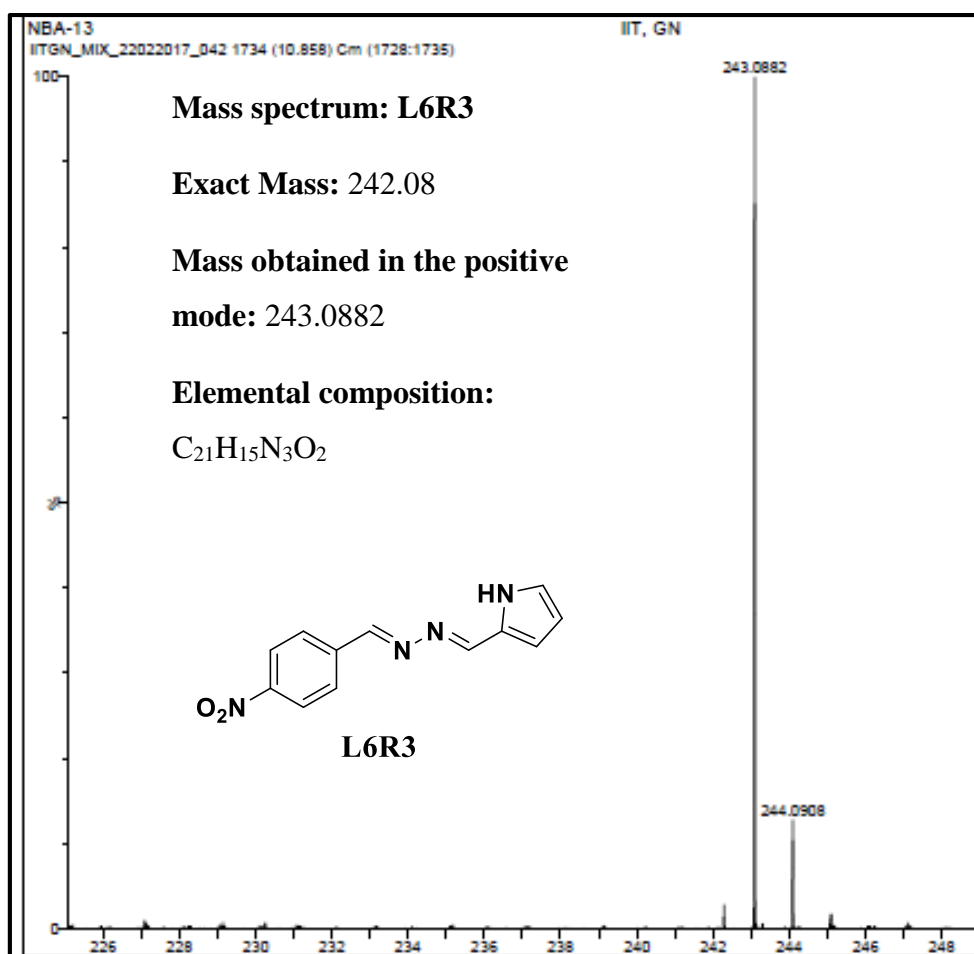
Fig. 7.22 ESI-MS spectrum of receptor **L6R3**

7.3 RESULTS AND DISCUSSIONS

7.3.1 Colorimetric detection of anions

The sensing ability of the receptors **L6R1**, **L6R2,** and **L6R3** (1×10^{-5} M in DMSO) was analyzed with the addition of a series of tetrabutylammonium salts of the anions ([Bu4N]$^+$X$^-$, X= F$^-$, Cl$^-$, Br$^-$, I$^-$, NO$_3^-$. HSO$_4^-$, H$_2$PO$_4^-$, and AcO$^-$ (1×10^{-2}M). **L6R1**, **L6R2,** and **L6R3** exhibited color change from pale yellow to orange, purple, and magenta, respectively, with the addition of 2 equiv. of F$^-$, AcO$^-$, and H$_2$PO$_4^-$ ions as depicted in Fig. 7.23. The colorimetric selectivity of the receptors **L6R1**, **L6R2,** and **L6R3** for the detection of F$^-$, AcO$^-$, and H$_2$PO$_4^-$ ions was further confirmed by using the UV-Vis spectroscopy as represented in Fig. 7.24, Fig. 7.25, and Fig. 7.26. The results indicated that **L6R1**, **L6R2,** and **L6R3** could be good sensors for multiple anions like F$^-$, AcO$^-$, and H$_2$PO$_4^-$ over competing anions in the DMSO.
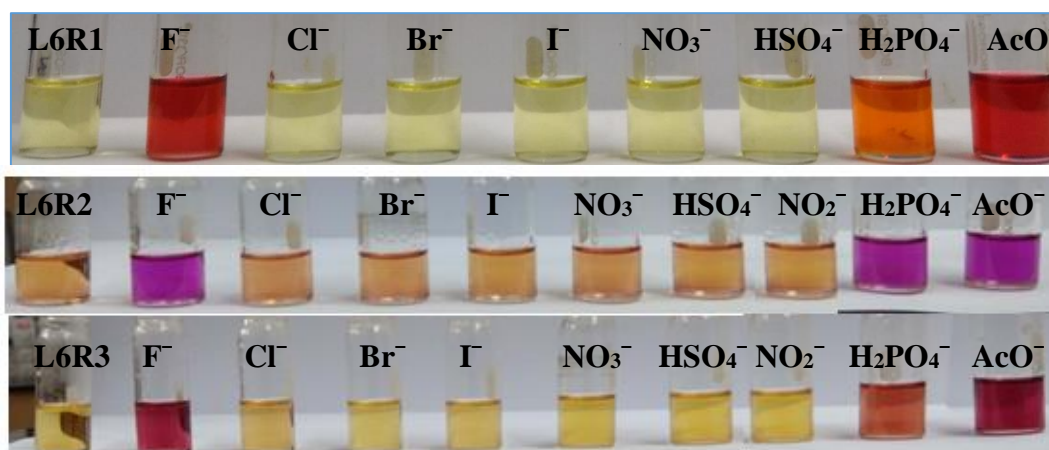
Fig. 7.23 Color change of the receptors **L6R1**, **L6R2** and **L6R3** (1×10^{-5} M in DMSO) with the addition of TBA salts of anions (1×10^{-2} M in DMSO)
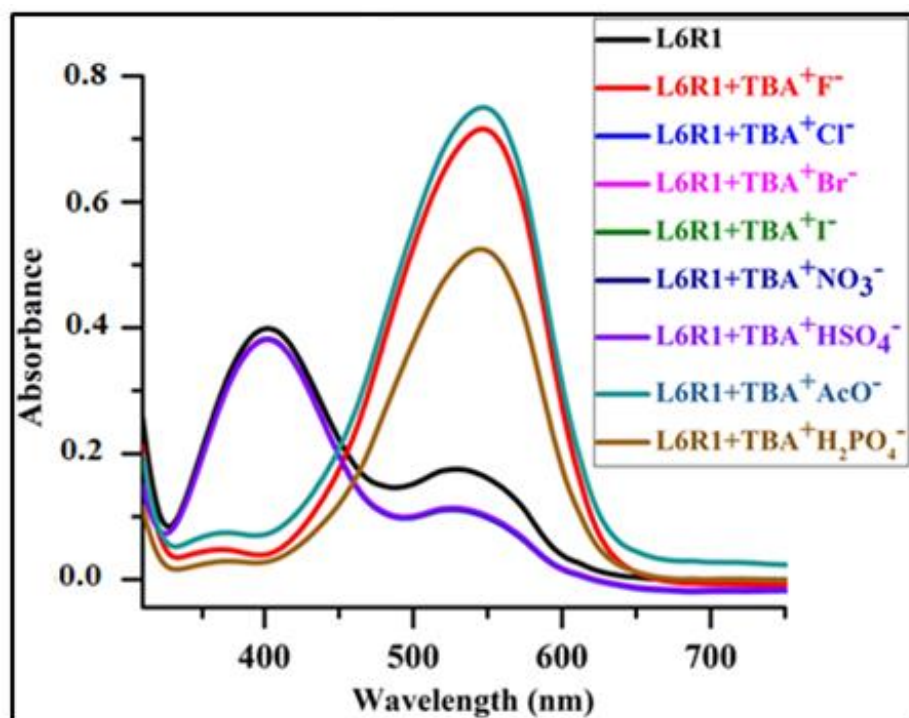
Fig. 7.24 UV-Vis absorption spectra of the receptor **L6R1** (1×10^{-5} M in DMSO) upon addition of 2 equiv of various anions as TBA salts (1×10^{-2}M in DMSO)
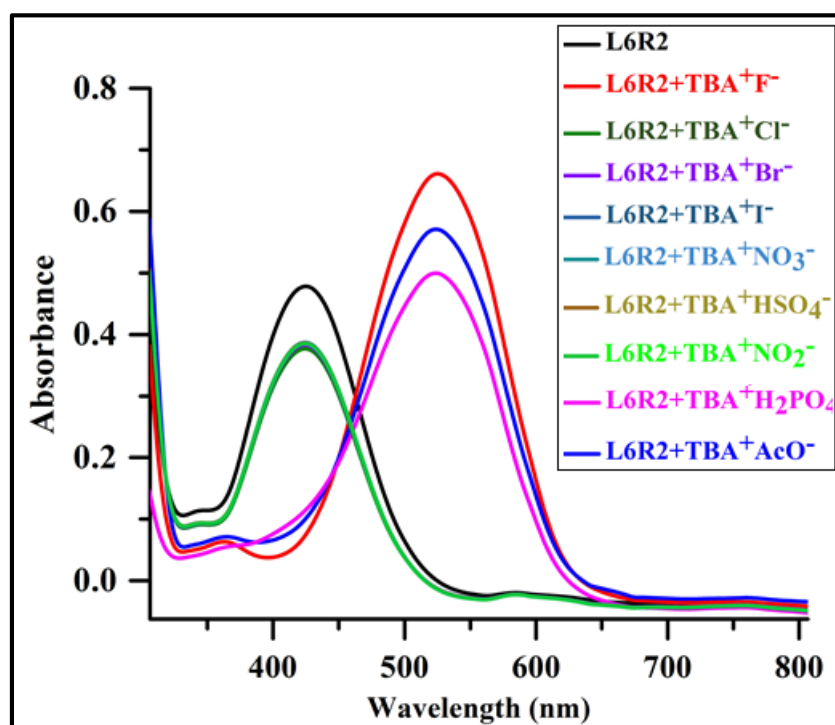
Fig. 7.25 UV-Vis absorption spectra of the receptor **L6R2** (1×10^{-5}M in DMSO) upon addition of 2 equiv of various anions as TBA salts (1×10^{-2}M in DMSO)
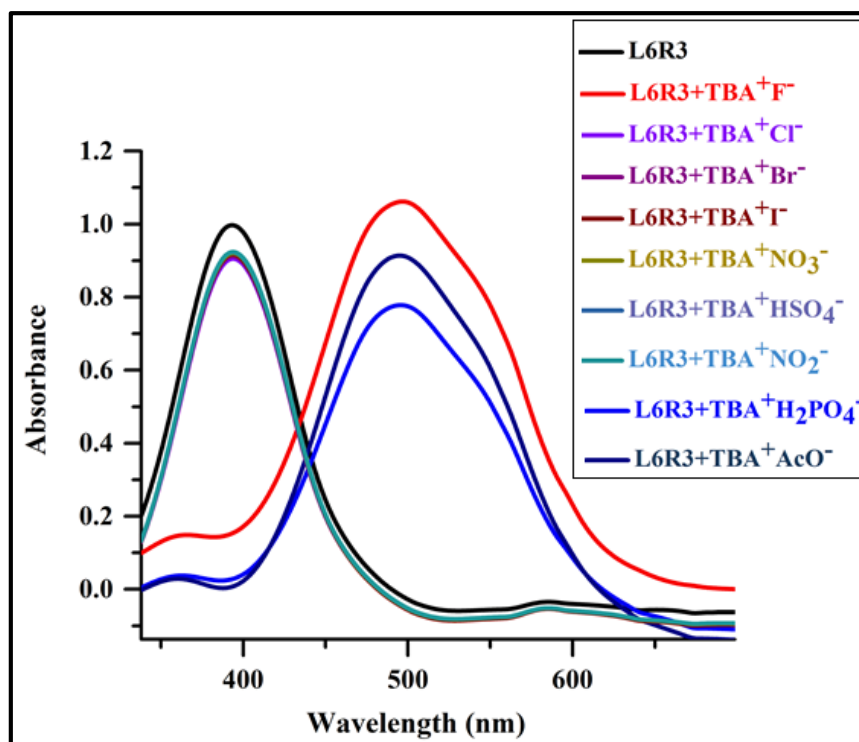
Fig. 7.26 UV-Vis absorption spectra of the receptor **L6R3** (1×10^{-5}M in DMSO) upon addition of 2 equiv of various anions as TBA salts (1×10^{-2}M in DMSO)

7.3.2 UV-Vis titration studies of receptors L6R1-L6R3 in DMSO

To further investigate the binding property of **L6R1** with F^-, AcO^-, and $H_2PO_4^-$ ions, UV-Vis titration experiments were performed. The absorption spectrum of the free receptor **L6R1** displayed a strong absorption band at 405 nm. The incremental addition of 0.1 equiv. of F^-, AcO^-, and $H_2PO_4^-$ ions to **L6R1** resulted in decrease in the band centred at 405 nm and growth of new bands at 551 nm 555 nm, and 545 nm. Bathochromic shift ($\Delta\lambda_{max}$) of 146 nm, 150 nm, and 140 nm was observed, which was attributed to the H-bonding interaction between the OH protons and the added anions. The occurrence of isosbestic points at 442 nm, 444 nm and 440 nm represented a strong complex formation between the receptor **L6R1** and the anions F^-, AcO^-, and $H_2PO_4^-$ in the DMSO. The titration profile of the receptor **L6R1** with F^-, AcO^-, and $H_2PO_4^-$ ions is presented in Fig. 7.27, Fig. 7.28, and Fig. 7.29. The plot of $1/(A-A_0)$ vs. $1/[Anions]^1$ gave a straight line confirming 1:1 binding ratio between the receptor **L6R1** and the anions (Anions= TBA^+F^-, TBA^+AcO^-, and $TBA^+H_2PO_4^-$) in the DMSO as depicted in Fig. 7.30.
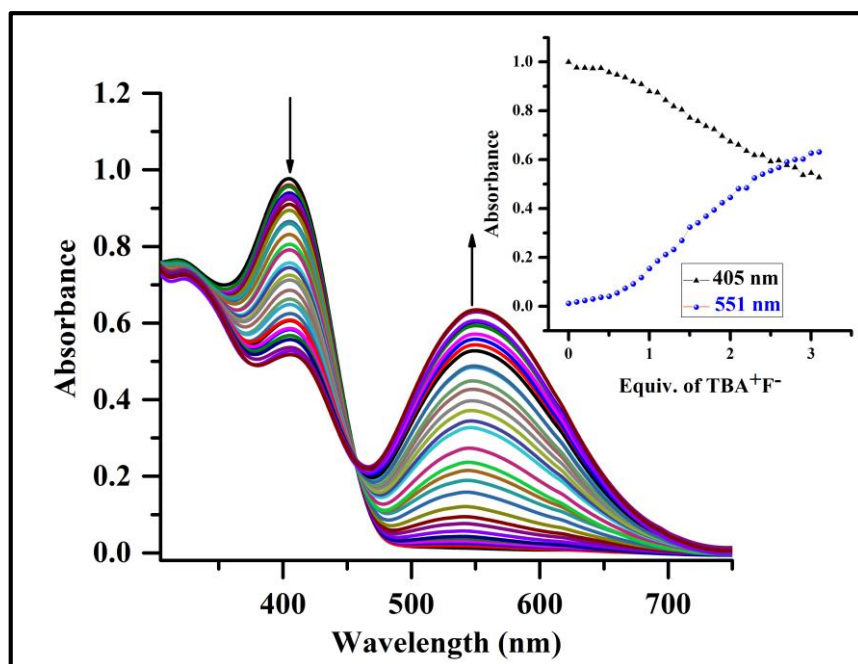
Fig. 7.27 UV- Vis titration spectra of the receptor **L6R1** (1×10^{-5} M in DMSO) with step-wise addition of 0.1 equiv. of TBA$^+$F$^-$ ion (1×10^{-2} M in DMSO); Inset plot represents the binding isotherm at 405 nm and 551 nm

Fig. 7.28 UV- Vis titration spectra of the receptor **L6R1** (1×10^{-5} M in DMSO) with step-wise addition of 0.1 equiv. of TBA$^+$AcO$^-$ ion (1×10^{-2} M in DMSO); Inset plot represents the binding isotherm at 405 nm and 555 nm
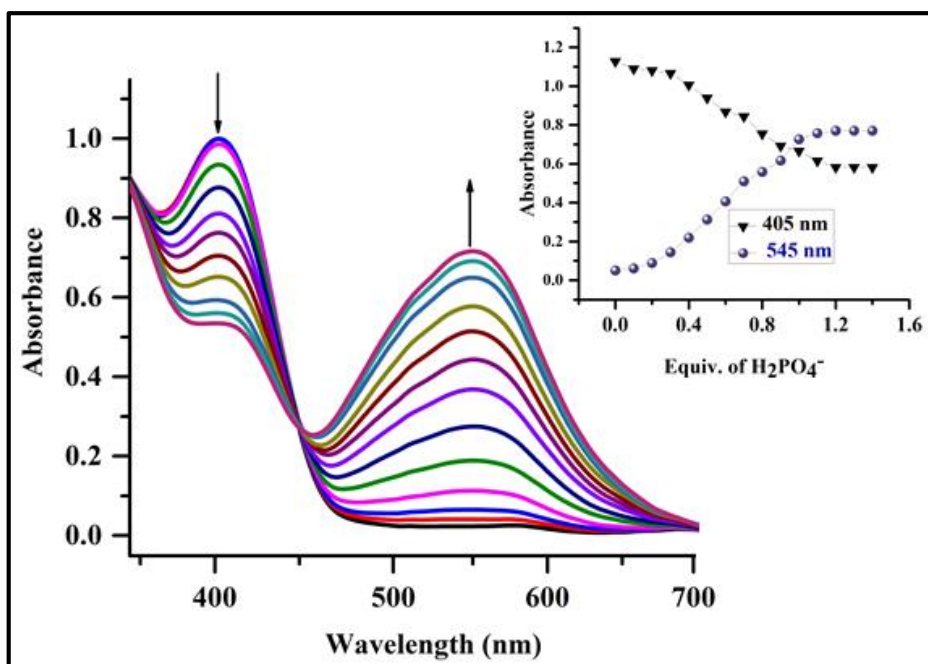
Fig. 7.29 UV- Vis titration spectra of the receptor **L6R1** (1×10^{-5} M in DMSO) with step-wise addition of 0.1 equiv. of $TBA^+H_2PO_4^-$ ion (1×10^{-2} M in DMSO); Inset plot represents the binding isotherm at 405 nm and 545 nm

Equation	y = a + b*x		
Plot	L6R1-TBAF	L6R1-TBAAcO	L6R1-TBAH2PO4
Intercept	0.26462 ± 0.03033	0.15707 ± 0.03116	1.81552 ± 0.09952
Slope	5.29562E-7 ± 1.74698E-8	1.24302E-6 ± 2.12082E-8	2.52098E-6 ± 6.57808E-8
Residual Sum of Squares	0.05379	0.13909	1.21822
Pearson's r	0.9946	0.99782	0.99527
R-Square(COD)	0.98923	0.99565	0.99056
Adj. R-Square	0.98816	0.99536	0.98988
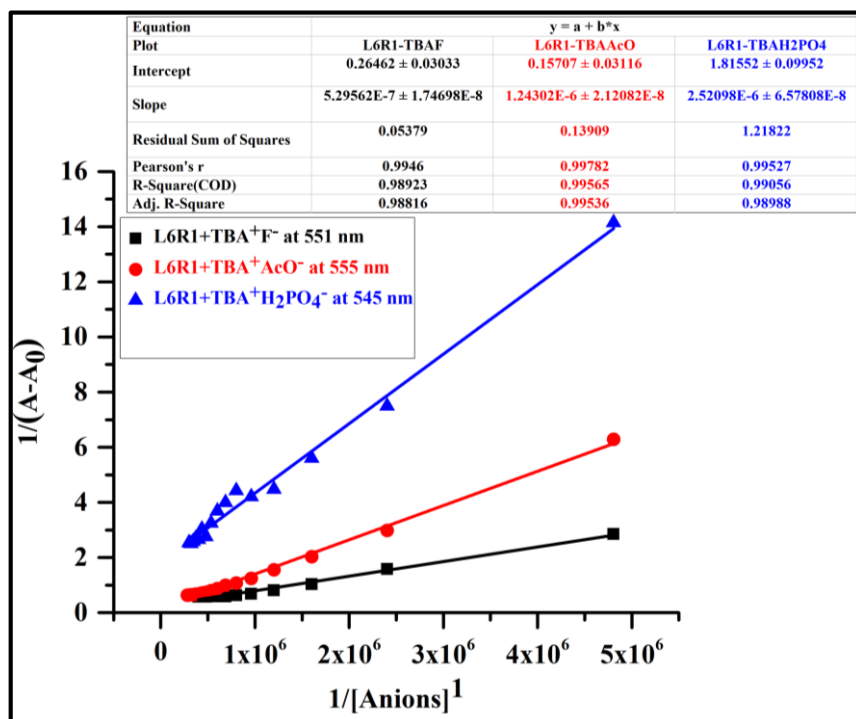
Fig. 7.30 B-H plot of receptor **L6R1**-F^-, **L6R1**-AcO^-, and **L6R1**-$H_2PO_4^-$ (TBA^+) complex at a selective wavelength of 551nm, 555 nm, and 545 nm

---

For further investigation of the complex formation, UV-Vis titration experiment was carried out with the incremental addition of F⁻, AcO⁻, and $H_2PO_4^-$ ions to the solution of the receptor **L6R2**. With the sequential addition of 0.1 equiv. of F⁻, AcO⁻, and $H_2PO_4^-$ ions to **L6R2**, the band centred at 390 nm decreased in intensity with the gradual appearance of new red shift bands at 544 nm, 542 nm, and 538 nm. The presence of isosbestic points at 444 nm, 442 nm, and 440 nm indicated that only one product was generated from **L6R2** upon binding to F⁻, AcO⁻, and $H_2PO_4^-$ ions in the binding process. This bathochromic shift of ($\Delta\lambda_{max}$) of 154 nm, 152 nm, and 148 nm was assigned to the intramolecular charge transfer (ICT) between the electron-rich (NH) and electron-deficient (NO_2) moieties in the receptor on anions binding, resulting in visible color change through the push-pull mechanism. The titration profiles are represented in Fig. 7.31, Fig. 7.32, and Fig. 7.33. The B-H plot for the **L6R2**- F⁻, **L6R2**-AcO⁻, and **L6R2**- $H_2PO_4^-$ complexes yielded a linear plot with second power concentration of the anions indicating strong hydrogen-bond formation, followed by deprotonation of the receptor. The B-H plot with F⁻, AcO⁻, and $H_2PO_4^-$ ions is shown in Fig. 7.34.
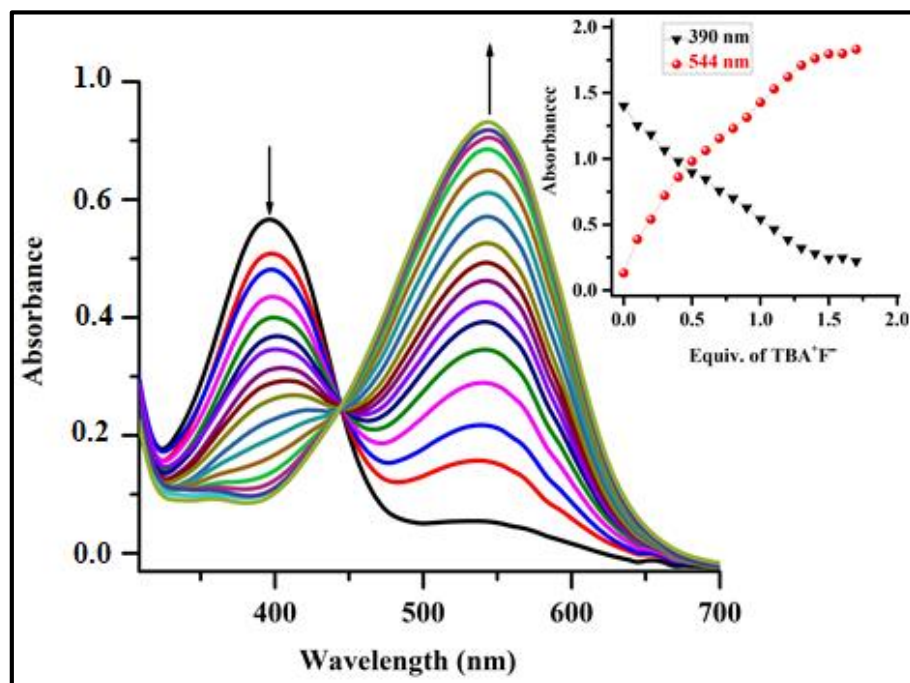
Fig. 7.31 UV- Vis titration spectra of the receptor **L6R2** (1×10^{-5} M in DMSO) with step-wise addition of 0.1 equiv. of TBA^+F^- ion (1×10^{-2} M in DMSO); Inset plot represents the binding isotherm at 390 nm and 544 nm
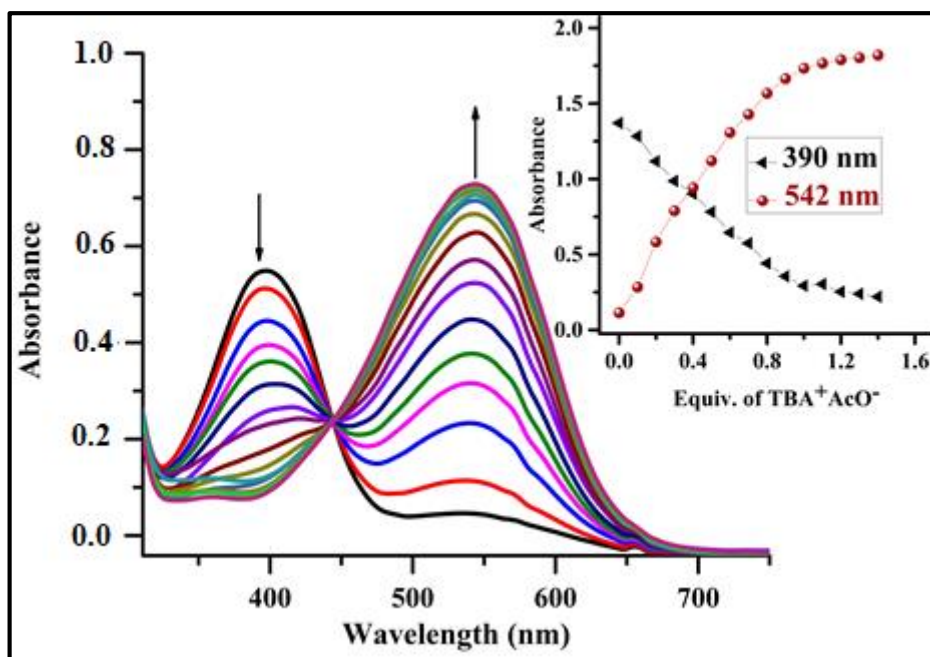
Fig. 7.32 UV- Vis titration spectra of the receptor **L6R2** (1×10^{-5} M in DMSO) with step-wise addition of 0.1 equiv. of TBA^+AcO^- ion (1×10^{-2} M in DMSO); Inset plot represents the binding isotherm at 390 nm and 542 nm
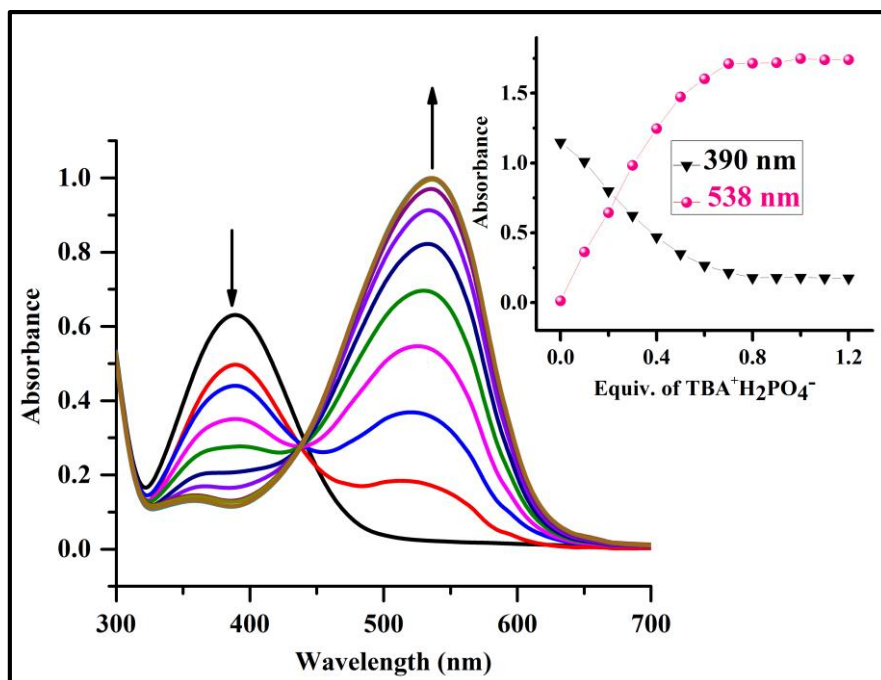
Fig. 7.33 UV- Vis titration spectra of the receptor **L6R2** (1×10^{-5} M in DMSO) with step-wise addition of 0.1 equiv. of $TBA^+H_2PO_4^-$ ion (1×10^{-2} M in DMSO); Inset plot represents the binding isotherm at 390 nm and 538 nm

Equation	y = a + b*x		
Plot	L6R2-TBAF	L6R2-TBAAcO	L6R2-TBAH2PO4
Intercept	0.54007 ± 0.01293	0.39793 ± 0.06456	0.34739 ± 0.04291
Slope	1.31391E-12 ± 1.64038E-14	8.98094E-13 ± 3.64427E-14	9.1658E-13 ± 4.57964E-14
Residual Sum of Squares	0.02767	0.49534	0.12169
Pearson's r	0.99883	0.99026	0.98775
R-Square(COD)	0.99767	0.98062	0.97564
Adj. R-Square	0.99751	0.97901	0.97321
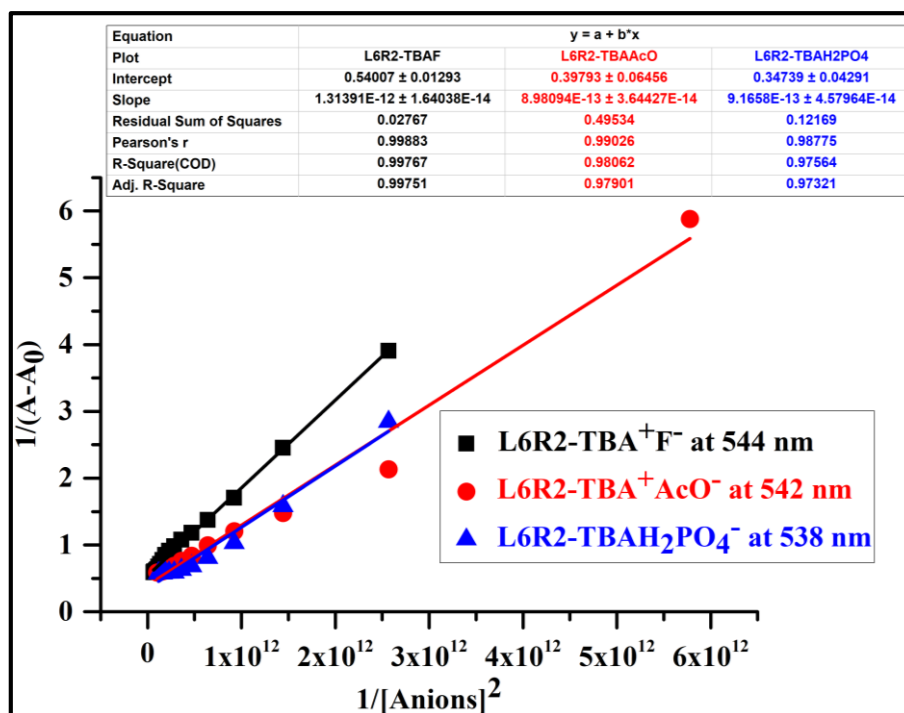
Fig. 7.34 B-H plot of receptor **L6R2**-F⁻, **L6R2**-AcO⁻, and **L6R2**-$H_2PO_4^-$ (TBA⁺) complex at a selective wavelength of 544 nm, 542 nm, and 538 nm

Further to confirm the anion binding modes of the receptor **L6R2**, UV-Vis titration was performed with the incremental addition of TBA⁺OH⁻ in the DMSO. As illustrated in Fig. 7.35, the absorption band induced by TBA⁺OH⁻ matched well with the band formed in the presence of TBA⁺F⁻ and TBA⁺AcO⁻. The result clearly demonstrated that both anions functioned here as base, giving rise to deprotonation upon interaction with the receptor **L6R2**. This reflected the deprotonation process of NH by basic F⁻ and AcO⁻ ions in the DMSO, resulting in colorimetric response.
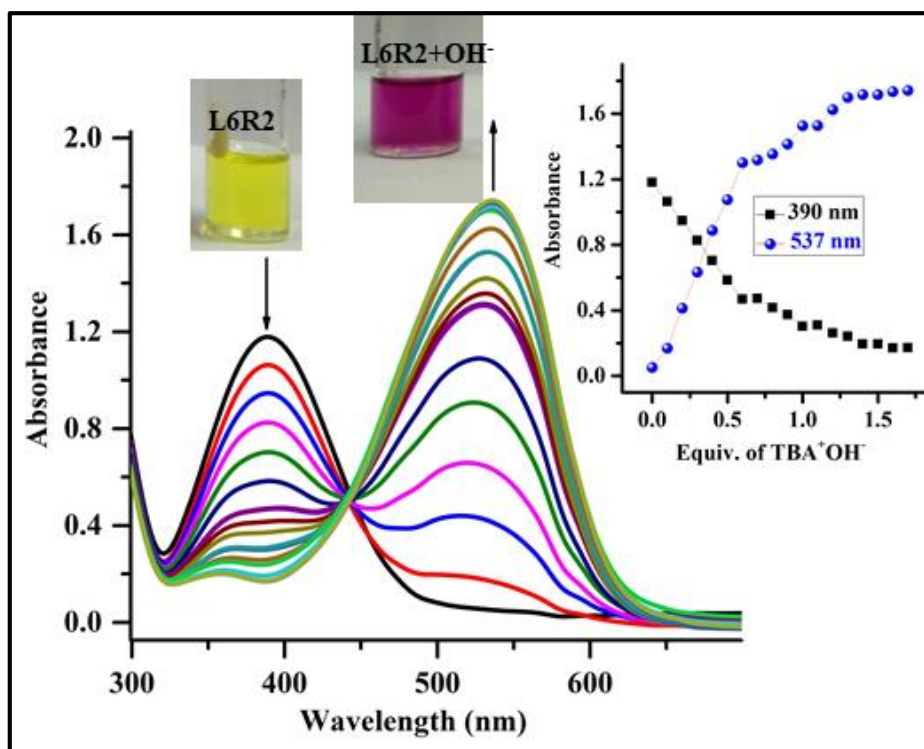
Fig. 7.35 UV- Vis titration spectra of receptor the **L6R2** (1×10^{-5} M in DMSO) with step-wise addition of 0.1 equiv. of TBA^+OH^- ion (1×10^{-2} M in DMSO); Inset plot represents the binding isotherm at 390 nm and 537 nm

To understand the nature of the receptor-anion interaction, UV-Vis titration experiment was conducted by incremental addition of F^-, AcO^-, and $H_2PO_4^-$ ions to **L6R3** in the DMSO. The constant increase in equiv. of F^-, AcO^-, and $H_2PO_4^-$ ions resulted in steady decrease in intensity of the absorbance band at 385 nm. Meanwhile, new absorption bands at 514 nm, 510 nm, and 485 nm appeared and intensity of the absorption bands increased continuously with the increasing concentration of F^-, AcO^-, and $H_2PO_4^-$ ions. The titration spectra are represented in Fig. 7.36, Fig. 7.37, and Fig. 7.38. The bathochromic shift ($\Delta\lambda_{max}$) of 129 nm, 125 nm, and 100 nm in the absorption maxima was due to intramolecular charge transfer. The presence of well-defined isosbestic points at 436 nm, 434 nm, and 429 nm suggested the complex formation process and equilibrium between the free receptor **L6R3** and the anion-receptor complex with F^-, AcO^-, and $H_2PO_4^-$ in the DMSO. The B-H plot indicating 1:2 binding ratio of **L6R3** with F^-, AcO^-, and $H_2PO_4^-$ ions is shown in Fig. 7.39.
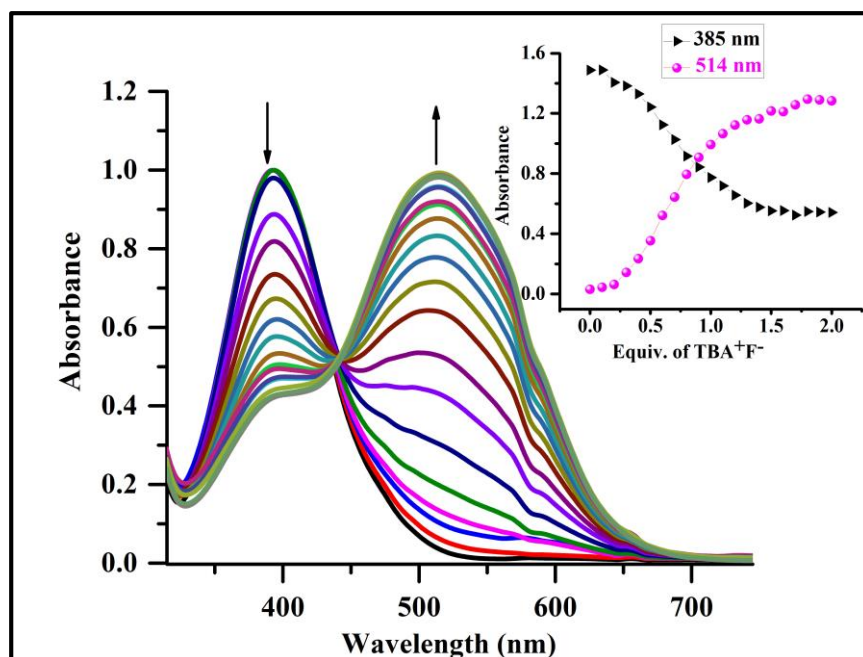
Fig. 7.36 UV- Vis titration spectra of the receptor **L6R3** (1×10^{-5} M in DMSO) with step-wise addition of 0.1 equiv. of TBA$^+$F$^-$ ion (1×10^{-2} M in DMSO); Inset plot represents the binding isotherm at 385 nm and 514 nm
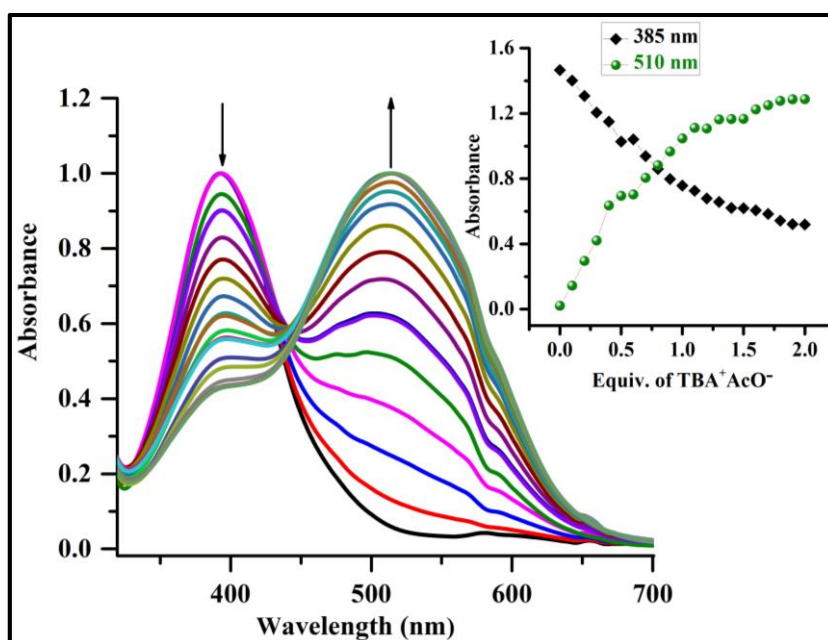
Fig. 7.37 UV- Vis titration spectra of the receptor **L6R3** (1×10^{-5} M in DMSO) with step-wise addition of 0.1 equiv. of TBA$^+$AcO$^-$ ion (1×10^{-2} M in DMSO); Inset plot represents the binding isotherm at 385 nm and 510 nm
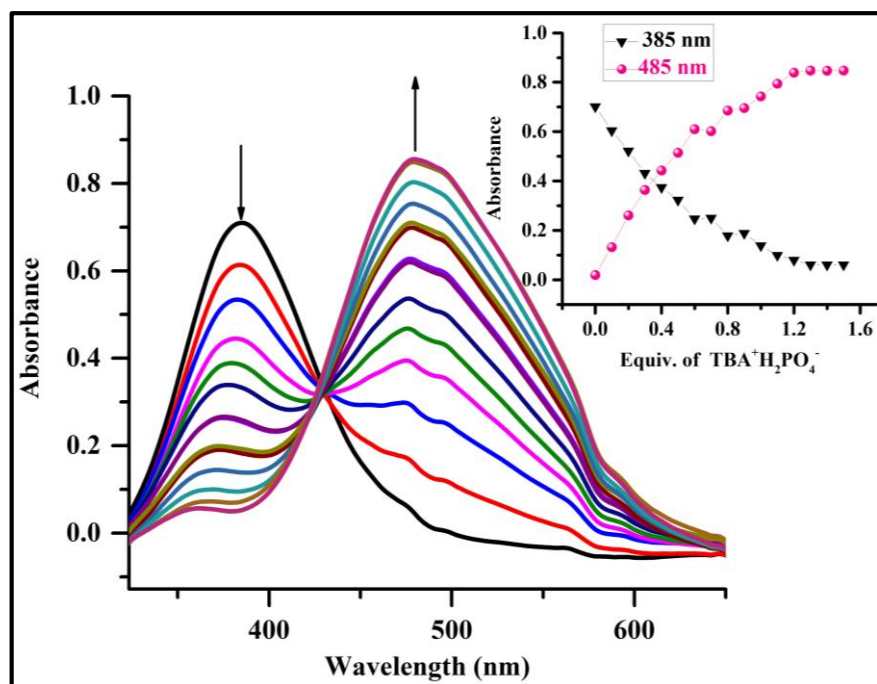
Fig. 7.38 UV- Vis titration spectra of the receptor **L6R3** (1×10^{-5} M in DMSO) with step-wise addition of 0.1 equiv. of TBA$^+$H$_2$PO$_4^-$ ion (1×10^{-2} M in DMSO); Inset plot represents the binding isotherm at 385 nm and 485 nm

Equation	y = a + b*x		
Plot	L66R3+TBAF	L6R3+TBAAcO	L6R3+TBAH2PO4
Intercept	1.01521 ± 0.24186	0.64466 ± 0.0277	0.77892 ± 0.11876
Slope	1.18514E-11 ± 3.0672	2.0849E-12 ± 3.8084	2.88251E-12 ± 1.415
Residual Sum of S	9.67578	0.19046	1.6914
Pearson's r	0.99501	0.99701	0.98469
R-Square(COD)	0.99005	0.99403	0.96961
Adj. R-Square	0.98939	0.9937	0.96727
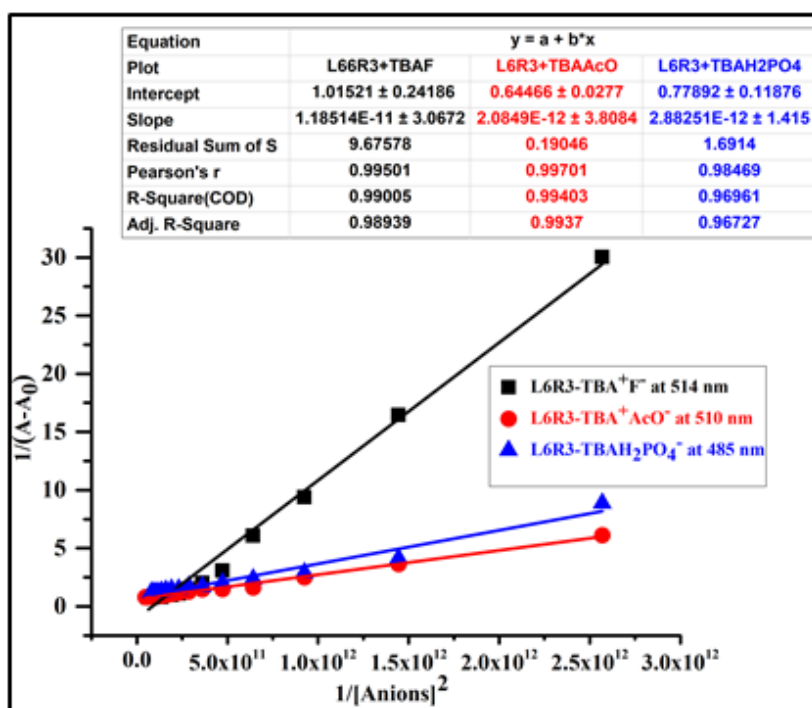
Fig. 7.39 B-H plot of receptor **L6R3**-F$^-$, **L6R3**-AcO$^-$, and **L6R3**-H$_2$PO$_4^-$ (TBA$^+$) complex at a selective wavelength of 514 nm, 510 nm, and 485 nm

7.3.3 UV-Vis titration studies of receptors L6R1-L6R3 in organo-aqueous medium DMSO: H₂O (9:1 v/v)

Generally, protic solvents such as water compete with anions for the host binding sites, and thereby, impede the interaction between the host and guest. That is why the direct sensing of anions in aqueous media has proved to be quite difficult. Moreover, the detection of sodium salts of anions by the receptors is highly necessary as it paves the way for practical application. Fluoride, acetate, and phosphate are found in the form of sodium salts at the physiological level. These have encroached into household usage in the form of food, medicine, and cosmetics. Beyond an optimum amount, anions can lead to health issues. With this in view, proves to be of essence to develop sensors, which can detect anions in aqueous media. In this regard, anion binding studies were performed in the organo-aqueous medium DMSO: H₂O (9:1 v/v) with the addition of sodium salts of F^-, AcO^-, $H_2PO_4^-$, and AsO_2^-.

UV-Vis titration studies were conducted with the sequential addition of F^- and AcO^- ions (1×10^{-2}M in distilled water) to a measured quantity of the receptor **L6R1** solution of (1×10^{-5} M) in aqueous DMSO (9:1 v/v). The absorption band at 405 nm decreased at the expense of new bands at 543 nm and 542 nm and accounted for vivid color change from pale yellow to pink as illustrated in Fig. 7.40. The titration profiles are shown in Fig. 7.41 and Fig. 7.42. The B-H plot is shown in Fig. 7.43 for **L6R1**-F^- and **L6R1**-AcO^- complex suggesting 1:1 binding ratio.
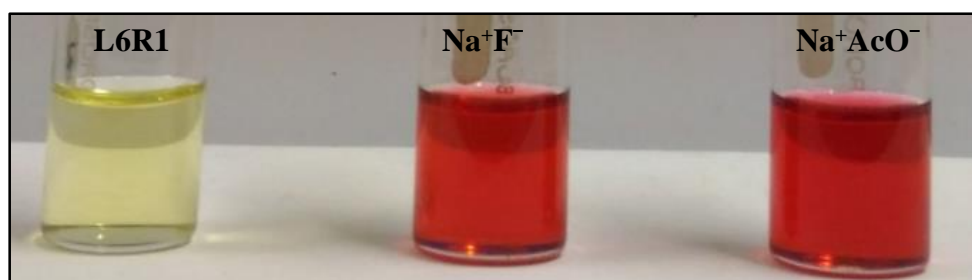
Fig. 7.40 Color change of the receptor **L6R1** (1×10^{-5} M in DMSO) upon addition of 2 equiv. of sodium salts of F^- and AcO^- (1×10^{-2}M in distilled water) in DMSO: H₂O (9:1 v/v)
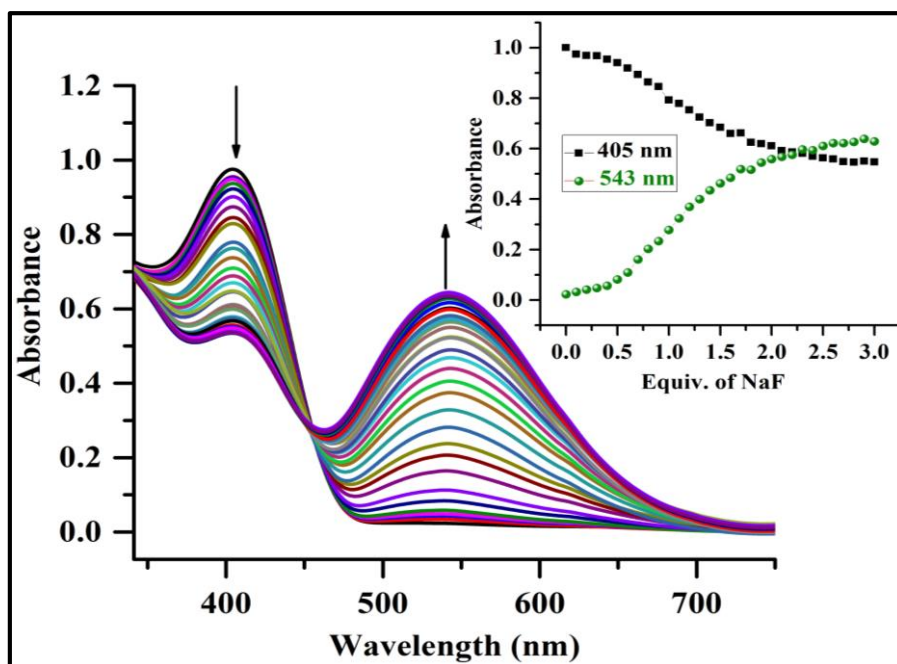
Fig. 7.41 UV- Vis titration spectra of the receptor **L6R1** (1×10^{-5} M in DMSO) with step-wise addition of 0.1 equiv. of Na^+F^- ion (1×10^{-2} M H_2O) in DMSO: H_2O (9:1 v/v); Inset plot represents the binding isotherm at 405 nm and 543 nm
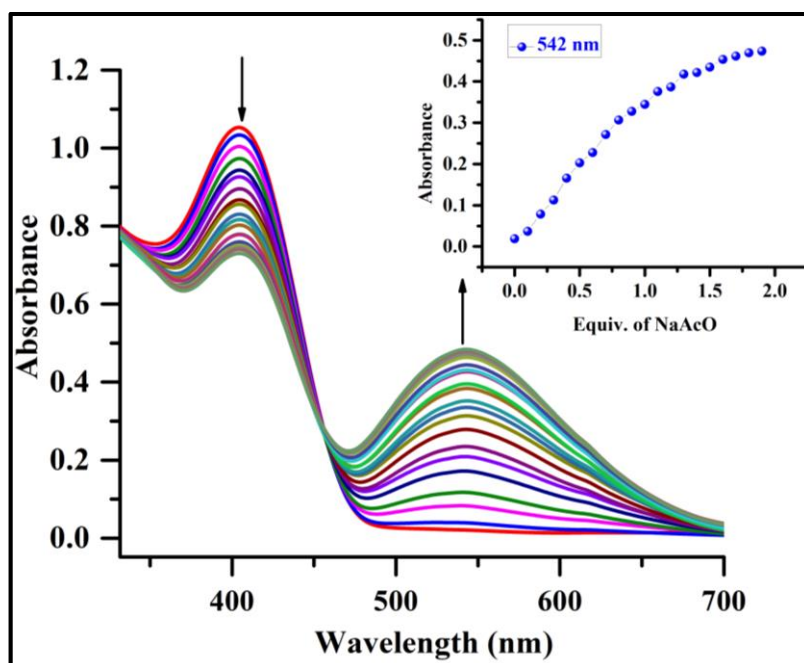
Fig. 7.42 UV- Vis titration spectra of the receptor **L6R1** (1×10^{-5} M in DMSO) with step-wise addition of 0.1 equiv. of Na^+AcO^- ion (1×10^{-2} M H_2O) in DMSO: H_2O (9:1 v/v); Inset plot represents the binding isotherm at 542 nm

Equation	y = a + b*x	
Plot	L6R1+NaF	L6R1+NaAcO
Intercept	0.51827 ± 0.06487	0.88149 ± 0.02599
Slope	1.6566E-6 ± 4.15667E-8	1.42971E-6 ± 1.61095E-8
Residual Sum of Squares	0.43942	0.05908
Pearson's r	0.99593	0.99924
R-Square(COD)	0.99188	0.99848
Adj. R-Square	0.99126	0.99835
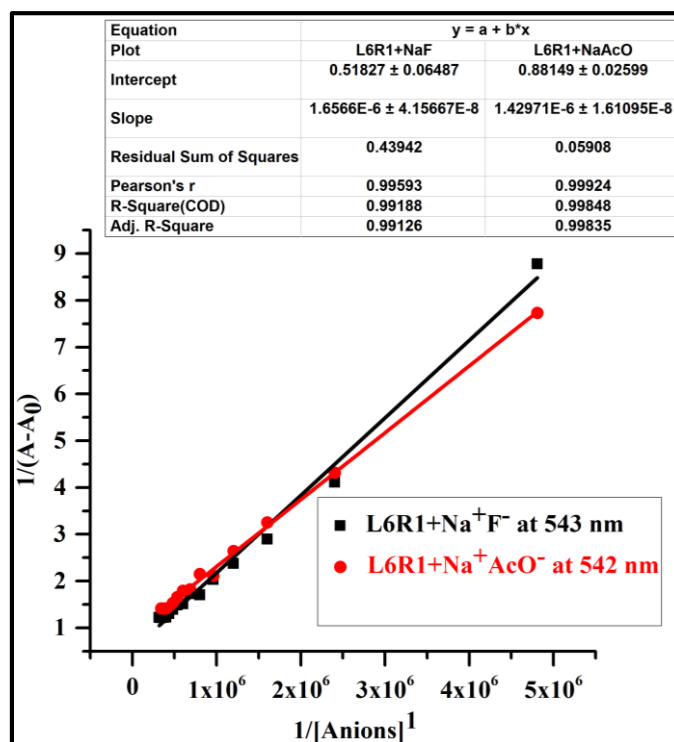
Fig. 7.43 B-H plot of receptor **L6R1**-F⁻ and **L6R1-**AcO⁻ (Na⁺) complex at a selective wavelength of 543 nm and 542 nm

Interestingly, the introduction of the electron-withdrawing substituent into the receptors significantly increased the acidity of the binding sites and selectivity towards the anions. Therefore, the receptors **L6R2** and **L6R3** can more effectively compete with water for the naked eye detection of Na^+F^-, Na^+AcO^-, $Na^+H_2PO_4^-$, and $Na^+AsO_2^-$ via dramatic color change as shown in Fig. 7.44. The receptors **L6R2** and **L6R3** showed significant red shift, which was comparable to the titration studies performed in 100 % DMSO solvent. The titration profiles of the receptors **L6R2,** and **L6R3** with the addition of active sodium anions in the DMSO: H_2O (9:1 v/v) are represented in Fig. 7.45, Fig. 7.46, Fig. 7.47, Fig. 7.48, Fig. 7.49, Fig. 7.50, Fig. 7.51, and Fig. 7.52. The appearance of clear isosbestic point indicates complex formation between the receptor and the anion surpassing the solvent interference in the binding process. The B-H plots represents 1:2 binding ratio between the receptors and target anions complex in DMSO: H_2O (9:1 v/v). The B-H plots of **L6R2**-Na^+F^-, **L6R2**-Na^+AcO^-, **L6R2**-$Na^+H_2PO_4^-$, **L6R2**- $Na^+AsO_2^-$, **L6R3**-Na^+F^-, **L6R3**-Na^+AcO^-, **L6R3**- $Na^+H_2PO_4^-$, and **L6R3**-$Na^+AsO_2^-$ are shown in Fig. 7.5 and Fig. 7.54. The bathochromic shift ($\Delta\lambda_{max}$) of the

receptors **L6R1**, **L6R2,** and **L6R3** in the presence of the TBA salts of F^-, AcO^-, and $H_2PO_4^-$ in DMSO and the sodium salts of F^-, AcO^-, $H_2PO_4^-$, and AsO_2^- ions in DMSO: H_2O (9:1 v/v) is summarized in Table 7.1.
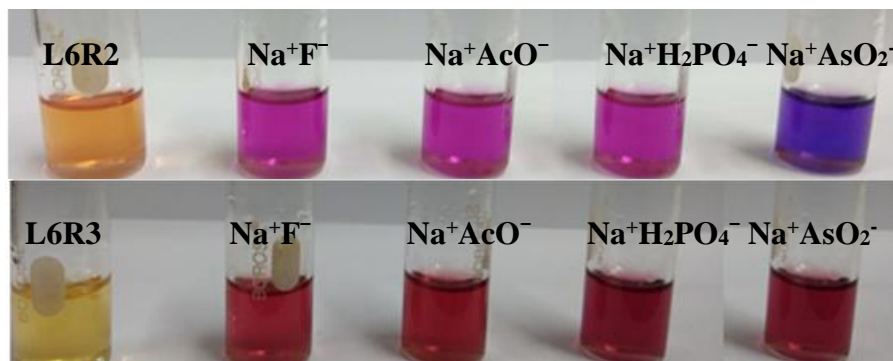
Fig. 7.44 Color change of receptor **L6R2** and **L6R3** (1×10^{-5} M) upon addition of 2 equiv. of sodium salts of F^-, AcO^-, $H_2PO_4^-$, and AsO_2^- (1×10^{-2}M in distilled water) in DMSO: H_2O (9:1 v/v)
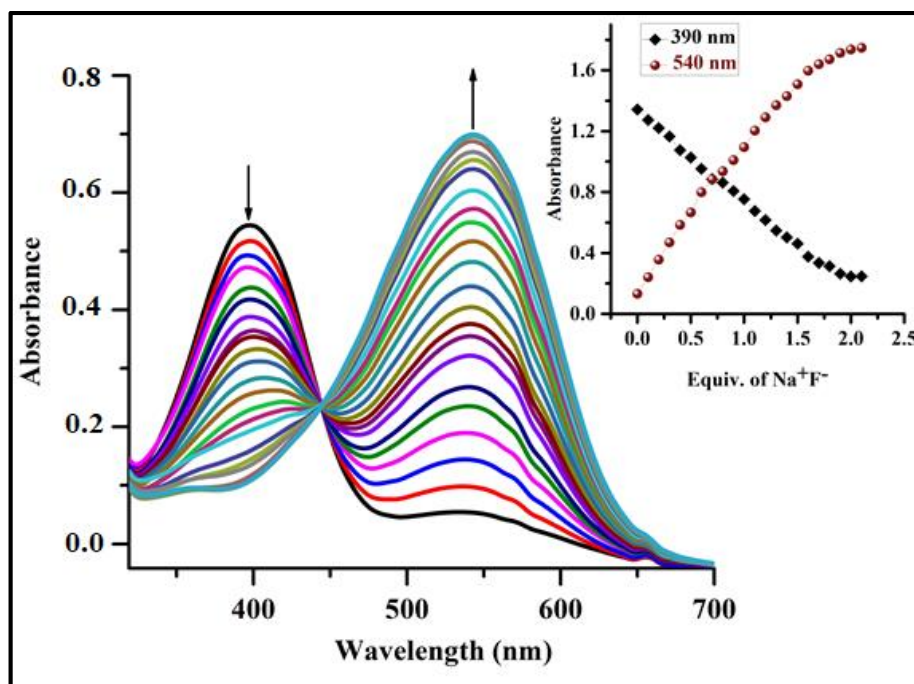
Fig. 7.45 UV- Vis titration spectra of receptor **L6R2** (1×10^{-5} M in DMSO) with step-wise addition of 0.1 equiv. of Na^+F^- ion (1×10^{-2} M H_2O) in DMSO: H_2O (9:1 v/v); Inset plot represents the binding isotherm at 390 nm and 540 nm
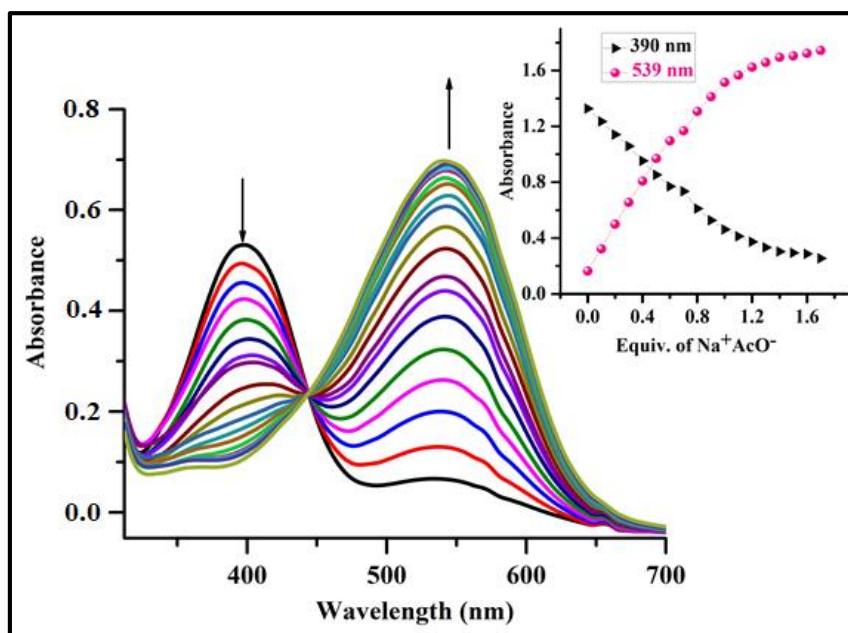
Fig. 7.46 UV- Vis titration spectra of receptor the **L6R2** (1×10^{-5} M in DMSO) with step-wise addition of 0.1 equiv. of Na^+AcO^- ion (1×10^{-2} M H_2O) in DMSO: H_2O (9:1 v/v); Inset plot represents the binding isotherm at 390 nm and 539 nm
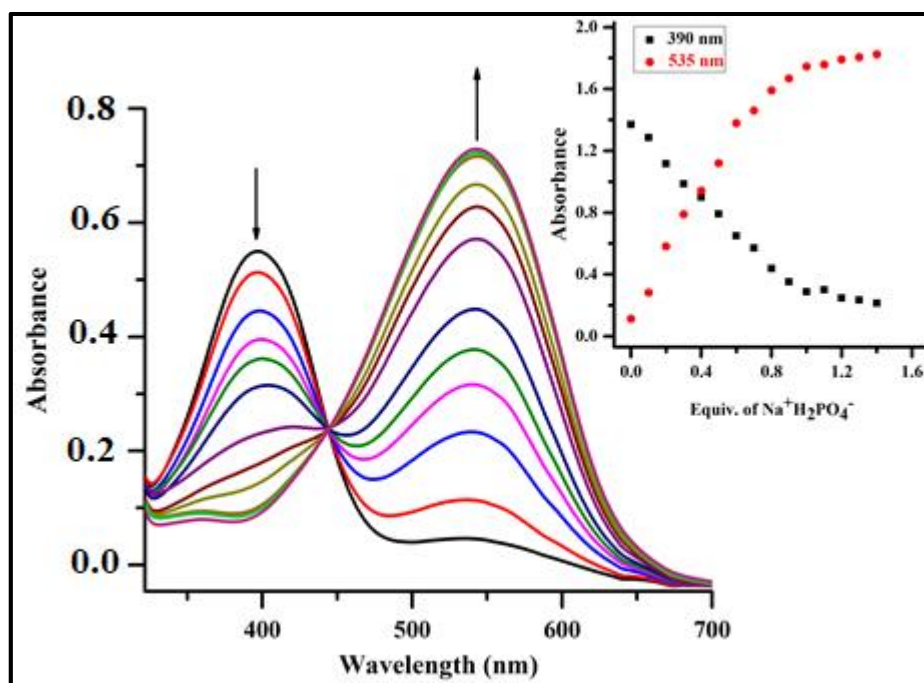
Fig. 7.47 UV- Vis titration spectra of receptor the **L6R2** (1×10^{-5} M in DMSO) with step-wise addition of 0.1 equiv. of $Na^+H_2PO_4^-$ ion (1×10^{-2} M H_2O) in DMSO: H_2O (9:1 v/v); Inset plot represents the binding isotherm at 390 nm and 535 nm
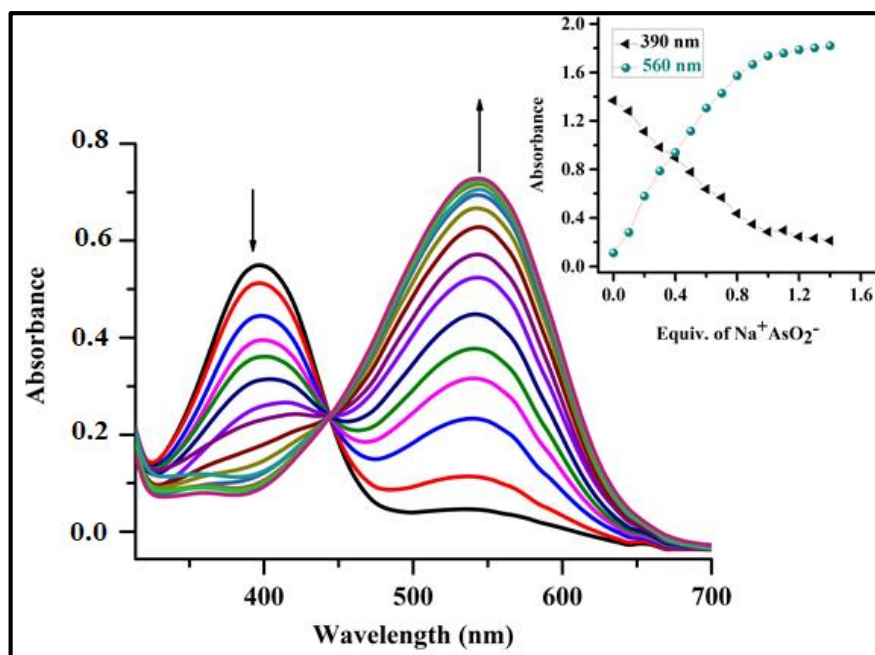
Fig. 7.48 UV- Vis titration spectra of receptor **L6R2** (1×10^{-5} M in DMSO) with step-wise addition of 0.1 equiv. of $Na^+AsO_2^-$ ion (1×10^{-2} M H_2O) in DMSO: H_2O (9:1 v/v); Inset plot represents the binding isotherm at 390 nm and 560 nm
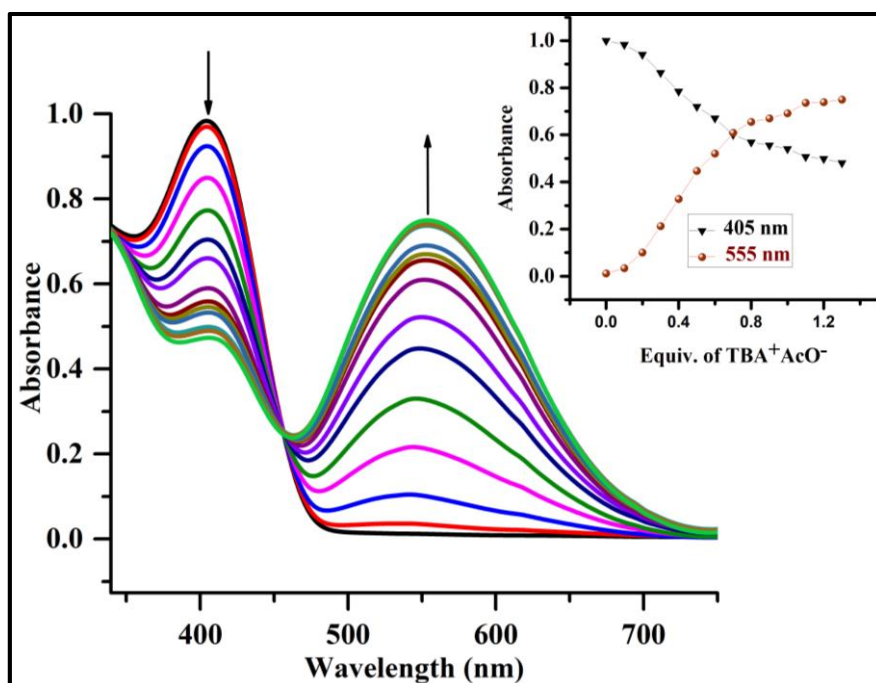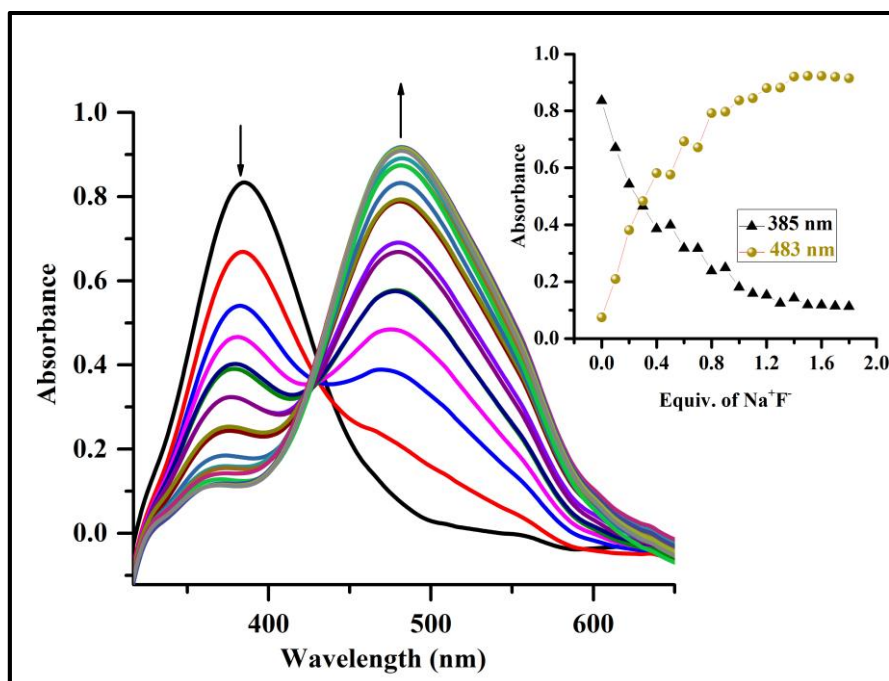

Fig. 7.49 UV- Vis titration spectra of the receptor **L6R3** (1×10^{-5} M in DMSO) with step-wise addition of 0.1 equiv. of Na^+F^- ion (1×10^{-2} M H_2O) in DMSO: H_2O (9:1 v/v); Inset plot represents the binding isotherm at 385 nm and 483 nm
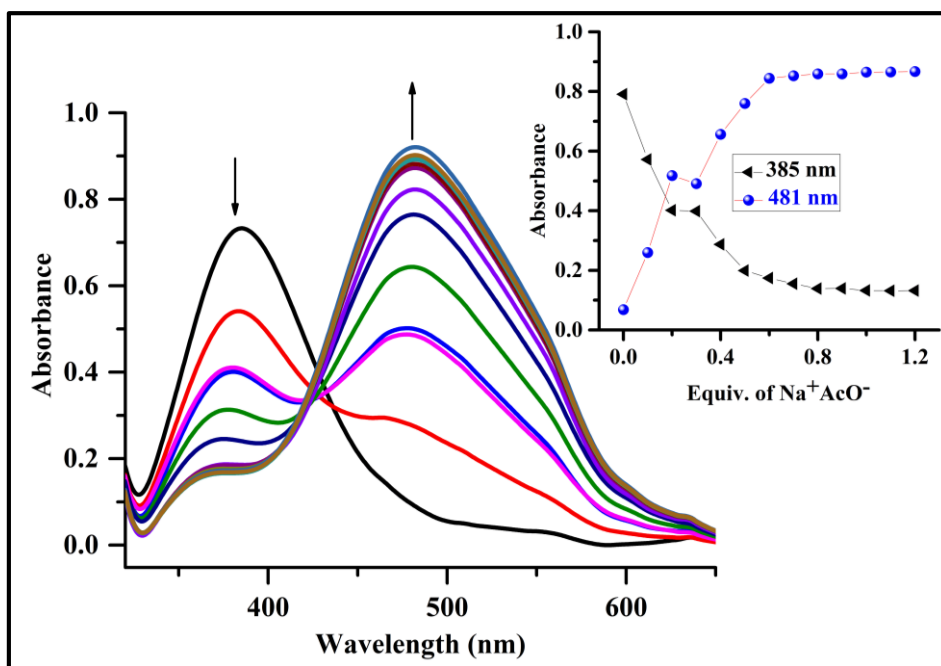
Fig. 7.50 UV- Vis titration spectra of receptor the **L6R3** (1×10^{-5} M in DMSO) with step-wise addition of 0.1 equiv. of Na^+AcO^- ion (1×10^{-2} M H_2O) in DMSO: H_2O (9:1 v/v); Inset plot represents the binding isotherm at 385 nm and 481 nm
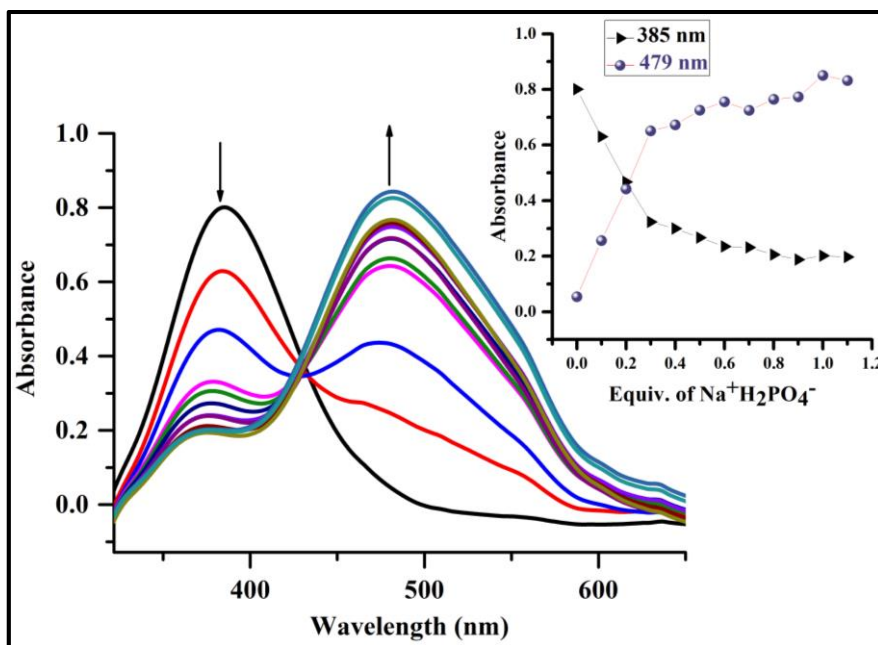
Fig. 7.51 UV- Vis titration spectra of receptor **L6R3** (1×10^{-5} M in DMSO) with step-wise addition of 0.1 equiv. of $Na^+H_2PO_4^-$ ion (1×10^{-2} M H_2O) in DMSO: H_2O (9:1 v/v); Inset plot represents the binding isotherm at 385 nm and 479 nm
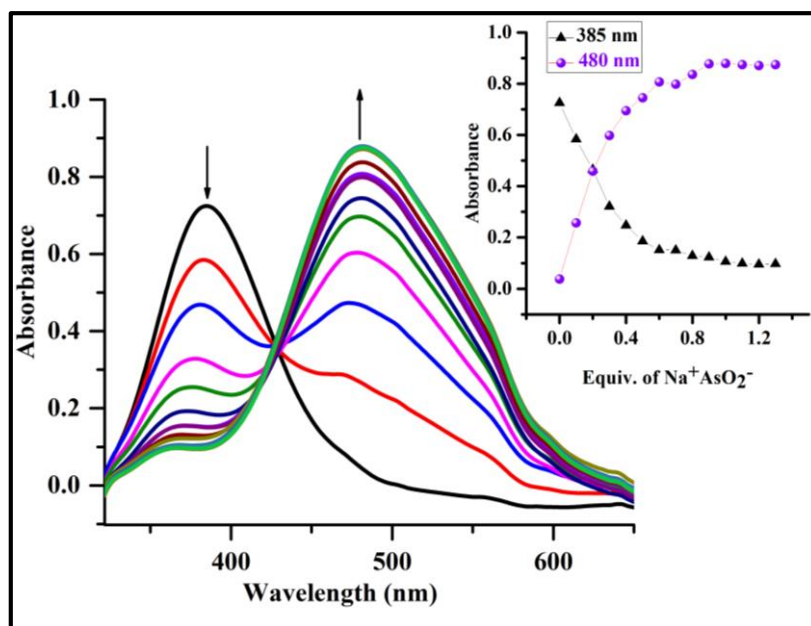
Fig. 7.52 UV- Vis titration spectra of receptor the **L6R3** (1×10^{-5} M in DMSO) with step-wise addition of 0.1 equiv. of $Na^+AsO_2^-$ ion (1×10^{-2} M H_2O) in DMSO: H_2O (9:1 v/v); Inset plot represents the binding isotherm at 385 nm and 480 nm

Equation		$y = a + b*x$		
Plot	L6R2-NaF	L6R2-NaAcO	L6R2-NaH2PO4	L6R2-NaAsO2
Intercept	0.63119 ± 0.01223	0.70375 ± 0.03492	0.69858 ± 0.02272	1.24176 ± 0.0492
Slope	2.12379E-13 ± 1.9	2.29144E-13 ± 5.4	1.85519E-13 ± 3.4	3.8181E-13 ± 8.1
Residual Sum of	0.02101	0.17127	0.06086	0.46429
Pearson's r	0.99952	0.99664	0.99815	0.99679
R-Square(COD)	0.99904	0.9933	0.9963	0.9936
Adj. R-Square	0.99896	0.99274	0.99597	0.99314
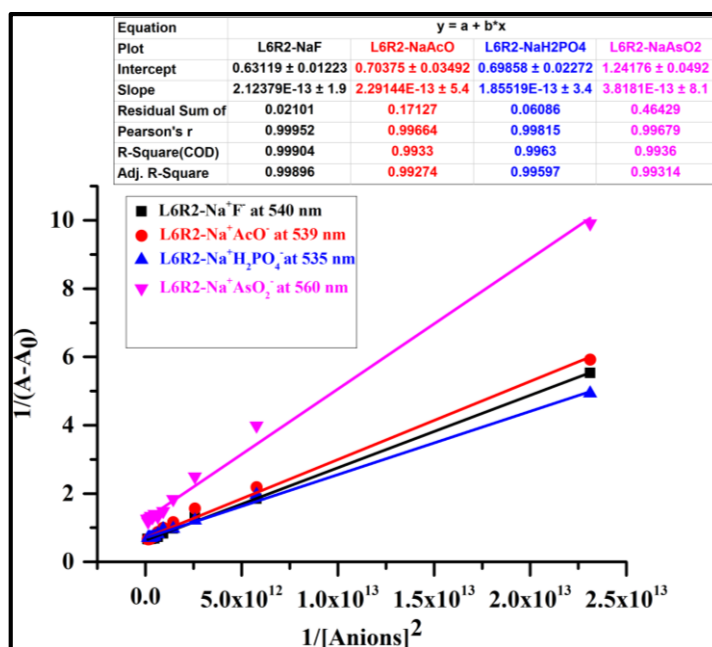
Fig. 7.53 B-H plot of receptor **L6R2**-F^-, **L6R2**-AcO^-, **L6R2**-$H_2PO_4^-$, and **L6R2**-AsO_2^- (Na^+) complex at a selective wavelength of 540 nm, 539 nm, 535 nm and 560 nm in DMSO: H_2O (9:1 v/v)
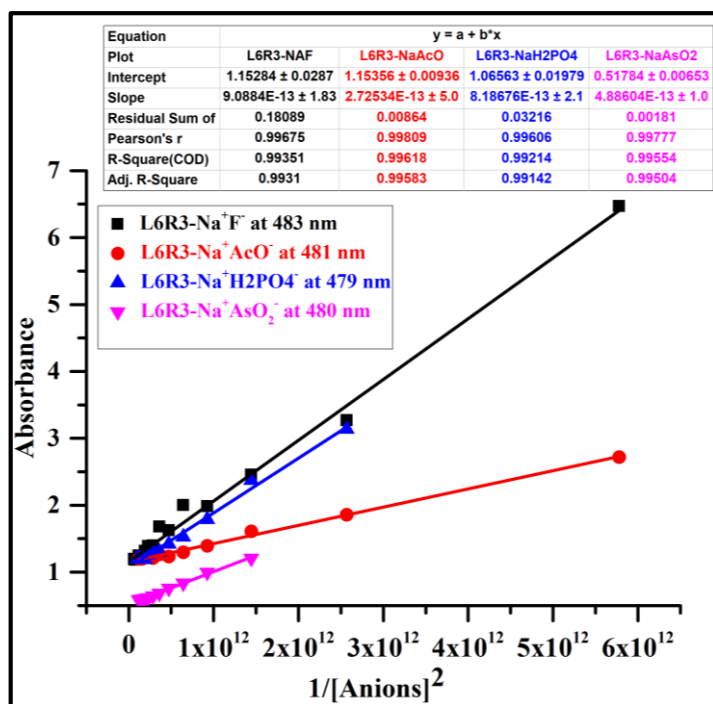
Fig. 7.54 B-H plot of receptor **L6R3**-F⁻, **L6R3**-AcO⁻, and **L6R3**-$H_2PO_4^-$ (Na^+) complex at a selective wavelength of 483 nm, 481 nm, 479 nm and 480 nm in DMSO: H_2O (9:1 v/v)

Table 7.1 Bathochromic shift ($\Delta\lambda_{max}$) of the receptor **L6R1, L6R2** and **L6R3** in the presence of 2 equiv. of sensed anions

S.No	Receptor +anion	Medium	$\Delta\lambda_{max}$ nm
1	**L6R1**+TBA^+F^-	DMSO	146
2	**L6R1**+TBA^+AcO^-	DMSO	150
3	**L6R1**+$TBA^+H_2PO_4^-$	DMSO	140
4	**L6R2**+TBA^+F^-	DMSO	154
5	**L6R2**+TBA^+AcO^-	DMSO	152
6	**L6R2**+$TBA^+ H_2PO_4^-$	DMSO	148
7	**L6R3**+TBA^+F^-	DMSO	129

8	**L6R3**+TBA$^+$AcO$^-$	DMSO	125
9	**L6R3**+TBA$^+$ H$_2$PO$_4$$^-$	DMSO	100
10	**L6R1**+ Na$^+$F$^-$	DMSO:H$_2$O (9:1 v/v)	138
11	**L6R1**+Na$^+$AcO$^-$	DMSO:H$_2$O (9:1 v/v)	137
12	**L6R2**+ Na$^+$F$^-$	DMSO:H$_2$O (9:1 v/v)	150
13	**L6R2**+Na$^+$AcO$^-$	DMSO:H$_2$O (9:1 v/v)	149
14	**L6R2**+ Na$^+$H$_2$PO$_4$$^-$	DMSO:H$_2$O (9:1 v/v)	145
15	**L6R2**+ Na$^+$AsO$_2$$^-$	DMSO:H$_2$O (9:1 v/v)	170
16	**L6R3**+ Na$^+$F$^-$	DMSO:H$_2$O (9:1 v/v)	100
17	**L6R3**+Na$^+$AcO$^-$	DMSO:H$_2$O (9:1 v/v)	96
18	**L6R3**+ Na$^+$H$_2$PO$_4$$^-$	DMSO:H$_2$O (9:1 v/v)	94
19	**L6R3**+ Na$^+$AsO$_2$$^-$	DMSO:H$_2$O (9:1 v/v)	95

The titration of the receptors **L6R1- L6R3** in the DMSO:H$_2$O (9:1 v/v) medium showed a slight less red shift compared with the DMSO solvent with F$^-$, AcO$^-$ and H$_2$PO$_4$$^-$ ions, presumably due to the solvation of the anions in an aqueous medium. Interestingly, the titration of **L6R1- L6R3** in the DMSO: H$_2$O (9:1 v/v) media with the anions afforded spectral and color changes similar to those observed in the organic media. In fact, it is worth mentioning that the receptors could detect anions in both the DMSO and the organo-aqueous media.

The calibration of the detection limit of anions (Anions= TBA$^+$F$^-$, TBA$^+$AcO$^-$, TBA$^+$H$_2$PO$_4$$^-$, Na$^+F^-$, Na$^+AcO^-$, and Na$^+AsO_2$$^-$) vs. absorbance of the receptors-anions complex at selective wavelength are depicted in Fig. 7.55, Fig. 7.56, Fig. 7.57, Fig. 7.58, Fig. 7.59, and Fig. 7.60. The corresponding binding ratio, binding constant, and detection limit is presented in Table 7.2.
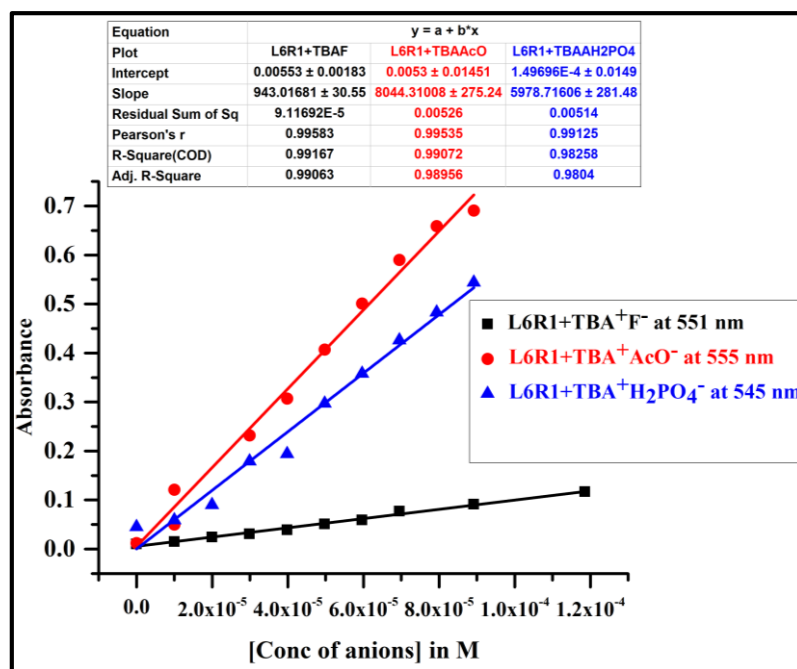
Fig. 7.55 Linear calibration curve between the concentration of the TBA salts of F⁻, AcO⁻ and H₂PO₄⁻ions and the absorbance of the receptor **L6R1**-anion complex monitored at a specific wavelength
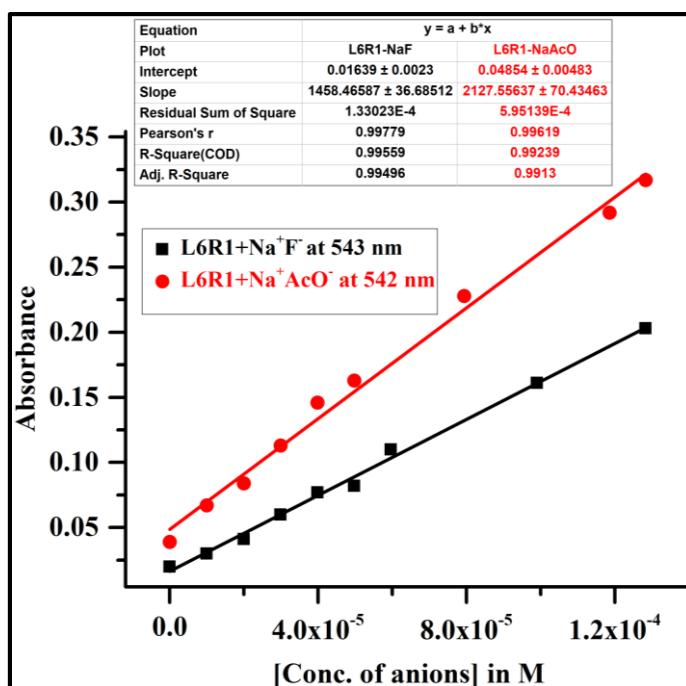
Fig. 7.56 Linear calibration curve between the concentration of the Na⁺ salts of F⁻ and AcO⁻ ions and the absorbance of the receptor **L6R1**-anions complex monitored at a specific wavelength
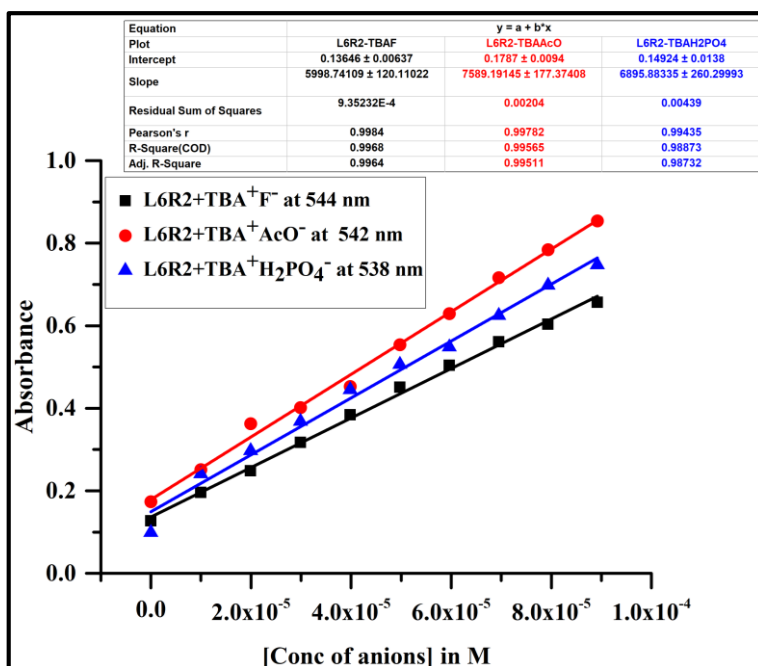
Fig. 7.57 Linear calibration curve between the concentration of the TBA salts F⁻, AcO⁻, and H₂PO₄⁻ and the absorbance of the receptor **L6R2**-anions complex monitored at a specific wavelength
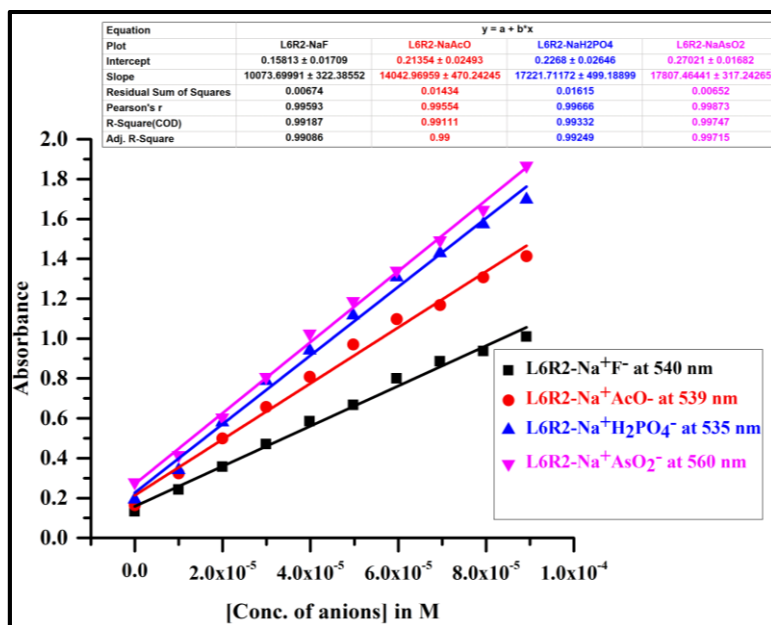
Fig. 7.58 Linear calibration curve between the concentration of the sodium salts F⁻, AcO⁻, H₂PO₄⁻ and AsO₂⁻) and the absorbance of the receptor **L6R2**-anion complex monitored at a specific wavelength

Equation	y = a + b*x		
Plot	L6R3-TBAF	L6R3-TBAAcO	L6R3-TBAH2PO4
Intercept	0.24549 ± 0.00611	0.56271 ± 0.01228	0.23201 ± 0.01464
Slope	5674.18031 ± 115.32802	10730.64819 ± 231.7491	7850.57325 ± 276.18876
Residual Sum of Square	8.62242E-4	0.00348	0.00495
Pearson's r	0.99835	0.99814	0.99509
R-Square(COD)	0.99671	0.99628	0.9902
Adj. R-Square	0.99629	0.99582	0.98897
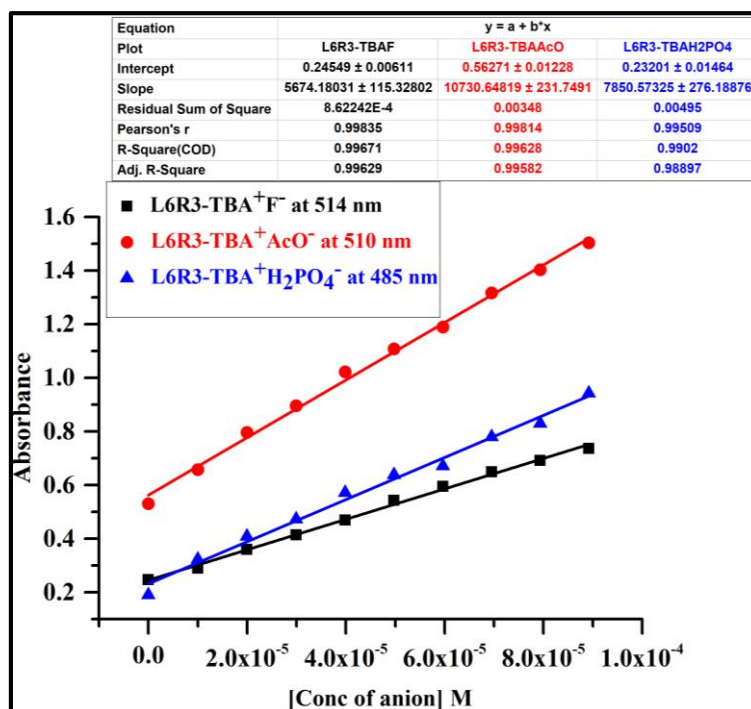
Fig. 7.59 Linear calibration curve between the concentration of the TBA salts F^-, AcO^-, and $H_2PO_4^-$ and the absorbance of the receptor **L6R3-** anion complex monitored at a specific wavelength

Equation	y = a + b*x			
Plot	L6R2-NaF	L6R2-NaAcO	L6R2-NaH2PO4	L6R2-NaAsO2
Intercept	0.14042 ± 0.02001	-0.08243 ± 0.03022	0.00825 ± 0.02164	0.24702 ± 0.01365
Slope	8528.31822 ± 377.4566	13726.88719 ± 570.0047	12667.85088 ± 408.1847	11613.50996 ± 257.5925
Residual Sum of Squar	0.00924	0.02106	0.0108	0.0043
Pearson's r	0.99226	0.99317	0.99587	0.99804
R-Square(COD)	0.98457	0.98639	0.99176	0.99608
Adj. R-Square	0.98264	0.98469	0.99073	0.99559
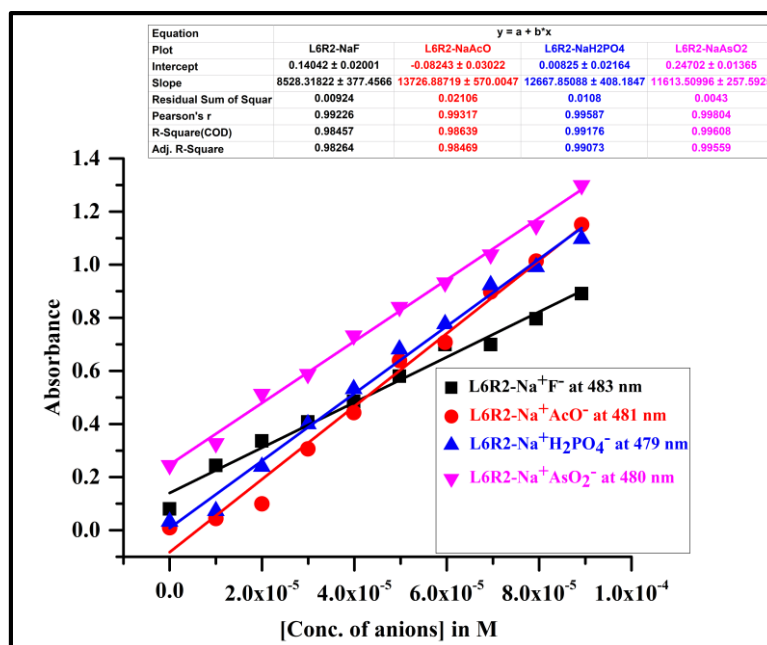
Fig. 7.60 Linear calibration curve between the concentration of the sodium salts F^-, AcO^-, $H_2PO_4^-$ and AsO_2^-) and the absorbance of the receptor **L6R3**- anion complex monitored at a specific wavelength

---

Table 7.2 Calculation of binding constant, detection limits and stoichiometry of receptors **L6R1**, **L6R2** and **L6R3**

S.No	Receptor +anion	Binding Constant	Stoichiometry	LOD (ppm)	Medium
1	**L6R1**+TBA$^+$F$^-$	3.3×10^4 M^{-1}	1:1	1.3	DMSO
2	**L6R1**+TBA$^+$AcO$^-$	5.0×10^4 M^{-1}	1:1	0.9	DMSO
3	**L6R1**+TBA$^+$H$_2$PO$_4^-$	1.3×10^3 M^{-1}	1:1	1.7	DMSO
4	**L6R1**+ Na$^+$F$^-$	7.6×10^2 M^{-1}	1:1	7	DMSO:H$_2$O (9:1 v/v)
5	**L6R1**+Na$^+$AcO$^-$	3.5×10^3 M^{-1}	1:1	2.3	DMSO:H$_2$O (9:1 v/v)
6	**L6R2**+TBA$^+$F$^-$	7.8×10^5 M^{-2}	1:2	0.20	DMSO
7	**L6R2**+TBA$^+$AcO$^-$	3.1×10^5 M^{-2}	1:2	0.31	DMSO
8	**L6R2**+TBA$^+$H$_2$PO$_4^-$	2.7×10^5 M^{-2}	1:2	0.57	DMSO
9	**L6R2**+ Na$^+$F$^-$	8.8×10^5 M^{-2}	1:2	0.08	DMSO: H$_2$O (9:1 v/v)
10	**L6R2**+Na$^+$AcO$^-$	7.1×10^5 M^{-2}	1:2	0.21	DMSO: H$_2$O (9:1 v/v)
11	**L6R2**+ Na$^+$H$_2$PO$_4^-$	2.4×10^5 M^{-2}	1:2	1.11	DMSO: H$_2$O (9:1 v/v)
12	**L6R2**+ Na$^+$AsO$_2^-$	9.3×10^5 M^{-1}	1:2	0.143	DMSO:H$_2$O, (9:1 v/v)
13	**L6R3**+TBA$^+$F$^-$	4.8×10^4 M^{-2}	1:2	0.71	DMSO
14	**L6R3**+TBA$^+$AcO$^-$	4.5×10^4 M^{-2}	1:2	0.76	DMSO
15	**L6R3**+ TBA$^+$H$_2$PO$_4^-$	2.2×10^4 M^{-2}	1:2	1.23	DMSO
16	**L6R3**+ Na$^+$F$^-$	9.9×10^4 M^{-1}	1:2	0.459	DMSO:H$_2$O (9:1 v/v)
17	**L6R3**+Na$^+$AcO$^-$	9.1×10^4 M^{-1}	1:2	0.498	DMSO:H$_2$O (9:1;v/v)
18	**L6R3**+ Na$^+$H$_2$PO$_4^-$	4.11×10^1 M^{-1}	1:2	1.3	DMSO:H$_2$O (9:1 v/v)
19	**L6R3**+ Na$^+$AsO$_2^-$	7.9×10^4 M^{-1}	1:2	0.32	DMSO:H$_2$O (9:1 v/v)

Importantly, the receptors **L6R2** and **L6R3** could detect F⁻ in water even at 0.08 ppm and 0.459 ppm, which is lower than the WHO permissible level (1 ppm) in drinking water (Avvannavar 2007; Status and Use 1994).

7.3.4   Electrochemical studies

Further, the sensing properties of the receptors **L6R2** and **L6R3** were investigated using the cyclic voltammetric studies. The cyclic voltammetric of the receptors **L6R2** and **L6R3** was recorded in ACN with the three-electrode system with tetrabutylammonium perchlorate as the supporting electrolyte in the presence and absence of anions. The free receptors **L6R2** and **L6R3** exhibited anodic peaks at 1.15 V and 0.81 V indicating the role of NH functionality, and cathodic peaks at -0.79 V and -0.98 V signifying the role of NO_2 functionality. With the incremental addition of F⁻ ion to the solutions of **L6R2** and **L6R3**, there was substituent shift in the oxidation and reduction peak with the increase in intensity of the peak as illustrated in Fig. 7.61 and Fig. 7.62. The shift in oxidation peak was attributed to the deprotonation of the NH proton by the basic F⁻ ions leaving behind N⁻ species. The energy bandgap of the receptors **L6R2** and **L6R3** and the anions complexes was calculated from the cyclic voltammetric experimental data using Eq. 7.3. The HOMO, LUMO, and energy gap of the receptors **L6R2** and **L6R3** and their complex with anions is represented in Fig. 7.63. The values obtained are given in Table 7.3.

$$\mathbf{I_p= -(E_{ox}+4.4)\ eV\text{-----------}(1)}$$
$$\mathbf{E_a=-(E_{red}+4.4)\ eV\text{-----------}(2)}$$
$$\mathbf{E_g= E_a\text{-}I_p\text{----------------------}Eq.\ 7.3}$$
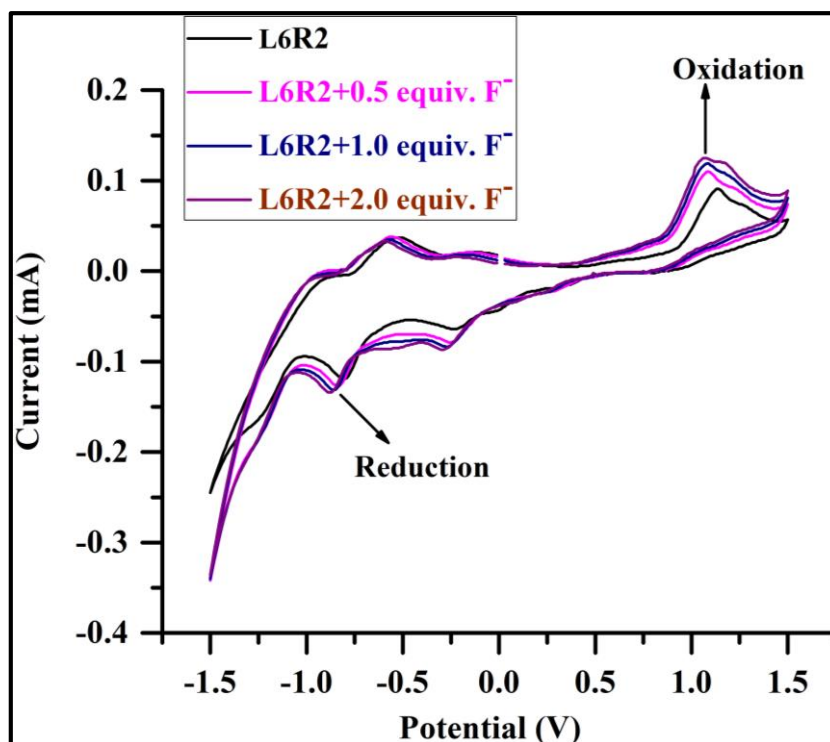
Fig. 7.61 Cyclic voltammetric (CV) of the receptor **L6R2** with sequential addition of F⁻ ion (0.5 equiv.-2.0 equiv.)
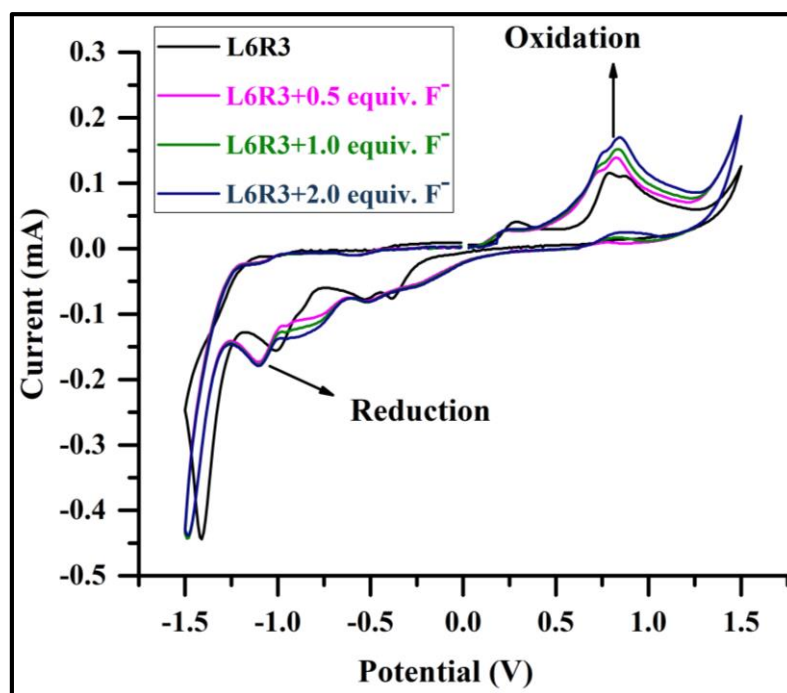
Fig. 7.62 Cyclic voltammetric (CV) of the receptor **L6R3** with sequential addition of F⁻ ion (0.5 equiv.-2.0 equiv.)
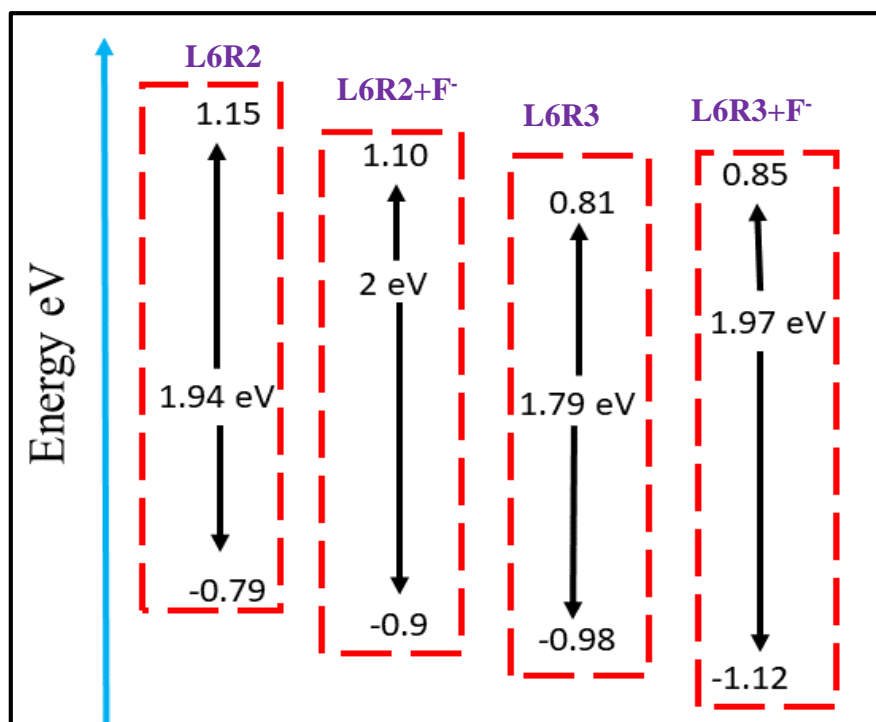
Fig. 7.63 Band gap values obtained from the receptors **L6R2** and **L6R3** and their complex with anions

Table 7.3 Band gap values obtained from receptors **L6R2** and **L6R3** and their complexes with anions

Receptors	Oxidation (V)	Reduction (V)	Bandgap (eV)
L6R2	1.15	-0.79	1.94
L6R2+F⁻	1.10	-0.9	2
L6R3	0.81	-0.98	1.79
L6R3+F⁻	0.85	-1.12	1.97

7.3.5 ^{1}H-NMR titrations studies

To gain deep insight into the actual mode of interaction of receptor **L6R2** with anions, ^{1}H-NMR titration experiment was studied in DMSO-d_6. The systematic changes of ^{1}H-NMR signals of **L6R2** upon incremental addition of F⁻, AcO⁻ and $H_2PO_4^-$ ions is depicted in (Fig. 7.64, Fig. 7.65 and Fig. 7.66). Upon addition of (0.5-1.0) equiv. of F⁻, AcO⁻ and $H_2PO_4^-$ ions, the peak at 12 ppm assigned to NH proton experienced downfield shift of about 13.0 ppm, 12.8 ppm and 12.6 ppm with decrease in it intensity

of the peak which reflecting the strong hydrogen bonding between added anions and NH moiety. On the further addition of 2 equiv. of anions, the peak at 13.0 ppm, 12.8 ppm and 12.6 ppm completely disappears which signifies the deprotonation of NH proton and leaves behind N^- species. The aromatic protons in receptor **L6R2** exhibited a gradual decrease in intensity signifying the charge transfer interaction occurring in the presence of added anions. We have noted that when we add 2 equiv. for F^-, AcO^- and $H_2PO_4^-$ ions, no upfield was observed that proves that the complex reached an equilibrium proposing 1:2 stoichiometry for receptor- anions interaction. These results reveal that the binding process includes two stage (i) hydrogen bonding interactions (for small quantities of anions (anions $=F^-$, AcO^-, and $H_2PO_4^-$) and (ii) proton transfer between the receptor **L6R2** and the coordinated anion (for high quantities of anions (anions $=F^-$, AcO^-, and $H_2PO_4^-$) yields in deprotonation of -NH proton.
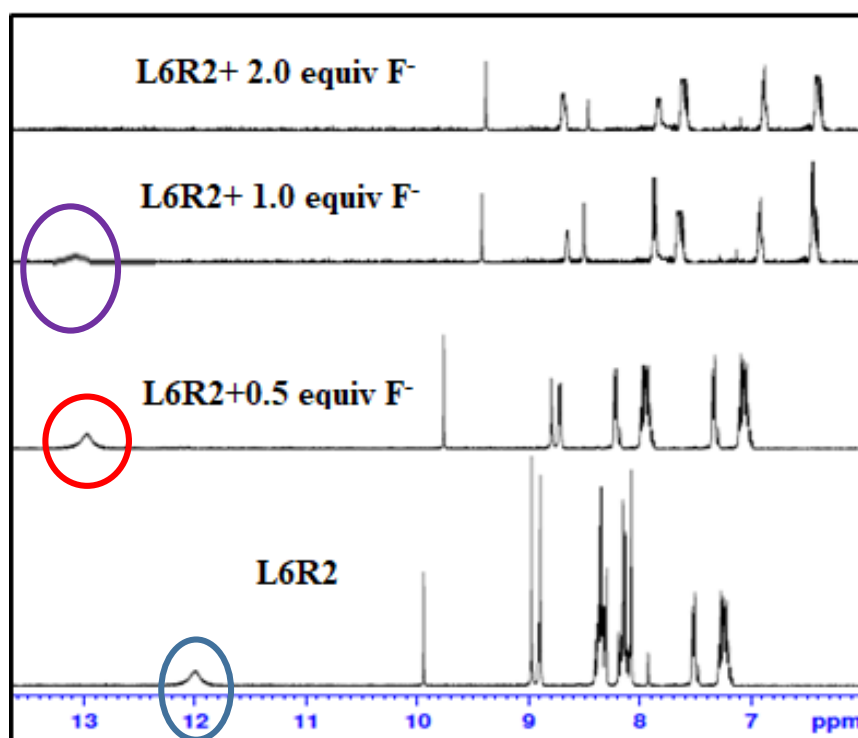
Fig. 7.64 ^{1}H-NMR titration spectra of **L6R2** on incremental addition of F^- ion
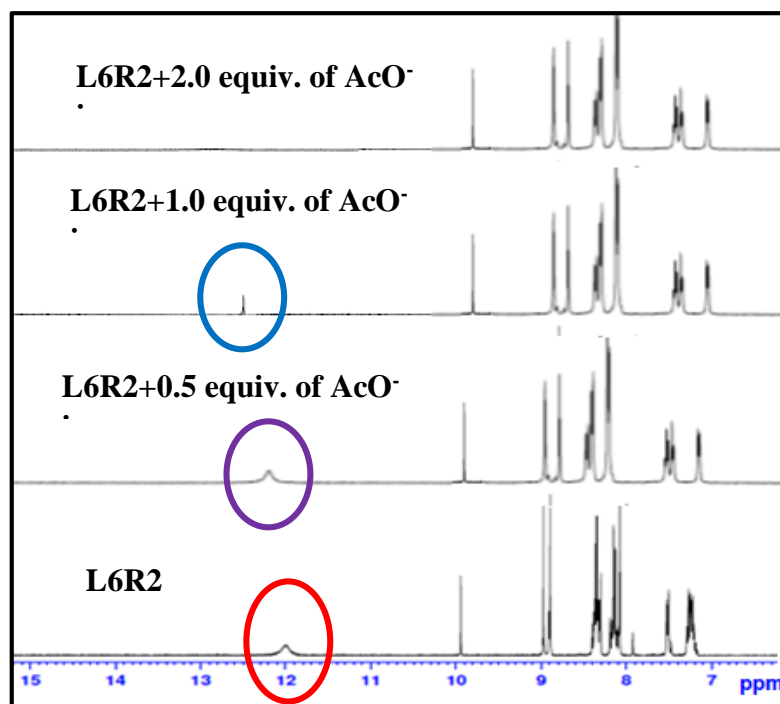
Fig. 7.65 ^{1}H-NMR spectra of receptor **L6R2** in DMSO-d$_6$ in the absence and presence of different amount of TBA$^+$AcO$^-$
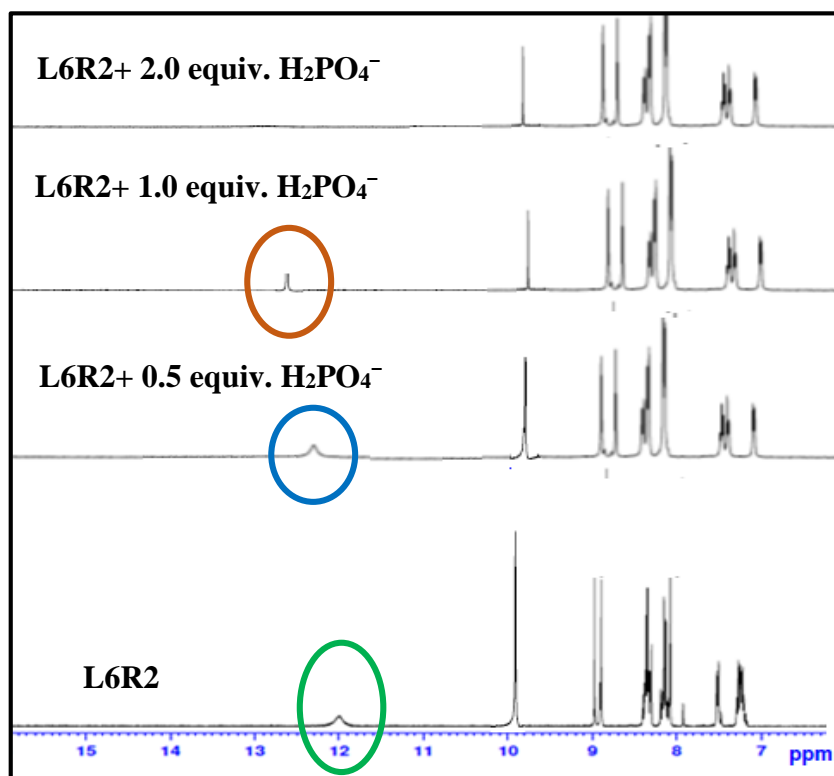
Fig. 7.66 ^{1}H-NMR spectra of receptor **L6R2** in DMSO-d$_6$ in the absence and presence of different amount of TBA$^+$H$_2$PO$_4^-$

7.3.6　Binding mechanism

The presence of NO_2 functionality at para position to the imine linked extended π-conjugation is known to promote strong hydrogen bond complex between the receptor and anions (anions=F^-, AcO^-, and $H_2PO_4^-$). Based on the ^{1}H-NMR studies the binding mechanism of the anions (anions=F^-, AcO^-, and $H_2PO_4^-$) to the receptor **L6R2** can be proposed as shown in Scheme 7.5 result reveals, initially at lower concentration of anions binds the receptor with hydrogen bond and at higher concentration of anions the receptor experience the deprotonation. As a result of the ICT transition between the electron-deficient NO_2 group at p-position and the electron-rich $–N^-$, the charging separation in the receptor leads to intense colorimetric change.
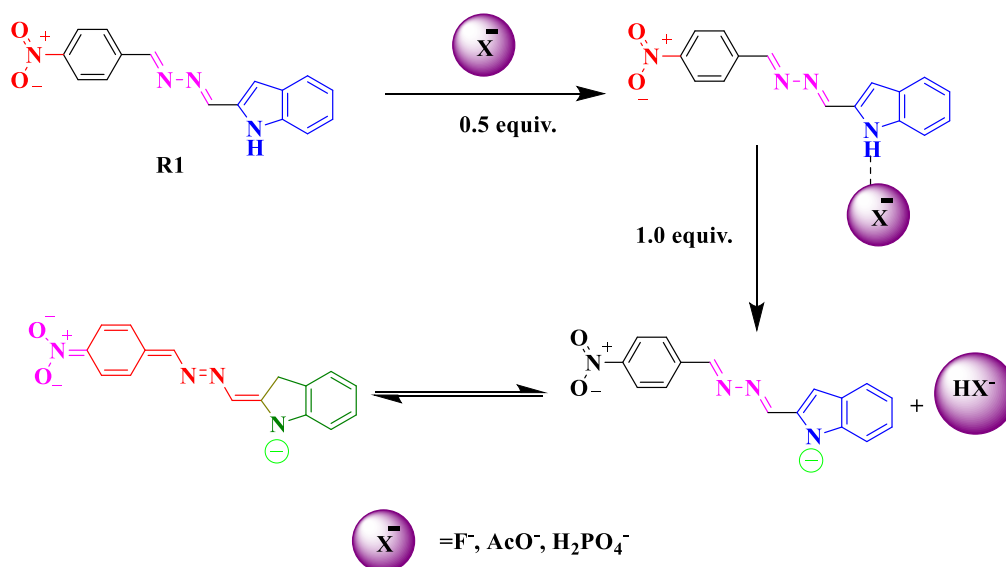
Scheme 7.5 Proposed mechanism of receptor **L6R2** with F^- ion

7.3.7　pH study

In order to analyze the selective detection of the ions, anion binding studies of the receptor were carried out in the presence of the HEPES buffer (0.05 M). Surprisingly, the receptor **L6R2** exhibited excellent pH response over a wide range of pH from 6 to pH: 11 with distinct color change as shown in Fig. 7.67. In order to quantify the observed color change, the UV-Vis experiment was recorded at 544 nm with the addition of 2 equiv. of AcO^- ion to the receptor **L6R2** (1×10^{-5} M in DMSO: HEPES buffer; 9:1, v/v), in different pH range from 6-11. As the pH started to rise from

6 to 11, the intensity of the absorbance bands increased due to the presence of strong basic species such as the NH proton, which competed with the AcO⁻ ion for the binding site. As shown in Fig. 7.68, in more basic conditions (pH 11), the absorption band intensity is higher, which could be due to deprotonation of the NH proton by AcO⁻. Thus, the pH study confirmed the color change originating from the ICT transition from the donor (-NH) to the acceptor (-NO$_2$) moiety through the deprotonation mechanism by the basic AcO⁻ ion.
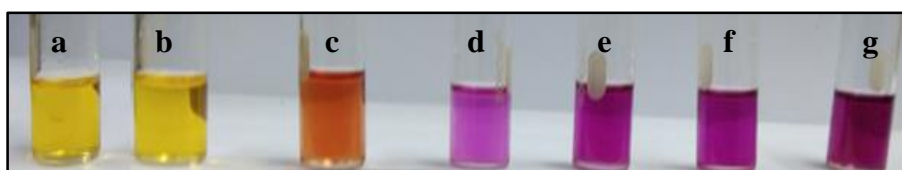
Fig. 7.67 Color change of the receptor **L6R2** (1×10^{-5}M in DMSO: HEPES buffer; 9:1, v/v) (a) **L6R2**, (b) **L6R2**+pH 6, (c) **L6R2**+pH 7, (d) **L6R2**+ pH 8, (e) **L6R2**+ pH 9, (f) **L6R2**+ pH 10, and (g) **L6R2**+ pH 11 upon addition of 2 equiv. of AcO⁻ ion
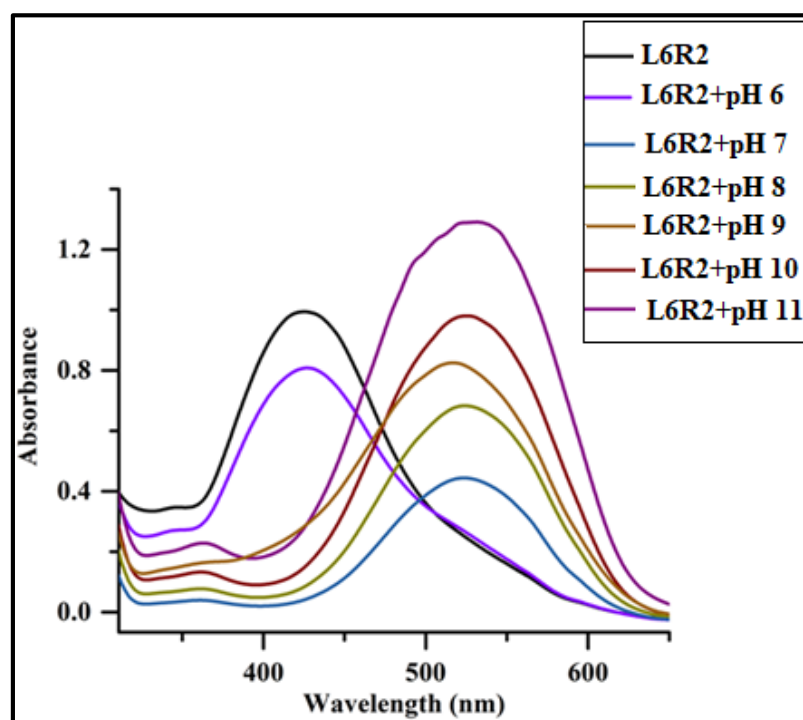
Fig. 7.68 Change in UV-Vis spectra of the receptor **L6R2** (1×10^{-5}M in DMSO: HEPES buffer; 9:1, v/v) in different pH range from 6-11 upon addition of 2 equiv. of AcO⁻ ion

7.3.8 Reversibility test on receptor L6R2

The reversibility of the chemosensor is an essential phenomenon in the analytical method. In the present study, the interaction between **L6R2** and F⁻ was reversible as confirmed by the addition of $Ca(NO_3)_2$ into the receptor solution containing **L6R2**+F⁻ ion. After the addition of $Ca(NO_3)_2$ to the **L6R2**+F⁻ solution, the color reverted to its original shade from purple to pale yellow as shown in Fig. 7.69. To further elucidate the reversibility test, UV-Vis absorption spectra were recorded as depicted in Fig.7.70, upon the addition of 2 equiv. of $Ca(NO_3)_2$ to the mixture containing 2 equiv of **L6R2**+F⁻, which displayed the original absorption band of the free receptor **L6R2**, thus confirming reversibility in binding as shown in Scheme 7.6. Moreover, the diminution of the absorption band intensity at 530 nm could be due to the displacement of F⁻ from the receptor unit by the Ca^{2+} ion. Additionally, with the addition of 2 equiv. of $Ca(NO_3)_2$ into the solution containing **L6R2**+AcO⁻ ion (2 equiv.), there neither complete restoration of color nor the original absorption band of the free receptor could be observed as seen in Fig. 7.71 and Fig. 7.72. The AcO⁻ triangular Y shape form structure firmly bonded with the receptor's binding site. This may be one of the reasons why the anion detection system is not completely reversible. The study clearly shows that the F⁻ ion binding mechanism had reversed successfully.
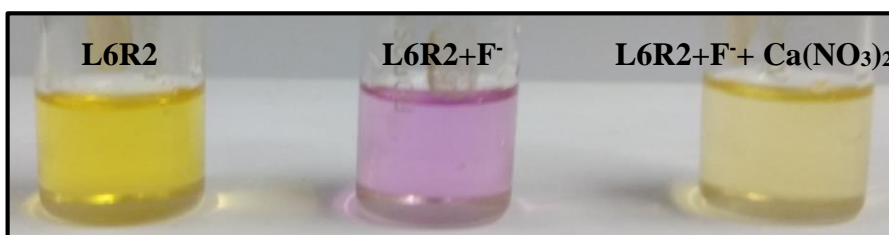
Fig. 7.69 Color change of the receptor **L6R2**+F⁻ complex in the presence of 2 equiv. of $Ca(NO_3)_2$
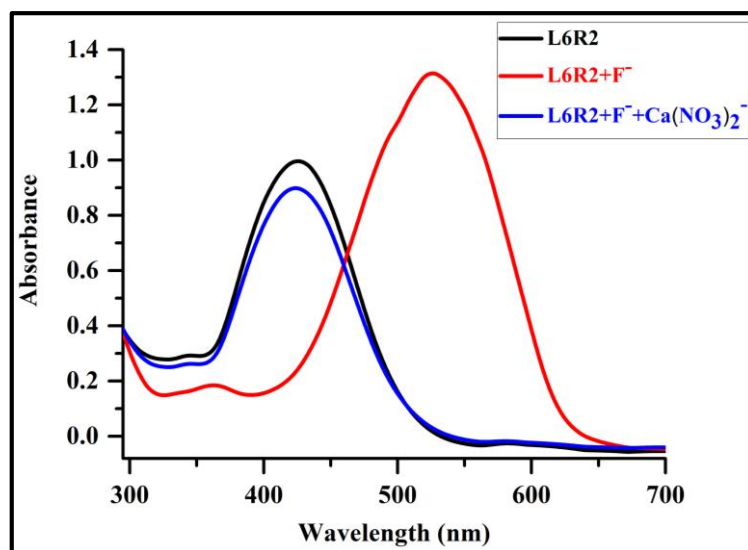
Fig. 7.70 UV-Vis spectra representing reversibility of the receptor **L6R2** +F⁻ complex in the presence of 2 equiv. of Ca(NO$_3$)$_2$
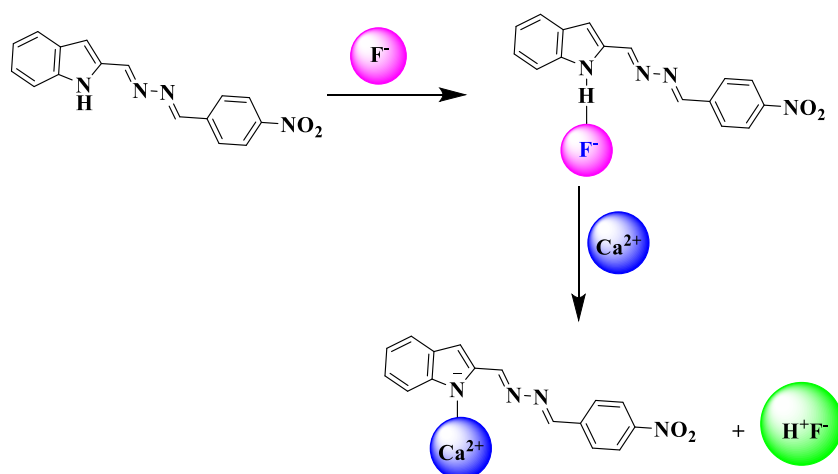
Scheme 7.6 Binding mechanism of receptor **L6R2** with F⁻ ion in in the presence of Ca(NO$_3$)$_2$⁻
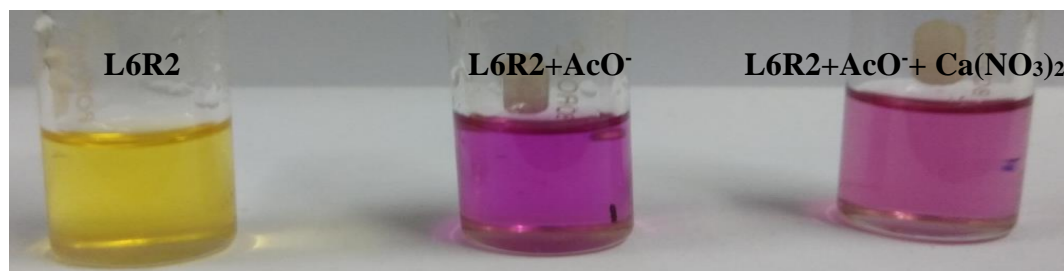
Fig. 7.71 Color change of the receptor **L6R2**+AcO⁻ complex in the presence of 2 equiv. of Ca(NO$_3$)$_2$
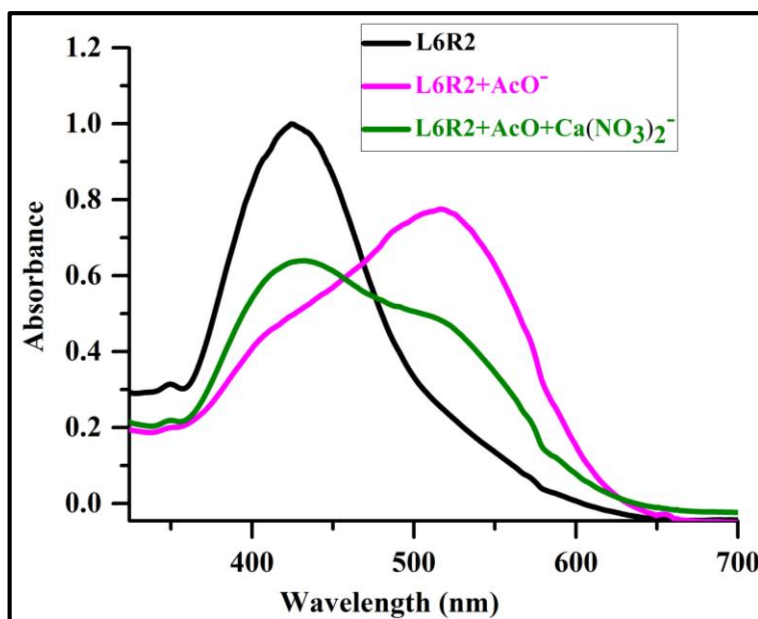
Fig. 7.72 UV-Vis spectra representing reversibility of **L6R2**+ AcO⁻ complex in the presence of 2 equiv. of $Ca(NO_3)_2$

7.3.9 Analytical application

7.3.9.1 Fluoride and acetate detection in toothpaste and vinegar

Sodium fluoride and sodium acetate are essential parts of the biological system and must be present in optimum amount to maintain the physiological process. Any deficiency or excess can lead to disorders in the ecosystem. In this regards, the detection of F⁻ and AcO⁻ ions is essential. Accordingly, 25 mg of toothpaste was dissolved in 10 ml of distilled water and filtered. The filtrate was used for the quantitative analysis of F⁻ ion. As shown in Fig. 7.73, the receptors **L6R2** and **L6R3** exhibited significant color change from yellow to purple and from pale yellow to wine red by the addition of the prepared toothpaste solution and 5µl of commercially available vinegar solution.
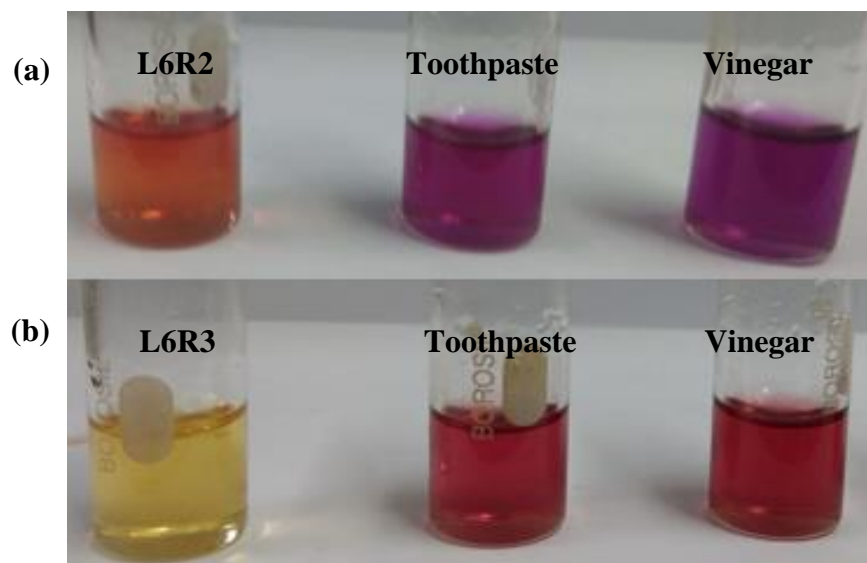
Fig. 7.73 Colorimetric changes of the receptor (1×10^{-5}M in DMSO) (a) **L6R2** with toothpaste and vinegar (b) **L6R3** with toothpaste and vinegar in aqueous medium

As a quantification procedure, UV-Vis titration analysis was carried out with the sequential addition of toothpaste and vinegar solution prepared in distilled water to the solutions of the receptors **L6R2** and **L6R3**. The titration spectra revealed shift in original absorption band to 536 nm and 528 nm (**L6R2**) and to 482 nm and 479 nm (**L6R3**) upon the addition of F$^-$ and AcO$^-$ ions present in toothpaste and vinegar. The titration profiles are illustrated in Fig. 7.74, Fig. 7.75, Fig. 7.76, and Fig. 7.77. The spectral change exhibited similar titration profiles as observed with the addition of TBA$^+$F$^-$ and TBA$^+$AcO$^-$. This reflects the property of the receptors to detect F$^-$ and AcO$^-$ ions present in an aqueous medium. The calibration curve of absorbance vs. concentration of F$^-$ and AcO$^-$ ions was plotted to determine the amount of F$^-$ and AcO$^-$ ions in toothpaste and vinegar. The detection limits (LOD= 3σ/s) of the receptors **L6R2** and **L6R3** were found to be 0.067 ppm and 0.097 ppm (for F$^-$ and AcO$^-$ ions) and 0.21 ppm and 0.27 ppm (for F$^-$ and AcO$^-$ ions), as illustrated in as shown Fig. 7.78 and Fig. 7.79. Consequently, the chromogenic receptors **L6R2** and **L6R3** can be used for the quantitative analysis of F$^-$ and AcO$^-$ ions in toothpaste and vinegar in absolute aqueous medium.
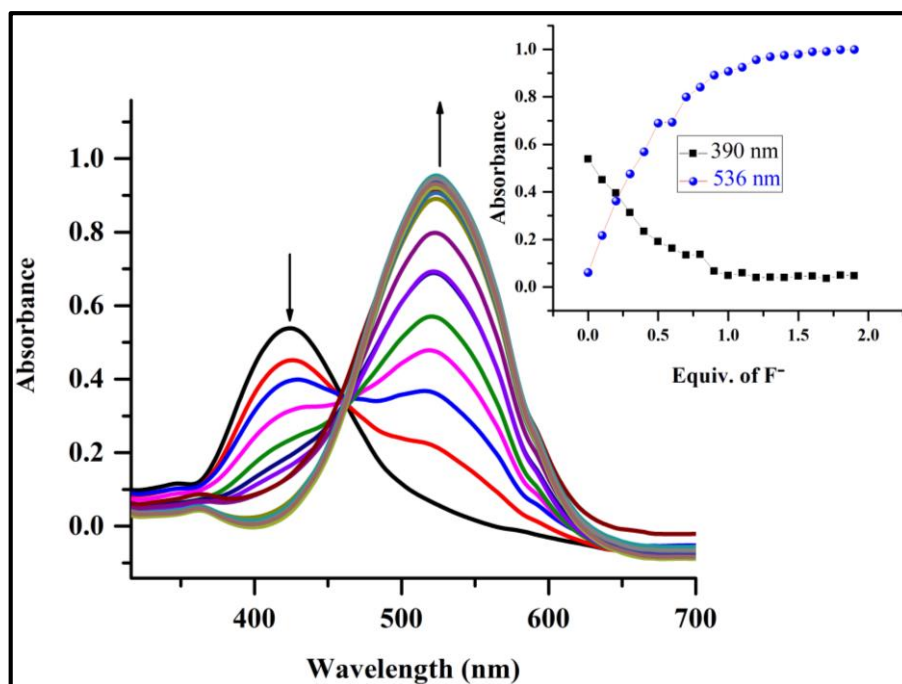
Fig. 7.74 Change in absorption spectra of the receptor **L6R2** (1×10^{-5}M in DMSO) upon incremental addition of toothpaste (source of F⁻ ion); Inset plot signifying the binding isotherm at 390 nm and 536 nm
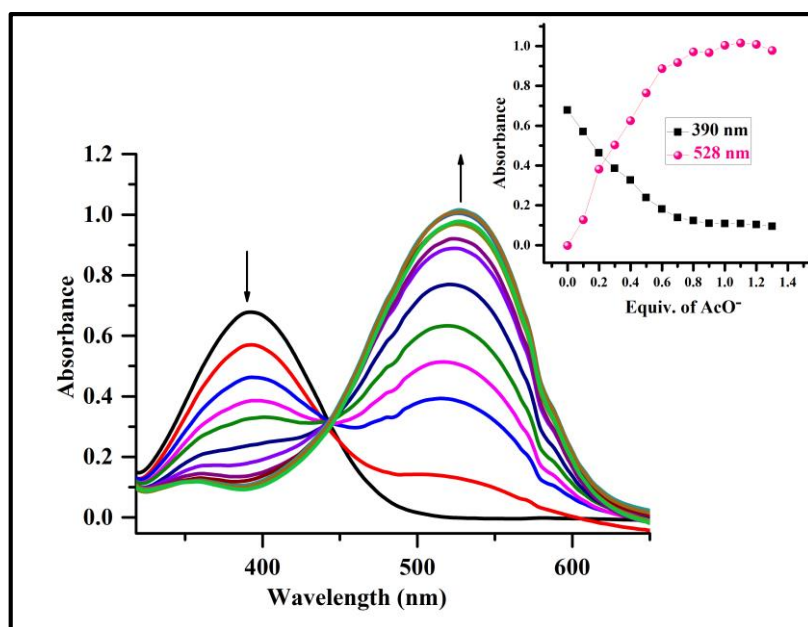
Fig. 7.75 Change in absorption spectra of the receptor **L6R2** (1×10^{-5}M in DMSO) upon incremental addition of vinegar (source of AcO⁻ ion); Inset plot signifying the binding isotherm at 390 nm and 528 nm
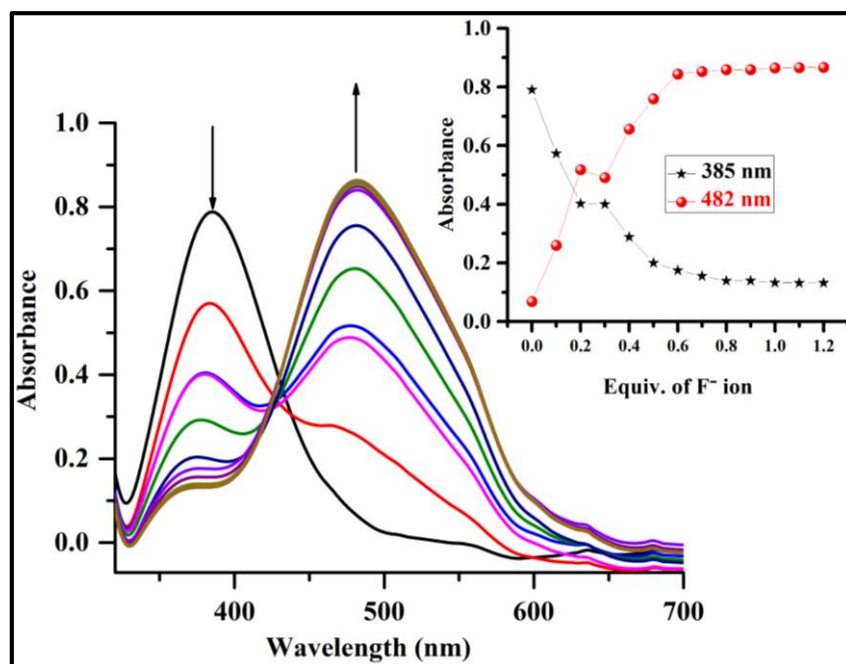
Fig. 7.76 Change in absorption spectra of the receptor**L6R3** (1×10^{-5}M in DMSO) upon incremental addition of vinegar (source of F⁻ ion); Inset plot signifying the binding isotherm at 385 nm and 482 nm
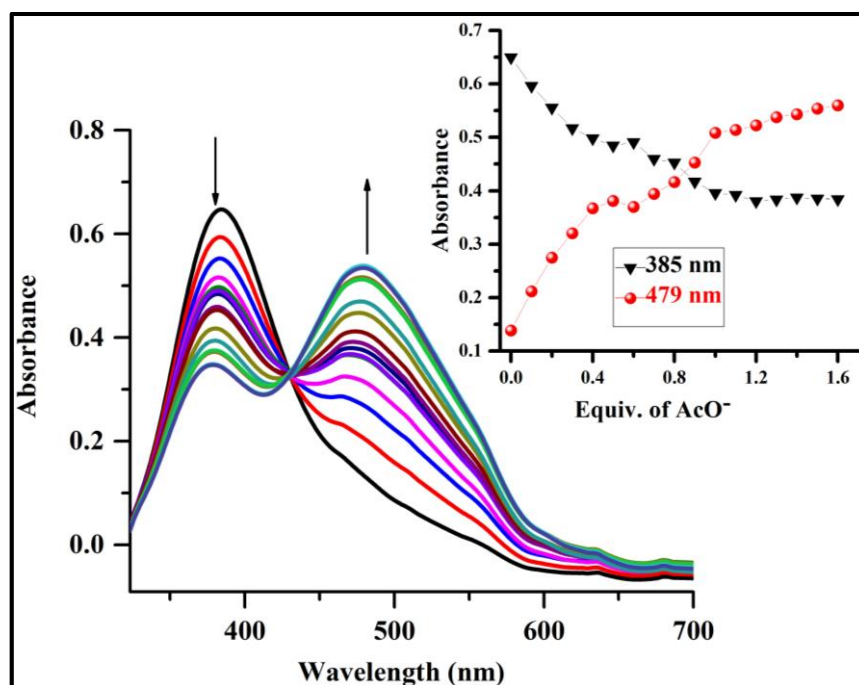
Fig. 7.77 Change in absorption spectra of the receptor **L6R3** (1×10^{-5}M in DMSO) upon incremental addition of vinegar (source of AcO⁻ ion); Inset plot signifying the binding isotherm at 385 nm and 479 nm
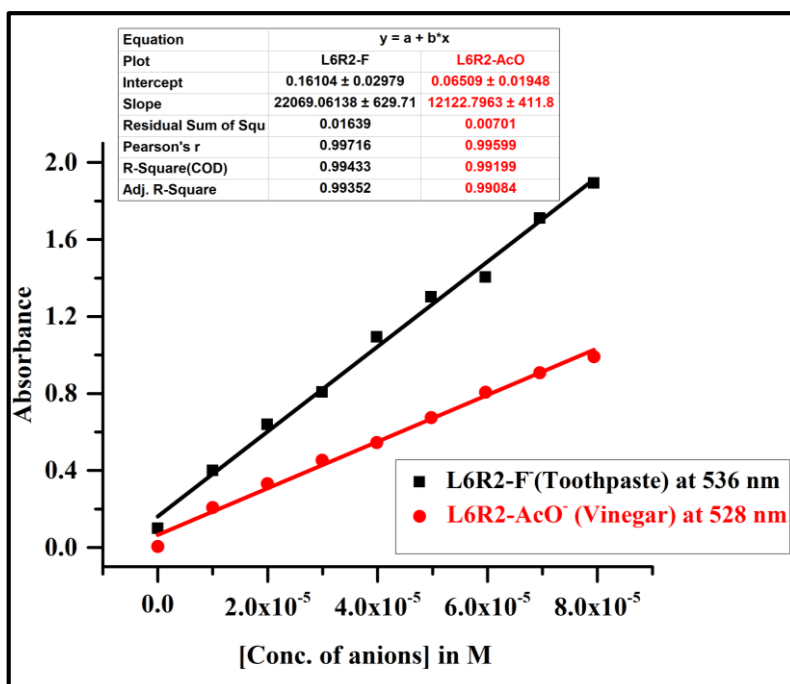
Fig. 7.78 Calibration curve of absorbance of the receptor **L6R2-**anion complex v/s concentration of anion
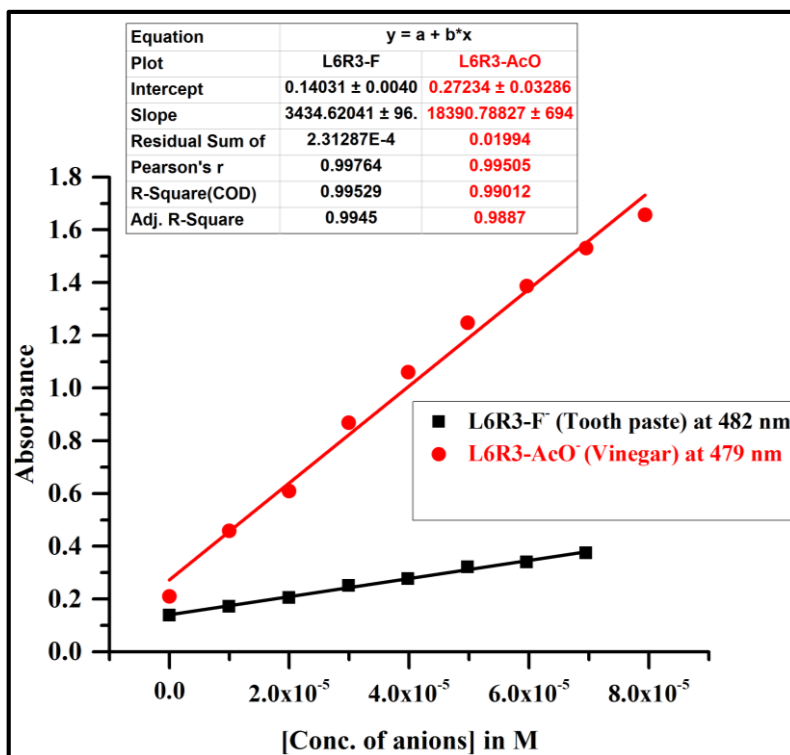
Fig. 7.79 Calibration curve of absorbance of the receptor **L6R3-**anion complex v/s concentration of anions

7.3.9.2 Color changing ability of L6R2 on test papers

The potential utility and applicability of the receptor **L6R2** for the detection of F^-, AcO^-, and $H_2PO_4^-$ was checked by using a test strip. The test strip was prepared using the Whatman-40 test paper, which was immersed in the solution of the receptor **L6R2** (1×10^{-5} M in DMSO) and then dried in a hot oven for 3 h at 45^0C. After complete drying, the color of the test strip changed to yellow. When 2 equiv. F^-, AcO^-, and $H_2PO_4^-$ stock solutions of the anion were added to the coated test strip, it immediately turned from yellow to purple as shown in Fig.7.80. Therefore, the receptor **L6R2** proved to be potentially useful for real-life applications by detecting biologically important F^-, AcO^-, and $H_2PO_4^-$ ions using a test strip. In addition, it is efficient, less expensive, and easy to handle.

Fig. 7.80 Color changes observed on addition of TBA salts of F^-, AcO^-, and $H_2PO_4^-$ anion to test strips coated with the receptor **L6R2** solution

7.3.9.3 Color changing ability test of L6R2 on cotton swabs

In addition, cotton swabs were used for the analytical application of the receptor **L6R2** for F^-, AcO^-, and $H_2PO_4^-$ anion in the present study. Initially, the cotton swabs were soaked in a solution of the receptor (1×10^{-5} M in DMSO) and dried in a hot oven. The cotton swabs coated with **L6R2** were immersed in different anion solutions such as F^-, Cl^-, Br^-, I^-, NO_3^-, HSO_4^-, $H_2PO_4^-$, and AcO^- (1×10^{-2} M in DMSO). Remarkable color change was observed from light brown to purple only in the presence of F^-, AcO^-, and $H_2PO_4^-$ anions, whereas the other anions did not show any color change as depicted in Fig. 7.81. Thus, the receptor **L6R2** showed high selectivity towards F^-, AcO^-, and $H_2PO_4^-$ anions over the other interference anions in the DMSO.
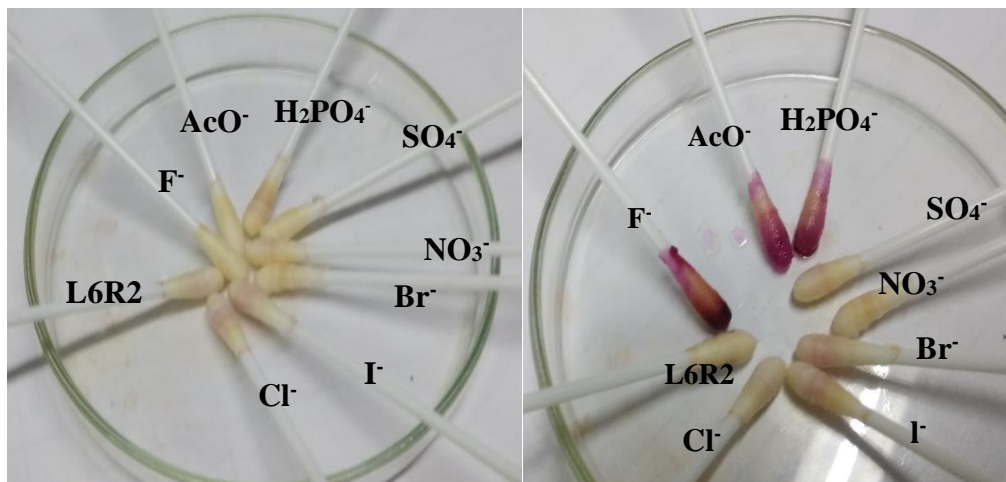
Fig. 7.81 Color change of receptor **L6R2** with anions on cotton swabs

7.4 CONCLUSIONS

In conclusion, the chromogenic receptors **L6R1**, **L6R2,** and **L6R3** were synthesized in good yields via the Schiff base condensation. The receptors **L6R2** and **L6R3** exhibited excellent colorimetric sensing behaviour towards multiple anions such as F^-, AcO^-, and $H_2PO_4^-$ in the DMSO and the sodium salts of F^-, AcO^-, $H_2PO_4^-$, and AsO_2^- in the DMSO: H_2O, (9:1; v/v) proving their utility as chemosensors. The lower detection limit of 0.143 ppm and 0.32 ppm for the sodium salt of AsO_2^- reflected the sensitivity of the receptors **L6R2** and **L6R3** in anion detection as surpassing the constraints of the aqueous media. The receptor **L6R2** demonstrated high affinity towards AcO^- ion in the DMSO/HEPES (9:1, v/v) at different pH range of 6 to 11. The ^{1}H-NMR titration confirmed hydrogen bonding between the NH proton and the F^- ion, followed by deprotonation of the NH proton by the excess addition of fluoride ion leaving behind N^- species. The receptors **L6R2** and **L6R3** possessed high sensitivity for the inorganic F^- ion with detection limit of 0.08 ppm and 0.459 ppm in the aqueous media, which is much less than the WHO permissible level (1 ppm) in drinking water. The applicability of the receptors **L6R2** and **L6R3** for detecting F^- and AcO^- ions in toothpaste and vinegar makes them appropriate as real- time colorimetric sensors. Overall, the receptors served as multi- anion chemosensors with interesting real-life practical applications.

CHAPTER 8

SUMMARY AND CONCLUSIONS

This chapter describes in brief the results and the conclusion of the present research work.

8.1 SUMMARY

Among the wide range of anions, the detection of fluoride ion has gained much attention because of its privileged usage in clinical applications, which makes it beneficial to human health. However, an excess of fluoride ion consumption can cause many lethal diseases, including bone cancer. Owing to this dual functionality, it is significant to detect fluoride ion. More precisely, it is more advantageous if one can detect the presence of fluoride ion colorimetrically using organic receptors. Likewise, the importance of acetate ion is also to be considered as they are present in the human body as acetyl coenzyme A. Looking at the literature, the design and synthesis of new receptors has been aimed, which can colorimetrically detect fluoride and acetate ions over other anions, not only in organic media but also in aqueous media in the form of sodium salts.

Apart from the detection of fluoride and acetate ions the detection of dicarboxylates is also important as they play a vital role in numerous metabolic processes such as glyoxalate cycle, generation of high energy phosphate bonds, and in dicarboxylate cycle for autotrophic carbon dioxide (CO_2) fixation. Among the widespread organic anions, the discrimination of geometrical isomers such as cis/trans dicarboxylates (maleate and fumarate ions) attains significance because of their different biological behaviours and similar chemical and physical properties. It will be gainful to discriminate these isomeric dicarboxylates with the colorimetric approach.

Among various anions, the detection of Arsenic (As) in the form of arsenite (AsO_2), and arsenate (AsO_4^{2-}) needs urgent attention in view of public health and environmental problems. Similarly, phosphate plays an important role in the living systems, but high amounts of phosphate can disrupt the balance of the ecosystem.

On the other hand, carbonates are main component of shells and the skeleton in aquatics. Despite the fact that CO_3^{2-} ions are beneficial in many aspects, material safety data sheet states that their strong caustic effect to the gastro-intestinal tract may cause

severe abdominal pain, vomiting, diarrhoea, collapse, and even death, if ingested in excess.

Considering the significance of the field, it has been decided to develop new receptors for the colorimetric detection of fluoride (F), acetate (AcO), dihydrogen phosphate ($H_2PO_4^-$), carbonate (CO_3^{2-}), arsenite (AsO_2), arsenate (AsO_4^{2-}), and dicarboxylates. The overall research work is summarized below.

- ❖ Six different series of receptors possessing signalling units and anion binding sites have been synthesized and designed for the colorimetric detection of anions

- ❖ All the receptors and intermediates were well- characterized using different techniques such as ^{1}H-NMR, ^{13}C-NMR, FT-IR, and ESI-MS.

- ❖ The binding of F^-, AcO^-, $H_2PO_4^-$, AsO_2^-, and AsO_4^{2-} by different receptors in the series in organic and semi-aqueous media has been qualitatively and quantitatively assessed by UV-Vis spectroscopic, ^{1}H-NMR titration, Cyclic voltammetric, and DFT studies.

- ❖ The stoichiometric ratios of the anion to the receptor have been determined with the help of either the Job's Plot method or via the Benesi–Hildebrand method. Applying the stoichiometric ratios and quantitative studies, the binding mechanisms of the anion to the receptor have been derived. These binding mechanisms were justified by the ^{1}H NMR titration of the receptors with the anions.

- ❖ All the receptors were tested for different practical applications such as detection of inorganic F^- and AcO^- ions in aqueous media, solvatochromic and HEPES buffer behaviour of the receptor upon adding AcO^- ions, and test strip application for naked-eye detection of anions without use of any spectroscopic instrument.

- ❖ The practical applicability of the receptor was tested by detecting and quantifying the amount of F^- and AcO^- ions present in commercial mouthwash, sea water, toothpaste, and vinegar.

8.2 CONCLUSION

The present research work has been merged in the field of anion receptor chemistry with the design strategy paving the way for the detection of a multitude of anions such as F^-, AcO^-, $H_2PO_4^-$, AsO_2^-, and AsO_4^{2-}. The practical utility of the designed receptors in real-life applications has enriched the early explorations leading to successful physiological applications.

Six different series of organic receptors were synthesized, characterized by standard spectroscopic techniques, and evaluated for their anion sensing properties. Based on the evaluation of the anion binding behaviour by UV-Vis, ^{1}H-NMR, Cyclic voltammetric and DFT, the following conclusions were derived.

➤ The influence of the positional substitution of nitro functionality in the series of the six colorimetric receptors **L1R1-L1R6** on anion detection was confirmed. Receptor **L1R1** exhibited excellent colorimetric selectivity towards F^- and AcO^- ions in the DMSO with purple colouration and revealed sharp bathochromic shifts of 141 nm and 143 nm in the absorption maxima due to the presence of the electron-withdrawing effect of NO_2 group at the para position, which strengthened the binding ability of the receptor with the anions. The receptor **L1R1** was able to colorimetrically detect the TBAF and NaF with minimum concentration of 7.4 $\times 10^{4}$ and 6.6$\times 10^{3}$ M^{-1} in the organo-aqueous mixture, and proved that it was highly capable of competing with the water molecules to detect inorganic anions in an aqueous medium. The ^{1}H-NMR titration and DFT calculation emphasized the hydrogen bond formation, followed by deprotonation of the OH proton by the ICT mechanism. The receptor **L1R1** showed unique solvatochromic properties in different polar aprotic solvents in the presence of AcO^- ions. The colorimetric response of the receptor **L1R1** towards F^- and AcO^- ions in the organic, aqueous, and solid phase signified its practical utility as a chemosensor.

➤ In a series of novel colorimetric receptors **L2R1**, **L2R2**, **L2R3,** and **L2R3** with different substituents for the optical measurement of anions was developed based on the hydrazide derivatives. The DMSO solution of the receptor **L2R1**

exhibited colorimetric response and red shift band in the presence of F⁻, AcO⁻, and $H_2PO_4^-$ ions with remarkable colour change from pale yellow to blue. The UV-Vis spectra of the receptor **L2R1** revealed positive solvatochromism confirming the vivid colour changes observed with the addition of AcO⁻ ion to the receptor in a solvent of varying polarities. The anion binding studies of the receptor **L2R1** in the DMSO: HEPES buffer (9:1, v/v) media exhibited selective detection of AcO⁻ ion with blue colouration. The **L2R1** receptor proved to be highly capable of sensing F⁻, AcO⁻, AsO_2^-, and AsO_4^{2-} sodium salts in an aqueous medium with lower detection limit of 0.392 ppm, 0.823 ppm, 0.643 ppm, and 0.721 ppm, which highlighted the efficacy of the nitro group in fine tuning the colorimetric response of the receptor **L2R1**.

➢ The impact of the positional substitution of the -OH functionality in the series of anion receptors **L3R1**, **L3R2**, and **L3R3** was definite. The receptor **L3R1** exhibited excellent colorimetric sensing behaviour towards F⁻ and AcO⁻ ions in the DMSO with blue colouration. The receptor **L3R2** was successfully applied to the detection of Na^+F^-, Na^+AcO^-, and $Na^+AsO_2^-$ in the organic-aqueous mixture DMSO: H_2O (9:1 v/v) with higher binding constant of 8.79×10^7 M⁻¹, 9.34×10^7 M⁻¹, and 8.12×10^7 M⁻¹ compared with **L3R1** owing to the presence of the -OH group at the para position, suggesting stable receptor-anion complexation in the organo-aqueous media. To sum up, based on the UV-Vis, spectroscopic studies, ¹H-NMR titration studies, and electrochemical studies, the receptor **L3R2** can be considered as an effective colorimetric chemosensor for anions.

➢ The receptors **L4R1** and **L4R2** based on the pyridine derivative **L4R1** showed high selectivity for F⁻ ions, whereas **L4R2** efficiently distinguished between F⁻ and AcO⁻ ions by displaying distinct colour change from pale yellow to aqua and green in the presence of various competitive anions in the DMSO. The receptors **L4R1** and **L4R2** bound to the CO_3^{2-} ion in a 2:1 stoichiometric manner, induced fast colour change from yellow to aqua for CO_3^{2-} ion over other anions with significant bathochromic ($\Delta\lambda_{max}$) of 210 nm and 219 nm in the absorbance spectra. The lower detection limit of 0.47 ppm and higher

binding constant value of 8.72×10^4 M^{-2} for **L4R2-** CO_3^{2-} complex indicated its practical utility.

- The new receptors **L5R1** and **L5R2** were able to discriminate between isomeric dicarboxylate anions, namely, maleate ions over fumarate ions by the colorimetric approach. The colour change was owing to the formation of the intermolecular hydrogen bond complex between the maleate ion and the receptors, which was confirmed by ^{1}H NMR titration. In addition, the receptors **L5R1** and **L5R2** showed remarkable colorimetric response to the biologically important anions F$^-$ and AcO$^-$ ions in the DMSO and inorganic F$^-$, AcO$^-$, and AsO$_2^-$ in the organo-aqueous (DMSO: H$_2$O; 9:1 v/v). The ^{1}H-NMR and DFT calculations further confirmed the anion binding process of the receptor L5R1 with the F$^-$ ion and the maleate ion.

- The receptors **L6R1**, **L6R2,** and **L6R3** proved the colorimetric detection of F$^-$, AcO$^-$, and H$_2$PO$_4^-$ ions with sharp colour change in the DMSO. Studies in DMSO/HEPES (9:1, v/v) in different pH range of 6 to 11 confirmed the selective detection of AcO ions by the receptor **L6R2.** In addition, the electrochemical studies conducted for the receptors **L6R2** and **L6R3** in the presence of the F$^-$ ion, revealed the deprotonation of the N-H proton in the anion binding process. The applicability of the receptors **L6R2** and **L6R3** for detecting F$^-$ and AcO$^-$ ions in toothpaste and vinegar made them real- time colorimetric sensors. The receptor **L6R2** also displayed rapid colorimetric response that could be observed by the naked eye and good reversibility between **L6R2+CO₃²⁻** and F$^-$ ion. The receptors **L6R2** and **L6R3** possessed high sensitivity for inorganic F$^-$ ion with a detection limit of 0.08 ppm and 0.459 ppm in an aqueous media, which is much less than the WHO permissible level (1 ppm) in drinking water. Overall, the receptors served as multi-anion chemosensors with interesting real-life practical applications.

8.3 DATA OF COMPARISON (SOLVENT AND LOD) OF ALL SYNTHESIZED RECEPTORS IN THE PRESENCE OF F⁻ IN ORGANIC AND ORGANO-AQUEOUS MEDIA

S.No	Receptors	Anions	LOD (ppm)	Solvent
Chapter 2	**L1R1**	TBA^+F^-	2.8	DMSO
	L1R2	TBA^+F^-	12.3	DMSO
	L1R4	TBA^+F^-	5.2	DMSO
	L1R5	TBA^+F^-	15.4	DMSO
	L1R1	Na^+F^-	0.35	DMSO:H_2O (9:1 v/v)
	L1R4	Na^+F^-	3.0	DMSO:H_2O (9:1 v/v)
Chapter 3	**L2R1**	TBA^+F^-	0.514	DMSO
	L2R2	TBA^+F^-	2.33	DMSO
	L2R3	TBA^+F^-	3.76	DMSO
	L2R4	TBA^+F^-	4.32	DMSO
	L2R1	Na^+F^-	0.392	DMSO:H_2O (9:1 v/v)
Chapter 4	**L3R1**	TBA^+F^-	2.81	DMSO
	L3R2	TBA^+F^-	0.98	DMSO
	L3R1	Na^+F^-	2.56	DMSO:H_2O (9:1 v/v)
	L3R2	Na^+F^-	0.53	DMSO:H_2O (9:1 v/v)
Chapter 5	**L4R1**	TBA^+F^-	0.9	DMSO
	L4R1	TBA^+F^-	0.74	DMSO
Chapter 6	**L5R1**	TBA^+F^-	0.160	DMSO
	L5R2	TBA^+F^-	0.231	DMSO
	L5R1	Na^+F^-	0.181	DMSO:H_2O (9:1 v/v)
	L5R2	Na^+F^-	1.81	DMSO:H_2O (9:1 v/v)
Chapter 7	**L6R1**	TBA^+F^-	1.3	DMSO
	L6R2	**TBA^+F^-**	**0.20**	**DMSO**
	L6R3	**TBA^+F^-**	**0.71**	**DMSO**
	L6R1	**Na^+F^-**	**7**	**DMSO:H_2O (9:1 v/v)**
	L6R2	**Na^+F^-**	**0.08**	**DMSO:H_2O (9:1 v/v)**
	L6R3	Na^+F^-	0.449	DMSO:H_2O (9:1 v/v)

Among all the synthesized receptors, the receptor **L6R2** exhibited high selectivity for TBA^+F^- in the organic (DMSO) medium with a lower detection of 0.20 ppm. In addition, the receptor **L6R2** showed a high sensitivity towards inorganic F⁻ ion with a lower detection limit of 0.08 ppm in organic aqueous media which is much lower than the WHO permissible amount (1 ppm) in drinking water.

Here, the comparative study reflects the stability of receptor **L6R2**— F⁻ ion complex in both organic and organo-aqueous media.

8.4   SCOPE FOR FUTURE WORK

The present research work has been successful in the detection of biologically and environmentally important anions, thus paving the way for practical applications. Yet, the selective and sensitive detection of anions has to be addressed in the future as it can lead to device applications. The reproducibility and reversibility of the sensors has to be optimized by the rational design of a receptor with appropriate binding sites. If a receptor can be designed such that it exhibits vivid colour change in the presence of different anions, it can certainly be utilized in the detection and extraction of anions from groundwater source and industrial effluents.

REFERENCES

Agarwalla, H., Jana, K., Maity, A., Kesharwani, M. K., Ganguly, B., and Das, A. (2014). "Hydrogen bonding interaction between active methylene hydrogen atoms and an anion as a binding motif for anion recognition: experimental studies and theoretical rationalization." The Journal of Physical Chemistry A, 118(14), 2656–2666.

Ajayakumar, M. R., Hundal, G., and Mukhopadhyay, P. (2013). "A tetrastable naphthalenediimide: anion induced charge transfer, single and double electron transfer for combinational logic gates." Chemical Communications, 49(70), 7684–7686.

Alberts, B., Bray, D., Lewis, J., Raff, M., Roberts K. and Watson, J.D. (1994). "Molecular Biology of the Cell, 3rd. edn, Garland Science, New York.

Ali, H. D. P., Kruger, P. E., and Gunnlaugsson, T. (2008). "Colorimetric 'naked-eye'and fluorescent sensors for anions based on amidourea functionalised 1, 8-naphthalimide structures: anion recognition via either deprotonation or hydrogen bonding in DMSO." New Journal of Chemistry, 32(7), 1153–1161.

Alreja, P., & Kaur, N. (2019). "Test kit" of chromogenic and ratiometric 1, 10-phenanthroline based chemosensor for the recognition of F^- and CN^- ions. Inorganic Chemistry Communications, 110, 107600.

Amendola, V., Bergamaschi, G., Boiocchi, M., Fabbrizzi, L. and Mosca, L. (2013). "The interaction of fluoride with fluorogenic ureas: An ON1 –OFF–ON2 response." J. Am. Chem. Soc., 135 (16), 6345–6355.

Amendola, V., Esteban-Gómez, D., Fabbrizzi, L., Licchelli, M. (2006). "What anions do to N− H-containing receptors." Accounts of chemical research., 39(5), 343-353.

Amundson, R. G., Trask, J., and Pendall, E. (1988). "A rapid method of soil carbonate analysis using gas chromatography." Soil Science Society of America Journal, 52(3), 880–883.

Anderson, M.P., Gregory, R.J., Thompson, S., Souza, D.W., Paul, S., Mulligan, R.C., Smith, A.E. and Welsh, M.J. (1991). "Demonstration that CFTR is a chloride channel by alteration of its anion selectivity." Science, 253, 202-205.

Anuradha, C. D., Kanno, S., and Hirano, S. (2000). "Fluoride induces apoptosis by caspase-3 activation in human leukemia HL-60 cells." Archives of toxicology, 74(4–5), 226–230.

Anzenbacher, P., Try, A. C., Miyaji, H., Jursíková, K., Lynch, V. M., Marquez, M., & Sessler, J. L. (2000). "Fluorinated calix [4] pyrrole and dipyrrolylquinoxaline: neutral anion receptors with augmented affinities and enhanced selectivities." Journal of the American Chemical Society., 122(42), 10268-10272.

Arabahmadi, R., Orojloo, M., and Amani, S. (2014). "Azo Schiff bases as colorimetric and fluorescent sensors for recognition of F−, Cd 2+ and Hg 2+ ions." Analytical Methods, 6(18), 7384–7393.

Arslan, Ö., Aydıner, B., Yalçın, E., Babür, B., Seferoğlu, N., and Seferoğlu, Z. (2017). "8-Hydroxyquinoline based push-pull azo dye: Novel colorimetric chemosensor for anion detection." Journal of Molecular Structure, 1149, 499–509.

Asadollahzadeh, M., Niksirat, N., Tavakoli, H., Hemmati, A., Rahdari, P., Mohammadi, M., and Fazaeli, R. (2014). "Application of multi-factorial experimental design to successfully model and optimize inorganic arsenic speciation in environmental water samples by ultrasound assisted emulsification of solidified floating organic drop microextraction." Analytical Methods, 6(9), 2973–2981.

Ashley, K., Agrawal, A., Cronin, J., Tonazzi, J., McCleskey, T. M., Burrell, A. K., and Ehler, D. S. (2007). "Ultra-trace determination of beryllium in occupational hygiene samples by ammonium bifluoride extraction and fluorescence detection using hydroxybenzoquinoline sulfonate." Analytica chimica acta, 584(2), 281–286.

Aurbach, D., Gnanaraj, J. S., Geissler, W., and Schmidt, M. (2004). "Vinylene carbonate and Li salicylatoborate as additives in LiPF3 (CF 2 CF 3) 3 solutions for rechargeable Li-ion batteries." Journal of The Electrochemical Society, 151(1), A23–A30.

Avvannavar, S. M. (2007). "J. Fawell, K. Bailey, J. Chilton, E. Dahi, L. Fewtrell and Y. Magara, Fluoride in drinking-water, WHO, IWA Publishers, London (2006) ISBN: 1900222965, US $100.00, 141 pp." Science of the Total Environment, 382, 388–388.

Basu, A., Dey, S. K., and Das, G. (2013). "Amidothiourea based colorimetric receptors for basic anions: evidence of anion induced deprotonation of amide–NH proton and hydroxide induced anion··· π interaction with the deprotonated receptors." RSC Advances, 3(18), 6596–6605.

Batista, R. M., Oliveira, E., Costa, S. P., Lodeiro, C., and Raposo, M. M. M. (2007). "Synthesis and ion sensing properties of new colorimetric and fluorimetric chemosensors based on bithienyl-imidazo-anthraquinone chromophores." Organic letters, 9(17), 3201–3204.

Beer, P. D., and Gale, P. A. (2001). "Anion recognition and sensing: the state of the art and future perspectives." Angewandte Chemie International Edition, 40(3), 486–516.

Beer, P. D., and Hayes, E. J. (2003). "Transition metal and organometallic anion complexation agents." Coord. Chem. Rev.., 240(1-2), 167-189.

Beer, P. D., Graydon, A. R., Johnson, A. O., and Smith, D. K. (1997). "Neutral ferrocenoyl receptors for the selective recognition and sensing of anionic guests." Inorganic chemistry, 36(10), 2112–2118.

Bencini, A., Coluccini, C., Garau, A., Giorgi, C., Lippolis, V., Messori, L., Pasini, D., and Puccioni, S. (2012). "A BINOL-based chiral polyammonium receptor for highly enantioselective recognition and fluorescence sensing of (S, S)-tartaric acid in aqueous solution." Chemical Communications, 48(84), 10428–10430.

Benesi, H. A., and Hildebrand, J. H. J. (1949). "A spectrophotometric investigation of the interaction of iodine with aromatic hydrocarbons." Journal of the American Chemical Society, 71(8), 2703–2707.

Berg, J.M., Tymoczko, J.L., Stryer, L. and Gatto, Jr, G.J. (2012). "Biochemistry" W. H. Freeman and Company, New York.

Berryman, O. B., and Johnson, D. W. (2009). "Experimental evidence for interactions between anions and electron-deficient aromatic rings." Chemical Communications, (22), 3143–3153.

Berryman, O. B., Sather, A. C., Hay, B. P., Meisner, J. S., and Johnson, D. W. (2008). "Solution phase measurement of both weak σ and C− H··· X− hydrogen bonding interactions in synthetic anion receptors." Journal of the American Chemical Society, 130(33), 10895–10897.

Bhardwaj, V. K., Hundal, M. S., and Hundal, G. (2009). "A tripodal receptor bearing catechol groups for the chromogenic sensing of F− ions via frozen proton transfer." Tetrahedron, 65(41), 8556–8562.

Bianchi, A., Bowman-James, K., and Garcìa-España, E. (1997). Supramolecular chemistry of anions. Vch Pub.

Bose, P., Ahamed, B. N., and Ghosh, P. (2011). "Functionalized guanidinium chloride based colourimetric sensors for fluoride and acetate: single crystal X-ray structural evidence of-NH deprotonation and complexation." Organic & biomolecular chemistry, 9(6), 1972–1979.

Bratthall, D., Hänsel-Petersson, G., and Sundberg, H. (1996). "Reasons for the caries decline: what do the experts believe?" European journal of oral sciences, 104(4), 416–422.

Cametti, M., and Rissanen, K. (2013). "Highlights on contemporary recognition and sensing of fluoride anion in solution and in the solid state." Chemical Society Reviews, 42(5), 2016–2038.

Cances, E., Mennucci, B., and Tomasi, J. (1997). "A new integral equation formalism for the polarizable continuum model: Theoretical background and applications to isotropic and anisotropic dielectrics." The Journal of chemical physics, 107(8), 3032–3041.

Chauhan, K., Singh, P., Kumari, B., and Singhal, R. K. (2017). "Synthesis of new benzothiazole Schiff base as selective and sensitive colorimetric sensor for arsenic on-site detection at ppb level." Analytical Methods, 9(11), 1779–1785.

Chen, L. D., Mandal, D., Pozzi, G., Gladysz, J. A., and Bühlmann, P. (2011). "Potentiometric sensors based on fluorous membranes doped with highly selective

ionophores for carbonate." Journal of the American Chemical Society, 133(51), 20869–20877.

Chen, M. L., Gu, C. B., Yang, T., Sun, Y., Wang, J. H. (2013). "A green sorbent of esterified egg-shell membrane for highly selective uptake of arsenate and speciation of inorganic arsenic." Talanta., 116, 688-694.

Chen, X., Leng, T., Wang, C., Shen, Y., and Zhu, W. (2017). "A highly selective naked-eye and fluorescent probe for fluoride ion based on 1, 8-naphalimide and benzothizazole." Dyes and Pigments, 141, 299–305.

Chifotides, H. T., Schottel, B. L., and Dunbar, K. R. (2010). "The π-Accepting Arene HAT (CN) 6 as a Halide Receptor through Charge Transfer: Multisite Anion Interactions and Self-Assembly in Solution and the Solid State." Angewandte Chemie International Edition, 49(40), 7202–7207.

Cho, E. J., Ryu, B. J., Lee, Y. J., and Nam, K. C. (2005). "Visible colorimetric fluoride ion sensors." Organic letters, 7(13), 2607–2609.

Choi, P. J., Petterson, K. A., and Roberts, J. D. (2002). "Ionization equilibria of dicarboxylic acids in dimethyl sulfoxide as studied by NMR." Journal of physical organic chemistry, 15(5), 278–286.

Choi, Y. S., Lvova, L., Shin, J. H., Oh, S. H., Lee, C. S., Kim, B. H., Cha, G. S., and Nam, H. (2002). "Determination of oceanic carbon dioxide using a carbonate-selective electrode." Analytical chemistry, 74(10), 2435–2440.

Christensen, D. (1984). "Determination of substrates oxidized by sulfate reduction in intact cores of marine sediments 1." Limnology and Oceanography, 29(1), 189–191.

Cossi, M., Persico, M., and Tomasi, J. (1994). "Aspects of Electrophilic Bromination of Alkenes in Solution. Theoretical Calculation of Atomic Charges in Bromonium Ions." Journal of the American Chemical Society, 116(12), 5373–5378.

Costero, A. M., Colera, M., Gavina, P., and Gil, S. (2006). "Fluorescent sensing of maleate versus fumarate by a neutral cyclohexane based thiourea receptor." Chemical Communications, (7), 761–763.

Cui, Y., Mo, H. J., Chen, J. C., Niu, Y. L., Zhong, Y. R., Zheng, K. C., & Ye, B. H. (2007). "Anion-Selective Interaction and Colorimeter by an Optical Metalloreceptor Based on Ruthenium (II) 2, 2 '-Biimidazole: Hydrogen Bonding and Proton Transfer." Inorganic chemistry., 46(16), 6427-6436.

Cullen, W. R., and Reimer, K. J. (1989). "Arsenic speciation in the environment." Chemical reviews, 89(4), 713–764.

Czarnik, A. W. (1994). "Chemical communication in water using fluorescent chemosensors." Acc.Chem.Res., 27(10), 302-308.

Dalapati, S., Alam, M. A., Jana, S., Karmakar, S., and Guchhait, N. (2013). "'Test kit' for detection of biologically important anions: A salicylidene-hydrazine based Schiff base." Spectrochimica Acta Part A: Molecular and Biomolecular Spectroscopy, 102, 314–318.

Dalapati, S., Alam, M. A., Jana, S., Saha, R., and Guchhait, N. (2012). "Reusable anion detection kit: An aqueous medium anion detection." Sensors and Actuators B: Chemical, 162(1), 57–62.

Dwivedi, S. K., Razi, S. S., & Misra, A. (2019). "Sensitive colorimetric detection of CN^- and AcO^- anions in a semi-aqueous environment through a coumarin–naphthalene conjugate azo dye". New Journal of Chemistry, 43(13), 5126-5132.

Devuyst, O., Christie, P.T., Courtoy, P.J., Beauwens, R. and Thakker, R.V. (1999). "Intra-Renal and subcellular distribution of the human chloride channel, CLC-5, reveals a pathophysiological basis for dent's disease" Hum. Mol. Genet., 8, 247-257.

Dey, S. K., and Das, G. (2011). "A selective fluoride encapsulated neutral tripodal receptor capsule: solvatochromism and solvatomorphism." Chemical Communications, 47(17), 4983–4985.

Dey, S. K., Chutia, R., and Das, G. (2012). "Oxyanion-Encapsulated Caged Supramolecular Frameworks of a Tris (urea) Receptor: Evidence of Hydroxide-and Fluoride-Ion-Induced Fixation of Atmospheric CO2 as a Trapped CO32–Anion." Inorganic chemistry, 51(3), 1727–1738.

Ding, Y., Li, T., Zhu, W., Xie, Y. (2012). "Highly selective colorimetric sensing of cyanide based on formation of dipyrrin adducts." Organic & biomolecular chemistry., 10(21), 4201-4207.

Dini, S., and Khanmohammadi, H. (2019). "A new azo-azomethine sensor for detection of CN− and AcO⁻ anions: Highly selective chemosensor for naked eye detection of sodium diclofenac." Spectrochimica Acta Part A: Molecular and Biomolecular Spectroscopy, 117157.

Divya, K. P., Sreejith, S., Balakrishna, B., Jayamurthy, P., Anees, P., Ajayaghosh, A. (2010). "A Zn2+-specific fluorescent molecular probe for the selective detection of endogenous cyanide in biorelevant samples." Chemical Communications., 46(33), 6069-6071.

Du, J., Hu, M., Fan, J., and Peng, X. (2012). "Fluorescent chemodosimeters using 'mild' chemical events for the detection of small anions and cations in biological and environmental media." Chemical Society Reviews, 41(12), 4511–4535.

Duke, R. M., and Gunnlaugsson, T. (2011). "3-Urea-1, 8-naphthalimides are good chemosensors: a highly selective dual colorimetric and fluorescent ICT based anion sensor for fluoride." Tetrahedron letters, 52(13), 1503–1505.

Duke, R. M., O'Brien, J. E., McCabe, T., and Gunnlaugsson, T. (2008). "Colorimetric sensing of anions in aqueous solution using a charge neutral, cleft-like, amidothiourea receptor: tilting the balance between hydrogen bonding and deprotonation in anion recognition." Organic & biomolecular chemistry, 6(22), 4089–4092.

Duke, R. M., Veale, E. B., Pfeffer, F. M., Kruger, P. E., and Gunnlaugsson, T. (2010). "Colorimetric and fluorescent anion sensors: an overview of recent developments in the use of 1, 8-naphthalimide-based chemosensors." Chemical society reviews, 39(10), 3936–3953.

Dwivedi, S. K., Razi, S. S., and Misra, A. (2019). "Sensitive colorimetric detection of CN− and AcO− anions in a semi-aqueous environment through a coumarin–naphthalene conjugate azo dye." New Journal of Chemistry, 43(13), 5126–5132.

Dydio, P., Lichosyt, D., and Jurczak, J. (2011). "Amide-and urea-functionalized pyrroles and benzopyrroles as synthetic, neutral anion receptors." Chemical Society Reviews, 40(5), 2971–2985.

Edition, F. (2011). "Guidelines for drinking-water quality." WHO chronicle, 38(4), 104–108.

Eiam-Ong, S., Spohn, M., Kurtzman, N. A., and Sabatini, S. (1995). "Insights into the biochemical mechanism of maleic acid-induced Fanconi syndrome." Kidney international, 48(5), 1542–1548.

EiamOng, S., Spohn, M., Kurtzman, N.A. and Sabatini, S. (1995). "Insights into the biochemical mechanism of maleic acid-induced Fanconi syndrome." Kidney Int., 48, 1542–1548.

El-Sherif, A. A. (2010). "Synthesis, solution equilibria and antibacterial activity of Co (II) with 2-(aminomethyl)-benzimidazole and dicarboxylic acids." Journal of solution chemistry, 39(10), 1562–1581.

Esteban-Gomez, D., Fabbrizzi, L., and Licchelli, M. (2005). "Why, on interaction of urea-based receptors with fluoride, beautiful colors develop." The Journal of organic chemistry, 70(14), 5717–5720.

Evans, L. S., Gale, P. A., Light, M. E., and Quesada, R. (2006). "Anion binding vs. deprotonation in colorimetric pyrrolylamidothiourea based anion sensors." Chemical Communications, (9), 965–967.

Evans, R. W., and Darvell, B. W. (1995). "Refining the estimate of the critical period for susceptibility to enamel fluorosis in human maxillary central incisors." Journal of Public Health Dentistry, 55(4), 238–249.

Fawell, J., Bailey, K., Chilton, J., Dahi, E., Fewtrell, L. and Magara, Y. (2001) Fluoride in Drinking-water, IWA Publishing, London, 32.

Fegade, U., Sharma, H., Tayade, K., Attarde, S., Singh, N., and Kuwar, A. (2013). "An amide based dipodal Zn 2+ complex: nano-molar detection of HSO 4− in a semi-aqueous system." Organic & biomolecular chemistry, 11(39), 6824–6828.

Fejerskov, O., Stephen, K. W., Richards, A., and Speirs, R. (1987). "Combined effect of systemic and topical fluoride treatments on human deciduous teeth–case studies." Caries research, 21(5), 452–459.

Ferguson, J. F., and Gavis, J. (1972). "A review of the arsenic cycle in natural waters." Water research, 6(11), 1259–1274.

Fitzmaurice, R. J., Kyne, G. M., Douheret, D., and Kilburn, J. D. (2002). "Synthetic receptors for carboxylic acids and carboxylates." Journal of the Chemical Society, Perkin Transactions 1, (7), 841–864.

Frisch, M., Trucks, G. W., Schlegel, H. B., Scuseria, G. E., Robb, M. A., Cheeseman, J. R., Scalmani, G., Barone, V., Mennucci, B., and Petersson, Ga. (2009). "Gaussian 09, revision a. 02, gaussian." Inc., Wallingford, CT, 200, 28.

Frisch, M., Trucks, G. W., Schlegel, Hb., Scuseria, G. E., Robb, M. A., Cheeseman, J. R., Montgomery Jr, J. A., Vreven, T., Kudin, K. N., and Burant, Jc. (2004). "Gaussian 03, revision c. 02; Gaussian." Inc., Wallingford, CT, 4.

Gale, P. A. (2001). "Anion receptor chemistry: highlights from 1999." Coordination chemistry reviews, 213(1), 79–128.

Gale, P. A. (2010). "Anion receptor chemistry: highlights from 2008 and 2009." Chemical Society Reviews., 39(10), 3746-3771.

Gale, P. A., Gunnlaugsson, T. (2010). "Preface: supramolecular chemistry of anionic species themed issue." Chemical Society Reviews., 39, 3595-3596.

Gaussian, R. A. (2003). "03, MJ Frisch, GW Trucks, HB Schlegel, GE Scuseria, MA Robb, JR Cheeseman, JA Montgomery, Jr." T. Vreven, KN Kudin, JC Burant, JM Millam, SS Iyengar, J. Tomasi, V. Barone, B. Mennucci, M. Cossi, G. Scalmani, N. Rega, GA Pet.

Gaussian09, R. A. (2009). "1, mj frisch, gw trucks, hb schlegel, ge scuseria, ma robb, jr cheeseman, g. Scalmani, v. Barone, b. Mennucci, ga petersson et al., gaussian." Inc., Wallingford CT, 121, 150–166.

Gholivand, M. B., Rahimi-Nasrabadi, M., Ganjali, M. R., and Salavati-Niasari, M. (2007). "Highly selective and sensitive copper membrane electrode based on a new synthesized Schiff base." Talanta, 73(3), 553–560.

Ghorai, A., Mondal, J., Chandra, R., and Patra, G. K. (2016). "A reversible fluorescent-colorimetric chemosensor based on a novel Schiff base for visual detection of $CO_3{}^{2-}$ in aqueous solution." RSC Advances, 6(76), 72185–72192.

Ghosh, A., Ta, S., Ghosh, M., Karmakar, S., Banik, A., Dangar, T. K., Mukhopadhyay, S. K., and Das, D. (2016). "Dual mode ratiometric recognition of zinc acetate: nanomolar detection with in vitro tracking of endophytic bacteria in rice root tissue." Dalton Transactions, 45(2), 599–606.

Ghosh, K., and Majumdar, A. (2013). "Enantioselective sensing of lactate by pyridinium-based chiral receptor." Tetrahedron Letters, 54(42), 5686–5689.

Ghosh, K., Saha, I., Masanta, G., Wang, E. B., & Parish, C. A. (2010). "Triphenylamine-based receptor for selective recognition of dicarboxylates." Tetrahedron Letters, 51(2), 343-347.

Ghosh, K., Saha, I., Masanta, G., Wang, E. B., and Parish, C. A. (2010). "Triphenylamine-based receptor for selective recognition of dicarboxylates." Tetrahedron Letters, 51(2), 343–347.

Ghosh, P., Roy, B. G., Mukhopadhyay, S. K., and Banerjee, P. (2015). "Recognition of fluoride anions at low ppm level inside living cells and from fluorosis affected tooth and saliva samples." RSC Advances, 5(35), 27387–27392.

Ghosh, T., and Maiya, B. G. (2004). "Visual sensing of fluoride ions by dipyrrolyl derivatives bearing electron-withdrawing groups." Journal of Chemical Sciences, 116(1), 17–20.

Ghule, N. V., Bhosale, S. V., and Bhosale, S. V. (2014). "Dipyrrolyl-bis-sulfonamide chromophore based probe for anion recognition." RSC Advances, 4(52), 27112–27115.

Gougoux, A., Lemieux, G. and Lavoie, N. (1976). "Maleate-induced bicarbonaturia in the dog: a carbonic anhydrase-independene effect." Am. J. Physiol., 231, 1010–1017.

Greenhalgh, S., and Selman, M. (2012). "Comparing water quality trading programs: what lessons are there to learn?" Journal of Regional Analysis and Policy, 42(1100-2016–89913).

Grice, M. M., Alexander, B. H., Hoffbeck, R., Kampa, D. M. (2007). "Self-reported medical conditions in perfluorooctanesulfonyl fluoride manufacturing workers." Journal of occupational and environmental medicine, 49(7), 722-729.

Gunnlaugsson, T., Davis, A. P., O'Brien, J. E., and Glynn, M. (2002). "Fluorescent sensing of pyrophosphate and bis-carboxylates with charge neutral PET chemosensors." Organic Letters, 4(15), 2449–2452.

Gunnlaugsson, T., Glynn, M., Tocci, G. M., Kruger, P. E., Pfeffer, F. M. (2006). "Anion recognition and sensing in organic and aqueous media using luminescent and colorimetric sensors." Coordination chemistry reviews., 250(23-24), 3094-3117.

Gunnlaugsson, T., Kruger, P. E., Jensen, P., Tierney, J., Ali, H. D. P., and Hussey, G. M. (2005). "Colorimetric 'naked eye' sensing of anions in aqueous solution." The Journal of organic chemistry, 70(26), 10875–10878.

Gunupuru, R., Kesharwani, M. K., Chakraborty, A., Ganguly, B., and Paul, P. (2014). "Dipicrylamine as a colorimetric sensor for anions: experimental and computational study." RSC Advances, 4(95), 53273–53281.

Guo, C., Sun, S., He, Q., Lynch, V. M., and Sessler, J. L. (2018). "Pyrene-Linked Formylated Bis (dipyrromethane): A Fluorescent Probe for Dihydrogen Phosphate." Organic letters, 20(17), 5414–5417.

Guo, Z., Shin, I., and Yoon, J. (2012). "Recognition and sensing of various species using boronic acid derivatives." Chemical communications, 48(48), 5956–5967.

Gupta, V. K., Singh, A. K., Bhardwaj, S., and Bandi, K. R. (2014). "Biological active novel 2, 4-dinitro phenyl hydrazones as the colorimetric sensors for selective detection of acetate ion." Sensors and Actuators B: Chemical, 197, 264–273.

Hadjmohammadi, M. R., Chaichi, M. J., and Yousefpour, M. (2008). "Solvatochromism effect of different solvents on UV-Vis spectra of flouresceine and

its derivatives." Iranian Journal of Chemistry and Chemical Engineering (IJCCE), 27(4), 9–14.

Han, C., Cui, Z., Zou, Z., Tian, D., and Li, H. (2010). "Urea-type ligand-modified CdSe quantum dots as a fluorescence 'turn-on' sensor for CO 3 2− anions." Photochemical & Photobiological Sciences, 9(9), 1269–1273.

Han, F., Bao, Y., Yang, Z., Fyles, T. M., Zhao, J., Peng, X., Fan, J., Wu, Y., and Sun, S. (2007). "Simple Bisthiocarbonohydrazones as Sensitive, Selective, Colorimetric, and Switch-On Fluorescent Chemosensors for Fluoride Anions." Chemistry–A European Journal, 13(10), 2880–2892.

Hanwell, M. D., Curtis, D. E., Lonie, D. C., Vandermeersch, T., Zurek, E., and Hutchison, G. R. (2012). "Avogadro: an advanced semantic chemical editor, visualization, and analysis platform." Journal of cheminformatics, 4(1), 17.

Hariharan, P. C., and Pople, J. A. (1973). "The influence of polarization functions on molecular orbital hydrogenation energies." Theoretica chimica acta, 28(3), 213–222.

Hasegawa, H., Matsui, M., Okamura, S., Hojo, M., Iwasaki, N., and Sohrin, Y. (1999). "Arsenic speciation including 'hidden'arsenic in natural waters." Applied Organometallic Chemistry, 13(2), 113–119.

Hehre, W. J., Ditchfield, R., and Pople, J. A. (1972). "Self—consistent molecular orbital methods. XII. Further extensions of Gaussian—type basis sets for use in molecular orbital studies of organic molecules." The Journal of Chemical Physics, 56(5), 2257–2261.

Hennrich, G., Sonnenschein, H., and Resch-Genger, U. (2001). "Fluorescent anion receptors with iminoylthiourea binding sites—selective hydrogen bond mediated recognition of CO32−, HCO3− and HPO42−." Tetrahedron Letters, 42(15), 2805–2808.

Hijji, Y. M., Barare, B., Kennedy, A. P., and Butcher, R. (2009). "Synthesis and photophysical characterization of a Schiff base as anion sensor." Sensors and Actuators B: Chemical, 136(2), 297–302.

Hofmeister, F. (1888). "About the science of the effects of salts: About the water withdrawing effect of the salts." Arch. Exp. Pathol. Pharmacol., 24, 247–260.

Homocianu, M. (2011). "Solvent effects on the electronic absorption and fluorescence spectra." Journal of Advanced Research in Physics, 2(1).

Hou, P., Chen, S., and Song, X. (2014). "A colorimetric and fluorescent probe for fluoride ions based on 6-acetyl-2-naphthol." Luminescence, 29(5), 423–426.

Hu, R., Long, G., Chen, J., Yin, Y., Liu, Y., Zhu, F., Feng, J., Mei, Y., Wang, R., and Xue, H. (2015). "Highly sensitive colorimetric sensor for the detection of H2PO4− based on self-assembly of p-sulfonatocalix [6] arene modified silver nanoparticles." Sensors and Actuators B: Chemical, 218, 191–195.

Huang, F., Cheng, C., and Feng, G. (2012). "Introducing ligand-based hydrogen bond donors to a receptor: both selectivity and binding affinity for anion recognition in water can be improved." The Journal of organic chemistry, 77(24), 11405–11408.

Huang, W., Yu, X., Lin, H., Lin, H. (2011). "A colorimetric sensor for the recognition of biologically important anions." Journal of Inclusion Phenomena and Macrocyclic Chemistry., 69(1-2), 69-73.

Huang, C.-Y., Wan, C.-F., Chir, J.-L., and Wu, A.-T. (2013). "A Schiff-based colorimetric fluorescent sensor with the potential for detection of fluoride ions." *Journal of fluorescence*, 23(6), 1107–1111.

Hughes, M. F., Beck, B. D., Chen, Y., Lewis, A. S., and Thomas, D. J. (2011). "Arsenic exposure and toxicology: a historical perspective." Toxicological Sciences, 123(2), 305–332.

Huheey, J. E., Keiter, E. A., Keiter, R. L., and Medhi, O. K. (2006). Inorganic chemistry: principles of structure and reactivity. Pearson Education India.

Jadhav, V. D., and Schmidtchen, F. P. (2006). "Judging on Host− Guest Binding Mode Uniqueness: Association Entropy as an Indicator in Enantioselection." Organic letters, 8(11), 2329–2332.

Jain, A. K., Gupta, V. K., and Raisoni, J. R. (2006). "Anion recognition using newly synthesized hydrogen bonding diamide receptors: PVC based sensors for carbonate." Electrochimica acta, 52(3), 951–957.

Jiang, Q. Q., Darhkijav, B., Liu, H., Wang, F., and Li, Z. (2009). "Chem An Asian J. 2010; 5: 543–549.[PubMed](b) Liu WX, Yang R, Li AF, Li Z, Gao YF, Luo XX, Ruan YB, Jiang YB." Organic and Biomol Chem, 7, 4021–4028.

Jiang, Y., Sun, L.-L., Ren, G.-Z., Niu, X., and Hu, Z.-Q. (2016). "A novel colorimetric and fluorescent iminocoumarin-based chemosensor for acetate ion and its application to living cell imaging." Talanta, 146, 732–736.

Jin, C., Zhang, M., Wu, L., Guan, Y., Pan, Y., Jiang, J., Lin, C., and Wang, L. (2013). "Squaramide-based tripodal receptors for selective recognition of sulfate anion." Chemical Communications, 49(20), 2025–2027.

Jo, T. G., Na, Y. J., Lee, J. J., Lee, M. M., Lee, S. Y., and Kim, C. (2015). "A diaminomaleonitrile based selective colorimetric chemosensor for copper (II) and fluoride ions." New Journal of Chemistry, 39(4), 2580–2587.

Joo, T. Y., Singh, N., Lee, G. W., and Jang, D. O. (2007). "Benzimidazole-based ratiometric fluorescent receptor for selective recognition of acetate." Tetrahedron Letters, 48(50), 8846–8850.

Jose, D. A., Kumar, D. K., Ganguly, B., and Das, A. (2004). "Efficient and simple colorimetric fluoride ion sensor based on receptors having urea and thiourea binding sites." Organic letters, 6(20), 3445–3448.

Jose, D. A., Kumar, D. K., Ganguly, B., and Das, A. (2005). "Urea and thiourea based efficient colorimetric sensors for oxyanions." Tetrahedron letters, 46(32), 5343–5346.

Jose, D. A., Singh, A., Das, A., and Ganguly, B. (2007). "A density functional study towards the preferential binding of anions to urea and thiourea." Tetrahedron letters, 48(21), 3695–3698.

Jung, H. S., Kim, H. J., Vicens, J., Kim, J. S. (2009). "A new fluorescent chemosensor for F− based on inhibition of excited-state intramolecular proton transfer." Tetrahedron Letters., 50(9), 983-987.

Kaifer, A. E., and Gómez-Kaifer, M. (2008). Supramolecular electrochemistry. John Wiley & Sons.

Kalluri, J. R., Arbneshi, T., Afrin Khan, S., Neely, A., Candice, P., Varisli, B., Washington, M., McAfee, S., Robinson, B., and Banerjee, S. (2009). "Use of gold nanoparticles in a simple colorimetric and ultrasensitive dynamic light scattering assay: selective detection of arsenic in groundwater." Angewandte Chemie International Edition, 48(51), 9668–9671.

Kata, J.E., Dumlao, S.D., Wasserman, J.I., Lansdown, M.G., Jung, M.E., Faull, K.F. and Clarke, S. (2004). "3-Isopropylmalate is the major endogenous substrate of the saccharomyces cerevisiae trans-aconitate methyltransferase." Biochemistry, 43, 5976–5986.

Keefe, M. H., Benkstein, K. D., and Hupp, J. T. (2000). "Luminescent sensor molecules based on coordinated metals: a review of recent developments." Coordination Chemistry Reviews, 205(1), 201–228.

Kigga, M., Trivedi, D. R. (2014). "Naked-eye" detection of inorganic fluoride ion in aqueous media using base labile proton: A different approach." Journal of Fluorine Chemistry., 160, 1-7.

Kim, H. J., Lee, J. H., Lee, M., and Lee, T. S. (2008). "Optical switching and anion-induced chromogenic application in conjugated polyazomethine derivatives." Reactive and Functional Polymers, 68(12), 1696–1703.

Kim, K. B., Kim, H., Song, E. J., Kim, S., Noh, I., Kim, C. (2013). "A cap-type Schiff base acting as a fluorescence sensor for zinc (II) and a colorimetric sensor for iron (II), copper (II), and zinc (II) in aqueous media." Dalton Transactions., 42(47), 16569-16577.

Kirk, K. L. (1991). "Biochemistry of inorganic fluoride." Biochemistry of the Elemental Halogens and Inorganic Halides, Springer, 19–68.

Kodlady, S. N., Narayana, B., Sarojini, B. K., and Gauthama, B. U. (2019). "Aromatic aldehyde based chemosensors for fluoride and cyanide detection in organic and aqueous media: Ascertained by characterization, spectroscopic and DFT studies." Inorganica Chimica Acta, 494, 245–255.

Kornak, U., Kasper, D., Bosl, M.R., Kaiser, E., Schweizer, M., Schulz, A., Friedrich, W., Delling, G. and Jentsch, T.J. (2001). "Loss of the ClC-7 chloride channel leads to osteopetrosis in mice and man." Cell, 104, 205-215.

Korte, N. E., and Fernando, Q. (1991). "A review of arsenic (III) in groundwater." Critical Reviews in Environmental Science and Technology, 21(1), 1–39.

Kral, V., Andrievsky, A., and Sessler, J. L. (1995). "A covalently linked sapphyrin dimer. a new receptor for dicarboxylate anions." Journal of the American Chemical Society, 117(10), 2953–2954.

Kubik, S. (2010). "Anion recognition in water." Chemical Society Reviews, 39(10), 3648–3663.

Kumar, R., Jain, H., Gahlyan, P., Joshi, A., Ramachandran, C. N. (2018). "A highly sensitive pyridine-dicarbohydrazide based chemosensor for colorimetric recognition of Cu 2+, AMP 2−, F− and AcO− ions." New Journal of Chemistry., 42(11), 8567-8576.

Kumar, S., Luxami, V., and Kumar, A. (2008). "Chromofluorescent probes for selective detection of fluoride and acetate ions." Organic letters, 10(24), 5549–5552.

Kumari, N., Jha, S., and Bhattacharya, S. (2011). "Colorimetric probes based on anthraimidazolediones for selective sensing of fluoride and cyanide ion via intramolecular charge transfer." The Journal of organic chemistry, 76(20), 8215–8222.

Larsen, K. R., Johnsen, C., Hammerich, O., and Jeppesen, J. O. (2013). "Selective redox-active molecular receptors for K+ and Ag+." Organic letters, 15(7), 1452–1455.

Lavigne, J. J., and Anslyn, E. V. (1999). "Teaching old indicators new tricks: A colorimetric chemosensing ensemble for tartrate/malate in beverages." Angewandte Chemie International Edition, 38(24), 3666–3669.

Lawrence, K., Flower, S. E., Kociok-Kohn, G., Frost, C. G., and James, T. D. (2012). "A simple and effective colorimetric technique for the detection of boronic acids and their derivatives." Analytical Methods, 4(8), 2215–2217.

Lee, C., Yang, W., and Parr, R. G. (1988). "Density-functional exchange-energy approximation with correct asymptotic behaviour." Phys. Rev. B, 37, 785–789.

Lee, C., Yang, W., and Parr, R. G. (1988). "Development of the Colle-Salvetti correlation-energy formula into a functional of the electron density." Physical review B, 37(2), 785.

Lee, D. H., Lee, K. H., and Hong, J.-I. (2001). "An azophenol-based chromogenic anion sensor." Organic letters, 3(1), 5–8.

Lee, G. W., Kim, N.-K., and Jeong, K.-S. (2010). "Synthesis of biindole− diazo conjugates as a colorimetric anion receptor." Organic letters, 12(11), 2634–2637.

Lee, H. J., Yoon, I. J., Yoo, C. L., Pyun, H.-J., Cha, G. S., and Nam, H. (2000). "Potentiometric evaluation of solvent polymeric carbonate-selective membranes based on molecular tweezer-type neutral carriers." Analytical chemistry, 72(19), 4694–4699.

Lee, H. K., Oh, H., Nam, K. C., and Jeon, S. (2005). "Urea-functionalized calix [4] arenes as carriers for carbonate-selective electrodes." Sensors and Actuators B: Chemical, 106(1), 207–211.

Lee, J. Y., Kim, S. K., Jung, J. H., and Kim, J. S. (2005). "Bifunctional fluorescent calix [4] arene chemosensor for both a cation and an anion." The Journal of organic chemistry, 70(4), 1463–1466.

Li, A.-F., Wang, J.-H., Wang, F., and Jiang, Y.-B. (2010). "Anion complexation and sensing using modified urea and thiourea-based receptors." Chemical Society Reviews, 39(10), 3729–3745.

Li, A.-F., Wang, J.-H., Wang, F., and Jiang, Y.-B. (2010). "Anion complexation and sensing using modified urea and thiourea-based receptors." Chemical Society Reviews, 39(10), 3729–3745.

Li, J.-Q., Wei, T.-B., Lin, Q., Li, P., and Zhang, Y.-M. (2011). "Mercapto thiadiazole-based sensor with colorimetric specific selectivity for AcO− in aqueous solution." Spectrochimica Acta Part A: Molecular and Biomolecular Spectroscopy, 83(1), 187–193.

Li, P., Zhang, X. Q., Chen, Y. J., Lian, H. Z., & Hu, X. (2014). "A sequential solid phase microextraction system coupled with inductively coupled plasma mass spectrometry for speciation of inorganic arsenic." Analytical Methods., 6(12), 4205-4211.

Li, S.-H., Yu, C.-W., Yuan, W.-T., and XU, J.-G. (2004). "A lanthanide hybrid cluster as a selective optical chemosensor for phosphate-containing anions in aqueous solution." Analytical sciences, 20(10), 1375–1377.

Li, Z., Liu, C., Wang, S., Xiao, L., and Jing, X. (2019). "Visual detection of cyanide ion in aqueous medium by a new chromogenic azo-azomethine chemosensor." Spectrochimica Acta Part A: Molecular and Biomolecular Spectroscopy, 210, 321–328.

Li, Z., Wang, S., Xiao, L., Li, X., Jing, X., Peng, X., and Ren, L. (2018). "An efficient colorimetric and absorption ratiometric anion sensor based on a simple azo-azomethine receptor." Inorganica Chimica Acta, 479, 148–153.

Li, Z., Wang, S., Xiao, L., Li, X., Shao, X., Jing, X., Peng, X., and Ren, L. (2018). "An efficient colorimetric probe for fluoride ion based on schiff base." Inorganica Chimica Acta, 476, 7–11.

Lin, Y.-D., Pen, Y.-S., Su, W., Liau, K.-L., Wen, Y.-S., Tu, C.-H., Sun, C.-H., and Chow, T. J. (2012). "Reaction-Based Colorimetric and Ratiometric Fluorescence Sensor for Detection of Cyanide in Aqueous Media." Chemistry–An Asian Journal, 7(12), 2864–2871.

Lin, Z. H., Xie, L. X., Zhao, Y. G., Duan, C. Y., Qu, J. P. (2007). "Thiourea-based molecular clips for fluorescent discrimination of isomeric dicarboxylates." Organic & biomolecular chemistry, 5(21), 3535-3538.

Little, M. J., and Wentzell, P. D. (1995). "Evaluation of acoustic emission as a means for carbonate determination." Analytica chimica acta, 309(1–3), 283–292.

Liu, S.-Y., Fang, L., He, Y.-B., Chan, W.-H., Yeung, K.-T., Cheng, Y.-K., and Yang, R.-H. (2005). "Cholic-acid-based fluorescent sensor for dicarboxylates and acidic amino acids in aqueous solutions." Organic letters, 7(26), 5825–5828.

Liu, W. X., Jiang, Y. B. (2007). "N-Amidothiourea based PET chemosensors for anions." Organic & biomolecular chemistry., 5(11), 1771-1775.

Liu, W., Sun, Z., Ranheimer, M., Forsling, W., and Tang, H. (1999). "A flexible method of carbonate determination using an automatic gas analyzer equipped with an FTIR photoacoustic measurement chamber." Analyst, 124(3), 361–365.

Lv, X., Liu, J., Liu, Y., Zhao, Y., Chen, M., Wang, P., Guo, W. (2011). "Rhodafluor-based chromo-and fluorogenic probe for cyanide anion." Sensors and Actuators B: Chemical., 158(1), 405-410.

Mahapatra, A. K., Manna, S. K., and Sahoo, P. (2011). "Color response of tri-armed azo host colorimetric sensors and test kit for fluoride." Talanta, 85(5), 2673–2680.

Mallick, A., Katayama, T., Ishibasi, Y., Yasuda, M., and Miyasaka, H. (2011). "Norharmane: Old yet highly selective dual channel ratiometric fluoride and hydrogen sulfate ion sensor." Analyst, 136(2), 275–277.

Manivannan, R., Satheshkumar, A., El-Mossalamy, E.-S. H., Al-Harbi, L. M., Kosa, S. A., and Elango, K. P. (2015). "Design, synthesis and characterization of indole based anion sensing receptors." New Journal of Chemistry, 39(5), 3936–3947.

March, J. (1992). Advanced organic chemistry: reactions, mechanisms, and structure. John Wiley & Sons,.

Marcotte, N., Plaza, P., Lavabre, D., Fery-Forgues, S., and Martin, M. M. (2003). "Calcium Photorelease from a Symmetrical Donor− Acceptor− Donor Bis-crown-fluoroionophore Evidenced by Ultrafast Absorption Spectroscopy." The Journal of Physical Chemistry A, 107(14), 2394–2402.

Marcus, Y. (1991). "Thermodynamics of solvation of ions. Part 5.—Gibbs free energy of hydration at 298.15 K." Journal of the Chemical Society, Faraday Transactions, 87(18), 2995–2999.

Margolis, H. C., and Moreno, E. C. (1990). "Physicochemical perspectives on the cariostatic mechanisms of systemic and topical fluorides." Journal of dental research, 69(2_suppl), 606–613.

Marini, A., Munoz-Losa, A., Biancardi, A., and Mennucci, B. (2010). "What is solvatochromism?" The Journal of Physical Chemistry B, 114(51), 17128–17135.

Marks, J., Debnam, E. S., and Unwin, R. J. (2010). "Phosphate homeostasis and the renal-gastrointestinal axis." American Journal of Physiology-Renal Physiology, 299(2), F285–F296.

Martinez-Manez, R., and Sancenón, F. (2003). "Fluorogenic and chromogenic chemosensors and reagents for anions." Chemical reviews, 103(11), 4419–4476.

Masscheleyn, P. H., Delaune, R. D., and Patrick, W. H. (1991). "Arsenic and selenium chemistry as affected by sediment redox potential and pH." Journal of Environmental Quality, 20(3), 522–527.

Matthews, S. E., and Beer, P. D. (2005). "Calixarene-based anion receptors." Supramolecular Chemistry, 17(6), 411–435.

Miao, H., Wuer, G., Shuangshuang, X. (2014). "On-line electrokinetic extraction and electrochemical hydride generation coupled with atomic fluorescence spectrometry for inorganic arsenic speciation in water samples." Analytical Methods., 6(6), 1796-1801.

Miehlich, B., Savin, A., Stoll, H., and Preuss, H. (1989). "Results obtained with the correlation energy density functionals of Becke and Lee, Yang and Parr." Chemical Physics Letters, 157(3), 200–206.

Miyaji, H., Sato, W., & Sessler, J. L. (2000). Naked-eye detection of anions in dichloromethane: colorimetric anion sensors based on calix [4] pyrrole. Angewandte Chemie International Edition, 39, 1777-1780.

Mohadesi, A., and Taher, M. A. (2007). "Voltammetric determination of Cu (II) in natural waters and human hair at a meso-2, 3-dimercaptosuccinic acid self-assembled gold electrode." Talanta, 72(1), 95–100.

Morris, R. V., Ruff, S. W., Gellert, R., Ming, D. W., Arvidson, R. E., Clark, B. C., Golden, D. C., Siebach, K., Klingelhöfer, G., and Schröder, C. (2010). "Identification of carbonate-rich outcrops on Mars by the Spirit rover." Science, 329(5990), 421–424.

Moss, B. (1996). "A land awash with nutrients-The problem of eutrophication." Chem. Ind., 11, 407-411.

Mukherjee, S. C., Saha, K. C., Pati, S., Dutta, R. N., Rahman, M. M., Sengupta, M. K., Ahamed, S., Lodh, D., Das, B., and Hossain, M. A. (2005). "Murshidabad—one of the nine groundwater arsenic-affected districts of West Bengal, India. Part II: dermatological, neurological, and obstetric findings." Clinical Toxicology, 43(7), 835–848.

Murray, J. J. (1993). "Efficacy of preventive agents for dental caries." Caries Research, 27(Suppl. 1), 2–8.

Murugesan, K., Jeyasingh, V., Lakshminarayanan, S., Narayanan, S., Ramasamy, S., Enoch, I. M. V., and Piramuthu, L. (2019). "Simple and highly electron deficient Schiff-base host for anions: First turn-on colorimetric bifluoride sensor." Spectrochimica Acta Part A: Molecular and Biomolecular Spectroscopy, 209, 165–169.

Nie, L., Li, Z., Han, J., Zhang, X., Yang, R., Liu, W.-X., Wu, F.-Y., Xie, J.-W., Zhao, Y.-F., and Jiang, Y.-B. (2004). "Development of N-benzamidothioureas as a new generation of thiourea-based receptors for anion recognition and sensing." The Journal of organic chemistry, 69(19), 6449–6454.

Nie, L., Zhang, Q., Hu, L., Liu, Y., & Yan, Z. (2017). "Modified hydrazone derivatives for ratiometric and colorimetric F− recognition: Relationship between architectures and performances". Sensors and Actuators B: Chemical, 245, 314-320.

Nisbet, D. J., Callaway, T. R., Edrington, T. S., Anderson, R. C., and Krueger, N. (2009). "Effects of the Dicarboxylic Acids Malate and Fumarate on E. coli O157: H7 and Salmonellaenterica Typhimurium Populations in Pure Culture and in Mixed Ruminal Microorganism Fermentations." Current microbiology, 58(5), 488–492.

Nishiyabu, R., and Anzenbacher, P. (2005). "Sensing of antipyretic carboxylates by simple chromogenic calix [4] pyrroles." Journal of the American Chemical Society, 127(23), 8270–8271.

Nishiyabu, R., and Anzenbacher, P. (2006). "1, 3-Indane-based chromogenic calixpyrroles with push− pull chromophores: synthesis and anion sensing." Organic letters, 8(3), 359–362.

Niu, H.-T., Su, D., Jiang, X., Yang, W., Yin, Z., He, J., and Cheng, J.-P. (2008). "A simple yet highly selective colorimetric sensor for cyanide anion in an aqueous environment." Organic & biomolecular chemistry, 6(17), 3038–3040.

Odago, M. O., Colabello, D. M., and Lees, A. J. (2010). "A simple thiourea based colorimetric sensor for cyanide anion." Tetrahedron, 66(38), 7465–7471.

Ogata, F., Ueda, A., Tanei, S., Imai, D., and Kawasaki, N. (2016). "Simultaneous removal of phosphate and nitrite ions from aqueous solutions using modified soybean waste." Journal of industrial and engineering chemistry, 35, 287–294.

Ozsvath, D. L. (2009). "Fluoride and environmental health: a review." Reviews in Environmental Science and Bio/Technology., 8(1), 59-79.

Pangannaya, S., Thimaradka, V., and Trivedi, D. R. (2018). "Electroanalytical and spectral investigation of organic receptors as colorimetric and absorption ratiometric anion chemosensor." Supramolecular Chemistry, 30(2), 103–114.

Park, G. J., Jo, H. Y., Ryu, K. Y., Kim, C. (2014). "A new coumarin-based chromogenic chemosensor for the detection of dual analytes Al 3+ and F−." RSC Advances., 4(109), 63882-63890.

Park, J. J., Kim, Y.-H., Kim, C., and Kang, J. (2011). "Naked eye detection of fluoride and pyrophosphate with an anion receptor utilizing anthracene and nitrophenyl group as signaling group." Tetrahedron letters, 52(21), 2759–2763.

Park, S., Hong, K.-H., Hong, J.-I., and Kim, H.-J. (2012). "Azo dye-based latent colorimetric chemodosimeter for the selective detection of cyanides in aqueous buffer." Sensors and Actuators B: Chemical, 174, 140–144.

Pasias, I. N., Thomaidis, N. S., Bakeas, E. B., Piperaki, E. A. (2013). "Application of zirconium–iridium permanent modifier for the simultaneous determination of lead, cadmium, arsenic, and nickel in atmospheric particulate matter by multi-element electrothermal atomic absorption spectrometry." Environmental monitoring and assessment., 185(8), 6867-6879.

Patil, P., Ajeya, K. V., Bhat, M. P., Sriram, G., Yu, J., Jung, H.-Y., Altalhi, T., Kigga, M., and Kurkuri, M. D. (2018). "Real-Time Probe for the Efficient Sensing of Inorganic Fluoride and Copper Ions in Aqueous Media." ChemistrySelect, 3(41), 11593–11600.

Peng, X., Wu, Y., Fan, J., Tian, M., and Han, K. (2005). "Colorimetric and ratiometric fluorescence sensing of fluoride: tuning selectivity in proton transfer." The Journal of organic chemistry, 70(25), 10524–10531.

Pérez-Casas, C., and Yatsimirsky, A. K. (2008). "Detailing hydrogen bonding and deprotonation equilibria between anions and urea/thiourea derivatives." The Journal of organic chemistry, 73(6), 2275–2284.

Piątek, P., and Jurczak, J. (2002). "A selective colorimetric anion sensor based on an amide group containing macrocycle." Chemical Communications, (20), 2450–2451.

Pramanik, K., Ghosh, P., Dey, D., Malpaharia, P., Chandra, S. K., Mukhopadhyay, S. K., and Banerjee, P. (2018). "Chelator Probe with Exceptionally High Stokes Shift for Selective Detection of OAc⁻ with Red Emission: Application as a Biosensor." ChemistrySelect, 3(4), 1151–1156.

Preiss, J., and Handler, P. (1958). "Biosynthesis of diphosphopyridine nucleotide I. Identification of intermediates." Journal of Biological Chemistry, 233(2), 488–492.

Quinlan, E., Matthews, S. E., and Gunnlaugsson, T. (2007). "Colorimetric recognition of anions using preorganized tetra-amidourea derived calix [4] arene sensors." The Journal of organic chemistry, 72(20), 7497–7503.

Raker, J., and Glass, T. E. (2002). "Selectivity via cooperative interactions: detection of dicarboxylates in water by a pinwheel chemosensor." The Journal of organic chemistry, 67(17), 6113–6116.

Reclaru, L., and Meyer, J.-M. (1998). "Effects of fluorides on titanium and other dental alloys in dentistry." Biomaterials, 19(1–3), 85–92.

Reena, V., Suganya, S., Velmathi, S. (2013). "Synthesis and anion binding studies of azo-Schiff bases: Selective colorimetric fluoride and acetate ion sensors." Journal of Fluorine Chemistry., 153, 89-95.

Ren, J., Wu, Z., Zhou, Y., Li, Y., and Xu, Z. (2011). "Colorimetric fluoride sensor based on 1, 8-naphthalimide derivatives." Dyes and Pigments, 91(3), 442–445.

Rezaeian, K., and Khanmohammadi, H. (2014). "Naked-eye detection of biologically important anions by a new chromogenic azo-azomethine sensor." Spectrochimica Acta Part A: Molecular and Biomolecular Spectroscopy, 133, 31–37.

Richards, M. W., Spitzer, J. C., and Warner, M. B. (1986). "Effect of varying levels of postpartum nutrition and body condition at calving on subsequent reproductive performance in beef cattle." Journal of Animal Science, 62(2), 300–306.

Ros-Lis, J. V., Martínez-Máñez, R., Sancenón, F., Soto, J., Rurack, K., and Weißhoff, H. (2007). "Signalling Mechanisms in Anion-Responsive Push-Pull Chromophores: The Hydrogen-Bonding, Deprotonation and Anion-Exchange Chemistry of Functionalized Azo Dyes." European journal of organic chemistry, 2007(15), 2449–2458.

Royzen, M., Durandin, A., Young, V. G., Geacintov, N. E., and Canary, J. W. (2006). "A sensitive probe for the detection of Zn (II) by time-resolved fluorescence." Journal of the American Chemical Society, 128(12), 3854–3855.

Saha, J., Roy, A. D., Dey, D., Nath, J., Bhattacharjee, D., and Hussain, S. A. (2017). "Development of arsenic (v) sensor based on fluorescence resonance energy transfer." Sensors and Actuators B: Chemical, 241, 1014–1023.

Saha, S., Ghosh, A., Mahato, P., Mishra, S., Mishra, S. K., Suresh, E., Das, A. (2010). "Specific recognition and sensing of CN− in sodium cyanide solution." Organic letters., 12(15), 3406-3409.

Sakai, R., Barasa, E. B., Sakai, N., Sato, S., Satoh, T., and Kakuchi, T. (2012). "Colorimetric detection of anions in aqueous solution using poly (phenylacetylene) with sulfonamide receptors activated by electron withdrawing group." Macromolecules, 45(20), 8221–8227.

Sancenón, F., Martínez-Máñez, R., Miranda, M. A., Seguí, M.-J., and Soto, J. (2003). "Towards the development of colorimetric probes to discriminate between isomeric dicarboxylates." Angewandte Chemie International Edition, 42(6), 647–650.

San-José, N., Gómez-Valdemoro, A., Ibeas, S., García, F. C., Serna, F., and García, J. M. (2010). "Colorimetric anion sensing by polyamide models containing urea-binding sites." Supramolecular Chemistry, 22(6), 325–338.

Santos-Figueroa, L. E., Moragues, M. E., Raposo, M. M. M., Batista, R. M., Costa, S. P., Ferreira, R. C. M., Sancenón, F., Martínez-Máñez, R., Ros-Lis, J. V., and Soto, J. (2012). "Synthesis and evaluation of thiosemicarbazones functionalized with furyl moieties as new chemosensors for anion recognition." Organic & biomolecular chemistry, 10(36), 7418–7428.

Saravanakumar, D., Sengottuvelan, N., Kandaswamy, M., Aravindan, P. G., and Velmurugan, D. (2005). "Amide-nitrophenyl based colorimetric receptors for selective sensing of fluoride ions." Tetrahedron letters, 46(42), 7255–7258.

Saroj, M. K., Sharma, N., and Rastogi, R. C. (2011). "Solvent effect profiles of absorbance and fluorescence spectra of some indole based chalcones." Journal of fluorescence, 21(6), 2213.

Schmidtchen, F. P., and Berger, M. (1997). "Artificial organic host molecules for anions." Chemical reviews, 97(5), 1609–1646.

Schumacher, A. L., Hill, J. P., Ariga, K., and D'Souza, F. (2007). "Highly effective electrochemical anion sensing based on oxoporphyrinogen." Electrochemistry Communications, 9(12), 2751–2754.

Scott, D.A., Wang, R., Kreman, T.M., Sheffield V.C. and Karniski, L.P. (1999). "The Pendred syndrome gene encodes a chloride-iodide transport protein." Nat. Genet., 21, 440- 443.

Sessler, J. L., Gale, P. A., and Cho, W.-S. (2006). Anion receptor chemistry. Royal Society of Chemistry.

Shang, X., Li, J., Guo, K., Dang, Q., Wang, T., Zhang, J., and Xu, X. (2018). "The Synthetic and Anion-binding Ability of Novel Colorimetric Chemosensors Based on Azobenzol Derivatives: Experimental and Theoretical." Current Organic Synthesis, 15(1), 143–149.

Shao, J., Yu, X., Lin, H., and Lin, H. (2008). "Colorimetric recognizing of biologically important anions based on anion-induced tautomerism of the sensor." Journal of Molecular Recognition: An Interdisciplinary Journal, 21(6), 425–430.

Sharma, D., Kumar, S. A., and Sahoo, S. K. (2014). "Vitamin B6 cofactor derived chemosensor for the selective colorimetric detection of acetate anions." Tetrahedron Letters, 55(4), 927–930.

Sharma, D., Moirangthem, A., Sahoo, S. K., Basu, A., Roy, S. M., Pati, R. K., Patil, U. D. (2014). "Anion selective chromogenic and fluorogenic chemosensor and its application in breast cancer live cell imaging." RSC Advances., 4(78), 41446-41452.

Sharma, D., Sahoo, S. K., Bera, R. K., and Kamal, R. (2013). "Spectroscopic and computational study of a naphthalene derivative as colorimetric and fluorescent sensor for bioactive anions." Journal of fluorescence, 23(3), 387–392.

Sharma, D., Sahoo, S. K., Chaudhary, S., Bera, R. K., and Callan, J. F. (2013). "Fluorescence 'turn-on'sensor for F− derived from vitamin B6 cofactor." Analyst, 138(13), 3646–3650.

Sharma, R., Mittal, S. K., and Chhibber, M. (2015). "Voltammetric Sensor for Fluoride Ions Using Diphenylether Derivatives Supported by NMR and Theoretical Studies." Journal of The Electrochemical Society, 162(9), B248–B255.

Sharma, S., Hundal, M. S., and Hundal, G. (2013). "Dual channel chromo/fluorogenic chemosensors for cyanide and fluoride ions–an example of in situ acid catalysis of the Strecker reaction for cyanide ion chemodosimetry." Organic & biomolecular chemistry, 11(4), 654–661.

Sharma, V. K., and Sohn, M. (2009). "Aquatic arsenic: toxicity, speciation, transformations, and remediation." Environment international, 35(4), 743–759.

Shannon, R. D. (1976). "Revised effective ionic radii and systematic studies of interatomic distances in halides and chalcogenides." *Acta crystallographica section A: crystal physics, diffraction, theoretical and general crystallography*, 32(5), 751–767.

Shin, J. H., Lee, H. J., Kim, C. Y., Oh, B. K., Rho, K. L., Nam, H., and Cha, G. S. (1996). "ISFET-based differential pCO2 sensors employing a low-resistance gas-permeable membrane." Analytical Chemistry, 68(18), 3166–3172.

Shin, Y.-J., Jang, S.-A., Song, H.-Y., Song, H.-J., and Song, K. B. (2011). "Effects of combined fumaric acid-UV-C treatment and rapeseed protein-gelatin film packaging on the postharvest quality of 'Seolhyang'strawberries." Food Science and Biotechnology, 20(4), 1161.

Shiraishi, Y., Adachi, K., Itoh, M., and Hirai, T. (2009). "Spiropyran as a selective, sensitive, and reproducible cyanide anion receptor." Organic letters, 11(15), 3482–3485.

Simon, D.B., Bindra, R.S., Mansfield, T.A., Nelson-Williams, C., Mendonca, E., Stone, R., Schurman, S., Nayir, A., Alpay, H., Bakkaloglu, A., Rodriguez-Soriano, J., Morales, J.M., Sanjad, S.A., Taylor, C.M., Pilz, D., Brem, A., Trachtman, H., Griswold, W., Richard, G.A., John, E. and Lifton, R.P. (1997). "Mutations in the chloride channel gene, CLCNKB, cause Bartter's syndrome type III." Nat. Genet. 17, 171 – 178.

Simon, M. J., Beil, F. T., Riedel, C., Lau, G., Tomsia, A., Zimmermann, E. A., Ignatius, A. (2016). "Deterioration of teeth and alveolar bone loss due to chronic environmental high-level fluoride and low calcium exposure." Clinical oral investigations., 20(9), 2361-2370.

Singh, P., Barjatiya, M., Dhing, S., Bhatnagar, R., Kothari, S., Dhar, V. (2001). "Evidence suggesting that high intake of fluoride provokes nephrolithiasis in tribal populations." Urological research., 29(4), 238-244.

Sivakumar, R., Reena, V., Ananthi, N., Babu, M., Anandan, S., and Velmathi, S. (2010). "Colorimetric and fluorescence sensing of fluoride anions with potential salicylaldimine based schiff base receptors." Spectrochimica Acta Part A: Molecular and Biomolecular Spectroscopy, 75(3), 1146–1151.

Smedley, P. L., and Kinniburgh, D. G. (2002). "A review of the source, behaviour and distribution of arsenic in natural waters." Applied geochemistry, 17(5), 517–568.

Snowden, T. S., and Anslyn, E. V. (1999). "Anion recognition: synthetic receptors for anions and their application in sensors." Current opinion in chemical biology, 3(6), 740–746.

Sørensen, J., Christensen, D., and Jørgensen, B. B. (1981). "Volatile fatty acids and hydrogen as substrates for sulfate-reducing bacteria in anaerobic marine sediment." Appl. Environ. Microbiol., 42(1), 5–11.

Srikala, P., Tarafder, K., Shetty, A. N., and Trivedi, D. R. (2016). "Insights into the electrooptical anion sensing properties of a new organic receptor: solvent dependent chromogenic response and DFT studies." RSC Advances, 6(78), 74649–74653.

Status, W. E. C. on O. H., and Use, F. (1994). Fluorides and Oral Health: Report of the WHO Expert Committee on Oral Health Status and Fluoride Use. World Health Organization.

Steed, J. W. (2010). "Anion-tuned supramolecular gels: a natural evolution from urea supramolecular chemistry." Chemical Society Reviews, 39(10), 3686–3699.

Stepiński, J., Pawłowska, D., and Angielski, S. (1984). "Effect of lithium on renal gluconeogenesis." Acta Biochimica Polonica, 31(2), 229–240.

Su, H., Lin, H., Cai, Z.-S., and Lin, H. (2010). "Anion receptor based on thiourea: via hydrogen bonding interaction and efficient deprotonation." Journal of Inclusion Phenomena and Macrocyclic Chemistry, 67(1–2), 183–189.

Suganya, S., and Velmathi, S. (2013). "Simple azo-based salicylaldimine as colorimetric and fluorescent probe for detecting anions in semi-aqueous medium." Journal of Molecular Recognition, 26(6), 259–267.

Suganya, S., Park, J. S., and Velmathi, S. (2014). "Visual sensing of aqueous anions by C2-symmetric chemosensor and its application in real sample analysis." Sensors and Actuators B: Chemical, 190, 679–684.

Suganya, S., Velmathi, S., Venkatesan, P., Wu, S.-P., and Boobalan, M. S. (2015). "A highly fluorescent zinc complex of a dipodal N-acyl hydrazone as a selective sensor for H 2 PO 4− ions and application in living cells." Inorganic Chemistry Frontiers, 2(7), 649–656.

Suksai, C., and Tuntulani, T. (2003). "Chromogenic anion sensors." Chem. Soc. Rev., 32(4), 192-202.

Sun, S., Hu, X.-Y., Chen, D., Shi, J., Dong, Y., Lin, C., Pan, Y., and Wang, L. (2013). "Pillar [5] arene-based side-chain polypseudorotaxanes as an anion-responsive fluorescent sensor." Polymer Chemistry, 4(7), 2224–2229.

Tas, A. C. (2009). "Monodisperse calcium carbonate microtablets forming at 70° C in prerefrigerated CaCl2–gelatin–urea solutions." International Journal of Applied Ceramic Technology, 6(1), 53–59.

Tchounwou, P. B., Yedjou, C. G., Patlolla, A. K., and Sutton, D. J. (2012). "Heavy metal toxicity and the environment." Molecular, clinical and environmental toxicology, Springer, 133–164.

Thimaradka, V., Pangannaya, S., Mohan, M., and Trivedi, D. R. (2018). "Hydrazinylpyridine based highly selective optical sensor for aqueous source of carbonate ions: Electrochemical and DFT studies." Spectrochimica Acta Part A: Molecular and Biomolecular Spectroscopy, 193, 330–337.

Tomasi, J., and Persico, M. (1994). "Molecular interactions in solution: an overview of methods based on continuous distributions of the solvent." Chemical Reviews, 94(7), 2027–2094.

Trivedi, D. R. (2014). "A new colorimetric receptor for selective detection of maleate vs. fumarate and ratiometric detection of F− ions." Analytical Methods, 6(11), 3817–3825.

Tseng, Y. P., Tu, G. M., Lin, C. H., Chang, C. T., Lin, C. Y., Yen, Y. P. (2007). "Synthesis of colorimetric sensors for isomeric dicarboxylate anions: selective discrimination between maleate and fumarate." Organic & biomolecular chemistry, 5(22), 3592-3598.

Tsukada, K., Miyahara, Y., Shibata, Y., and Miyagi, H. (1990). "An integrated chemical sensor with multiple ion and gas sensors." Sensors and Actuators B: Chemical, 2(4), 291–295.

Vázquez, M., Fabbrizzi, L., Taglietti, A., Pedrido, R. M., González-Noya, A. M., and Bermejo, M. R. (2004). "A colorimetric approach to anion sensing: a selective chemosensor of fluoride ions, in which color is generated by anion-enhanced π delocalization." Angewandte Chemie International Edition, 43(15), 1962–1965.

Vella, F. (1990). "Biochemistry: By CK Mathews and KE van Holde. pp 1299. Benjamin/Cummings Publishing Co, Redwood City, CA, USA. 1990.£ 24.95 ISBN 0-8053-5015-2." Biochemical Education, 18(3), 154–154.

Villamil-Ramos, R., and Yatsimirsky, A. K. (2011). "Selective fluorometric detection of pyrophosphate by interaction with alizarin red S–dimethyltin (IV) complex." Chemical Communications, 47(9), 2694–2696.

Wang, L., Fang, G., and Cao, D. (2014). "A reversible and reusable selective chemosensor for fluoride detection using a phenolic OH-containing BODIPY dye by both colorimetric 'naked-eye'and fluorometric modes." Journal of fluorescence, 24(6), 1757–1766.

Wang, L., He, X., Guo, Y., Xu, J., and Shao, S. (2011). "Tris (indolyl) methene molecule as an anion receptor and colorimetric chemosensor: tunable selectivity and sensitivity for anions." Organic & biomolecular chemistry, 9(3), 752–757.

Wang, Q., Xie, Y., Ding, Y., Li, X., Zhu, W. (2010). "Colorimetric fluoride sensors based on deprotonation of pyrrole–hemiquinone compounds." Chemical Communications., 46(21), 3669-3671.

Wang, Q.-Q., Day, V. W., and Bowman-James, K. (2011). "Tunable, shape-shifting capsule for dicarboxylates." Chemical Science, 2(9), 1735–1738.

Wang, R., Shu, X., Fan, Y., Li, S., Jin, Y., and Huang, C. (2018). "Visible colorimetric fluoride and hydroxide sensing by asymmetric tris-urea receptors: combined experimental and theoretical studies." RSC advances, 8(69), 39394–39407.

Wang, Y., Song, R., Guo, K., Meng, Q., Zhang, R., Kong, X., and Zhang, Z. (2016). "A gadolinium (iii) complex based dual-modal probe for MRI and fluorescence sensing of fluoride ions in aqueous medium and in vivo." Dalton Transactions, 45(44), 17616–17623.

Whitford, G. M. (1996). "Overview of fluoride metabolism and intake." The Metabolism and Toxicity of Fluoride, Karger Publishers, 1–9.

WHO Technical Report Series- 846, Fluoride and Oral Health, Geneva, 1994.

Wu, J.-L., He, Y.-B., Wei, L.-H., Liu, S.-Y., Meng, L.-Z., and Hu, L. (2004). "Anionic fluororeceptors based on thiourea and hydrazide: Synthesis and recognition properties." Supramolecular Chemistry, 16(5), 353–359.

Wu, L., Liu, L., Fang, R., Deng, C., Han, J., Hu, H., Lin, C., and Wang, L. (2012). "New P-bridgehead urea-based tripodal anion receptors for $H_2PO_4^-$ recognition." Tetrahedron Letters, 53(28), 3637–3641.

Wu, Y.-C., You, J.-Y., Jiang, K., Xie, J.-C., Li, S.-L., Cao, D., and Wang, Z.-Y. (2017). "Colorimetric and ratiometric fluorescent sensor for F^- based on benzimidazole-naphthalene conjugate: reversible and reusable study & design of logic gate function." Dyes and Pigments, 140, 47–55.

Xiao, L., Ren, L., Jing, X., Li, Z., Wu, S., & Guo, D. (2020). "A selective naphthalimide-based colorimetric and fluorescent chemosensor for "naked-eye" detection of fluoride ion". Inorganica Chimica Acta, 500, 119207.

Xu, G., Liu, L., and Chen, J. (2012). "Reconstruction of cytosolic fumaric acid biosynthetic pathways in Saccharomyces cerevisiae." Microbial cell factories, 11(1), 24.

Xu, X., Lin, L., Papelis, C., and Xu, P. (2018). "Sorption of arsenic from desalination concentrate onto drinking water treatment solids: operating conditions and kinetics." Water, 10(2), 96.

Xu, Z., Chen, X., Kim, H. N., & Yoon, J. (2010). "Sensors for the optical detection of cyanide ion." Chem. Soc. Rev., 39(1), 127-137.

Xu, Z., Chen, X., Kim, H. N., and Yoon, J. (2010). "Sensors for the optical detection of cyanide ion." Chemical Society Reviews, 39(1), 127–137.

Yao, S.-Z., Nie, L.-H., and Mo, Z.-H. (1989). "Determination of picomolar concentrations of bromide with a piezoelectric detector by catalysis of the permanganate/iodide reaction." Analytica Chimica Acta, 217, 327–334.

Yen, Y.-P., and Ho, K.-W. (2006). "Synthesis of colorimetric receptors for dicarboxylate anions: a unique color change for malonate." Tetrahedron letters, 47(7), 1193–1196.

Yogarajah, N., and Tsai, S. S. (2015). "Detection of trace arsenic in drinking water: challenges and opportunities for microfluidics." Environmental Science: Water Research & Technology, 1(4), 426–447.

Yong, X., Su, M., Wang, W., Yan, Y., Qu, J., and Liu, R. (2013). "A naked-eye chemosensor for fluoride ions: a selective easy-to-prepare test paper." Organic & biomolecular chemistry, 11(14), 2254–2257.

Yoo, J., Kim, M.-S., Hong, S.-J., Sessler, J. L., and Lee, C.-H. (2008). "Selective sensing of anions with calix [4] pyrroles strapped with chromogenic dipyrrolylquinoxalines." The Journal of organic chemistry, 74(3), 1065–1069.

Yoshida, A., Taniguchi, S., Hisatome, I., Royaux, I.E., Green, E.D., Kohn, L.D. and Suzuki, K. (2002). "Pendrin is an iodide-specific apical porter responsible for iodide efflux from thyroid cells." J. Clin. Endo. Metab., 87, 3356-3361.

Yoshino, J., Kano, N., Kawashima, T. (2009). "Fluorescence properties of simple N-substituted aldimines with a B− N interaction and their fluorescence quenching by a cyanide ion." The Journal of organic chemistry., 74(19), 7496-7503.

Yu, H., Fu, M., & Xiao, Y. (2010). "Switching off FRET by analyte-induced decomposition of squaraine energy acceptor: A concept to transform 'turn off' chemodosimeter into ratiometric sensors." Physical Chemistry Chemical Physics., 12(27), 7386-7391.

Yu, M., Lin, H., Zhao, G., Lin, H. (2007). "A benzimidazole-based chromogenic anion receptor." Journal of Molecular Recognition: An Interdisciplinary Journal., 20(1), 69-73.

Yu, Y., Yang, W., Dong, Z., Wan, C., Zhang, J., Liu, J., Guizhou, B. (2008). "Neurotransmitter and receptor changes in the brains of fetuses from areas of endemic fluorosis." Fluoride., 41(2), 134-138.

Zang, L., and Jiang, S. (2015). "Substituent effects on anion sensing of salicylidene Schiff base derivatives: Tuning sensitivity and selectivity." Spectrochimica Acta Part A: Molecular and Biomolecular Spectroscopy, 150, 814–820.

Zapata, F., Caballero, A., Espinosa, A., Tárraga, A., and Molina, P. (2008). "Cation coordination induced modulation of the anion sensing properties of a ferrocene–imidazophenanthroline dyad: multichannel recognition from phosphate-related to chloride anions." The Journal of organic chemistry, 73(11), 4034–4044.

Zhang, D., and Jin, W. (2012). "Highly selective and sensitive colorimetric probe for hydrogen sulfide by a copper (II) complex of azo-dye based on chemosensing ensemble approach." Spectrochimica Acta Part A: Molecular and Biomolecular Spectroscopy, 90, 35–39.

Zhang, S.-W., and Swager, T. M. (2003). "Fluorescent detection of chemical warfare agents: functional group specific ratiometric chemosensors." Journal of the American Chemical Society, 125(12), 3420–3421.

Zhang, X., Wu, Y., Ji, S., Guo, H., Song, P., Han, K., Wu, W., Wu, W., James, T. D., and Zhao, J. (2010). "Effect of the electron donor/acceptor orientation on the fluorescence transduction efficiency of the d-PET effect of carbazole-based fluorescent boronic acid sensors." The Journal of organic chemistry, 75(8), 2578–2588.

Zhang, Y.-M., Lin, Q., Wei, T.-B., Wang, D.-D., Yao, H., and Wang, Y.-L. (2009). "Simple colorimetric sensors with high selectivity for acetate and chloride in aqueous solution." Sensors and Actuators B: Chemical, 137(2), 447–455.

Zhao, J., Fyles, T. M., and James, T. D. (2004). "Chiral binol–bisboronic acid as fluorescence sensor for sugar acids." Angewandte Chemie International Edition, 43(26), 3461–3464.

Zhao, L., Liu, G., & Zhang, B. (2016). A colorimetric and fluorescence enhancement anion probe based on coumarin compounds. Spectrochimica Acta Part A: Molecular and Biomolecular Spectroscopy, 169, 45-49.

Zhao, Y., and Truhlar, D. G. (2008). "Density functionals with broad applicability in chemistry." Accounts of chemical research, 41(2), 157–167.

Zhao, Y., Li, Y., Qin, Z., Jiang, R., Liu, H., and Li, Y. (2012). "Selective and colorimetric fluoride anion chemosensor based on s-tetrazines." Dalton Transactions, 41(43), 13338–13342.

Zou, L., Yan, B., Pan, D., Tan, Z., & Bao, X. (2015). "A colorimetric and absorption ratiometric anion sensor based on indole & hydrazide binding units". Spectrochimica Acta Part A: Molecular and Biomolecular Spectroscopy, 148, 78-84.

Zougagh, M., Ríos, A., and Valcárcel, M. (2005). "Direct determination of total carbonate salts in soil samples by continuous-flow piezoelectric detection." Talanta, 65(1), 29–35.

PUBLICATIONS

&

CONFERENCES

LIST OF PUBLICATION

Papers published/communicated in international journals

- **Singh, A.,** & Trivedi, D. R. (2017). "Naked-eye'detection of biologically important anions in aqueous media by colorimetric receptor and its real life applications". *Spectrochimica Acta Part A: Molecular and Biomolecular Spectroscopy*, 179, 95-103.

- **Singh, A.,** Sahoo, S. K., & Trivedi, D. R. (2018). "Colorimetric anion sensors based on positional effect of nitro group for recognition of biologically relevant anions in organic and aqueous medium, insight real-life application and DFT studies". *Spectrochimica Acta Part A: Molecular and Biomolecular Spectroscopy*, 188, 596-610.

- **Singh, A.,** Gowda, R. G., & Trivedi, D. R. (2019). "Substituent effect on colorimetric detection of biologically and environmentally relevant anions: Insight in real-life applications". *Spectrochimica Acta Part A: Molecular and Biomolecular Spectroscopy*, 219, 517-529.

- **Singh, A.,** Mohan, M., & R. Trivedi, D. (2019). Chemosensor Based on Hydrazinyl Pyridine for Selective Detection of F^- Ion in Organic Media and CO_3^{2-} Ions in Aqueous Media: Design, Synthesis, Characterization and Practical Application. *ChemistrySelect*, *4*(48), 14120-14131.

- **Singh, A.,** Mohan, M., & Trivedi, D. R. (2020). "Design and synthesis new colorimetric receptors for naked-eye detection of biologically important fluoride and acetate anions in organic and arsenite in aqueous medium based on ICT mechanism: DFT study and test strip application". *Spectrochimica Acta Part A: Molecular and Biomolecular Spectroscopy*, 225, 117522.

- **Singh, A.,** Mohan, M., & Trivedi, D. R. (2020). Design and synthesis of malonohydrazide based colorimetric receptors for discrimination of maleate over fumarate and detection of F^-, AcO^- and AsO_2^- ions. *Spectrochimica Acta Part A: Molecular and Biomolecular Spectroscopy*, 229, 117883.

- **Singh, A.,** Nishith, U., & Trivedi, D. R. (2020). Spectroscopic studies of colorimetric receptors for detection of biologically important inorganic F^-,

AcO⁻ and $H_2PO_4^-$ anions in organo-aqueous medium: Real-life application. Inorganic Chemistry Communications, 107874.

Papers presented in national/international conferences

❖ **Archana Singh,** Darshak R. Trivedi. (2016). "Schiff Base Colorimetric Chemosensor for the Detection of Biologically Important Anions". Paper presented in "International Conference on Science & Technology: Futher Challenge and Solutions (STFCS-2016)" August 8-9, Mysore.

❖ **Archana Singh,** Darshak R. Trivedi. (2017). "Naked-Eye Detection of Bioactive Anion with A Colorimetric Anion Sensor: Insight Real Life Application". Paper presented in "International Conference On Crystal Ball Vision On Science & Engineering For Societal Upliftment" August 7-8, Goa.

❖ **Archana Singh,** Makesh Mohan, Darshak R.Trivedi (2018). "Colorimetric detection of biologically important anion based on ICT Between Donor– Acceptor (D–A): Experimental and DFT studies" paper presented in "International Conferences on advanced materials, energy & environmental substainablity (ICAMEES-2018)" 14-15 December 2018, Dehradun.

❖ **Archana Singh,** Darshak R.Trivedi (2019). "Design and synthesis of colorimetric anion chemosensor for naked-eye detection of biologically important fluoride and acetate ion" paper presented in national conference on "synthesic, spectroscopic and structural chemistry (SSSC-2019) " 15-16 March 2019, govinda dasa collage. **(First Prize in poster presentation).**

❖ **Archana Singh,** Darshak R.Trivedi (2019). "Naked-eye detection of inorganic fluoride and acetate ion in an aqueous medium using Organic receptor: Real life application" paper presented in international conference on advance in basic science (ICABS19) 7-9, February 2019, GDC memorial collage, bahal, district bhiwani (Haryana) india.

❖ **Archana Singh,** Darshak R.Trivedi (2019). "Naked-eye detection of biologically important anions based on a new colorimetric receptors and its application in real sample analysis" paper presented in national conference on national symposium on environmental pollution prevention and control: further perspective (EPPC:FP-2019)" 23-25, August 2019. **(Best Paper Award).**

❖ **Archana Singh,** Darshak R.Trivedi (2019). "Synthesis and spectroscopic study of simple naked-eye colorimetric chemosensor for bioactive anions in organic and aqueous medium: Real-life application" paper presented in international conference on emerging advancement in science & technology& 10th India-Japan science & technology conclave September 5-6, 2019 New Delhi.

Papers published in conference proceedings

1. **Singh, A**., & Trivedi, D. R. (2019, August). Naked-eye detection of inorganic fluoride and acetate ion in an aqueous medium using organic receptor: Real life application. In AIP Conference Proceedings (Vol. 2142, No. 1, p. 190009). AIP Publishing LLC.

2. Trivedi, D. R., **Singh, A**., & Mohan, M. (2019). Colorimetric detection of biologically important anion based on ICT Between Donor–Acceptor (D–A): Experimental and DFT studies. International Journal of Photochemistry, 5(1), 49-56.

CURRICULUM VITAE

<h1 style="text-align:center">CURRICULUM VITAE</h1>

Name: ARCHANA SINGH

Email: archu.svnit@gmail.com, archu.nitk@gmail.com

Mobile: +91-8762902293

Research Interests

Design, synthesis and characterization of colorimetric receptors for the detection of biologically and environmentally important anion and its application

Academic qualifications

July 2015 – December 2019	Ph.D. in chemistry under the guidance of Dr. Darshak R. Trivedi, (**Associate Professor**) Department of Chemistry, National Institute of Technology Karnataka, Surathkal, Mangalore, Karnataka, INDIA
October 2013-June 2015	JRF, (IIT GN) Indian Institute of Technology, Palaj, Gujarat 382355 under Dr. Sudhanshu Sharma & Dr. Sriram Kanvah Gundimeda
June 2008 - May 2013	Five year integrated M.Sc Chemistry (SVNIT Surat) Sardar Vallabhbhai National Institute of Technology, Surat

Achievements and Awards

1. First Prize in poster presentation "Synthetic spectroscopic and structural chemistry (SSSC-2019)" conducted by Govinda Dasa College Surathkal, 15-16 March 2019

2. Best Paper Award in "Nation Conference On National Symposium On Environmental Pollution Prevention and Control: Further Perspective (EPPC:FP-2019)" 23-25, August 2019

Papers published/communicated in international journals

1. **Singh, A.,** Tom, S., & Trivedi, D. R. (2018). Aminophenol based colorimetric chemosensor for naked-eye detection of biologically important fluoride and acetate ions in organo-aqueous medium: Effective and simple anion sensors. *Journal of Photochemistry and Photobiology A: Chemistry*, 353, 507-520.

2. **Singh, A.,** & Trivedi, D. R. (2017). 'Naked-eye' detection of biologically important anions in aqueous media by colorimetric receptor and its real life applications. *Spectrochimica Acta Part A: Molecular and Biomolecular Spectroscopy*, 179, 95-103.

3. **Singh, A.,** Sahoo, S. K., & Trivedi, D. R. (2018). Colorimetric anion sensors based on positional effect of nitro group for recognition of biologically relevant anions in organic and aqueous medium, insight real-life application and DFT studies. *Spectrochimica Acta Part A: Molecular and Biomolecular Spectroscopy*, 188, 596-610.

4. **Singh, A.,** Gowda, R. G., & Trivedi, D. R. (2019). Substituent effect on colorimetric detection of biologically and environmentally relevant anions: Insight in real-life applications. *Spectrochimica Acta Part A: Molecular and Biomolecular Spectroscopy,* 219, 517-529.

5. **Singh, A.,** Mohan, M., & R. Trivedi, D. (2019). Chemosensor Based on Hydrazinyl Pyridine for Selective Detection of $\bar{F}$ Ion in Organic Media and CO_3^{2-} Ions in Aqueous Media: Design, Synthesis, Characterization and Practical Application. *ChemistrySelect*, 4(48), 14120-14131.

6. **Singh, A.,** Mohan, M., & Trivedi, D. R. (2020). "Design and synthesis new colorimetric receptors for naked-eye detection of biologically important fluoride and acetate anions in organic and arsenite in aqueous medium based on ICT mechanism: DFT study and test strip application". *Spectrochimica Acta Part A: Molecular and Biomolecular Spectroscopy*, 225, 117522.

7. **Singh, A.,** Mohan, M., & Trivedi, D. R. (2020). Design and synthesis of malonohydrazide based colorimetric receptors for discrimination of maleate

over fumarate and detection of F^-, AcO^- and AsO_2^- ions. *Spectrochimica Acta Part A: Molecular and Biomolecular Spectroscopy*, *229*, 117883.

8. **Singh, A.,** Nishith, U., & Trivedi, D. R. (2020). Spectroscopic studies of colorimetric receptors for detection of biologically important inorganic F^-, AcO^- and $H_2PO_4^-$ anions in organo-aqueous medium: Real-life application. *Inorganic Chemistry Communications,* 107874.

9. **Singh, A.,** Palakollu, V., Pandey, A., Kanvah, S., & Sharma, S. (2016). Green synthesis of 1, 4-benzodiazepines over La_2O_3 and $La(OH)_3$ catalysts: possibility of Langmuir–Hinshelwood adsorption. *RSC Advances*, 6(105), 103455-103462.

10. Gangwar, B. P., Palakollu, V., **Singh, A.,** Kanvah, S., & Sharma, S. (2014). Combustion synthesized La_2O_3 and $La(OH)_3$: recyclable catalytic activity towards Knoevenagel and Hantzsch reactions. *RSC Advances*, 4(98), 55407-55416.

11. Malek, N. I., **Singh, A.,** Surati, R., & Ijardar, S. P. (2014). Study on thermo physical and excess molar properties of binary systems of ionic liquids. I:[Cnmim][PF6](n= 6, 8) and alkyl acetates. *The Journal of Chemical Thermodynamics*, 74, 103-118.

Papers published in conference proceedings

1. **Singh, A**., & Trivedi, D. R. (2019, August). Naked-eye detection of inorganic fluoride and acetate ion in an aqueous medium using organic receptor: Real life application. In AIP Conference Proceedings (Vol. 2142, No. 1, p. 190009). AIP Publishing LLC.

2. Trivedi, D. R., **Singh, A**., & Mohan, M. (2019). Colorimetric detection of biologically important anion based on ICT Between Donor–Acceptor (D–A): Experimental and DFT studies. International Journal of Photochemistry, 5(1), 49-56.

Instrumentation skills

Hands-on experience in handling and usage of UV-Vis spectrophotometer (analytic jena Specord S-600, Thermo scientific Genesys 10s), Cyclic voltammetry-IVIUM electrochemical workstation (Vertex), FT-IR (Bruker) spectrophotometer, Cyclic voltammetry-lvium electrochemical workstation (Vertex) and Fluorescence spectrophotometer (JASCO-FP-6200).

Specialized skills

- Mentored three post graduate project students and assisting practical laboratory for engineering graduates and post graduate science students
- Software Sills: Microsoft, Origin
- Turbomole

Workshop attended

- National workshop on "Nano-structural material and their application in catalysis & Fuel Cells" organized by Department of Chemical Engineering NITK Surthkal from Semptember 29^h -1th, 2016
- Software and Application of Single Crystal X-Ray Diffraction, 29th– 31th August 2019 at Department of Chemistry, Smt. S.S.Patel Nootan Science& Commerce Colleage Visnagar, Dist-Mehsana, Gujarat-384315
- National workshop on "Recent Advances in Material Chemistry (RAMC)" organized by Department of Chemistry NITK Surthkal on 26 Semptember 2019

Personal Details

Date of birth	18th September 1988
Nationality	Indian
Marital Status	Single
Languages known	English, Hindi, Tamil,
Permanent address	A 32, Siddharth Kunj, Veer savarkar nagar
	100 futta road, Dist-Bareilly, Uttar Pradesh-243001

References

Dr. Darshak R. Trivedi

(Associate Professor)

(Research supervisor)

Department of Chemistry,

National Institute of Technology Karnataka

(NITK), Surathkal-575025,

Mangalore, Karnataka, India

Mob: +91-9481271272; Tel.: +91-824-

2473205; Fax: +91 824 2474033

E-mail: darshak_rtrivedi@yahoo.co.in